

MARINE & COASTAL HARTIAF MANAGEMENT
ALASKA DEPT. OF FISHERY & GAME
333 Raspberry Road
Anchorage, Alaska 99502

Environmental Assessment of the Alaskan Continental Shelf

Annual Reports of Principal Investigators
for the year ending March 1979

Volume VII. Transport



U.S. DEPARTMENT OF COMMERCE
National Oceanic and Atmospheric Administration



U.S. DEPARTMENT OF INTERIOR
Bureau of Land Management

VOLUME I	RECEPTORS -- MAMMALS BIRDS
VOLUME II	RECEPTORS -- BIRDS
VOLUME III	RECEPTORS -- FISH, LITTORAL, BENTHOS
VOLUME IV	RECEPTORS -- FISH, LITTORAL, BENTHOS
VOLUME V	RECEPTORS -- MICROBIOLOGY CONTAMINANT BASELINES
VOLUME VI	EFFECTS
VOLUME VII	TRANSPORT
VOLUME VIII	TRANSPORT
VOLUME IX	HAZARDS
VOLUME X	HAZARDS DATA MANAGEMENT

ARLIS

Alaska Resources
Library & Information Services
Anchorage, Alaska

Environmental Assessment of the Alaskan Continental Shelf

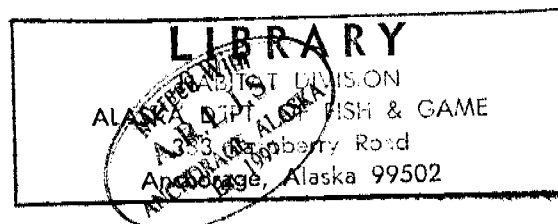
GC
85.2
.A4
E57
1979
v.7

Annual Reports of Principal Investigators
for the year ending March 1979

Volume VII. Transport

Outer Continental Shelf Environmental Assessment Program
Boulder, Colorado

October 1979



U.S. DEPARTMENT OF COMMERCE
National Oceanic and Atmospheric Administration

U.S. DEPARTMENT OF INTERIOR
Bureau of Land Management

ARLIS
Alaska Resources
Library & Information Services
Anchorage, Alaska

DISCLAIMER

Mention of a commercial company or product does not constitute an endorsement by National Oceanic and Atmospheric Administration. Use for publicity or advertising purposes of information from this publication concerning proprietary products or the tests of such products is not authorized.

ACKNOWLEDGMENT

These annual reports were submitted as part of contracts with the Outer Continental Shelf Environmental Assessment Program under major funding from the Bureau of Land Management.

TRANSPORT

CONTENTS

<u>RU #</u>	<u>PI - Agency</u>	<u>Title</u>	<u>Page</u>
48	Barrick, D. - Wave Propagation et al. Lab, ERL, NOAA, Boulder, CO	Data Processing and Analysis from H-F Radar Data Obtained in Cook Inlet Alaska During Summers 1977 and 1978	1
59	Hayes, M. - Univ. of South Ruby, C. Carolina, Columbia, SC	Oil Spill Vulnerability, Coastal Morphology, and Sedimentation of Kotzebue Sound	115
87	Martin, S. - Univ. of Washington, Seattle, WA	The Interaction of Oil with Sea Ice in the Arctic Ocean	171
88	Kovacs, A. - Cold Regions Weeks, W. Research & Engineering Lab, Hanover, NH	Dynamics of Near-Shore Ice	181
91	Aagaard, K. - Univ. of Washington, Seattle, WA	Current Measurement in Possible Dispersal Regions of the Beaufort Sea	208
138	Muench, R. - Pacific Marine Schumacher, J. Environmental Lab, Sillcox, R. Seattle, WA	Northwest Gulf of Alaska Shelf Circulation	232
141/ 549	Charnell, R. - Pacific Marine Schumacher, J. Environmental Lab, Coachman, L. U. of Washington, Seattle, WA	Bristol Bay Oceanographic Processes (B-BOP)	249
289	Royer, T. - Institute of Marine Science, U. of Alaska, Fairbanks	Circulation and Water Masses in the Gulf of Alaska	320
367	Reynolds, R. - Pacific Marine et al. Environmental Lab Seattle, WA	Near-Shore Meteorology	384
430	Cacchione, D. - U.S. Geological Drake, D. Survey, Menlo Park, CA	Bottom and Near-Bottom Dynamics in Lower Cook Inlet	505
435	Leendertse, J. - The Rand Corp. Liu, S. Santa Monica, CA	Modeling of Tides and Circulation of the Bering Sea	547

QUARTERLY REPORT

Project No: RW0000 R

Research Unit: No. 48

Reporting Period:

April 1, 1979 thru June 30, 1979

No. of Pages:

Data Processing and Analysis from H-F Radar Data
Obtained in Cook Inlet Alaska During Summers 1977 and 1978

Principal Investigators: Donald E. Barrick
Shelby Frisch
Robert Weber

Submitted: June 30, 1979

Wave Propagation Laboratory
Environmental Research Laboratories
National Oceanic and Atmospheric Administration

Data Processing and Analysis from H-F Radar Data
Obtained in Cook Inlet During Summers 1977 and 1978

Progress Report - 30 June 1979

I. Abstract

During the summer of 1977 the H-F Doppler surface current radar system was deployed in Lower Cook Inlet, Alaska at Anchor Point and Seldovia. Several time series of data were collected during the deployment period. A representative 24-hour data set has been extensively analyzed. A paper by Frisch and Weber based on the tidal analysis of these data has been submitted to JGR. A copy of the manuscript draft is included as the first section of this report.

During the summer of 1978, the radar system was successfully operated in western Lower Cook Inlet, Alaska, for a period of two weeks. We collected about 8 days of data during this time. The radar sites were located at Cape Douglas and Augustine Island for these experiments. These data have been processed and current vector maps have been plotted. These results appear in the second section of the report.

II. Objectives

The FY 79 objectives of this project are to analyze the 1978 data and to provide a Final Report containing analysis and interpretation of data collected during 1977 and 1978. Specific objectives for analysis of the 1978 data include the following:

1. Produce an observed current map for each usable data sample.
2. Produce non-tidal current maps, in which the tidal effects have been filtered out. This will result in a time-averaged map every 12 hours over the 8-day data collection period. These maps will be generated from 24-hour data segments least squares fit for the 0 frequency.
3. Produce x and y components of flow in a suitable format for trajectory calculations and comparison with model results (RU 436) over the entire 1978 data period.
4. Attempt to correlate the non-tidal current results with the local meteorology prevailing during the observation period. We will investigate effects of storms and prevailing winds on the surface currents by using observations from the Lower Cook Inlet data buoy and other meteorological data such as RU 367 can provide.

5. Compare the tidal and non-tidal currents and time series data with the results of moored current meter observations provided by RU 138. Compare the low passed time series every 12 hours.

III. Field Activities

None for this year.

IV. Results

The results of Objective 1 are presented in the second report section in the form of chronological current vector maps covering the eight-day observation period. Interpretation of these results is presently underway and will be included in the Final Report. Even though the interpretation cannot be presented at this time, we believe that the current maps, in themselves, are of sufficient interest to warrant inclusion in the present report.

The analyses for Objectives 2-5 are proceeding according to schedule.

SECTION I: ANALYSIS OF 24-HOUR TIME SERIES, EASTERN LOWER
 COOK INLET, JULY 1977

A NEW TECHNIQUE FOR MEASURING TIDAL CURRENTS
USING A TWO-SITE HF DOPPLER RADAR SYSTEM

A. S. Frisch and B. L. Weber
NOAA/ERL/Wave Propagation Laboratory
Boulder, Colorado 80302

Abstract

We have measured surface currents using a newly developed H-F (High Frequency) Doppler radar technique. The system was operated in lower Cook Inlet, Alaska in July, 1977. During one particular day, (13 July), we analyzed the radar data collected every 30 minutes for 24 hours. By least squares fitting these data to two of the dominate tidal periods 12.31 and 24.6 hours, we determined the spatial distribution of the tidal currents for each of these two periods. In addition, we determined the spatial distribution of the mean surface currents for this 24 hour period.

Our analysis of this data shows that near Kachemak Bay, there is a distinct difference of the east-west component of tidal flow compared to regions further from Kachemak. In addition, we observed longer period components that we cannot determine the period for. These components exhibited gyre-like spatial patterns. Our results demonstrates the use of H-F radar techniques for resolving spatial and temporal currents which affect the nearshore environment.

Acknowledgment

This study was partially supported by the Bureau of Land Management through interagency agreement with the National Oceanic and Atmospheric Administration, under which a multi-year program responding to needs of petroleum development of the Alaska Continental shelf is managed by the Outer Continental Shelf Environmental Assessment Program (OCSEAP) office. We would also like to thank the personnel of Alaska Fish and Game and all the personnel in the Wave Propagation Laboratory's Sea State Studies Program under the direction of Dr. D. E. Barrick for their help in this study.

A NEW TECHNIQUE FOR MEASURING TIDAL CURRENTS
USING A TWO-SITE HF DOPPLER RADAR SYSTEM

A. S. Frisch and B. L. Weber
NOAA/ERL/Wave Propagation Laboratory
Boulder, Colorado 80302

Introduction

Until recently, surface current observations have been made using either moored current meters or any of a variety of drifters (McCullough, 1977). For practical reasons, these observations were limited in their sampling both temporally and spatially. However, the use of High-Frequency (HF) Doppler radar techniques (Barrick and Evans, 1976; Barrick et al., 1977) now allows one to determine the surface currents over an area of about 2500 km² on a continuous basis in time. With such measurements it is possible to determine the tidal structure of the surface currents and the residual effects such as wind driven currents, net water outflow etc. In July of 1977, two of these radar units were employed to study the currents in the Lower Cook Inlet near Kachemak Bay. This paper shows some results of the analysis of this data during one 24-hour period on 13 July 1977.

Background

The initial discovery of surface-current effects on backscattered HF electromagnetic waves was made by Crombie (Crombie, 1972). Since then, theoretical and experimental studies of surface-current effects have been conducted by Barrick, et al. (1974), Stewart and Joy (1974), and Barrick et al. (1977). Stewart and Joy (1974) have shown that the radial component of surface current measured by the HF radar compares well with radial velocities determined by tracking a float by conventional techniques. Barrick and Evans (1976) describe a two-site technique which

provides both components of surface currents rather than just the radial component. This technique was tested in Florida using two shore-based, transportable HF radars at Fort Lauderdale and Miami Beach (Barrick et al. 1977).

Each radar does not measure the radial current directly but, rather, measures the phase velocity of certain ocean waves which are propagating radially toward or away from the radar. These ocean waves must have wavelengths exactly one-half of the HF wavelength because of the scattering mechanism. This mechanism is called Bragg scattering because of the close analogy with the diffraction of light by optical gratings and the diffraction of x-rays by crystals. The scattering process allows the radar to selectively measure the phase velocity of these particular ocean waves. Since this velocity is known with a great deal of accuracy when there is no current, any significant deviation from this value is therefore attributed to currents.

The accuracy of the radar-measured currents depends upon a number of experimental and theoretical parameters. When the radar measurements were compared with drifter measurements (using a "Hi-Fix" radio-positioning system) of the Gulf Stream (Barrick et al. (1977)), it was found that the two sets of measurements agreed to within 0.5 knots. The currents ranged from near zero up to values in excess of 4 knots, and the agreement was often much better than 0.5 knots. Later, it was determined that experimental errors in both sets of measurements were the limiting factors and not any inherent limitation in either method. Theoretically, the accuracy of the radar measurements can be expected to be within 10 cm/s. However, near perfect agreement between radar and conventional techniques should not be expected since they do not measure the same quantity. By virtue of the scattering process, the radar measures the current averaged over several square kilometers in area, whereas, the drifter technique averages a trajectory over some time interval. Therefore, caution must be exercised in the interpretation of any discrepancy between these different sets of measurements.

Method of Tidal Analysis

For the experiment described here two radars were operated simultaneously at Seldovia ($59^{\circ} 27' 30''$ N, $151^{\circ} 42' 30''$ W) and Anchor Point ($59^{\circ} 46' 18''$ N, $151^{\circ} 52' 6''$ W) which are located on the Eastern side of the Lower Cook Inlet, Alaska (Fig. 1). Operating each radar alternately for 15 minutes every half hour over a 24-hour period, we obtained a data base from which were computed (by the least-squares method) estimates of the nominal 12- and 24-hour tidal components for the surface currents as a function of position. The current velocity at selected locations were decomposed into semi-diurnal and diurnal components, which show a considerable but orderly amplitude and phase variation over the radar coverage area.

To obtain the tidal parts of the surface currents, we used results of Doodson (1921) who examined all the frequencies of importance in the moon-sun-earth system. Neumann and Pierson (1966) pointed out that, no matter how complex the boundary conditions or how strong or weak the effects of friction, the solution for the tidal amplitudes and tidal currents must contain these same periodic terms. However, the amplitudes and phases of these components will be dependent upon the geometry of the location, such as the length and depth of a particular embayment. Some of the important frequencies are listed in Defant (1961) and Neumann and Pierson (1966). Since we have a limited data set timewise (24 hours), we cannot separate out any amplitude coefficients falling within the semi-diurnal or diurnal components. What we have done is to take the principal solar and lunar frequencies and average them with weights proportional to the coefficients given in Defant's (1961) table on page 267 for the open ocean. The semi-diurnal period then became approximately 12.31 hours. Similarly, we have taken the Luni-solar diurnal and the principle lunar diurnal and averaged them to obtain approximately 24.6 hr. It should be noted that the relative weights of these coefficients will depend upon the particular location in coastal waters, so that these two averaged frequencies would not be strictly constant throughout Cook Inlet.

We least-squares fitted the N-S and E-W components of the data to the sine and cosine terms with these two periods as follows:

$$u = u_0 + \sum_{n=1}^2 [u'_n \cos(2\pi \frac{t}{\tau_n}) + u''_n \sin(2\pi \frac{t}{\tau_n})]$$

$$v = v_0 + \sum_{n=1}^2 [v'_n \cos(2\pi \frac{t}{\tau_n}) + v''_n \sin(2\pi \frac{t}{\tau_n})]$$

where u is the north component, v is the west component, and $n=1$ and 2 indicate the nominal 24-hour and 12-hour periods, respectively. The leading "DC" or constant terms are used to pull out any bias in the data due to long term trends and the coefficients were computed simultaneously using the least-squares technique.

Results

The data can be viewed in one of two ways depending upon whether the time dependence or space dependence is to be illustrated. First, we selected a small set of locations (Fig. 2) at which the tidal flow will be pictured as a function of time. These particular locations were selected in order to illustrate the strong spatial variability introduced by bathymetric variation within the region being studied. Figure 3 gives the north and west components of the tidal flow along five cuts through Kachemak Bay. These results clearly reveal that the west component exhibits much more spatial dependence in phase and amplitude than does the north component. For all five cuts, the north component of current assumes its maximum and minimum values at nearly the same time for all of the locations. The only significant spatial variation is in the amplitude of this component. The amplitude generally increases smoothly going from east to west and from south to north. On the other hand, the occurrence in time of the extremal values for the west component shows a high degree of spatial variability and the amplitude exhibits a dramatic position dependence.

The east-west cuts EW1 in Fig. 3a and EW2 in Fig. 3b reveal large amplitudes in the west component at opposite ends of these cuts with

very diminished values at intermediate locations. In addition, the sense of direction is reversed at opposite ends of these cuts. In contrast, the northernmost cut EW3 in Fig. 3c, does not exhibit this degree of variation. One should also note that, in the majority of cases, the 12-hour tidal component dominates, the most noteworthy exception being the second position along EW2 going from east to west.

The south-north cuts SN1 in Fig. 3d and SN2 in Fig. 3e also display a contrast in behavior for the west component. The eastmost cut SN1 shows the amplitude to be larger near the end points and smaller at intermediate locations, while the cut SN2 shows the amplitude increasing going from south to north. More dramatic though is the gradual shift in phase as one moves from position to position along these cuts, suggesting a travelling-wave-like feature. In addition, the phase change is much greater along cut SN1 than along cut SN2.

Another very useful format for this data is in the form of an area map which represents a "snapshot" of the flow at some time during the 24-hour period. For example, the time sequence of maps in Fig. 4 shows the dominance of the north-south flow in Cook Inlet and also reveals how the intricate bottom topography of Kachemak Bay diverts a portion of this flow, setting up the west-east patterns seen in Fig. 3. According to tide tables for Seldovia, the high water levels were reached around 00, 12, and 24 hours (see Table I). From these maps, it is clear that slack water does not occur at the same time as the occurrence of high or low water, which would be expected in the open ocean. This fact was also confirmed by tracking drifters in this area, but not on this same day.

The next map sequence (Fig. 5) shows the 12-hour tidal component alone over the first half of the day (i.e., one complete cycle). The flow due to this component would, of course, be the same during the second half of the day. These maps illustrate that the flow into and out of Kachemak Bay tends to follow the trough at the southern end of the bay. Also, we see that the current vectors do indeed reverse their

directions at 6-hour intervals, whereas the composite flow in Fig. 4 would not be expected to show this behavior because of the presence of other current components. The 24-hour tidal component is given in the sequence of maps in Fig. 6 which reveal that the 12-hour and 24-hour components are nearly 180° out of phase at 00 hours (Figs. 5a and 6a) and nearly in phase at 12 hours (Figs. 5a and 6d). This would explain the stronger composite flow at 12 hours (Fig. 4d) compared with 00 hours (Fig. 4a). One interesting point is evident when we compare the 24-hour maps with the 12-hour maps. The former maps show greater spatial variability than do the latter. In particular, the 24-hour component exhibits a greater portion of its energy flowing east and west than does the 12-hour component.

In addition to the tidal induced flow, we also computed the longer-period flow (Fig. 7) which would be caused by seasonal runoff, storm surge, winds, etc. that create a circulation pattern peculiar to Cook Inlet. The current vectors are plotted at a greater spatial density and with larger vectors in this figure in order to emphasize the circulation pattern in Kachemak Bay. The largest current magnitude in this component is about 25 cm/s compared with a maximum velocity of nearly 150 cm/s in Fig. 4d for the composite. A significant feature of the steady flow is the region of very weak current which seems to form a boundary between a predominately northerly flow inside Kachemak Bay and a more or less westerly flow farther out in Cook Inlet.

Errors

During the collection of this particular set of data, there was no effort made to make measurements with drifters or current meters for purposes of comparison. Furthermore, it is not really the purpose of this paper to make or evaluate such comparisons. However, since tides are well understood physical phenomena and since the tidal frequencies are well documented, we believe that a fit of the radar measurements to

these tidal frequencies should provide some indication of the reliability of these measurements. For example, in Fig. 8, the raw radar data is shown with the composite tidal curve which was computed using the least squares method. With few exceptions, the raw data falls within 15 cm/s of the tidal curve, giving an exceptionally close fit. This result would indicate that the flow was due mostly to tides and other low frequency mechanisms and that the radar measurements are very accurate. However, caution should be exercised in interpreting any difference between the data and the curves to be due to measurement errors alone because there are a number of other agents such as local winds which would cause deviations from the simple tidal flow modeled here.

Since we lacked any independent measurements of error, we used the goodness of fit to map the region (Fig. 9) of acceptable radar data. It is an important point that most of the area over water covered by the radar system fell within this region. At the greatest ranges (beyond 36 km) from each of the sites, the signal-to-noise ratio of the HF Doppler spectra became so small that we did not expect reliable measurements. Actually, improvements on the radar system should its subsequent capability of mapping currents out to 70 km in range. Later experiments in Cook Inlet, off the Atlantic coast of Georgia, and in Washington Sound better demonstrated the real potential of this radar system as an important oceanographic tool for probing ocean currents. Also, we knew that the two-site vector composition would become very unstable near the baseline drawn between the sites. Furthermore, a significant comment can be made about the quality of the data by noting that there was no spatial filtering used so that each of the vectors in Figs. 3 through 7 are independent of one another. The consistency of the spatial distribution along with the close fit as a function of time gives us confidence in these results.

The radar system has been shown in other experiments to measure surface currents to an accuracy of ~ 15 cm/s, by comparisons with surface drifters.

Florida Gulf Stream experiments (Barrick et al., 1978) showed rms differences between radar and drifter measurements of ~ 10 cm/s during the period when the drifter was functioning properly. Although drifter measurements could not be made during all of our Alaskan operations, a fairly extensive set of such comparisons was done on July 1, 1977 over a large part of the radar coverage area and over nearly one complete semi-diurnal tidal cycle. Figure 10 is a correlogram of these comparisons; later analyses of these same radar data (based on software improvements) showed the rms difference to be ~ 15 cm/s for July 1.

Discussion and Conclusions

The analysis presented here illustrates a very useful feature of the HF Doppler radar technique for measuring ocean currents: that is, the spatial and temporal patterns can be easily separated from one another. In order to obtain similar results with conventional techniques, one would require the use of hundreds of moored current meters or the simultaneous tracking of hundreds of drifters. One example of the insight provided by this analysis is the observation that Kachemak Bay apparently modifies the spatial pattern of the flow at the 24-hour period to a greater extent than it does at the 12-hour period. This is evident if we compare the map sequences in Figs. 5 and 6 which show that the 24-hour period contains a greater proportion of east-west flow relative to the south-north flow than does the 12-hour period. Since Kachemak Bay is oriented with its axis nearly along an east-west line, we should expect some east-west flow. However, it is not immediately obvious that the 24-hour period should exhibit a higher percentage of east-west flow.

Another possible use for this type of data would be as input to or verification of tidal models such as that developed by Matthews and Mungall (1972) for Cook Inlet. Since their model only covered Cook Inlet north of Anchor Point, we could not make a quantitative comparison.

But, we do see that our currents south of Anchor Point are reasonably consistent with the currents of 100 cm/s to 120 cm/s predicted by their model. A further possible use is the detection of gyre-like features (Fig. 7) which could trap debris, oil, or fish larvae and which, as a result, were of interest to Burbank (1977) and Muench et al. (1978). Their observations of drifters and flotsam (Burbank) along with current meter measurements (Muench et al.) have allowed them to infer the presence of gyres in and around Kachemak Bay even though they could not observe the gyres directly.

In addition, it is worth mentioning that, while the HF Doppler technique only measures currents within a meter or so of the surface, the tidal flow behaves nearly independently of depth because tides are shallow water waves. In those near-shore regions where the tidal currents dominate (as in the present case), the radar measurements, in conjunction with the tidal analysis, actually provides sub-surface currents which are important for stress considerations of off-shore oil platforms. And finally, radar data should prove useful in the study of the tides themselves in coastal and estuarial zones where bathymetry and nonlinear behavior (Munk and Cartwright, 1966) become important.

References

- Crombie, D. C., in Proceedings of IEEE Ocean '72 Conference (IEEE Publ. 72 CHO 660-10CC Institute of Electrical and Electronics Engineers, New York 1972), pp 173-179.
- Barrick, D. E., Headrick, J. M., Bogle, R. W. and Crombie, D. D., 1974, Sea Backscatter at HF: interpretation and utilization of the echo, Proc: IEEE, Vol 62 pp 673-680.
- Stewart, R. H., and Joy, J. W., 1974, HF radio measurements of surface currents, Deep Sea Research, 21, 1039-1049.
- Barrick, D. E., Evans, M. W., and Weber, B. L., 1977, Ocean surface currents mapped by radar, Vol 198, No. 4313 Science. 14, Oct. 1977.
- Barrick, D. E., Evans, M. W., and Weber, B. L., 1978, Ocean surface currents mapped by radar (revised), W. Woodward, C.N.K. Mooers, and K. Jensen (eds.), Proc. of a Working Conference on Current Measurement. Tech. Report DEL-SG-3-78, College of Marine Studies, University of Delaware, Newark, DE 19711, 372 pp., June 1978.
- Barrick, D. E., and Evans, M. W., 1976, Implementation of coastal current-mapping HF radar system, Progress Report No. 1, NOAA Tech. Report ERL 373-WPL 47.
- Matthews, J. B., and Mungall, J. C. H., 1972, A numerical tidal model and its application to Cook Inlet, Alaska, Journal of Marine Research 30, 1 p 27-38.
- Doodson, A. T., 1921, The harmonic development of the tide-generating potential. Proc. Roy. Soc., A, Vol. 100 pp. 305-329 (London).

Neumann, G. and Pierson, W. J., Jr., 1966, Principles of Physical Oceanography. Prentice-Hall, Inc., 545 pp.

Defant, A., 1961, Physical Oceanography, Vol. II. Pergammon Press, 598 pp.

Burbank, D. C., 1977, Cumulation Studies in Kachemak Bay and Lower Cook Inlet Alaska, Dept. of Fish and Game, Anchorage, Alaska.

Muench, R. D., Mofjeld, H. O., and Charnell, R. L., 1978, Oceanographic conditions in Lower Cook Inlet: Spring and Summer 1973. J. of Phys. Oceanography, Vol. 83, p. 5090-98.

Munk, W. H., and Cartwright, D. E., 1966, Tidal spectroscopy and prediction. Proc. Roy. Soc. A, Vol. 253, pp 533-581.

Figure Captions

Figure 1. The currents were remotely measured in the lower Cook Inlet, Alaska (boxed area) during July 1977. Two radar units were located on the Kenai Peninsula to the right of this area. One unit was positioned at Anchor Point, just north of Kachemak Bay, and the other was placed at Seldovia on the southern side of the bay. The town of Homer is located on the eastern edge of the bay and Anchorage is at the northern end of Cook Inlet. The larger island just south of the box is Kodiak. The prevailing winds came from the southwest, up the Shelikof Strait between Kodiak and the Alaskan Peninsula, driving the ocean waves that produced the sea echoes from which the currents were extracted.

Figure 2. The tidal currents were analyzed in time along three east-west cuts (EW1, EW2, and EW3) and two south-north cuts (SN1 and SN2). These currents were computed at the indicated locations which were spaced 3 km apart along each of the cuts. All locations were referenced to the radar site near Seldovia at lat. $59^{\circ}27'30''$ north and longitude $151^{\circ}42'30''$ west.

Figure 3a. The north and west components of current due to tides are shown for positions along the east-west cut EW1 in Fig. 2. From bottom to top, the locations shift by 3 km intervals going from east to west along the cut. The bottommost curves correspond to a location situated 6 km north and 6 km west of the Seldovia radar site.

Figure 3b. The north and west components of current due to tides are shown for positions along the east-west cut EW2 in Fig. 2. From bottom to top, the locations shift by 3 km intervals going from east to west along the cut. The bottommost curves correspond to a location situated 15 km north and 9 km west of the Seldovia radar site.

Figure 3c. The north and west components of current due to tides are shown for positions along the east-west cut EW3 in Fig. 3. From bottom to top, the locations shift by 3 km intervals going from east to west along the cut. The bottommost curves correspond to a location situated 27 km north and 15 km west of the Seldovia radar site.

Figure 3d. The north and west components of current due to tides are shown for positions along the south-north cut SN1 in Fig. 2. From bottom to top, the locations shift by 3 km intervals going from south to north along the cut. The bottommost curves correspond to a location situated 18 km due west of the Seldovia radar site.

Figure 3e. The north and west components of current due to tides are shown for positions along the south-north cut SN2 in Fig. 2. From bottom to top, the locations shift by 3 km intervals going from south to north along the cut. The bottommost curves correspond to a location situated 30 km due west of the Seldovia radar site.

Figure 4. This sequence of 6 maps depicts the tidal currents in the vicinity of Kachemak Bay at 4-hour intervals starting at 00 hours on 13 July 1977. The current vectors are plotted at 3 km intervals relative to the southern radar site near Seldovia. The bathymetry contours (in fathoms) were taken from a U.S.G.S. chart.

Figure 5. This sequence of 6 maps depicts the 12-hour tidal component in the vicinity of Kachemak Bay at 2-hour intervals starting at 00 hours on 13 July 1977. The current vectors are plotted in the same format used in Fig. 4.

Figure 6. This sequence of 6 maps depicts the 24-hour tidal component in the vicinity of Kachemak Bay at 4-hour intervals starting at 00 hours on 13 July 1977. The current vectors are plotted in the same format used in Fig. 4.

Figure 7. This map illustrates the steady flow near Kachemak Bay based upon 24 hours of data. The current vectors are plotted at 1.5 km intervals even though the data is independent at intervals greater than 3 km. There is a gyre-like feature at the top of the map with a counterclockwise rotation. The largest currents are about 25 cm/s and are found inside of Kachemak Bay. Also, notice the line of weak flow going from south to north and ending in the gyre. The flow branches in two different directions on either side of this line, with the currents going north to northeast on the right and going south to west on the left. With as few as six radar units strategically placed, the entire circulation pattern of Cook Inlet could be mapped and better understood.

Figure 8a. The radar measurements (crosses) are shown with the tidal flow (curve) for the north component of current at the west location on cut EW1 in Fig. 2. The curve was fit, in a least squares sense, to the data using a three frequency Fourier expansion. The three frequencies correspond to periods with values of infinite, 24.6, and 12.31 hours.

Figure 8b. The radar measurements (crosses) are shown with the tidal flow (curve) for the west component of current at the west location on cut EW1 in Fig. 2. The curve was fit, in a least squares sense, to the data using a three frequency Fourier expansion. The three frequencies correspond to periods with values of infinite, 24.6, and 12.31 hours.

Figure 9. The shaded area indicates that region where the least squares fit of the radar measurements seemed to be particularly good. The maximum range from the radar units at Anchor Point and Seldovia for which the fit was satisfactory was about 36 km. This range was a function of the operation of the radar on this first experimental application of that system and is not a real limitation. Actually, the radar can map currents out to ranges of 70 km.

Figure 10. Correlogram of radar vs. drifter surface current velocities.

Table I

Tide Levels for Seldovia
13 July 1977

Time	Date	High (feet)	Low (feet)
2357	12 July	16.1	----
0642	13 July	----	.6
1311	13 July	14.9	----
1839	13 July	----	4.9
0039	14 July	16.9	----

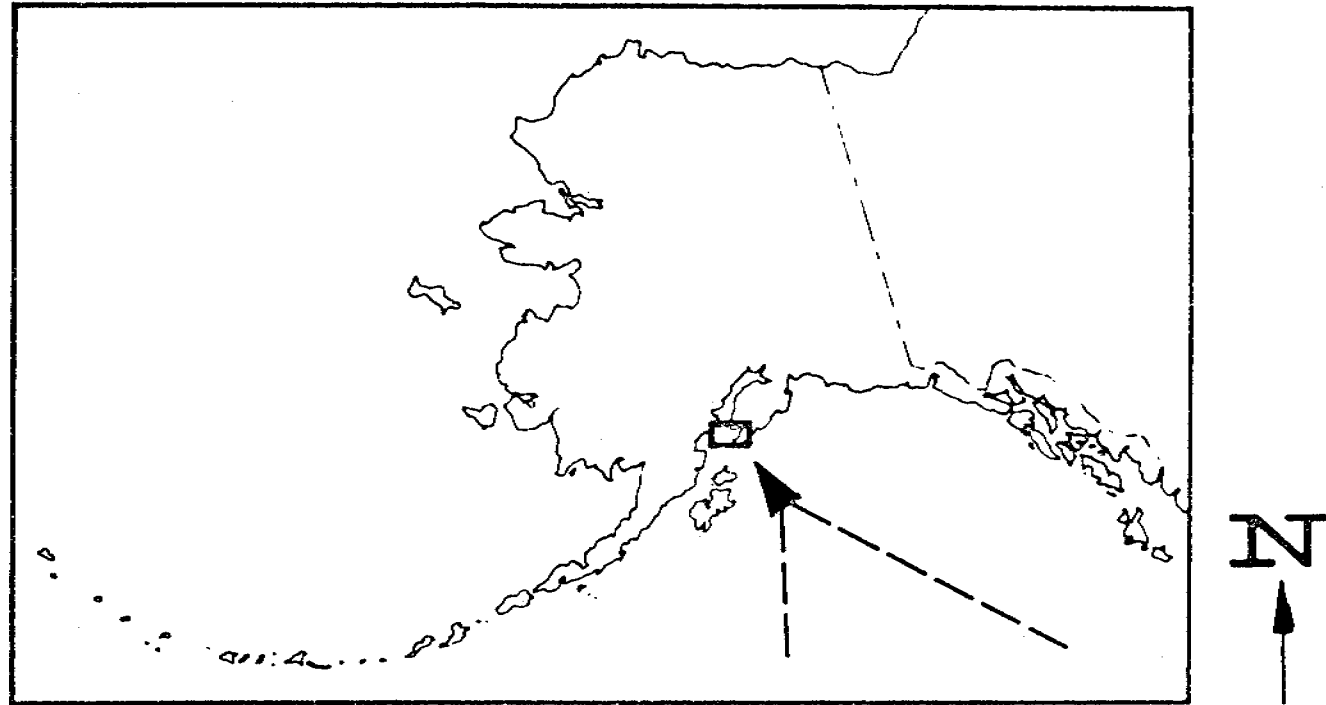


Figure 1.

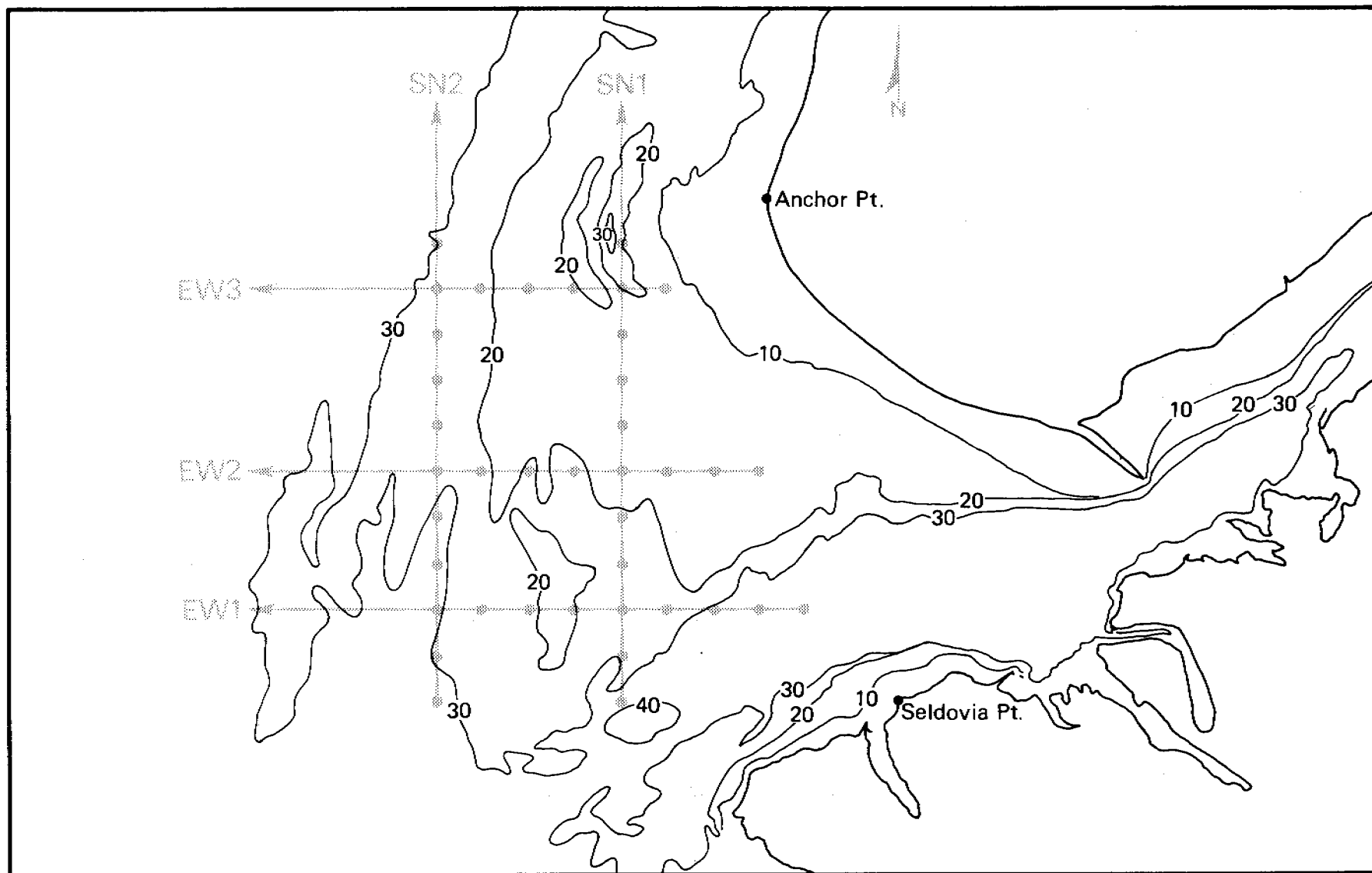


Figure 2.

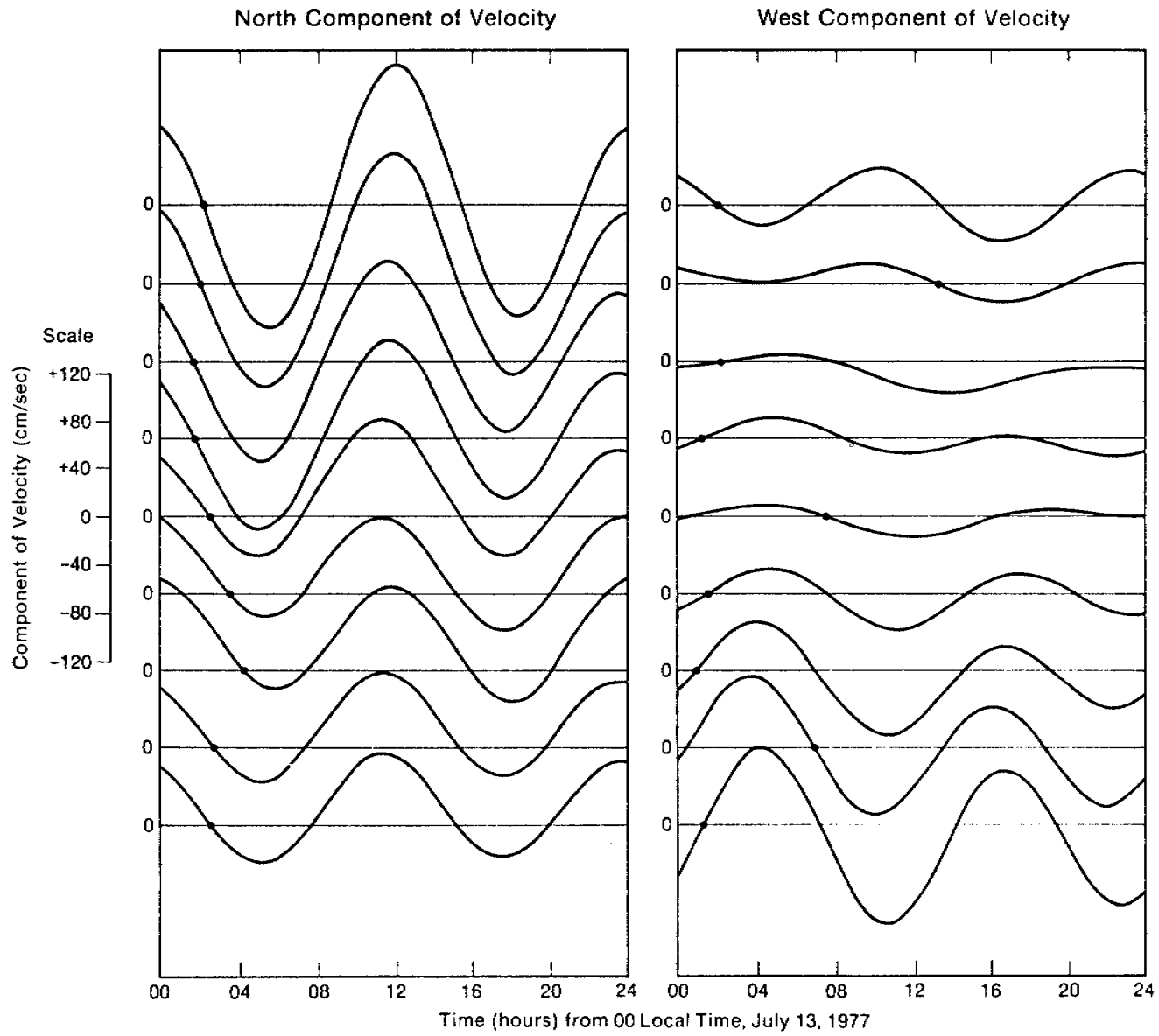


Figure 3a.

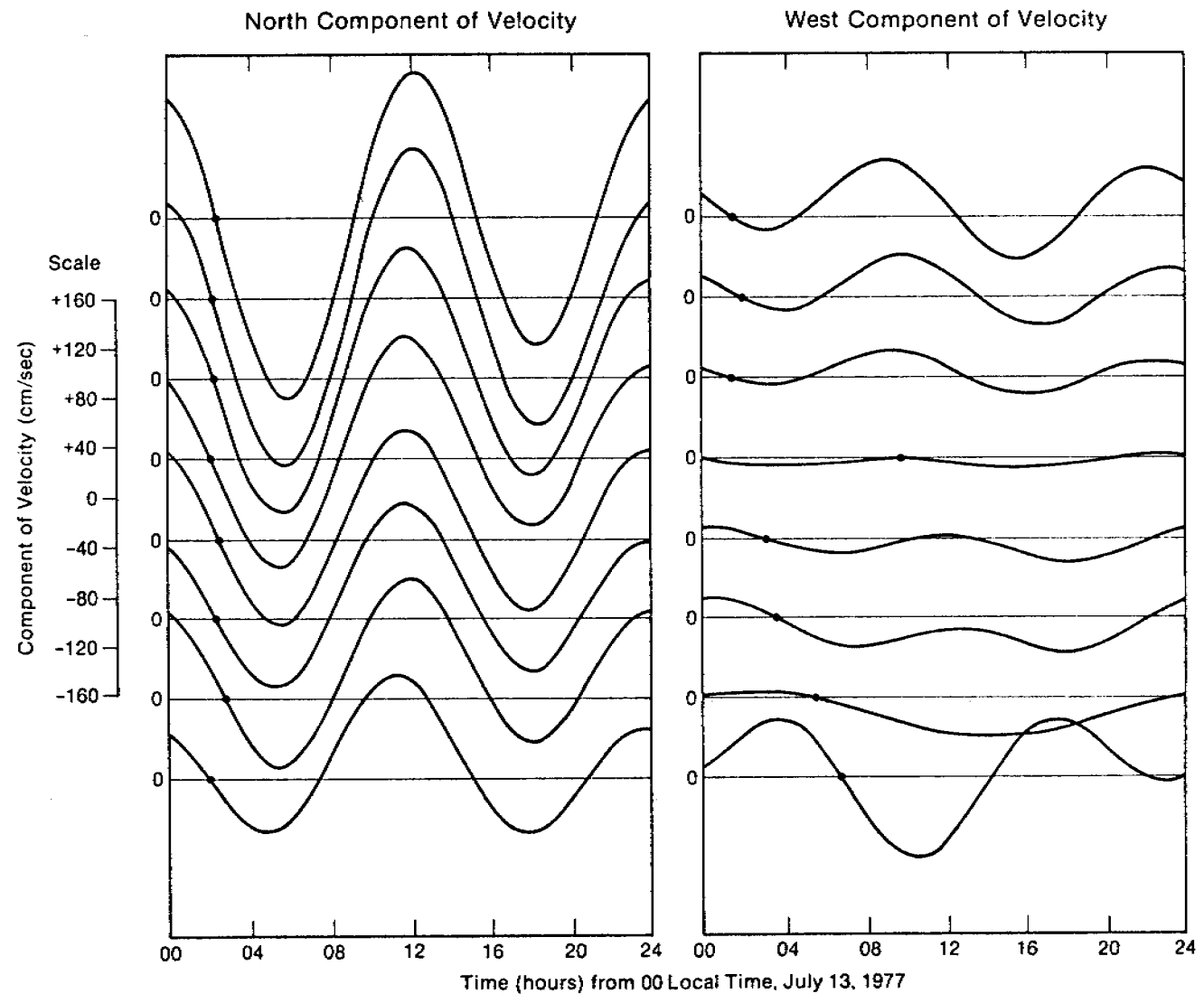


Figure 3b.

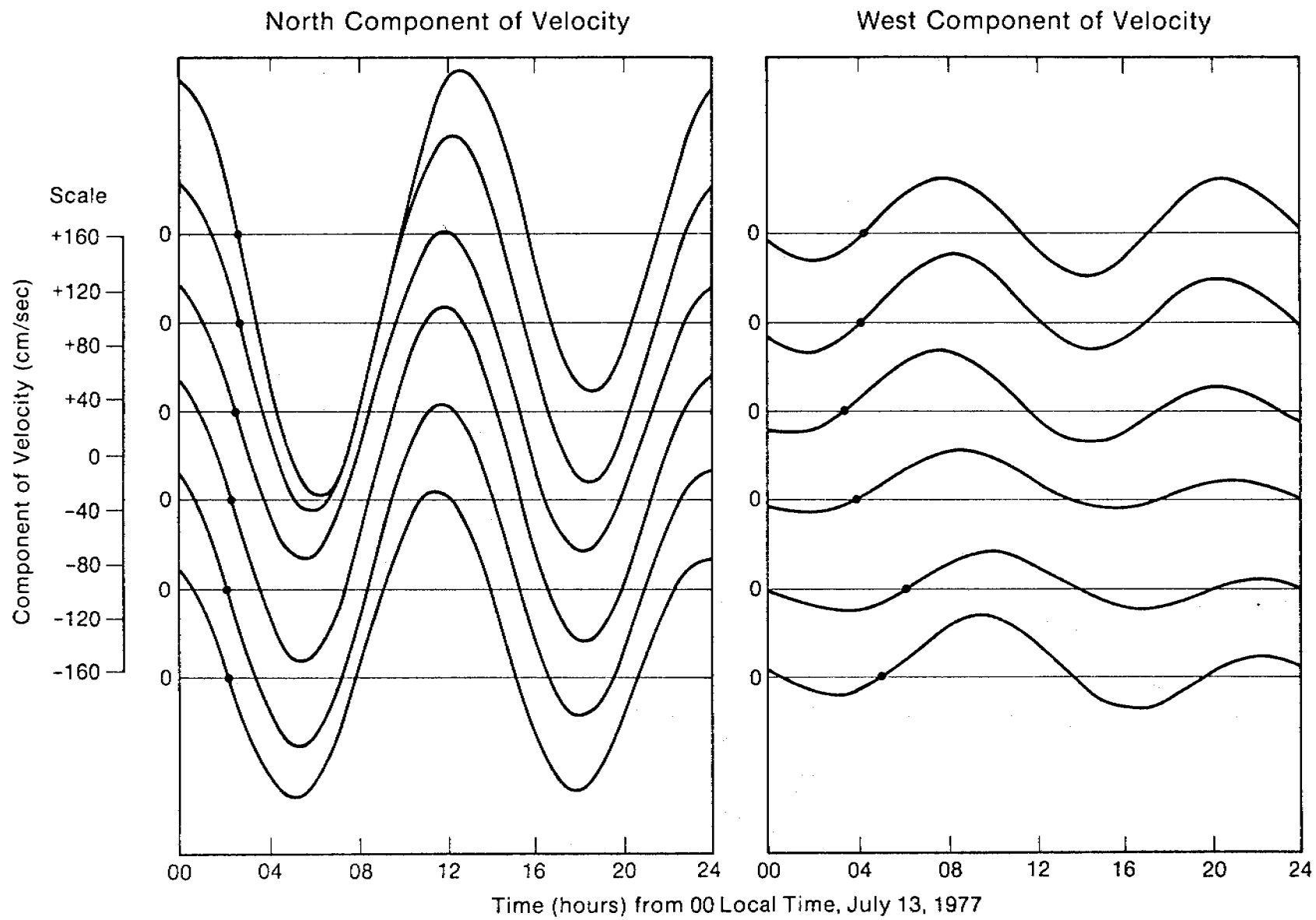


Figure 3c.

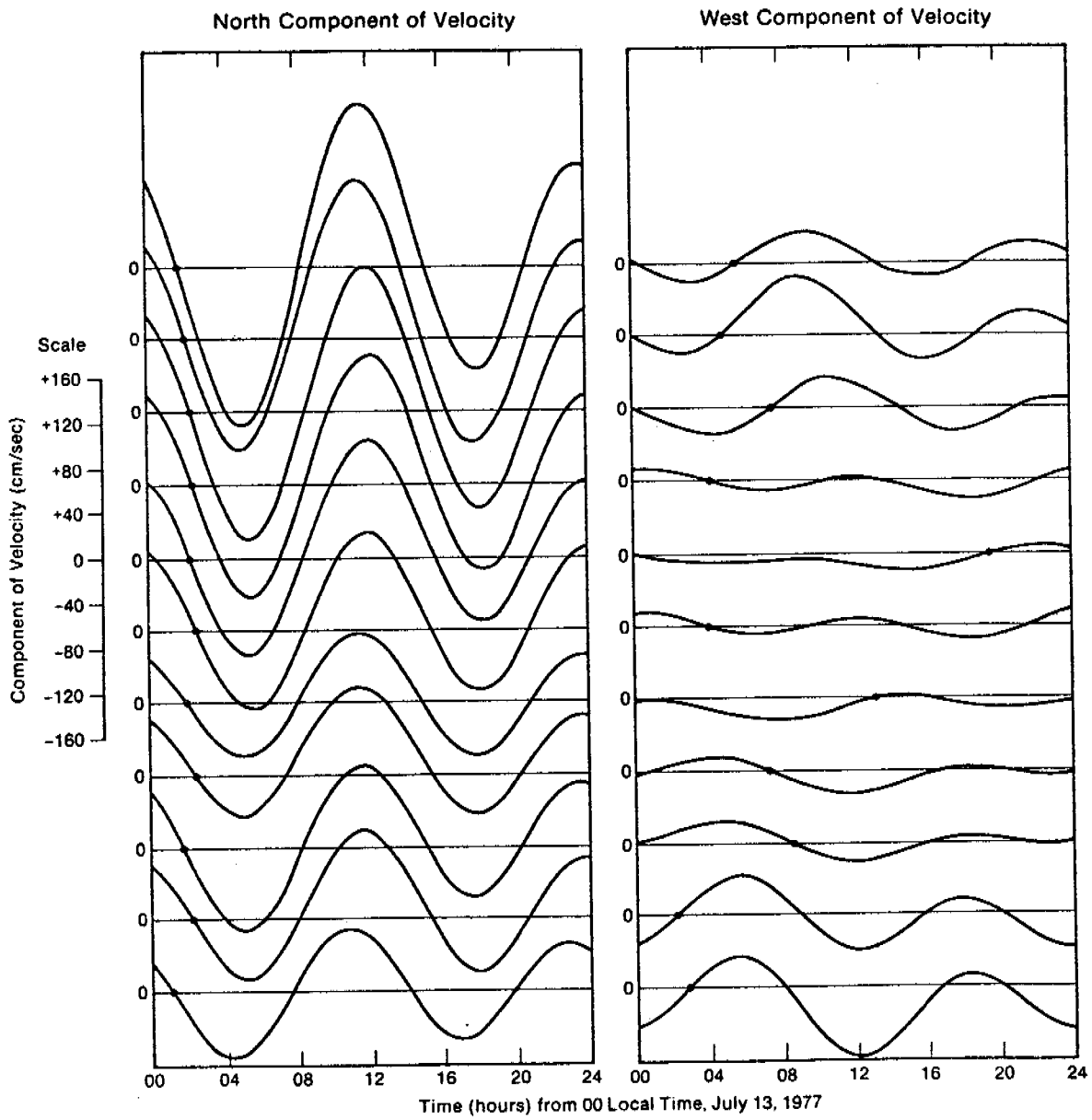


Figure 3d.

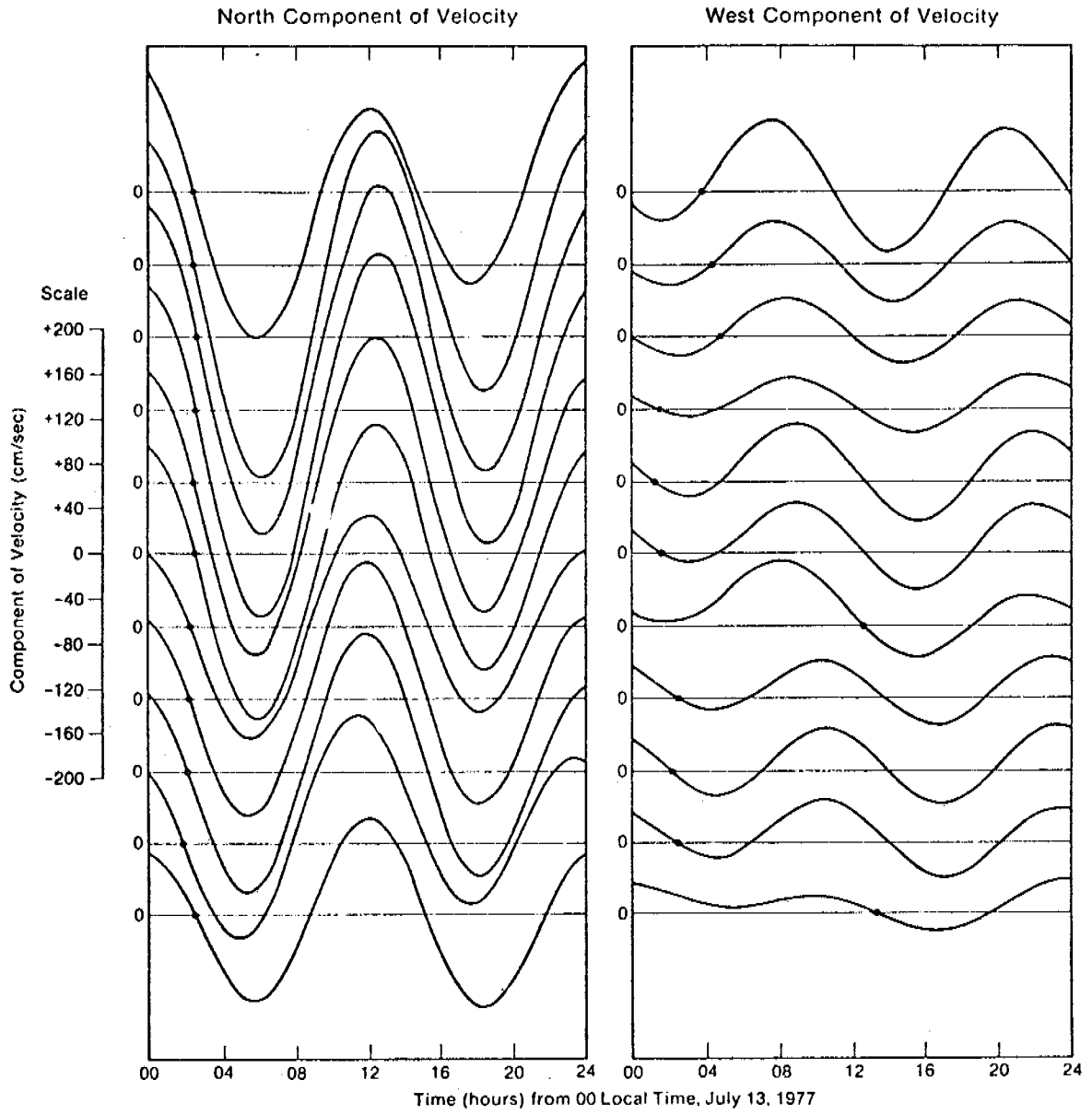


Figure 3e.

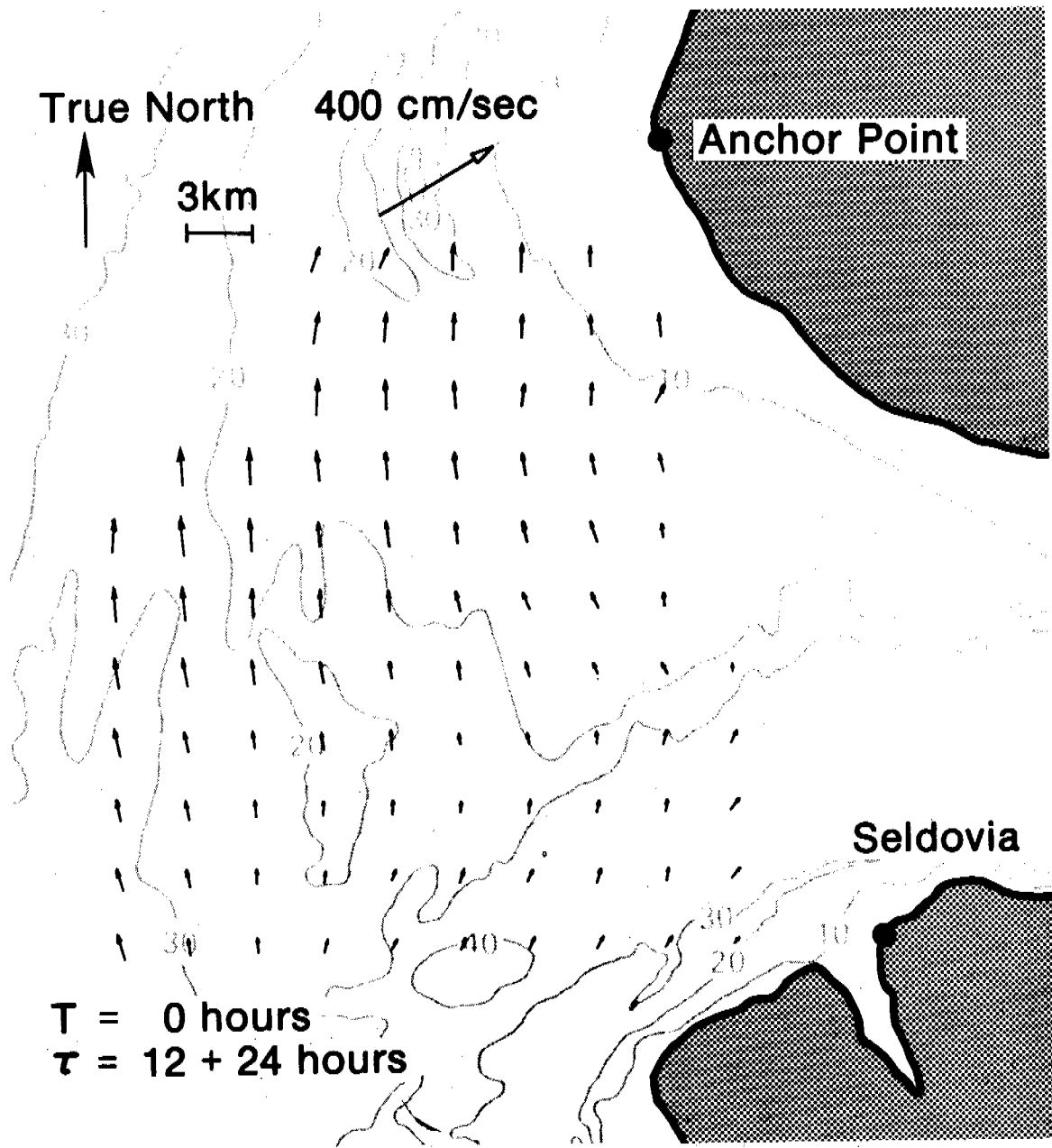


Figure 4a.

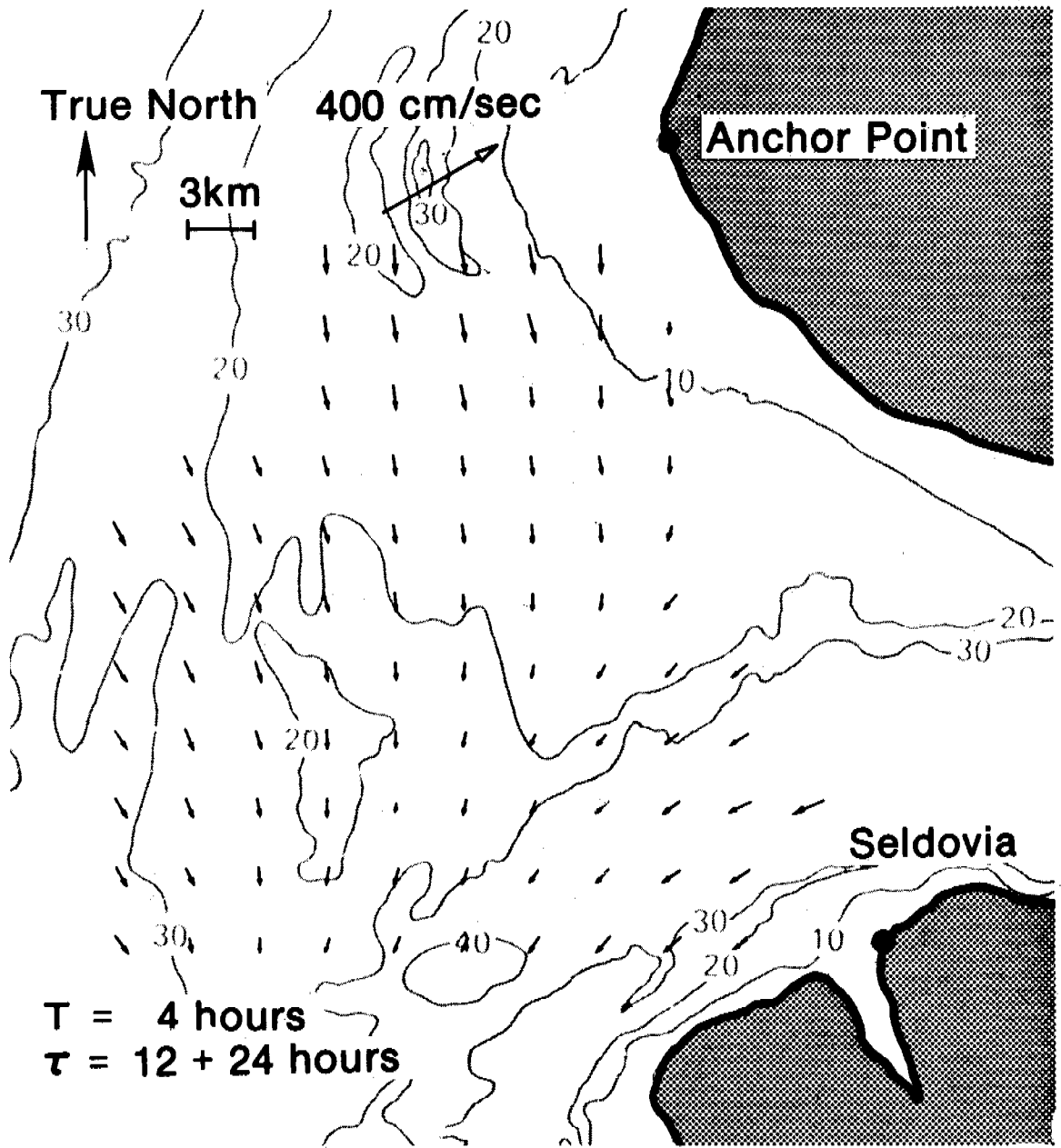


Figure 4b.

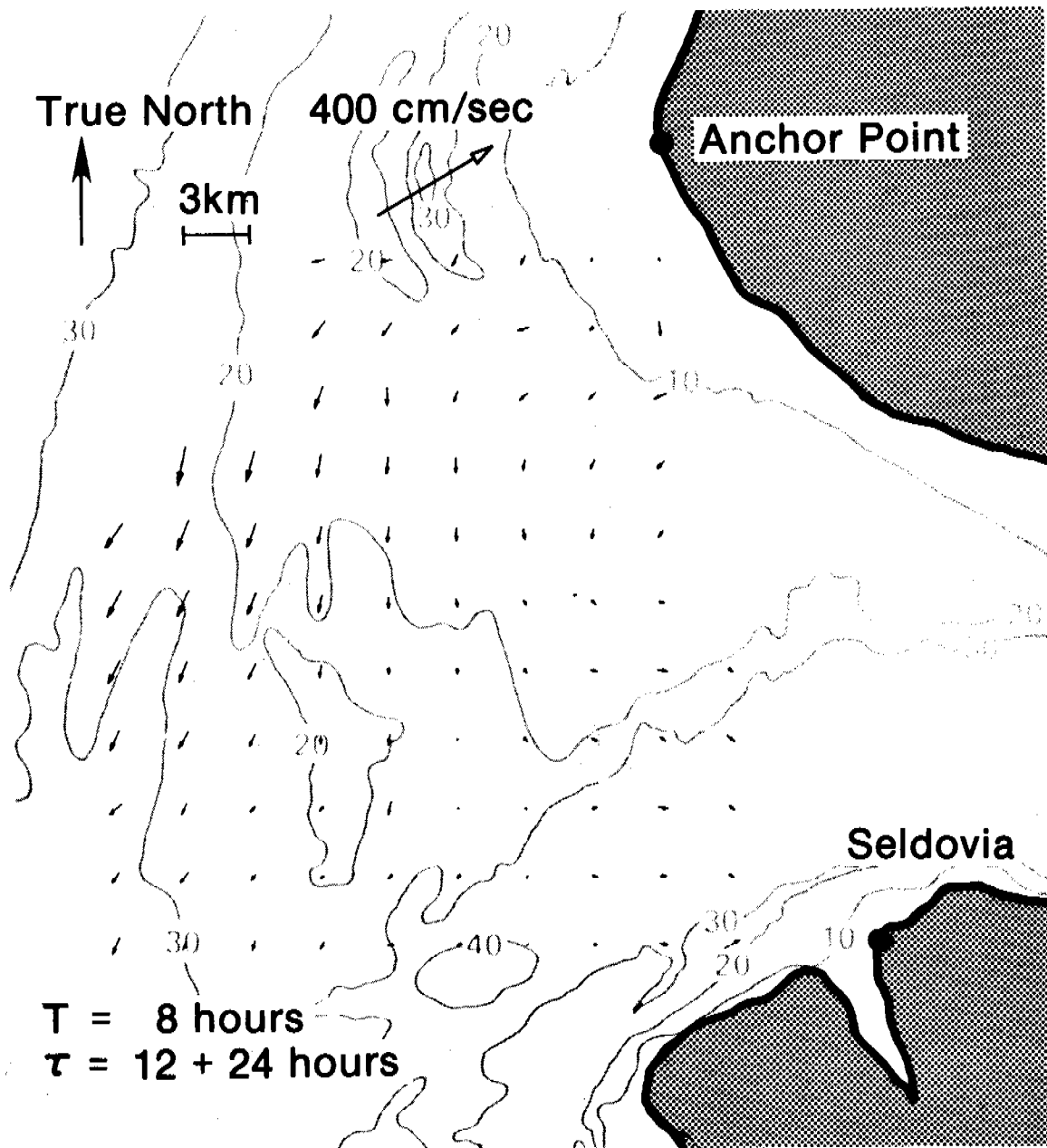


Figure 4c.

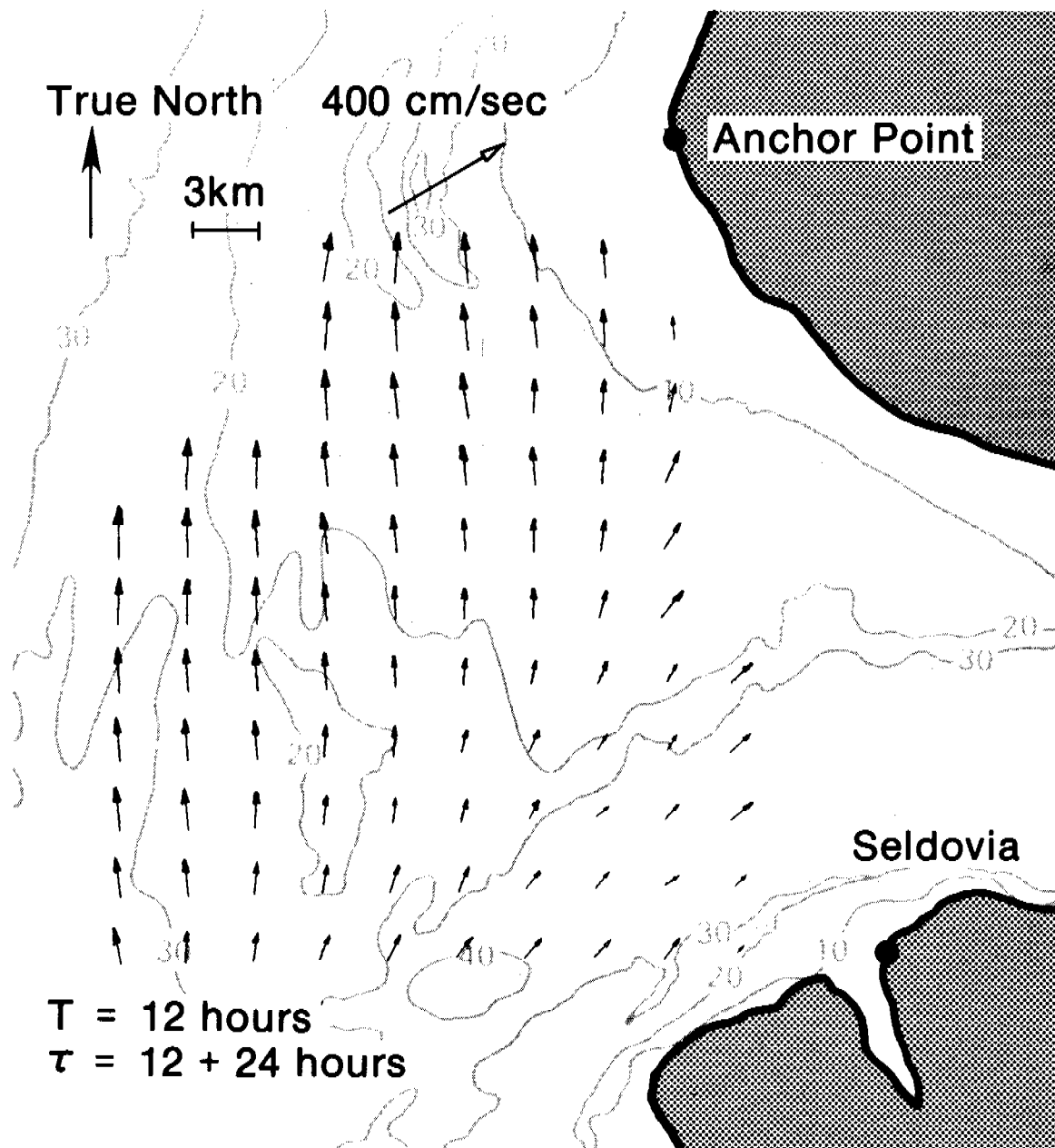


Figure 4d.

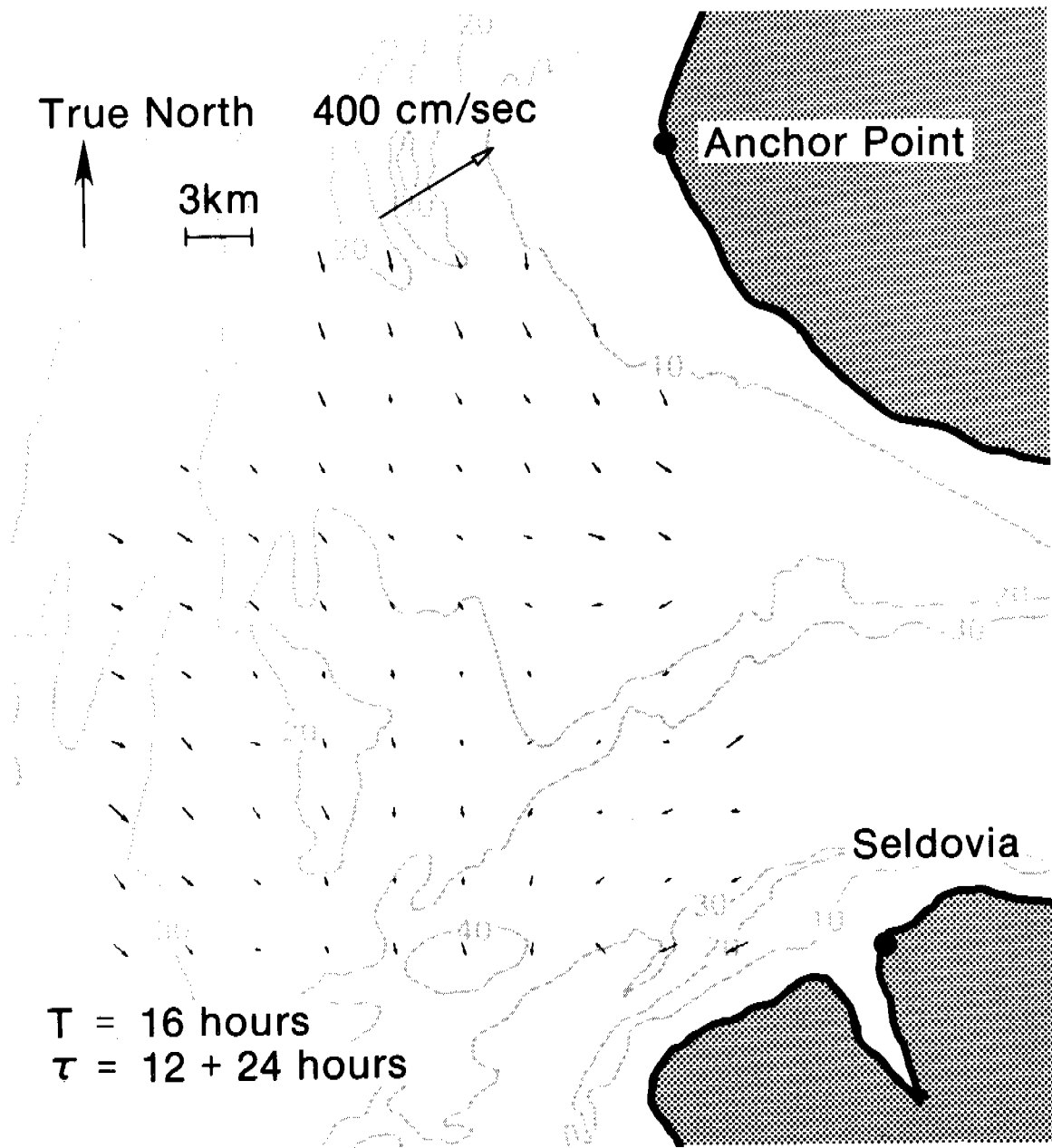


Figure 4e.

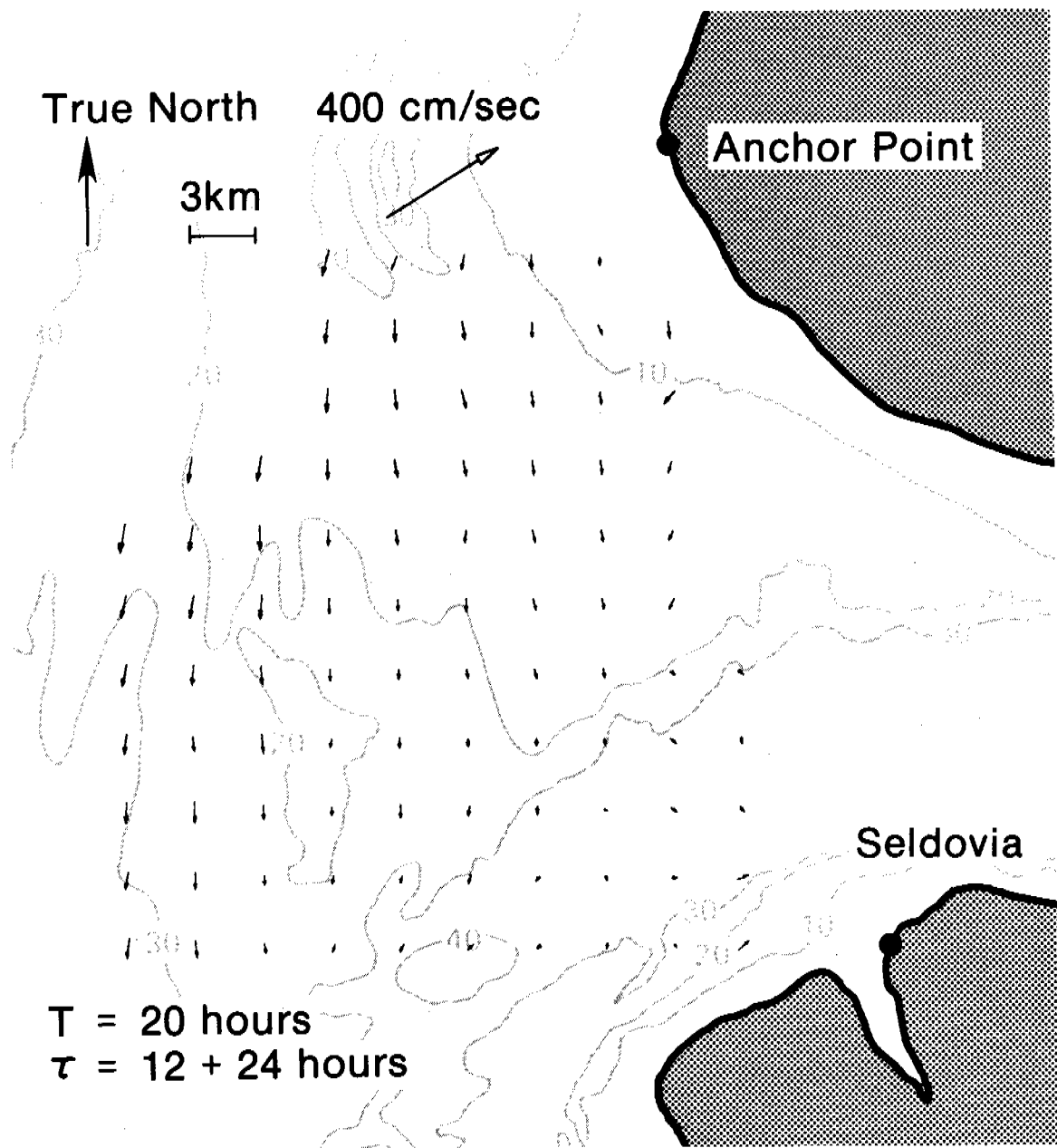


Figure 4f.

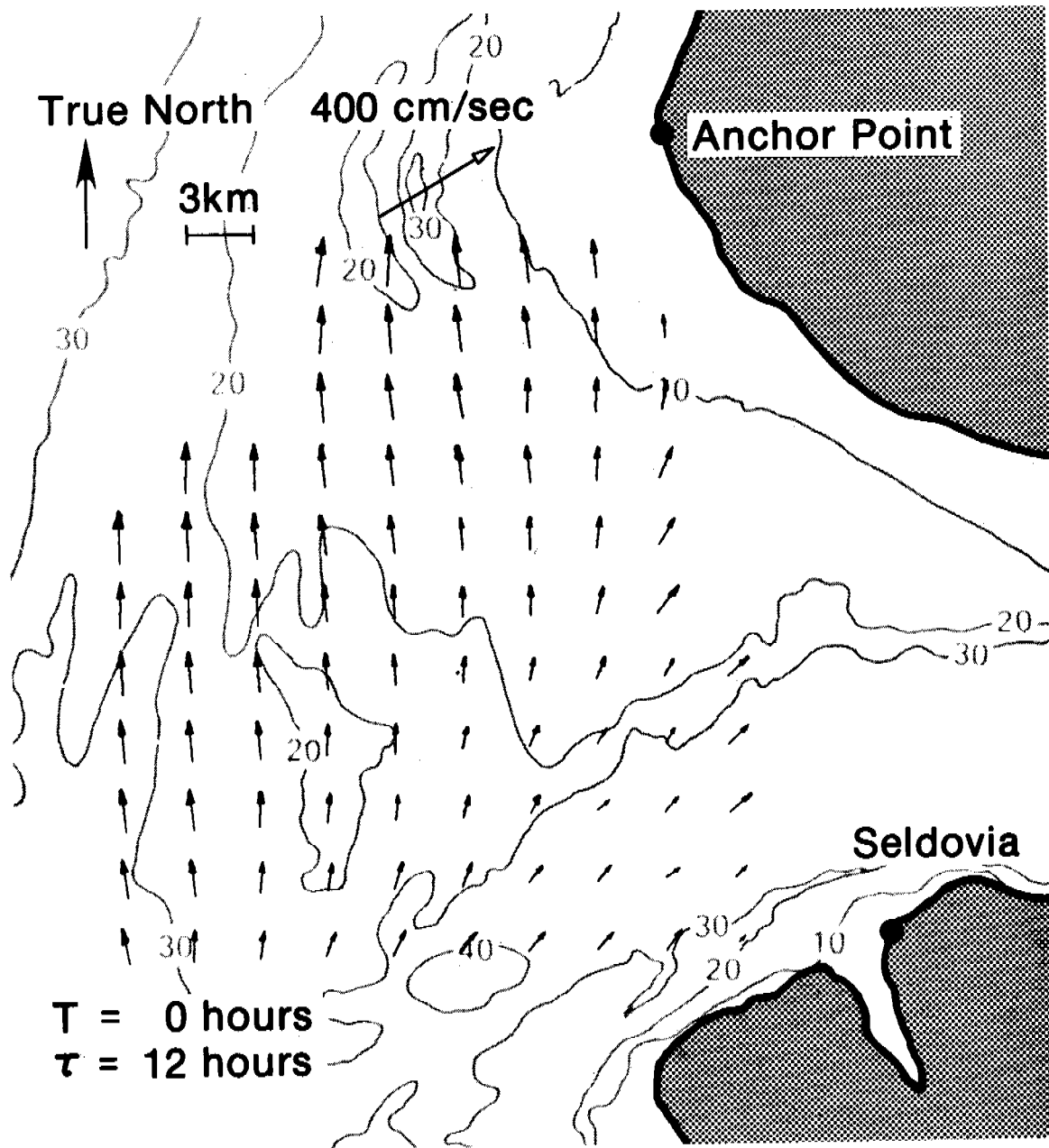


Figure 5a.

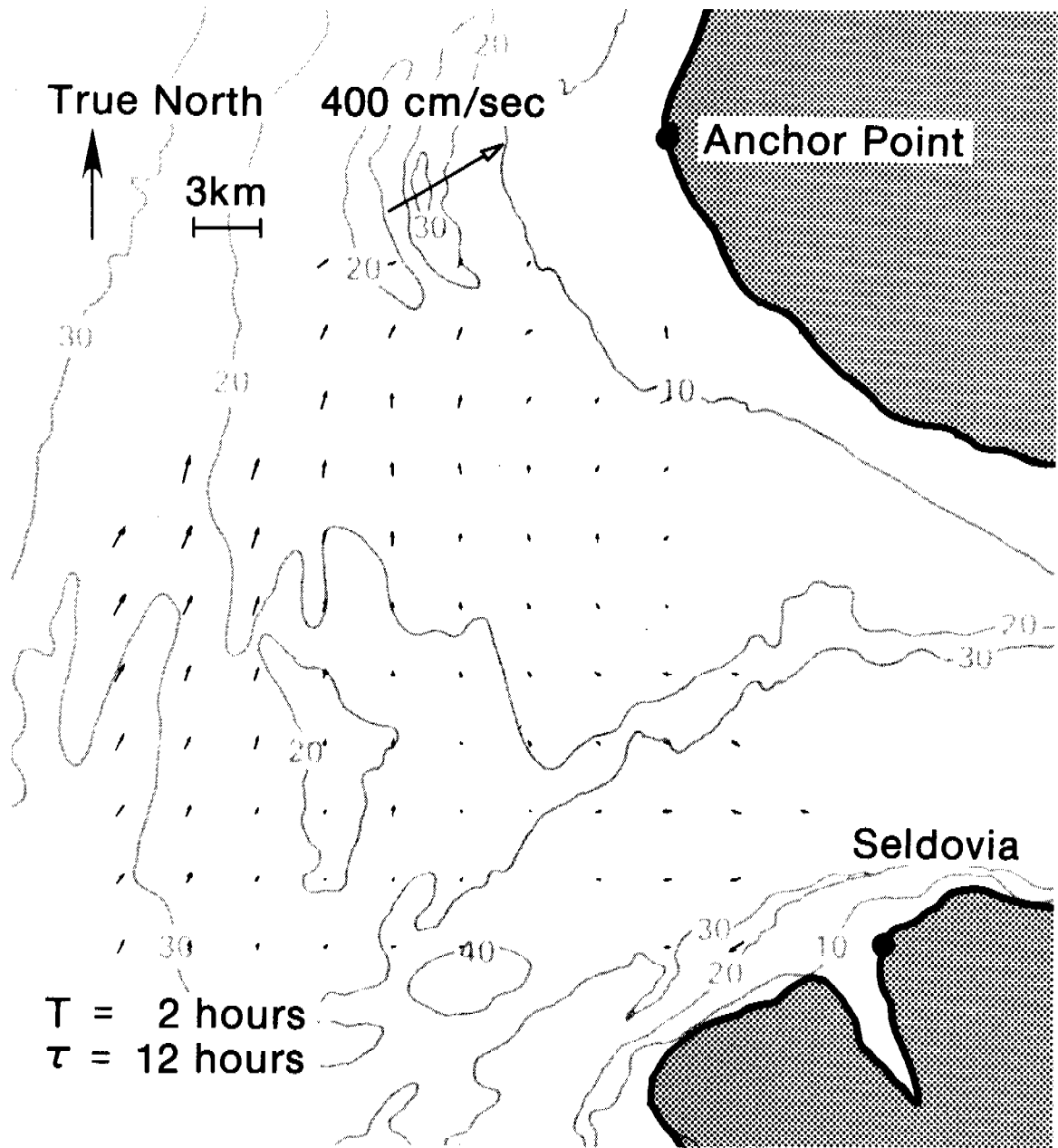


Figure 5b.

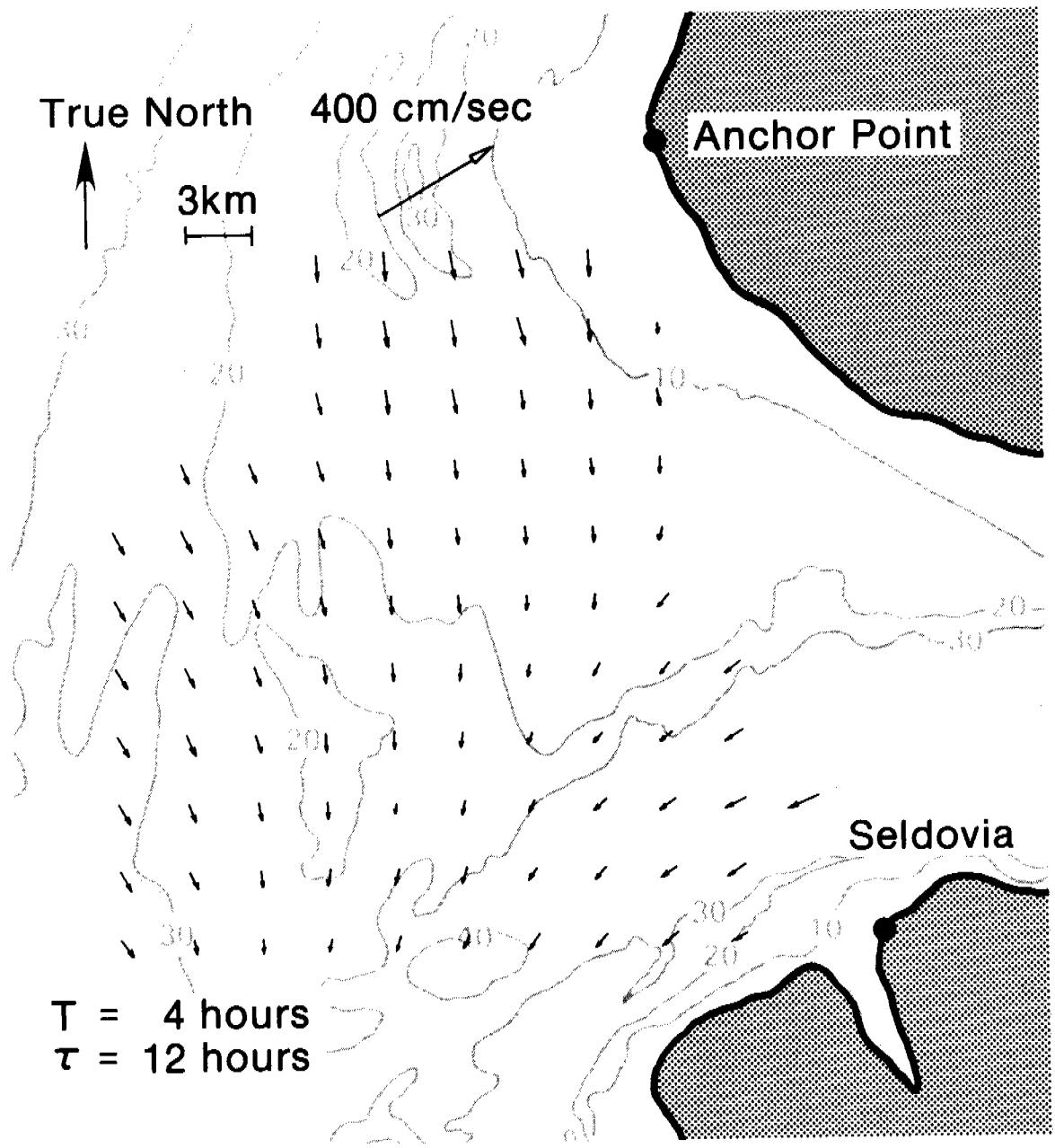


Figure 5c.

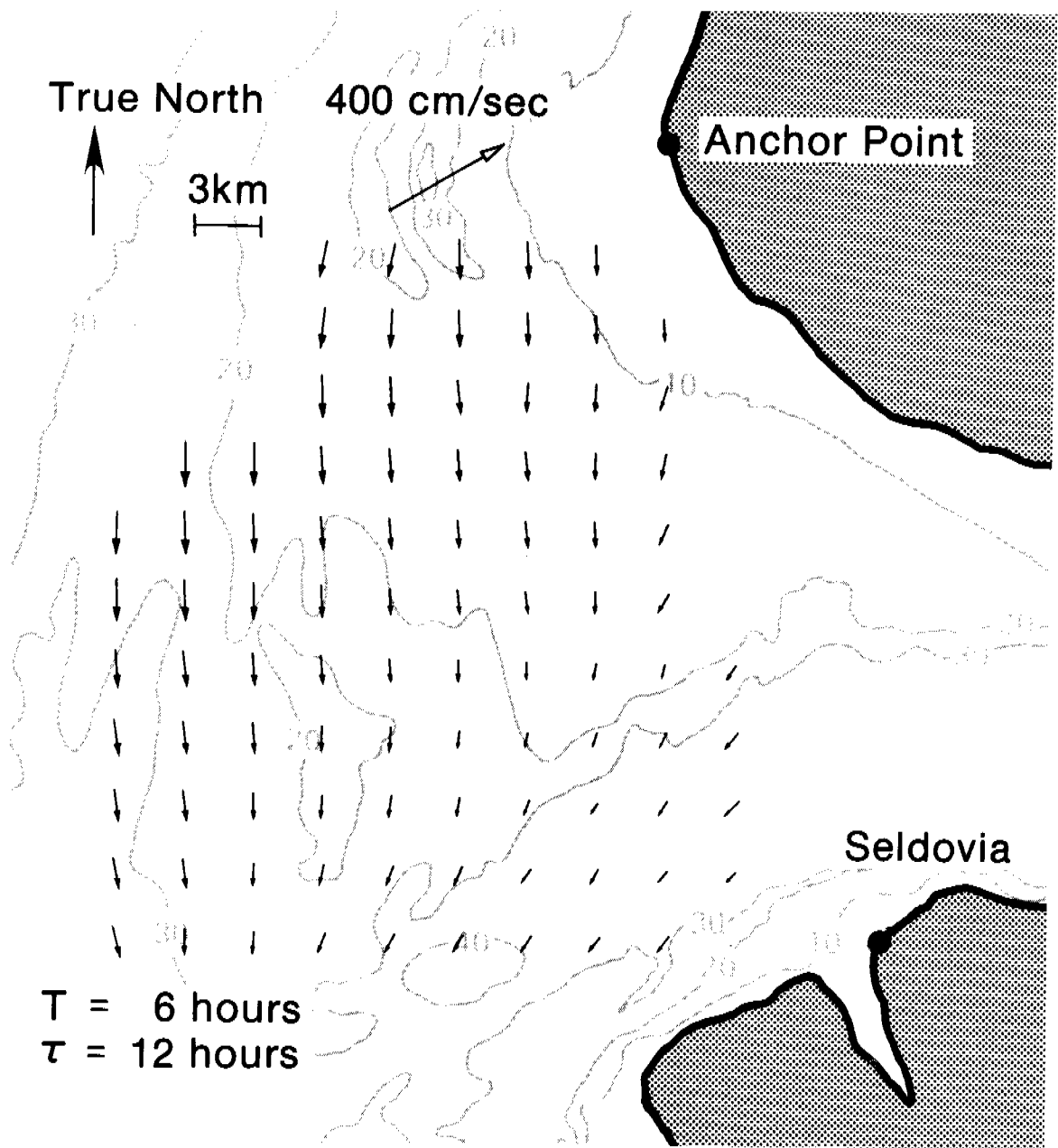


Figure 5d.

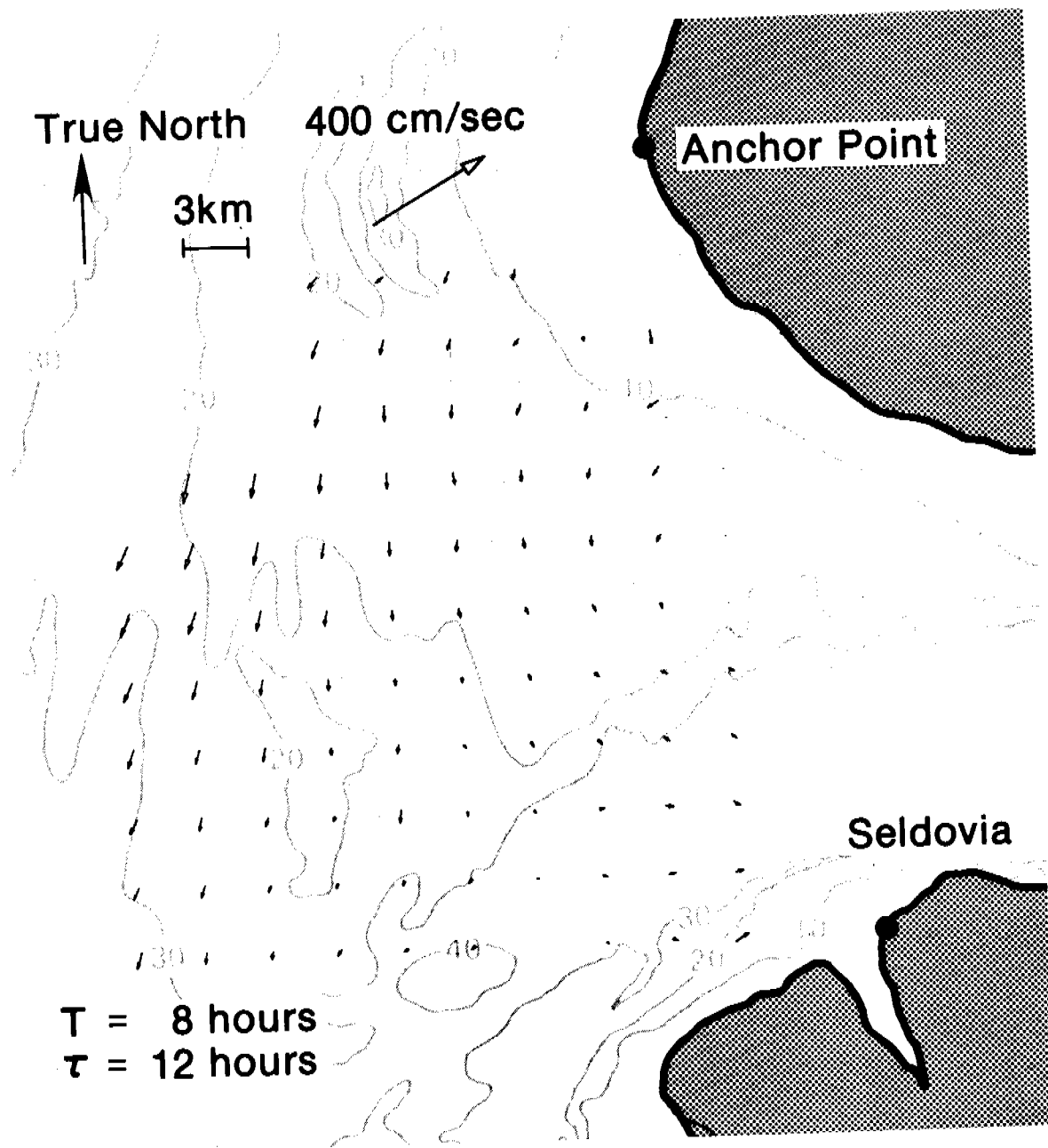


Figure 5e.

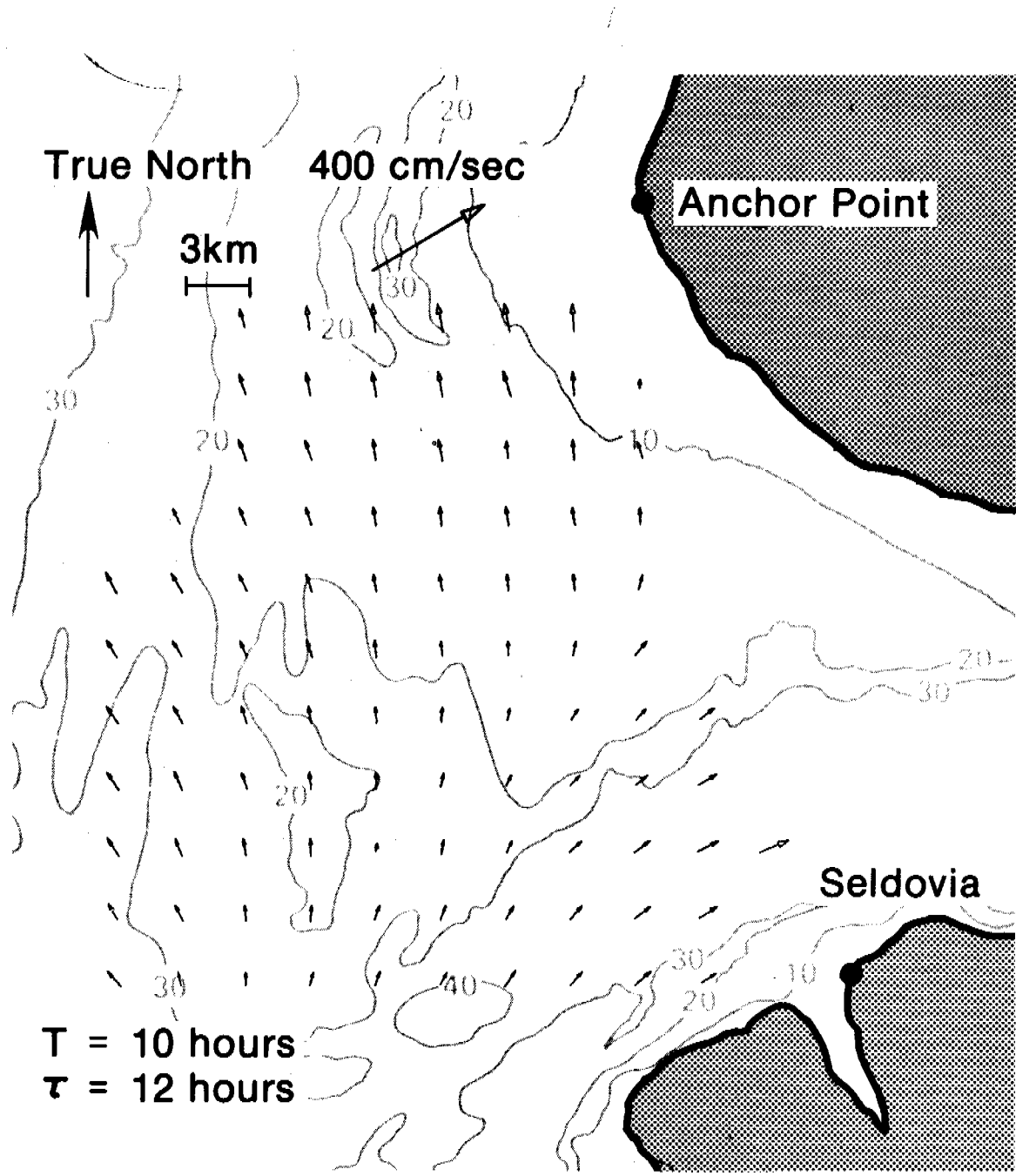


Figure 5f.

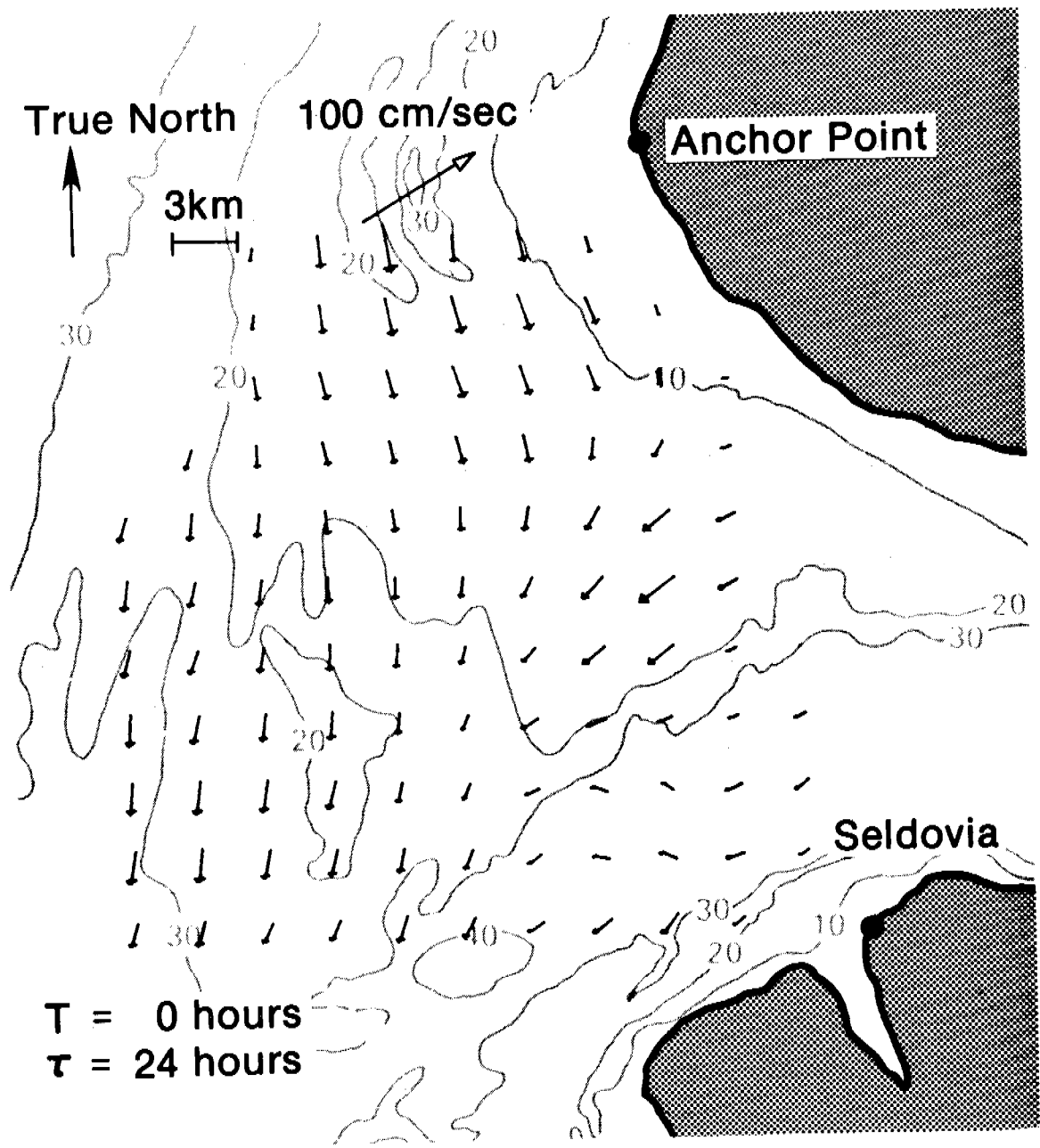


Figure 6a

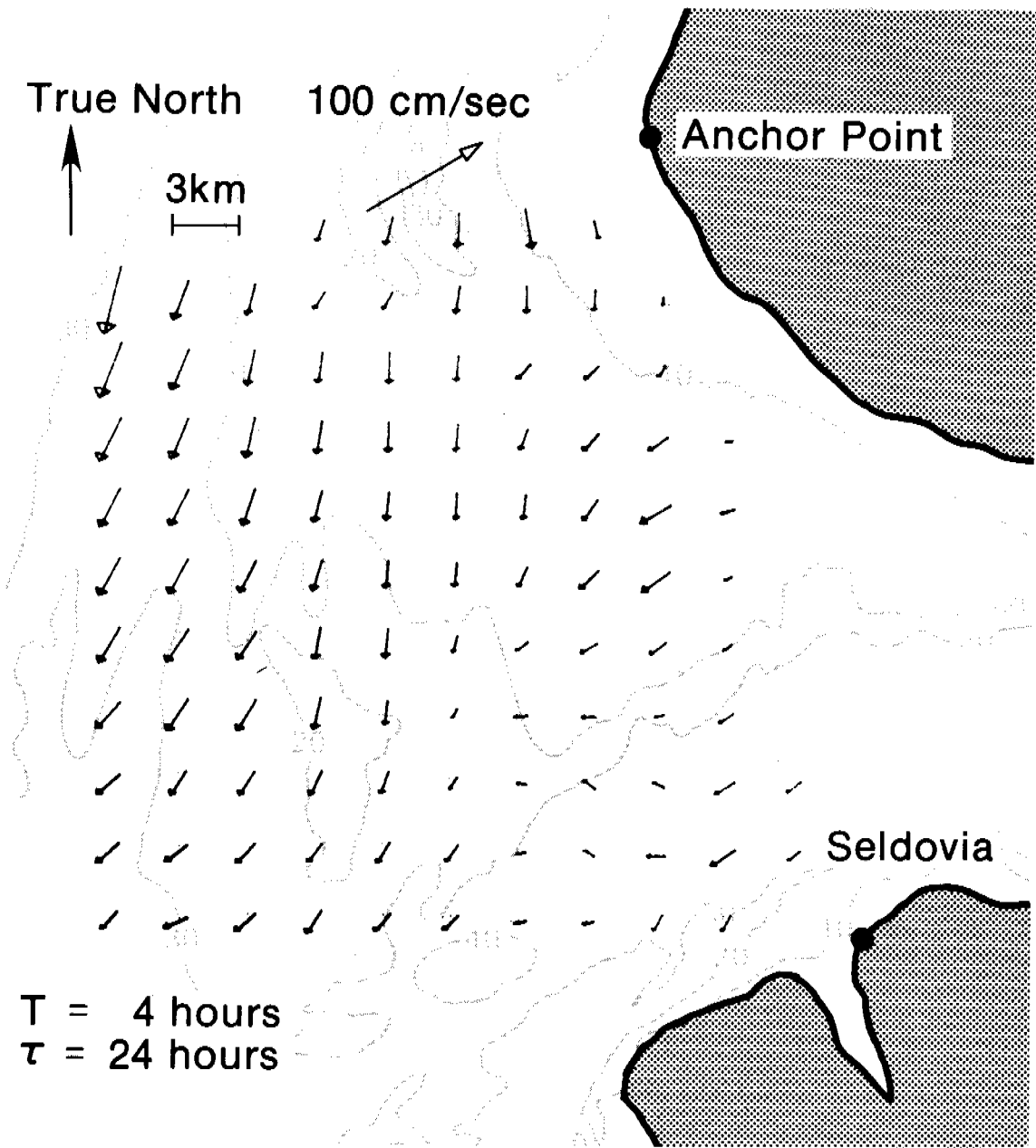


Figure 6b.

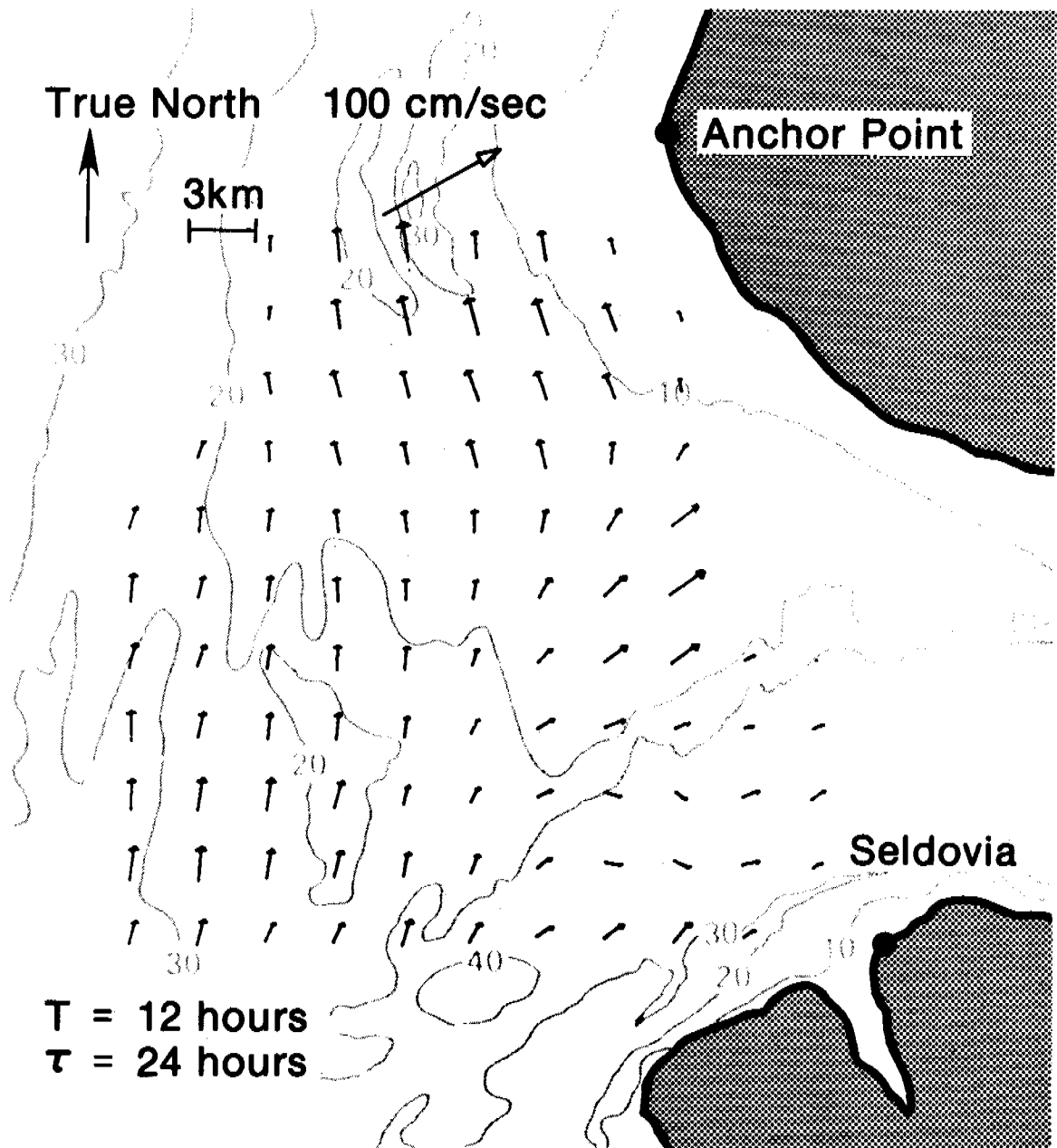


Figure 6d.

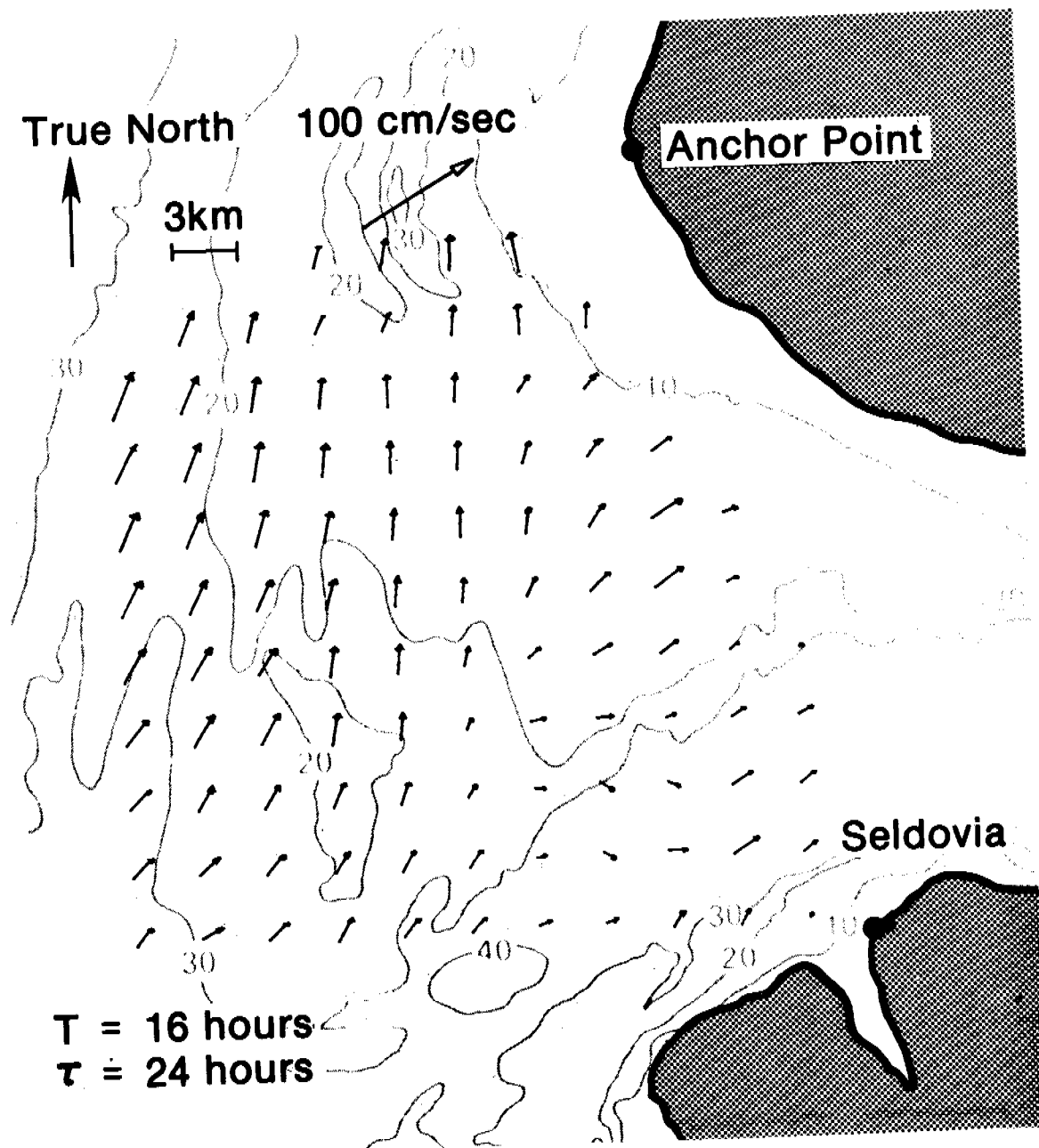


Figure 6e.

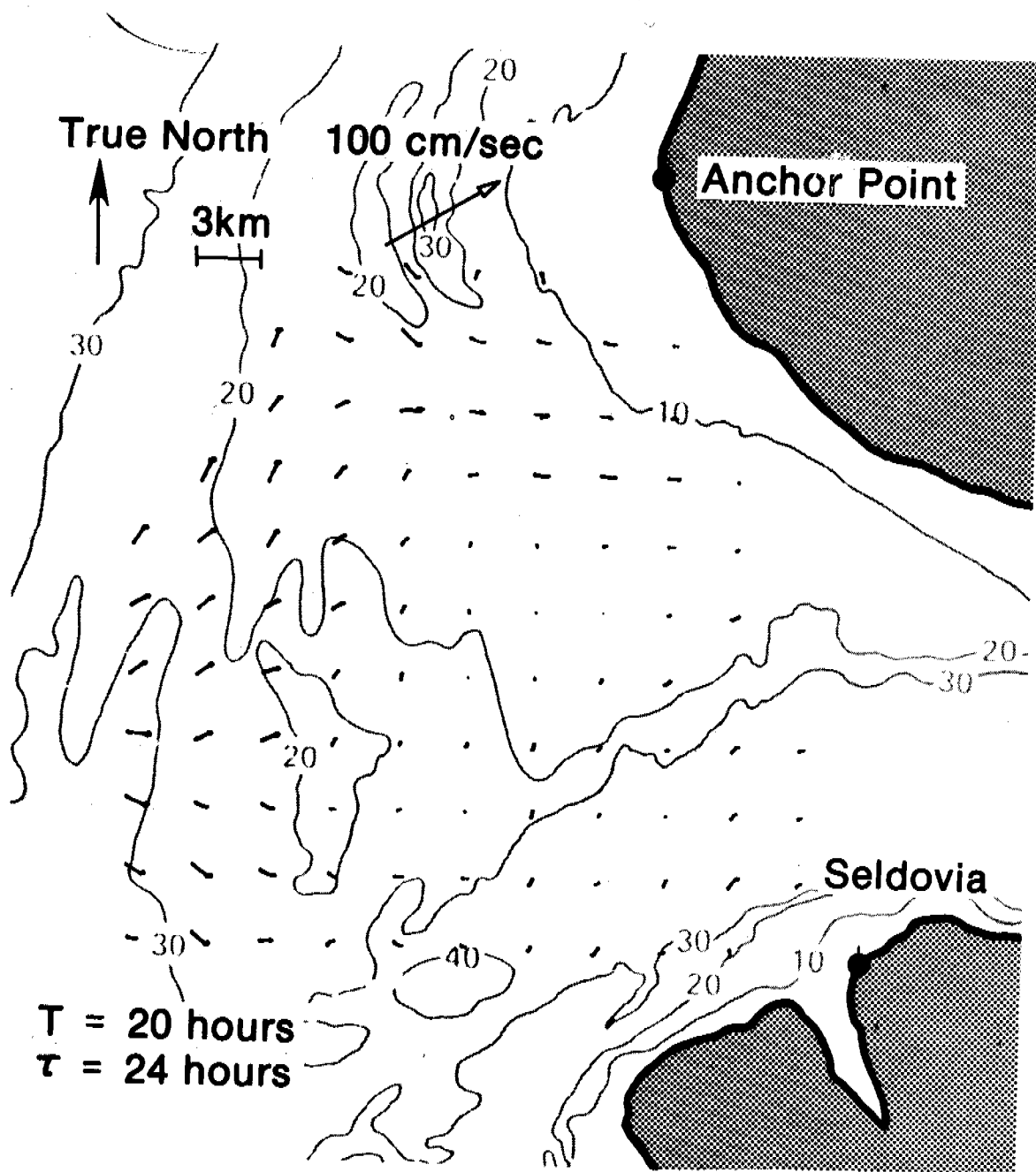


Figure 6f.

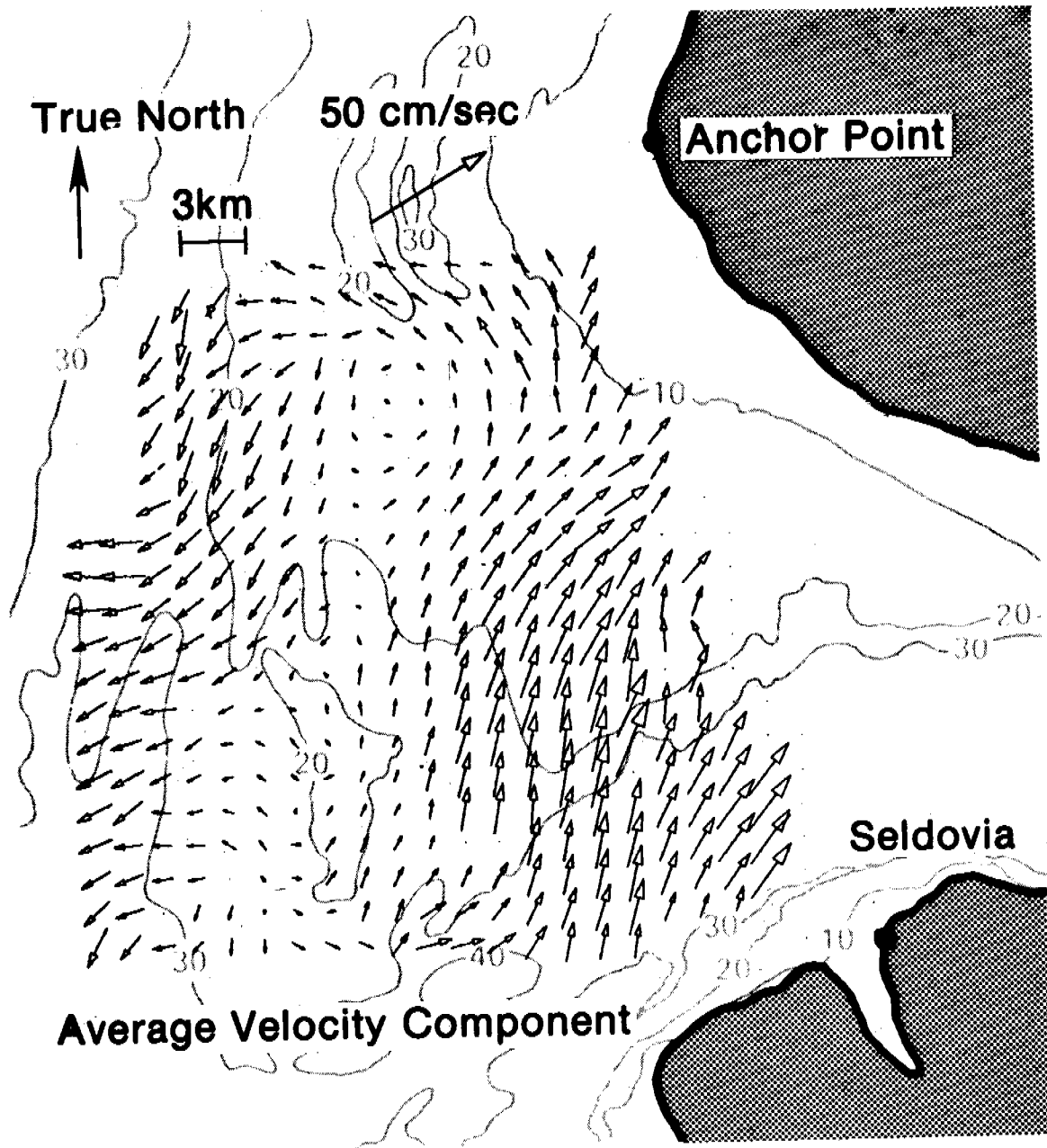
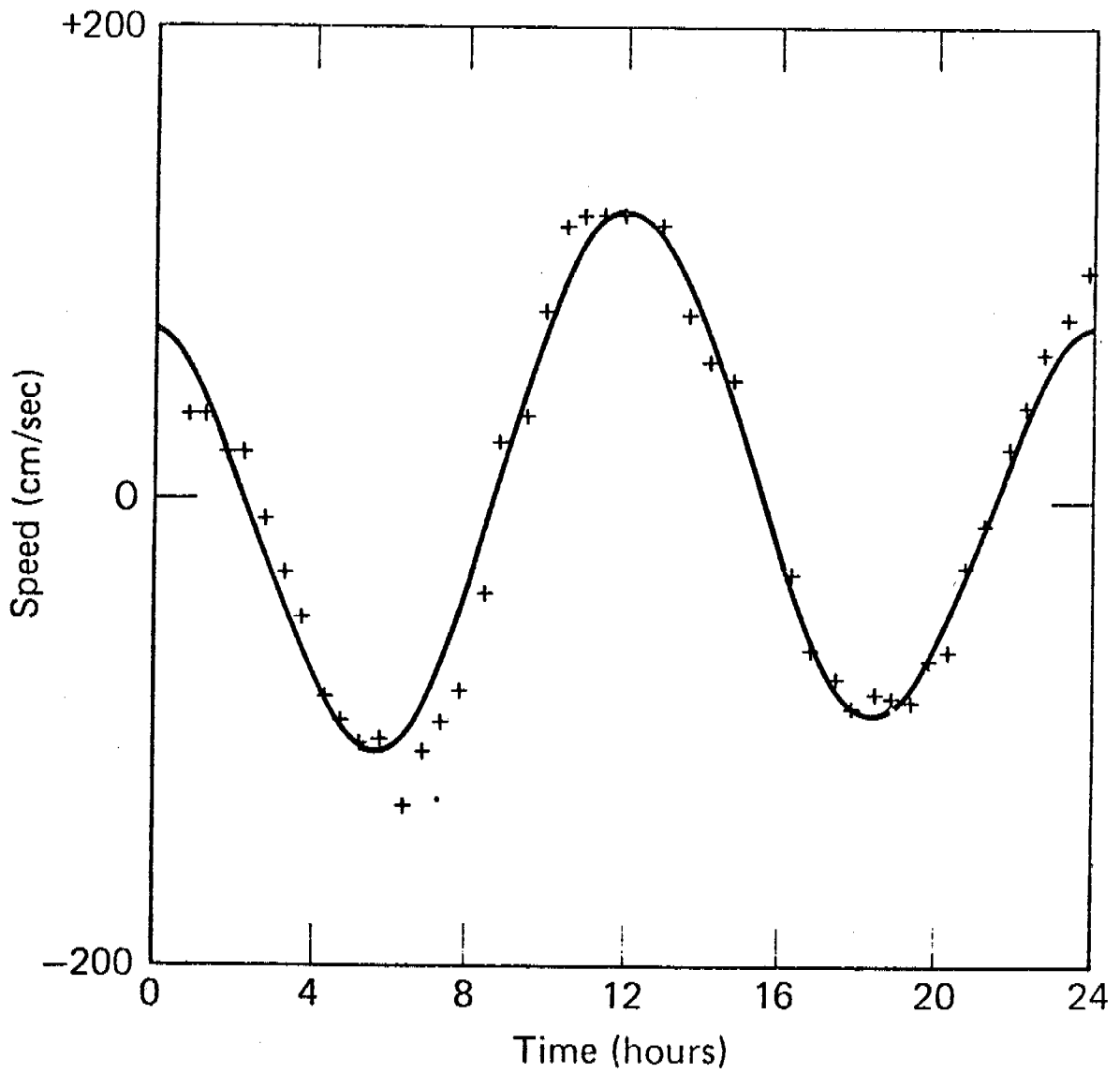
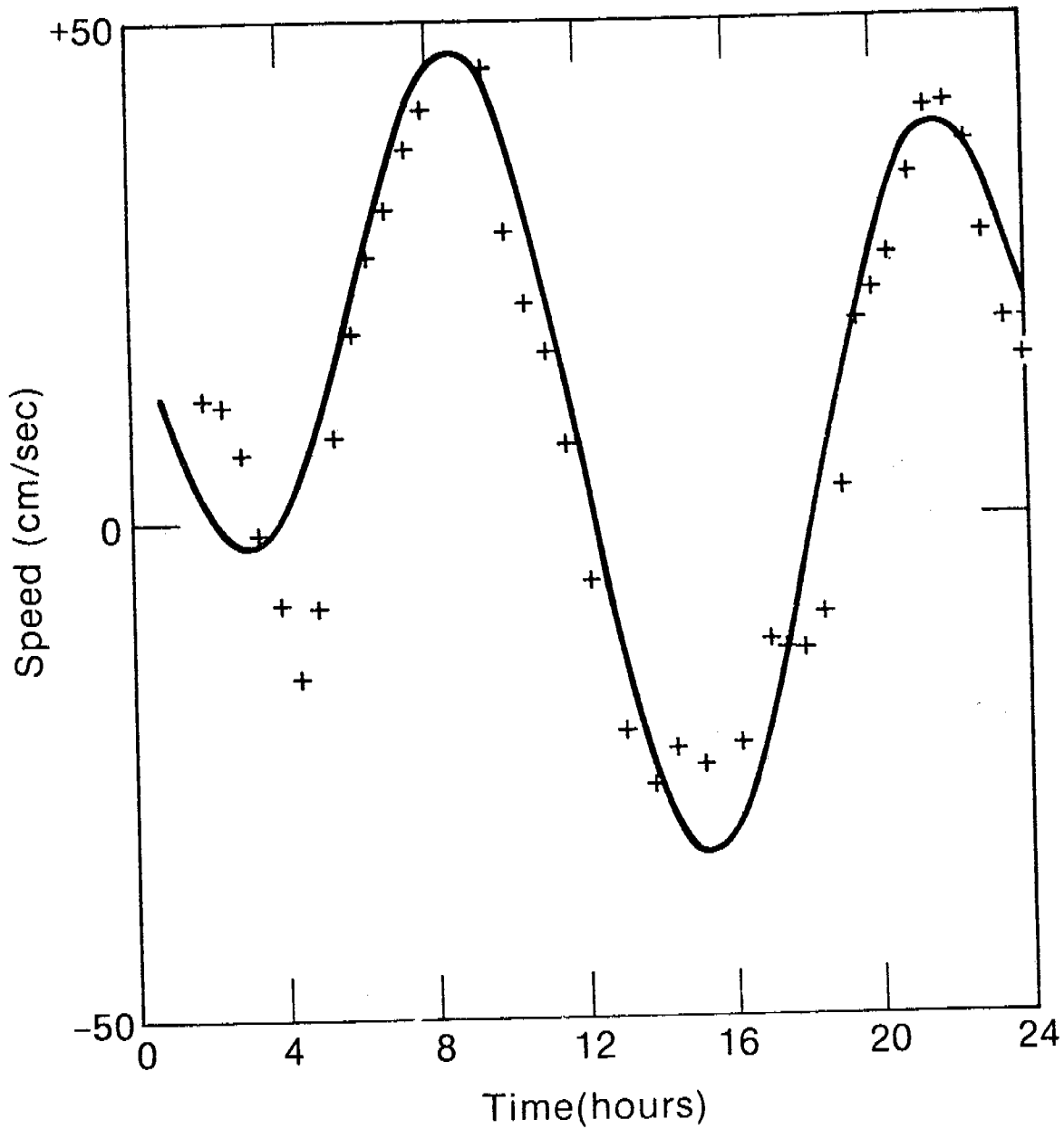


Figure 7.



North-South Component
At 6 km North and 30 km West of
Seldovia, Alaska

Figure 8a.



East-West Component
 AT 6 km North and 30 km West of
 Seldovia, Alaska

Figure 8b.

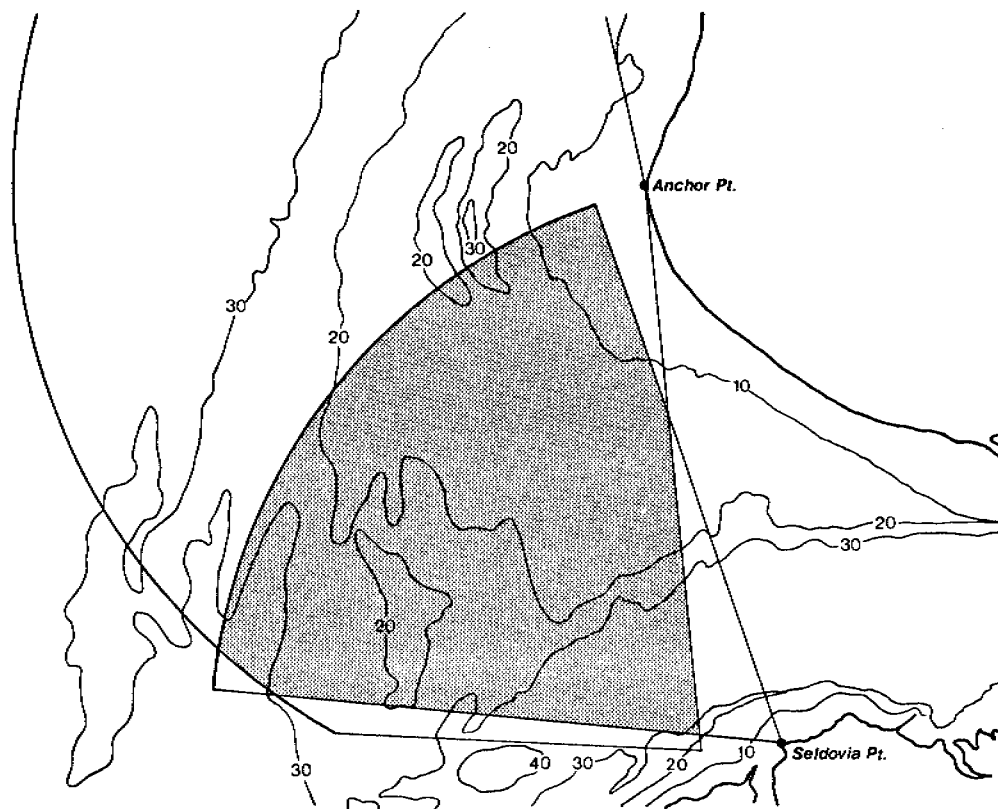


Figure 9.

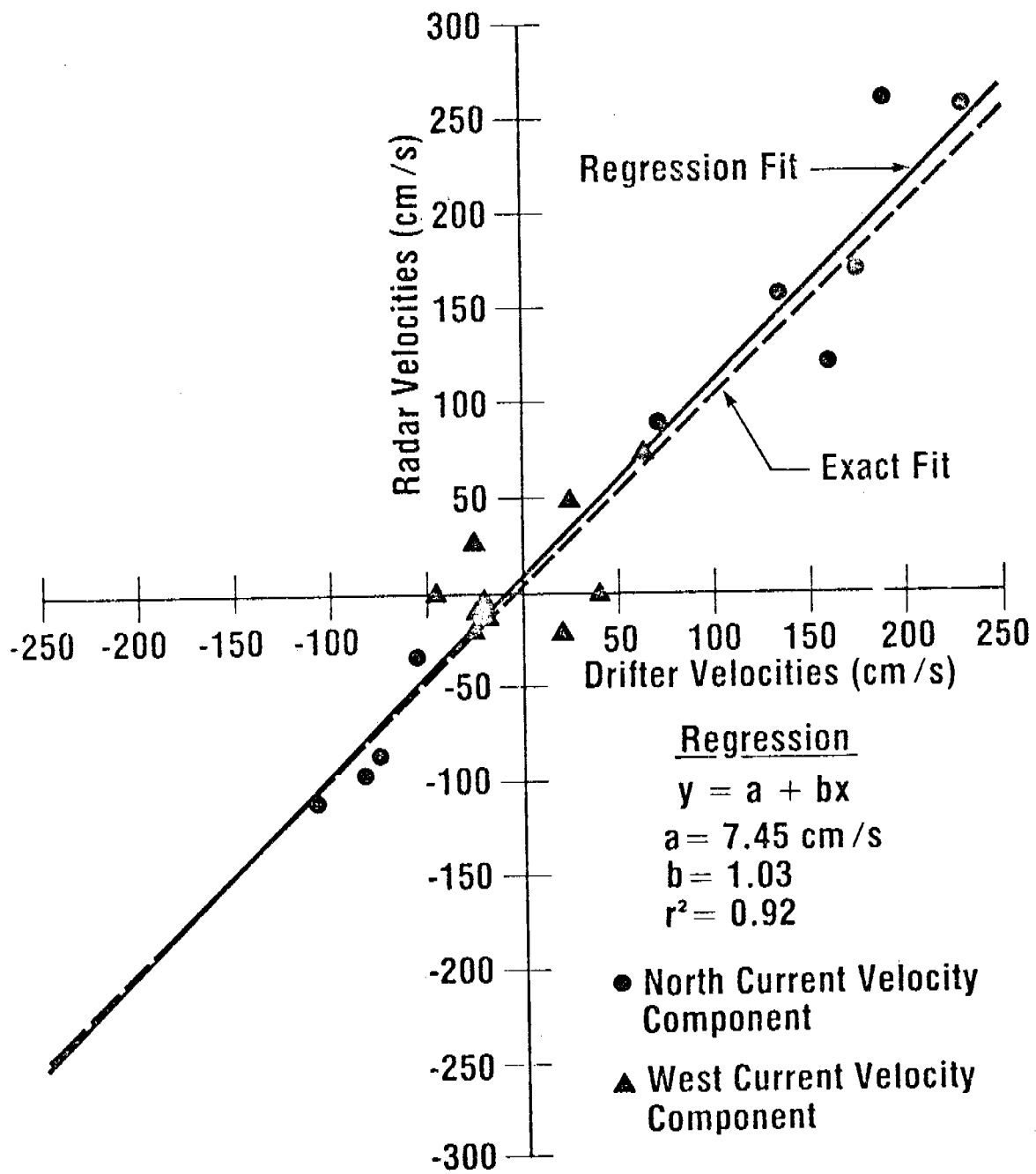
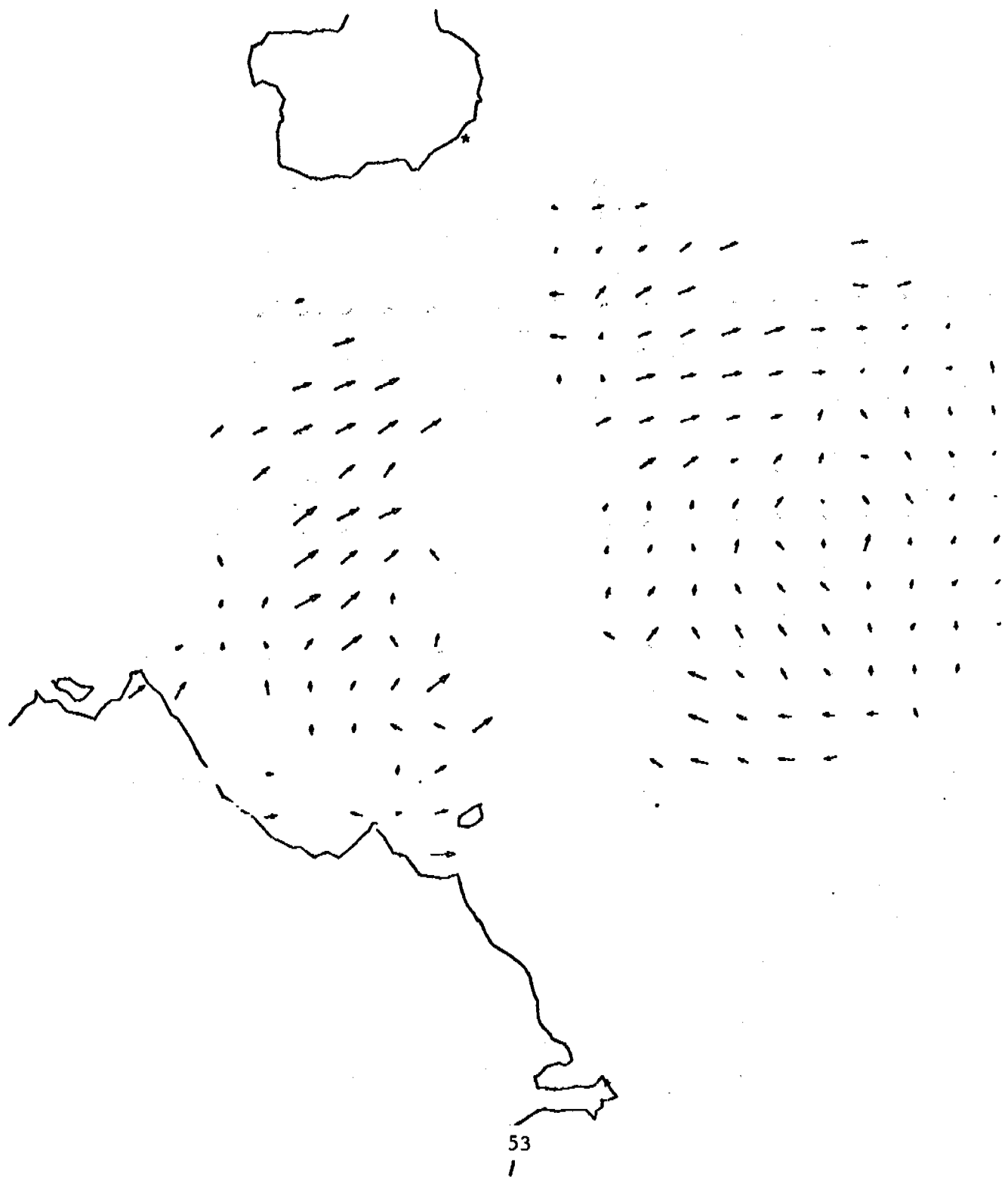


Figure 10. Correlogram of Radar vs Drifter Surface Current Velocities.

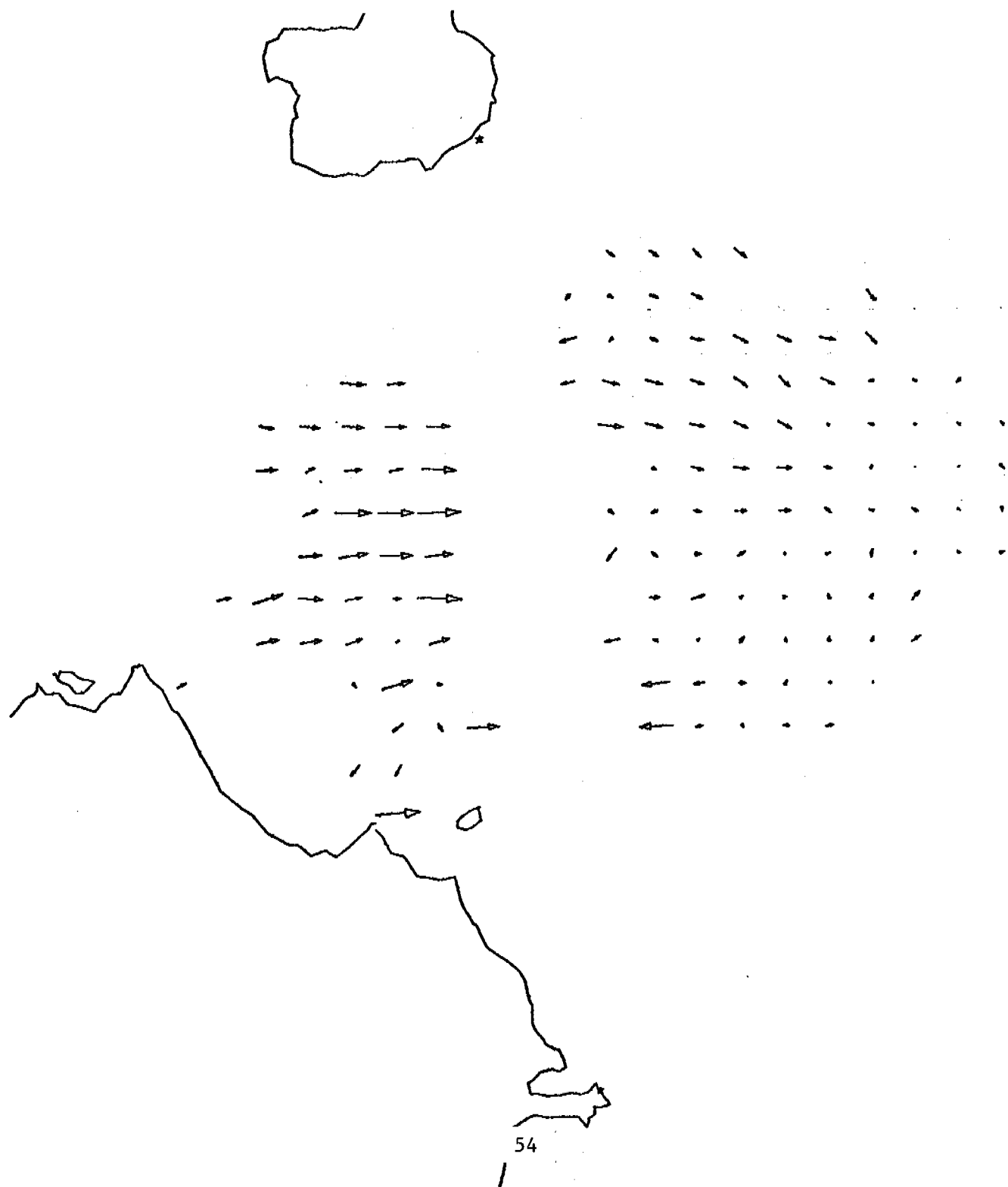
01-JUL-78 01:00:00
CAPE DOUGLAS AK.
AUGUSTINE IS. AK.

8 KM/IN
200 CM/S/IN
TRUE NORTH ↑



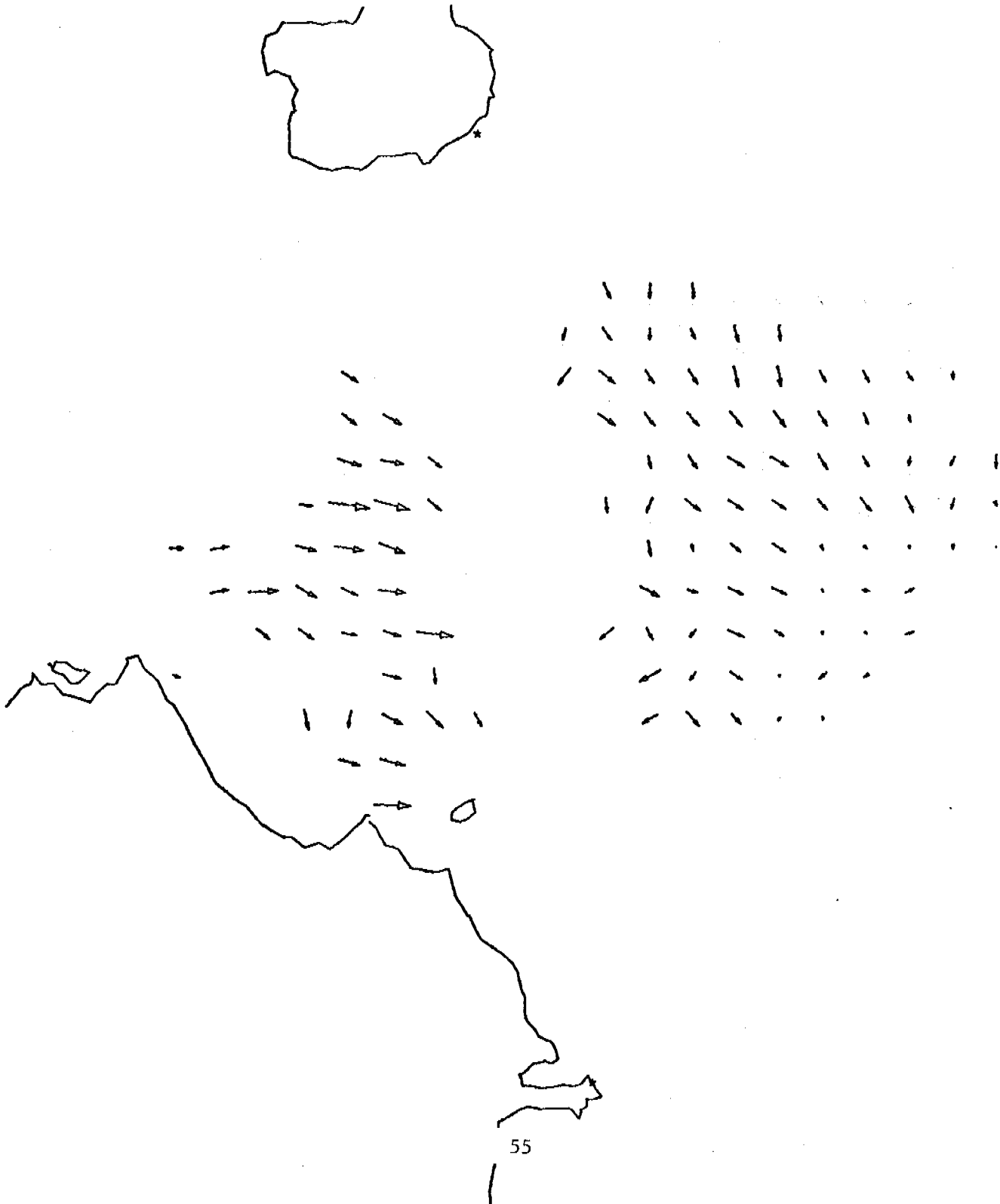
1 JUL 78 2: 0:00
CAPE DOUGLAS AK.
AUGUSTINE IS. AK.

8 KM/IN
200 CM/S/IN
TRUE NORTH ↑



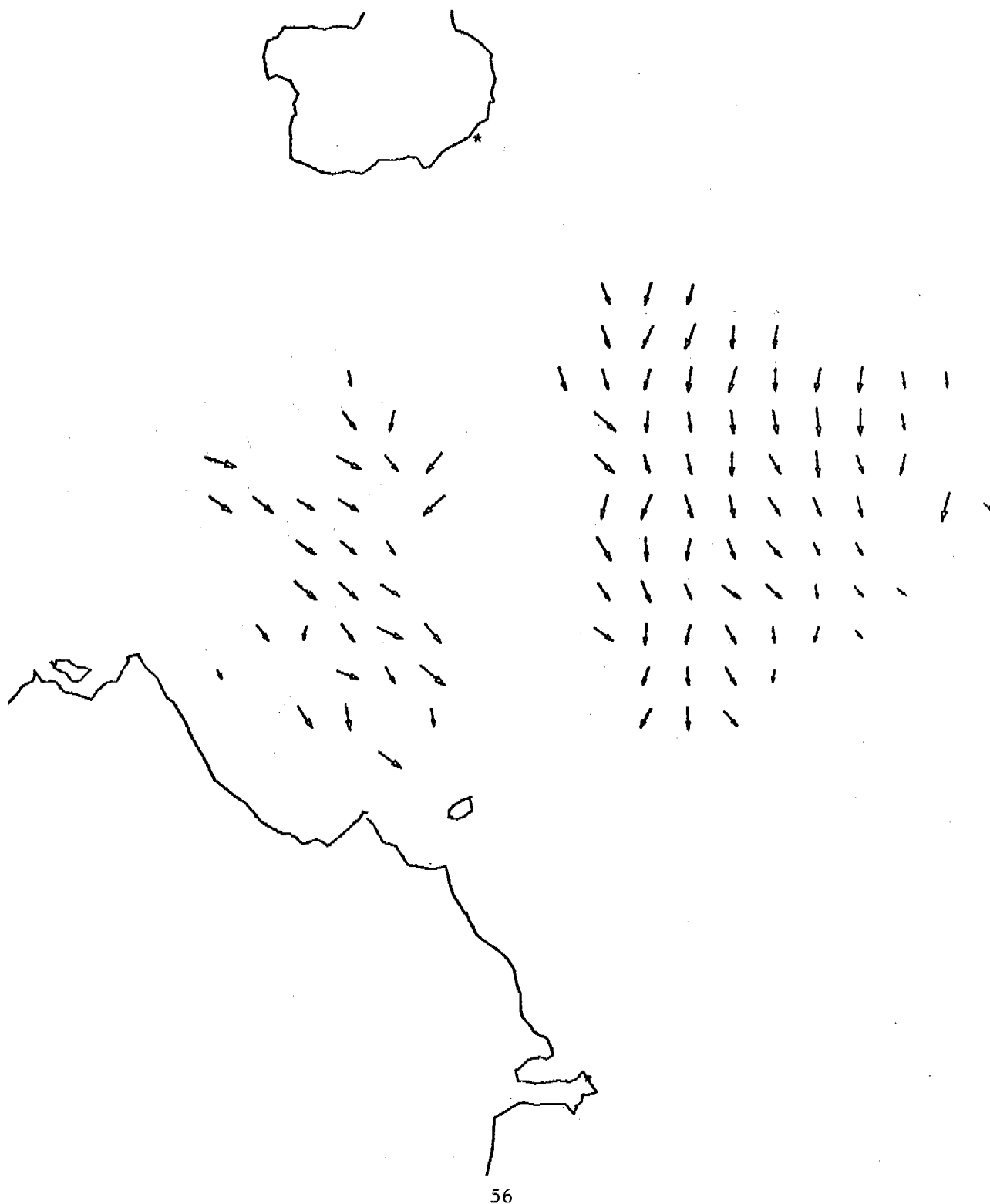
1 JUL 78 3: 0:00
CAPE DOUGLAS AK.
AUGUSTINE IS. AK.

8 KM/IN
200 CM/S/IN
TRUE NORTH ↑



CHIEF BOOBYING HIVE
AUGUSTINE IS. AK.

200 CM/S/IN
TRUE NORTH ↑

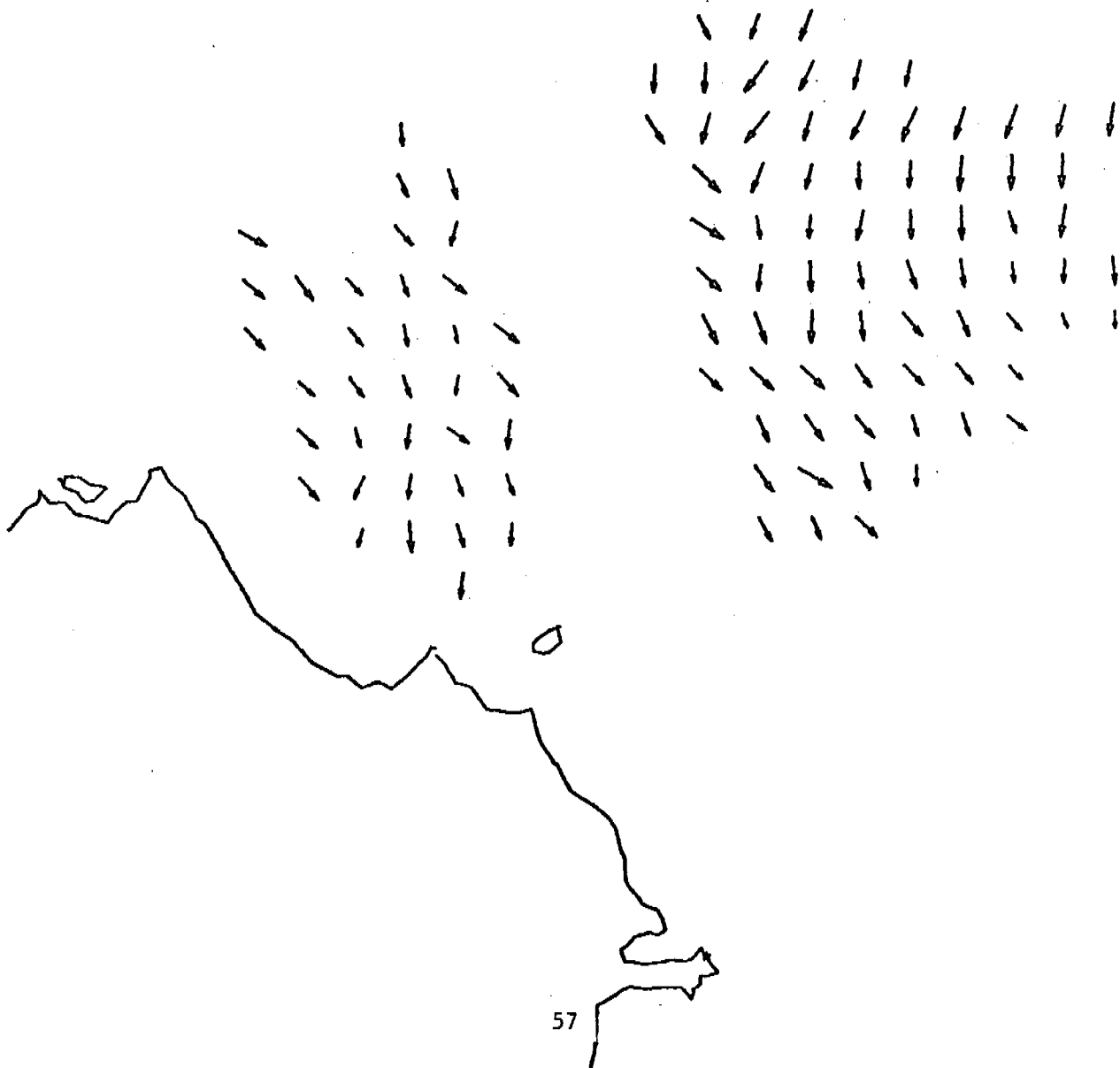


1 JUL 78 4: 0:00

8 KM/IN

1 JUL 78 5: 0:00
CAPE DOUGLAS AK.
AUGUSTINE IS. AK.

8 KM/IN
200 CM/S/IN
TRUE NORTH ↑



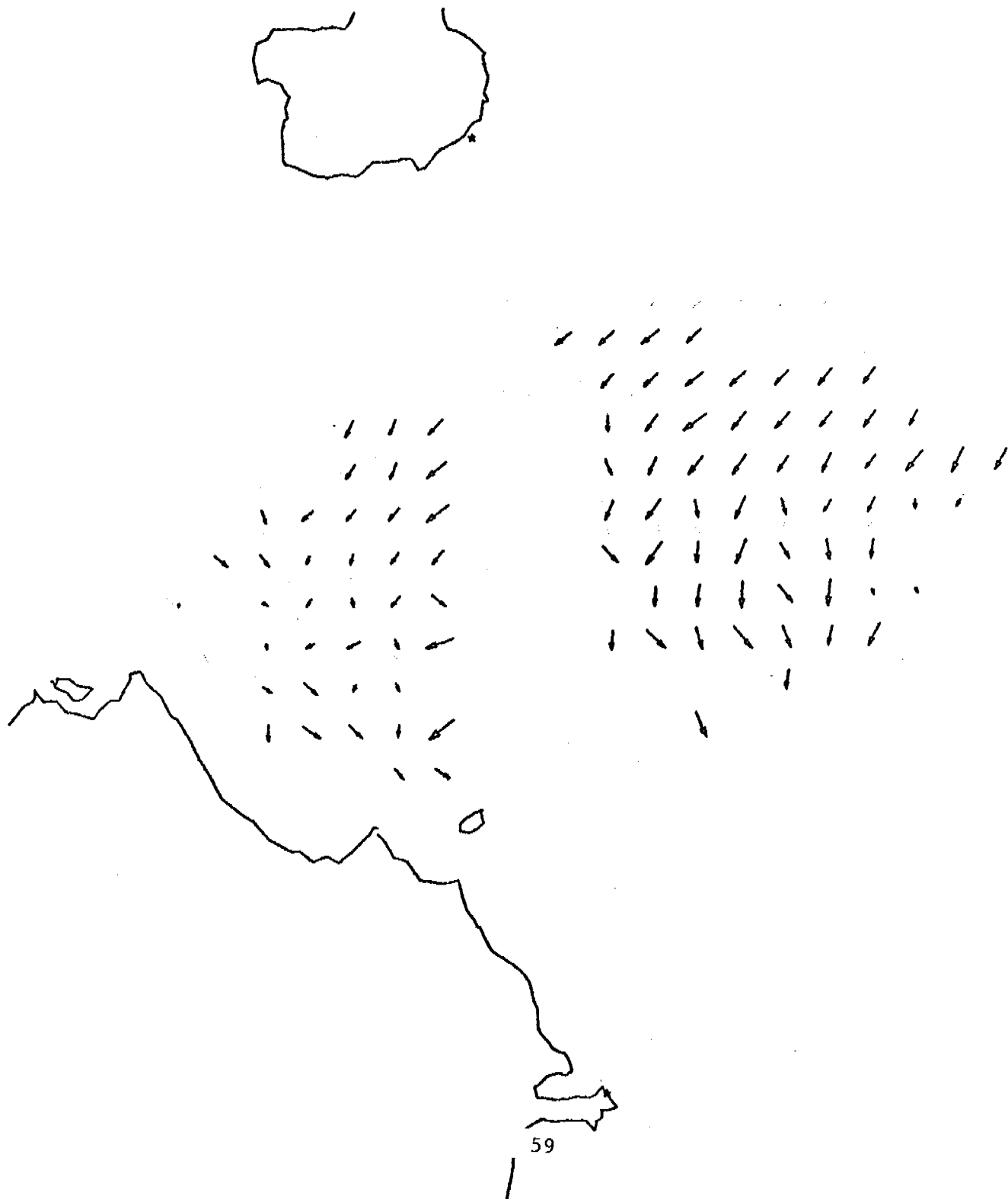
1 JUL 78 6: 0:00
CAPE DOUGLAS AK.
AUGUSTINE IS. AK.

8 KM/IN
200 CM/S/IN
TRUE NORTH ↑



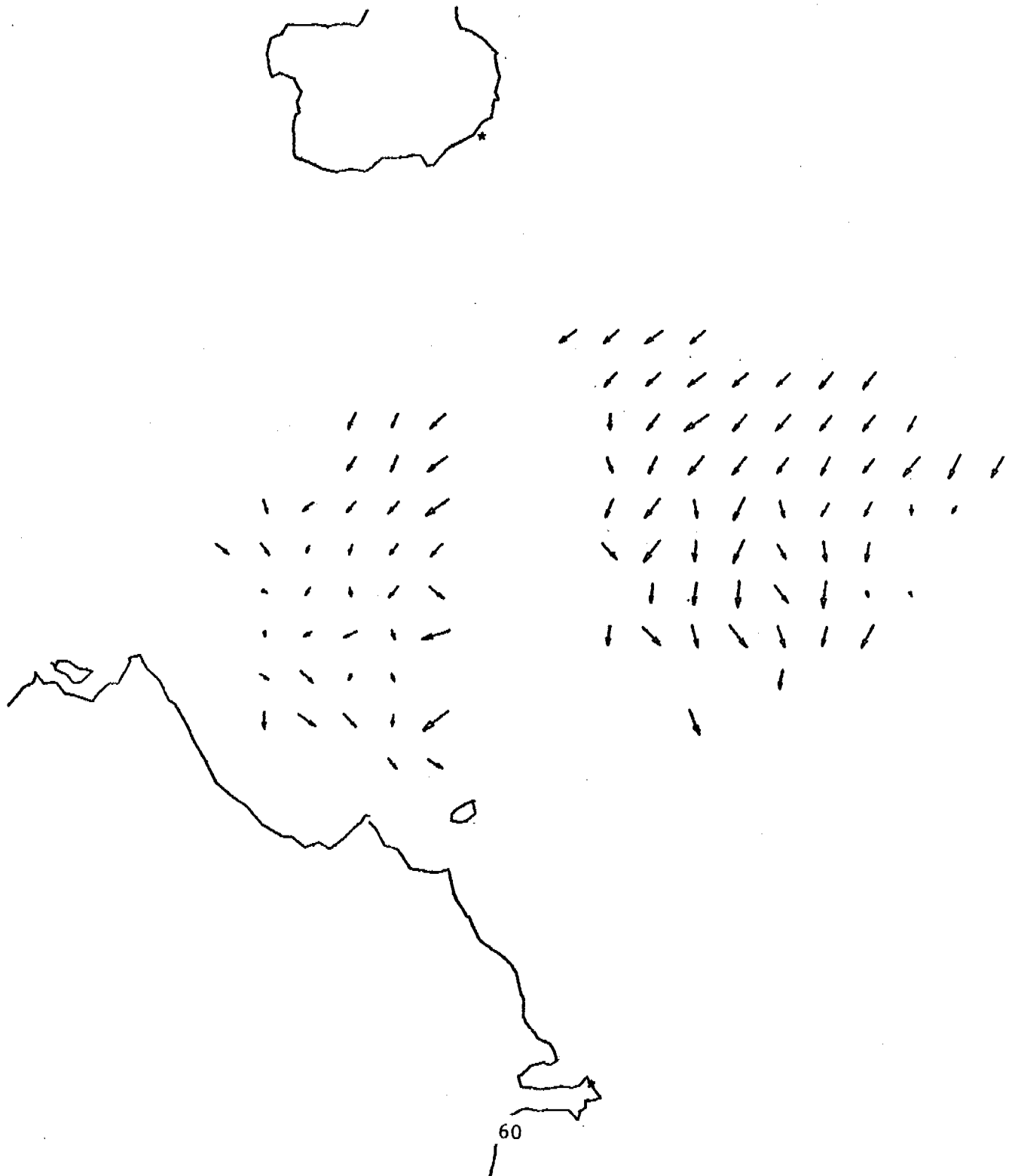
1 JUL 78 7: 0:00
CAPE DOUGLAS AK.
AUGUSTINE IS. AK.

8 KM/IN
200 CM/S/IN
TRUE NORTH ↑



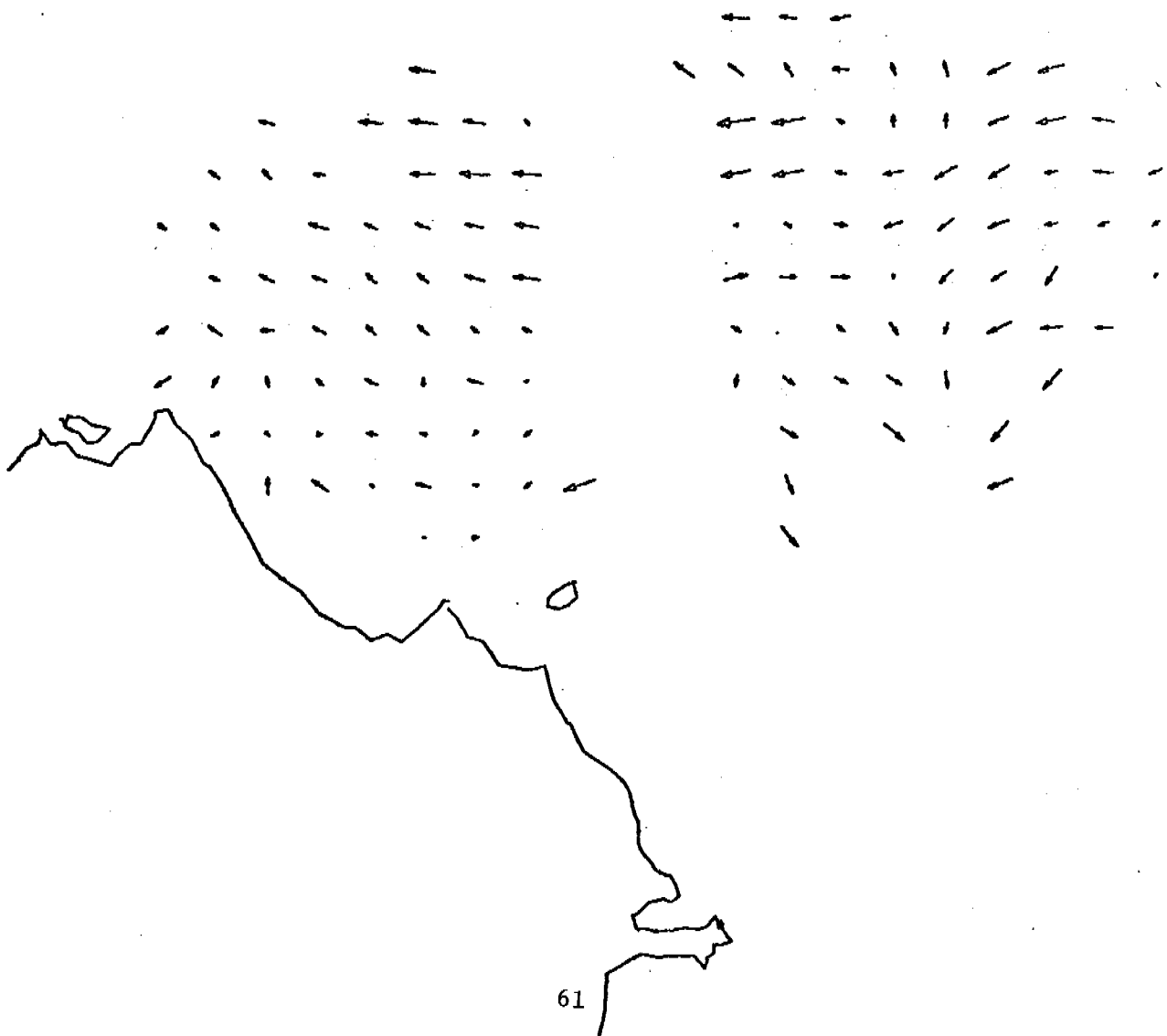
1 JUL 78 7: 0:00
CAPE DOUGLAS AK.
AUGUSTINE IS. AK. .

8 KM/IN
200 CM/S/IN
TRUE NORTH ↑



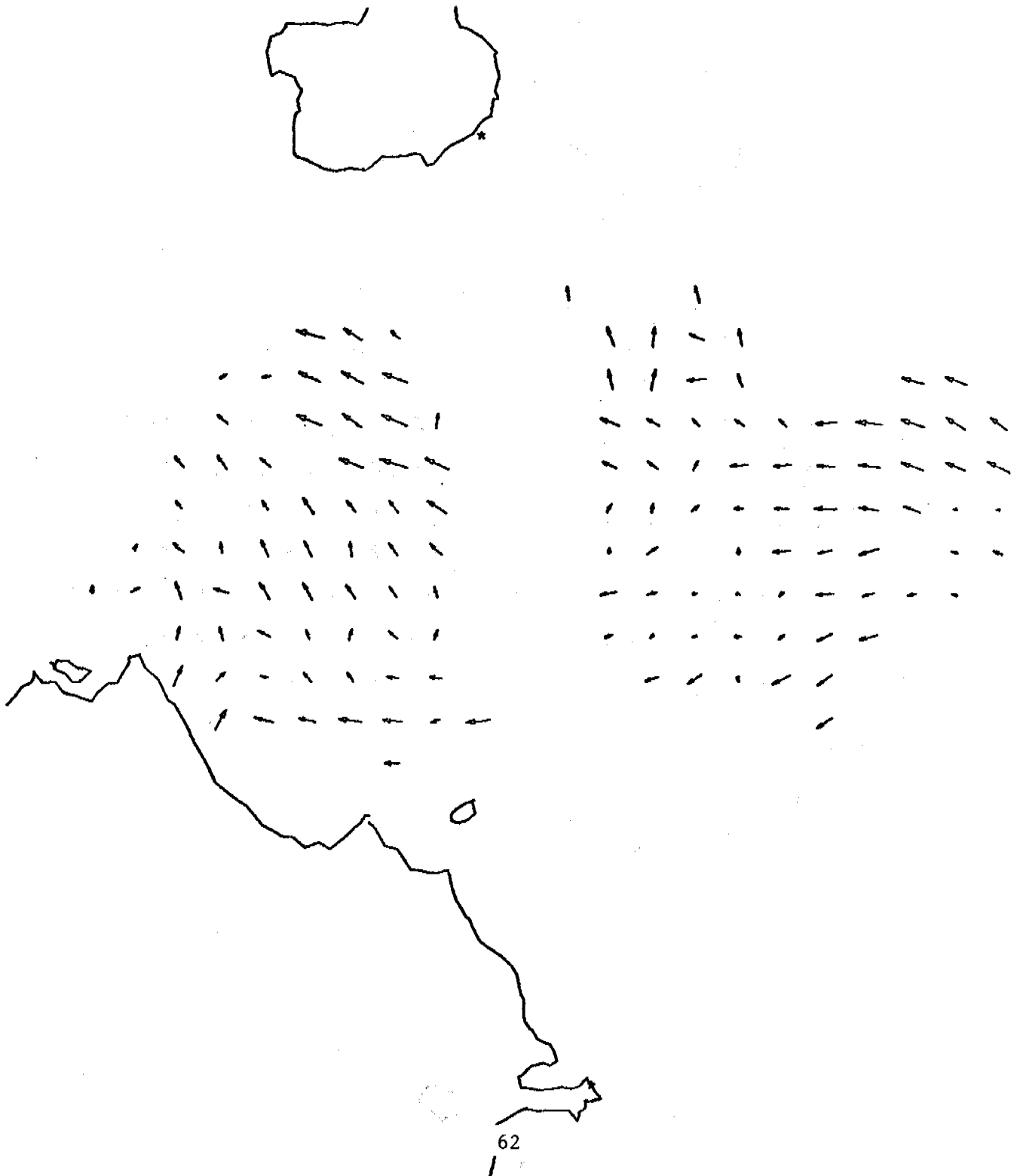
1 JUL 78 9: 0:00
CAPE DOUGLAS AK.
AUGUSTINE IS. AK.

8 KM/IN
200 CM/S/IN
TRUE NORTH ↑



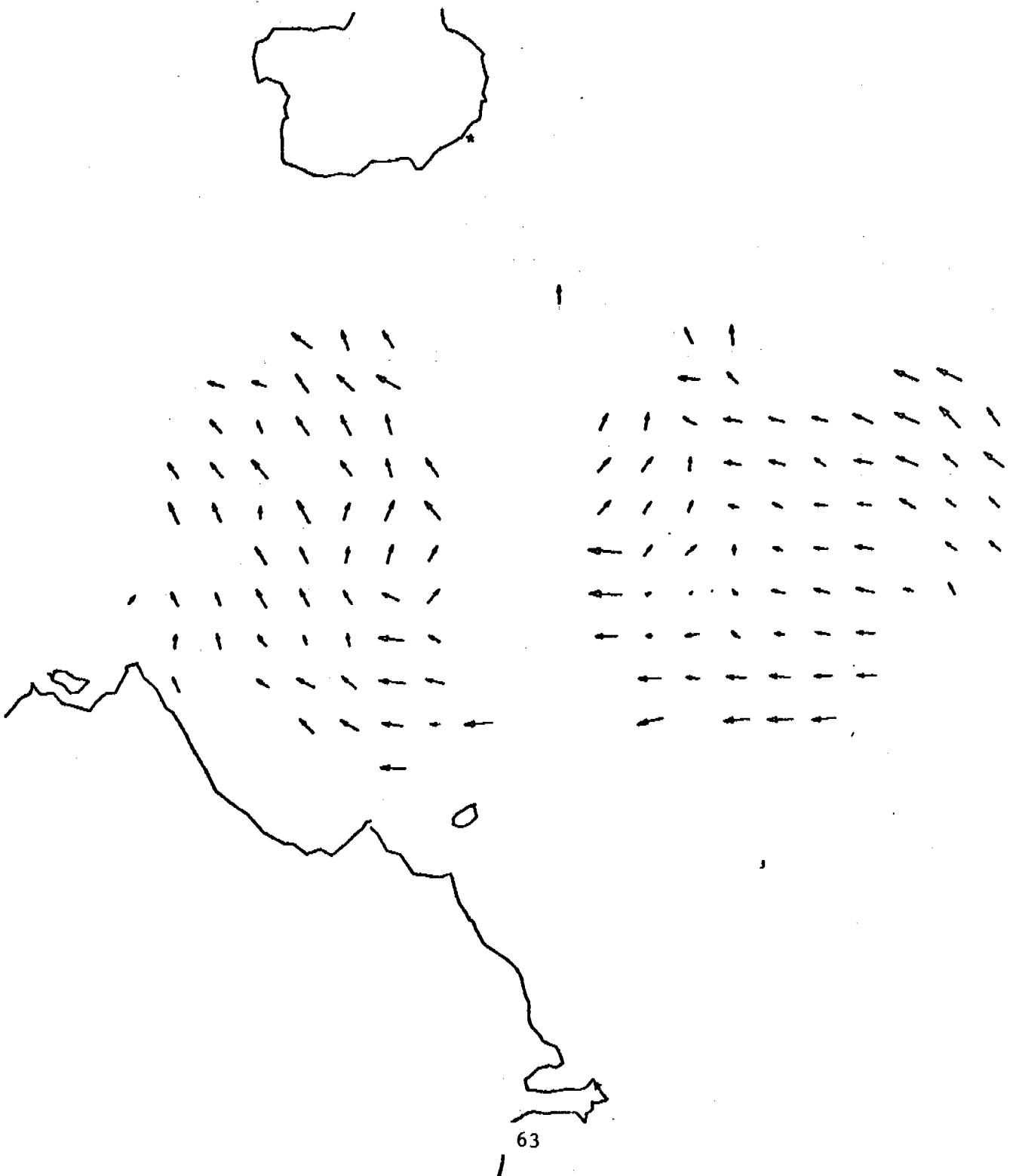
1 JUL 78 10: 0:00
CAPE DOUGLAS AK.
AUGUSTINE IS. AK.

8 KM/IN
200 CM/S/IN
TRUE NORTH ↑



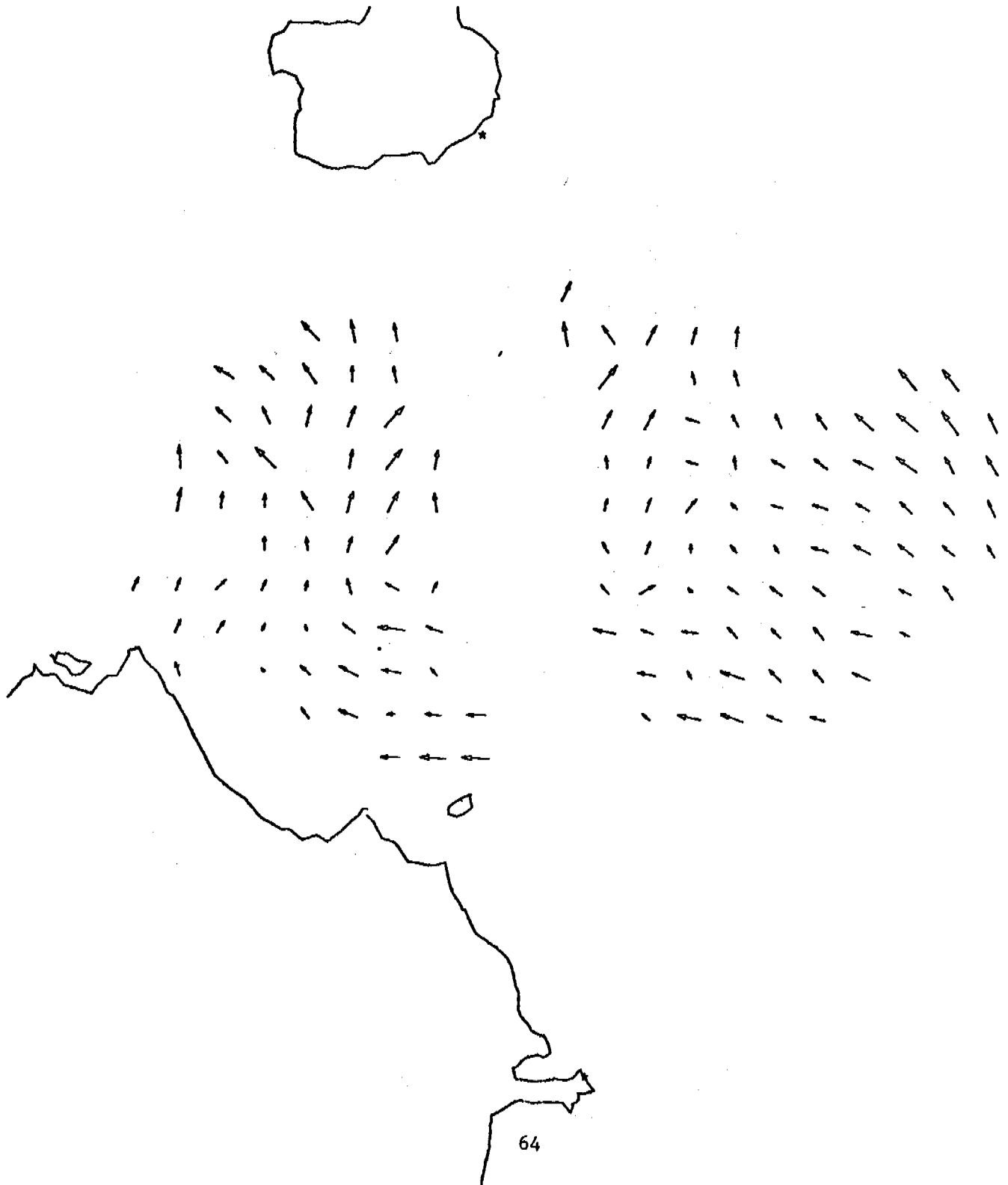
1 JUL 78 11: 0:00
CAPE DOUGLAS AK.
AUGUSTINE IS. AK.

8 KM/IN
200 CM/S/IN
TRUE NORTH ↑



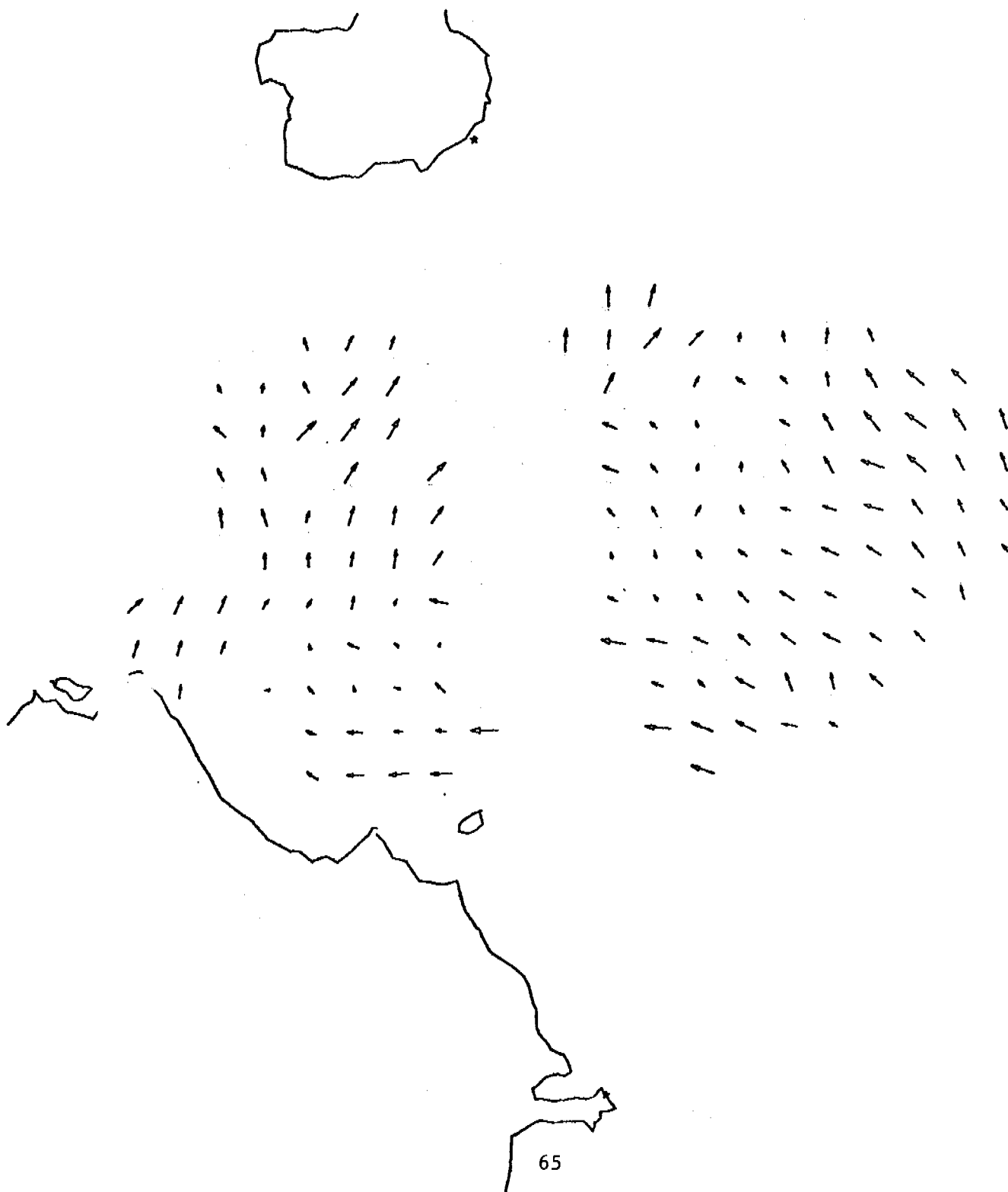
1 JUL 78 12: 0:00
CAPE DOUGLAS AK.
AUGUSTINE IS. AK.

8 KM/IN
200 CM/S/IN
TRUE NORTH ↑



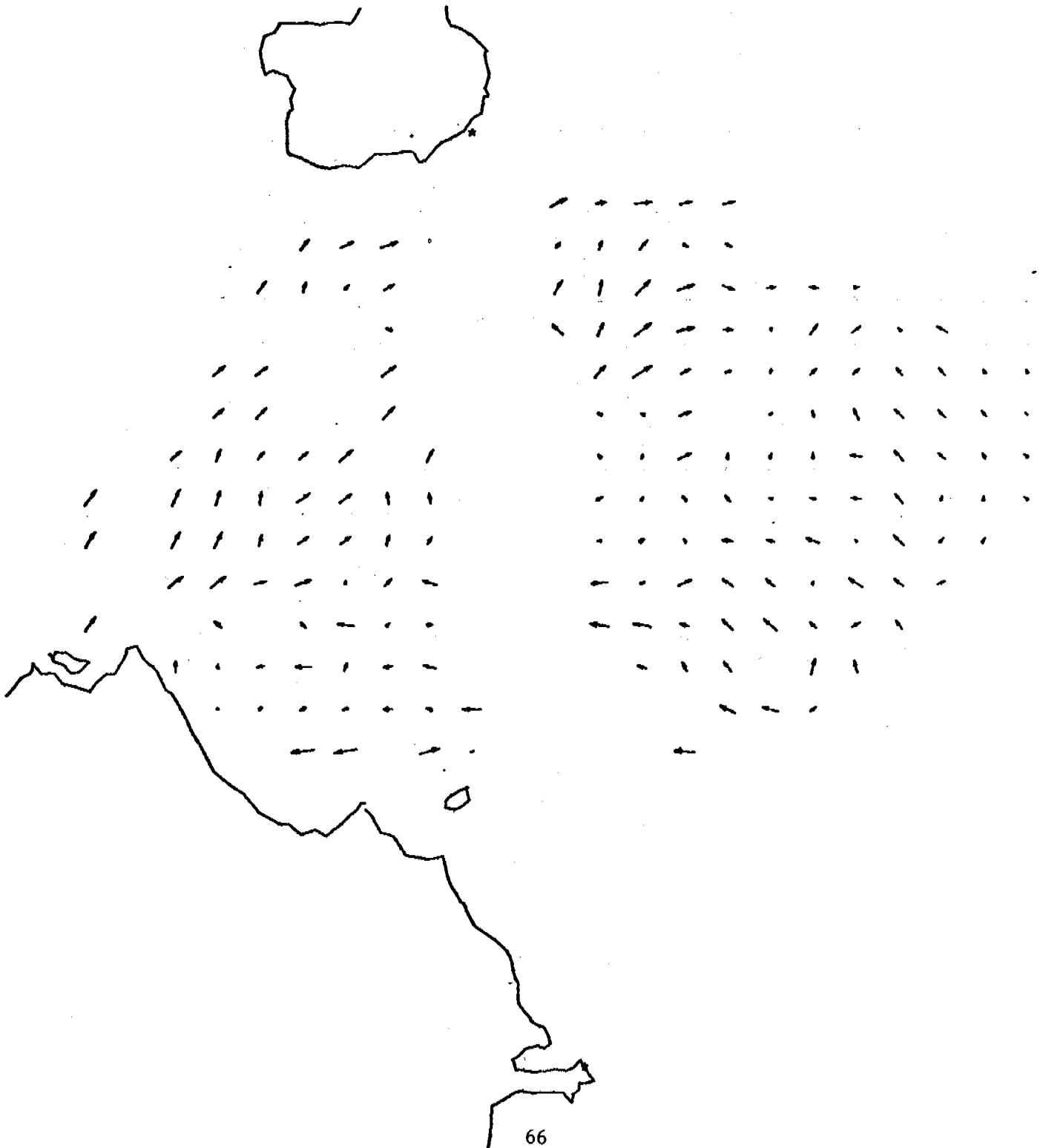
1 JUL 78 13: 0:00
CAPE DOUGLAS AK.
AUGUSTINE IS. AK.

8 KM/IN
200 CM/S/IN
TRUE NORTH ↑



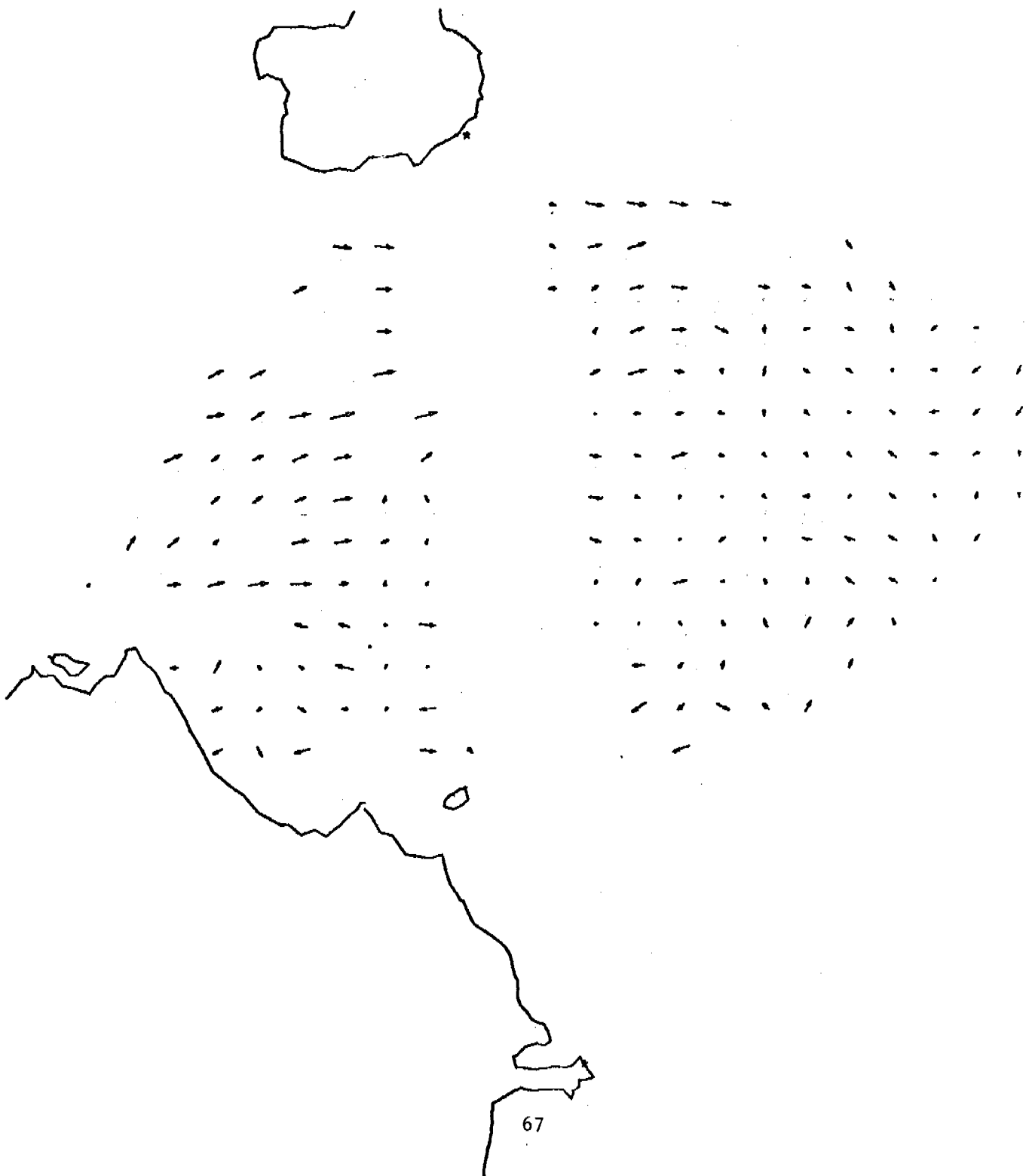
1 JUL 78 14: 0:00
CAPE DOUGLAS AK.
AUGUSTINE IS. AK.

8 KM/IN
200 CM/S/IN
TRUE NORTH ↑



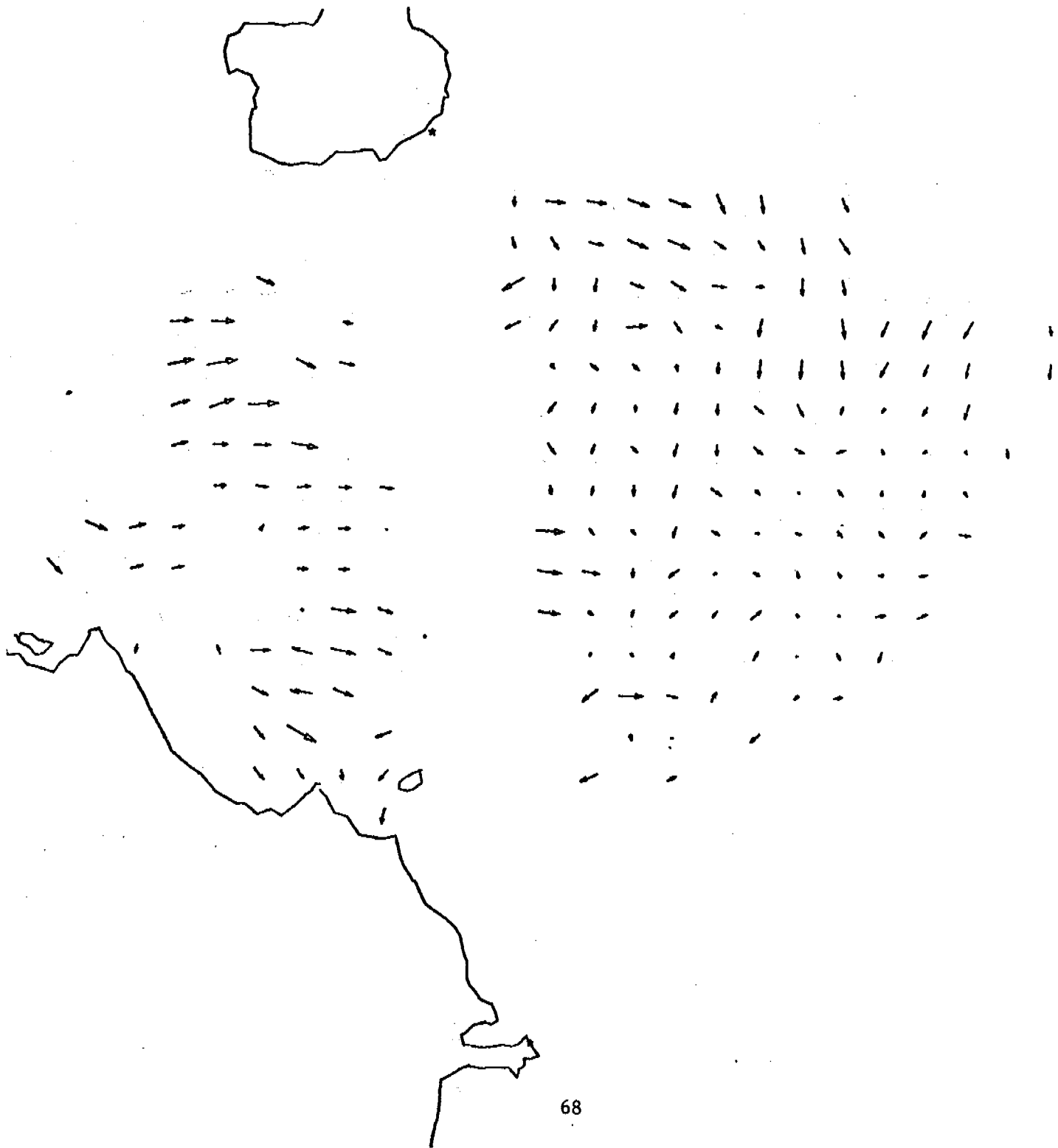
1 JUL 78 15: 0:00
CAPE DOUGLAS AK.
AUGUSTINE IS. AK.

8 KM/IN
200 CM/S/IN
TRUE NORTH ↑



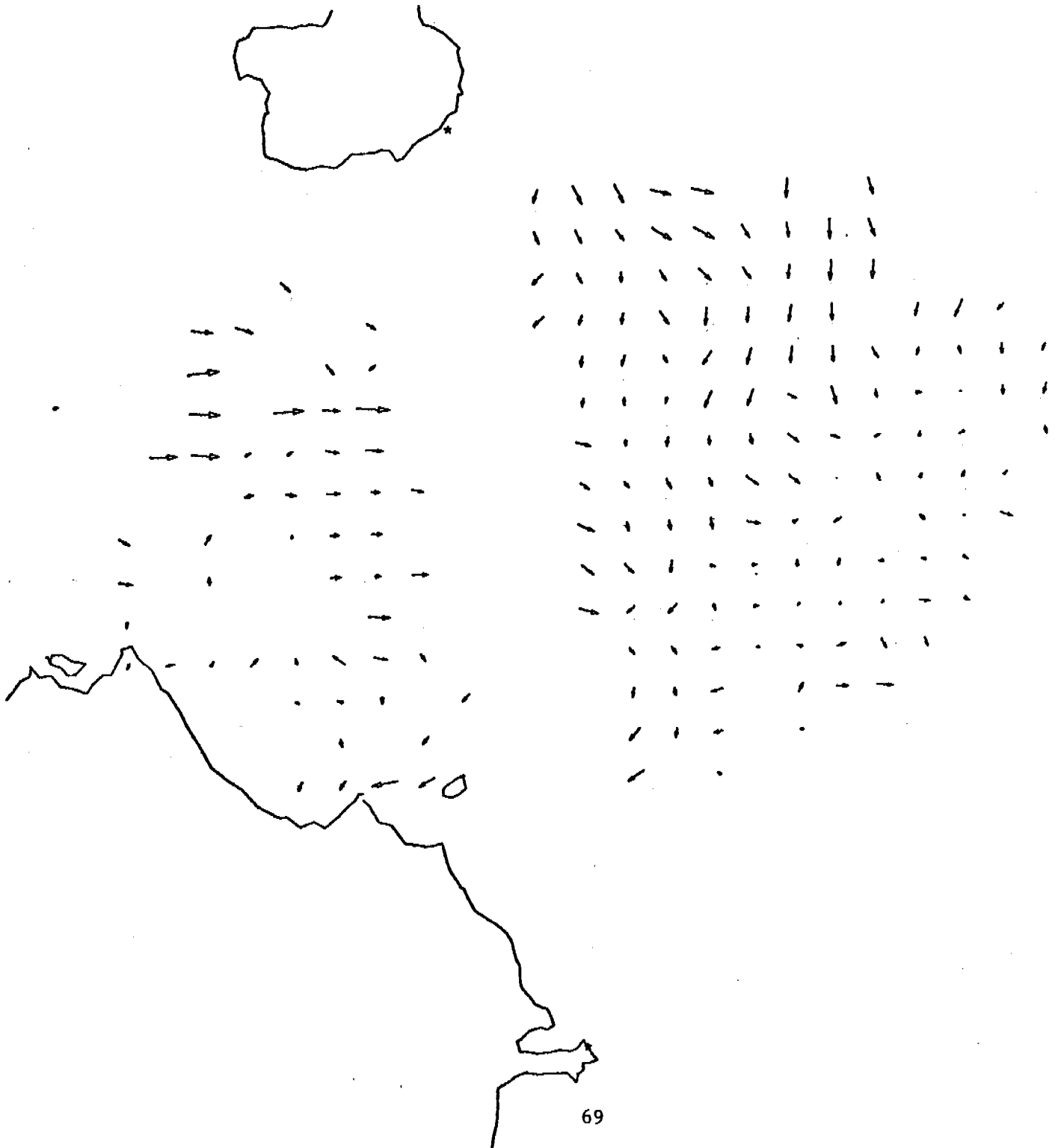
1 JUL 78 16: 0:00
CAPE DOUGLAS AK.
AUGUSTINE IS. AK.

8 KM/IN
200 CM/S/IN
TRUE NORTH ↑



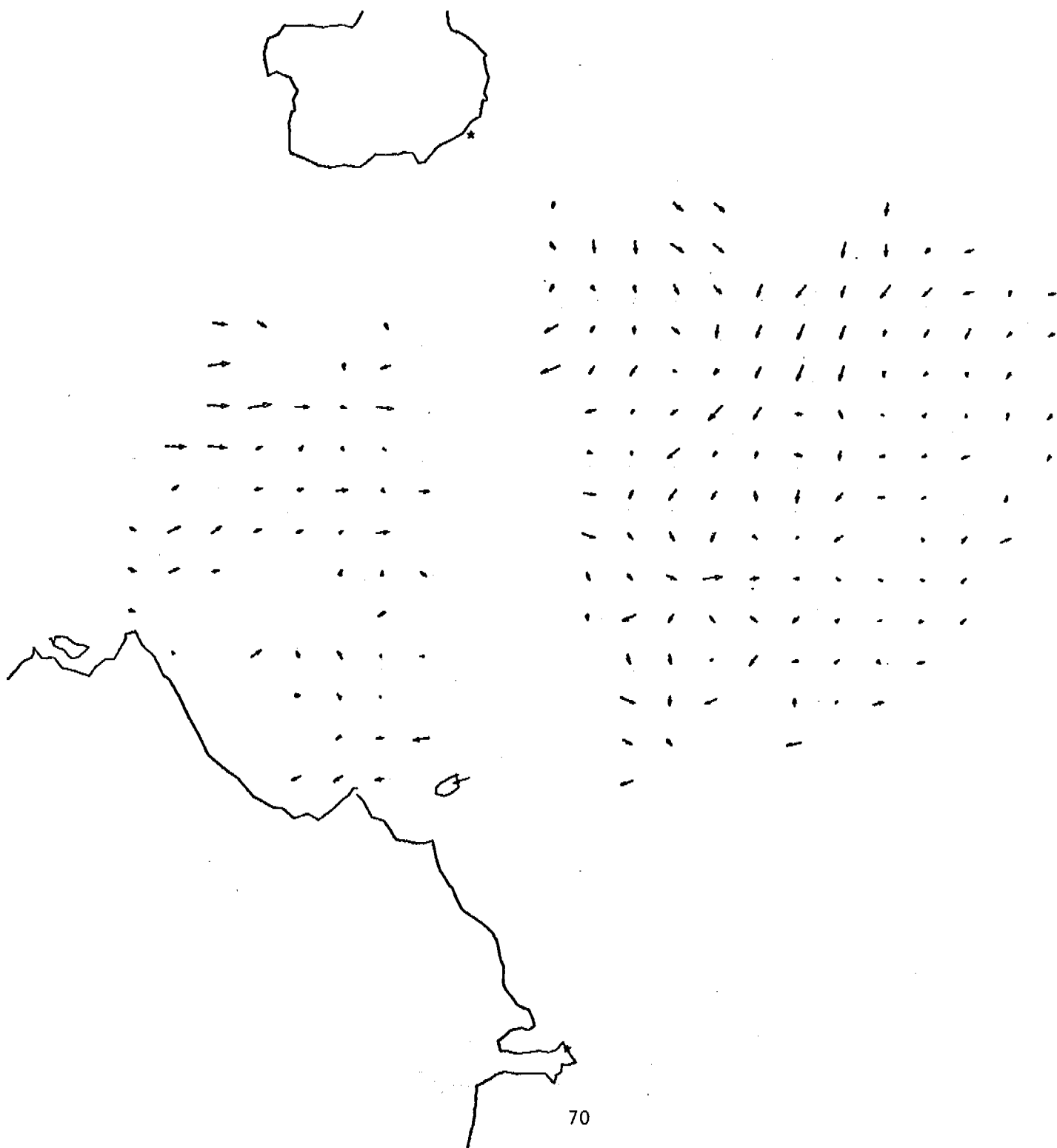
1 JUL 78 17: 0:00
CAPE DOUGLAS AK.
AUGUSTINE IS. AK..

8 KM/IN
200 CM/S/IN
TRUE NORTH ↑



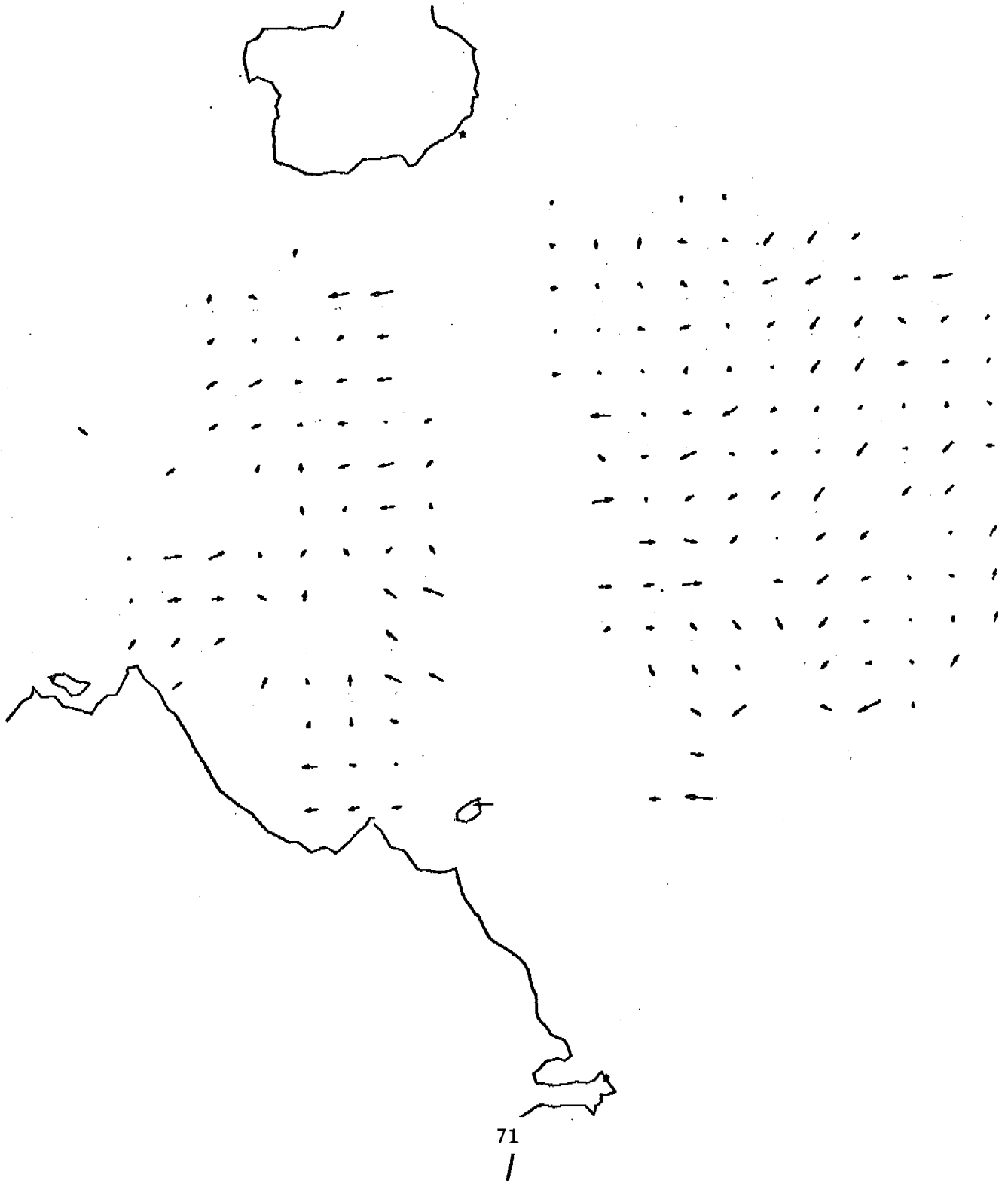
01-JUL-78 18:00:00
CAPE DOUGLAS AK.
AUGUSTINE IS. AK.

8 KM/IN
200 CM/S/IN
TRUE NORTH ↑



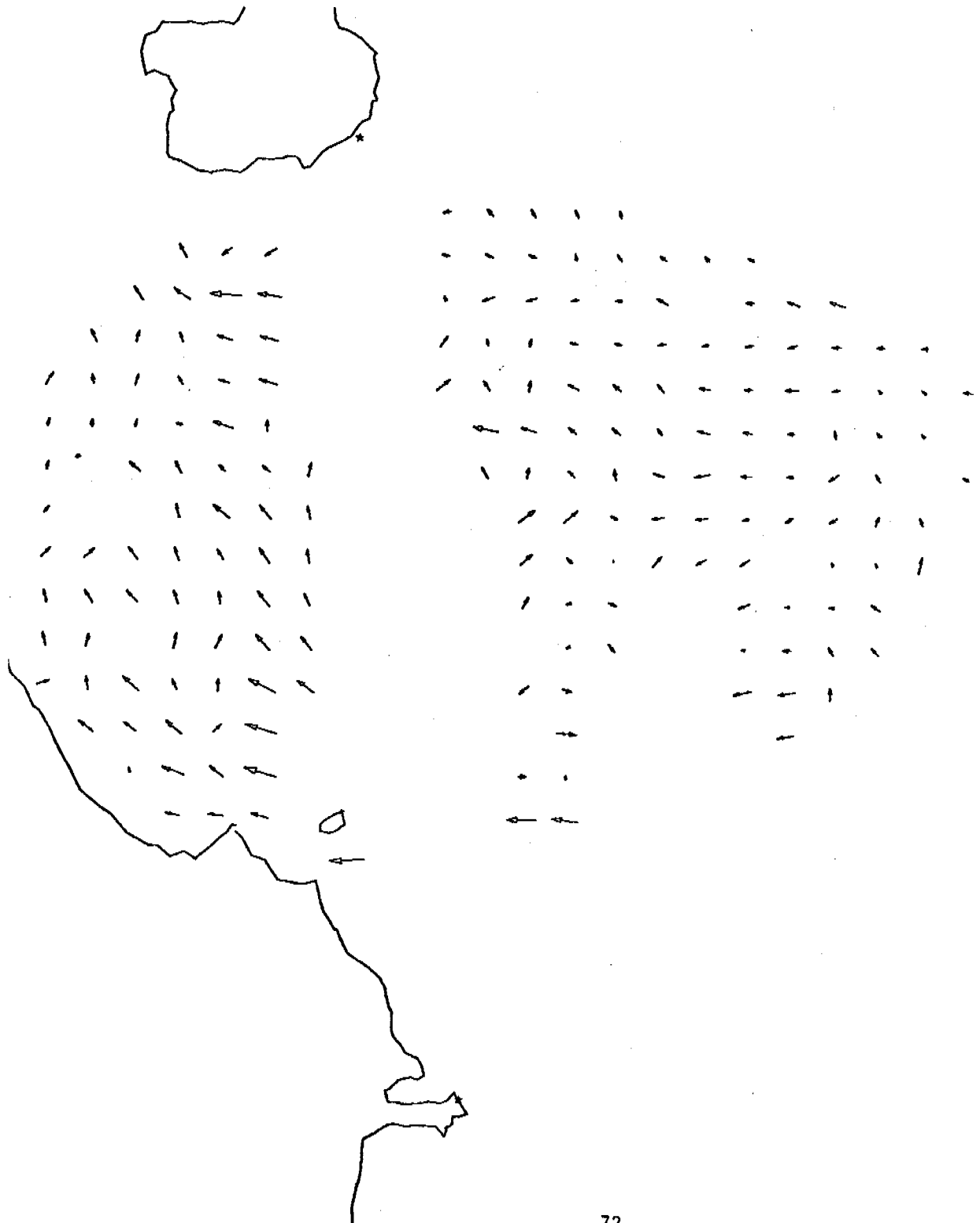
1 JUL 78 19: 0:00
CAPE DOUGLAS AK.
AUGUSTINE IS. AK:

8 KM/IN
200 CM/S/IN
TRUE NORTH ↑



DLHO HN.
IE IS. AK.

200 CM/SZ IN
TRUE NORTH ↑



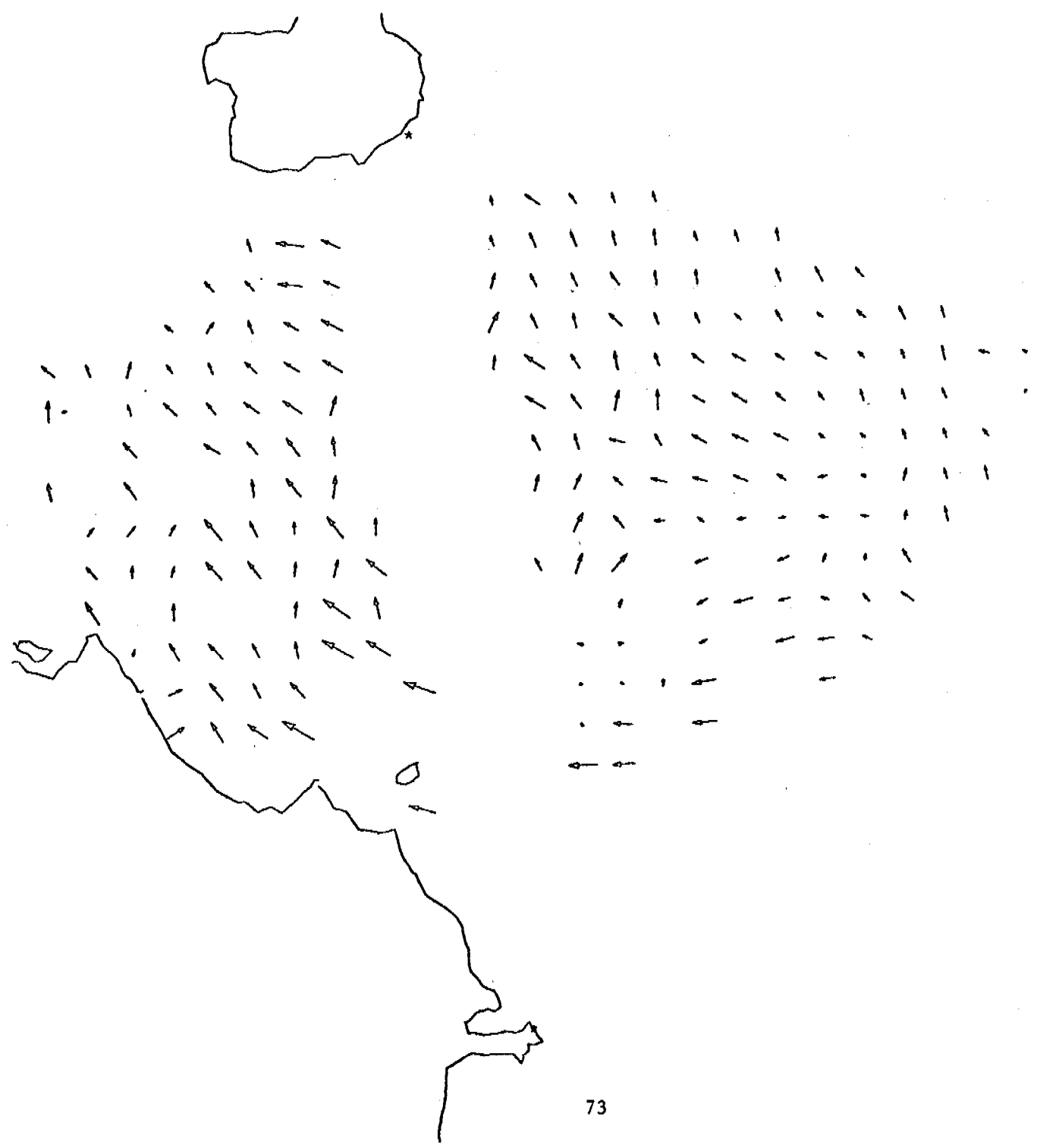
72

78 20:00:00

8 KM/IN

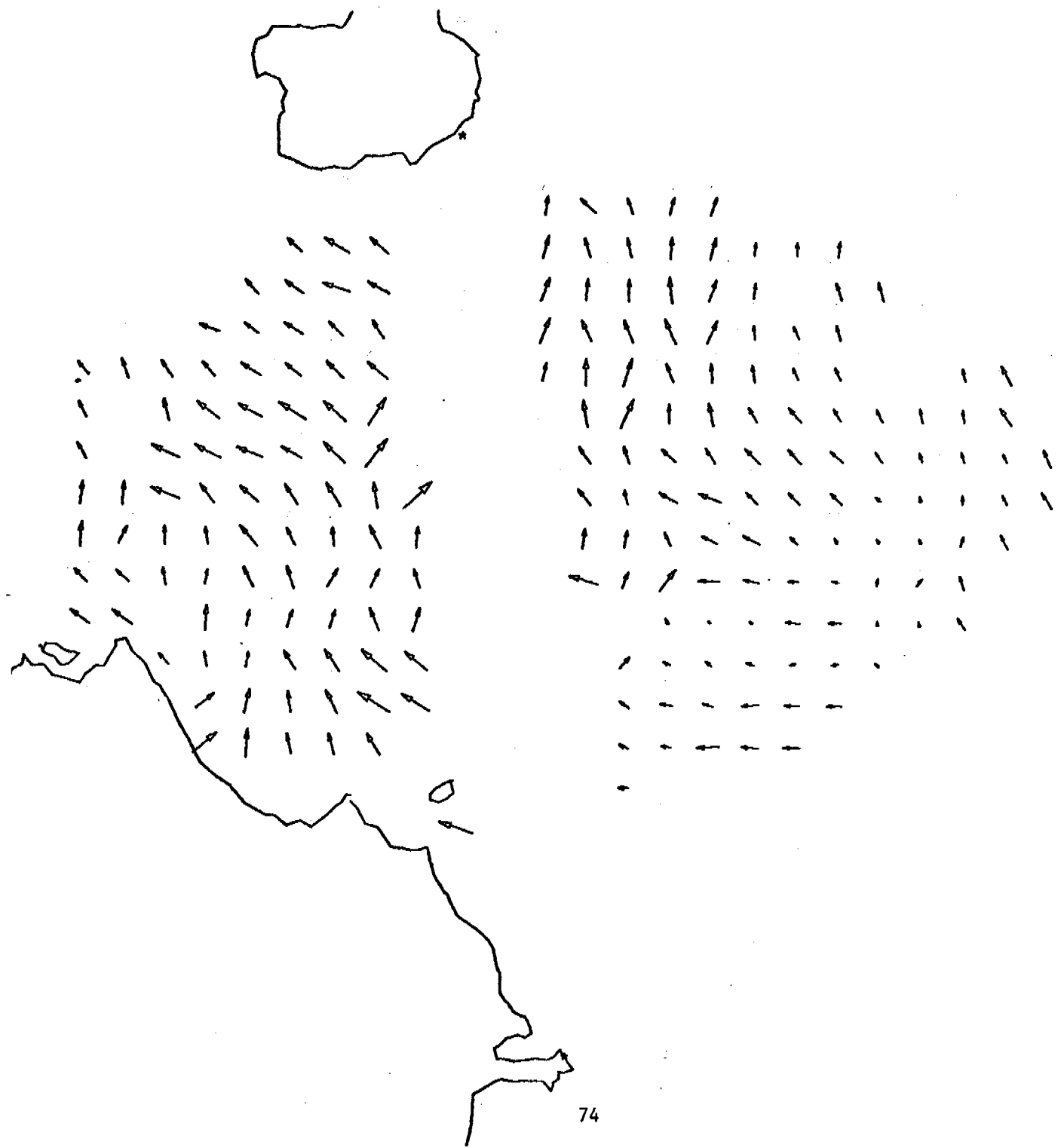
1 JUL 78 21: 0:00
CAPE DOUGLAS AK.
AUGUSTINE IS. AK.

8 KM/IN
200 CM/S/IN
TRUE NORTH ↑



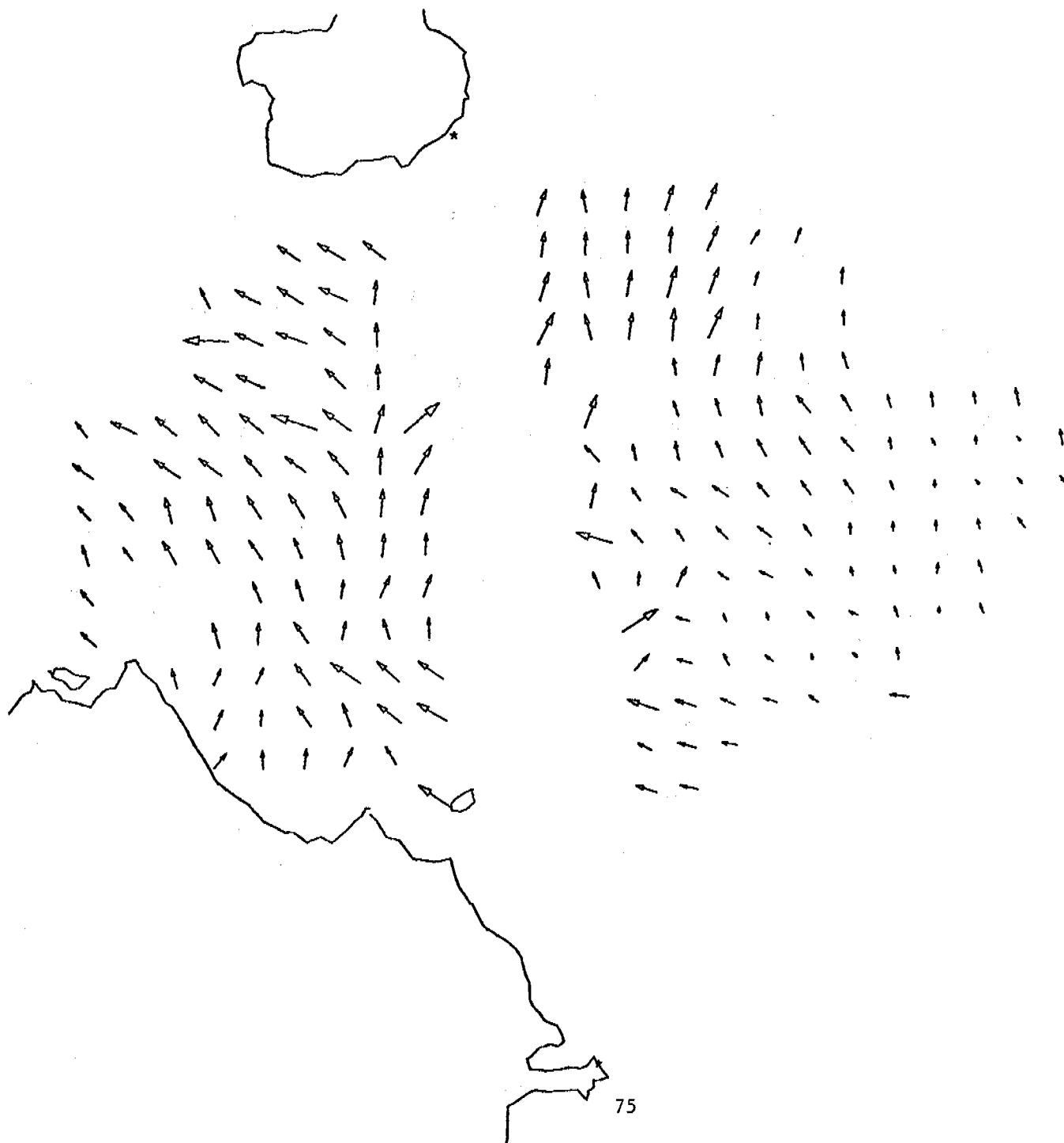
1 JUL 78 22: 0:00
CAPE DOUGLAS AK.
AUGUSTINE IS. AK.

8 KM/IN
200 CM/S/IN
TRUE NORTH ↑



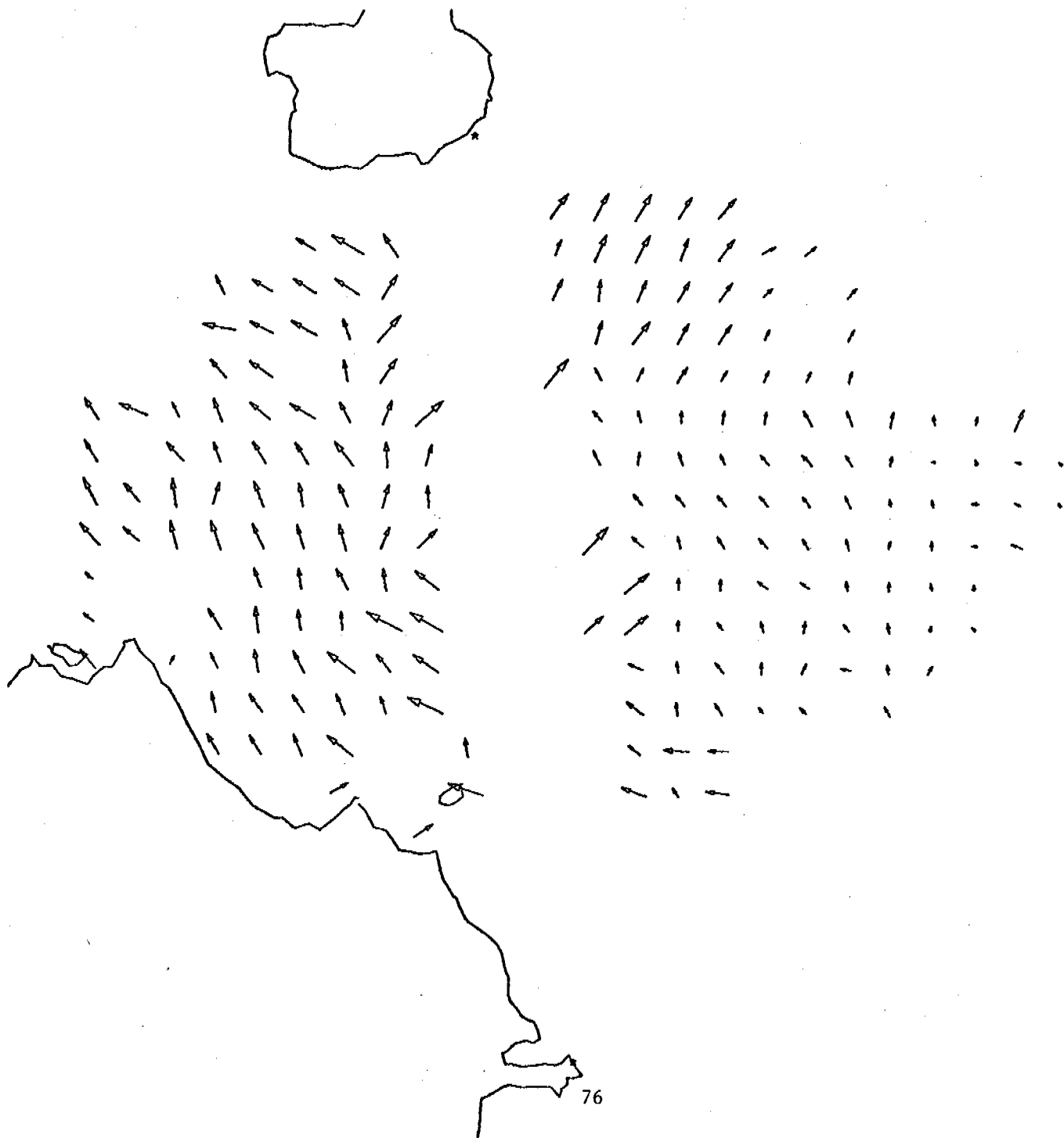
1 JUL 78 23: 0:00
CAPE DOUGLAS AK.
AUGUSTINE IS. AK.

8 KM/IN
200 CM/S/IN
TRUE NORTH ↑



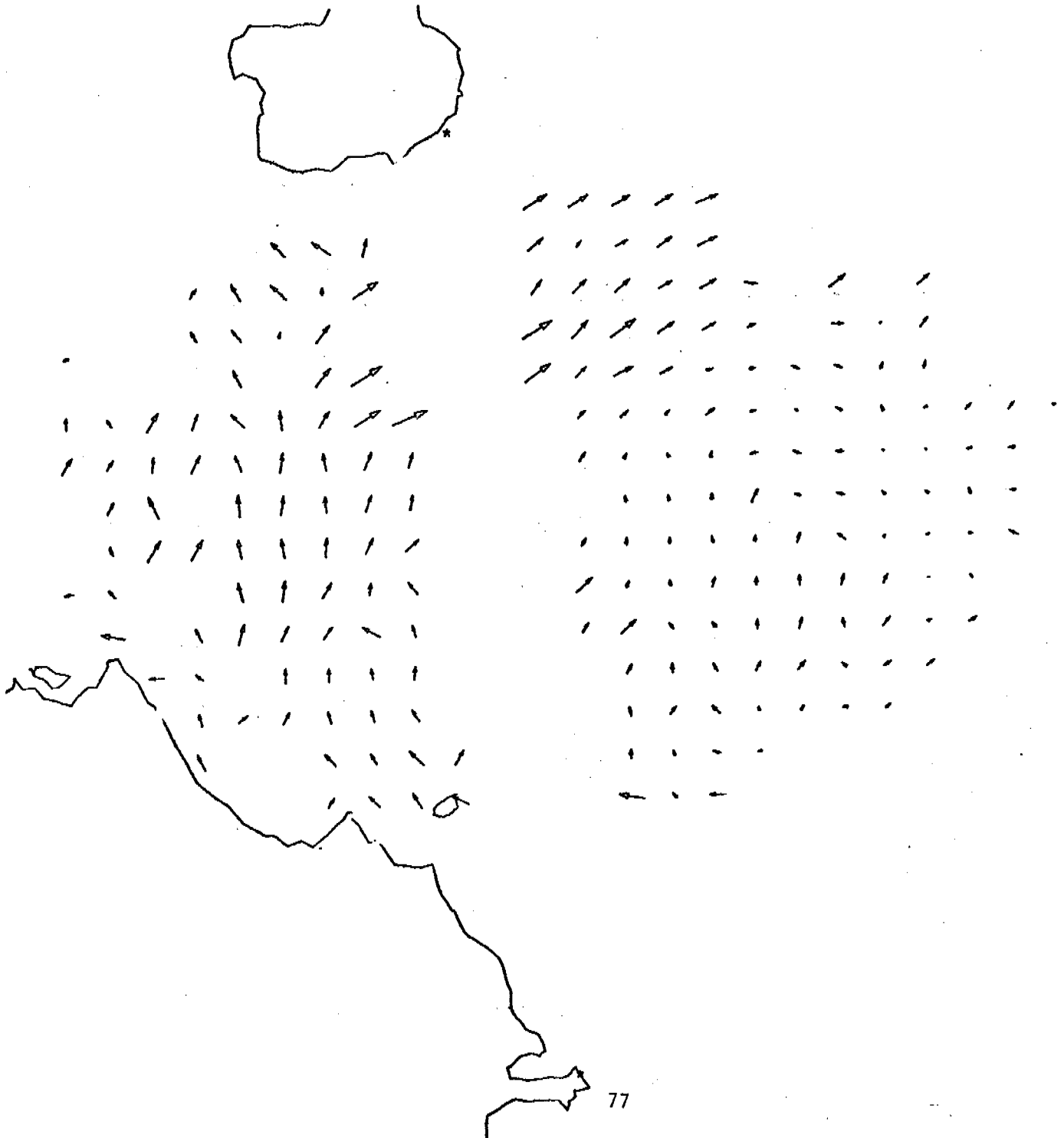
2 JUL 78 0: 0:00
CAPE DOUGLAS AK.
AUGUSTINE IS. AK.

8 KM/IN
200 CM/S/IN
TRUE NORTH ↑



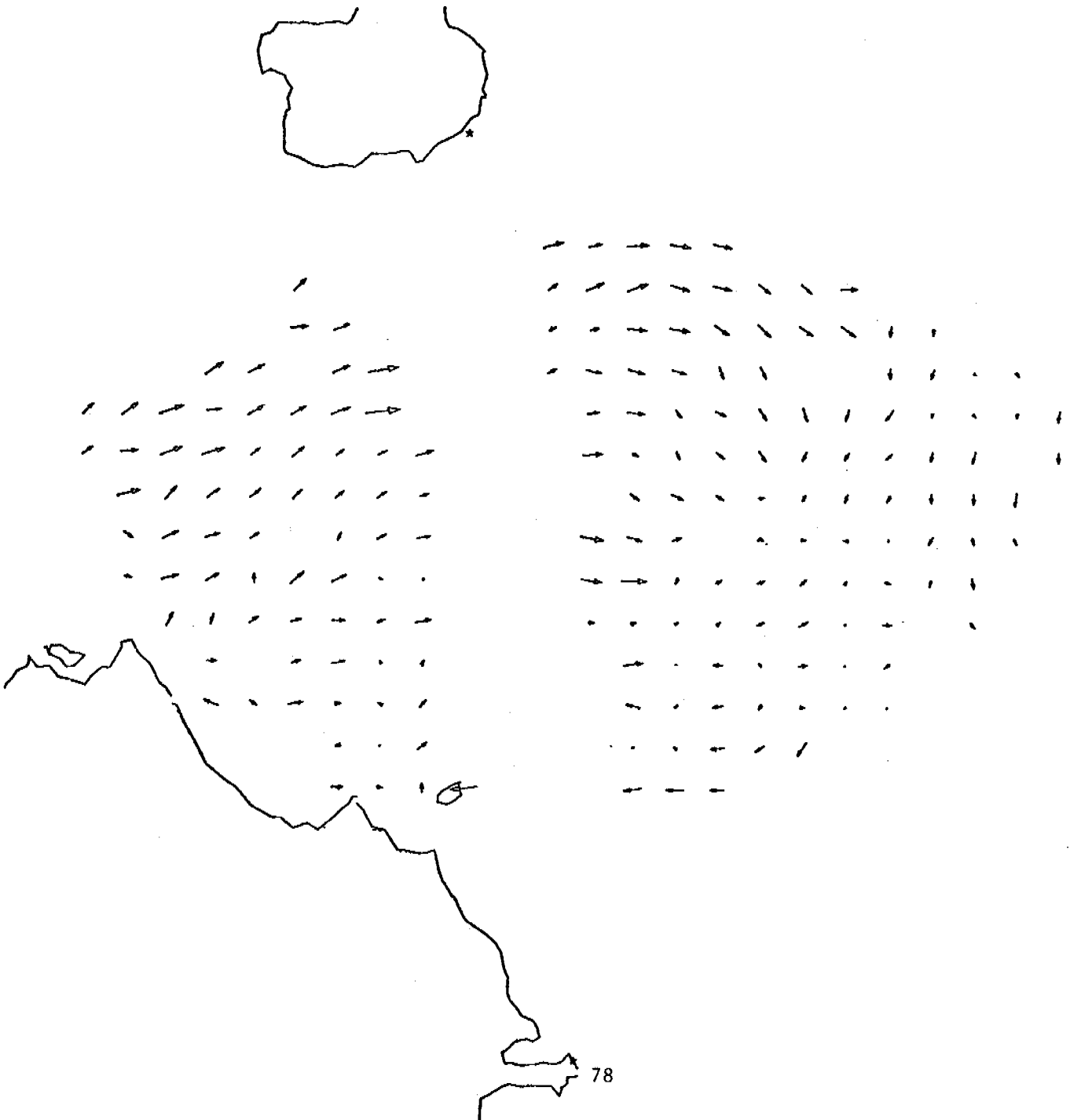
2 JUL 78 1: 0:00
CAPE DOUGLAS AK.
AUGUSTINE IS. AK.

8 KM/IN
200 CM/S/IN
TRUE NORTH ↑



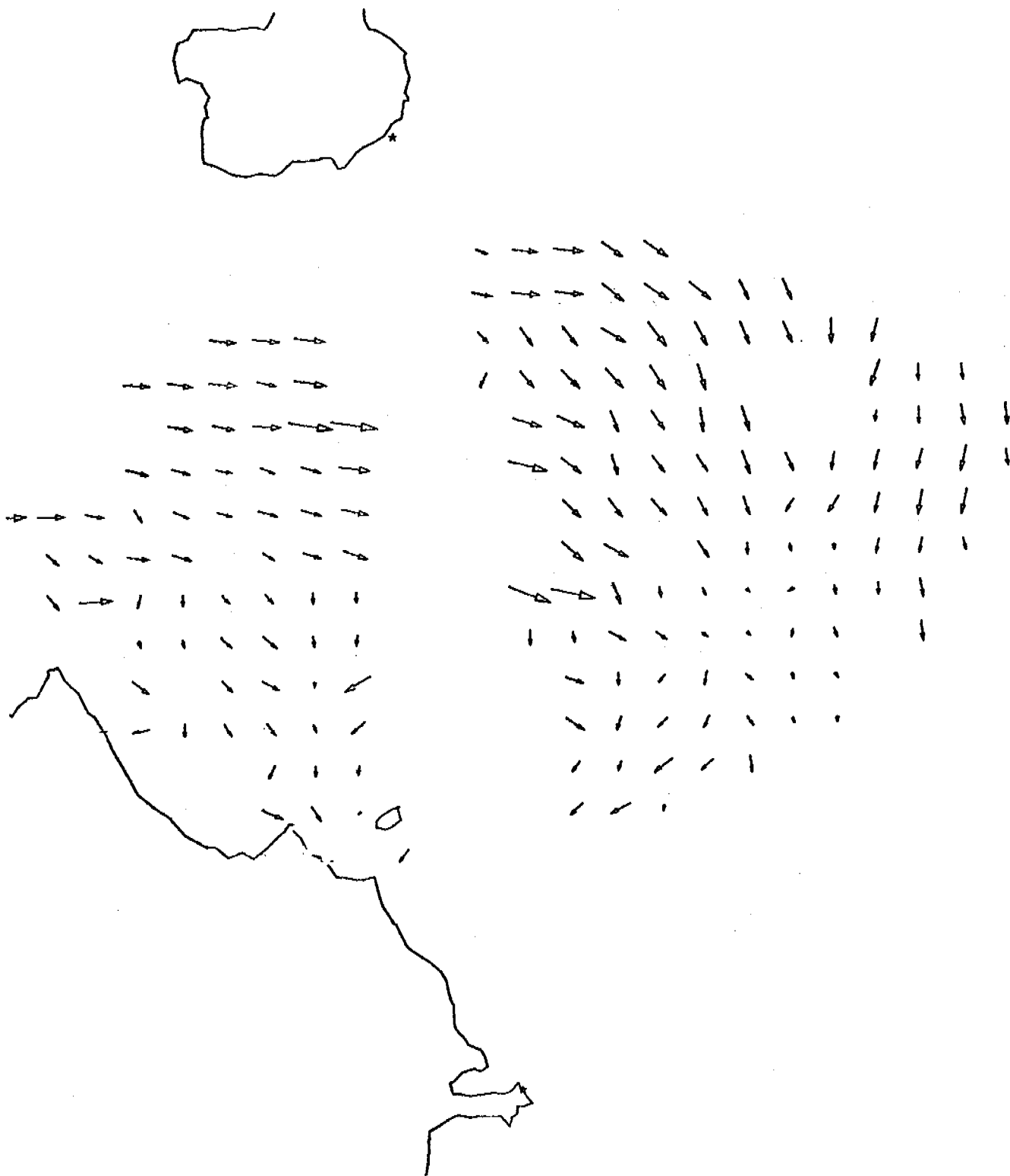
2 JUL 78 2: 0:00
CAPE DOUGLAS AK.
AUGUSTINE IS. AK.

8 KM/IN
200 CM/S/IN
TRUE NORTH ↑



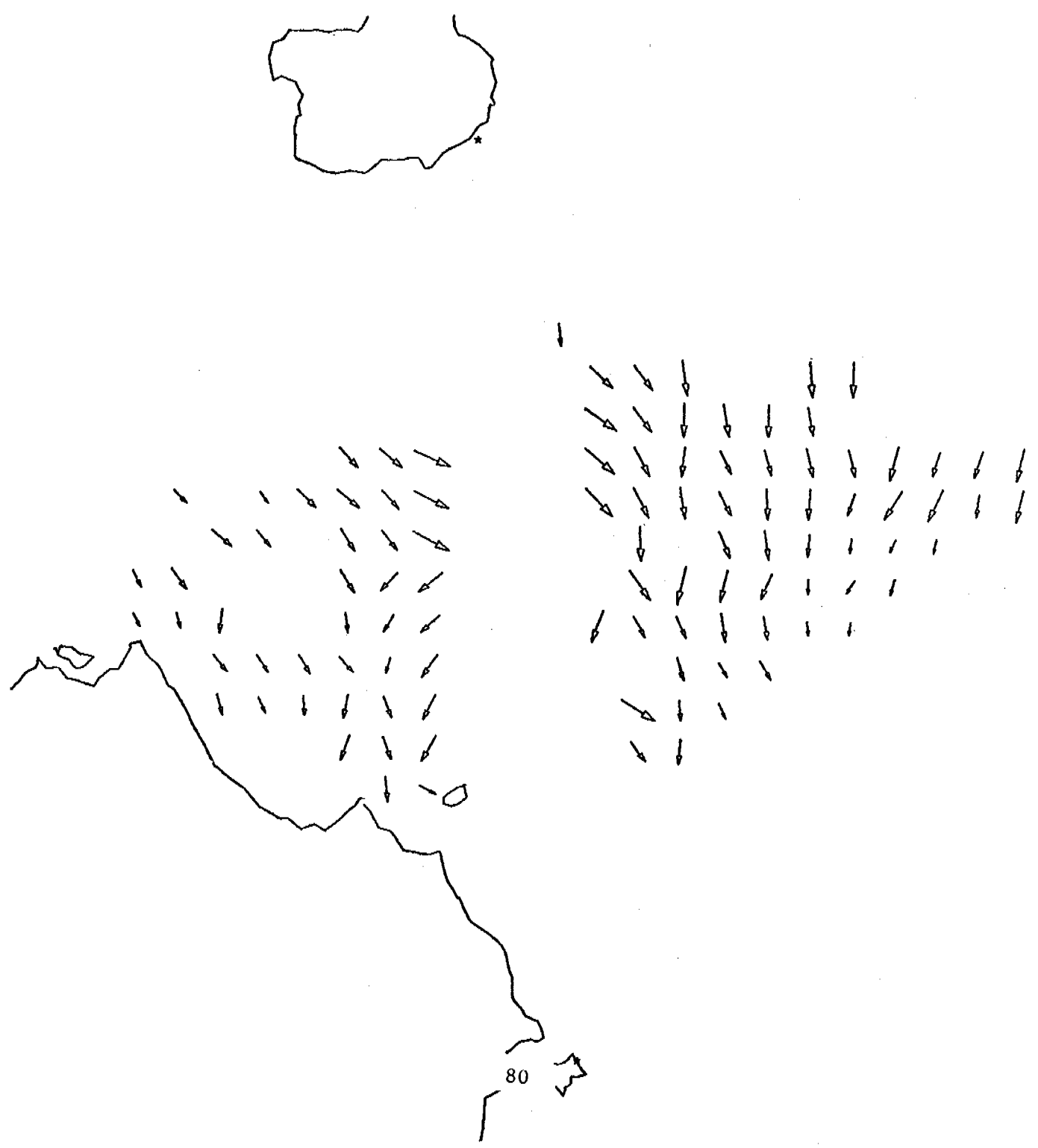
JUL 78 3: 0:00
DOUGLAS AK.
JUSTINE IS. AK.

8 KM/IN
200 CM/S/IN
TRUE NORTH ↑



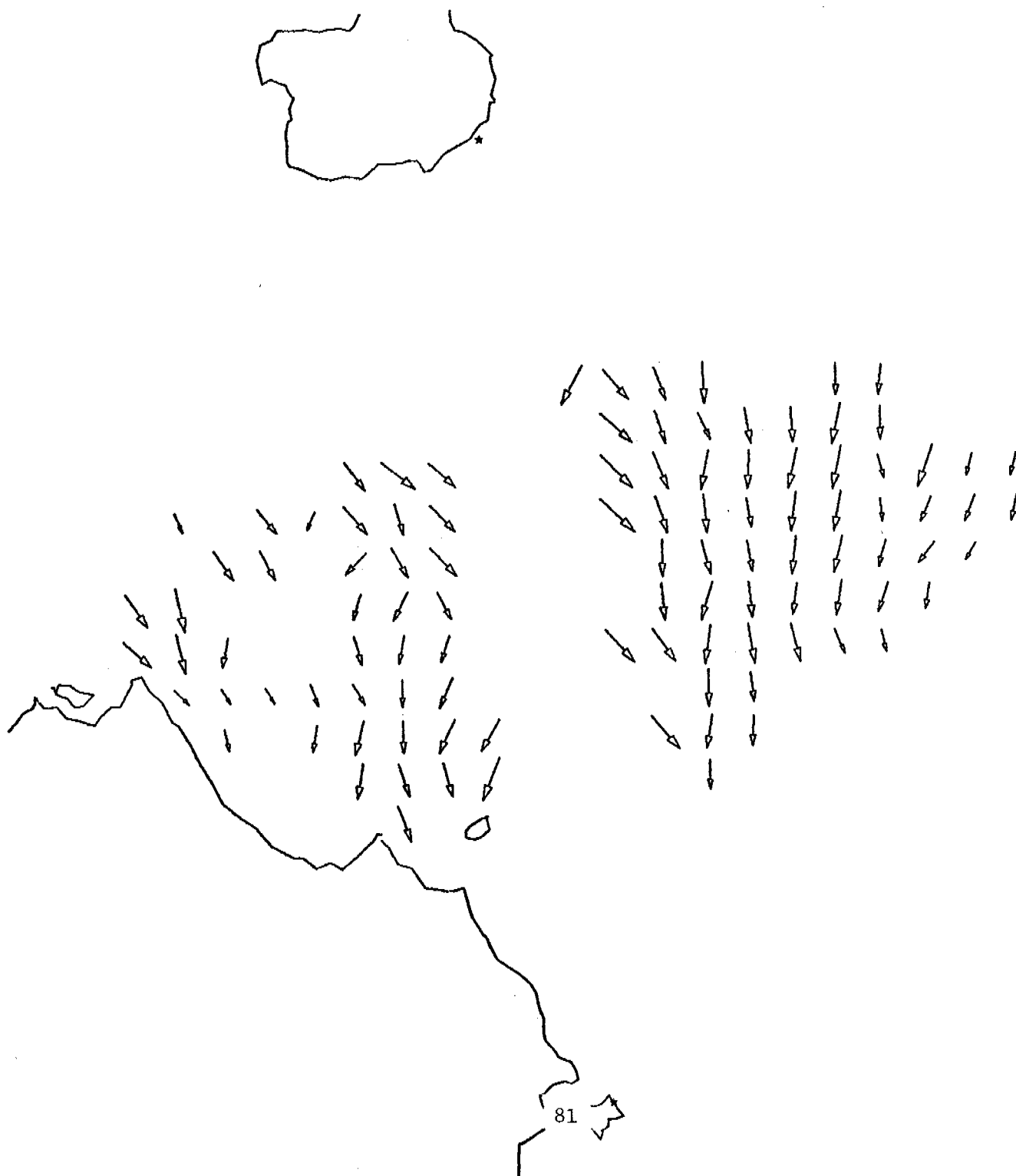
2 JUL 78 4:00:00
CAPE DOUGLAS AK.
AUGUSTINE IS. AK.

8 KM/IN
200 CM/S/IN
TRUE NORTH ↑



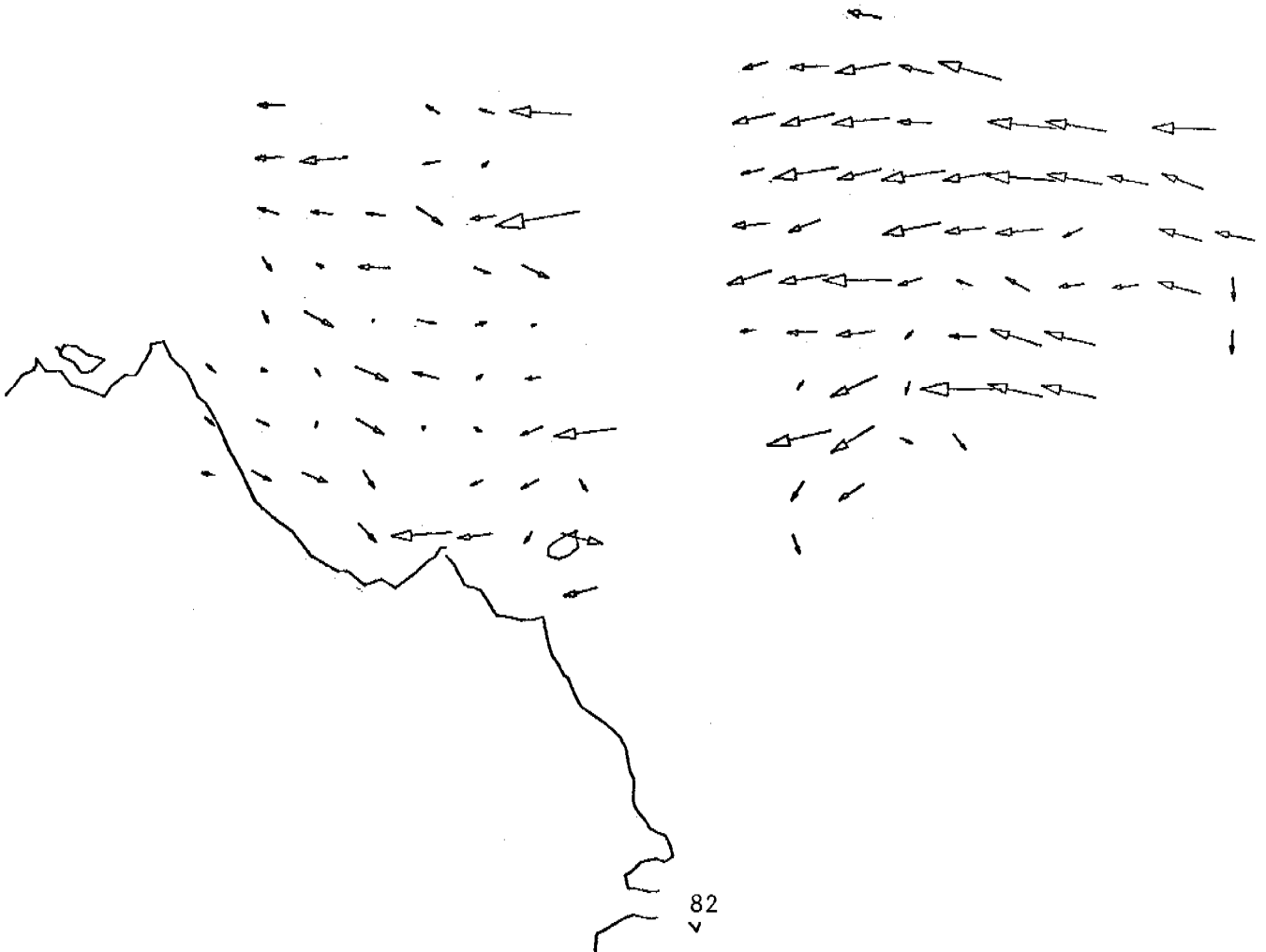
2 JUL 78 5: 0:00
CAPE DOUGLAS AK.
AUGUSTINE IS. AK.

8 KM/IN
200 CM/S/IN
TRUE NORTH ↑



4 JUL 78 11: 0:00
CAPE DOUGLAS AK.
AUGUSTINE IS. AK.

8 KM/IN
200 CM/S/IN
TRUE NORTH ↑



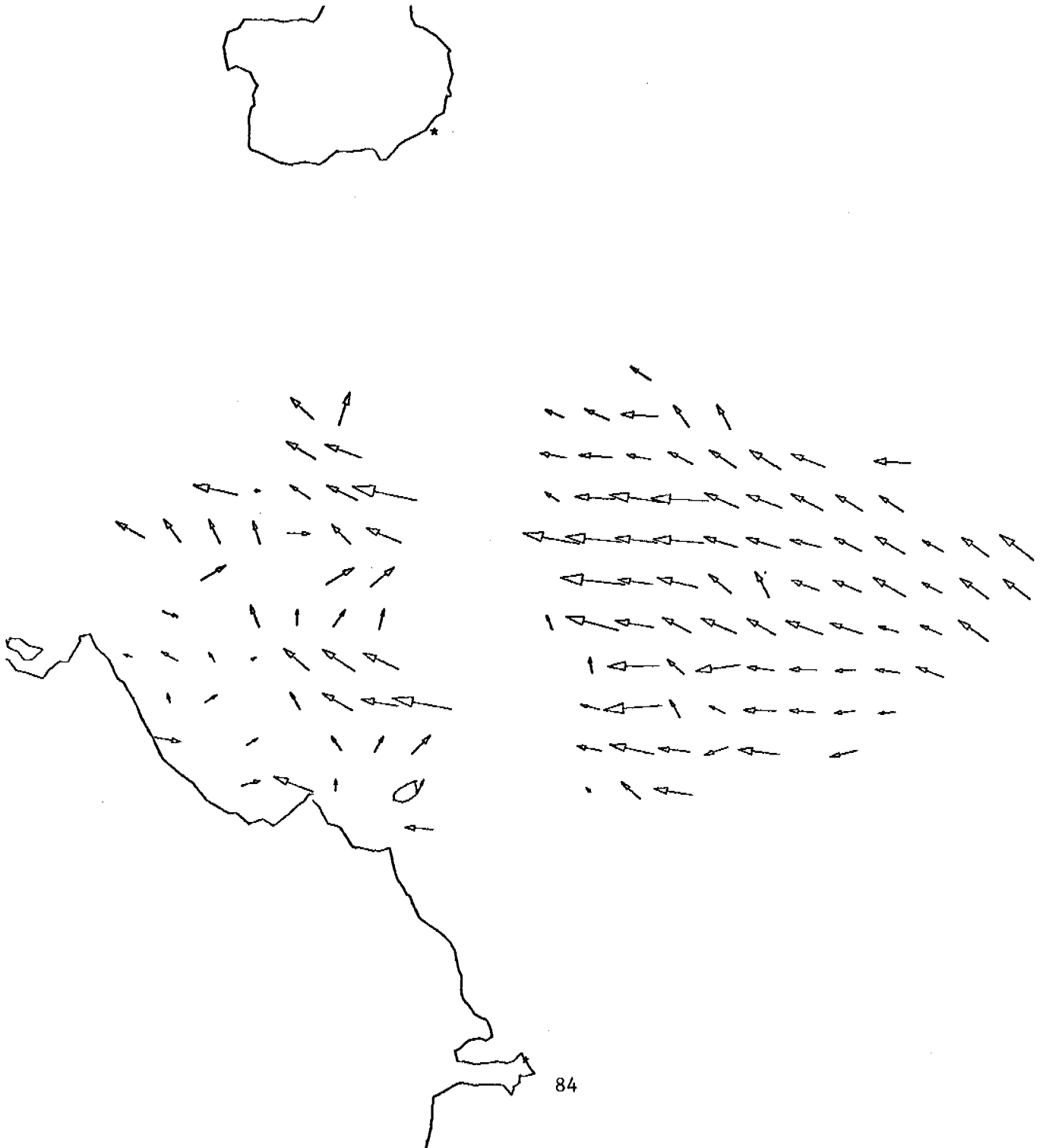
04-JUL-78 14:00:00
CAPE DOUGLAS AK.
AUGUSTINE IS. AK.

8 KM/IN
200 CM/S/IN
TRUE NORTH ↑



04-JUL-78 14:00:00
CAPE DOUGLAS AK.
AUGUSTINE IS. AK.

8 KM/IN
200 CM/S/IN
TRUE NORTH ↑



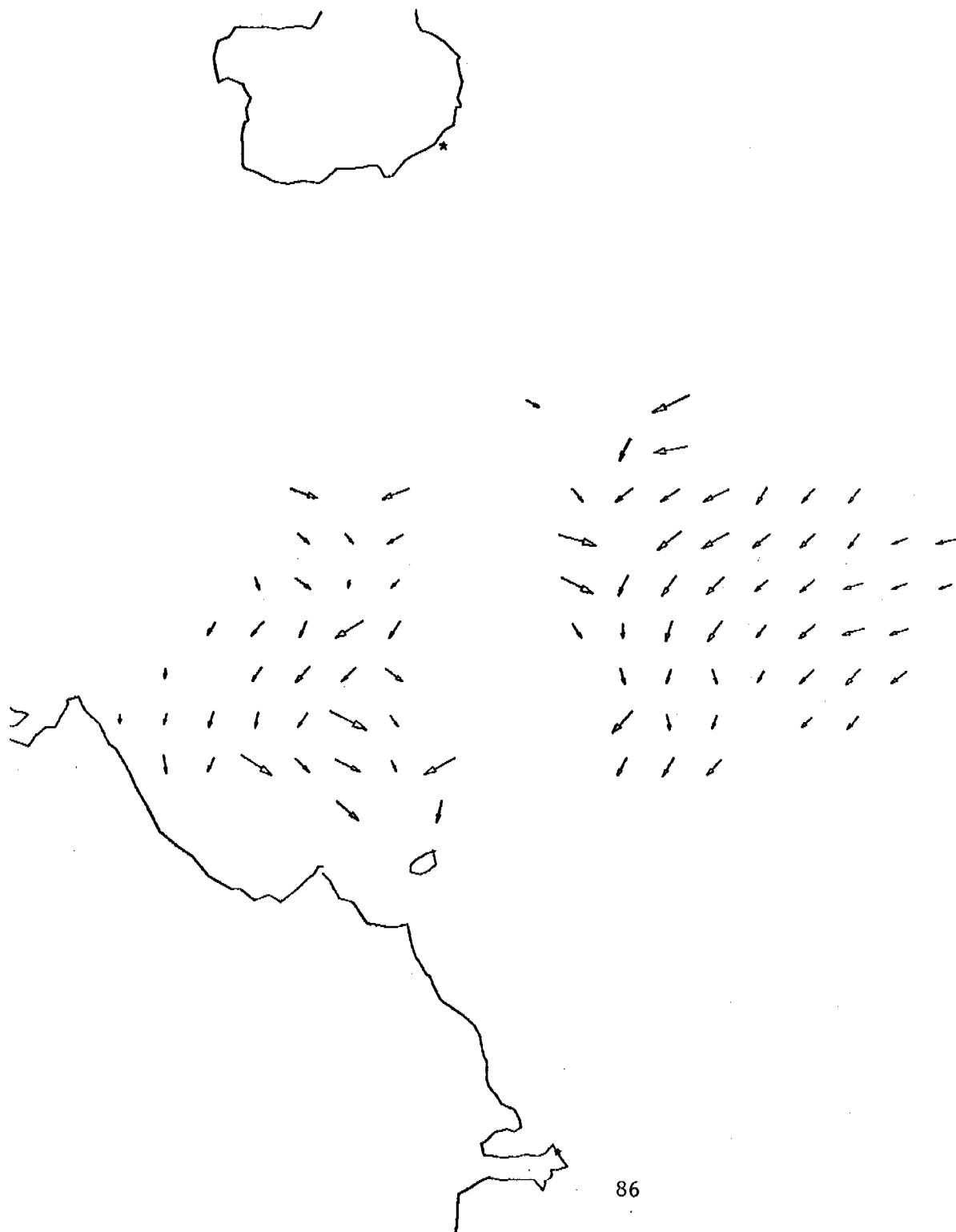
4 JUL 78 17: 0:00
CAPE DOUGLAS AK.
AUGUSTINE IS. AK.

8 KM/IN
200 CM/S/IN
TRUE NORTH ↑



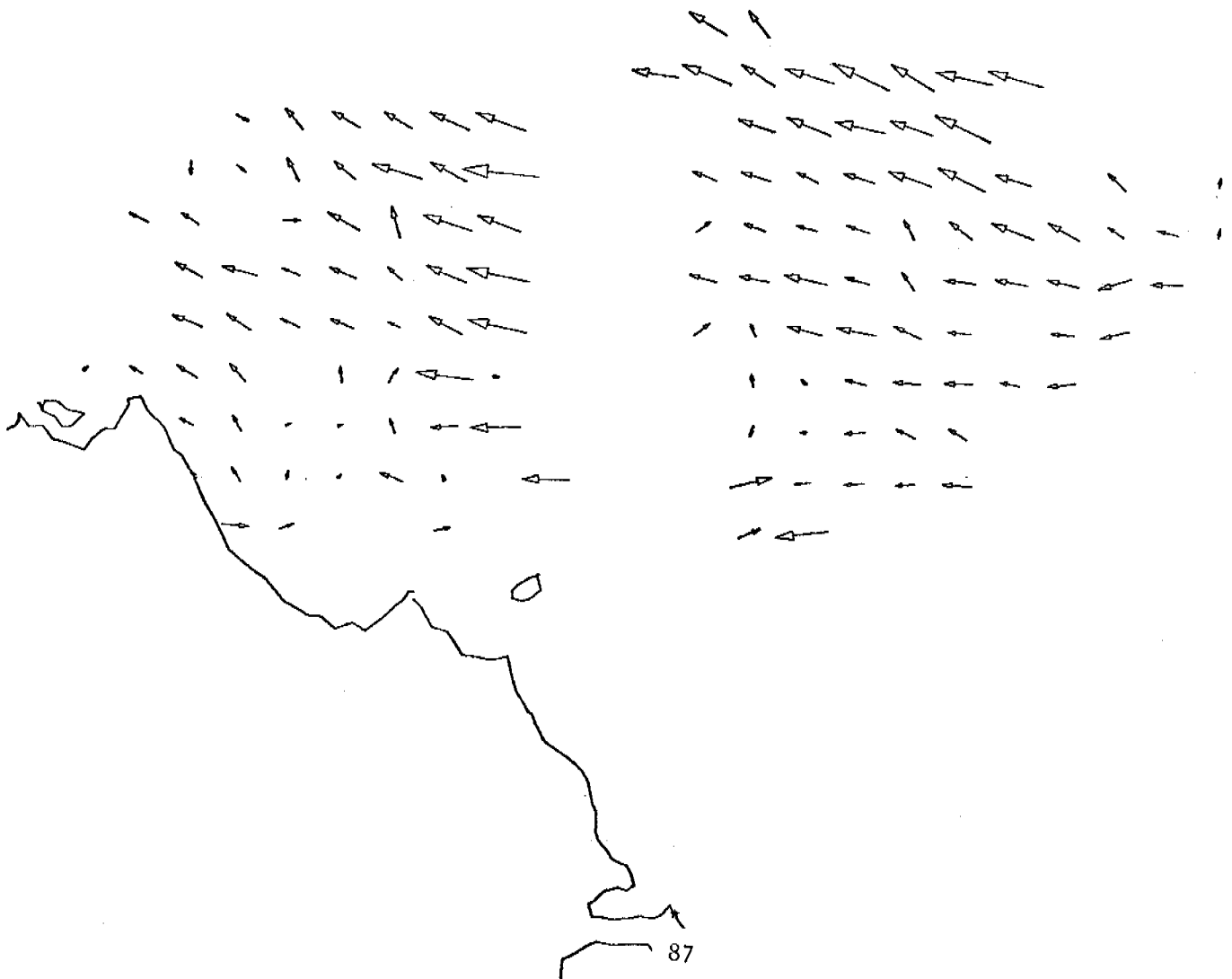
JUL 78 20: 0:00
E DOUGLAS AK.
USTINE IS. AK.

8 KM/IN
200 CM/S/IN
TRUE NORTH ↑



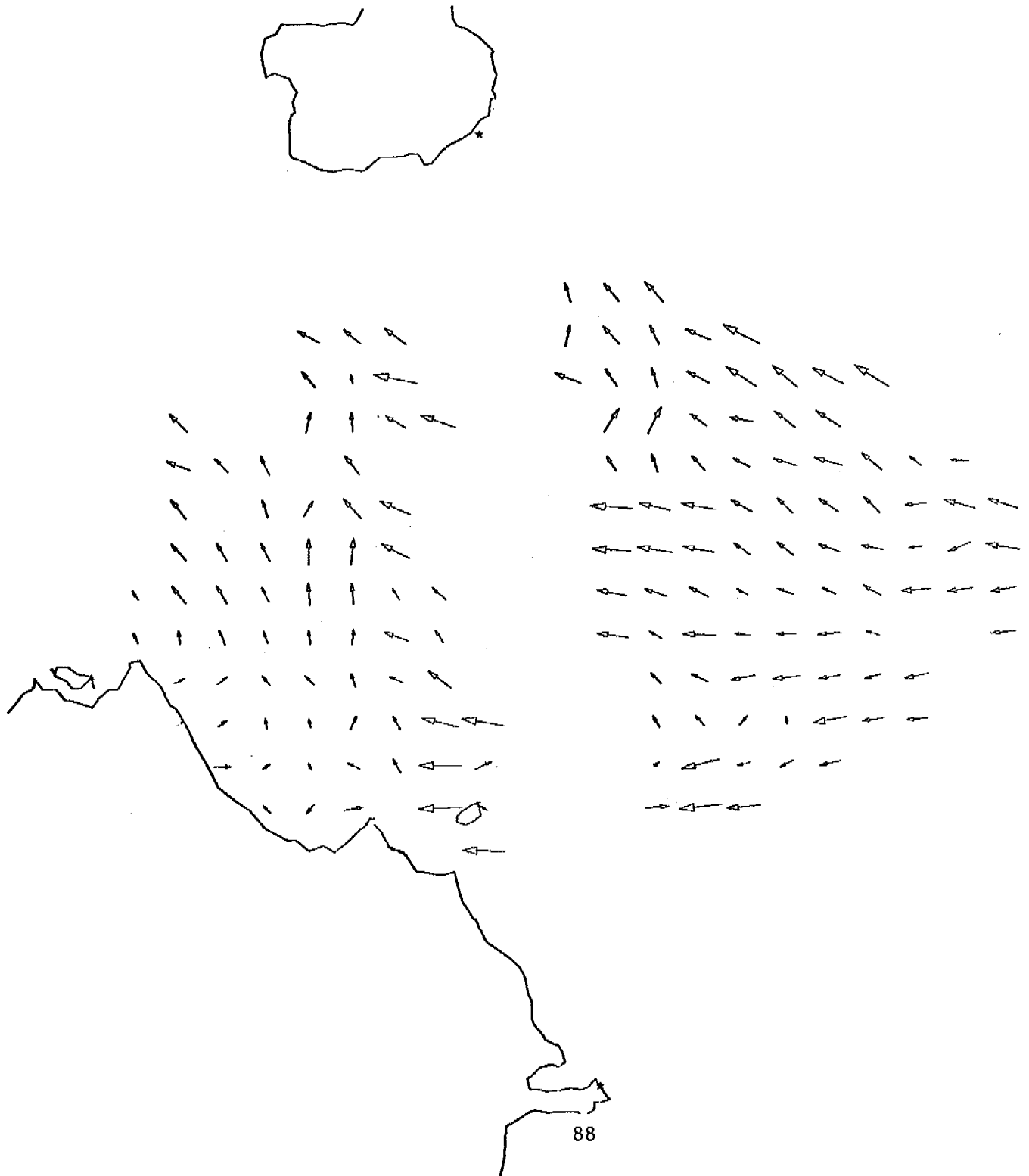
03:00:00
DOUGLAS AK.
ADLINE IS. AK.

8 KM/IN
200 CM/S/IN
TRUE NORTH ↑



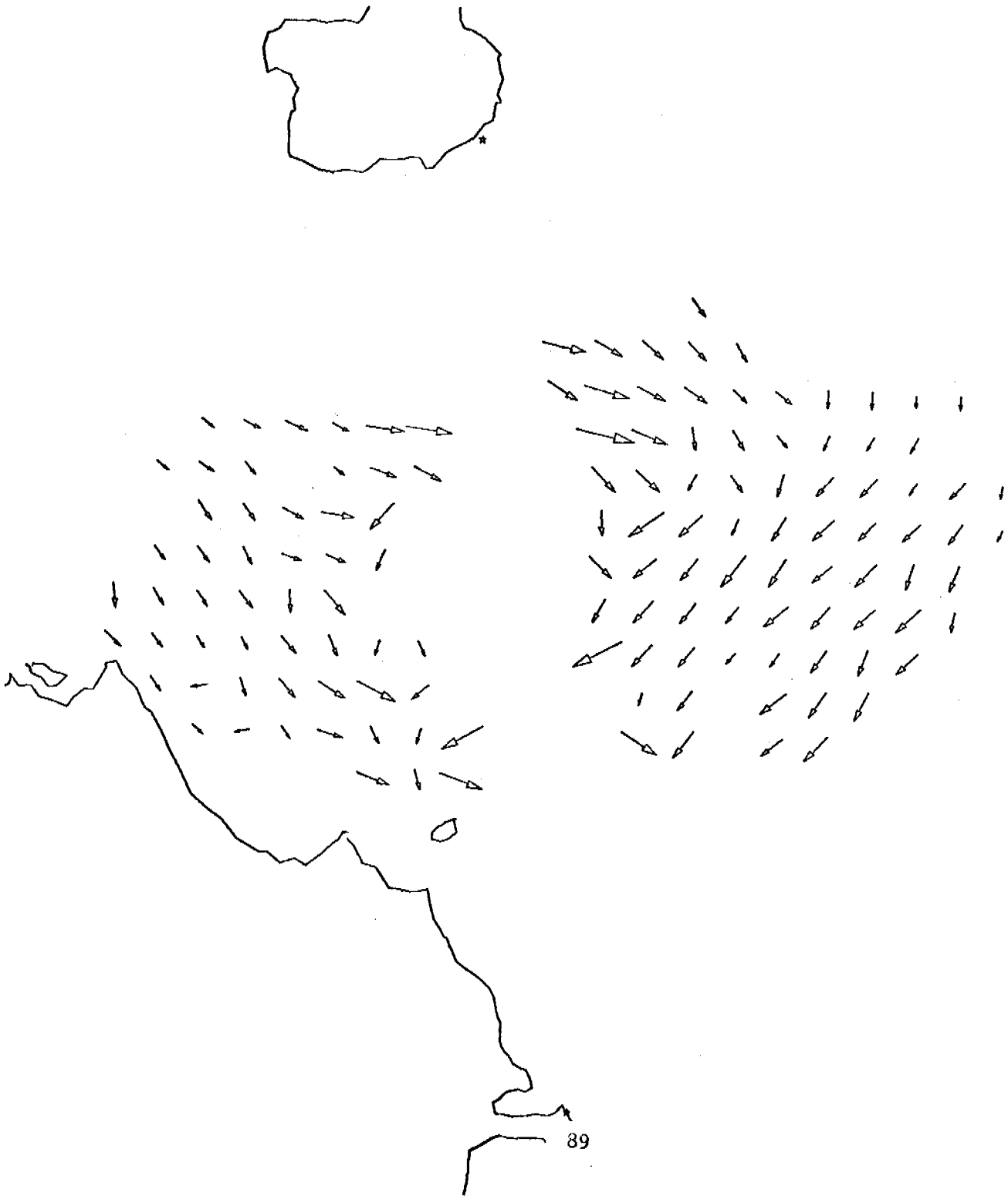
5 JUL 78 2: 0:00
CAPE DOUGLAS AK.
AUGUSTINE IS. AK.

8 KM/IN
200 CM/S/IN
TRUE NORTH ↑



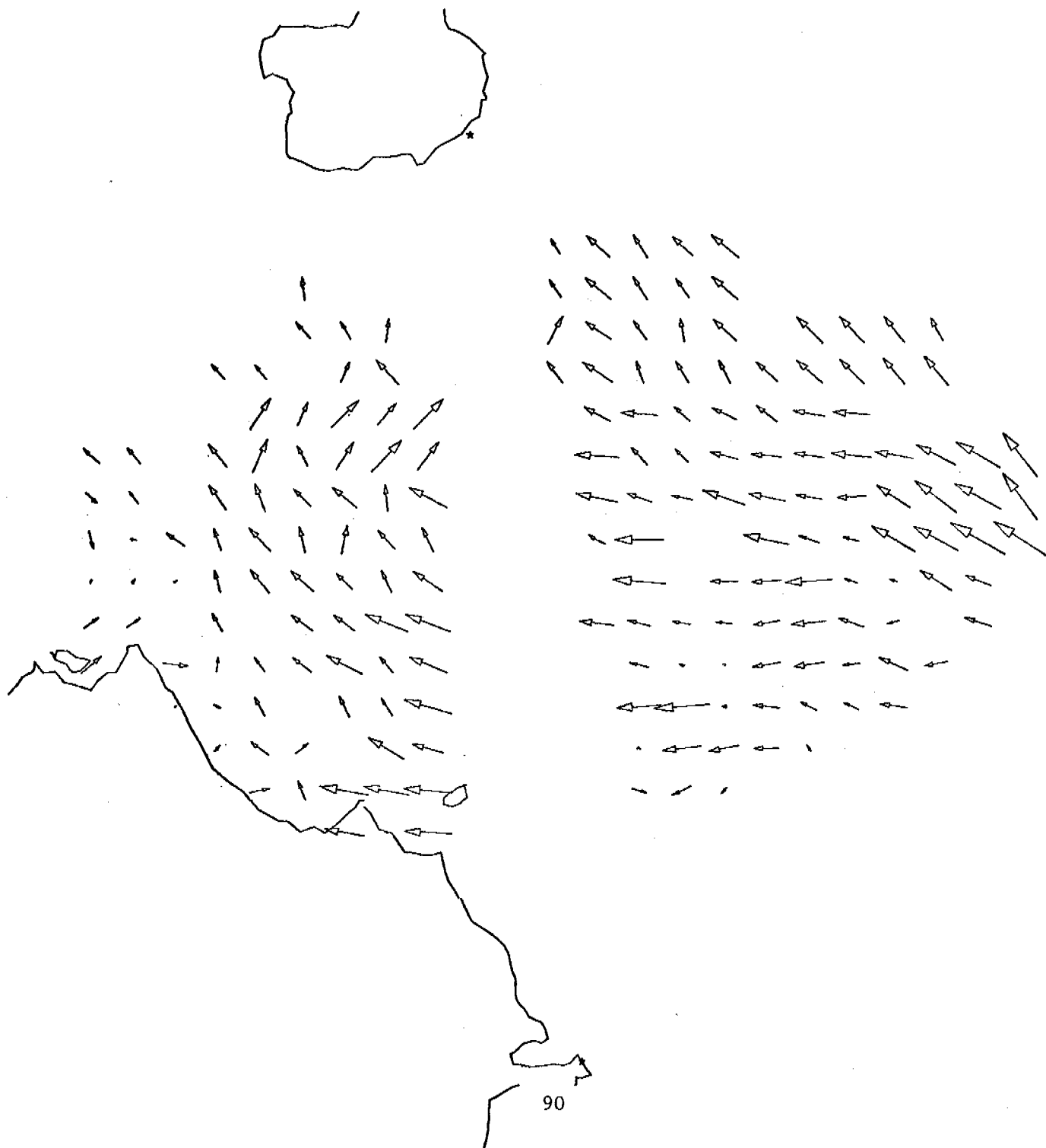
5 JUL 78 5: 0:00
CAPE DOUGLAS AK.
AUGUSTINE IS. AK.

8 KM/IN
200 CM/S/IN
TRUE NORTH ↑



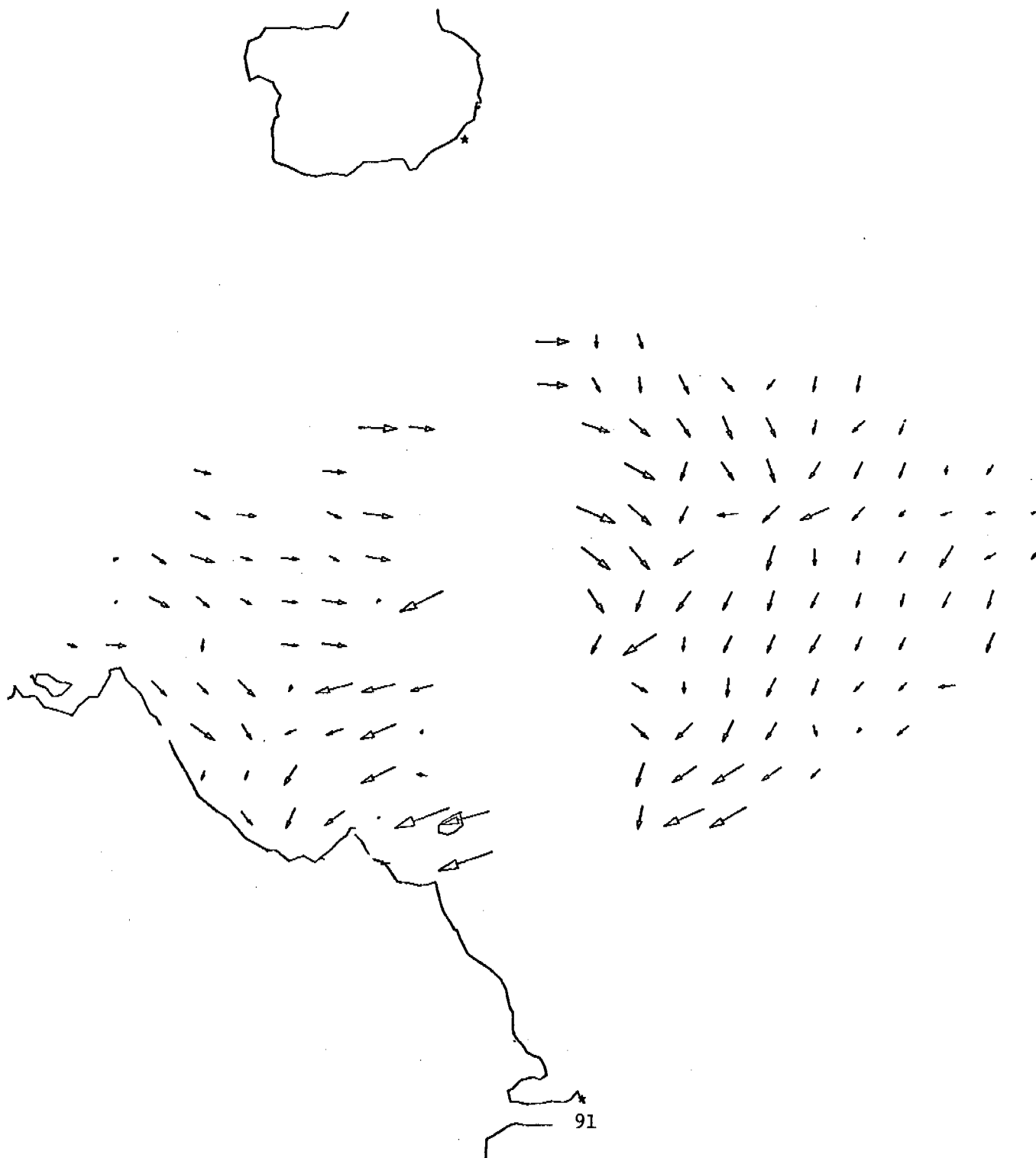
06-JUL-78 02:00:00
CAPE DOUGLAS AK.
AUGUSTINE IS. AK.

8 KM/IN
200 CM/S/IN
TRUE NORTH ↑



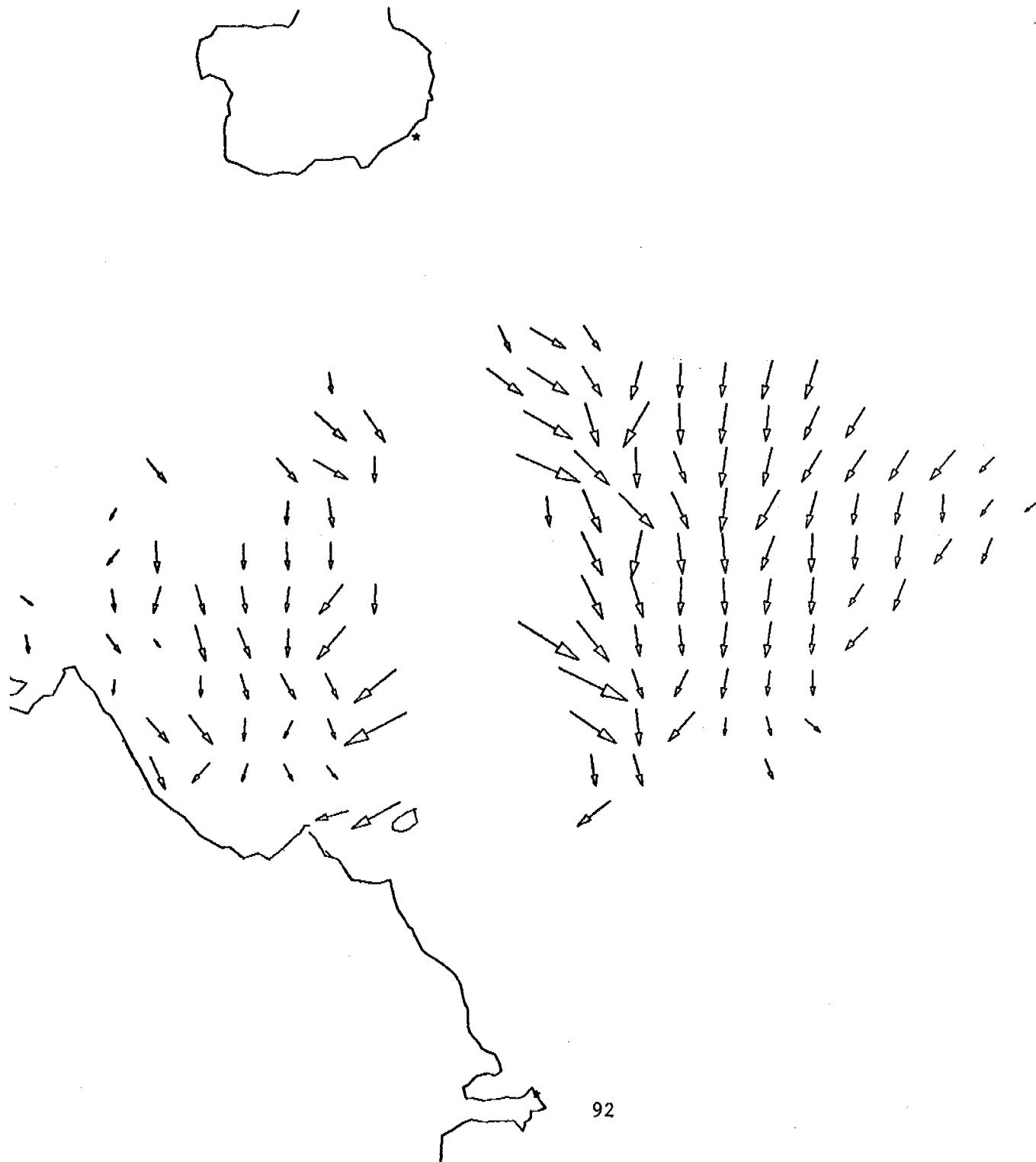
6 JUL 78 5: 0:00
CAPE DOUGLAS AK.
AUGUSTINE IS. AK.

8 KM/IN
200 CM/S/IN
TRUE NORTH ↑



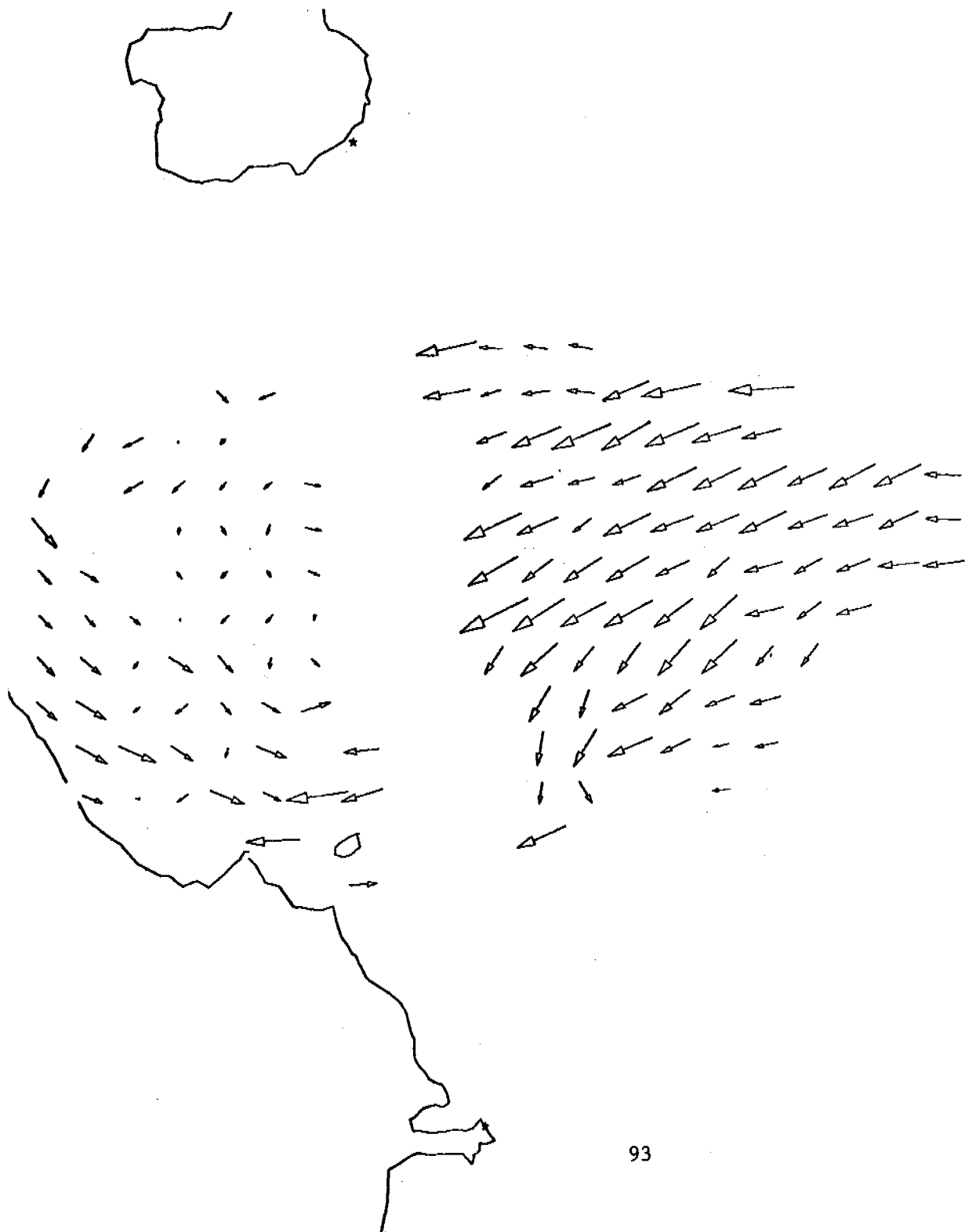
JUL 78 8: 0:00
E DOUGLAS AK.
JUSTINE IS. AK.

8 KM/IN
200 CM/S/IN
TRUE NORTH ↑



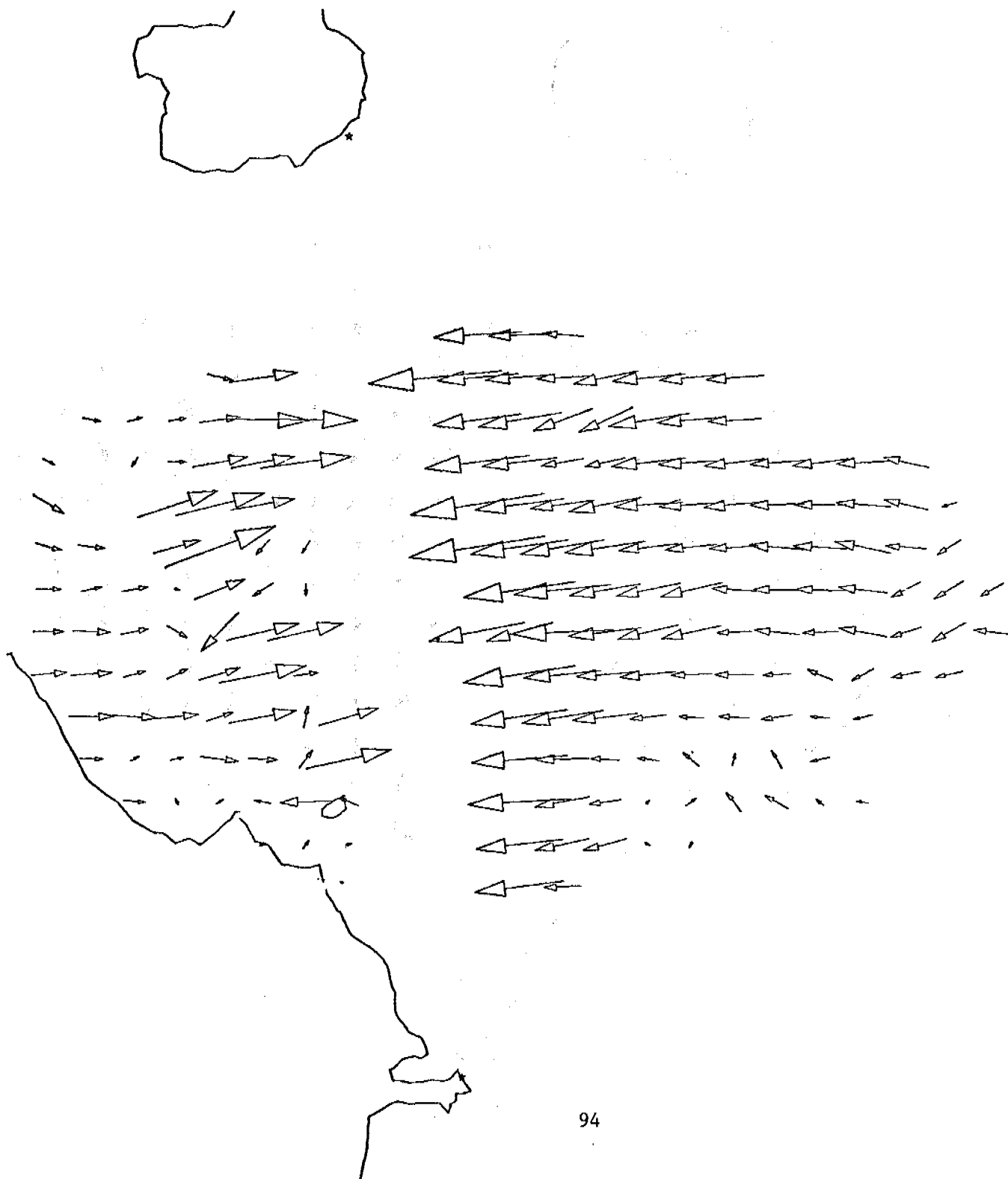
78 11: 0:00
UGLAS AK.
NE IS. AK.

8 KM/IN
200 CM/S/IN
TRUE NORTH ↑



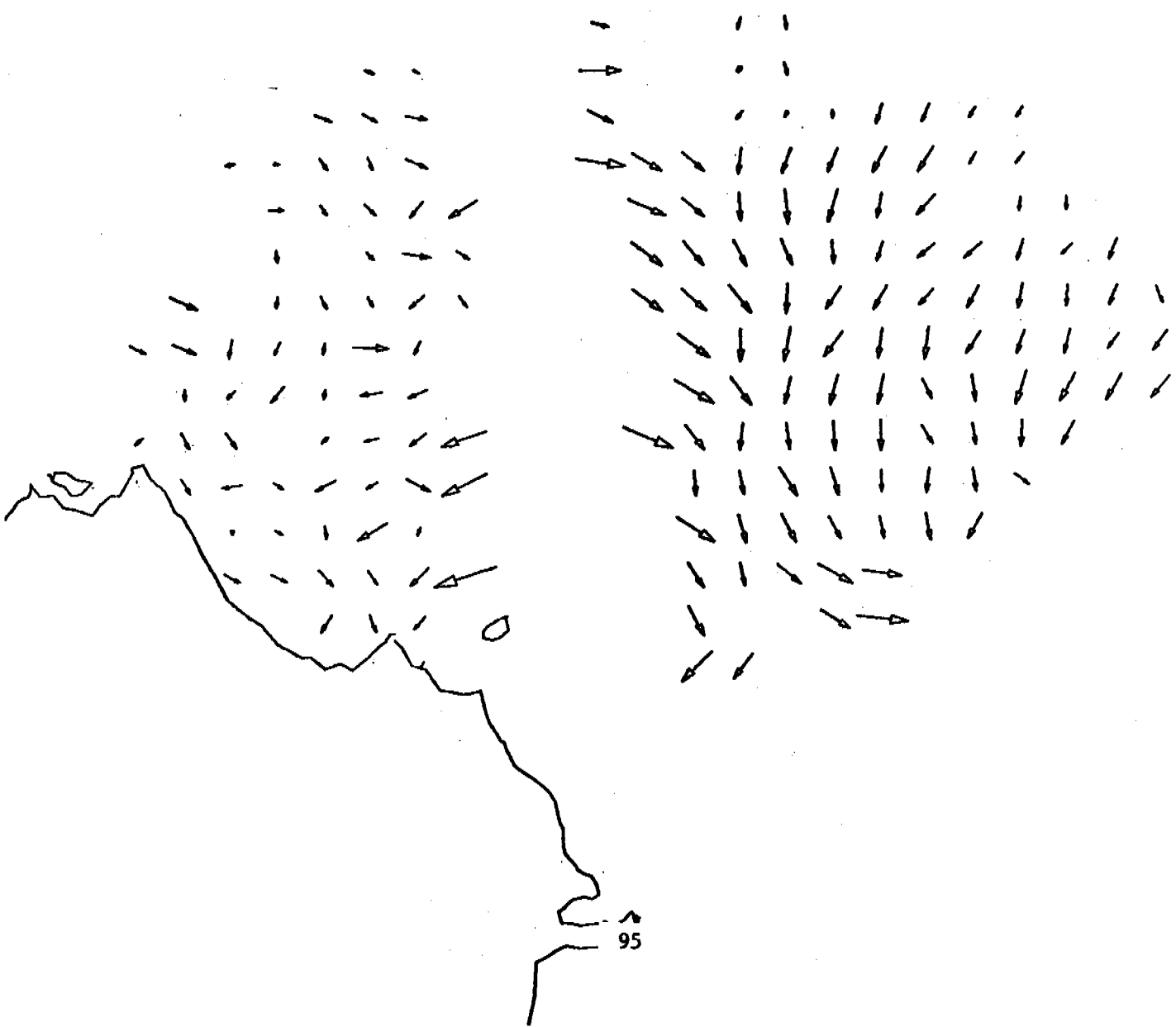
78° 14' 0:00
UGLAS AK.
NE IS. AK.

8 KM/IN
200 CM/S/IN
TRUE NORTH ↑



6 JUL 78 20: 0:00
CAPE DOUGLAS AK.
AUGUSTINE IS. AK.

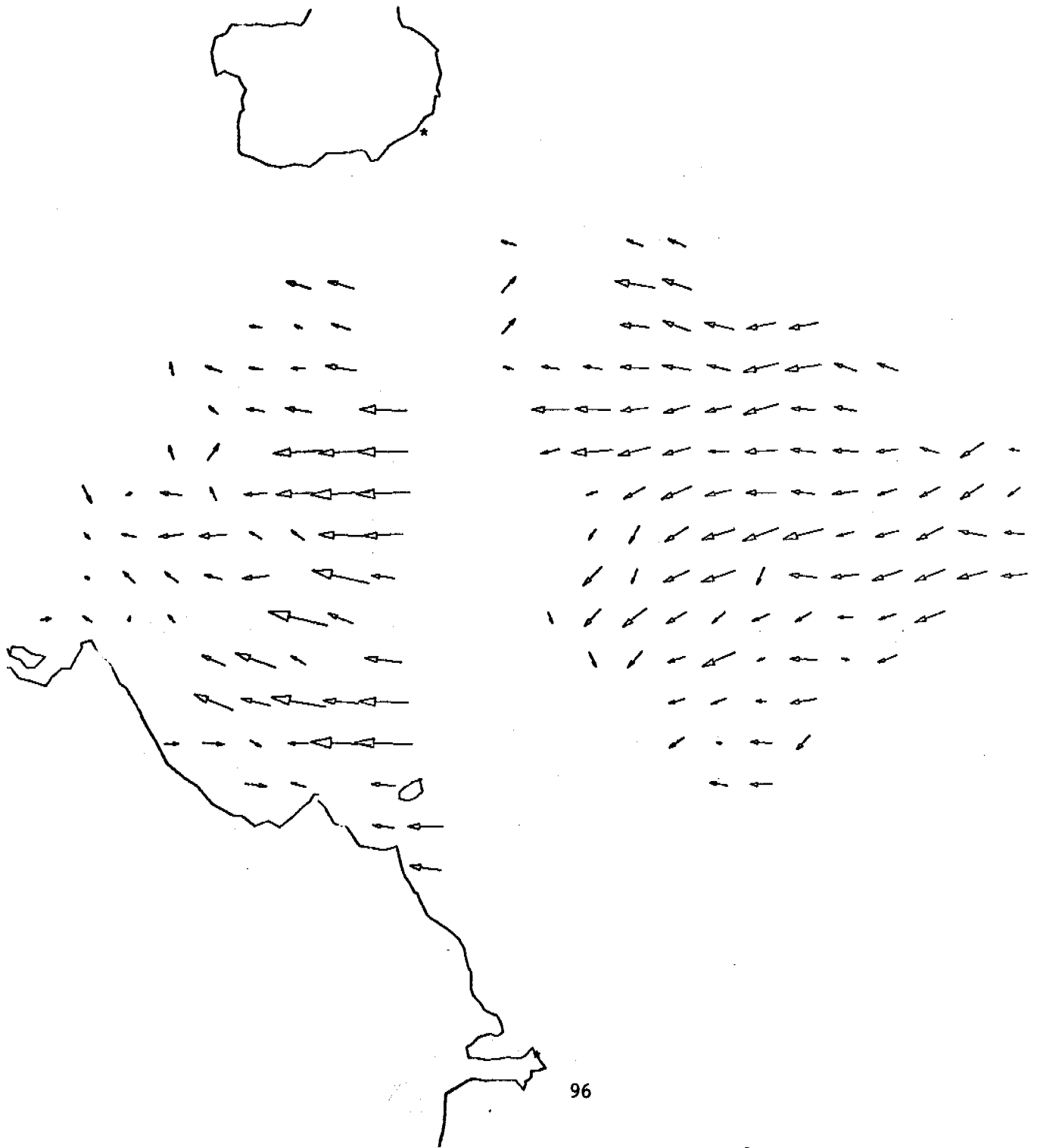
8 KM/IN
200 CM/S/IN
TRUE NORTH ↑



95

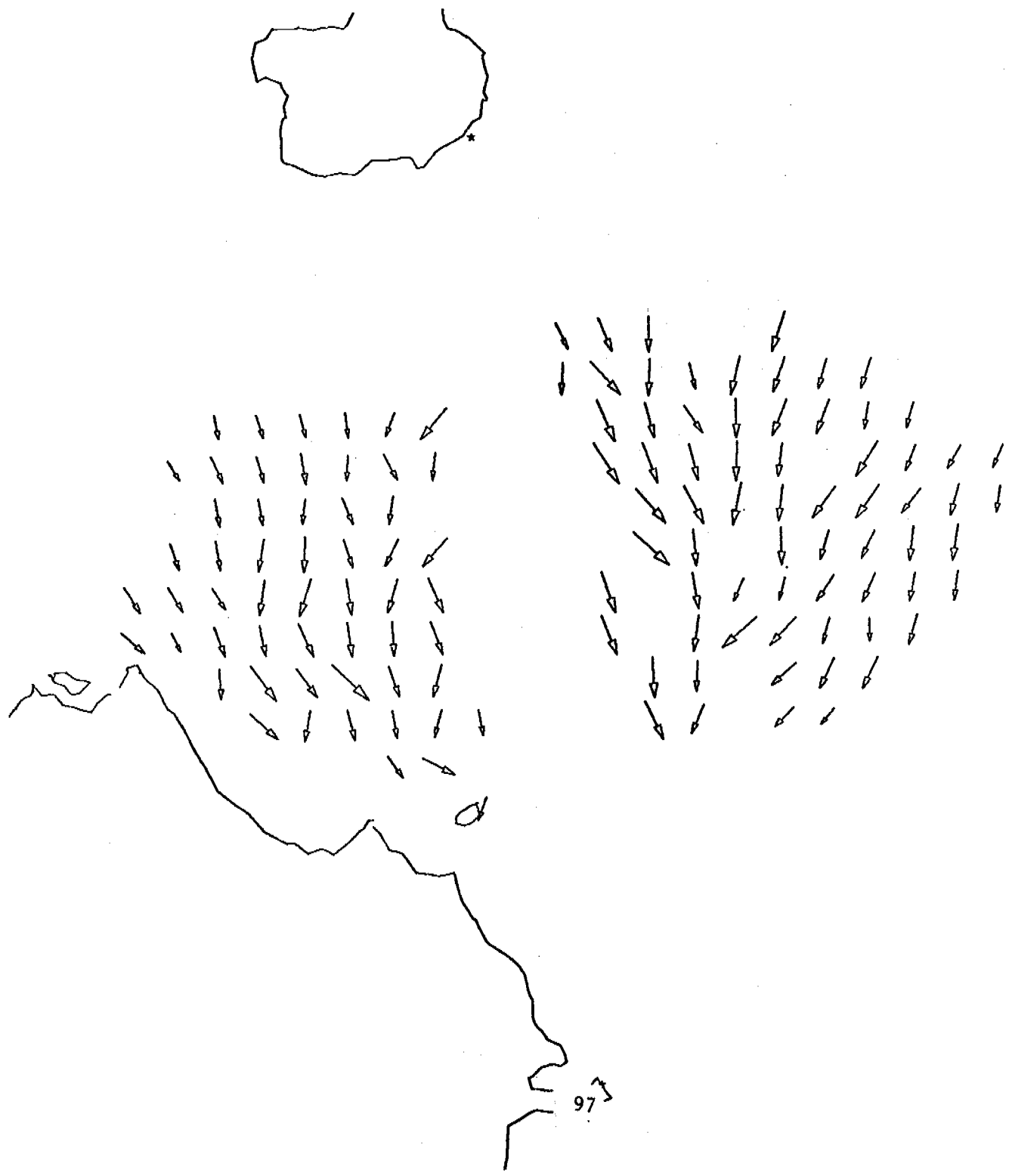
6 JUL 78 23: 0:00
APE DOUGLAS AK.
UGUSTINE IS. AK.

8 KM/IN
200 CM/S/IN
TRUE NORTH ↑



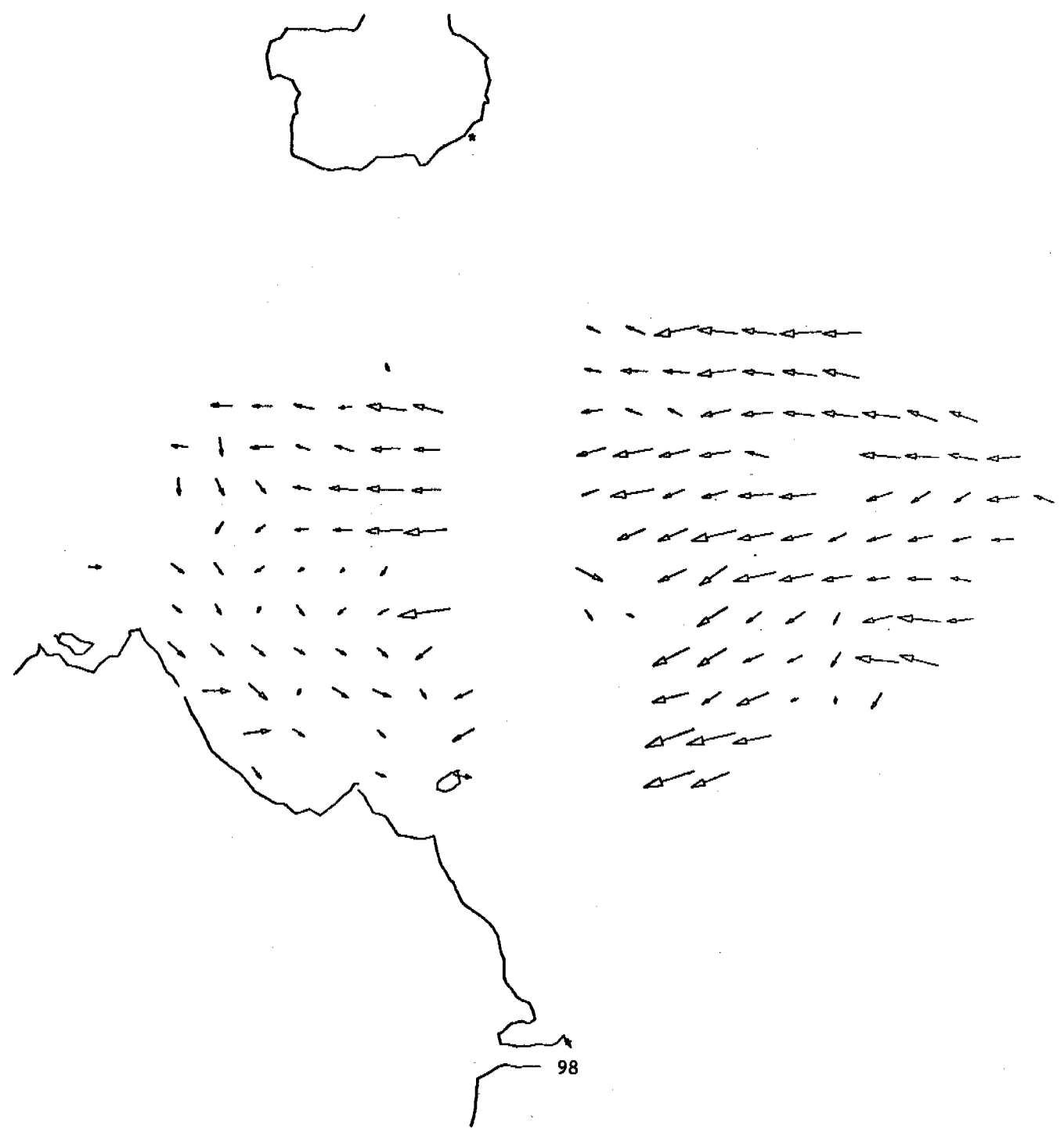
5 JUL 78 8: 0:00
CAPE DOUGLAS AK.
AUGUSTINE IS. AK.

8 KM/IN
200 CM/S/IN
TRUE NORTH ↑



5 JUL 78 11: 0:00
CAPE DOUGLAS AK. ·
AUGUSTINE IS. AK.

8 KM/IN
200 CM/S/IN
TRUE NORTH ↑



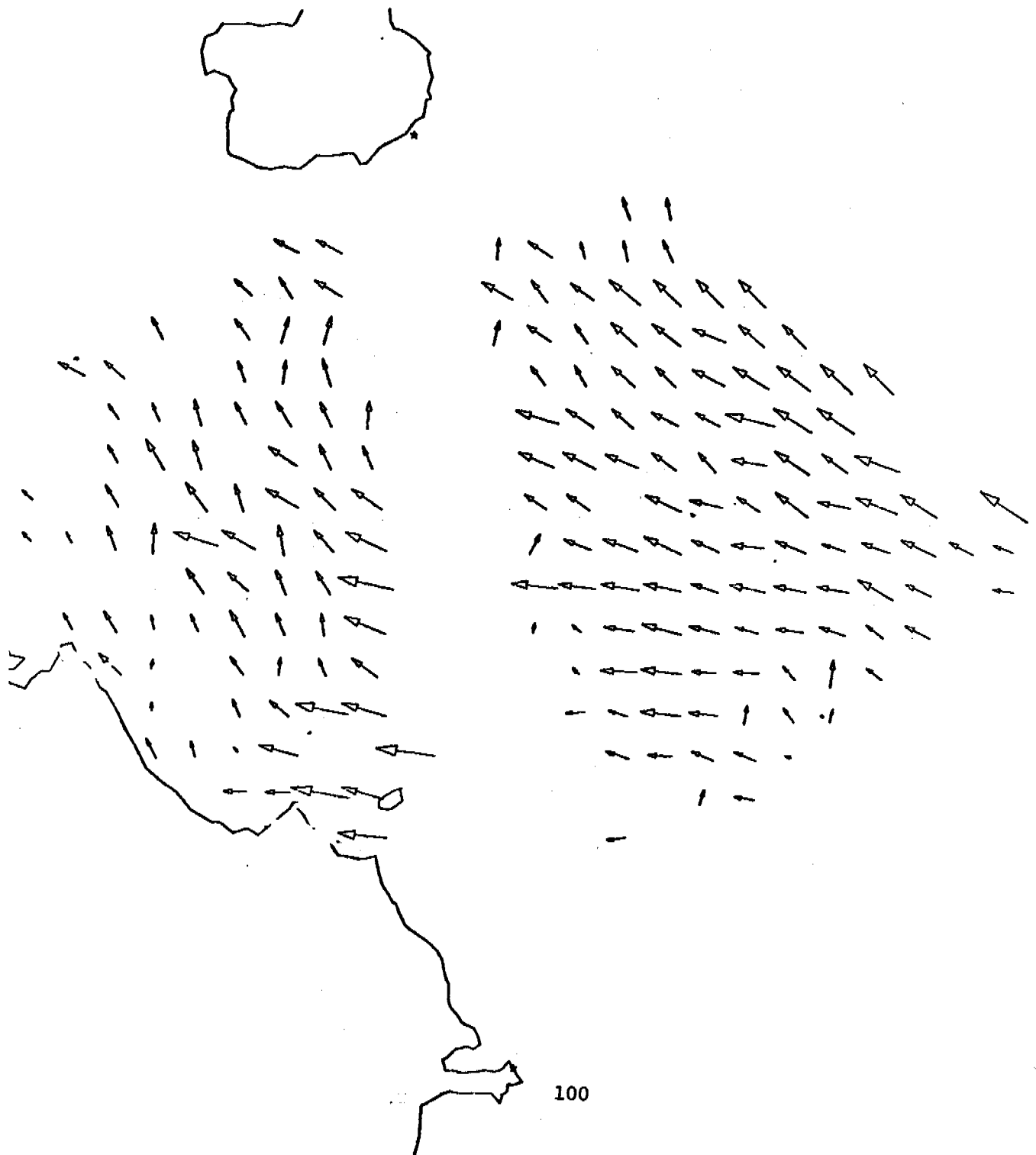
5 JUL 78 14: 0:00
CAPE DOUGLAS AK.
AUGUSTINE IS. AK.

8 KM/IN
200 CM/S/IN
TRUE NORTH ↑



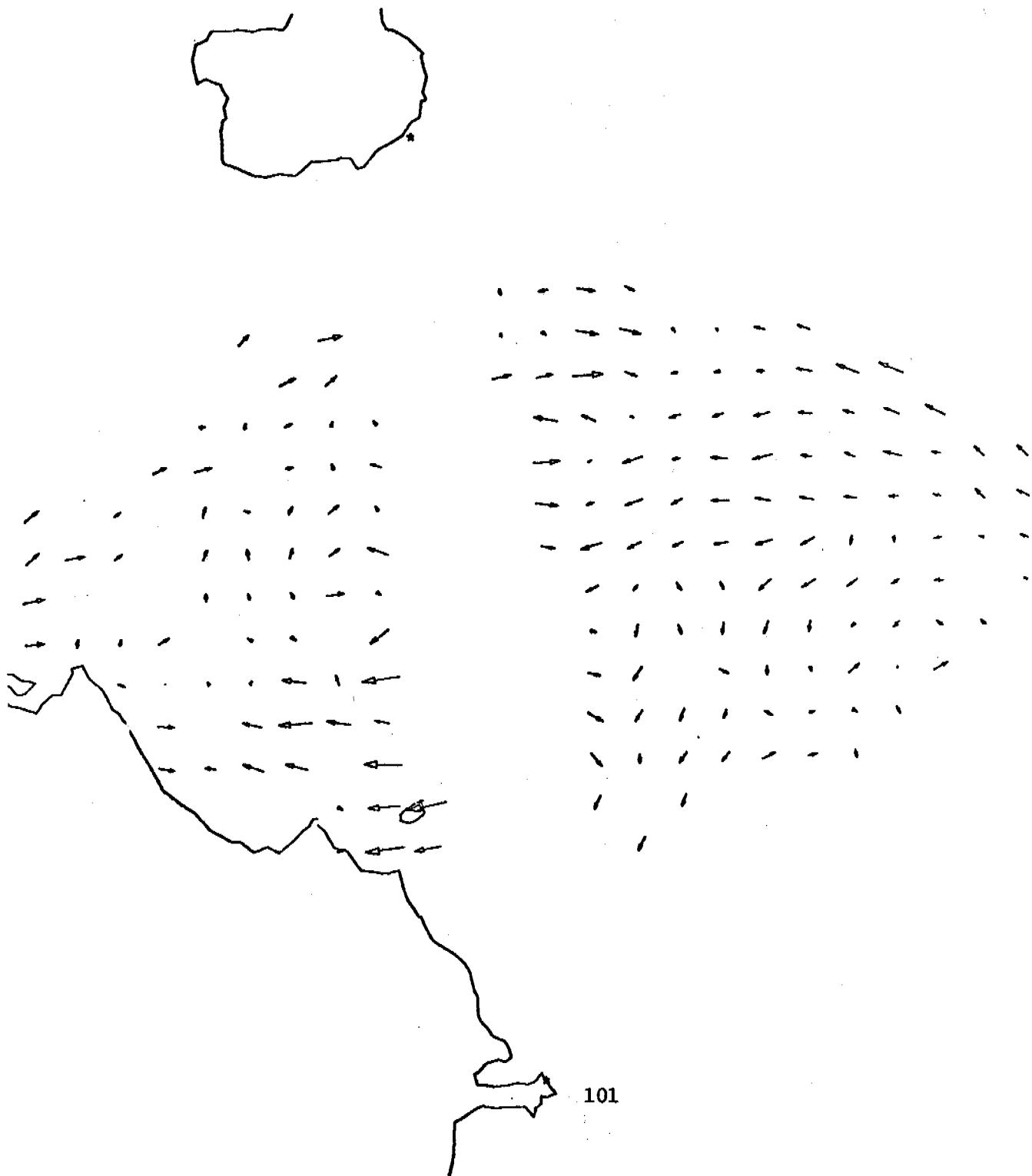
JUL 78 2: 0:00
E DOUGLAS AK.
USTINE IS. AK.

8 KM/IN
200 CM/S/IN
TRUE NORTH ↑



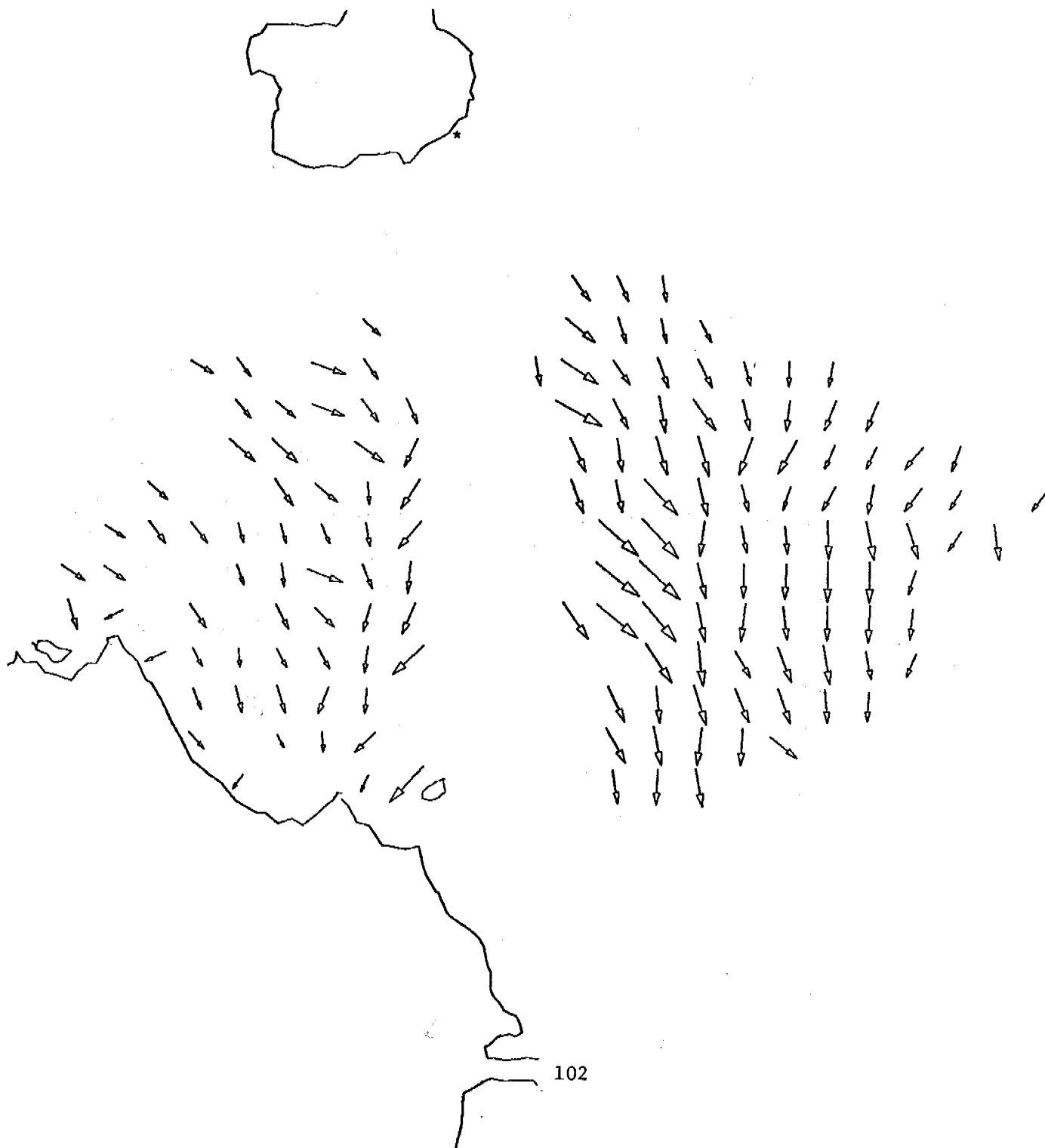
JUL 78 5: 0:00
CAPE DOUGLAS AK.
GUSTINE IS. AK.

8 KM/IN
200 CM/S/IN
TRUE NORTH ↑



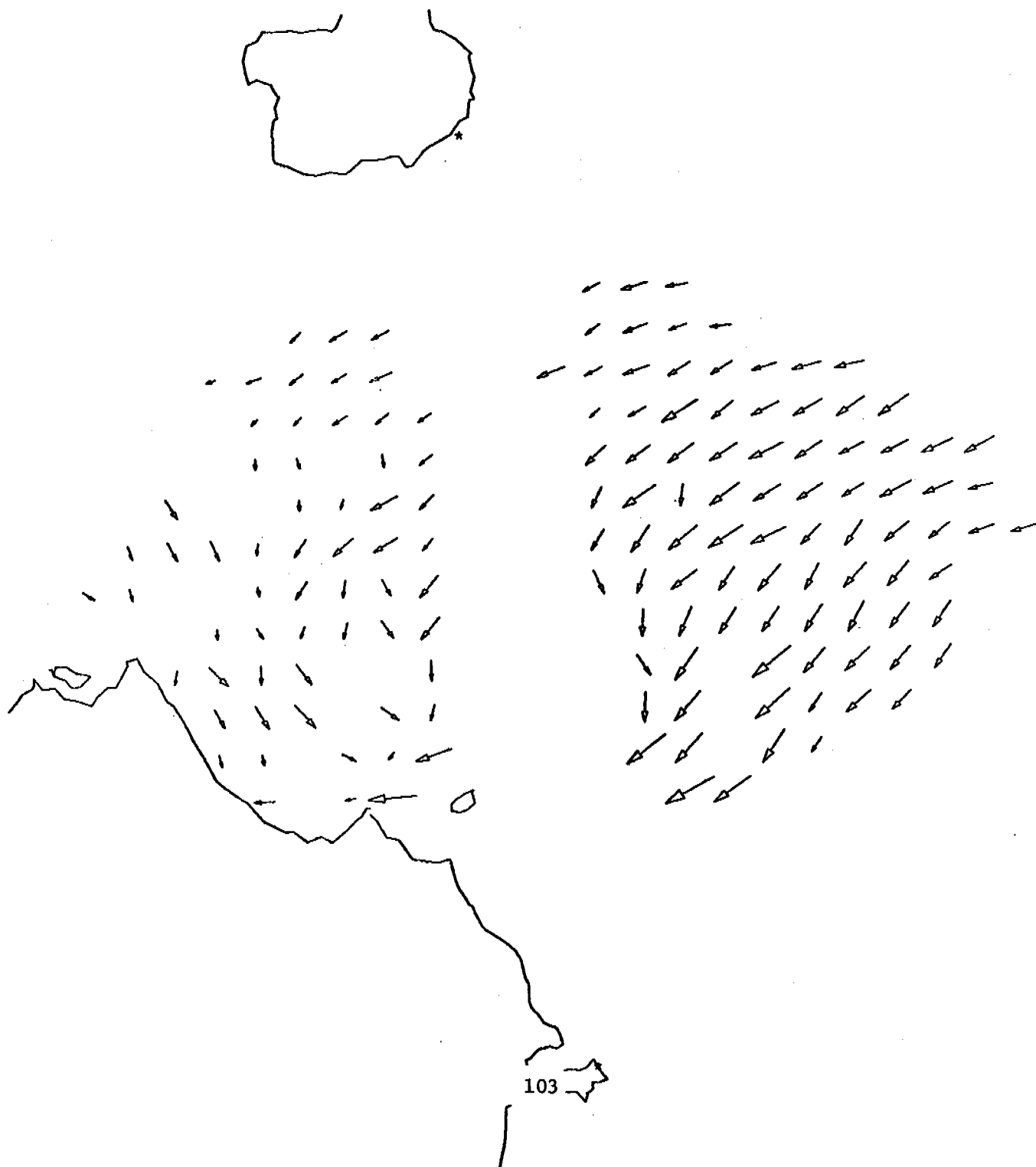
7 JUL 78 8: 0:00
CAPE DOUGLAS AK.
AUGUSTINE IS. AK.

8 KM/IN
200 CM/S/IN
TRUE NORTH ↑



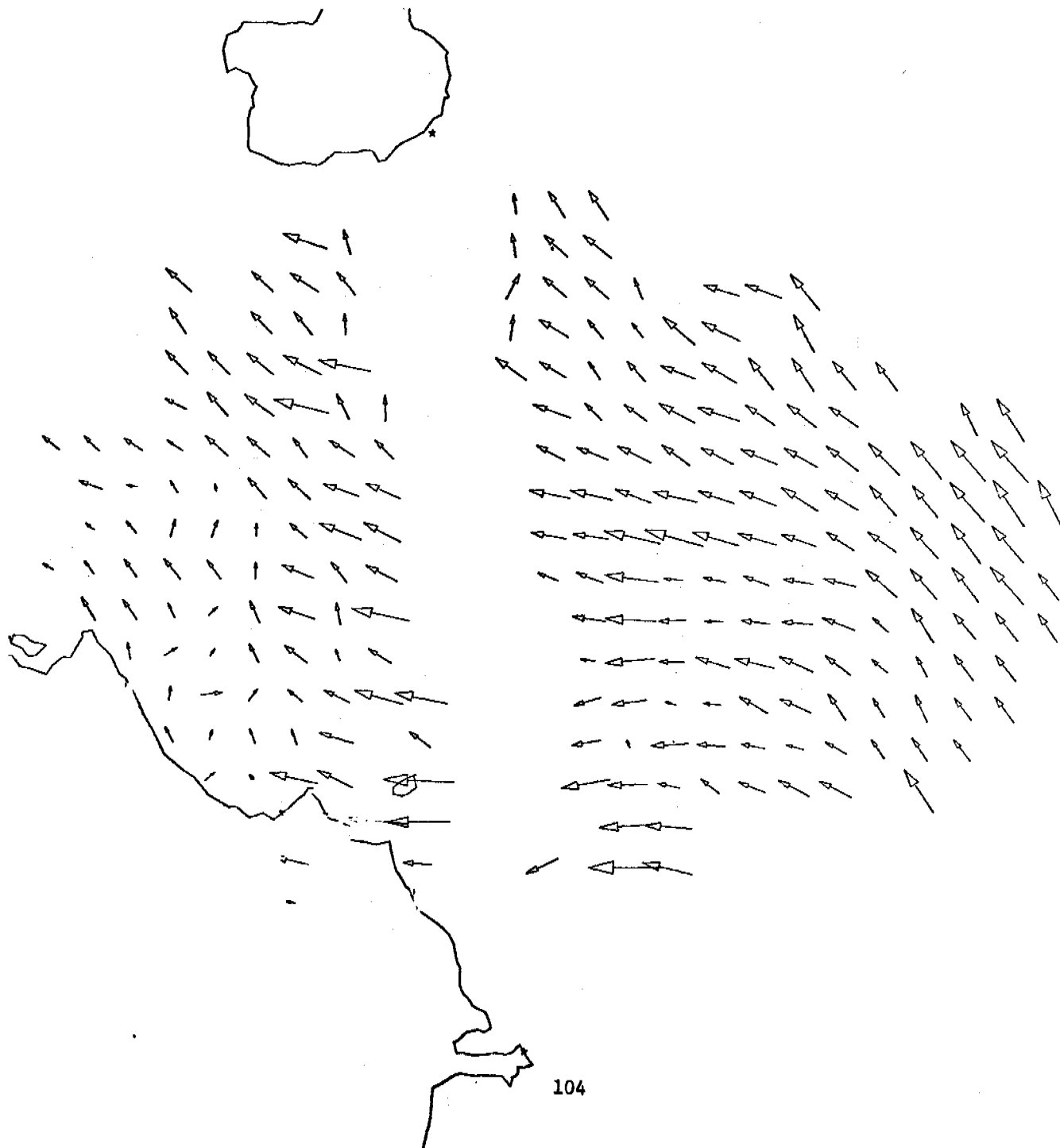
7 JUL 78 11: 0:00
CAPE DOUGLAS AK.
AUGUSTINE IS. AK.

8 KM/IN
200 CM/S/IN
TRUE NORTH ↑



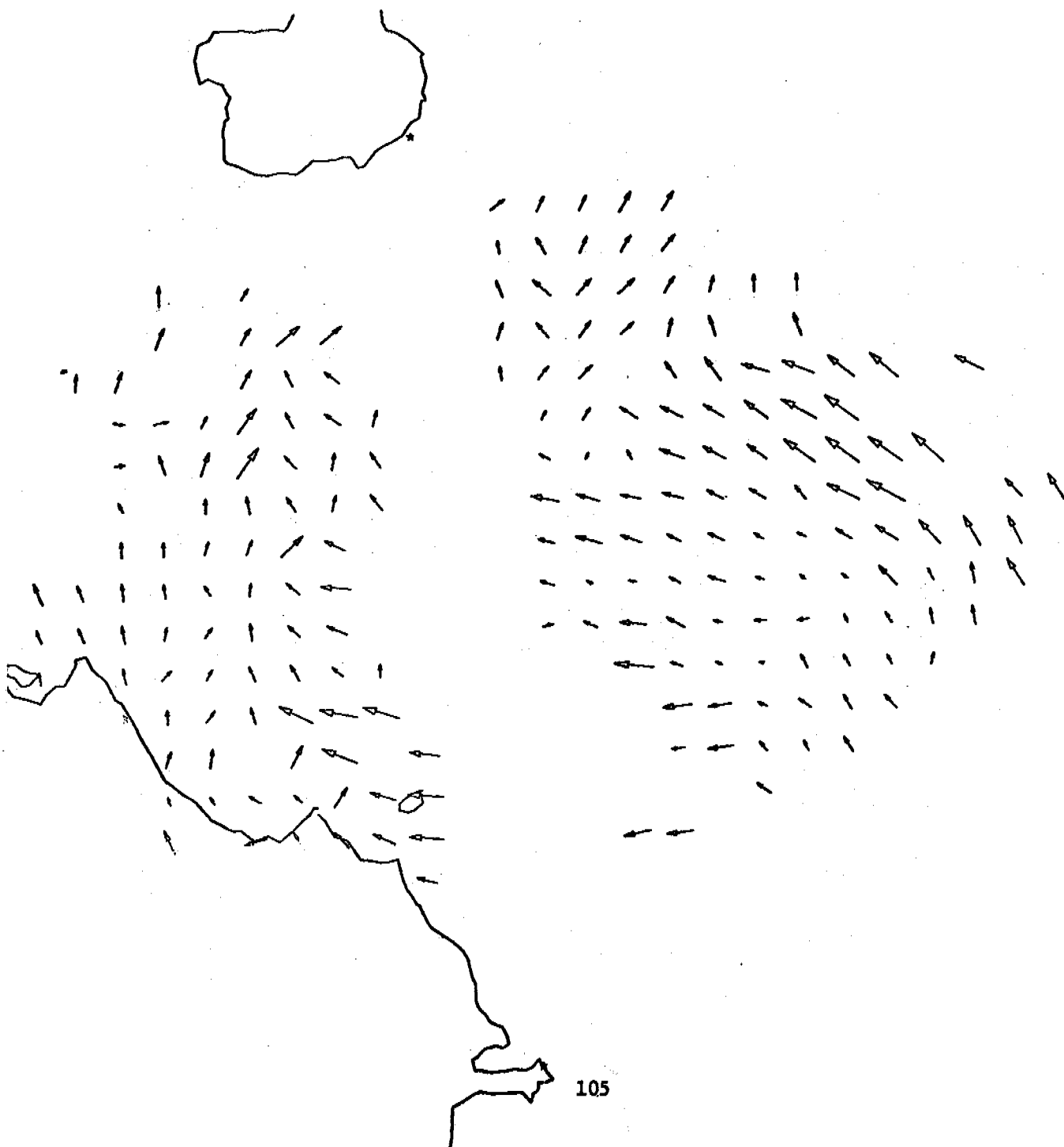
7 JUL 78 14: 0:00
APE DOUGLAS AK.
UGUSTINE IS. AK.

8 KM/IN
200 CM/S/IN
TRUE NORTH ↑



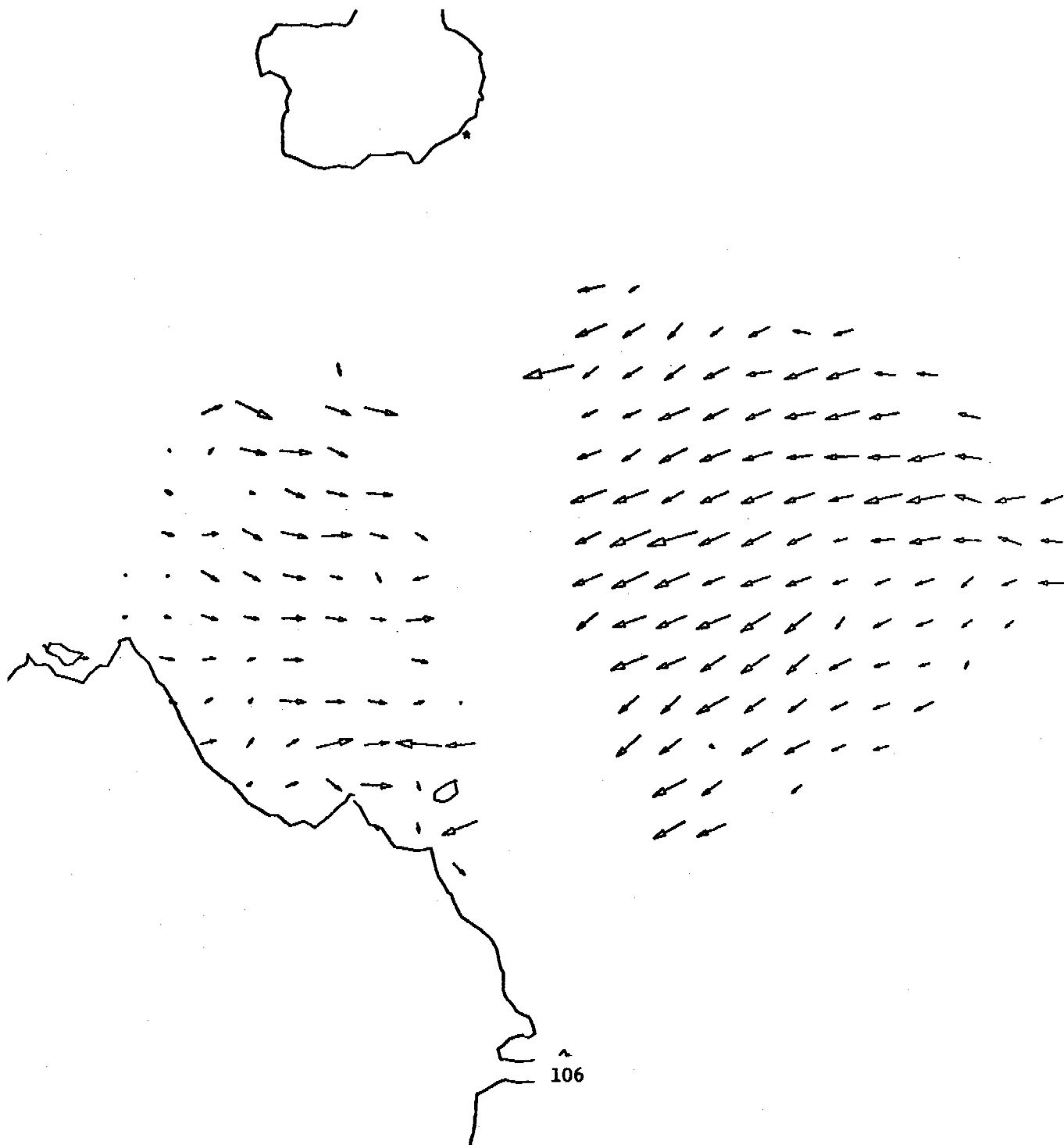
JUL 78 17: 0:00
PE DOUGLAS AK.
GUSTINE IS. AK.

.8 KM/IN
200 CM/S/IN
TRUE NORTH ↑



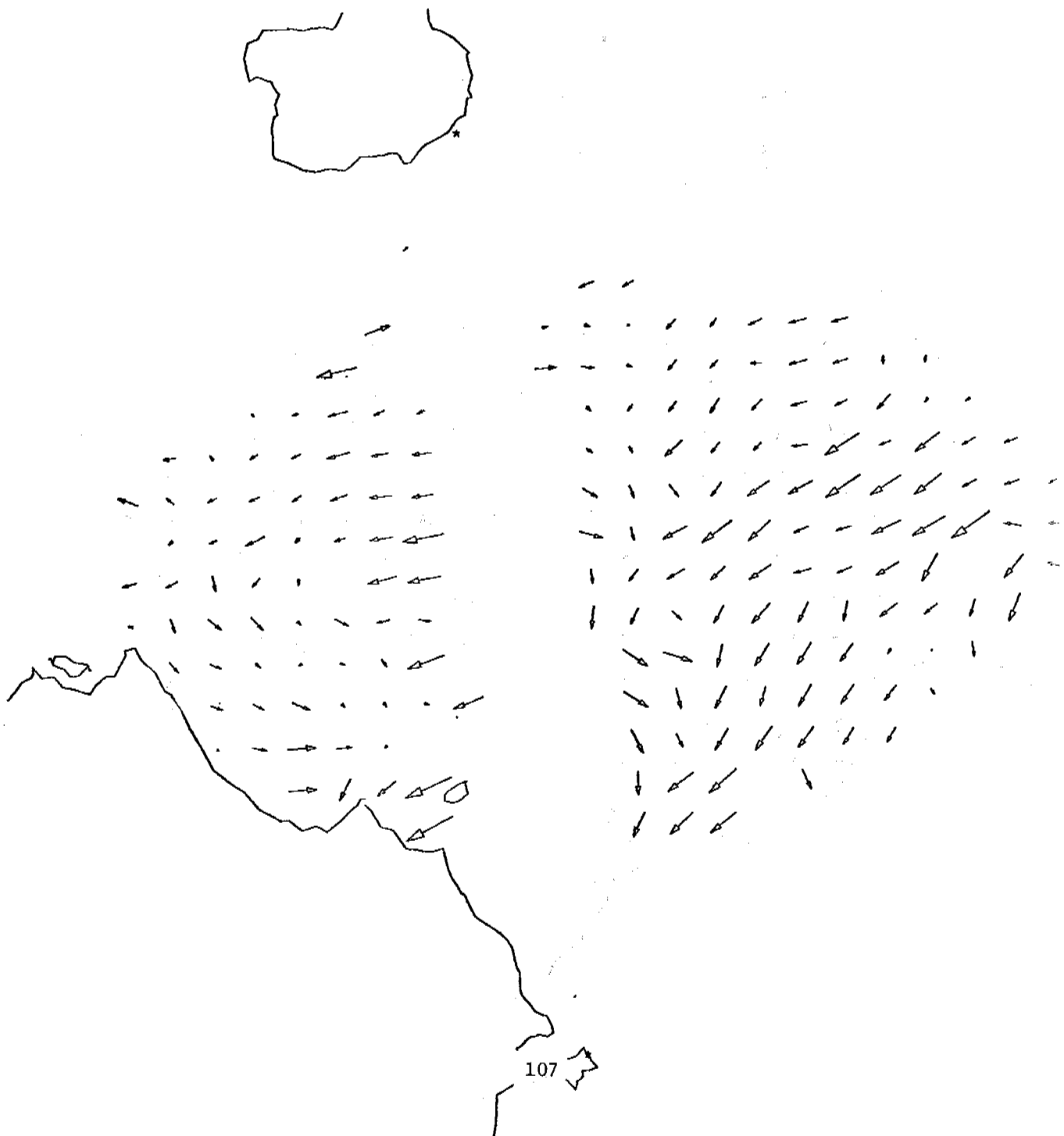
7 JUL 78 20: 0:00
CAPE DOUGLAS AK.
AUGUSTINE IS. AK.

8 KM/IN
200 CM/S/IN
TRUE NORTH ↑



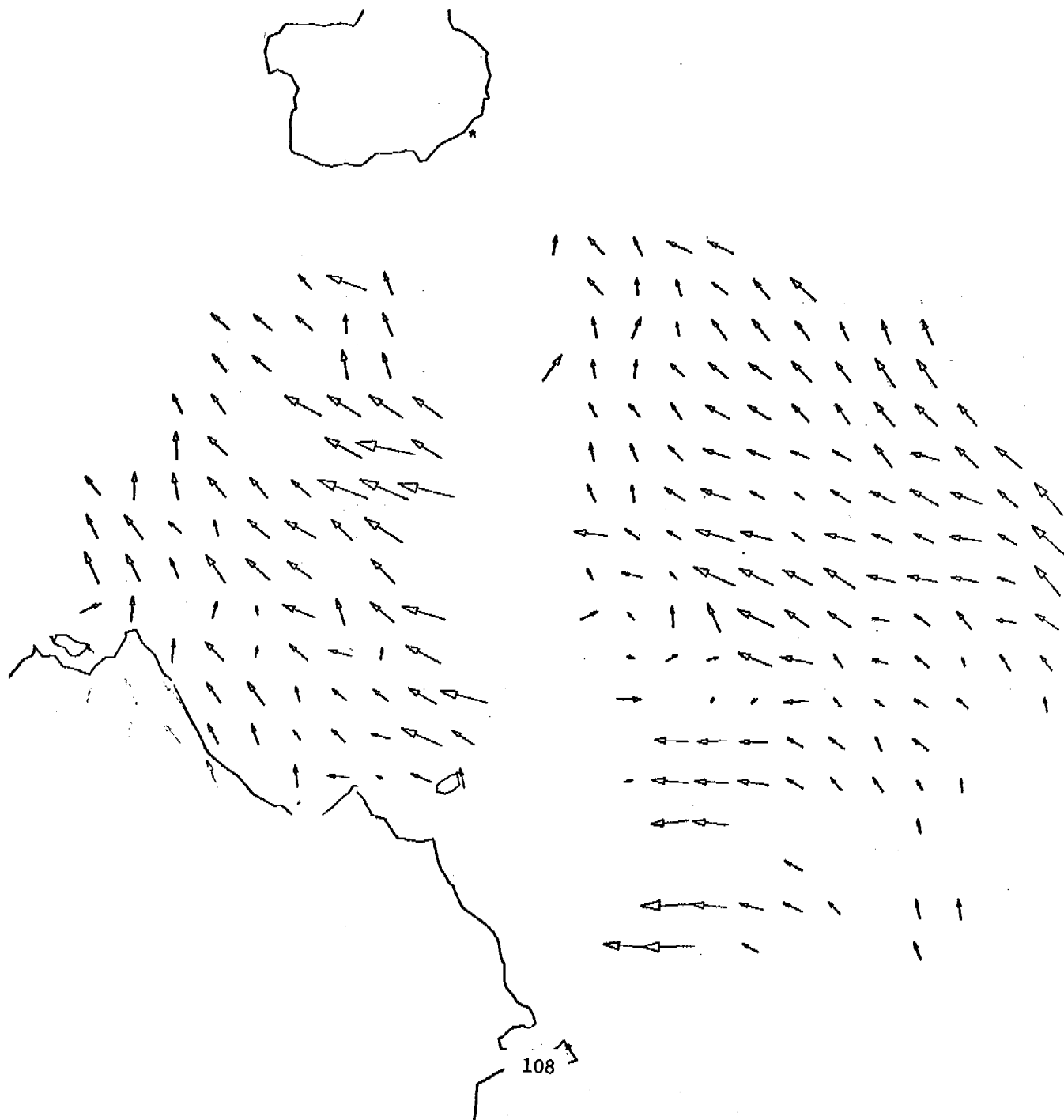
7 JUL 78 23: 0:00
CAPE DOUGLAS AK.
AUGUSTINE IS. AK.

8 KM/IN
200 CM/S/IN
TRUE NORTH ↑



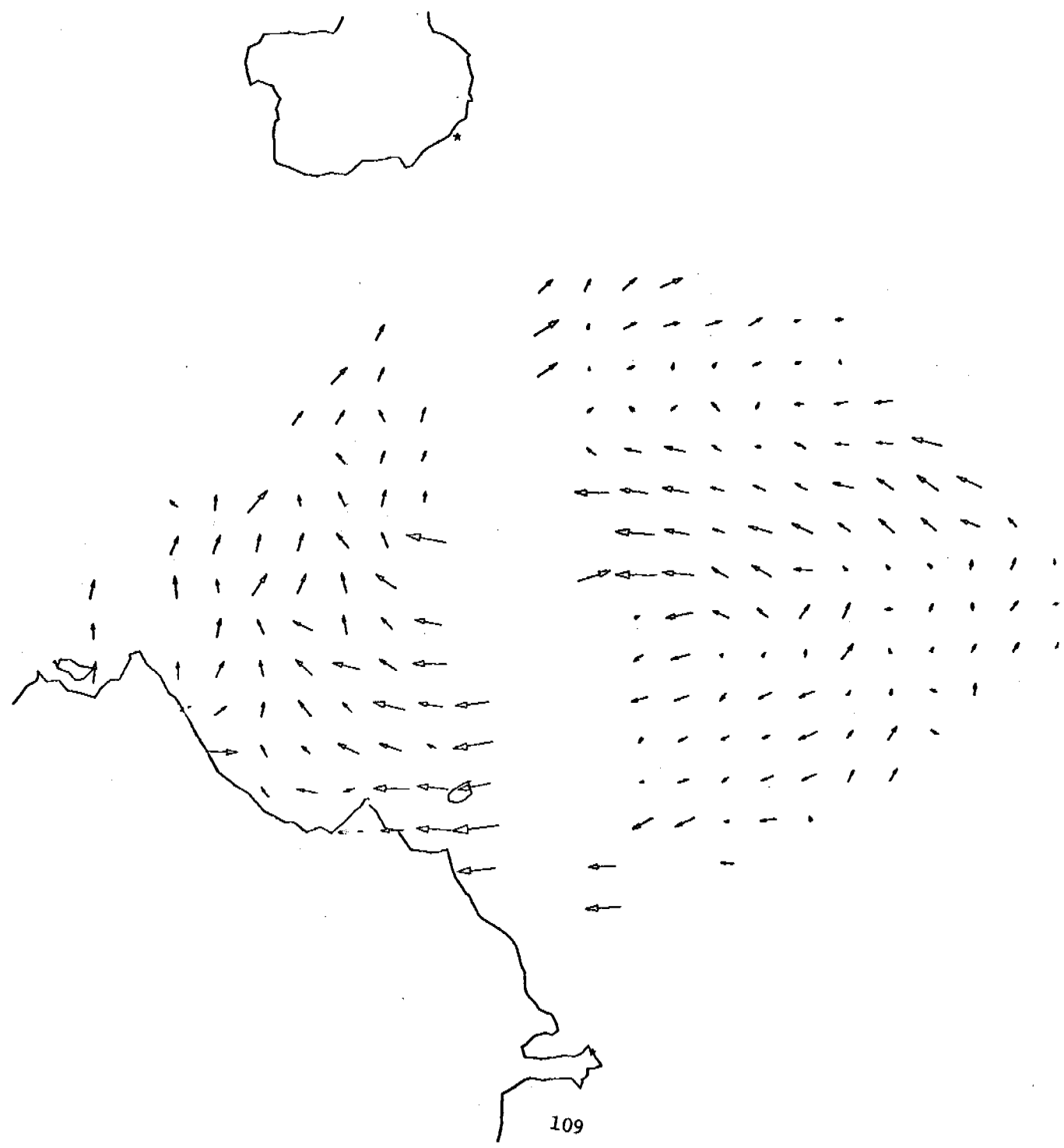
8 JUL 78 2: 0:00
CAPE DOUGLAS AK.
AUGUSTINE IS. AK.

8 KM/IN
200 CM/S/IN
TRUE NORTH ↑



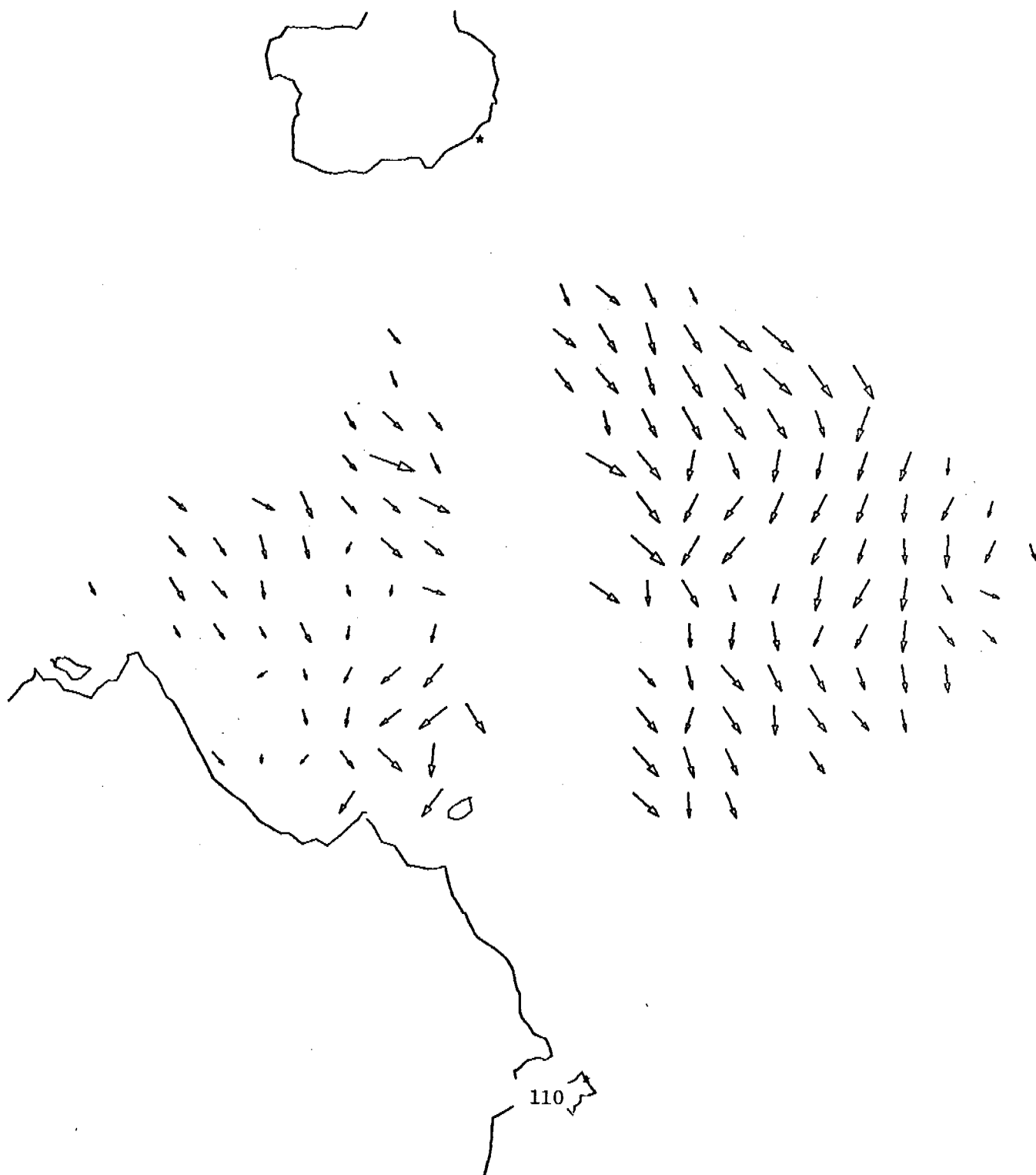
8 JUL 78 5: 0:00
CAPE DOUGLAS AK.
AUGUSTINE IS. AK.

8 KM/IN
200 CM/S/IN
TRUE NORTH ↑



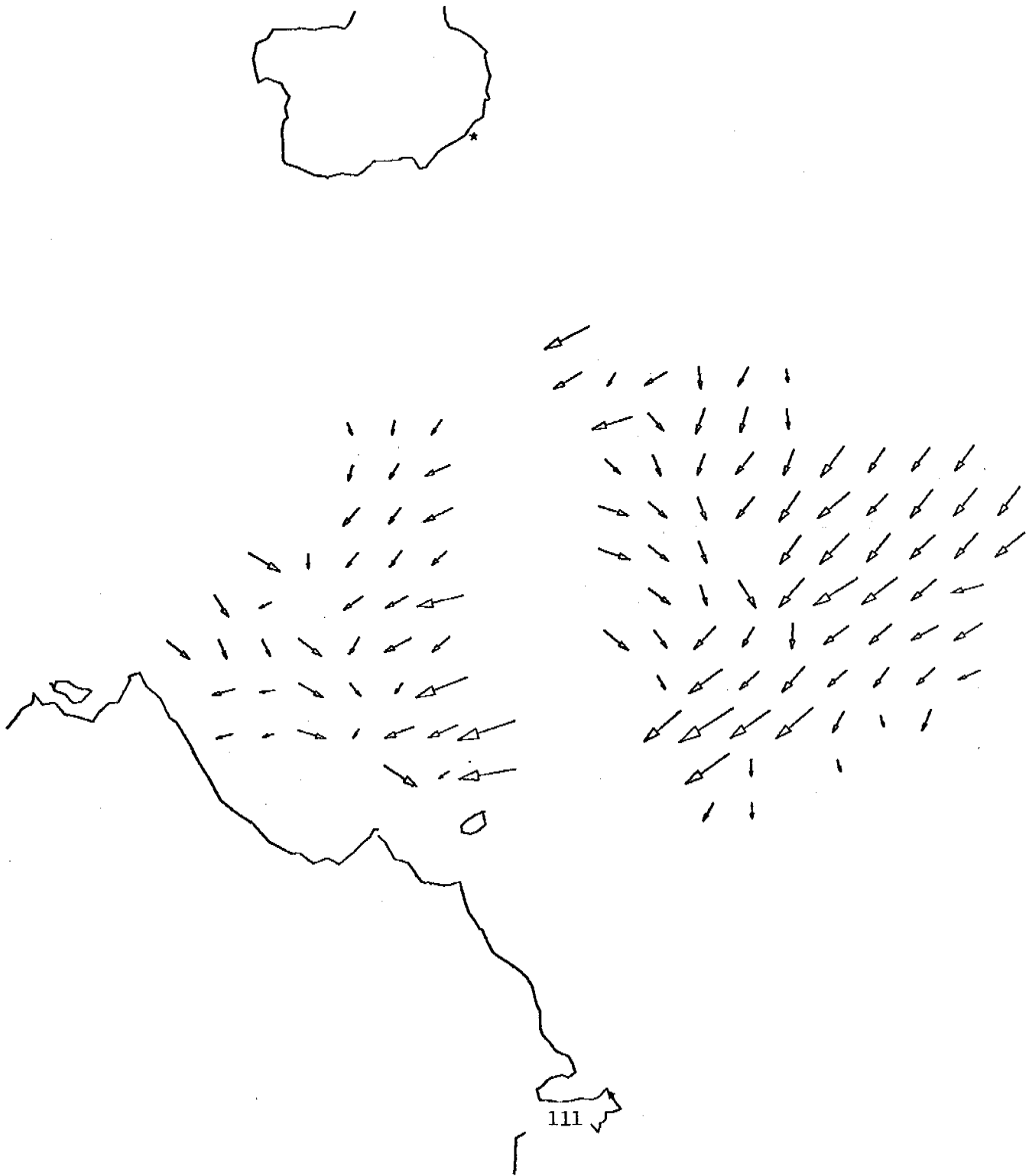
8 JUL 78 8: 0:00
CAPE DOUGLAS AK.
AUGUSTINE IS. AK.

8 KM/IN
200 CM/S/IN
TRUE NORTH ↑



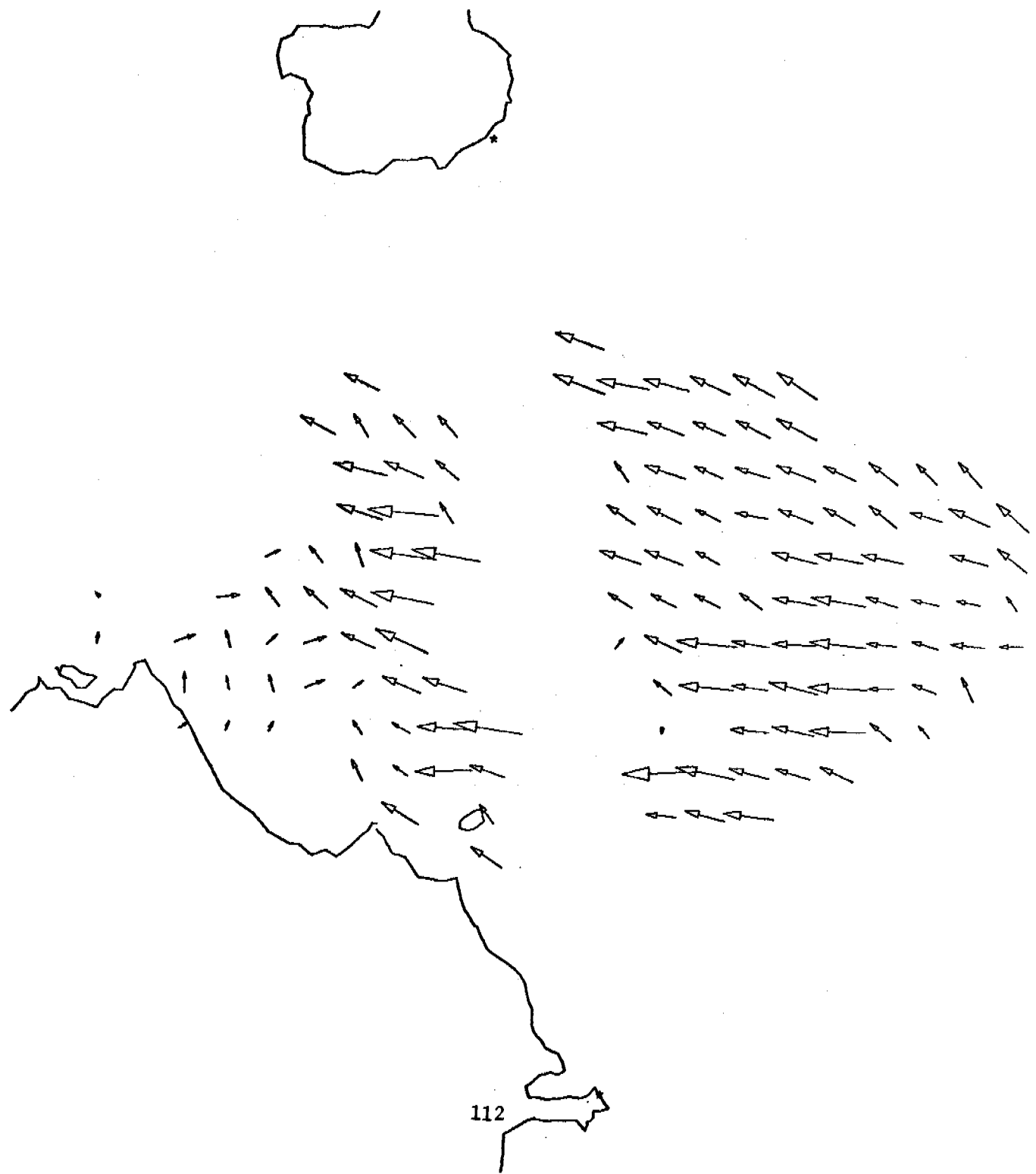
8 JUL 78 11: 0:00
CAPE DOUGLAS AK.
AUGUSTINE IS. AK.

8 KM/IN
200 CM/S/IN
TRUE NORTH ↑



8 JUL 78 14: 0:00
CAPE DOUGLAS AK.
AUGUSTINE IS. AK.

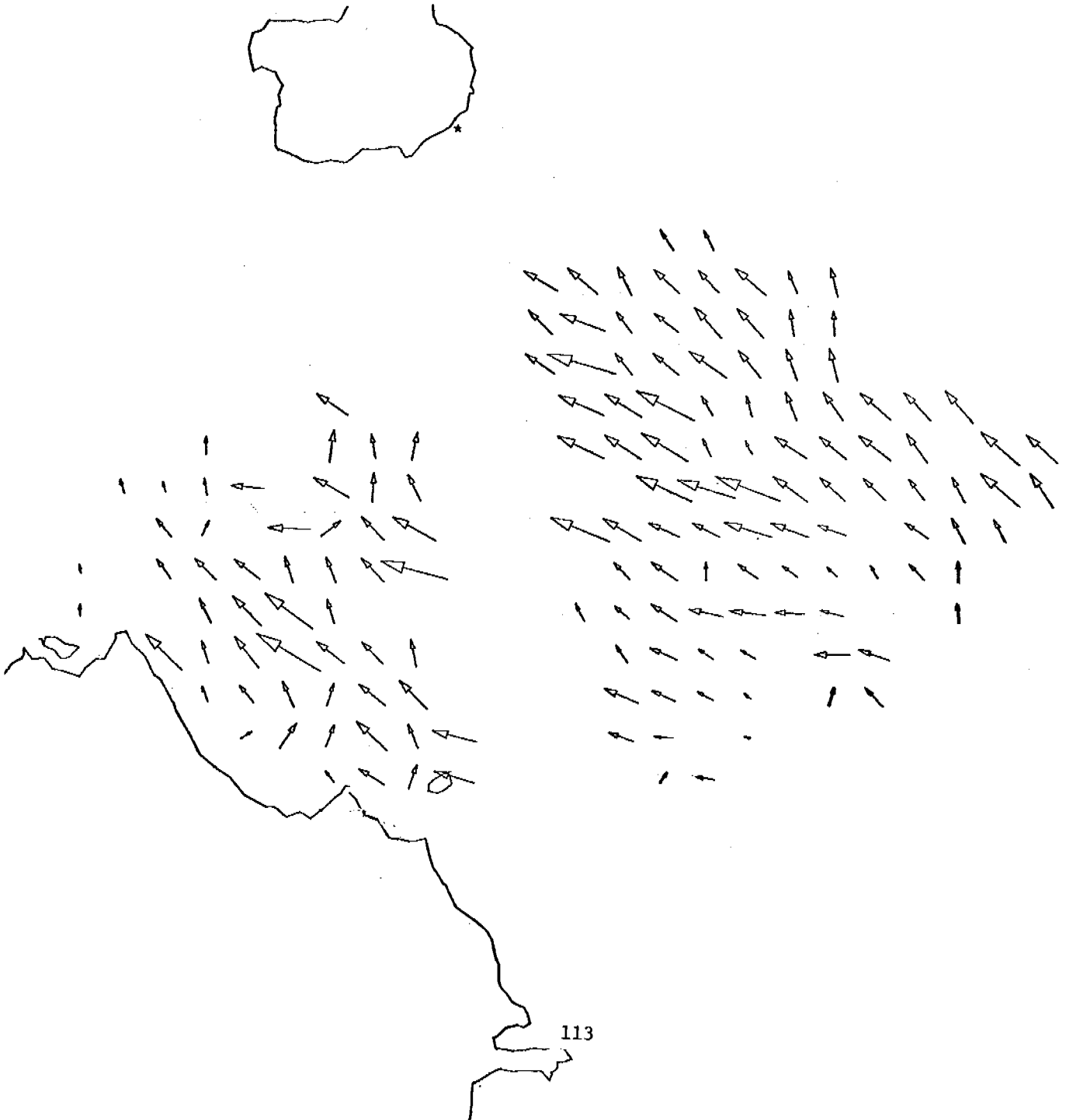
8 KM/IN
200 CM/S/IN
TRUE NORTH ↑



112

8 JUL 78 17: 0:00
CAPE DOUGLAS AK.
AUGUSTINE IS. AK.

8 KM/IN
200 CM/S/IN
TRUE NORTH ↑



8 JUL 78 20: 0:00
CAPE DOUGLAS AK.
AUGUSTINE IS. AK.

8 KM/IN
200 CM/S/IN
TRUE NORTH ↑



ANNUAL REPORT

Research Unit 59
Task D-4

OIL SPILL VULNERABILITY, COASTAL MORPHOLOGY, AND
SEDIMENTATION OF KOTZEBUE SOUND

Co-principal investigators: Miles O. Hayes
Christopher Ruby

Coastal Research Division
Department of Geology
University of South Carolina
Columbia, S.C. 29208

Date Submitted, April 27, 1979

I. Summary of Objectives and Conclusions

This material is contained within the body of the report which follows. The report contains the following:

1. A section detailing the coastal morphology of the Kotzebue Sound study area.
2. A section describing the Oil Spill Vulnerability of the study area shorelines.
3. A set of base maps on a 1:250,000 scale with a color-coded coastal geomorphology classification.
4. A set of base maps on a 1:250,000 scale with a color-coded Oil Spill Vulnerability Index classification.
5. A magnetic tape containing beach profiles and sediment grain size parameters for the Kotzebue Sound and Kodiak Island study areas.
6. An appendix showing each of the profile sites within Kotzebue Sound.

II. Introduction

During the summer of 1976, 89 profile and sample sites were analyzed in Kotzebue Sound from Cape Prince of Wales to Point Hope. These stations were spaced at a 10 km interval along all exposed shorelines. Each station consisted of the following:

1. Detailed line transect (surveyed), later reduced to digital form and plotted by computer;
2. Sediment sampling (3-5 samples on the beachface and back-beach areas);
3. Ground photos of morphologic features and general beachface;
4. Sketches of beach and backbeach zones;
5. Measures of wind direction, wave approach direction and height, temperature, width of surf zone, sediment transport direction;
6. Analysis of potential oil pooling areas and overwash areas;
7. Analysis of lagoon morphology and inlet flushing potential.

From this data, we have classified the shoreline with regard to its general geomorphology. Using the geomorphic classification, we have applied our Oil Spill Vulnerability Index (OSVI) which ranks the shoreline environments with regard to the expected impact of a potential oil spill. The OSVI is based primarily on the longevity of spilled oil within each coastal subenvironment. These data are shown in a coded form on overlays available under separate cover, (full scale overlays for standard 1:250,000 topographic charts). There are two sets of overlays for each chart, one for geomorphology and one for the OSVI.

This type of data may prove useful in the event of an oil spill in the Kotzebue Sound area. Additionally, specific areas to emplace

booms are indicated on the overlays. Longshore transport directions are also shown.

III. Current Knowledge

The overlays are considered our final classification; however, we are presently writing a report which will address the interaction of coastal ice and potential oil spills within the Sound. This report (to be submitted in June) can be used to modify the OSVI ratings on the overlays. Further, there are a number of areas which have been given an OSVI based on geomorphology but due to specific physical processes may require modification. These are addressed in the Discussion of this report.

IV. Study Area

The study area extends from Cape Prince of Wales to Point Hope, a shoreline distance of approximately 900 kilometers. We have also included Hotham Inlet. See Figure 1 in report.

V. Methods

During the summer of 1976 and 1978, 89 stations were established in the study area. At each of these stations, beach morphology, bedforms and bedform orientation, sediment grain size and shape characteristics, and composition of sediment were determined. Profiles were run in 1976 and re-run in 1978 to determine short term changes. All grain size data and profile data has been put onto magnetic tapes and sent to the NODC.

Aerial and ground photos were taken during both of these study periods. Analysis of vertical aerial photos from a number of sources has been used to study ice movement and resultant potential oil pathways.

VI. Results, Discussion and Conclusions

See the report which follows.

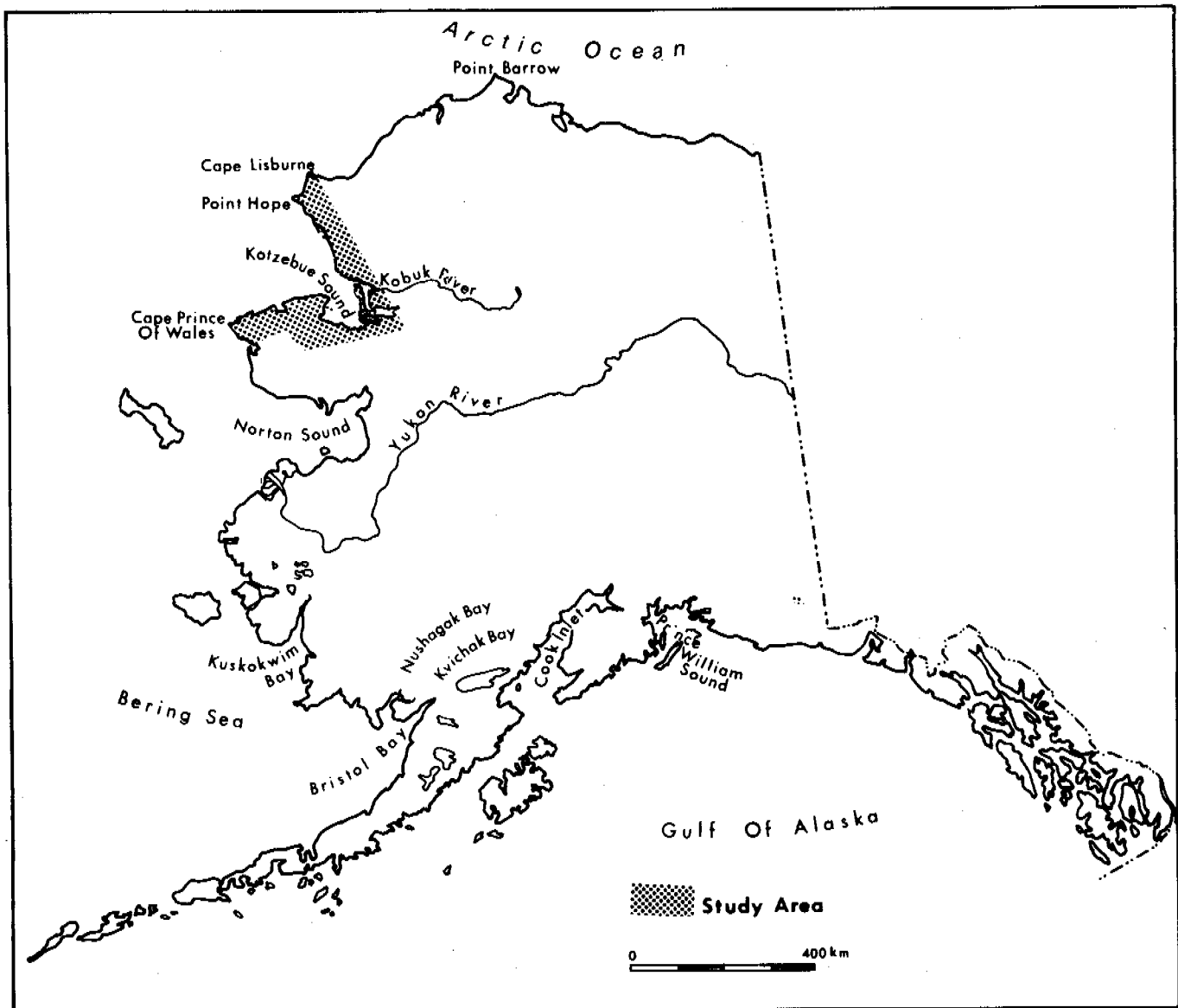


Figure 1. Kotzebue Sound study area. Includes the shoreline from Cape Prince of Wales to Point Hope, as well as all coastal lagoons and the delta of Hotham Inlet.

COASTAL GEOMORPHOLOGY AND OIL SPILL VULNERABILITY
OF KOTZEBUE SOUND

INTRODUCTION

Geology

The general form of Kotzebue Sound and the neighboring Chukchi Sea is the result of the mountains forming the Seward Peninsula to the south and the Brooks Range (De Long Mountain spur and Baird Mountain spur) to the north. These have been highly modified by later glacial, fluvial, marine, and aeolian deposits. These deposits have formed a wide coastal plain backing the barrier islands on the southern shore and a narrow coastal plain backing Cape Krusenstein on the northern shore. Additionally, the Baldwin Peninsula is primarily of glacial origin and is backed by a broad delta complex.

The majority of the shoreline environments consist of marine reworked glacial, fluvial, and aeolian deposits. The surficial geology is discussed below. The area has been subdivided into similar provinces.

Cape Prince of Wales to Goodhope Bay. - Cape Prince of Wales is a high bedrock outcrop of crystalline intrusive rocks. It occupies the westernmost end of the Seward Peninsula mountain range. This Cape, which forms the southern boundary of our study area, is characterized by high bedrock cliffs with some gravel beaches at their base. From the Cape to Goodhope Bay is a continuous low coastal plain of Quaternary gravel, sand, silt, and mud. In areas, it is as much as 60 km wide. These sediments are generally interstratified marine and alluvial deposits with some glacial drift. They are more than 150 ft. thick; the total depth to bedrock is not known. They are very poorly

drained, covered by boggy tundra, streams and lakes. Frost action is intense, posing many engineering problems.

The beaches fronting this section are uniform fine sand barrier islands. The barriers are broken by numerous narrow inlets and usually have a broad shallow lagoon behind them.

The only exception to this classification is the Devil Mountain area just southwest of Cape Espenberg. Devil Mountain is a volcanic cone now filled with water. There are a number of smaller cones surrounding it. The tundra in this area is underlain by Quaternary and Tertiary volcanics, mostly pumice and volcanic ash more than 150 ft. thick, overlain by about 10 feet of silt. This zone is well drained and better suited for engineering structures. It intersects the shoreline along about 10 km of shoreline where it is covered by a veneer of sand. This section of shoreline is slightly more resistant than the surrounding area and forms a small bulge, projecting into the Sound. There are short stretches of beach between Cape Espenberg and Goodhope Bay that are composed primarily of reworked pumice; otherwise, the volcanoes play a very minor role in the general coastal morphology. Most of the shoreline between Cape Espenberg and Goodhope Bay is characterized by low (10-40') scarps into tundra with narrow, low energy sand, mud, and gravel beachfaces.

Goodhope Bay to eastern end Eschsholtz Bay. - There is a narrow or absent coastal plain in this area. The shorelines are backed by interbedded marine and alluvial sediments and basaltic lava flows, or by crystalline or high grade metamorphic rocks covered with frost-shattered gravel. Further inland are low rolling hills underlain by Paleozoic limestone slate, schist and other high grade metamorphic rocks and still further inland, Tertiary and Quaternary volcanics.

The southern entrance to Eschscholtz Bay is backed primarily by marine and alluvial sediments interbedded with basalt flows. In some areas, these volcanics form rock headlands at the shoreline. Most of this area has steep narrow beaches of sands and locally derived gravels. Scarps into the bedrock are quite common. Small sand spits are prograding into river mouths and estuaries. On the inner east side of Eschscholtz Bay, the Buckland River has formed a small delta of sand and mud.

Baldwin Peninsula and Hotham Inlet. - The Baldwin Peninsula is composed of Quaternary glacial deposits greater than 150 feet thick. The southern tip of the peninsula has a bedrock island complex of high grade metamorphic Paleozoic rocks. In general, the shorelines are backed by moderately steep scarps into the unconsolidated glacial sediments. Beaches are composed of sands and gravels. The eastern side of the Baldwin Peninsula is similar, although the beaches are narrower and more poorly sorted because of the very low wave energies in Hotham Inlet.

The eastern side of Hotham Inlet is dominated by the Kobuk and Selawik River deltas. The Kobuk Delta is the largest and most active. This stretch of shoreline is extremely low, composed of sands and mud and subject to very low wave energy. Vegetation covers the surface almost to the waterline. True beaches are rare, occurring where the delta has been abandoned and is being transgressed by a narrow zone of sand and shells. The Noatak River empties into the northern end of Hotham Inlet and has a shoreline similar to the rest of the area, although beaches are better developed because of the greater wave energies. These areas are backed by thick sequences of alluvial and glacial deposits associated with the river deltas.

Sheshalik Spit to Cape Thompson. - Most of this area is backed by glacial deposits (10-150 feet thick) over crystalline bedrock. In local

areas, river drainage has resulted in fluvial sediments overlying the glacial sediments or directly overlying bedrock. The Kivalina area is underlain by aeolian silts on bedrock. Landward of these deposits are the Baird Mountains exposing metamorphic rocks of Paleozoic age.

The beaches in this area are almost exclusively mixes of sand and gravel. Often, they form narrow confining barriers fronting shallow coastal lagoons. Gravels are locally derived. Some small rivers drain into these lagoons and have formed minor delta sequences.

Cape Thompson to Point Hope. - The Cape Seppings to Cape Thompson area is primarily high bedrock cliffs dropping vertically into the Chukchi Sea. The De Long Mountains trend offshore at this location. Bedrock is Jurassic and Cretaceous sandstone, shale, and conglomerate. There is a thin blanket of sand, silt and gravel (10 feet thick) over the bedrock except in the Cape Seppings area where the blanket is considerably thicker.

Closer to Point Hope, the bedrock is older Permo-Triassic shale, chert and limestone ending in Mississippian to Permian rocks just east of the Point Hope cusped foreland. The blanket of unconsolidated sediments overlying the bedrock thickens toward the west. Beaches are generally absent at the bases of these sea cliffs. In some cases, locally derived gravels have formed steep pure gravel beaches as at Chariot.

Point Hope is a very large cusped foreland formed of gravel and sand. The steep beaches are backed by a Pleistocene delta complex which abuts Jurassic and Cretaceous rocks to the north and east. These sediments are more than 150 feet thick. Depth to bedrock is unknown.

The Arctic Information and Data Center has detailed maps of the areas described above, summarizing Geology, Oceanography, Biology, etc. Those maps have been the primary source for this section.

Climate

The general climate in the Kotzebue Sound - Chukchi Sea area is transitional. Thus, it may have characteristics of Continental climate or Maritime climate, or it may share characteristics of both. Overall, the climate is more extreme and variable than in maritime areas, but less extreme and variable than in the continental areas. Surface winds are generally light with numerous exceptions.

Precipitation. - Snowfall in the study area averages about 40 inches per year. The first snows generally fall in September. Heaviest falls (about 10 inches per month) occur during December and January. Most of that snow will remain on the ground until April and will generally melt by June.

Rainfall in the area is very light. In an average year, about 8 inches will fall, mostly during July - September. The total precipitation for the area, including the water equivalent of the snow, is about 10 inches. Thus, the area is quite arid, although there are numerous lakes and boggy tundra which might give an observer the impression that there is considerable precipitation. These surface waters are the result of the summer melt on the continuous permafrost surface.

Temperature. - The study area's location just south of the arctic North Slope results in rather low temperatures throughout the year. However the Brooks Range to the north generally separates the area from the colder arctic air mass during the summer; this results in considerably higher mid-summer temperatures. In general, the maximum temperature for July will be in the 50's; while the maximum for January will be about 0°F. Minimum July temperatures are in the 40's; while minimum January temperatures are in the minus teens F. Table 1 below shows the mean monthly temperatures for Kotzebue for 29 years between 1941 and 1970. The mean annual temperature for the 29 year period is 20.9°F.

Table 1. Mean temperature 1941 - 1970 (Degrees F)

Jan. -3.7	April 13.0	July 52.9	Oct. 23.6
Feb. -4.3	May 30.8	Aug. 50.7	Nov. 7.7
Mar. -0.5	June 43.5	Sept. 41.1	Dec. -3.9

One of the more useful derivatives of temperature is the Degree Day. A degree day is the departure of the mean daily temperature from a standard. For "Heating Degree Days", that standard is 65^oF. For "Thawing Degree Days", the standard is greater than 32^oF; "Freezing Degree Days", less than 32^oF.

Heating Degree Days: Mean temperatures below 65^oF accumulate heating degree days. Kotzebue averages about 17,000 heating degree days per year. By way of comparison, Barrow has 21,000; Anchorage 11,000, and Juneau, 9,000. Table 2 below shows the monthly averages from 1941 - 1970.

Table 2. Heating Degree Days (1941-1970)

Jan. 2130	April 1960	July 375	Oct. 1283
Feb. 1940	May 1060	Aug. 443	Nov. 1719
Mar. 2031	June 645	Sept. 717	Dec. 2136

Thawing Degree Days: Mean temperature above 32^oF accumulates thawing degree days. Kotzebue averages between 800 - 1800 per year. For comparison, Barrow averages 400, Anchorage 3,000 and Juneau, 4,000.

Freezing Degree Days: Mean temperature below 32^oF accumulate freezing degree days. Kotzebue averages between 5,500 - 6,500 per year. Barrow averages about 8,500, Anchorage 2,000 and Juneau about 0. In general, areas with more freezing degree days than thawing degree days will have some permafrost. Low thawing degree days and high freezing degree days will result in continuous permafrost.

Wind. - The winds in the study area are bi-directional, generally blowing out of the west or the east. There is a strong seasonal effect

with mostly easterly winds during the winter and mostly westerly winds during the summer. August and September tend to be the windy months, and August is the only month during the year when primary storm tracks move into the area (by way of the Bering Strait). Secondary tracks enter the Strait during February and November.

August and September are about 5 times more likely to have a storm center passage than during December to May. The probability increases from June to August, then decreases from September to November. The Kotzebue-Chukchi Sea area has higher storm probability than any of the arctic areas to the north.

The strong winds almost always come from east or west, generally 20-30 kts. The highest winds of the year occur during the winter and come from the east at about 50 kts. Table 3 below shows the average wind velocity and direction by month for the period 1950-1970. There is a clear seasonal variation in direction.

Table 3. Mean wind velocity and direction

Jan. E/17.0	April NE/14.7	July W/12.8	Oct. NE/14.6
Feb. E/14.2	May W/9.1	Aug. NW/14.3	Nov. ESE/16.0
Mar. E/14.2	June W/11.1	Sept. ESE/14.4	Dec. ESE/16.6

The predominance of westerly winds during the summer (when the area is ice free) results in a general wave approach from the west which transports sediments east along the beaches into the Sound. The occurrence of single high wind events from the north just before freeze-up results in storm overwash of the barrier islands along the southern side of the study area. This will be discussed in more detail in another section of this report. There are a number of excellent climatic references available which give very detailed data (BLM-OCSEAP climatic atlas; Alaskan Regional Profiles). Additional data was collected from the National

Weather Service at Kotzebue.

GEOMORPHIC CLASSIFICATION

The primary purpose of this study has been to provide descriptive baseline data regarding the coastal morphology of the Kotzebue Sound area shorelines and then to apply an Oil Spill Vulnerability Index. The division of the area into different geomorphic units is based on analysis of changes in the permanent profile sites and general beach morphology. Generally, these classification schemes divide the shoreline into either erosional, neutral or depositional subclasses. However, almost the entire shoreline of Kotzebue is erosional to some extent; so a different method has been derived.

The shoreline is divided into six such classes:

1. Sand barrier islands and spits.
2. Sand and gravel barriers and spits.
3. Gravel beaches.
4. Tundra scarps.
5. Deltas and river mouth systems.
6. Rock headlands.

Sand barrier islands and spits. - This is one of the most common shoreline types representing 257.04 km of the total 2318.36 km of shoreline classified. The entire barrier complex from Cape Prince of Wales to Cape Espenberg falls into this class. These are the only purely sand barriers in the study area. Figure 2 shows profile site KBS-16 located about 30 km NE of Shishmaref on the barrier island chain. Note that the profile is quite flat and featureless. All of the beaches in this class are flat due to their very fine-grained sandy sediments. The profiles for this area (KBS1 - KBS24) appear in the appendix of

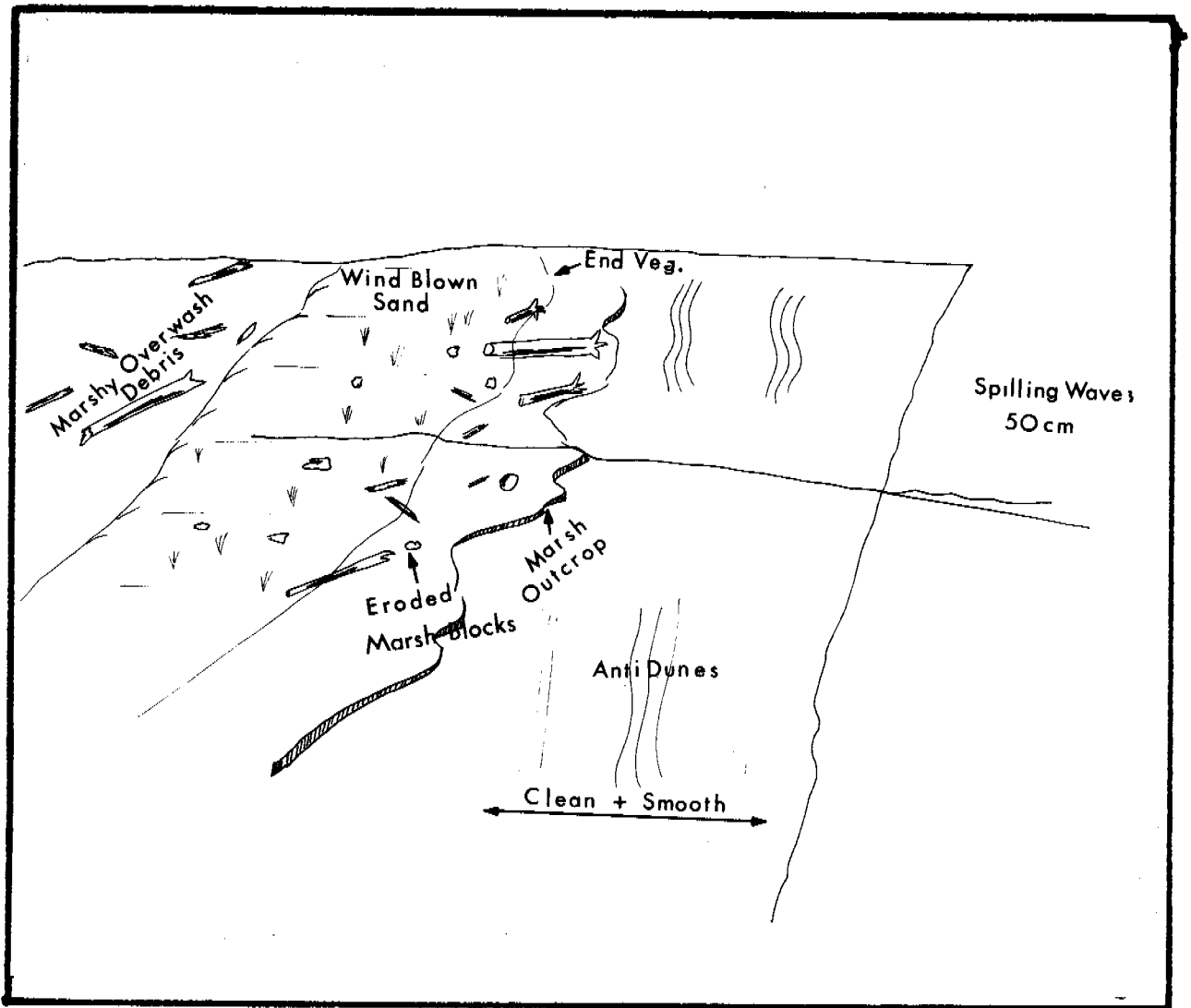


Figure 2. Profile site KBS-16 located about 30 km NE of Shishmaref on the fine sand barrier islands. These barriers are 100% fine mature sand and generally have very flat rather featureless profiles. Erosion along these shores is extreme. In many areas, rooted tundra muds outcrop on the beachface and are overlain by overwash fill and eroded tundra blocks. Overwash debris can be found well behind the normally active beachface. These areas are of intermediate vulnerability to oil spills. Their flat fine-grained character will, in general, prevent oil penetration into the beach. They should be cleaned by natural processes within about six months. They are, however, backed by very sensitive lagoonal environments.

this report. Note that they are all quite flat, sometimes with sharp scarps into earlier dune complexes.

Most of these beaches are erosional in character and show considerable evidence of this long-term erosion. Outcrops of tundra lake-rooted muds are very common on the beachface. In many areas, the beachface sands are migrating landward over the vegetated tundra behind them. Berms with aeolian sands and storm debris behind them are found "perched" on the older tundra deposits. Low wind shadow dunes with sparse vegetation cover some of the more stable areas.

At one time, this entire barrier chain was highly progradational. In some areas, the barrier is quite wide (2-3 km) and composed of multiple beach ridges with intervening swales filled with lakes or marshy vegetation. High dunes are common on these earlier beach ridges. Today, the area is undergoing erosion either due to a relative rise in sea level or a reduction in sediment supply, or both. Many of the houses in Shishmaref are at the edge of the dune scarp which has migrated landward since they were built. Some are in danger of falling over if a severe fall or summer storm develops in the Sound.

The general transport direction of sediment on this stretch of shoreline is NE into the Sound. As explained in the section on climate, the summer (when the Sound is ice free) wind direction is from the west. Thus, waves approach from the west and move the sediment along the beaches to the NE. Cape Espenberg has been built because of this long-term NE transport trend. However, there are exceptions and a number of smaller recurved spits have been built into the lagoons from the NE to the SW, thus documenting local reversals in transport direction.

Perhaps the most dramatic characteristic of these barriers are the numerous storm washover channels and wash-around features. The infrequent severe storms from the north and northwest during the latter sum-

mer - early fall generate high waves and storm surges which result in the total breaching of the barriers and the development of large deep washthrough channels. In some areas, broad unvegetated washover fans have been active for many years. These low areas tend to be overwashed repeatedly during storm events and do not have enough time to develop the required aeolian deposits between storm events to prevent washover during the next storm. Thus, many of them have remained active since they were first mapped. There are a large number of abandoned narrow washthrough channels indicating that they can be healed by the longshore transport of sediment and eventually prevent further breaching. The violence of the storm events is attested to by the presence of storm debris covering the barrier-top surface and into the backbarrier aeolian areas. If an oil spill were to take place during a storm event, severe, very long-term damage would result, because the oil would be emplaced high on the barriers above the normal "reach" of the waves.

Sand-gravel barriers and spits. - This category is one of the most common, comprising 610.47 km of shoreline, primarily on the northern side of the Sound. Figures 3, 4 and 5 show some typical examples. In general, these beaches are relatively narrow and considerably steeper than the fine-sand beaches. Cuspate multiple berms are common.

Figure 3 shows profile site KBS-66 on Cape Krusenstern. This profile run near the middle of the Cape has rather fine sediments with a dominance of sand over gravel. The sediments coarsen as the proximal end of the Cape is approached. The beachface is quite steep and shows a number of erosional indicators. The older ridge-and-swale topography intersects the coast at an angle where a perched storm berm has been deposited on top of the vegetated backbeach. Torn-up remnants of that vegetated mat outcrop on the beachface and are scattered on the top sur-

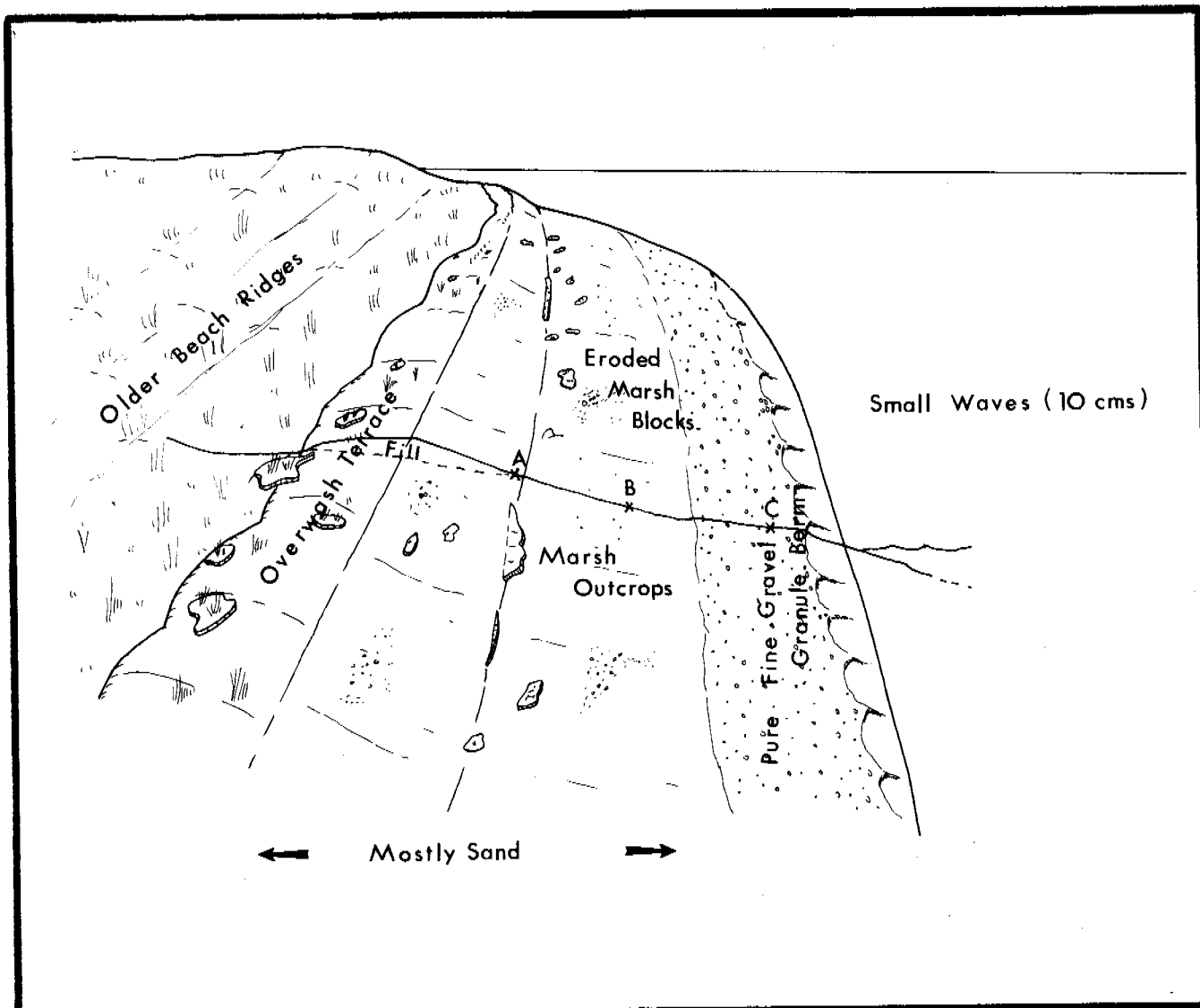


Figure 3. Profile site KBS-66, located on Cape Krusenstern. This area has beaches consisting of sand-gravel mixes. In this case, the sand is dominant, with the gravel being confined mostly to the lower beachface. Gravels here are generally quite fine (2-6 mm). The area is undergoing erosion, indicated by the oblique intersection of earlier ridge-and-swale topography and the shoreline. The sandy overwash terrace is migrating landward over the vegetated back beach. At the base of this terrace is a discontinuous outcrop of eroded vegetated tundra capping the older ridge-and-swale topography. Beach slope is of intermediate steepness. These beaches have an intermediate vulnerability to spilled oil. Penetration of oil into the substrate and burial of oil may be a problem due to the grain size; however, these areas should be cleaned by natural processes within a year. Oil spills during a storm or high spring tide could result in more long-term damage.

face of the beach. Long-term sediment transport direction is east, into the Sound.

Figure 4 shows profile KBS-72 located east of Cape Thompson. This is a very typical profile of a sand-gravel barrier enclosing a shallow coastal lagoon. The beachface is quite steep with two berms on it. The lower berm is cusate in form, with coarser sediments on the horns of the cusps. The berm top is covered by mostly sand and granules, and the higher berm has a berm face of sand and a coarser gravel trough. The above size characteristics are very common on these mixed sand and gravel berms. The backbeach area has a high vegetated storm berm, indicating very infrequent but severe storms. There is a minor beachface on the lagoon side of the barrier. Small cusate spits and flying spits are very common on these lagoon beaches. These small features indicate both westward and eastward sediment transport in the lagoons. Occasionally, there are washthrough channels on these beaches, but they are quite rare, indicating considerably less wave energy on this northern shore of the Sound compared to the southern shore.

Gravel beaches. - Pure gravel beaches occur rarely in the study area. Only 37.84 km of the study area are pure gravel beaches. They are generally located just downdrift of rock headlands or in areas of high wave energy and abundant glacially-derived gravels, as on the Baldwin Peninsula. The area around Chariot, just east of Cape Thompson, has a stretch of pure gravel beach. The beach is very steep with 2 to 4 berms. In general, there is a coarsening of the gravel size from the waterline to the top of the active beach. The upper berms are active only during storms. The beach on the northwest side of the Baldwin Peninsula also has almost pure gravel beaches. Most of the finer sediment has been winnowed out by wave activity, leaving only the gravels.

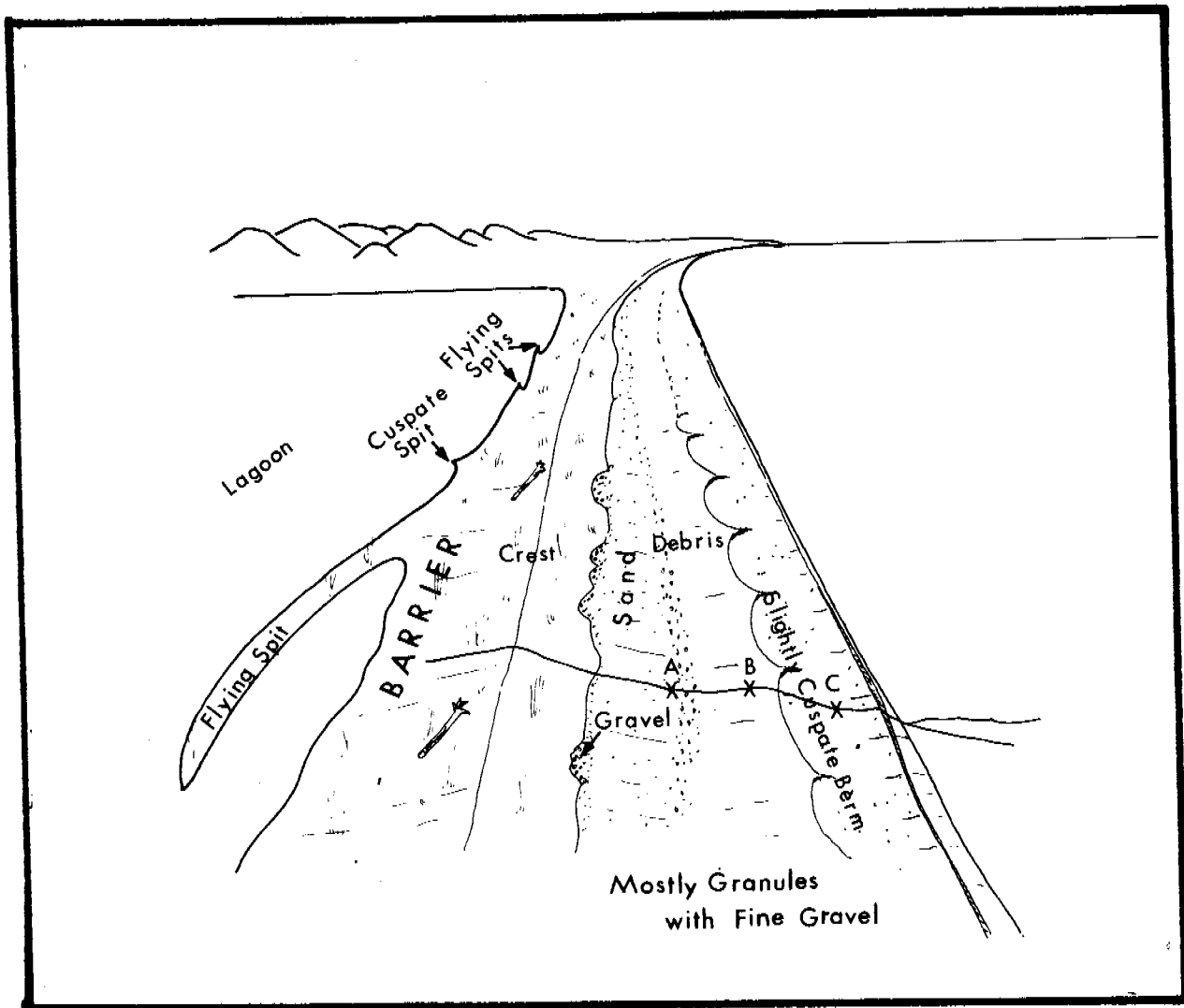


Figure 4. Profile site KBS-72, located east of Cape Thompson. This profile is composed of sand and gravel with gravel dominant. Most of the gravels are fine (2-10 mm). The beachface is of moderate steepness. Multiple berms are common. The beach is formed on a gravel barrier fronting a shallow coastal lagoon. The lagoonal side of the barrier has a narrow beachface with a number of depositional features (small flying spits and cusped spits). Most of these shorelines are anchored by bedrock and thus erosion rates are rather low. Thus, the back beach area is vegetated and generally unbroken by washovers. Oil spill vulnerability is intermediate. The coarse grain size will present problems with oil penetration and burial, but the beach should be cleaned by natural processes within about a year or two.

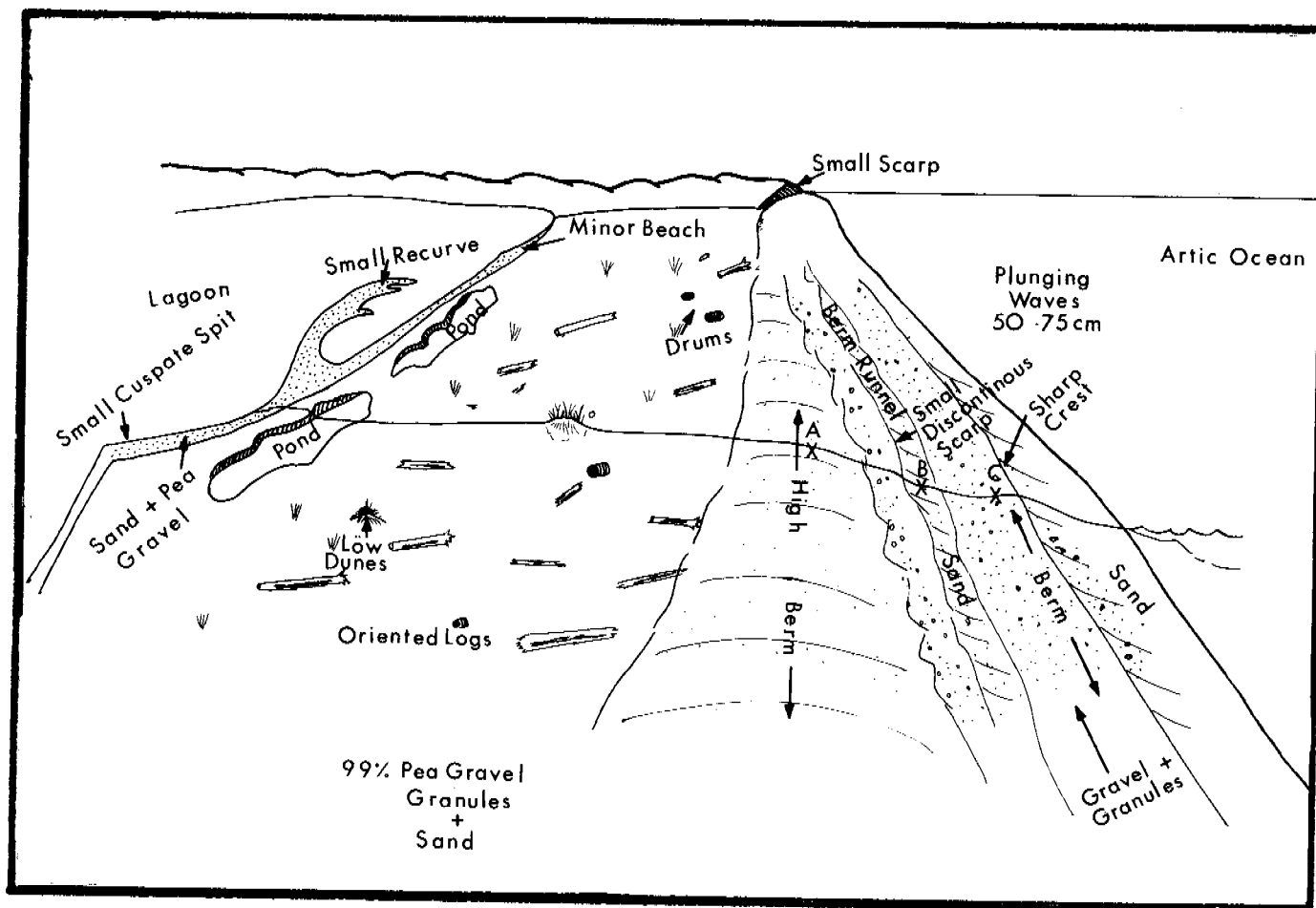


Figure 5. Profile site KBS-86, located on the NW shoreline of Point Hope. This area is one of the highest energy zones in the study area. The beachface is mostly fine gravel with some sands. The high wave energy results in a broad beachface with multiple berms. The back beach area is littered with storm debris and also has some low wind shadow dunes. The lagoonal beaches have a number of smaller depositional features (cusplate and flying spits). Oil spill vulnerability is intermediate. Penetration and burial of oil could be a problem due to the grain size; otherwise, the beach should be cleaned by natural processes in a year or two.

These beaches are highly susceptible to longer-term oil spill damage due to deep oil penetration into the sediment.

Tundra scarps. - Tundra scarps are very common in the study area comprising 671.16 km of the shoreline. They show a wide variety of heights and variable slope and vegetated covering generally as a function of wave energy. Figures 6, 7 and 8 show typical tundra scarp shorelines in Kotzebue Sound.

Figure 6 shows profile site KBS-26 located just south of Cape Espenberg. The scarp is about 4 m high, capped by vegetated tundra with well-developed polygonal topography. The face of the scarp is bare; however, there are numerous vegetated slump blocks fallen onto it. In places, the vegetated mat from the tundra cap overlaps the top portion of the scarp. This area is subject to relatively low wave energies during the ice free summer, except for winds from the east. The easterly winds are common enough to maintain the retreat rate of the scarp, and, thus, it remains unvegetated.

There is a narrow beachface at the base of the scarp. Organic plant detritus covers much of the upper beachface. A small low ridge was present on the lower beachface. The offshore slope is very low and contains abundant infauna (there are considerable shell swash lines on the ridge tops). Beach sediment is a fairly well-sorted coarse volcanic sand. The source of the sand is the Devil Mountain volcanic area to the west.

Figure 7 shows profile site KBS-42 located on the outer southern shore of Eschscholtz Bay. This is an area of relatively low wave energy. The very flat shallow offshore slope further reduces wave energy. The scarp is about 3 m high and is vegetated to the beachface indicating that it is not undergoing continuous erosion, but probably erodes only during

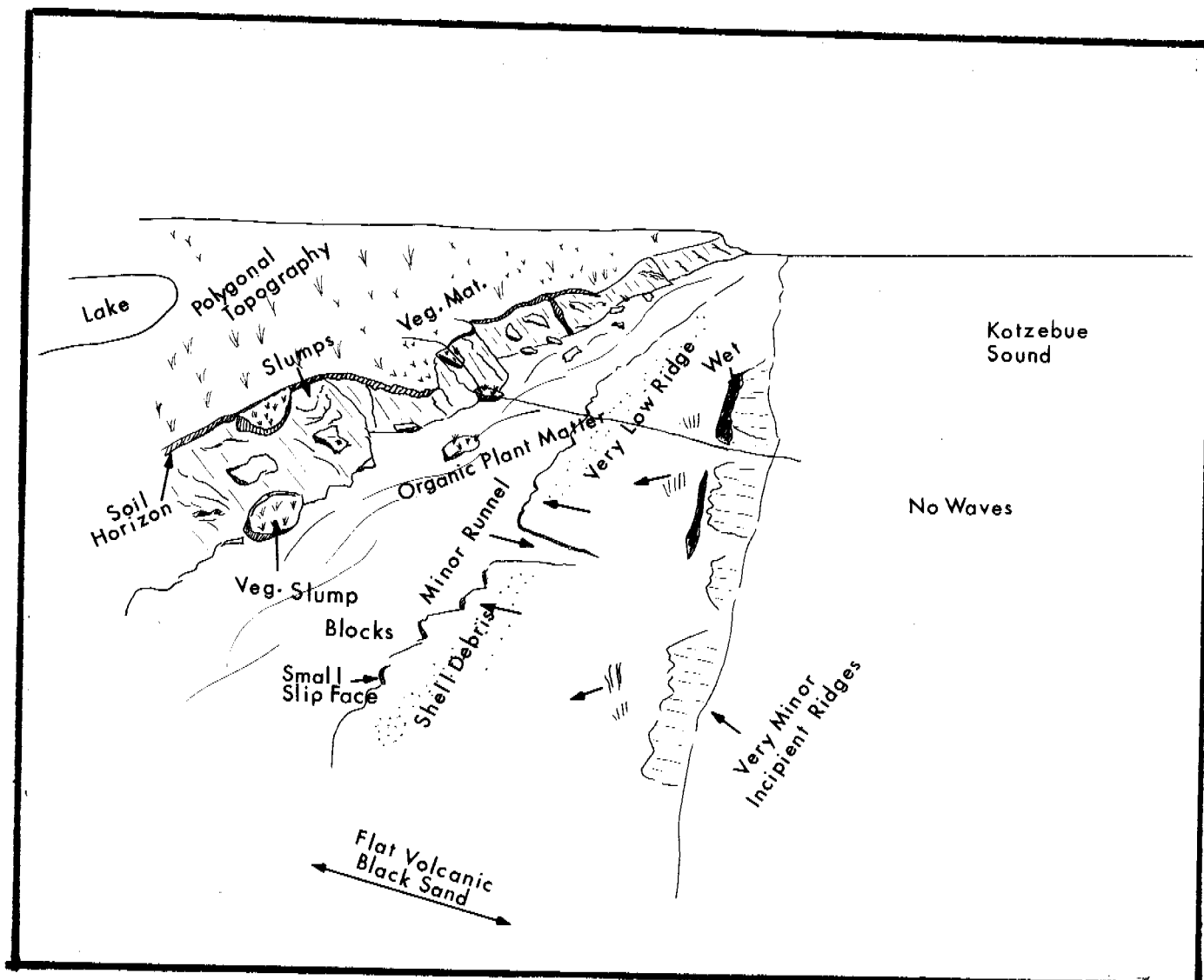


Figure 6. Profile site KBS-26, located just south of Cape Espenberg. The 4 m high scarp is unvegetated due to continual retreat. Slump blocks and hanging vegetated mats extend over the otherwise bare scarp. The beachface is composed of locally derived black volcanic sand with some mud from the scarp. The beach is narrow and of very low relief partly due to the fine grain size and partly due to low wave energy. Offshore slope is flat and shallow. The beachface is so low and narrow that even small storms will generate waves large enough to break on the scarp. Oil spill vulnerability is intermediate due to the grain size. The area should be cleaned within a year of a spill by natural processes. The low wave energies may increase that time slightly.

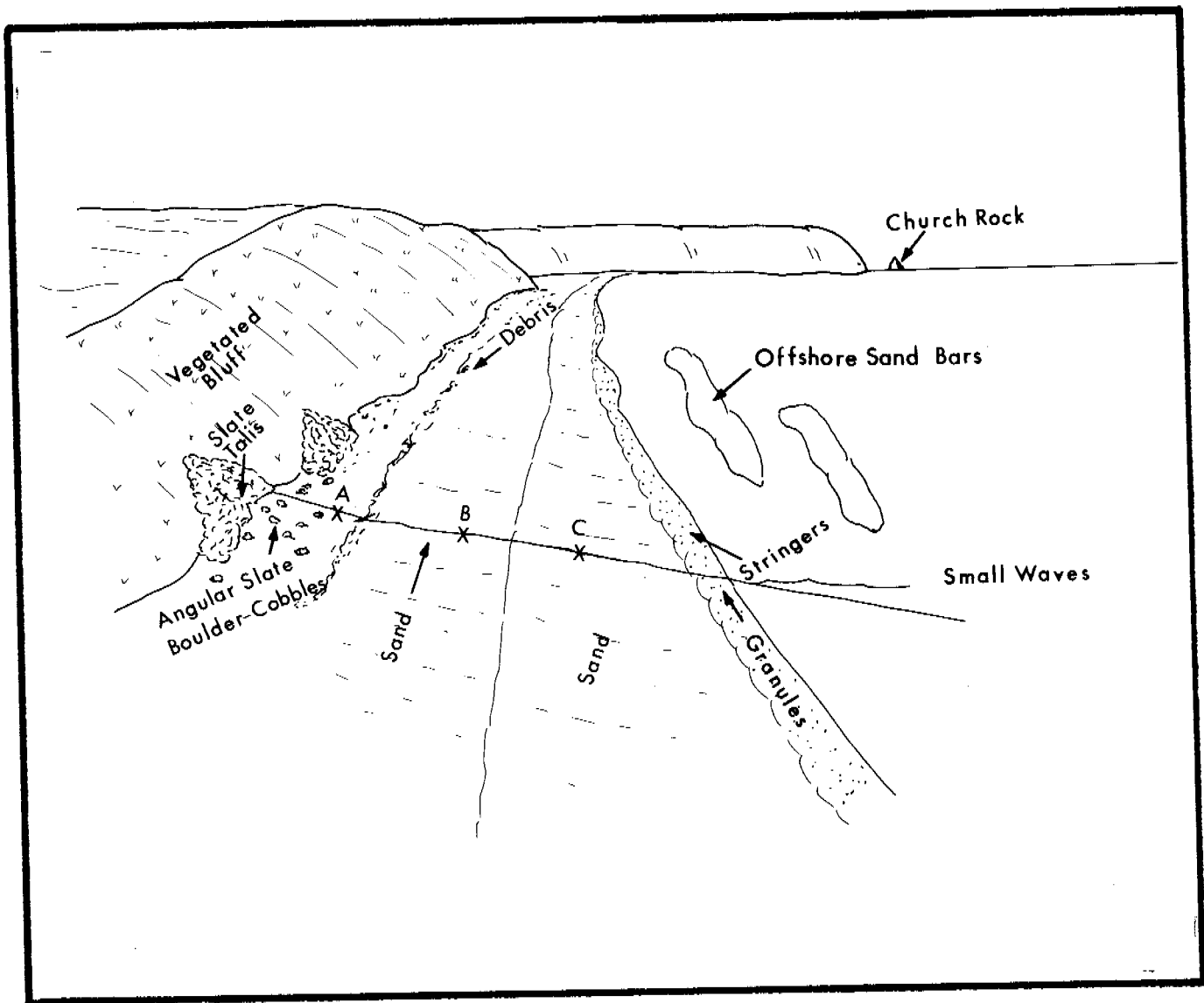


Figure 7. Profile site KBS-42, located on the southern shore of Eschsoltz Bay. This 3 m high scarp is completely vegetated, indicating very infrequent storms are responsible for its form. The beachface is predominantly sand with an accumulation of gravels on the lower beachface only. The offshore slope is extremely flat and covered with offshore bars composed of sand. There are some locally derived gravels at the base of the scarp; these are mostly frost-shattered bedrock outcrops. Oil spill vulnerability is moderate due to the fine grain size, but the very low wave energies could result in longer-term spill damage, up to about 2 or 3 years.

very infrequent severe storm events. The unconsolidated sediments of the tundra are quite thin in this area, and bedrock outcrops in many areas at the beachface. Small talus slopes of frost-shattered angular slate outcrop at the base of the scarp.

The upper beachface is sand covered with gravel derived from the talus slopes. The middle of the beachface is composed mostly of sand with very low relief. At the toe of the beachface, there is a narrow deposit of granules with small sand stringers arranged perpendicular to the shoreline. The offshore slope is very flat and shallow. A series of shore parallel swash bars or sand waves occur on the flat offshore platform, which tends to absorb much of the incoming wave energy.

Figure 8 shows profile site KBS-59 located on the exposed southern shore of the Baldwin Peninsula. The scarp is about 17 m high and covered with vegetation. Again, this indicates very infrequent severe storms from the west. At the base of the scarp, there are a number of unvegetated scarps cut into protruding sections which expose a predominantly mud sediment (glacial). In some areas, there are mud flows out onto the beachface. Where the unvegetated scarps do not occur, there is a perched gravel berm at the base of the vegetated scarp. Fronting the gravel zone is a sandy upper beachface. The lower beachface is dominated by a fine-gravel berm and a sandy zone at the waterline. The offshore slope is considerably steeper than the other scarp areas described above; thus, wave energy is considerably higher and has resulted in a broader beachface with better developed berms.

In general, the heavier the vegetation on the scarps, the less frequent are the storms responsible for their retreat. The normal "every day" energy is responsible for the width of the beachface at the base of the scarp and the sorting of the sediments.

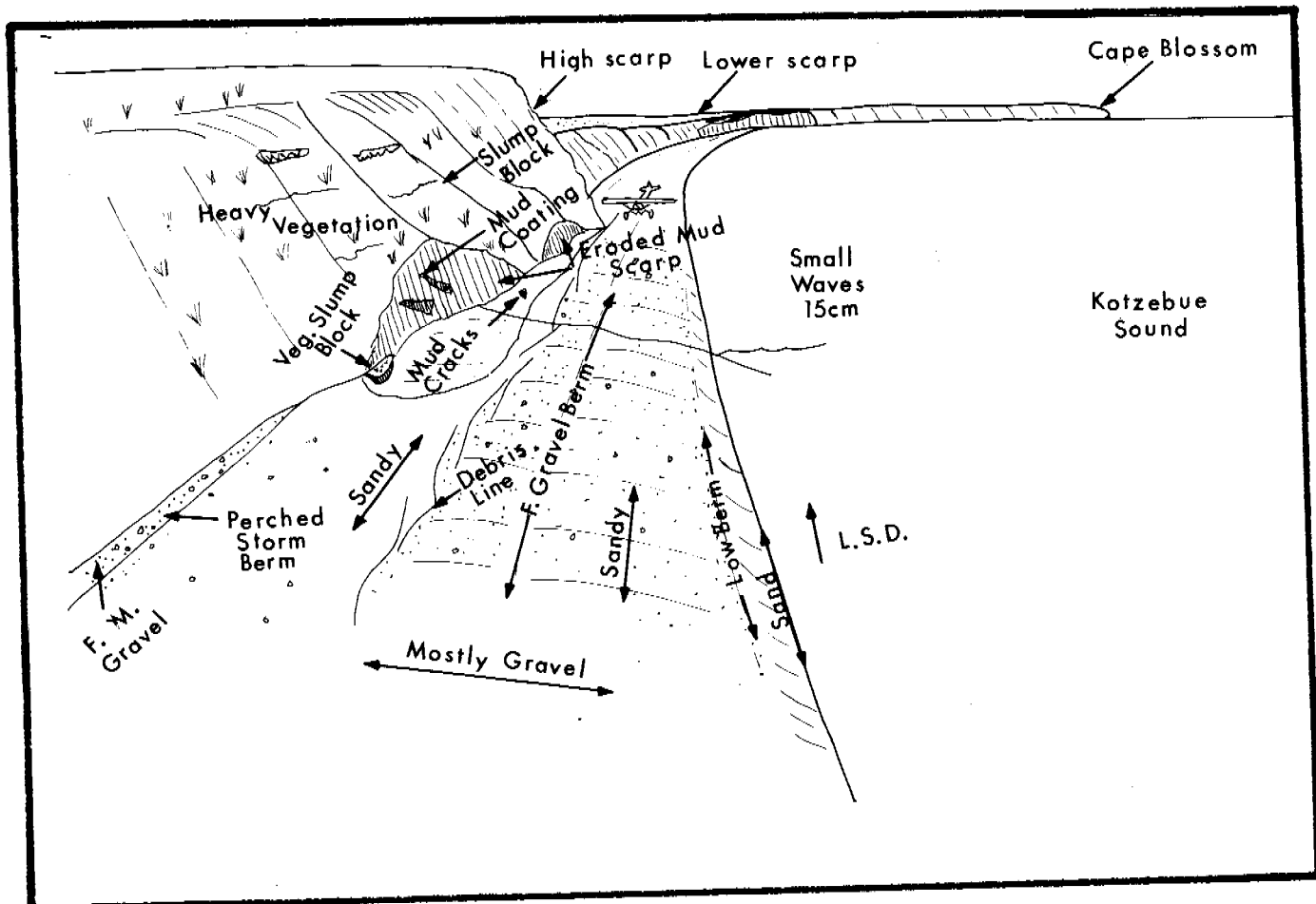


Figure 8. Profile site KBS-59, located on the Southern Baldwin Peninsula shore. This vegetated 17 m high scarp indicates infrequent but violent storms are responsible for its retreat. Some protruding areas are barren and eroding mud onto the upper beachface. Most of the lower beachface is composed of fine gravel, while the upper beachface is sandy. The relatively high wave energy slope is steep compared to the other tundra scarped shorelines. Offshore vulnerability is intermediate.

Finer sediments (silt and clay) are not found on beachfaces subjected to any consistent wave energy. Offshore slope plays an important role in decreasing incoming wave energy. All of the scarped shorelines occur on the inner portions of Kotzebue Sound, mostly on the Baldwin Peninsula and Eschscholtz Bay.

Deltas and river mouth systems. - The Hotham Inlet area is dominated by three major river deltas (the Selawik on the east, the Kobuk in the middle, and the Noatak on the west). Each of these rivers has built a delta into the inlet. The Kobuk River is the most active and has the largest delta; however, only a few of the distributary channels are active at any one time, while the others are abandoned and later became plugged.

In general, the shorelines adjacent to the active channels have very flat offshore slopes of sand and mud and extremely low wave energy. Vegetation grows almost to the waterline and no real beach is present. Where distributary channels have been abandoned for a long period, they become infilled with sand and silt. Since the sediment source to the adjacent shorelines is cut off, these areas of the marsh become erosional. Much of the clay and silt in the offshore is eroded, thus allowing small waves to break on the vegetation fronting the delta. The waves cut a low scarp into the vegetation and, in some cases, a sand and shell berm is formed on top of the eroding marsh front. If the area remains inactive for longer periods, the compaction of the sediment will result in subsidence of the area and the formation of small shallow bays as in front of the Selawik River.

There is a decrease in wave energy from the east to the west in Hotham Inlet, partly a function of fetch and partly a function of bathymetry. Thus, the Noatak Delta on the west has better developed beaches and a marine-dominant delta.

There are a number of smaller deltas and river mouth systems in the area, especially in Eschscholtz Bay. The Buckland River is one of the larger examples. There is a well-developed estuary mouth with surrounding marsh areas and river bars. Beaches are generally narrow, low and sandy. Offshore slopes are quite low with considerable attenuation of wave energy. There is often considerable fine sediment mixed with the river-derived sands. All of these delta environments are extremely vulnerable to severe long-term oil spill damage.

Rock headlands. - Rock headlands are rare in the study area, representing only 49.98 km of the shoreline. The primary area is Cape Thompson. Rock walls more than 1000' high drop directly into the sea. In general, there is no beach at their bases; however, gravel beaches have developed immediately downdrift. The headlands occur where the DeLong Mountains intersect the coast. Waves break directly on these cliffs during all stages of the tide. Erosion along these cliffs is extremely slow.

Discussion. - The six subclasses described above account for most of the variability of shoreline types in the study area. For the purposes of applying our Oil Spill Vulnerability Index, we have devised a coastal geomorphic classification with 10 subclasses. These will be discussed in detail in this report (Oil Spill Vulnerability Section). The 10 subclasses are used because they can describe almost any shoreline environment regardless of climate, wave energy, tidal range, etc. Thus, we use it as a standard for all oil spill-related projects. The base map overlays which have been color coded and enclosed under separate cover with this report use the 10 subclass classification given above. For the purpose of correlation, the following discussion is presented:

Oil Spill Vulnerability Coastal Morphology Classification

1. Exposed rocky headlands - this subclass agrees directly with the 6 subclass scheme given above.
2. Eroding wave-cut platforms - Since there are no shorelines of this type in the study area, they will not be discussed further.
3. Flat, fine-grained sandy beaches - This subclass agrees directly with the 6 subclass scheme given above.
4. Steeper, medium-coarse grained sandy beaches. - There are no shoreline areas in this subclass in the study area.
5. Impermeable exposed tidal flats - Since the study area is micro-tidal, there is only a very small area with shorelines of this type (1.5 km). It will not be discussed in this section (see next section).
6. Mixed sand and gravel beaches - This subclass agrees directly with the 6 subclass scheme given above. Many of the tundra scarps (under the 6 subclass scheme) have sand and gravel beaches fronting them. Where these occur, they have been classed #6.
7. Gravel beaches - This subclass agrees directly with the 6 subclass scheme given above.
8. Sheltered rocky headlands - The only area of this type (9.6 km) occurs in Eschsoltz Bay and will be discussed in the next section.
9. Protected estuarine tidal flats - Many of the tundra scarps (in the 6 subclass scheme) have very flat shallow offshore zones fronting them. Where these occur, they have been classed #9 on the charts.
10. Protected estuarine marshes - This subclass correlates with the delta and river mouth systems subclass given in the 6 subclass scheme. It also includes any lagoonal shorelines that have vegetation growing very close to the waterline or extremely sheltered low vegetated tundra scarps with narrow or absent beachfaces.

Table 4

Subclass	Kilometers of shoreline	% of total shoreline
1	49.98	2.2
2	0	0
3	257.04	11.1
4	0	0
5	1.428	.07
6	610.47	26.3
7	37.84	1.63
8	8.57	.4
9	671.16	28.9
10	<u>681.87</u>	<u>29.4</u>
	2318.36	100

Table 4 above shows the 10 subclasses used for the base map overlay sent with this report. It also shows the shoreline kilometers and percent of the total shoreline represented by each subclass.

OIL SPILL VULNERABILITY

Introduction

As oil exploration and development continue to escalate in Alaska, the potential for oil spills in the coastal environment increases. Any production facilities or support facilities located in the Kotzebue Sound area would subject the adjacent shorelines to potential oil spills. Large spills or chronic small spillages could result in serious environmental damage or alteration. Estuarine and open marine assemblages could be seriously affected by oil spills and resulting cleanup efforts, thus reducing or eliminating their productivity, and, therefore, affecting the food chain. It is unclear, at this time, what effect oil spills would have on economic species harvested by the small fishing villages within

the area.

Trends in sedimentation can also be altered by oil spills. Some of the more sensitive geomorphic environments can release oil for periods of time in excess of 10 years. Thus, development of this area will require careful evaluation of the possible impacts of potential oil spills. The Oil Spill Vulnerability Index developed by our group has been based on detailed field studies of 3 major oil spills (Urquiola - Spain; Metula - Chile; and Amoco Cadiz - France) and 7 minor spills in specific coastal environments (mangrove areas, frozen estuaries and river, coral reefs, etc.). Thus, we have had the opportunity to analyze the process-response of oil spills in a wide variety of coastal environments, with variable sediment types, marine energy, climate, and in various seasons.

Cold Water Spills

There is abundant literature dealing with case studies of the numerous major and minor oil spills that have taken place in the coastal waters of the lower 48 states and around the world. Predictive models for oil spill dispersal, spreading, bio-degradation and physical degradation have been developed from these studies. The Arctic and sub-Arctic areas, however, have been, to a large extent, omitted due to the difficulties inherent in any study of these environments and a general lack of actual oil spills in these environments from which to base detailed case studies. The Arrow oil spill in Chedabucto Bay, Nova Scotia, probably comes closest to a comparative model for the sub-Arctic. However, the cleanup effort and later studies (Owens and Drapeau, 1973; Owens, 1973; Drapeau, 1973; Owens, 1971; and Owens and Rashid, 1976) made very little reference to the special problems encountered as a result of the colder environment (i.e. oil on ice and snow; ice-oil interaction with beach sediments; oil dispersal in heavily-iced environments, etc.). Our investigation of the Buzzards Bay oil spill (Ruby et al., 1977) and the Ethyl H. spill in the frozen Hudson River have

given new insight into the extremely limiting effects of oil spills in ice-choked waters.

Further, evaporation losses and biodegradation are slower in colder environments. Biodegradation can be reduced as much as 90% in water of 0°C when compared to water of 25°C (Robertson, 1972). Isakson et al., (1975) states that burning may be the only feasible method of cleaning oil spills in iced areas; however, this may represent a trade of one type of pollution for another. During the Buzzards Bay spill cleanup, burning was an effective method for cleaning oil which was not accessible from the shore. Only a small amount of particulate matter resulting from the fires was noticed.

Finally, tidal currents and surface winds in the study area can disperse the spilled oil in an unpredictable manner, making it very difficult to recover before it impacts on nearby shorelines. A report addressing the problem of winter ice in Kotzebue Sound will be included with our next progress report. Although the ice plays a major role in containing and transporting spilled oil, it will not change the classification given in this report.

Conclusions

In summary, the potential for oil spills in Alaskan waters is increasing as exploration and development continue to escalate. There is a complex interaction of marine processes during an oil spill which can make it extremely difficult to predict the track and dispersal pattern of an oil spill. However, numerous case studies permit the construction of an oil spill vulnerability scale which is based primarily on the longevity of spilled oil within each geomorphic environment, and the biologic sensitivity and natural cleaning ability of those environments. This scale, developed by our group, has been applied to Lower Cook Inlet (Michel et al., 1977; Hayes et al., 1977); the Copper River delta (Ruby and Hayes, 1978); the Gulf of Alaska (Ruby, 1977) and is here modified for Kotzebue Sound. A

brief abstract of the earlier applications is also available (Gundlach et al., 1977).

Environmental Vulnerability to Oil Spills

This scale has been devised on the basis of the case studies mentioned above and a careful study of the literature. It is based primarily on the longevity of oil in each sub-environment, which is generally a function of the intensity of the marine processes, sediment size and transport trends. The biologic sensitivity has also been utilized to modify the ratings of the various environments.

Coastal environments are listed and discussed below in order of increasing vulnerability of oil spills. These subclasses correspond to the 10 subclasses given in the previous section.

Vulnerability Scale (OSVI)

1. Straight rocky headlands:

Most areas of this type are exposed to maximum wave energy. Waves reflect off of the rocky scarps with great force, readily dispersing the oil. In fact, waves reflecting off the scarps at high tide tend to generate a surficial return flow that keeps the oil off the rocks (observed at the Urquiola spill site in Spain). Cape Thompson is a typical example of this environment. Even if oiled, natural cleaning will only require a few days or weeks. No human intervention is necessary.

2. Eroding wave-cut platforms:

These areas are also swept clean by wave action. All of the areas of this type at the Metula spill site had been cleaned of oil after one year. The rate of removal of the oil is a function of wave climate. In general, no cleanup measures are needed for this type of coast. However, there can be large biologic populations in these areas. There are no wave cut platforms in the Kotzebue Sound area.

3. Flat, fine-grained sandy beaches:

Beaches of this type are generally flat and hardpacked. Oil that is emplaced on such beaches will not penetrate more than a few centimeters at most. Usually, the oil will be deposited on the surface of the sand where it can be removed by elevated scrapers or other road-grading machinery. Furthermore, these types of beaches change slowly, so sand deposition and resultant burial of oil will take place at a slow rate. If left to natural processes, these beaches will be cleaned within several months. Almost the entire southern arm of the Sound falls into this category.

4. Steeper, medium to coarse-grained sandy beaches:

On these beaches, the depth of penetration would be greater than for the fine-grained beaches (though still only a few centimeters), but rates of burial of the oil would be greatly increased. Based on our earlier studies, it is possible for oil to be buried as much as 50-100 cm within a period of a few days on beaches of this class. In this situation, removal of the oil becomes a serious problem, since removal of the oiled sediments will often result in large scale erosion, as the beach changes into a new equilibrium state. This was a common problem encountered during the clean-up of the Arrow oil spill in Chedabucto Bay, Nova Scotia (Owens and Rashid, 1976). Another problem is that burial of the oil preserves it for release at a later date when the beach erodes as part of the natural beach cycle, thus causing longer term pollution of the environment. There are a few beaches of this type in Kotzebue Sound.

5. Impermeable exposed tidal flats:

One of the major surprises of the study of the Metula site was the discovery that oil had not remained on the mud flats. At the Urquiola site, oil was observed as it became refloated with rising tides on the mud flats. Penetration of the oil is prevented by the extremely fine sediment size, saturated with water. Therefore, if an oiled tidal flat is

subject to winds and currents, the oil will tend to be removed, although not at the rapid rate encountered on exposed beaches. Mechanized cleanup is considered impossible. These are often areas of high biologic importance. There are no exposed tidal flat areas in the Kotzebue Sound study area.

6. Mixed sand and gravel beaches:

On beaches of this type, the oil may penetrate several centimeters, and rates of burial are quite high (a few days in Spain). Any attempt to remove the oiled sediment will result in considerable erosion. The longevity of the spilled oil at the Metula site, particularly on the low-tide terraces and berm top areas, attests to the high susceptibility of this type of beach to long-term oil spill damage. Natural cleaning may require many years. There are many long stretches of this type of shoreline along the northern side of Kotzebue Sound.

7. Gravel beaches:

Pure gravel beaches allow the oil to penetrate to considerable depth (up to 45 cm in Spain). Furthermore, rapid burial is also possible. A heavily-oiled gravel beach will be impossible to clean up without completely removing the gravel. Natural cleaning will be quite slow for this type of beach; the exact time required will depend on the intensity of the marine processes. Pure gravel beaches occur downdrift of many of the rocky headlands in the area, as well as on the Baldwin Peninsula and much of Point Hope.

8. Sheltered rocky headlands:

Our experience in Spain indicates that oil tends to stick to rough rocky surfaces. In the absence of abrasion by wave action, oil could remain on such areas for years, with only chemical and biological processes to degrade it. There are a number of sheltered rocky headlands and cliffs within Eschscholtz Bay. However, they represent a very small percentage of the total shoreline.

9. Protected estuarine tidal flats:

If oil reaches a quiet, protected estuarine tidal flat, it will remain there for long periods because natural cleaning progresses at an extremely slow rate. Because of the low intensity of marine process parameters, removal of the oil will have to be accomplished by natural chemical and biogenic processes. This will take many years, dependent on the amount of oil deposited. Because of their high biologic populations, these environments are very sensitive to the toxic effects of oil. A number of areas of this type exist in Eschscholtz Bay and in Hotham Inlet.

10. Protected estuarine salt marshes:

In sheltered estuaries, oil from a spill may have long-term deleterious effects. We observed oil from the Metula on the salt marshes of East Estuary, in the south shore of the Strait of Magellan, that had shown essentially no change in 1½ years. We predict a life span of at least 10 years for that oil. These areas are extremely important biologically, supporting large communities of organisms. The inner parts of Hotham Inlet and most of the river estuaries fall into this class.

Applications to Kotzebue Sound

Oil spill vulnerability. - Utilizing a combination of the vulnerability classification just described and a classification of coastal morphology described earlier, it is possible to delineate the coastal environments of Kotzebue Sound with respect to oil spill vulnerability. Generally, the Sound is a high risk area, especially in the backbarrier lagoons and delta areas. Many of the environments have a high risk rating as explained below. In addition, the entire study area is remote and almost inaccessible to standard clean-up operations. Of all the environments, the erosional shorelines in rock scarps near Cape Thompson are most apt to be rapidly cleaned by natural processes. The marsh and tidal flat areas in Hotham Inlet and behind barrier islands and associated with small rivers are

extremely high risk areas. The remainder of the beaches of the study area are variable, depending essentially upon the wave energy and beach grain size. Oil burial can be a problem with many of the sand and gravel beaches.

Using the ten morphological subdivisions just discussed, a risk classification has been devised and applied to Kotzebue Sound study area.

Oil longevity within these risk classifications is estimated as follows:

<u>Risk Class</u>	<u>Longevity</u>
1-2	A few days to a few weeks
3-4	A month to six months
5-6	Less than 12 months
7-8	A year or 2 to as much as 8 yrs
9-10	Up to 10 years

Notice, the risk class numbers correlate to the 10 geomorphic subclasses given above.

CONCLUSIONS

Table 5 shows that 60% of the 2318.65 km of shoreline classified falls into the high risk categories of 7-10. Oil longevity within these areas is estimated to be a few years to more than 10 years. However, in some instances, certain natural physical processes may act to prevent or limit oil spills from penetrating into these high risk zones. The barrier islands and spits in the area will act as natural barriers to spilled oil. Where they are continuous, they should totally prevent oil entering the lagoons behind them unless there is a severe storm with resultant overwash of the barriers. Those barriers with tidal inlets will act as natural barriers to spilled oil except for the tidal exchange through the inlets. Once oil gets into the lagoon, the barrier islands will then tend to hold it in these very sensitive areas. Thus, booming of these inlets is sug-

gested. Boom locations are indicated on the base maps.

Fluvial flushing may also help to prevent oiling of the river mouth areas and the Hotham Inlet shorelines. The fresh water surficial flow should act as a barrier to floating oil. Thus, the high and low risk environments must be analyzed in detail to ascertain the actual probability of spilled oil reaching them.

Finally, there is the problem of the study area's remoteness and relative inaccessability. Within the area, there are only 4 small towns. Only Kotzebue has a jet airport. Other than these villages, the area can be considered to be virtually uninhabited. Additionally, there are absolutely no roads connecting these towns to either broad sections of the coast or each other. Most of the land area is covered by tundra, lakes and rivers, or by mountains. Thus, any attempted mechanized cleanup of a potential oil spill will have to deal with rather severe logistical problems. All equipment will have to be transported by air or by ship considerable distances to the spill site.

Table 5.

<u>Km of shoreline</u>	<u>% of shoreline</u>	<u>Discussion</u>	<u>Risk Classification</u>
39.27	1.8	Oil easily removed by wave erosion; some problems in areas of gravel accumulation and pocket beaches. Cape Thompson area.	1-2
249.9	10.8	Generally low risk areas. Fine sands prevent penetration of oil. Possibility of oil burial. Barrier islands on southern Sound shoreline.	3-4
605.76	26.0	Mud tidal flats do not permit deep penetration of the oil, but the relatively low energies require as much as a year to remove the oil. Sand and gravel beaches are highly prone to oil burial and thus fall into this risk class. Almost the entire northern shore of the Sound falls into this class.	5-6
110.67	4.8	These areas include pure gravel beaches and sheltered rock headlands and cliffs. Oil will remain for periods of years in these areas. Most of these areas occur on the Baldwin Peninsula and downdrift of rock headlands.	7-8
1313.03	56.6	These highly sensitive marsh and lagoonal areas can retain oil for more than 10 years. In addition, these areas are of extreme biological importance. Most of Hotham Inlet, all coastal lagoons and most of the small river mouth areas fall into this class. Additionally, very sheltered poorly developed beaches with vegetations close to the waterline fall into this class.	9-10

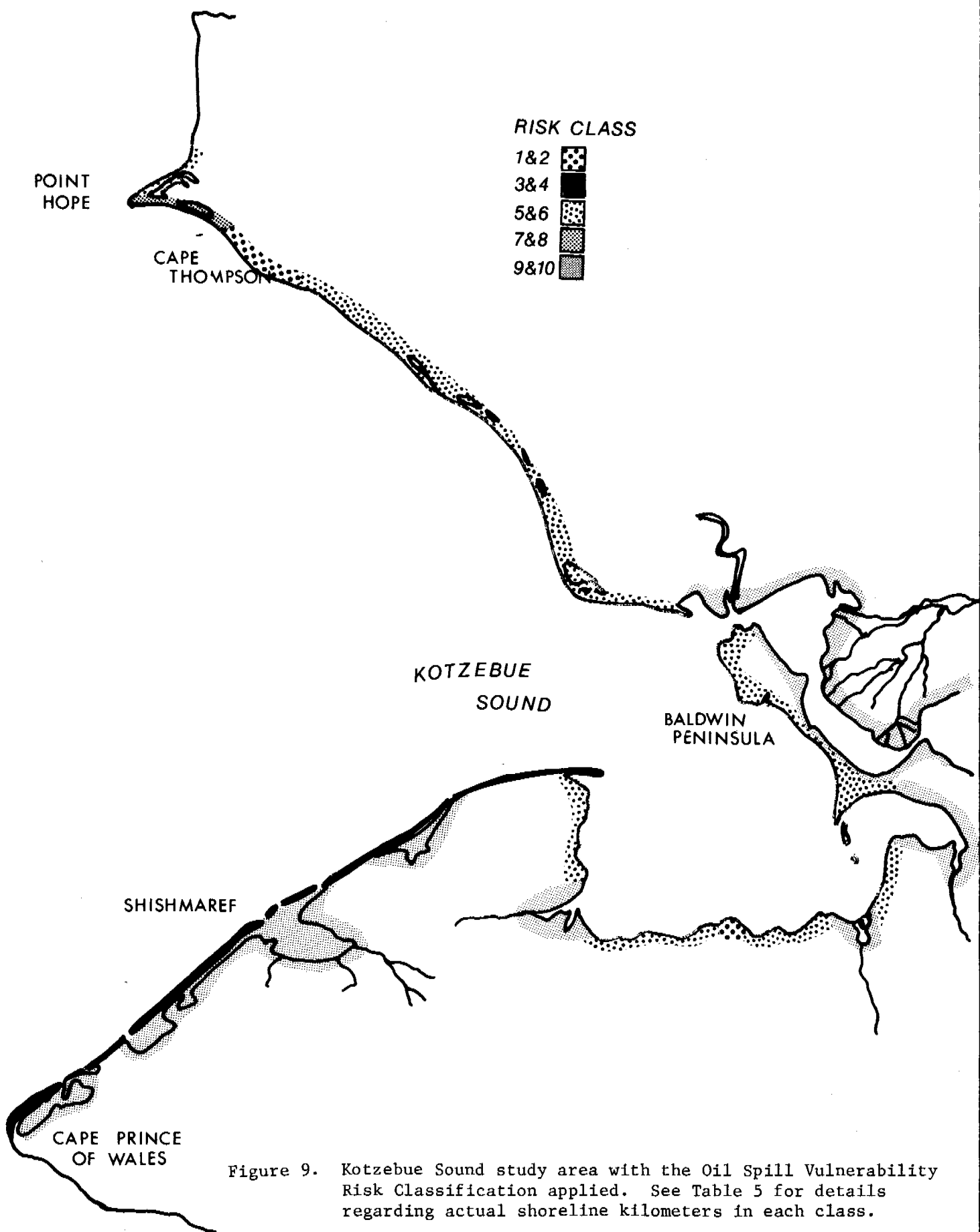


Figure 9. Kotzebue Sound study area with the Oil Spill Vulnerability Risk Classification applied. See Table 5 for details regarding actual shoreline kilometers in each class.

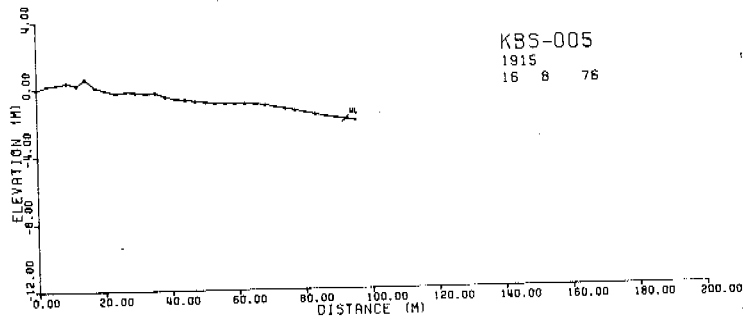
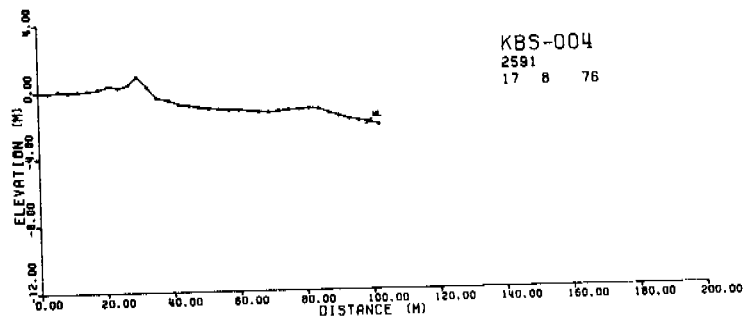
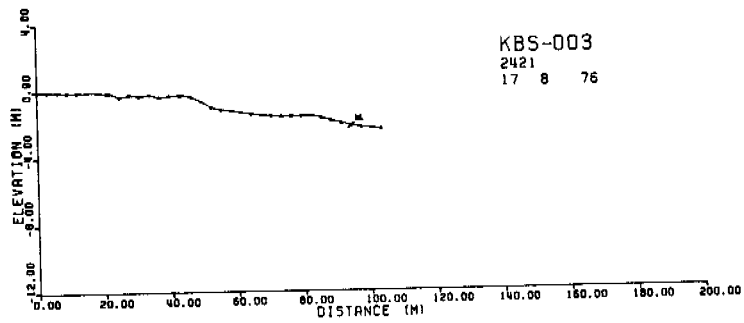
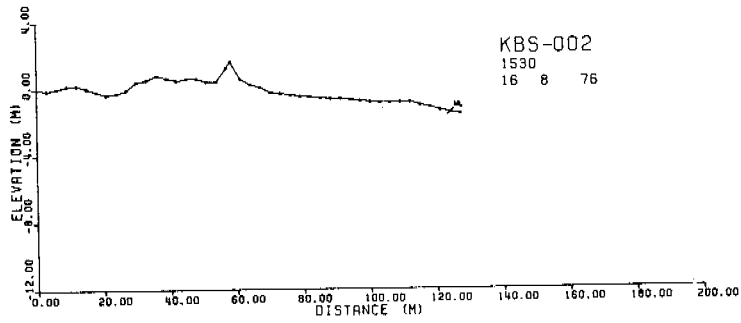
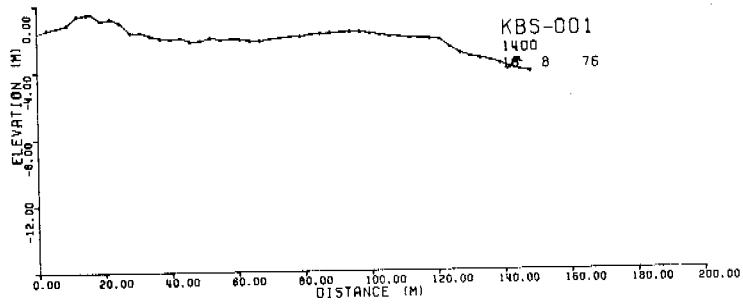
REFERENCES CITED

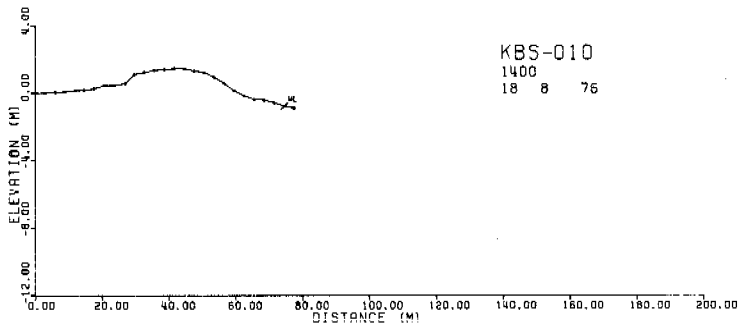
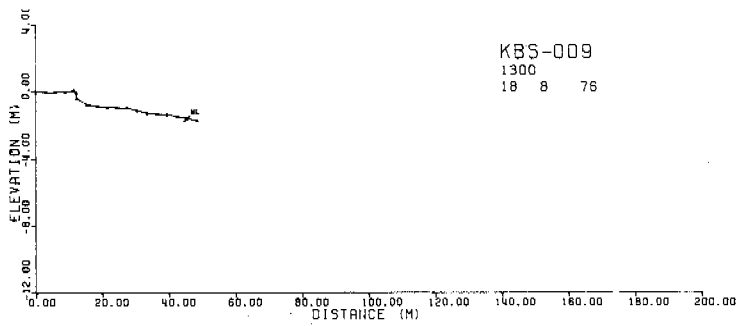
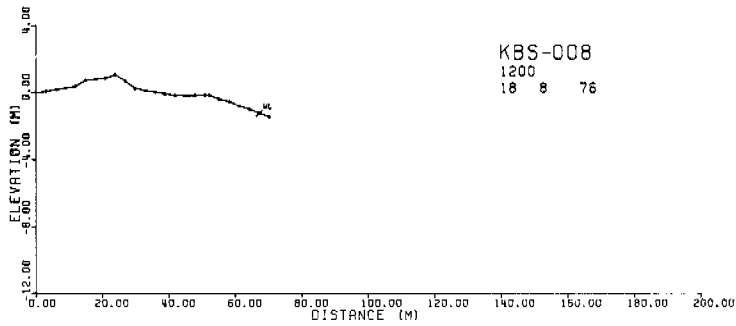
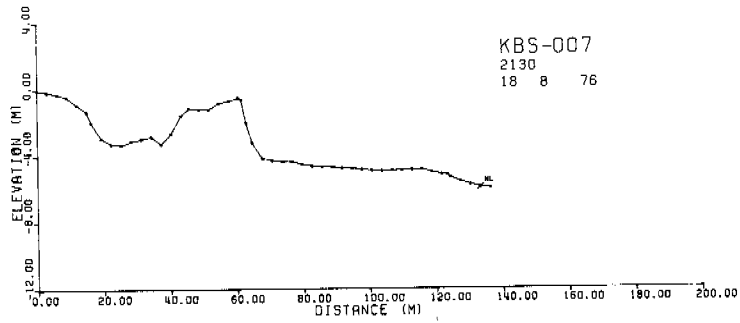
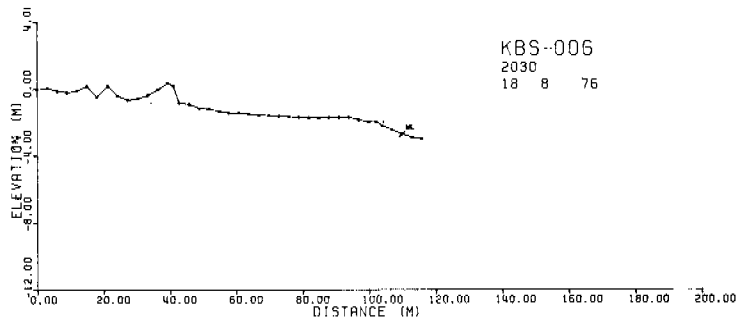
- Brower, William A., Searby, Harold W., Wise, James I., Diaz, Henry F. and Prechtel, Anton S., 1977, Climatic atlas of the outer continental shelf waters and coastal regions of Alaska, Vol. III, AEIDC, Anchorage, Alaska, 409p.
- Drapeau, G., 1973, Natural cleaning of oil polluted seashores: Proc. 13th Coastal Eng. Conf., Vancouver, B.C., p. 2557-2575.
- Gundlach, E. R., Hayes, M. O., Ruby, C. H., and Nummedal, D., 1977, Application of a shoreline vulnerability index for predicting oil spill impact: Abstr., Poster Session, Coastal Soc., Annual Meeting, Seattle, Washington.
- Hayes, M. O., Michel, J. and Brown, P.J., 1977, Lower Cook Inlet, Alaska: Application of oil spill vulnerability index: 4th Inter. Conf. on Port and Ocean Eng. under Arctic Conditions, St. Johns, Newfoundland, p. 832-843.
- Isakson, J.S., et al., 1975, Comparison of ecological impacts of postulated oil spills at selected Alaskan locations: USCG Rept. No. CG-D-155-75, Vol. 1, 633p., Vol. 2, 865p.
- Michel, J., Hayes, M. O. and Brown, P. J., 1978, Lower Cook Inlet - coastal morphology and vulnerability to oil spill damage: Environmental Geol., Vol. 2(2), p. 107-117.
- Owens, E.H., 1971, The restoration of beaches contaminated by oil in Chedabucto Bay, Nova Scotia: Marine Sci. Branch, Ottawa, Can., Manus. Rep. Serv., No. 19, 75p.
- Owens, E.H., 1973, The cleaning of gravel beaches polluted by oil: Proc. 13th Coastal Eng. Cong., Vancouver, B.C., p. 2543-2556.
- Owens, E.H., and Drapeau, G., 1973, Changes in beach profiles at Chedabucto Bay, Nova Scotia, following large scale removal of sediments: Can. Jour. Earth Sci., 10, p. 1226-1232.
- Owens, E.H., and Rashid, M.A., 1976, Coastal environments and oil spill residues in Chedabucto Bay, Nova Scotia: Can. Jour. Earth Sci., 13, p. 908-928.
- Robertson, B., Arhelger, S., Kinney, P.J., and Button, D. K., 1973, Hydrocarbon biodegradation in Alaskan waters: Center for Wetlands Resources, Louisiana State Univ., LSU-SG 73-01.
- Ruby, C.H., 1977, Coastal morphology, sedimentation and oil spill vulnerability - northern Gulf of Alaska, Tech. Rept. No. 15-CRD, Dept. of Geology, Univ. of South Carolina, 223p.

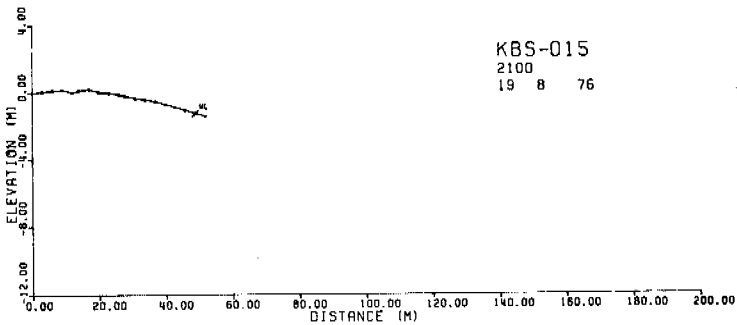
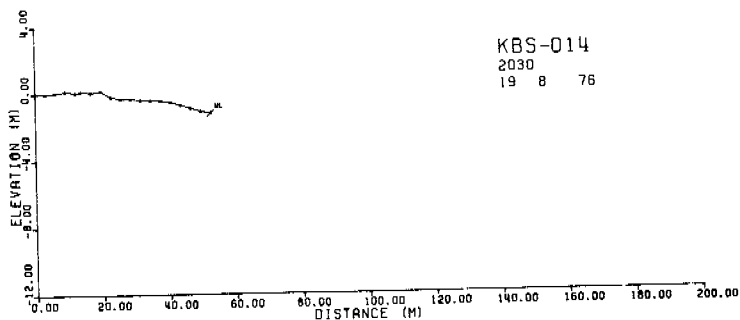
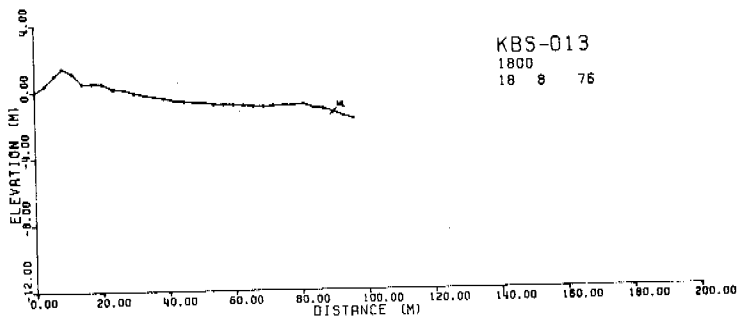
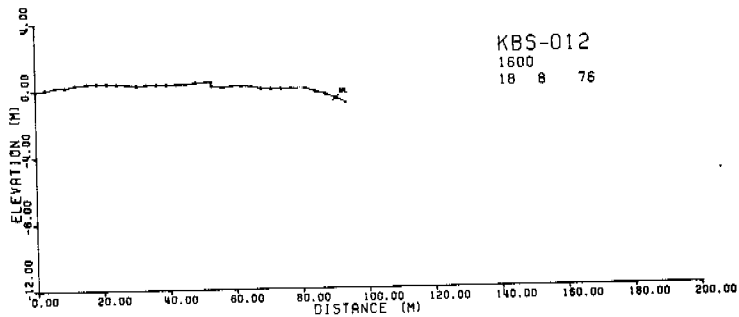
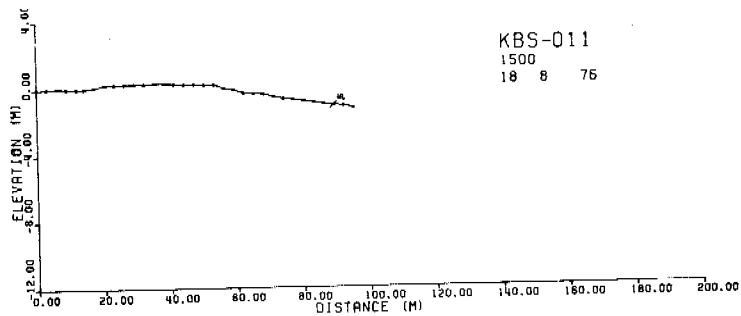
- Ruby, C.H. and Hayes, M. O., 1978, Application of an oil spill vulnerability index to the Copper River Delta, Alaska: Proceedings, Coastal Zone '78, San Francisco, Cal., March, p. 2204-2220.
- Ruby, C.H., Ward, L.G., Fischer, I.A. and Brown, P.J., 1977, Buzzards Bay oil spill - an Arctic analogue: 4th International Conf. on Port and Ocean Eng. under Arctic Conditions, St. Johns, Newfoundland, Sept., p. 844-856.
- Selkregg, L., 1975, Alaska regional profiles, Arctic region, AEIDC, Anchorage, Alaska, 218p.

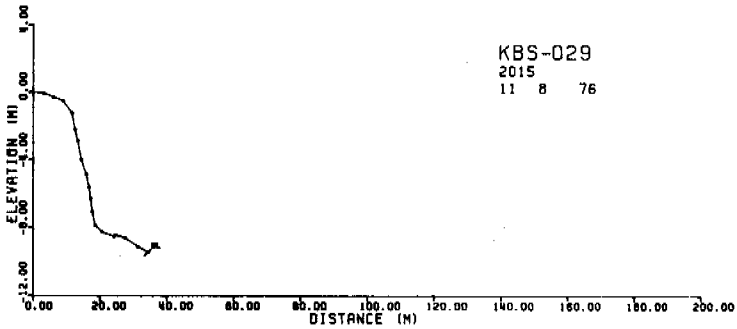
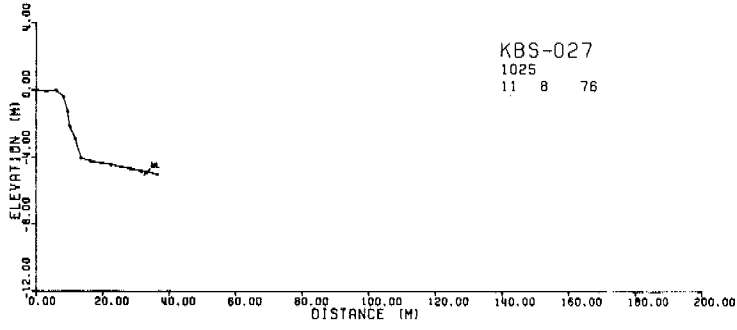
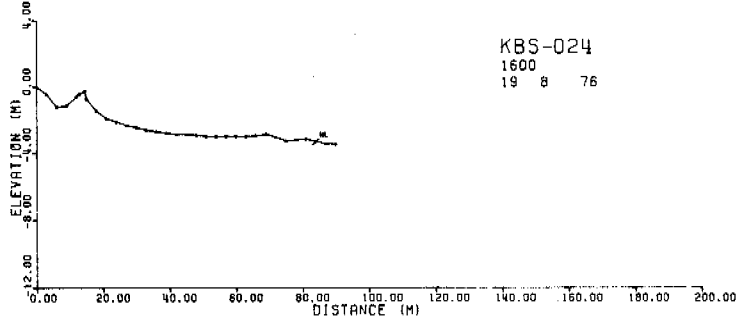
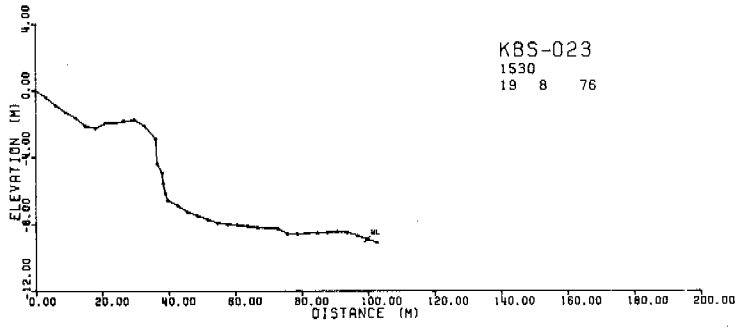
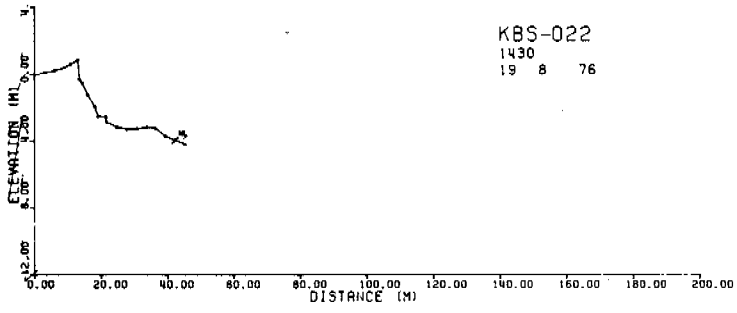
APPENDIX

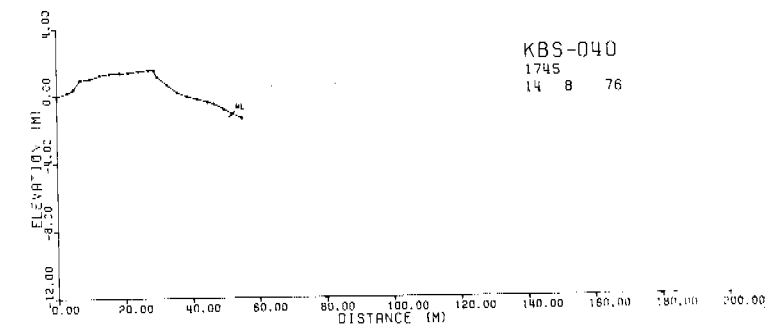
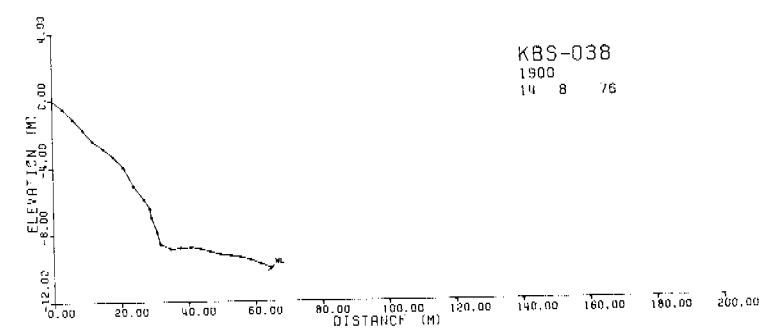
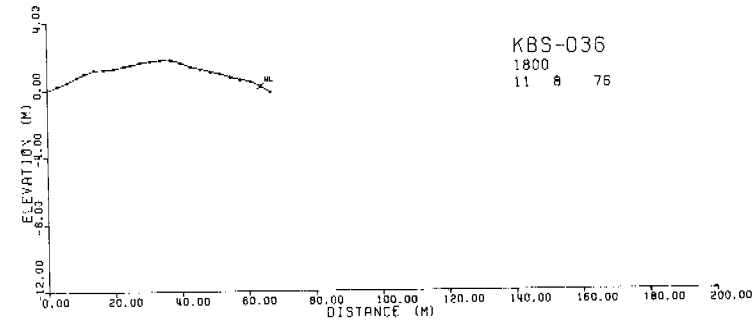
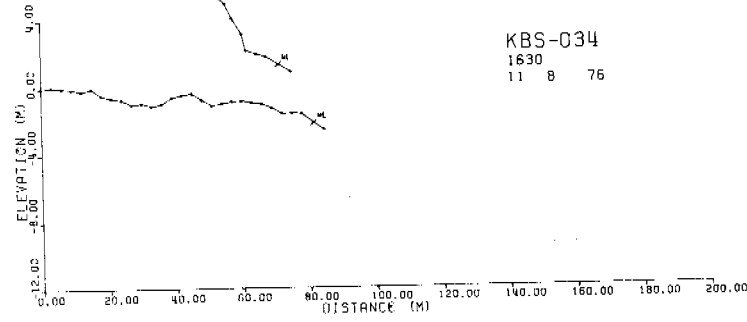
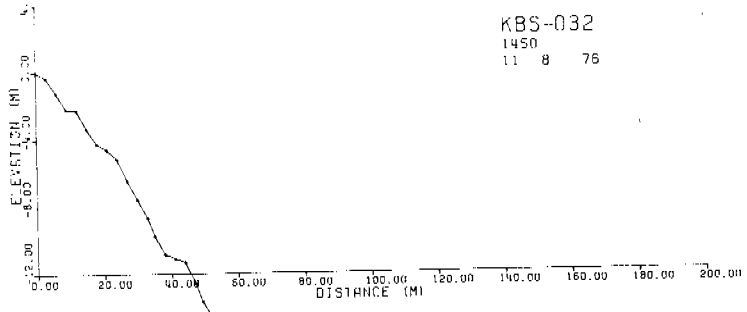
Computer Plotted Profiles from Kotzebue Sound

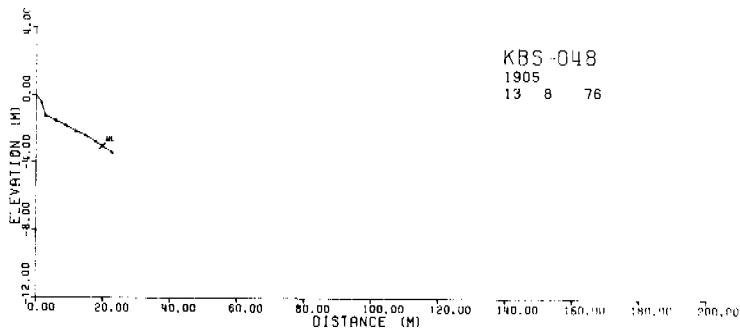
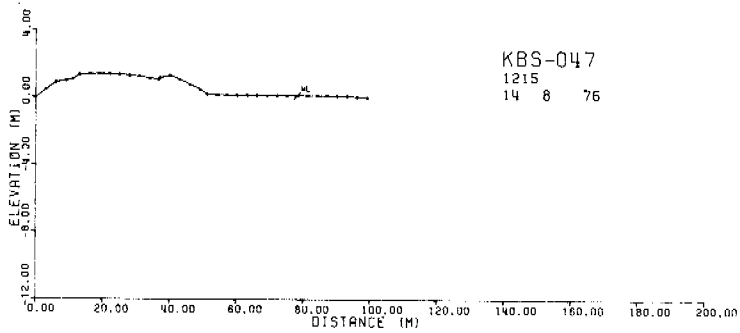
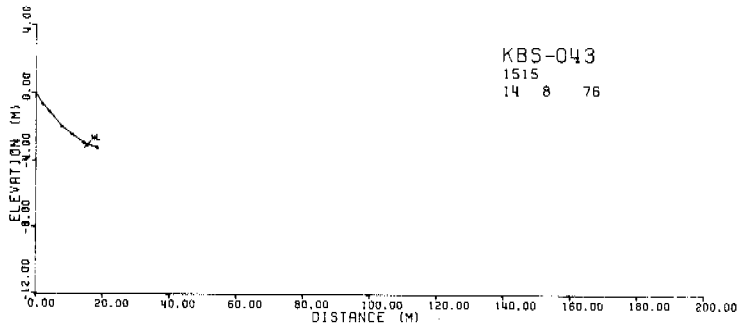
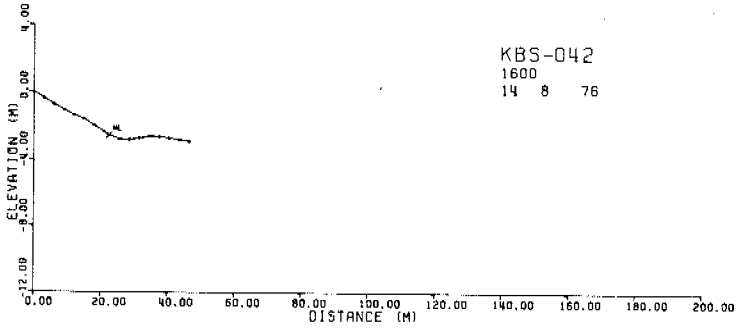
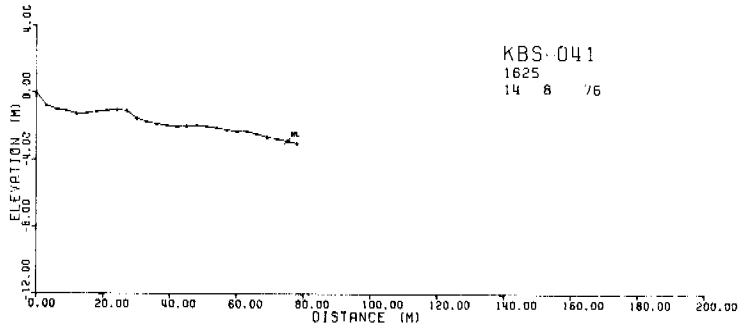


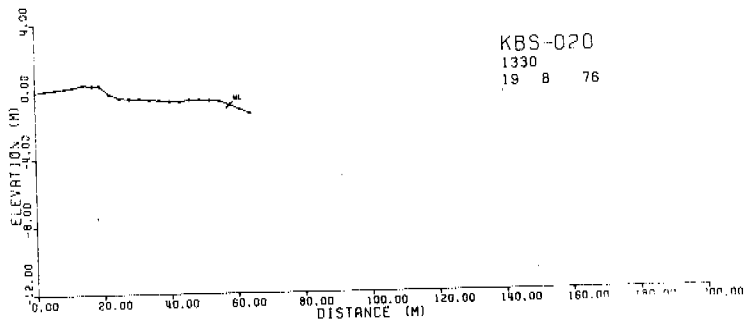
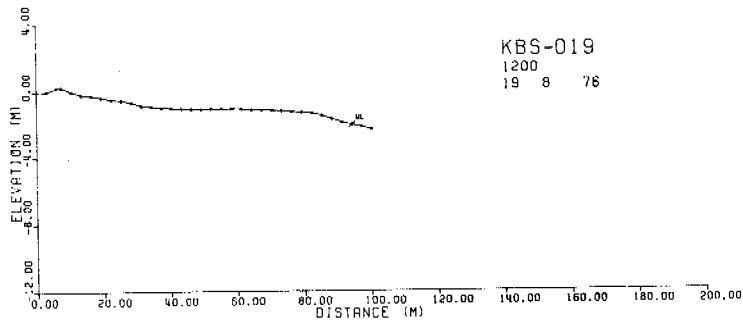
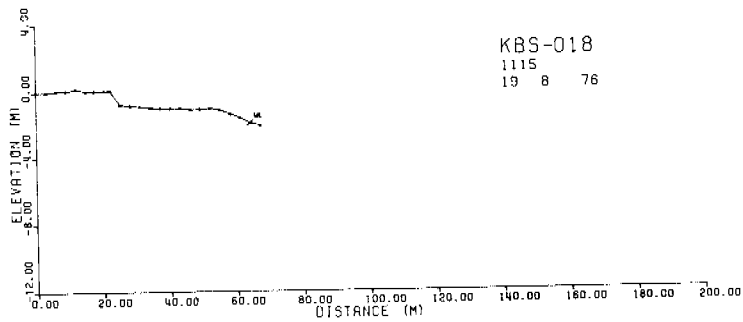
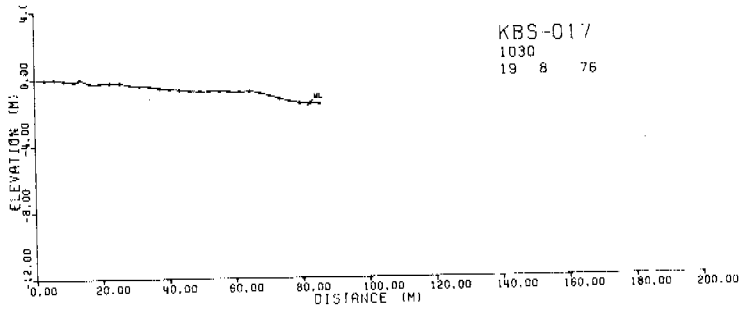
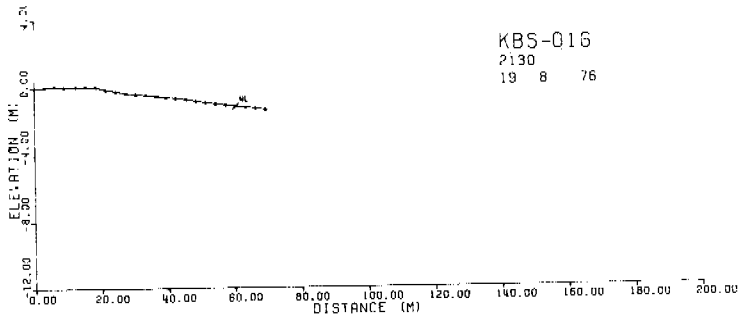


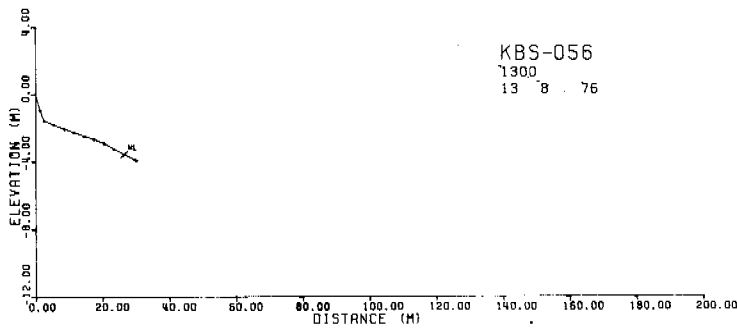
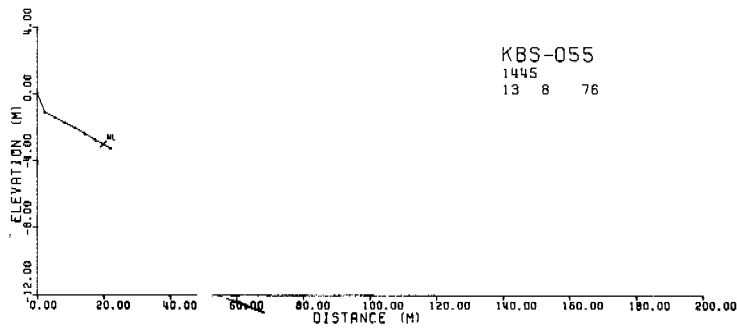
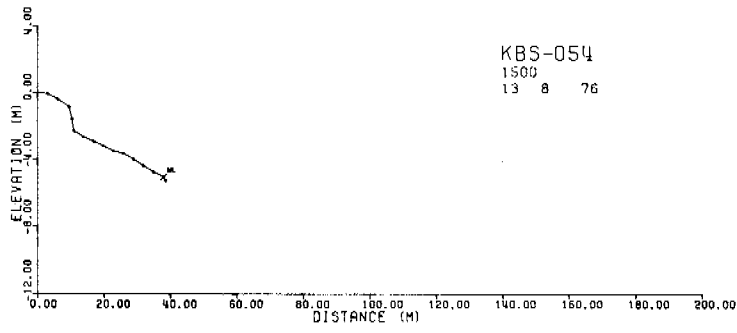
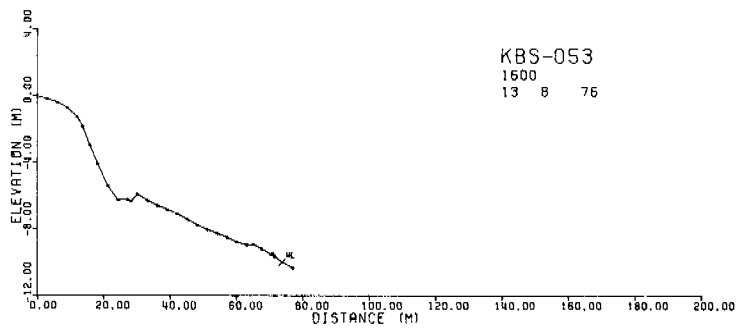
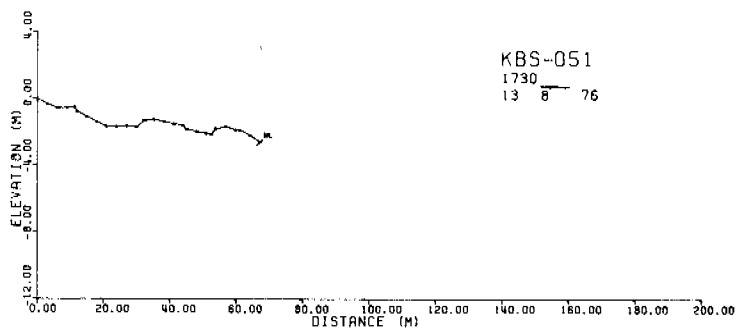


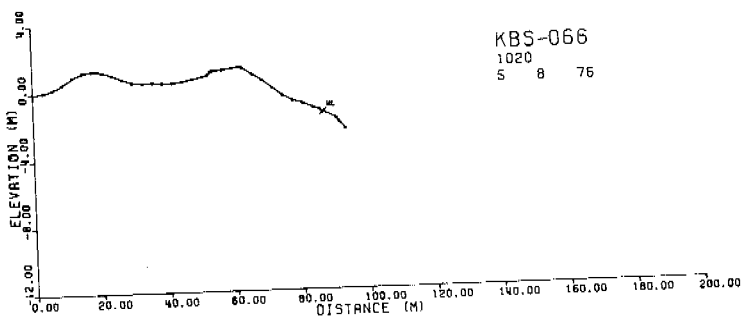
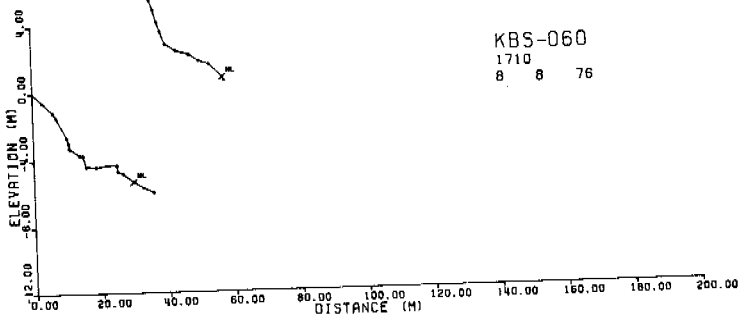
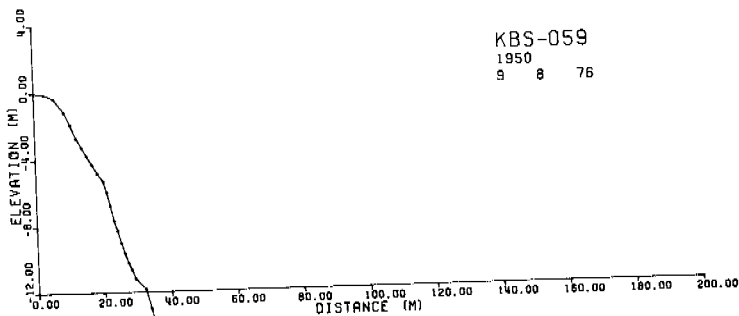
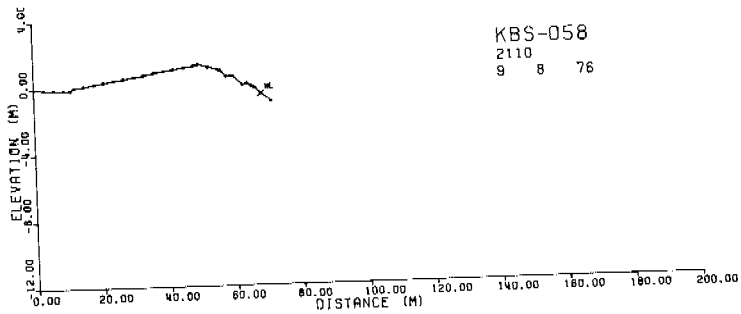
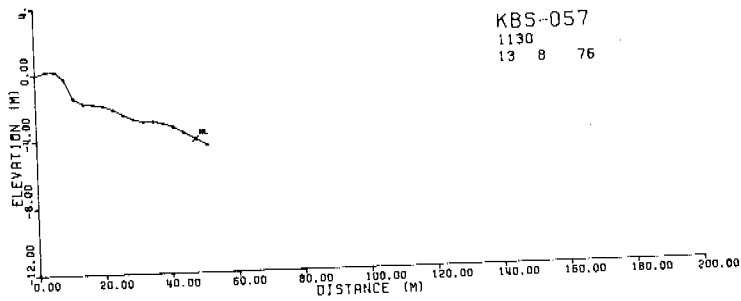


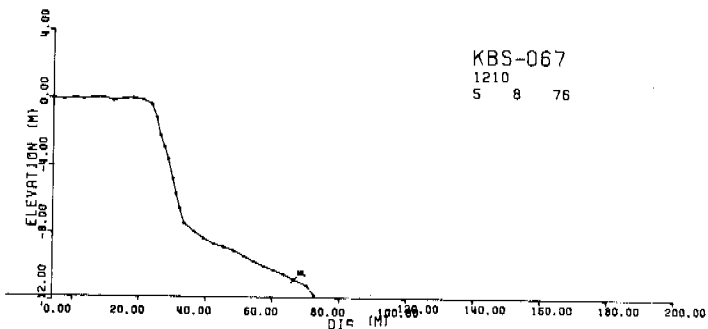
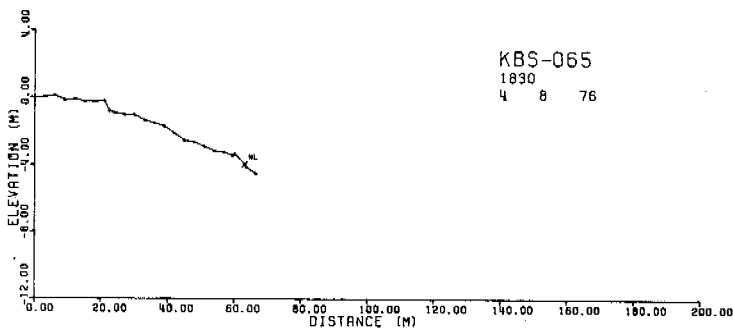
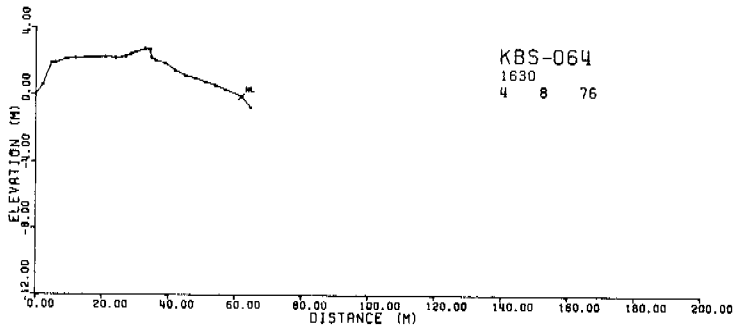
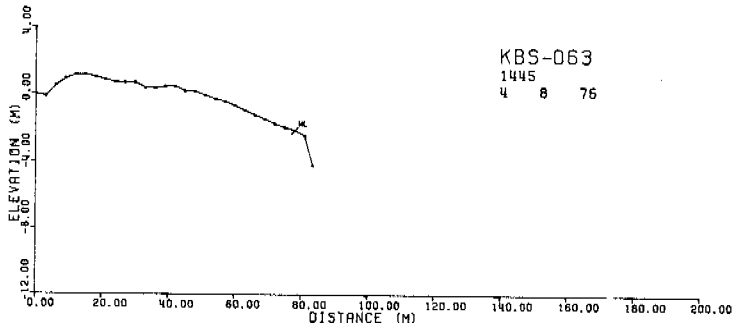
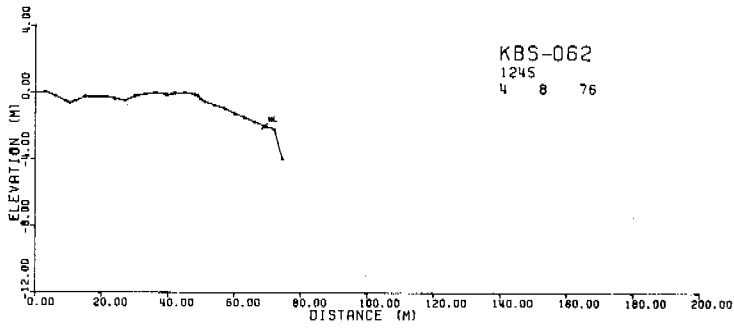


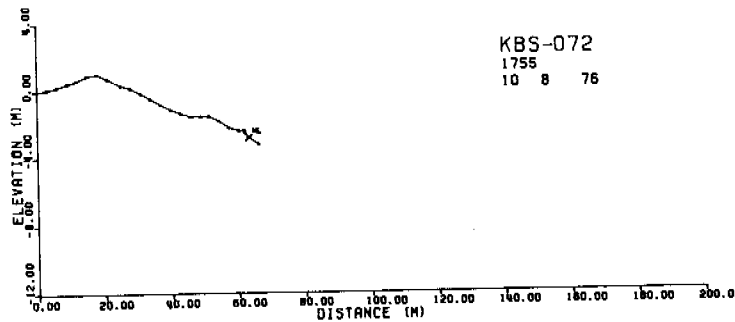
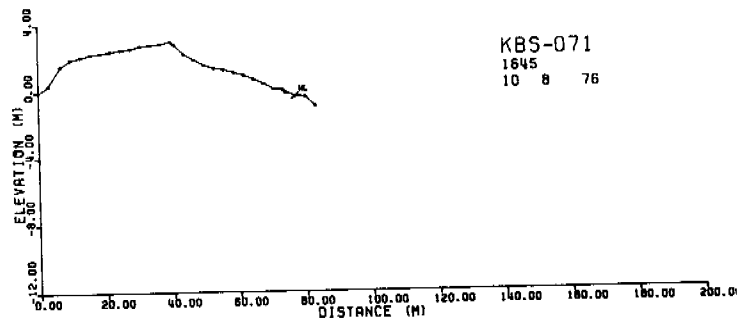
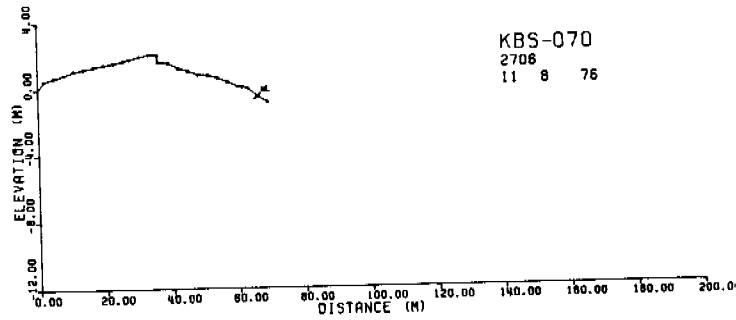
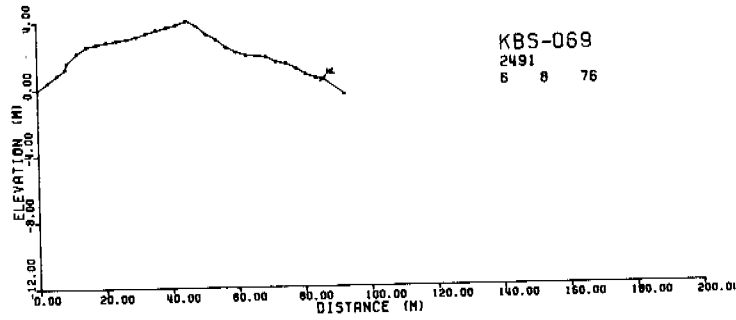
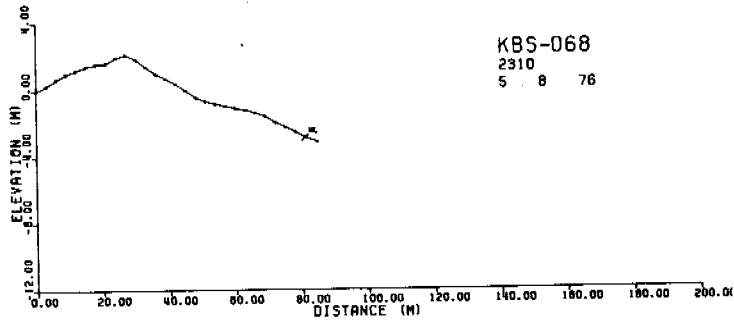


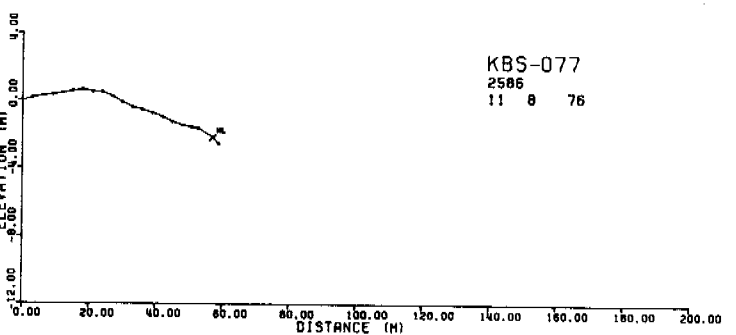
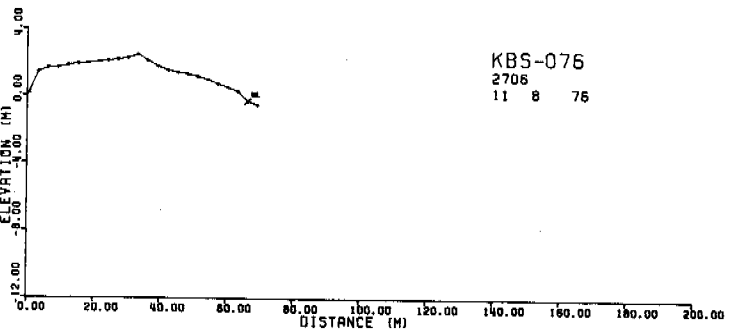
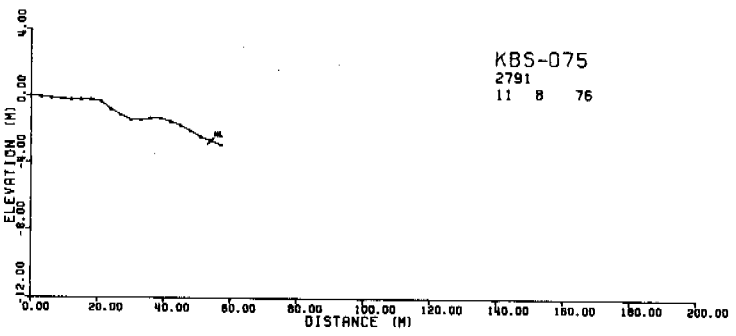
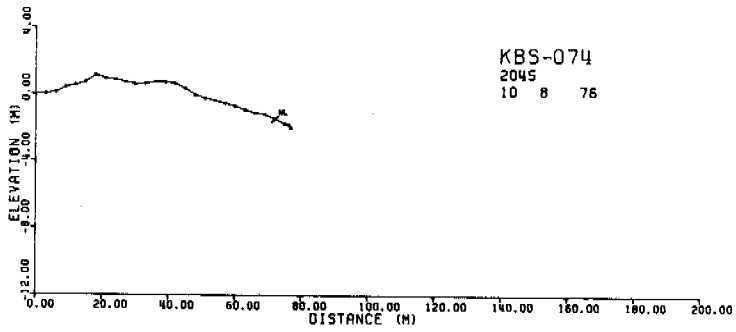
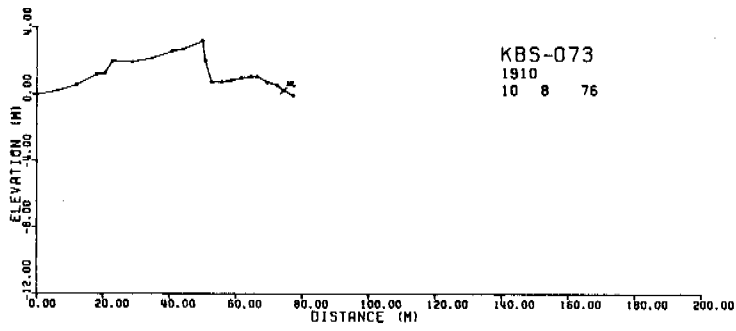


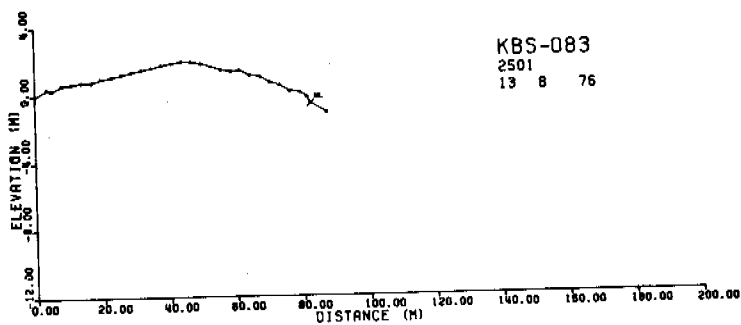
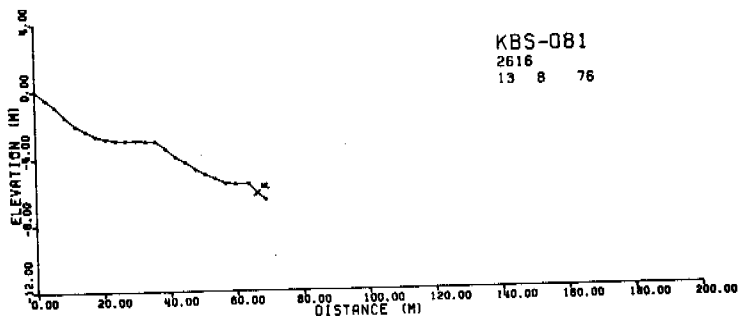
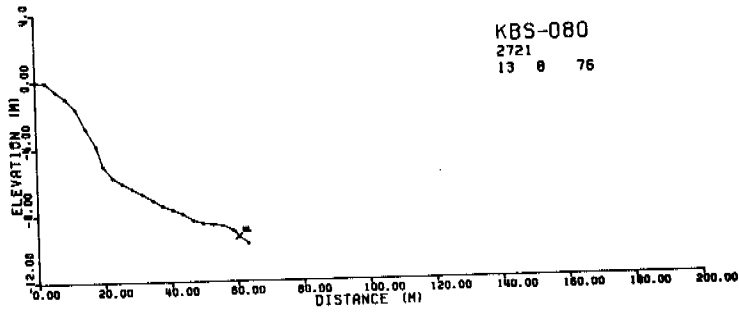
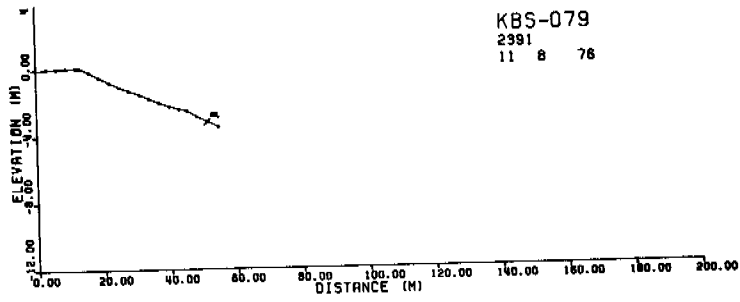
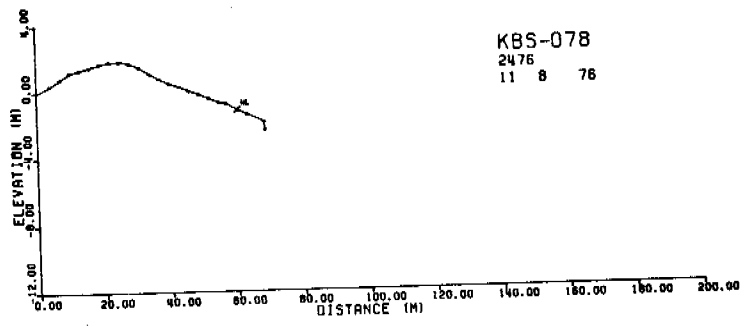


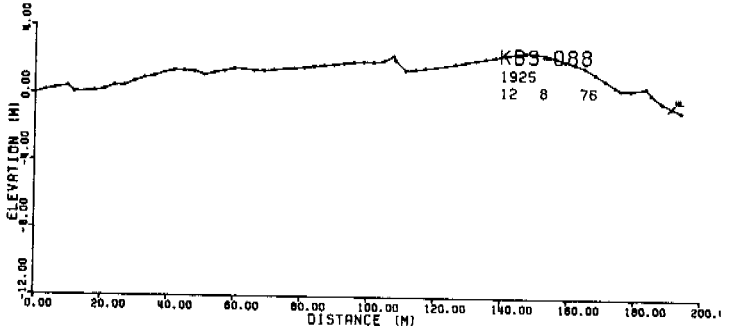
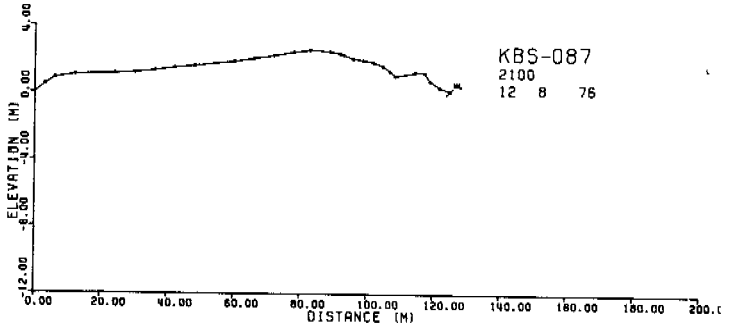
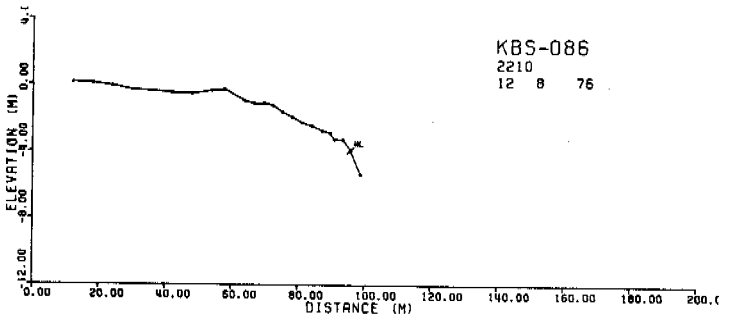
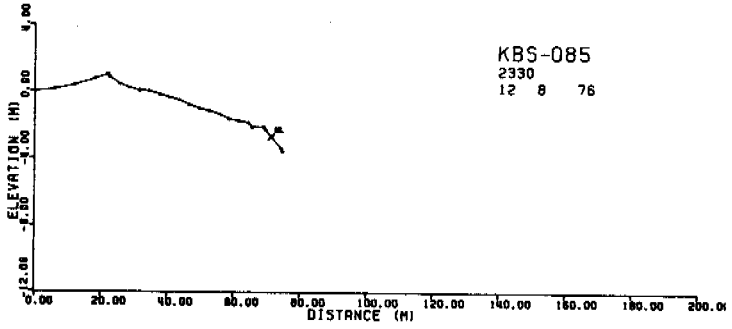
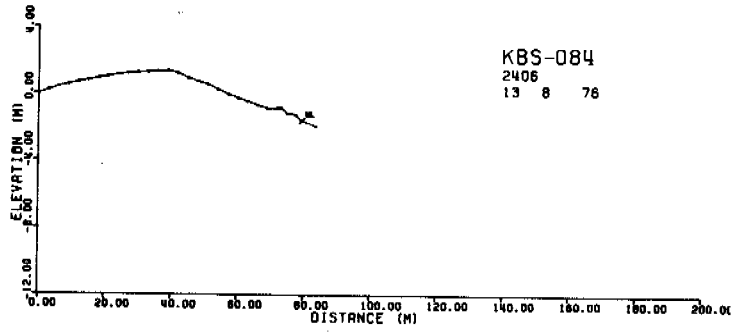












ANNUAL REPORT

Contract #03-5-022-67
Research Unit #87
Reporting Period:
1 April 1978 - 1 April 1979
Number of Pages: 9

THE INTERACTION OF OIL WITH SEA ICE IN THE ARCTIC OCEAN

Seelye Martin
Department of Oceanography
University of Washington
Seattle, Washington 98195

28 March 1979

REF: A79-07

I. Summary of Objectives:

Our purpose is to understand from laboratory experiments and field traverses how oil and sea ice would interact in an arctic oil spill.

II. Introduction:

A. General Nature and Scope of Study:

To understand how spilled oil might interact with the various kinds of ice in the Beaufort, Bering and Chukchi Seas, we have done field traverses in these regions, with particular emphasis on ice types which have previously not been studied. These include grease and pancake ice in Norton and Kotzebue Sound, and most recently a field investigation of the ice plumes which form at the pack ice edge in the Bering Sea. In the laboratory, we have carried out experiments on how spilled oil interacts with grease ice, pancake ice, and simulated multi-year ice.

B. Specific Objectives:

1. To understand how first-year sea ice entrains petroleum;
2. To understand from laboratory experiments the interaction of petroleum with grease and pancake ice;
3. To understand from field observations the behavior of the Bering Sea ice edge and the relevance of this behavior to oil entrainment from industrial development.

C. Relevance to Problems of Petroleum Development:

The above specific objectives have an obvious application to the impact and problems of oil spills in sea ice.

III. Current State of Knowledge:

I have published my laboratory and field results in two papers.

- A. Martin, S., and others. 1979. A laboratory study of the dispersion of crude oil within sea ice grown in a wave field, (by) S. Martin, P. Kauffman, and P. E. Welander. (In Science in Alaska, 1976, Proceedings of the Twenty-Seventh Alaska Science Conference, Fairbanks, Alaska, Volume II, Resource Development-Processes and Problems. Alaska Division, American Association for the Advancement of Science, Fairbanks, p. 261-287.)
- B. Martin, S. 1979. A field study of brine drainage and oil entrainment in first-year sea ice. Journal of Glaciology, in press.

The first paper summarizes our work on grease and pancake ice; the second is a review of both my work and other investigators' on oil entrainment and first-year ice.

IV. Study Areas:

We have worked in the Beaufort, Bering and Chukchi Seas. In the Beaufort, we worked on the ice over the Alaskan continental shelf, with particular emphasis on the Prudhoe Bay region. In the Bering and Chukchi, we concentrated on Norton and Kotzebue Sound, and most recently on the Bering Sea ice edge.

V. Methods:

In the field, we rely on working from helicopters, taking ice cores, then analyzing the cores for their salinity and temperature profiles, as well as their crystal structure. In the laboratory, we grow ice in our experimental tanks, spill oil both under and within the ice, then follow the evolution of the mixture. Our most recent work, which was a major study of the Bering Sea ice edge properties from the NOAA ship SURVEYOR, will be described below in the "Summary of the January-March Quarter".

VI. Results:

Our formal results are contained in the papers cited in Section III, above. We are presently writing one more report to summarize our laboratory work to date, and we plan a long report on our most recent Bering Sea ice edge cruise.

VII. Discussion:

I feel that the problem of the small-scale interaction of oil with first-year ice is well understood from both field and laboratory experiments. Also, my laboratory experiments give repeatable results for oil spilled in grease and pancake ice, although we have had no field verification. Our most recent work at the Bering Sea ice edge suggests that, because of the propagation of ocean swell into the pack, there are several new ways for oil and sea ice to interact, which we describe below.

VIII. Conclusions:

These are also summarized in the published papers.

IX. Needs for Further Study:

The problem of how the ice edge in the Bering and Chukchi Seas melt back during the spring and summer has not been addressed. This may be important for two reasons. First, any oil spilled during the winter would be released by the melting ice, then transported about by both the winds and the moving ice. Second, the large concentrations of marine mammals in these seas during this period would be affected by the released oil.

X. Summary of January-March Quarter:

A. Ship Activities:

1. Ship Schedule:

- a. Dates: Bering Sea Ice Edge Cruise; leave Kodiak, 26 February, return Kodiak, 17 March.
- b. Name of Vessel: NOAA Ship SURVEYOR.
- c. Aircraft: A Bell 206 "Jetranger" was onboard the ship.
- d. NOAA or Chartered: The ship is NOAA; the aircraft was chartered.

2. Scientific Party:

- a. Chief Scientist: Seelye Martin, University of Washington (UW).
- b. Peter Kauffman, UW, electronics, photographic and ice coring specialist.
- c. Jane Bauer, UW, carried out a relative ice motion study.
- d. Steven Tuell, UW, responsible for wave-rider buoy.
- e. Vernon Squire, Scott Polar Research Institute (SPRI), carried out studies of wave attenuation by pack ice.
- f. Stuart Moore, SPRI, worked with Dr. Squire.
- g. Carol Pease, Pacific Marine Environmental Laboratory (PMEL), supervised CTD operations and coordinated aircraft over-flights.
- h. Ronald Lindsay, PMEL, carried out airsonde work.

3. Methods:

A variety of instruments were deployed from the ship and helicopter to carry out this study. The ship-deployable instruments included the following:

- a. The CTD,
- b. Radiosonde balloons,
- c. A wave-rider buoy, which was launched from the ship and measured wave displacements which were telemetered back to the ship.

Other instruments were deployed from either the small boats or the helicopter. These instruments were used for the ice properties

study, the wave attenuation study, and for a study of the relative motion of ice floes. We next describe the procedure for each of these studies.

d. The Ice Properties Study:

To determine the ice properties which are physically important, we would land at different distances in from the ice edge in the helicopter, then take an ice core with a standard SIPRE corer. After recovering the core, we measured the ice thickness, then placed the core in an insulated box. Once the core was inside the box, we drilled into the core at either 5 or 10 cm intervals, and inserted thermistors into the holes inside the core. This allowed us to measure the ice temperature profile. We then cut the core in half longitudinally and determined with a dye technique its crystal properties. These properties are important in the determination of both the strength and radiometric properties of sea ice. We also cut the core into horizontal sections which generally measured 5 cm thick, put these samples into bags, and melted them down for a shipboard determination of salinity. We also separately measured the ice surface salinity and the snow thickness depth and salinity. Finally, we photographed the site from both the ground and the air, for later comparison with NIMBUS-G, LANDSAT-3 and TIROS-N satellite observations.

e. The SPRI Wave Attenuation Study:

This study involved two types of experiment; (a) an investigation of the attenuation of ocean swell by pack ice using accelerometers, and (b) a determination of the response of an individual floe to an incident swell field using strainmeters and accelerometers. In the first experiment, the instruments were transported to the ice by the helicopter, whereas in the second experiment, the ship's whaleboat was used. For each of these experiments, the open water wave conditions were monitored by means of the wave-rider buoy. The strainmeters consist of an Invar. rod connected to the ferrite core of a linear displacement transducer. The core is supported radially at its ends by three spring steel strips which ensure that it moves freely within the transducer. A rezero facility is included which drives the entire assembly relative to the core (and rod) should the measured signal drift off scale. When used to measure the flexure of ice floes, the instrument is screwed to the ice surface using coach bolts; then as the ice bends, the core moves within the transducer. This displacement is amplified electronically and recorded on digital tape, analogue tape or chart paper. Two accelerometers were used to record the heaving of floes due to incident swells. The first was mounted within a floating buoy and was deployed in any open water around the floe. The second was positioned on the floe surface to measure its heave. The output from the

accelerometers could be recorded on digital tape, analogue tape or chart paper.

f. The Relative Ice Motion Study:

This experiment, which was under the direction of Ms. Jane Bauer, involved placing radar targets and colored panels on the ice, so that their relative motion could be followed with the radar on the ship. The ice clutter made the radar targets invisible; however, it was possible to follow the relative panel motion over a 24 hr period with the helicopter.

4. Sample Localities:

The SURVEYOR worked at the ice edge between 2-14 March, beginning at longitude 165° and going west to 170°.

5. Data Collected:

- a. Ice cores: We took 24 ice cores operating on five separate days. The cores were taken along traverses which extended 50 km into the pack at 10 km intervals.
- b. Wave attenuation and floe flexure experiments: A total of 18 floes were occupied by the scientists from SPRI.
- c. CTD's: 41 CTD casts were taken at intervals along the ice front.
- d. Radiosondes: 21 balloons were released.
- e. Wave-rider buoy: We have five days of swell recordings from this buoy.

6. Chronology of the SURVEYOR cruise:

The following account is a summary of the work carried out during the cruise.

Monday, 26 February

SURVEYOR leaves Kodiak and picks up helicopter at Mormot Island, then begins cruise to ice edge.

Tuesday, 27 February - Thursday, 1 March

In transit to ice edge.

Friday, 2 March

Ship arrives ice edge approximately south of Nunivak Island. In afternoon, S. Martin and P. Kauffman fly out into the pack and take cores at two stations, code named S1 and S2. The Navy P-3 ice reconnaissance aircraft overflies the ship.

Saturday, 3 March

Too windy for helicopter operations; R. Lindsay does a weather balloon run downwind of the pack ice. The ice position data from the P-3 flight is transmitted to the SURVEYOR.

Sunday, 4 March

Too windy for helicopter operations, C. Pease organized a CTD survey at the ice edge. In the evening, R. Lindsay carries out a second downwind balloon run.

Monday, 5 March

Good weather. V. Squire and S. Moore fly in helicopter to occupy three stations within the pack with their strain gauge arrays. At the ship, we deploy the wave-rider buoy to record the ocean swell. J. Bauer and P. Kauffman take a small boat over to the ice edge and deploy two radar targets in three different configurations to see if the reflectors can be distinguished from the ice scatter. They found that the targets could not be distinguished from the ice clutter.

Tuesday, 6 March

Good weather. In the morning, S. Martin, P. Kauffman, V. Squire and S. Moore occupy a single floe, code-named "Scott", with all available coring, strainmeter and accelerometer instrumentation in an attempt to relate the physical ice properties to the floe flexure. At the ship, the wave-rider buoy is again deployed.

In the afternoon, S. Martin and P. Kauffman use helicopter to occupy four ice stations five nautical miles apart along a line, code-named "W" running to the NE from the ship. Also in the afternoon, LCDR Turnbull and LT Williscroft do diving survey of the floe "Scott", which reveals a rafted, irregular bottom topography.

Wednesday, 7 March

Good weather. S. Martin and P. Kauffman use helicopter, fly into pack ice in morning on a NE heading and occupy five ice stations along a transect code-named "B".

In the afternoon, second ice party consisting of V. Squire, S. Moore, C. Pease and S. Tuell deploy strainmeters on two floes from a small boat. On the return of Martin and Kauffman, Kauffman joins the ice floe party by helicopter and takes ice cores. Because the increasing ice density makes small boat operations impossible, the ice party was then evacuated by helicopter.

Thursday, 8 March

Good weather. V. Squire and S. Moore occupy nearby small floe by helicopter and deploy strain instrumentations. P. Kauffman,

S. Martin and J. Bauer join them by small boat with coring gear. The floe, code-named "Nansen", is small, measuring only 15 m across and is half awash. Squire and Moore finish their work, then use helicopter to fly into ice interior to occupy three additional stations. Coring party completes work and returns to ship by small boat.

In afternoon, wave-rider buoy is deployed by ship. Navy P-3 aircraft does second overflight of ship and radios ice edge location to ship. Also, four divers from ship, LCDR Turnbull, LT Williscroft, LT(jg) Fox, and Mr. Kramer, return in small boat to floe "Nansen" with S. Tuell to do another under-ice survey. Because of waves and warm weather, the floe breaks apart in the middle of the survey.

Friday, 9 March

Good weather. S. Martin and P. Kauffman using helicopter occupy four stations along a N-S line code-named "C". They occupy four stations at five n.m. intervals, beginning at eight n.m. from ship. Because of warm weather, the ice surface is soft and mushy.

In the afternoon, V. Squire and S. Moore attempt to occupy another floe by small boat, but floes nearby ship are too rotten. Using helicopter, J. Bauer does a photographic survey of an ice band, and P. Kauffman films ocean swell propagating into the pack.

Saturday, 10 March

Warm, blowing snow, poor visibility. Load helicopter for J. Bauer's experiment, but do not fly.

In afternoon, ship steams SE to longitude 170 along ice edge, deploying CTDs for Pease en route.

Sunday, 11 March

Good weather. Using helicopter, J. Bauer deploys radar and visual targets on ice in the shape of a large cross measuring about one km on each leg. At the same time, V. Squire and S. Moore begin an eight station wave attenuation experiment, wherein they deploy only their accelerometer. Their first station is occupied by small boat, the next seven stations by helicopter in an effort to study the effect of the ice cover on wave damping. When they are not working, J. Bauer flies out and surveys the relative motion of her targets. Operations this day end at 2000.

Monday, 12 March

J. Bauer and S. Tuell fly off in morning to map targets. In afternoon, ship begins to 166°W for joint operations with NASA aircraft planned for tomorrow.

Tuesday, 13 March

Ship sends weather message to NASA aircraft at 0600. Weather is good. In morning, J. Bauer deploys three radar targets on ice for overflights, ship deploys wave-rider buoy. At 1300, message received that NASA C-130 aircraft not flying because of broken laser. V. Squire and P. Kauffman fly into pack ice and take two cores, code-named "N"; also cut diving hole in interior floe in order for divers to observe the bottom topography. LCDR Turnbull and LT Williscroft fly in and do diving survey; interior floes are flat-bottomed. NASA re-schedules for tomorrow, same location.

Wednesday, 14 March

Good weather, clear skies. Ship sends weather message to NASA aircraft at 0600. At 0830, J. Bauer and R. Lindsay do a helicopter ice reconnaissance and an unsuccessful search for the radar targets. The ship deploys the wave-rider buoy at 0900. Bauer and Lindsay return at 1000; Lindsay begins launching radiosondes in support of NASA aircraft. Wave-rider buoy is recovered at 1120; at 1130, NASA C-130 makes first overflight. Between 1130 and 1300, C-130 makes at least two more overpasses. At 1300, SURVEYOR steaming for Unimak pass, with Lindsay releasing balloons.

Thursday, 15 March - Saturday, 17 March

In transit for Kodiak; arrive 1000, Saturday.

7. Preliminary Results of the Ice Core Observations:

The cores which we pulled lay within a 50 km wide band of the ice edge between Nunivak and St. Matthews Island. This data will be later related to microwave maps of the Bering Sea ice produced from the NIMBUS-7 satellite.

To summarize briefly our observations, the ice divides into three general types moving in from the pack edge.

- a. A zone of small, heavily rafted and ridged floes measuring between 10 and 20 m in diameter. This zone is of order 2-4 km wide. Two such floes in this region were investigated by divers and found to have rough bottoms with thicknesses as great as 3.5 m. The surface roughness of these floes varied between 0.5-1 m.
- b. A zone of thin recently cracked floes, which fit together like pieces in a jigsaw puzzle. This zone was between 10 and 20 km wide. The single dive under this sort of floe showed a flat bottom topography; coring observations showed a thickness of 0.3 m.
- c. The interior ice. In the region beyond the zone of recently

cracked floes, the ice floes were very large, on the order of 0.5-1 km across, with thickness of 0.3-0.5 m. To this observer, the ice in this zone resembled the winter ice in Kotzebue Sound, even though the ocean swell continued to propagate through it.

The cause of these three different zones appears to be the ocean swell. At the ice edge, where the swell is least damped, it causes rafting and ridging. Further in, the swell breaks the thin ice without rafting it. Beyond this region, the swell propagates into the pack without fracturing it. One surprising effect of these three zones is that within this 50 km region, the thickest ice occurs at the ice edge. This means that when the wind blows from the north, the increased surface roughness causes greater atmospheric drag and the roughened ice is blown away from the pack, where it forms the observed ice bands. When these bands are blown off the pack, they move into warmer water, where the combination of swell, wind-waves and warm water cause them to break up and disintegrate. This means that the swell is again free to propagate into the previously unrafted ice, and the process begins again.

In summary, this cruise appears to be the first to concentrate on the ice edge, with the conclusions listed above. At least one preconceived notion of mine was destroyed, namely that the thinnest ice occurs at the ice edge; instead, our observations show that the thickest ice occurs here. In the coming months, we hope, from a quantitative analysis of all of the data gathered on this cruise, to obtain a quantitative picture of the forces determining both the position and nature of the ice edge.

XI. Auxiliary Material:

A. Papers in Print or Preparation: See Section III.

B. Oral Presentations:

1. S. Martin presented a paper on oil pollution and grease ice at the Northwest regional meeting of the AAAS, on June 6, 1978 in Seattle.
2. S. Martin presented an expanded version of this talk to the Juneau Project Office on August 3, 1978, and to Flow Industries on December 20, 1978.

ANNUAL REPORT

R.U. #88: Dynamics of Near-Shore Ice

P.O.: 01-5-022-1651

Reporting Period: 1 April 1978 to
30 March 1979

No. of Pages: 52

DYNAMICS OF NEAR-SHORE ICE

Principal Investigators: A. Kovacs and W. Weeks

Cold Regions Research and Engineering Laboratory
Hanover, New Hampshire 03755

7 May 1979

I. SUMMARY OF OBJECTIVES, CONCLUSIONS AND IMPLICATIONS WITH RESPECT TO
OCS OIL AND GAS DEVELOPMENT

The purpose of this project is to:

- a. study the motion of the fast ice and near-shore sea ice north of Prudhoe Bay and in the vicinity of the Bering Strait,
- b. make observations on major ice deformation features that occur near the edge of the pack ice/fast ice boundary,
- c. explore the use of an airborne pulsed radar system to measure the thickness of sea ice,
- d. study the internal structure of near-shore sea ice,
- e. characterize the spatial and temporal variations in sea ice pressure ridging via the use of laser profilometry and side-looking airborne radar (SLAR).

At the present time our results (discussed more fully later in this report) suggest the following:

- a. during the late winter-early spring, fast ice motions within the barrier islands are small, however during the fall and early winter large (>1 km) ice motions may be encountered in such locations,
- b. fast ice motions outside the barrier islands increase with increasing distance from shore,
- c. the fast ice/pack boundary may at times be located a considerable distance offshore from the 18 m depth contour, where it is commonly assumed to be located,
- d. locally-formed multiyear pressure ridge systems can be a major hazard to offshore development in water depths in excess of 13 m,

- e. impulse radar systems can quite effectively obtain sea ice thickness information when operated from a helicopter,
- f. large areas of fast ice show the same crystal orientation year after year [The orientation is believed to be controlled by the current direction under the ice. The orientation makes the ice properties directionally dependent].
- g. remote sensing studies of ice deformation show a general decrease in the number of pressure ridges as one moves to the west from Barter Island and/or further north away from the edge of the fast ice. Also the ice along the north coast of Alaska is more highly deformed than the ice north of the Mackenzie Delta. The mean ridge height varies throughout the year and the distribution of sail heights appears to be exponential

II. INTRODUCTION

A. General Nature and Scope of Study.

The present program can be considered to be split into three main sub-projects:

1. The Coastal Ice Motion, Deformation and Structure

The purpose of this program is to obtain detailed information on the movement and deformation of both the near-shore pack ice and the fast ice along the coast of the Beaufort Sea (with particular emphasis on the region north of Prudhoe Bay). Studies have also been carried out on the nature of the ridge systems located near the edge of the fast ice, on lateral variations in the thickness of first and multiyear ice, and on the internal structure of sea ice.

2. The Bering Strait Program

This program is focused on one task; measuring the flux of sea ice through the Bering Strait in specific and developing theoretical models for the motion of ice through straits in general.

3. The Remote Sensing Program

This program attempts both to gather remote sensing data using a laser profilometer, a SLAR system and standard mapping cameras and to utilize this data to study the nature of pressure ridging and ice conditions along the coast of the Beaufort and Chukchi Seas. Studies have also been made of the nature of the radar return from sea ice and of the use of SLAR to reveal locations in the shallow lakes of the Northslope where water can be found at times of maximum ice thickness.

B. Specific Objectives

See previous section.

C. Relevance to Problems of Petroleum Development

A knowledge of motion, deformation and physical characteristics of both the near-shore pack ice and the fast ice is essential to adequately designing and estimating the hazards associated with a variety of engineering options that may be considered for offshore operations in the near coastal areas of the Beaufort and Chukchi Seas (e.g. construction of gravel islands, structural platforms, causeways, reinforced ice platforms, buried pipelines, or the utilization of the ice sheet itself to carry large, long-term loads). The present program contributes directly to the solution of this general class of engineering problems in that it will provide much of the geophysical and engineering data upon which sound engineering and regulatory decisions can be made. The area north of Prudhoe Bay that is being studied is currently being considered by the petroleum companies because it possesses favorable geologic structures and is a natural extension of the known Prudhoe Bay field. It is also a portion of the coming lease sale (December 1979).

Our interest in observing and in developing methods to predict the drift of pack ice through the Bering Strait is, as mentioned earlier, linked to the fact that ice flow through the Straits would be a key mechanism in dispersing

an oil spill occurring along the coastal areas of the Beaufort and Chukchi Seas. We also believe that a knowledge of the ice conditions in the Strait is essential to developing an adequate ice forecasting model for the Chukchi and Bering Seas. Such a model is required to predict the trajectories of potential oil spills.

The remote sensing program provides the basic information on the distribution of ice types and features and in particular ridges that will be required as one aspect of a risk analysis for the construction of an offshore drilling platform sited on the edge of the Arctic Ocean.

III. CURRENT STATE OF KNOWLEDGE

There has never been a comparable study of the motion of near-shore fast and pack ice to that carried out at Narwhal Island. The closest study is that of the University of Washington (R.U. #98) using drifting data buoys employed on the ice north of the Alaskan coast. These buoys are located further offshore than our study area. However, this data set will definitely prove to be useful to us in analyzing our results. The oil companies have also carried out studies of the motion of the fast ice in the vicinity of our operation. However, their results have not been made available to OCS program.

The Bering Strait Program is also quite different than existing programs. The most similar programs are R.U. #250 which uses a radar system to study the formation of near-shore ridges near Barrow, and the Japanese program using radar to study ice motion along the coast of Hokkaido. Neither of these efforts is focused on the problem of the passage of sea ice through restricted channels.

The laser profilometer program is the only such program currently underway. In the past there have been laser flights in the area of the Mackenzie Delta

carried out by the Beaufort Sea Program. This data will be most useful to us in making regional comparisons of ridging intensities.

IV. STUDY AREAS

Our detailed ice motion and ice deformation observations have been made at two principal locations; the Narwhal Island - Cross Island region north of Deadhorse and the Bering Strait between Wales and Little Diomedé Island. Our observations of ridging have included most of the Beaufort Sea coast and our remote sensing studies have ranged by Kaktovik on the Beaufort Sea to Point Lay on the Chukchi Sea. The crystal alignment study covered a 1300 km stretch of the Arctic coast between Shishmaref Inlet and Camden Bay.

V. RESULTS

1. Published reports (DB indicates availability in the OCS Data Bank)
 - a) Kovacs, A. (1976) Grounded ice in the fast ice zone along the Beaufort Sea Coast of Alaska. CRREL Report 76-32, 21 pp. (DB)
 - b) Kovacs, A. and Gow, A.J. (1976) Some characteristics of grounded floebergs near Prudhoe Bay, Alaska. CRREL Report 76-34, 10 pp.; also available in Arctic 29 (3), 169-73 (1976).
 - c) Weeks, W.F., Kovacs, A., Mock, S.H., Tucker, W.B., Hibler, W.D. and GOW, A.J. (1977) Studies of the movement of coastal sea ice near Prudhoe Bay, Alaska. Journal of Glaciology, Vol. 19, No. 81, p. 533-46 (DB)
 - d) Kovacs, A. (1977) Sea ice thickness profiling and under-ice oil entrapment. Offshore Technology Conference Paper OTC 29-49, (DB).
 - e) Schwarz, J. and Weeks, W.F. (1977) Engineering properties of sea ice. Journal of Glaciology, Vol. 19, No. 81, p. 499-531 (DB).
 - f) Gow, A.J. and Weeks, W.F. (1977) The internal structure of fast ice near Narwhal Island, Beaufort Sea, Alaska. CRREL Report 77-29, 9 p. (DB).
 - g) Sohdi, D.S. (1977) Ice arching and the drift of pack ice through restricted channels. CRREL Report 77-18, 14 p. (DB); also published by Sohdi, D.S. and Weeks, W.F. in Proceed. Part 2 IAHR Sympos. on Ice Problems, Lulea, Sweden, p. 415-32.

- h) Kovacs, A. (1977) Iceberg thickness profiling. In "Conference on Port and Ocean Engineering under Arctic Conditions" Memorial University of Newfoundland, St. Johns. (DB)
- i) Kovacs, A. (1978) Iceberg thickness and crack detection. Iceberg Utilization (A.A. Husseiny, ed.) Pergamon Press, p. 131-145.
- j) Weeks, W.F. and Gow, A.J. (1978). Preferred crystal orientations in the fast ice along the margins of the Arctic Ocean. CRREL Report 78-13, 24 pp.; also published in Journ. Geophys. Res. 83 (C 10), p. 5105-21 (1978).

2. Completed reports currently in press

- a) Kovacs, A. Radar profile of a multiyear pressure ridge. Arctic.
- b) Tucker, W.B., III, Weeks, W.F., Kovacs, A. and Gow, A.J., (1977) Near shore ice motion at Prudhoe Bay, Alaska. AIDJEX Sea Ice Symposium. Univ. of Washington Press.
- c) Weeks, W.F., Tucker, W.B. III, Frank, M. and Fungcharoen, S. (1977) Characterization of the surface roughness and floe geometry of the sea ice over the continental shelves of the Beaufort and Chukchi Seas. AIDJEX Sea Ice Symposium. Univ. of Washington Press.
- d) Tucker, W.B., Weeks, W.F. and Frank, M. (1979) Sea ice ridging over the Alaskan continental shelf. CRREL Report 79- , 24 pp.; also in press, Journal of Geophys. Res.
- e) Weeks, W.F. and Russer, J. (1979) Ice related environmental problems: Appendix D. In "Environmental Criteria for Design, Verification, Inspection of Offshore Structures Used in Exploration and Development of U.S. Offshore Continental Shelf Resources". Rept. of Environmental Criteria Working Group of the Committee on Offshore Energy Technology, Marine Board, National Research Council.
- f) Kovacs, A. and D.S. Sodhi (1979) Shore ice pile-up and ride-up; field observations, models, theoretical analyses. In "The Seasonal Sea Ice Zone" Cold Regions Science and Technology.
- g) Kovacs, A. Some problems associated with radar sea ice profiling. Cold Regions Research and Engineering Laboratory Tech. Note, 6 p.
- h) Kovacs, A. Remote detection of water under ice covered lakes on the North Slope. Cold Regions Research and Engineering Laboratory Report.

3. Reports currently in preparation

- a) Weeks, W.F. and Gow, A.J., Crystal alignments in the fast ice of Arctic Alaska. CRREL Rept. 79- ; also to be submitted to Journ. Geophys. Res.
- b) Gow, A.J., Weeks, W.F., Olheoft, G., Kohnen, H., Aota, M., Tabata, T., Onstott, R. and Moore, R. Interrelations between the internal structure and the physical properties of fast ice at Barrow, Alaska.

VI. CONCLUSIONS

- a) Laser observations during the winter and early spring months of fast ice motion at sites close to Narwhal Island show long term changes in the distance to targets located on the ice. These movements are believed to be primarily the result of the thermal expansion of the sea ice. The main ice motion was outward normal to the coast (in the least-constrained direction). The maximum movement was approximately 3 m with short term changes of 30 cm. Larger movements (up to 60 m) were associated with the formation of cracks and ridges within the fast ice.
- b) Field observations during freeze-up (early November) have now thoroughly documented large ice motions accompanied by ridge formation with sails of 4 m in the area between the barrier islands and the mainland. The ice at this time is, of course, relatively thin.
- c) Radar observations of fast ice sites further off-shore from the barrier islands do not permit the study of small motions (as do the laser records) because of insufficient measurement resolution. However, these records show many larger events with the standard deviation of the motion measured parallel to the coast increasing systematically with distance off-shore reaching a value of +6.6 m at 31 km. The ice motions show short term displacements of as much as 12 m at the sites furthest from the coast. The observations also show systematic changes in line length (up to 6 m over a distance of 30 km) that are believed to be the result of thermal expansion of the ice. Correlations between the wind and the ice movement are only appreciable for movements normal to the coast.

- d) Radar targets located within the pack ice showed large short term movements (up to 2.7 km) but negligible net motion along the coast. There was no significant correlation between the motion of the pack and the local wind suggesting the models for predicting coastal ice movement in the Beaufort Sea during the March-June time period can only succeed if they are handled as part of a regional model which incorporates the lateral transfer of stress through the pack ice.
- e) The stability and extent of the fast ice outside the barrier islands is to considerable degree controlled by the amount of grounded ice (ridges) that form early in the winter. When grounded ice is absent, the fast ice is not "protected" from the forces exerted by the moving pack, and significant shifts (hundreds of meters) in the fast ice cover are possible. The extreme case of such movements would be the destruction of the fast ice sheet outside of the barrier islands at the time of maximum ice thickness. When extensive grounded ice is present, the fast ice extension can extend to water depths of 30 to 35 m in the early spring (well seaward of the 18 m isobath that is usually assumed to correspond to the outer edge of the fast ice).
- f) The large grounded pressure ridge formations that occur along the Beaufort Sea coast must be considered as formidable obstacles in the development of off-shore operations in this region. In the design of off-shore drilling structures significant consideration must be given to not only the forces which can develop when these formations are pushed against the structures, but also to the potential for ice piling up and completely overriding the structures.

Based on our limited observational time series (4 years) we have found that during winters when there were very few grounded ridges stabilizing the edge of the fast ice, major shear ridges can form in water as shallow as 13 m (see Figures 6 and 7). This suggests that in the coming lease sale it might be prudent to limit production drilling to sites located in water less than 13 m deep (sites further seaward could presumably be reached by directional drilling). This restriction could be lifted in the future if additional data suggest that such a move is warranted.

- g) Shore ice pile-up and ride-up can occur at any time of the year but most commonly occurs during the spring or fall. The life-time of these events is usually brief (less than 30 min). Pile-ups seldom are found more than 10 m inland, but ride-ups frequently extend 50 m or more inland regardless of ice thickness.
- h) The dual antenna impulse radar system was highly effective in determining the thickness of both first-year and multiyear sea ice from the air. Good agreement was achieved between calculated and observed ice thicknesses and representative cross-sections of both ice types were obtained.
- i) Our observations coupled with published U.S. and Russian results show that very large areas (hundreds of kilometers) of sea ice have sufficiently similar c-axes orientations to act as a large single crystal (see Figure 8). Because of this, off-shore structures may have to be designed for "hard-fail" ice strengths which are 2 to 6 times the strength values normally used. Field evidence now strongly supports the hypothesis that the orientation direction is controlled by the current direction at the ice-water interface.

- j) The theory of the flow of granular media through chutes and hoppers has been applied with considerable success to ice motion through the Bering Strait. There is good correspondence between observed arching and lead patterns and those predicted by theory. In addition values determined via the theory for the angle of internal friction of pack ice (≈ 30 to 35°) and the cohesive strength ($\approx 2000 \text{ N/m}^3$) are similar to values obtained by other approaches. It is estimated that if the wind velocity parallel to the Bering Strait exceeds $\approx 6 \text{ m/s}$, there will be ice flow through the Strait.
- k) Based on laser profiles collected during the 1975-76 ice season the heaviest ridging occurred at Barter Island and there was a general decrease in the intensity of the ridging as one moves further east into the Chukchi Sea. Ridging also decreases as one moves further offshore. Individual frequency profiles fall off in an exponential manner as ridge height increases. There is no decrease in frequency at low ridge heights as has been suggested from the analysis of sonar profiles. Ridging intensity along the north coast of Alaska appears to be generally higher than off the Mackenzie Delta. Therefore it cannot be assumed that because a system was successful in Mackenzie Bay, it will be successful off the Northslope.
- l) Analysis of SLAR imagery shows that the area of ridged ice decreases in a linear manner as one moves away (North) from the coast into the pack ice. There is no obvious break corresponding to a seaward boundary of the so-called shear zone. The landward boundary is, however, reasonably well defined.

- m) The most common shape of multiyear ice floes is roughly circular. The largest length to width ratio observed was just over 5. The distribution of floe diameters shows an exponential decrease as floe size increases. The largest floe diameter observed was 3600 m.
- n) Although there have been many studies of the engineering properties of sea ice, there still is considerable uncertainty concerning the appropriate values to use in offshore design. This comment is particularly true of the mechanical properties where both the basic experimental measurements and their interpretation are not well resolved.

VII. FOURTH QUARTER OPERATIONS (1 Jan - 1 April)

a. Shore ice pile-up and ride-up (Kovacs)

Reconnaissance flights were made along the Beaufort Sea coast from Barrow to Konganevik Pt., Alaska, to observe coastal sea ice pile-up or ride-up occurrences. Larry Hester of Sea Ice Consultants made the observations from Barrow to Cape Halkett and reported the following.

On 19 October 1978 ice was observed thrust ashore on the northeast side of Plover Point (Figure 1) located southeast of Point Barrow, Alaska. Plover Point has a gravel beach which rises in a distance of 1.5 m to an abrupt crest about 0.5 m above sea level. The ice thrust was some 90 m wide and had an average inland advance of 10 m. A single tongue of ice extended about 25 m inland. The maximum height of pile-up on the land was about 1.5 m. The ice slabs in the pile-up were 16-17 cm thick. The winds during this ice movement were from the northeast at about 13 knots, gusting to 20 knots.

Ice was also observed pushed ashore at other sites on the Plover Islands and along the Alaska coast as shown in Figure 1. At site 13 the ice pile-up reached 2 m height.

The above findings also appear in the review report "Shore Ice Pile-up and Ride-up" by Kovacs and Sodhi (1979) which was completed during the 4th quarter.

From Cape Halkett to Konganevik Pt., Kovacs observed only one ice ride-up and pile-up event of any significance. This formation was on the northeast side of Thetis Island which is located on the eastern side of

of Harrison Bay. The ice was found to have either piled up or slid inland along some 400 m of the coastline. The maximum inland movement was somewhat more than 60 m and the ice came within 10 m of the Helmericks' cabin located on the island. The maximum height of the pile-up was on the order of 4 m.

From Jim Helmericks we found that the ice pile-up and ride-up occurred during a 4-9 November storm in which winds were from the northeast at 55 to 65 km/hr (35 to 40) with gusts to 110 km/hr (70). Temperature at the time was -29°C . Helmericks also believed that this pile-up on Thetis Island was the largest to occur in the last ten to fifteen years and reported that ice pile-up on Thetis Island occurs on the average of once every three years.

Our review of shore ice pile-up and ride-up which is referenced above may be briefly summarized as follows. Shore ice pile-up or ride-up appears to occur within a period of less than 30 minutes, at any time of year, but most often in the spring and fall. Pile-up seldom moves more than 10 m inland from the sea, but ride-up frequently extends 50 m or more inland, regardless of ice thickness. While steeply sloping shores do not favor ice ride-up, sea ice has nevertheless mounted the steep, 9-m high bluff at Barrow, Alaska, destroying structures and taking lives. From cross-sectional profiles of shore ice formations, models and theoretical analyses were made. Expressions derived give the force required to overcome gravitational potential and friction occurring during ice-piling and ride-up. The total force was found to be of the order of only 10 to 350 kPa (about 1.5 to 50 psi).

b. Ice morphology in the federal-state lease area (Kovacs)

During the March 1979 field season we noted that the fast ice inside the barrier islands from Reindeer Island eastward to Flexman Island had significant surface roughness. The broken and ridged ice relief was a result of the 4-9 November northeast storm mentioned above. During this storm, the fast ice was broken and driven shoreward, forming pressure ridges, some as high as 4 m, on shoals where we have not seen such formations before. On 10 November the winds changed quickly from the northeast to the southwest. These winds continued for three days at 25 to 40 km/hr. During this time, the previously broken fast ice was driven northward against the barrier islands where minor ice pile-up and ridge building occurred.

These observations revealed that even inside the barrier islands major ice displacements can occur during fall freeze-up.

Other interesting ice features noted were five floes north of Argo Island about 30 m in diameter, one 300 to 400-m diameter floe east of Argo Island, and one floe to the south of Reindeer Island consisting of a surface layer of clear "freshwater" ice 16 cm thick underlain by 1.70 m of sea ice. The freshwater ice surface was very smooth and mostly snow-free. Walking on this ice was exceedingly difficult because of its slick mirror surface. The salinity of this ice was 0.2% (2 parts per thousand), indicating that the melt would meet public health standards for potable water. Of the BLM/NOAA SLAR images taken during the winter of 1978-79 (up to 1 April) showing the Argo Island area, only the images of 28 November 78 and 3 January 79 (Figure 2) could be used to locate

the floes. The floes could be detected in the images because they appeared darker than the surrounding sea ice.

The freshwater ice portion of these floes undoubtedly formed in one of the coastal river deltas and was subsequently broken free and driven offshore during the November storm referred to above. The location of the "freshwater ice floes" from the nearest river delta clearly indicates that fall storms can break up and displace ice for great distances inside the barrier islands.

Beyond the barrier islands in early March we found very few grounded ridge areas and noted that the seasonal pack ice had been actively moving, as indicated by the many recently refrozen leads. In this respect, ice conditions in early March of this year were similar to those observed in the winter of 1974-75. During this winter the "shear zone" of the seasonal pack ice zone was active along the edge of the fast ice zone beginning at about the 15-m depth contour. In the winter of 1975-76 and to a lesser extent in 1976-77 large areas of grounded ice existed along the edge of the shore-fast ice zone, and as Kovacs (1976) has reported, this grounded ice zone protects the fast ice to the south from the forces induced by the moving pack ice to the north. In addition, the grounded ice zone provides anchorage for the fast ice and thus allows a seaward extension of it as depicted in Figure 3. The extent of this fast ice extension depends upon ice thickness, pack ice motion and the anchorage provided by the grounded ice zone. Thus in the winter of 1974-75 and 1978-79, without the anchorage and protection provided by large areas of grounded ice, no "stable" fast ice extension developed beyond about the 13-m depth contour and the seasonal pack ice was found actively moving along the fast ice edge.

A number of large grounded ridges did form during a major storm which struck the Prudhoe Bay area during 16-18 March. Storm winds were from the southwest at 32 to 50 km/hr on the 16th and 28 to 40 km/hr on the 17th. During this storm temperatures were between -30 and -35°C. Ice displacements occurred along the fast ice edge and in the seasonal pack ice zone. About 5 km northwest of Spy Island a grounded ridge area formed in 10 m of water. This ridge was about 30 m wide, 200 m long and had an elevation of 6 to 8 m along most of its length. Between Narwhal Island and Flexman Island four large grounded ridge areas formed in waters 16 to 19 m deep. These large formations varied from about 150 to 400 m long and rose above sea level from 7 to 12 m.

North of Narwhal Island at about 70°26.2'N, 147°23.6'W, a site inside the proposed 1979 federal-state lease area, a very high grounded ridge formed in 18.5 m of water. This formation was first discovered by Arny Hanson during an ice recon flight shortly after the 16-18 March storm (Figure 4). This ridge, the Hanson Ridge, developed when the corner of a large ice floe impinged against the coastal ice. The resulting ice rubble pile was about 350 m long and up to 100 m wide. Five impulse radar profiles over Hanson Ridge showed that the highest point on the ridge was 20.4 m above sea level (Figure 5). An elevation survey of the ridge which included the top of the highest ice block revealed a maximum height of 21.3 m (Vaudrey, personal communication). However, neither of these elevations are representative of the surrounding relief, which was generally 14 to 17 m high over a length of about 100 m.

Beyond this the ridge relief was progressively less until it became 3 to 4 m at the far ends.

Major movements of the seasonal pack ice along the shore-fast ice edge were also noted after the 16-18 March storm. At a location 5 to 10 km west of Hanson Ridge a movement of 1050 m occurred, which was clearly delineated by the lateral displacement of a seismic line ice road. The 1050-m distance was determined by the GSSI field crew who lost this quantity of seismic line cable as a result of the ice displacement.

As previously stated there were very few grounded ice formations along the seaward side of the shore-fast ice zone during the winter of 1978-79. The few locations where ice formations did exist which were believed grounded as determined by sail height and local water depth ratio considerations (Kovacs 1976), were along the shear boundary developed during a major seasonal pack ice displacement which occurred in November 1978 and can be seen in BLM/NOAA SLAR image B2 of 28 November (Figure 6). The location of the shear boundary is representative of the outer extent of the shore-fast ice zone for years when there are few areas of grounded ice along the shore-fast ice edge as in the winter of 1978-79. In other words, lack of grounded ice precluded a "stable" seaward extension of the fast ice zone as shown in Figure 3.

The water depth along the shore-fast ice zone, as clearly delineated by the long sinuous shear ridge (Figure 7) which developed during the displacement event shown in Figure 6, was measured at intervals of 15 minutes of longitude. The 17 measurement locations are shown in Figure 6 along with the tabulated water depth and local ice relief. As

the table in Figure 6 shows, the water depth varied from about 13 to 17 m. Also shown blacked out in Figure 6 is the proposed 1979 Beaufort Sea federal-state lease area. This area is seen to extend beyond the 1978-79 shore-fast ice zone. It is our recommendation that the seaward extent of the proposed 1979 lease area be moved southward inside the shore-fast ice area. Here ice movements are less severe and the possibility of ice pile-up or ride-up, and the forces exerted by the pack ice, on a manmade drilling structure would be greatly reduced. It is further recommended that if exploratory drilling is essential beyond the 13-m depth contour, and is to occur from gravel islands or similar low relief structures, such drilling only be allowed by directional drilling from structures founded inside the 13-m depth contour. The latter should remain a condition of the lease until such time that a test structure has been built and tested for resistance to the dynamic ice conditions which exist in the seasonal pack ice zone.

References

- Kovacs, A. (1976). Grounded ice in the fast ice zone along the Beaufort Sea coast of Alaska. CRREL Report 76-32.
- Kovacs, A. and D.S. Sodhi (1979). Shore ice pile-up and ride-up; field observations, models, theoretical analyses. ONR Workshop on Problems of the Seasonal Sea Ice Zone, Naval Postgraduate School, Monterey, California (in press).

b. Remote sensing and the structural properties of sea ice (Weeks)

1. The paper "Sea Ice Ridging Over the Alaskan Continental Shelf" by Tucker, Weeks and Frank has been completed (Appendix A). It includes a probabilistic study of the 1976 laser data and estimates the chances of encountering large ridges at specific sites.
2. The paper "Crystal Alignments in the Fast Ice of Arctic Alaska" by Weeks and Gow is in the final review process. By the time this annual report is published, it will be available in the OCS data bank. This paper includes data collected during March 1979.
3. Weeks and Gow participated in the NASA remote sensing program in Alaska (March 1979). Data collected include
 - (a) SLAR imagery of Northslope lakes located along a broad swath between Deadhorse and Teshekpuk Lake. Analysis of this imagery will allow us to prepare a map giving the locations of all coastal lakes that have depths greater than 2 m and contain fresh water during the time of maximum ice thickness. Ground truth observations were made to verify the interpretation of the imagery.
 - (b) laser profiles of sea ice off the Northslope and off Mackenzie Bay. This data will allow comparison to be made of similar profiles collected in 1976 and will be useful in estimating hazards caused by ridging.
4. Weeks and Gow returned to field sites off Barrow and Lonely and redetermined crystal alignments. Alignments were identical to measurements made the previous year to within 3 degrees (the experimental error).
5. Arcone and Delaney studied the electromagnetic characteristics of aligned sea ice at a wide range of frequencies. (items 4 and 5 were jointly funded by NSF).

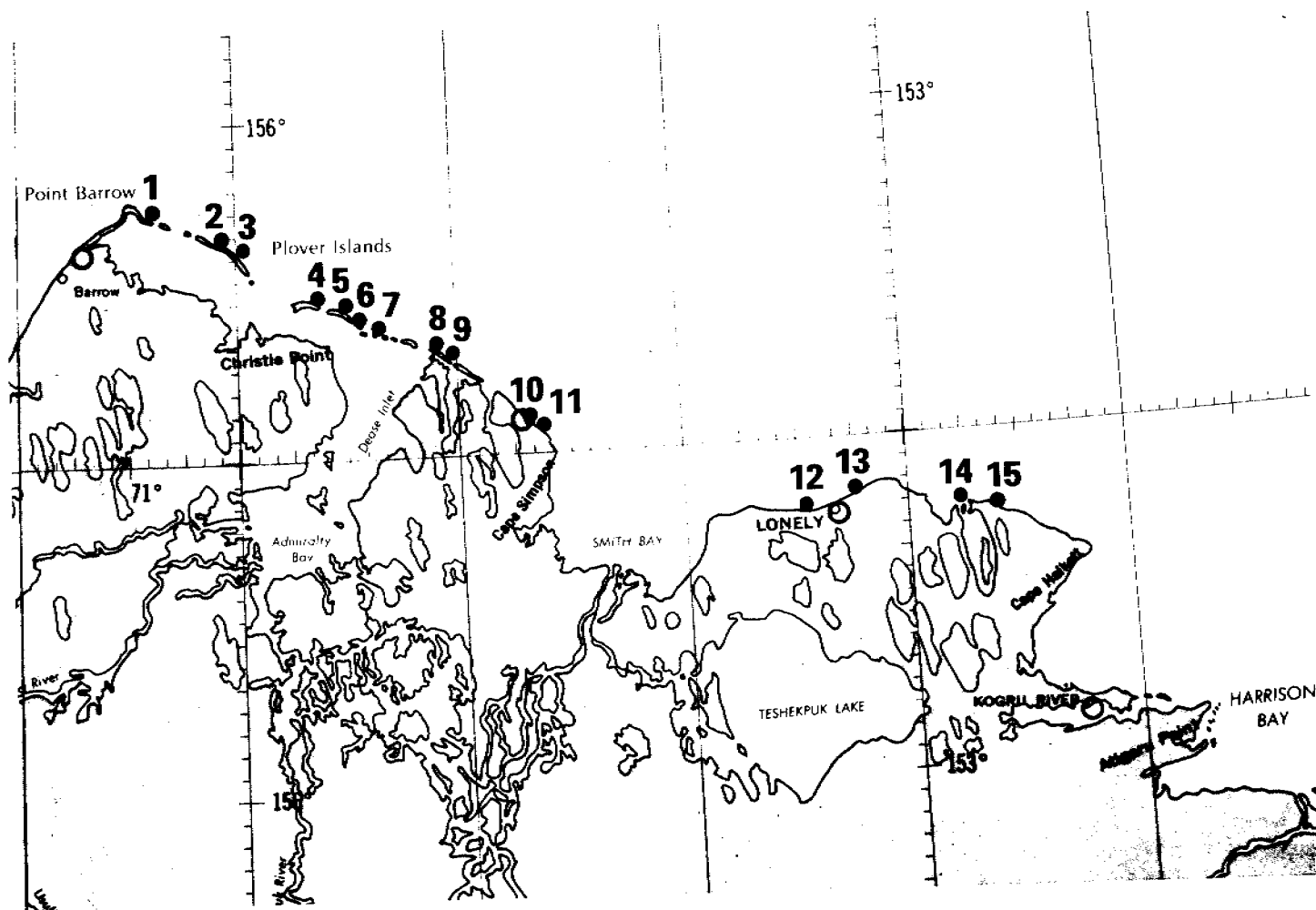


Figure 1. Ice observed ashore on 23-27 October 1978 and thought to have come ashore 19 October. At site 15 ice overrode an overhanging bluff approximately 2 m high. The width of the ice thrust was about 1 km. 1) Plover Point, 2), 3) Tapkaluk Island, 4) Cooper Island, 5), 6) Martin Island, 7) Sanigaruak Island, 8), 9) Kulgurak Island, 10), 11) Cape Simpson, 12), 13) near Lonely DEW Line station, 14) Pogik Point and 15) east of Pogik Point.

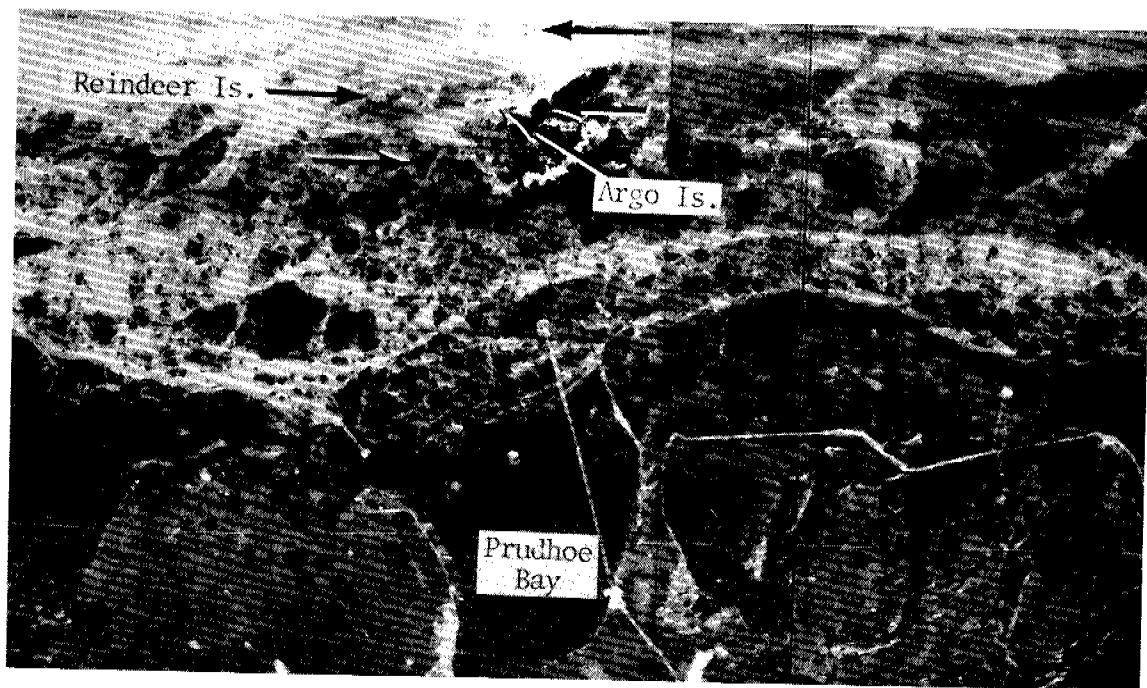


Figure 2. B1-6 SLAR image of 3 January 1979 with arrows pointing to sites of "freshwater ice" floes.

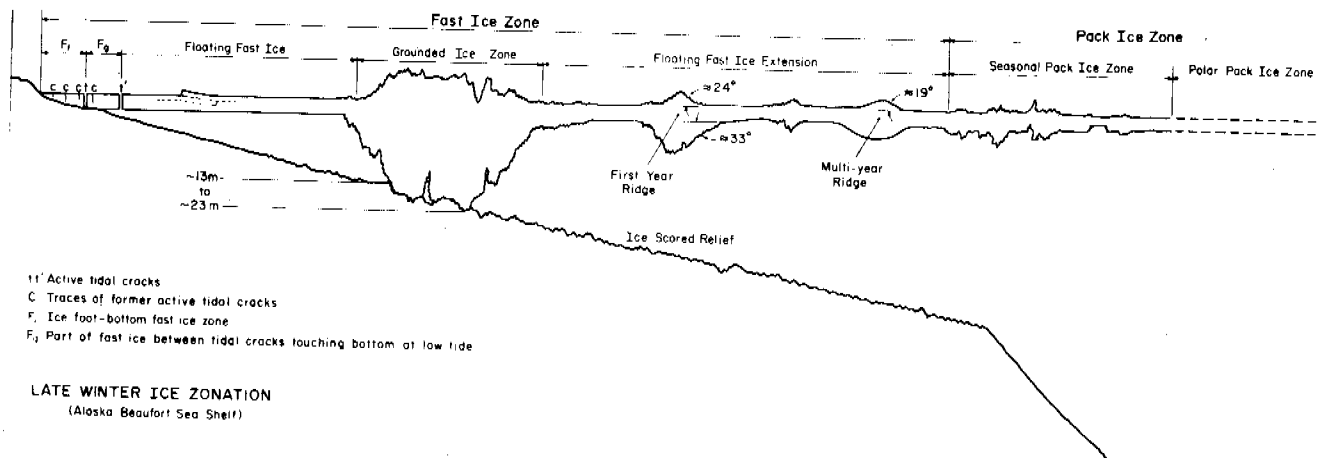


Figure 3. Late winter ice zonation along the Alaska Beaufort Sea Shelf.

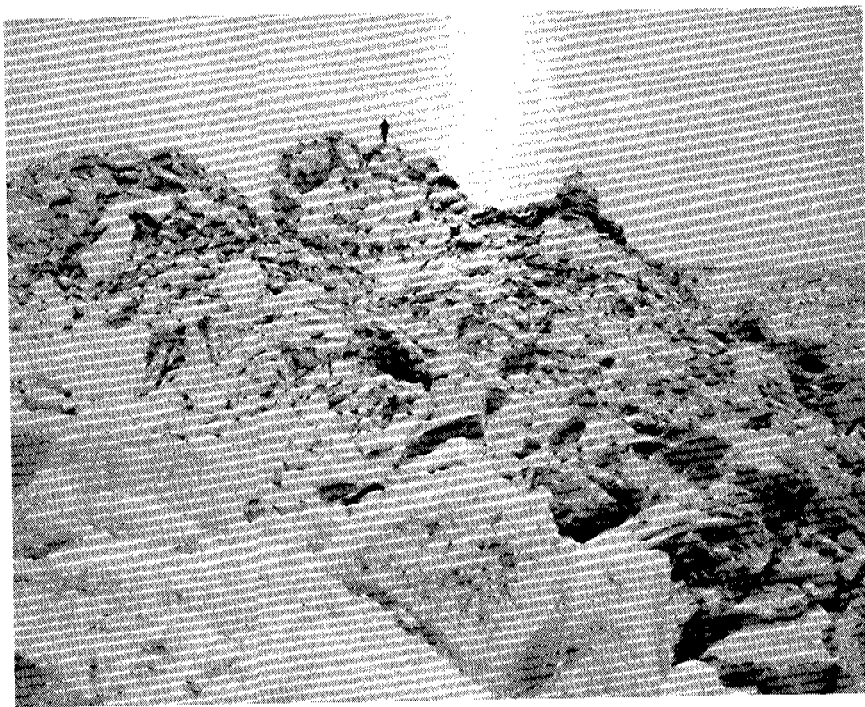


Figure 4. The Hanson Ridge. Note the dirt incorporated in many of the ice blocks.

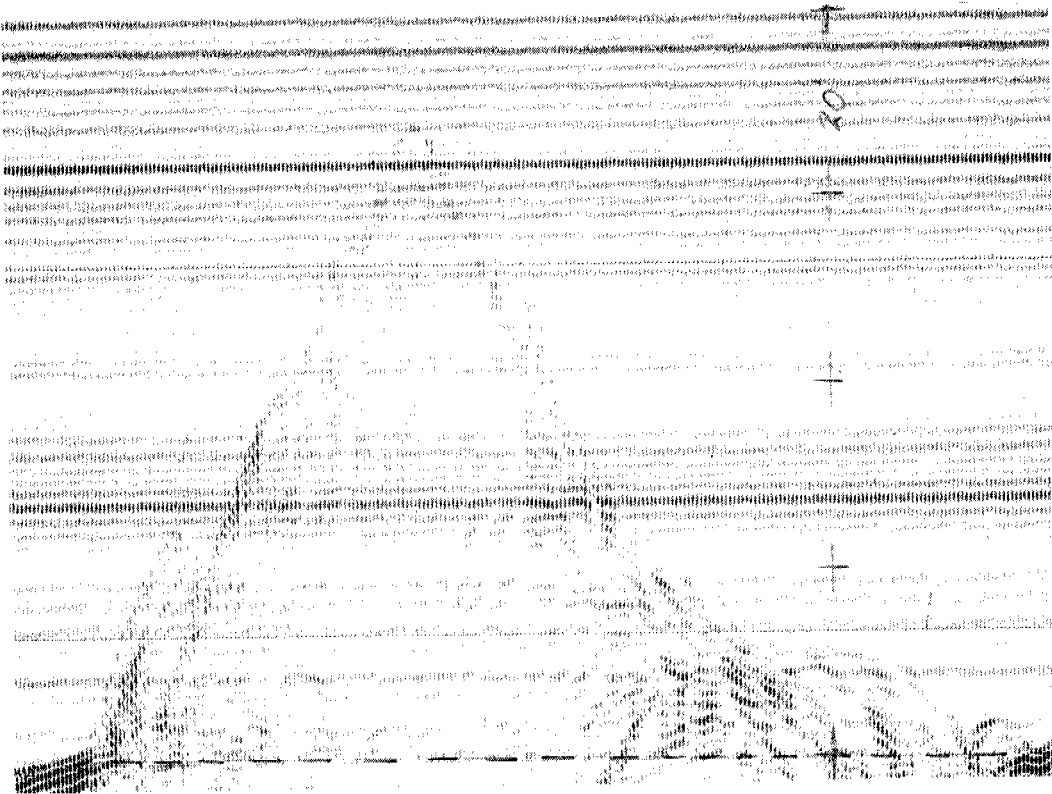


Figure 5. Graphic record of impulse radar profile over Hanson Ridge. The distance between the crosses is 20 ft (6.1 m). The dark banding on each side of the ridge is the return from undeformed first year sea ice. The dashed line represents sea level.

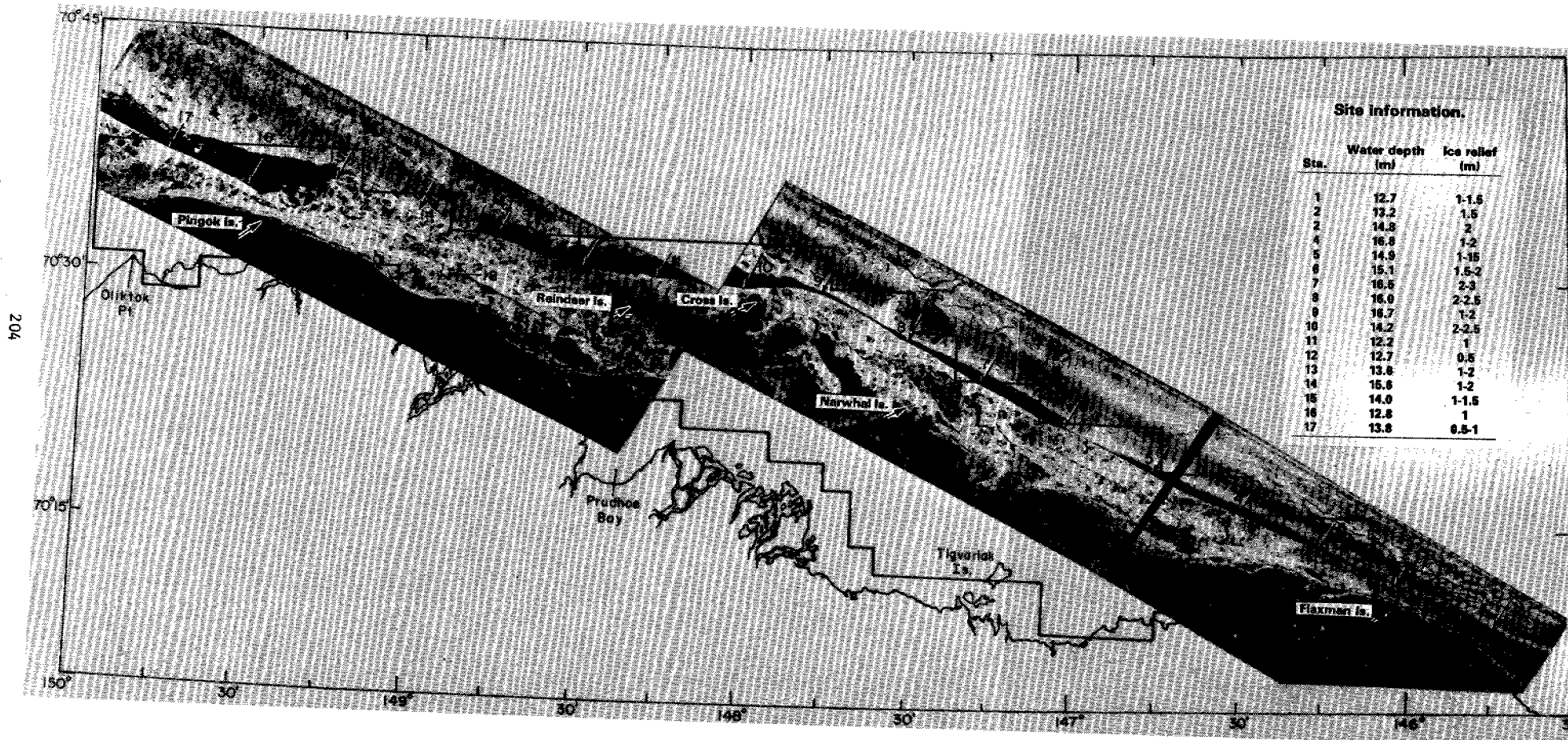


Figure 6. Proposed 1979 federal-state Beaufort Sea lease area (inside irregular outlined area) and the seaward edge of the shore-fast ice during the winter of 1978-79 as delineated by arrows 1-17. Position 18 is the location of a 12-m-high pressure ridge grounded in 8 m of water.

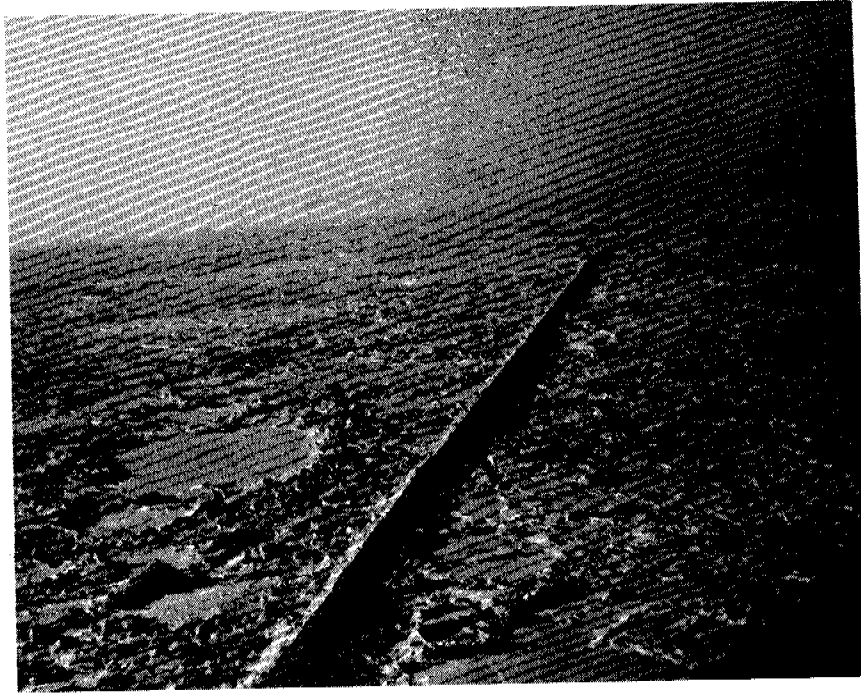


Figure 7. Example of the shear ridge at the shore-fast ice/seasonal pack ice zone boundary.

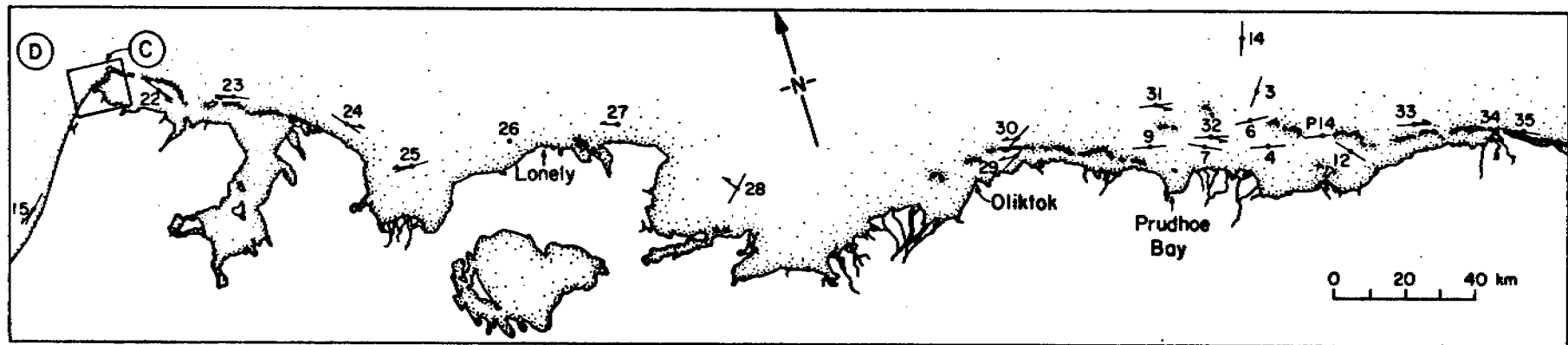


Figure 8. Sample site locations (dots), mean c-axis alignments (bars) and instantaneous current directions (arrows) determined along the coast of the Beaufort Sea in April 1978.

The following was submitted as part of this report:

Tucker, W.B.III, W.F. Weeks, and M. Frank (1979). Sea Ice Ridging
Over the Alaskan Continental Shelf, CRREL Report 79-8,
Cold Regions Research and Engineering Laboratory, Hanover,
New Hampshire. 24 pp.

Annual Report

Contract No.: 03-5-022-67, T.O.3
Research Unit No.: 91
Reporting Period: 1 April 1978-31 March 1979
Number of Pages: 23

Current Measurements in Possible Dispersal Regions
of the Beaufort Sea

Knut Aagaard

Department of Oceanography
University of Washington
Seattle, Washington 98195

27 March 1979



Knut Aagaard, Research Professor
Principal Investigator



George C. Anderson, Associate Chairman
for Research, Dept. of Oceanography

I. Summary

We have found that an energetic current regime over the outer shelf extends landward to at least the 100 m isobath. The flow is characterized by a series of pulses, in which the water alternately moves eastward or westward along the isobaths in a reciprocating fashion. The strength of these pulses is typically about 20 cm sec^{-1} , but can on occasion exceed 65 cm sec^{-1} , and their duration varies from a day to several weeks. The eastward pulses are generally stronger and longer-lasting. The long-term mean flow is therefore eastward (along the isobaths) and in the range of $5\text{-}10 \text{ cm sec}^{-1}$. There does not appear to be any seasonal cycle in the flow. These remarks apply to the motion below about 60 m; above this depth, the velocity field is unknown, as the drifting ice makes moored measurements at lesser depths extremely hazardous.

The thermal regime down to at least 65 m is largely advectively controlled, with the water bearing the mark of the freezing process until mid-summer. At that time, warm water is advected into the region, probably largely from the Bering Sea, and there are strong horizontal temperature differences. Under these circumstances, waters of different origin being advected past a given point cause a highly variable local temperature regime. Closer to the bottom there is a frequent invasion of warm and saline Atlantic water, occurring in a pulse-like manner and extending over large portions of the shelf. During such events the temperature increases to $1\text{-}2^\circ\text{C}$ or more above the freezing point. The pulses occur at all times of the year and have time scales similar to the reciprocating along-shelf motion discussed above. These are in effect upwelling events from 350 m or deeper offshore, and they must bring relatively large amounts of salt and sensible heat onto the shelf.

The significance of these results to the dispersion of plankton, pollutants, and substances of geological and biological consequence (below about 60 m) is as follows. (1) Material trajectories will nearly follow isobaths. (2) Over a period anywhere from 1-10 days, displacement may be either eastward or westward, and the magnitude of such displacement can exceed 40 km over 24 hours. (3) On time scales exceeding about one month, the net displacement will be westward, with mean speeds corresponding to typical monthly displacements in the range of 100-250 km. (4) Materials can also move on- and offshore on time scales of a few days. Such movements likely involve vertical displacements of several hundred meters. (5) The shelf is an energetic and variable environment even in winter.

II. Introduction

The objective of this work has been to obtain long-term Eulerian time series of currents at selected locations on the outer shelf of the Beaufort Sea. Such measurements are necessary to describe and understand the circulation on the shelf and the exchange between the shelf and the deep Arctic Ocean. It is this circulation and exchange which transports and disperses the plankton, substances of biological and geological consequence, and pollutants. The water motion also influences the ice distribution and drift. The current time series must be long enough to define the important temporal scales of motion.

III. Current state of knowledge

Much of what is known about the circulation on the outer shelf is in fact based on hydrography. Such inferences were discussed in last year's annual report for RU 151.

There have also been several direct measurements of currents on the outer shelf. Hufford (unpublished data) measured the flow at 25 m in water 54 m deep some 60 km east of Barrow for two weeks in August 1972. He found a strong eastward flow, averaging 60 cm sec^{-1} the first week. The current then decreased to less than 10 cm sec^{-1} , and on occasion reversed its direction, before resuming its eastward flow at more than 40 cm sec^{-1} a week later. The decrease during the second week occurred during a period of strong easterly winds.

In the annual report of two years ago for RU 91, we discussed a current series from 100 m, in water 225 m deep, north of Oliktok. The measurements extended from late May to the beginning of September 1976, during which time the velocity varied between 56 cm sec^{-1} easterly and 26 cm sec^{-1} westerly. The entire 95-day record was dominated by large low-frequency oscillations which had a typical peak-to-peak amplitude exceeding 50 cm sec^{-1} and a time scale of order 10 days. In effect, the oscillations represented long bursts of high easterly velocity separated by shorter periods of lesser flow toward the west. Between the easterly bursts, there were frequently smaller oscillations with amplitude and time scale of order 10 cm sec^{-1} and two days, respectively. August showed particularly large and long eastward bursts. The flow did not alternate strictly between east and west, for there were also appreciable north-south motions. Rather there was a tendency for the oscillations to be directed along the line 100° - 280° T. This is identical to the local isobath trend, so that the oscillations nearly represent alternating motion along the shelf edge. The mean motion also appears to be steered by the bathymetry. During 27 May-14 July the mean set was 0.7 cm sec^{-1} toward 100° T and during 16 July-1 September 18.5 cm sec^{-1} toward 98° T.

These same records show rather clear tidal signals, considerably larger than those recorded on the inner shelf and reported in the previous year's annual report for RU 91. The tidal amplitude was in the neighborhood of 5 cm sec^{-1} , and there appeared to be a diurnal inequality near the time of maximum lunar declination. Examination of the spectral estimates in the tidal band showed typical amplitudes of 2 - 4 cm sec^{-1} for the M_2 , S_2 , K_1 and O_1 constituents.

Neither the wind nor the surface pressure records from shore stations during the period of current measurements showed any convincing correlation with the flow measured in 1976.

Of the two instruments recovered in 1977, one recorded from 29 March to 21 October 1977. This meter was located at a nominal depth of 152 m NNE of Lonely in water 192 m deep. The second instrument was at 78 m and recorded from 29 March to 6 April.

As was the case on the shelf north of Oliktok the previous year, the flow was quite energetic over a broad range of subtidal frequencies. As an example, in the very low-frequency band, consider Table 1. This shows the mean current vector for consecutive time segments of three weeks each. The mean can vary by an order of magnitude and be in opposite directions.

Table 1

3-week time segment no.	Vector mean current magnitude cm sec ⁻¹	Vector mean current direction °T
1	11.2	305
2	1.5	257
3	1.8	180
4	9.4	139
5	2.0	219
6	12.4	136
7	3.2	127
8	9.3	131
9	6.3	127

Thus, even on this time scale the mean is clearly not a stationary statistic. Likewise, the variance of the flow is not stationary, as was discussed in last year's annual report. We are thus dealing with a highly variable and irregular flow.

There is, however, evidence for a certain amount of vertical coherence in the flow. The upper current meter recorded the events about 75 m higher in the water column during the first eight days of the long record discussed above. Both it and the lower meter showed northwesterly flow the first two to three days, followed by a reversal for a similar time, and then a return to northwesterly flow. The current vector at both meters appears to have rotated cyclonically. However, the records at the two levels are sufficiently different to indicate that the variability had a significant baroclinic component. For example, the initial northwesterly flow was as much as 25 cm sec⁻¹ at the lower meter, but less than 15 cm sec⁻¹ at the upper. On the other hand, during the reversal the upper meter showed speeds of 10 cm sec⁻¹, while the lower meter indicated threshold speeds (less than 2 cm sec⁻¹).

There is also evidence for topographic control of the flow. As can be seen from Table 1, the predominant direction was about 130°T; during the first three weeks the motion was strongly in the reciprocal direction. This is probably quite close to the local isobath trend, although the proximity of what is probably a sea valley complicates the picture somewhat. The vector mean flow over the entire record was also in about the same direction, *viz*, toward 145°T at 3.4 cm sec⁻¹.

On the whole there is in this record a sense of reciprocating motion along the shelf, much as was found north of Oliktok, with the north- and east-components of velocity being about 180° apart in phase over the coherent frequency bands. On the other hand, there were a few times during which the current was more nearly rotatory.

There were also considerable temperature fluctuations. However, the coherence between the velocity and temperature records was generally quite poor. The few cases that did show significant coherence differed among themselves in phase.

IV. Study area

The area of interest extends eastward from Point Barrow along the entire northern Alaska coast, *i.e.*, from about $156^\circ 30'W$ to $141^\circ W$, a lateral distance of 600 km. The shelf is narrow, with the shelf break typically 80-90 km offshore. The total runoff is small and highly seasonal. Tidal amplitudes are also small; they are mixed, predominantly semi-diurnal. Meteorological tides can exceed the astronomic tide by a factor of ten. The prevailing winds are from the ENE and are generally light. The entire area is covered by sea ice, both first- and multi-year, through all but two to three months. Even during the height of summer, ice is usually found well onto the shelf.

V. Data collection

The methods and rationale of data collection have been discussed at some length in earlier reports, both annual and quarterly.

VI. Results

The field work accomplished during this reporting period includes the recovery of three moorings in the Lonely section in October-November 1978, and the development of two moorings each in the Oliktok and Flaxman Island sectors in February, 1979. The recoveries were described in the quarterly report of 27 December 1978, while the deployments are described in the preliminary report (Ref M79-18) appended to this annual report.

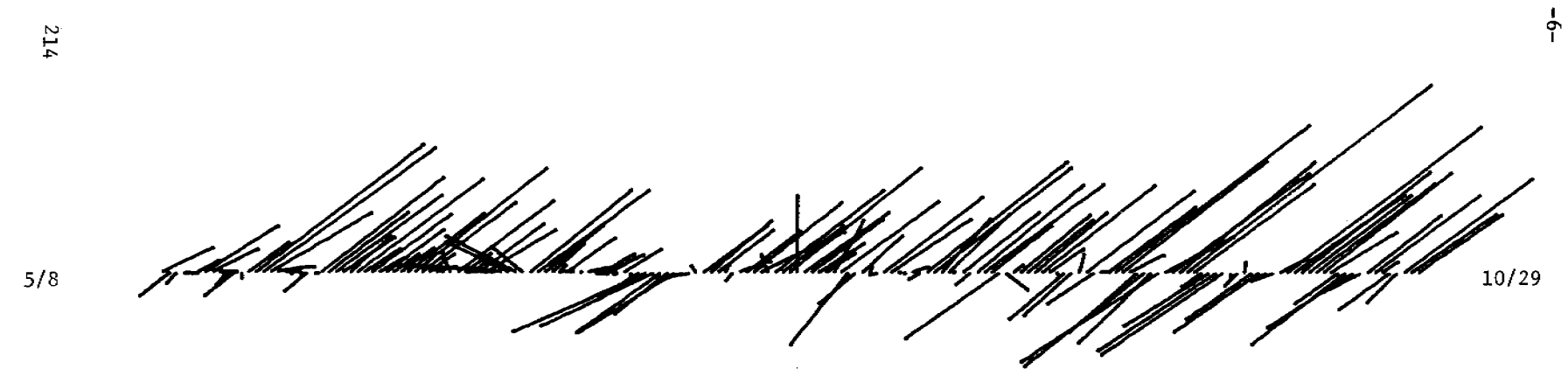
Table 2 summarizes the four current meter records from the fall mooring recoveries. There are a total of over 22,000 hours of clean data.

Table 2

Current meter	Lonely 4	Lonely 5	Lonely 6 upper	Lonely 6 lower
Latitude	71°31.8'N	71°17.0'N	71°17.7'N	71°17.7'N
Longitude	152°15.3'W	150°44.1'W	150°37.9'W	150°37.9'W
Sounding	192 m	99 m	203 m	203 m
Depth of meter	177 m	64 m	68 m	188 m
Date deployed	12 Nov 1977	12 Mar 1978	11 Mar 1978	11 Mar 1978
Date recovered	30 Oct 1978	2 Nov 1978	11 Nov 1978	11 Nov 1978
Start of record GMT	13 Nov 1977	13 Mar 1978	11 Mar 1978	11 Mar 1978
End of record GMT	30 Oct 1978	7 Oct 1978	4 Sept 1978	14 Sept 1978
Recording interval	60 min.	20 min.	20 min.	20 min.
No. of records	8,445	14,977	12,353	13,522

The daily mean velocity vectors and temperatures are shown in Figures 1-7. Note that in Figs. 1-3, the eastward current direction is normal to the time axis, so that the prevailing current direction shown is in the main along the east-west axis.

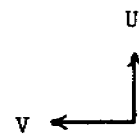
Lonely 4
131014
1 day means



N ←

Figure 1

20 cm/sec = 1 inch
20 days per 1 inch on X axis



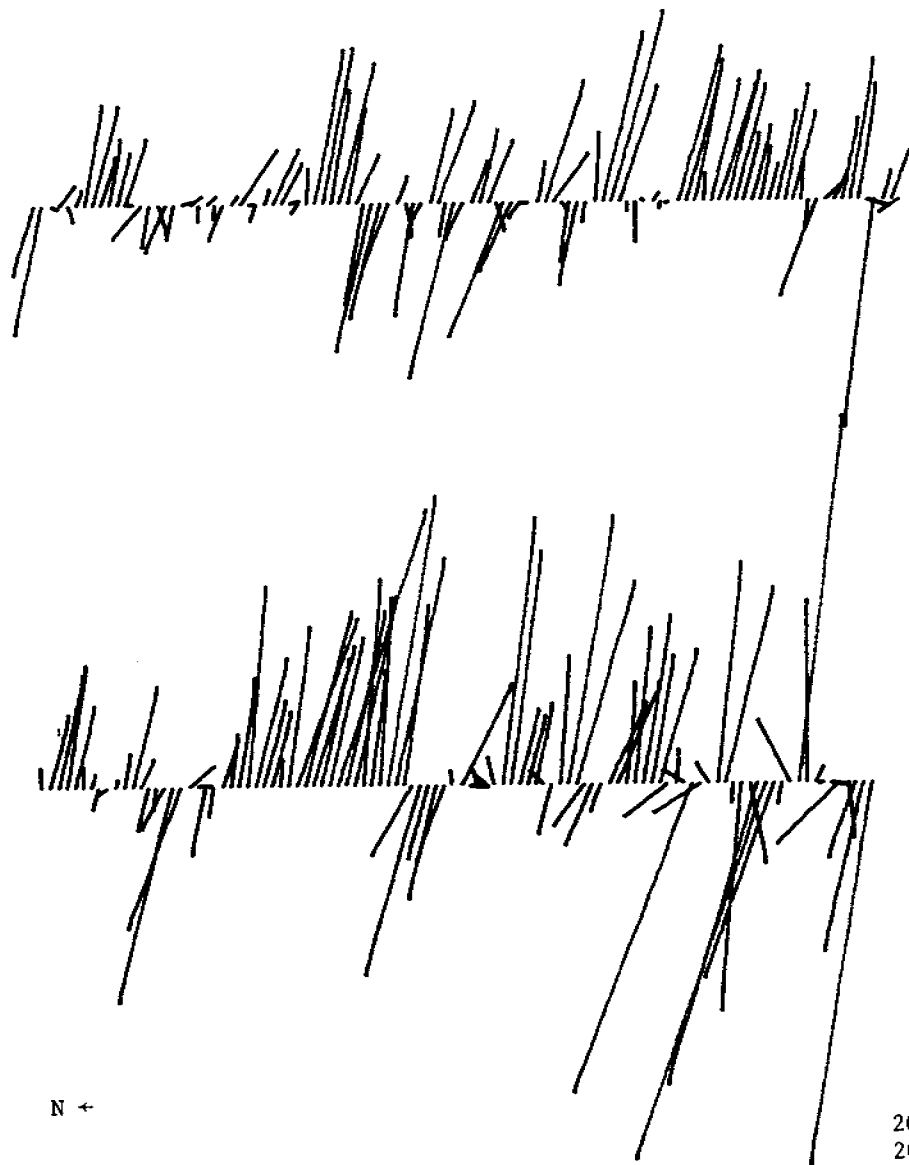
Lonely 5
CM 3169/1
1 day means

3/13 - 3/14

6/26 - 6/27

6/27 - 6/28

10/6 - 10/7



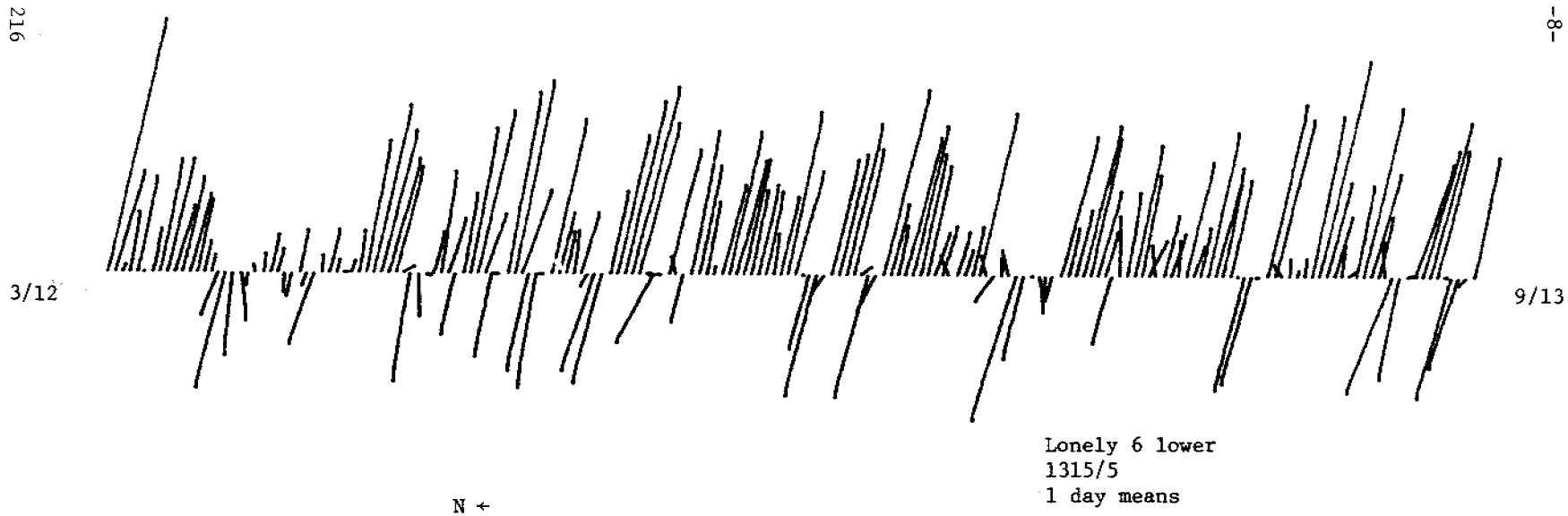
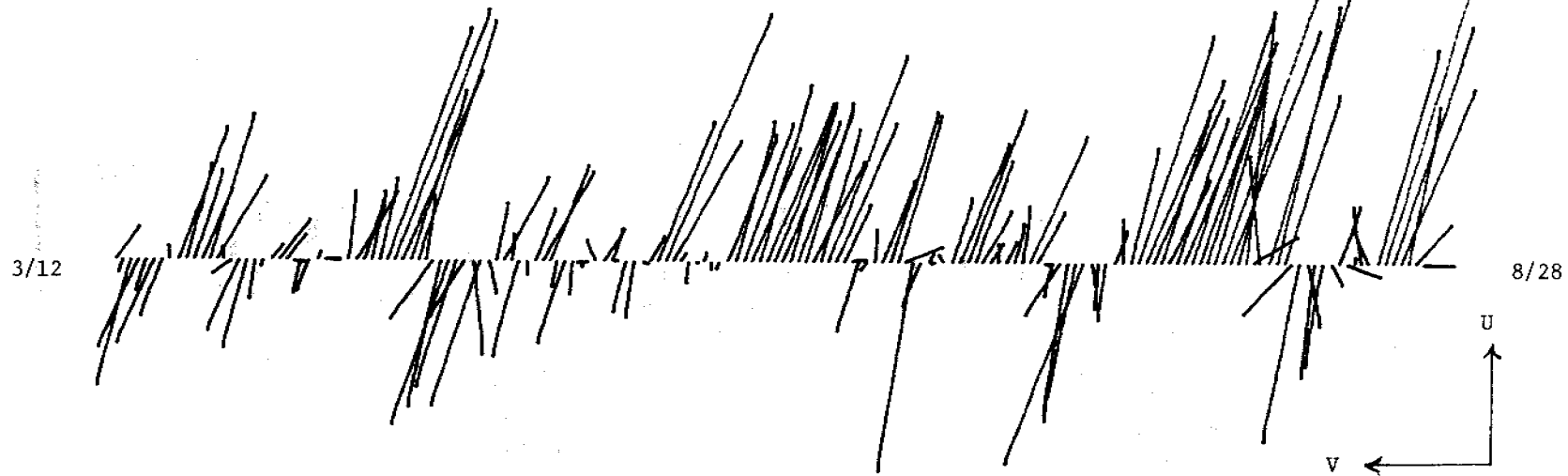
215

-7-

Figure 2

20 cm/sec/inch
20 days per inch

Lonely 6 upper
433/9
1 day means



Lonely 6 lower
1315/5
1 day means

Figure 3

20 cm/sec/inch
20 days per inch

1310/5
Lonely 4

177 m

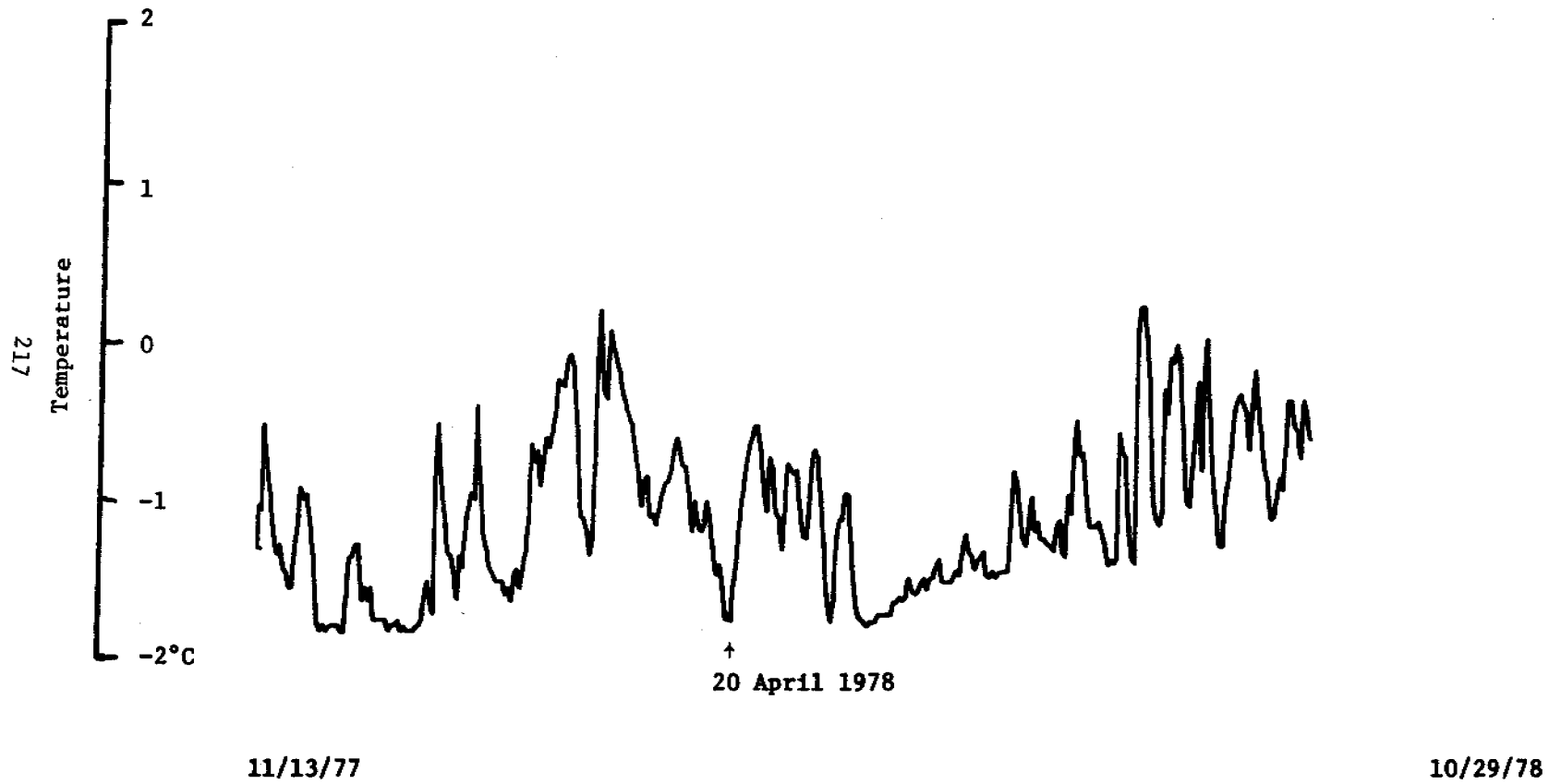


Figure 4

Lonely 5

64 m

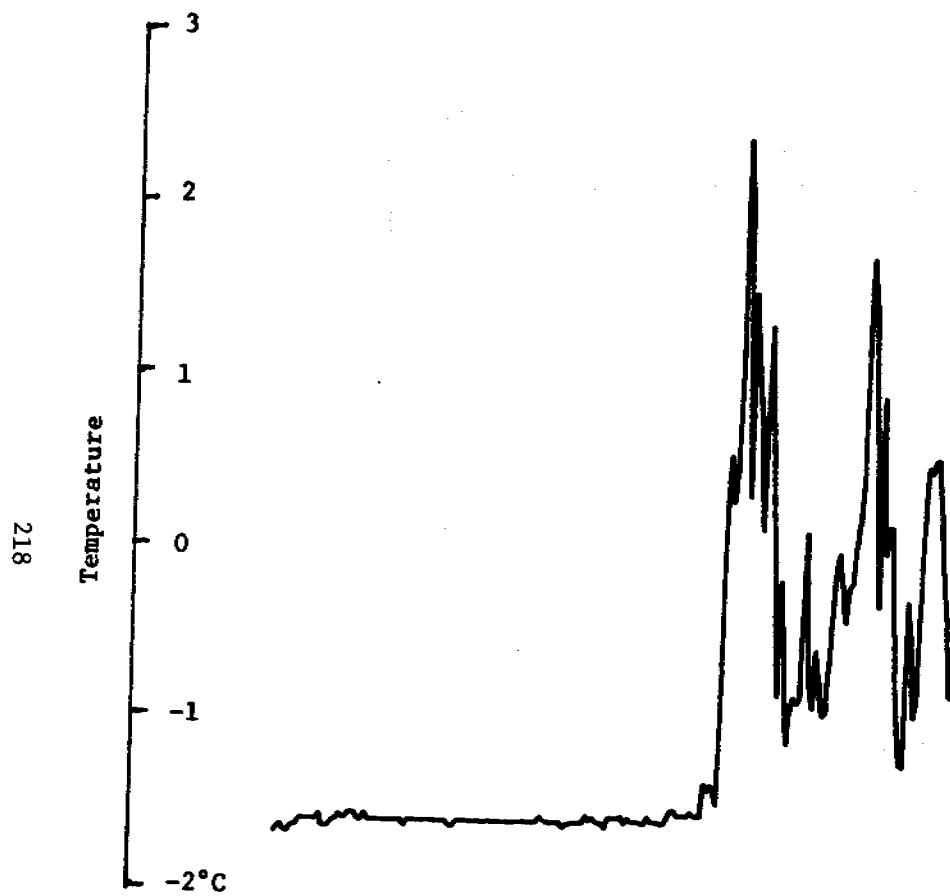


Figure 5

3/13/78

7/28/78

10/7/78

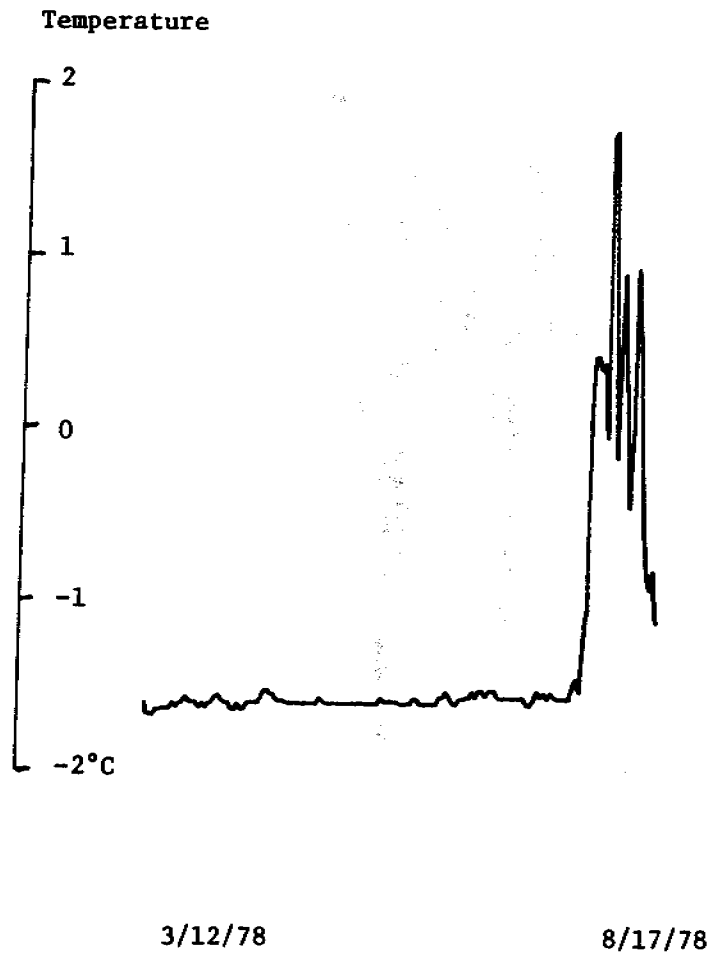


Figure 6

Lonely 6 188 m

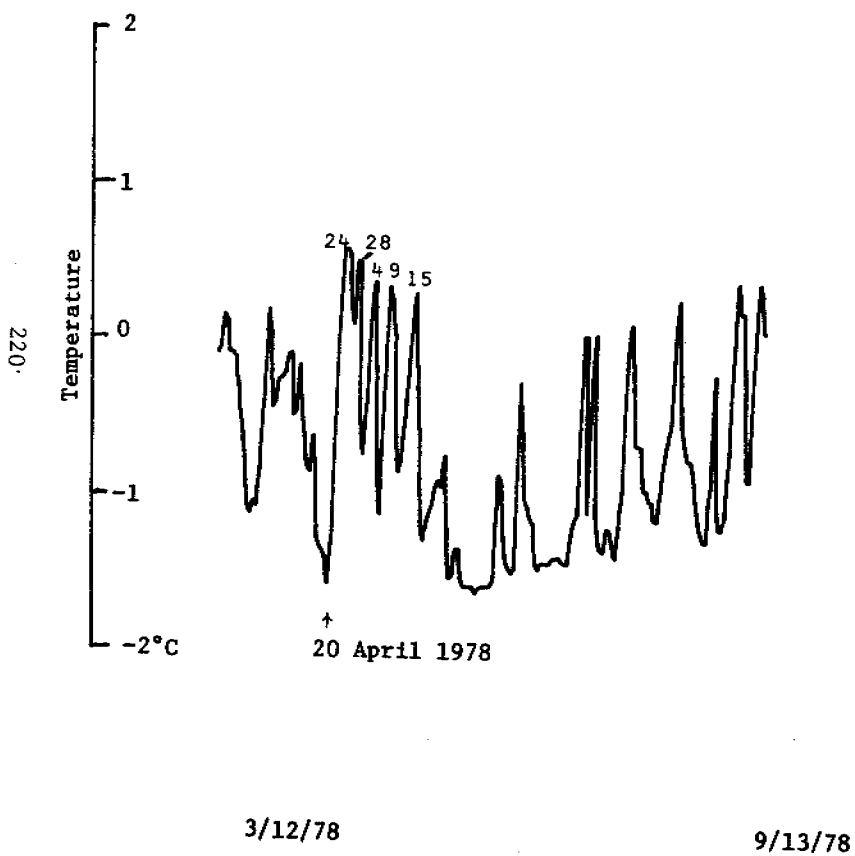


Figure 7

VII. Discussion

The flow is characterized by a series of pulses, in which the water alternately moves nominally eastward or westward along the isobaths in a reciprocating fashion (*cf.* Figs. 1-3). The strength of these pulses is typically 20 cm sec⁻¹ or so, but several pulses exceeded 50 cm sec⁻¹, with a maximum of over 65 cm sec⁻¹. The length of the pulses varies from a day to several weeks, with perhaps a week being a representative time scale. On the whole, the westward pulses are shorter and weaker than the eastward ones, so that the long-term mean flow is eastward.

This can be seen also in Table 3, showing the long-term mean velocity and temperature for these instruments. Note that the operating periods of the four instruments differ, as indicated in Table 2. The flow is on the

Table 3

Current meter	Lonely 4	Lonely 5	Lonely 6 upper	Lonely 6 lower
Vector mean speed	4.8 cm sec ⁻¹	3.8 cm sec ⁻¹	7.1 cm sec ⁻¹	6.9 cm sec ⁻¹
Vector mean direction	142°T	100°T	117°T	102°T
Mean temperature	-1.1°C	-1.0°C	-1.34°C	-0.7°C

whole quite similar to that measured in 1977 (*cf.* Section III, above), with long-term (several months) mean speeds in the range 4-7 cm sec⁻¹ and directed nominally eastward along the isobaths. (The 1977 mooring was in fact situated very close to Lonely 4.) Table 3 may possibly indicate that the mean flow increases as one proceeds seaward across the outer shelf. Nevertheless, instantaneous speeds (20-60 minute means) did not vary greatly from meter to meter, being in the range 57-66 cm sec⁻¹ for the various meters.

Table 4 shows the mean flow characteristics for 30-day intervals during the times that all four meters were operating. The instantaneous temperature range is shown in parentheses.

Table 4

Current meter	Lonely 4	Lonely 5	Lonely 6 upper	Lonely 6 lower
Period				
13 March-11 April	1.3 cm sec ⁻¹ toward 152°T (-1.4 to -0.1°C)	0.8 cm sec ⁻¹ toward 133°T (-1.7 to -1.5°C)	0.6 cm sec ⁻¹ toward 118°T (-1.7 to -1.5°C)	3.2 cm sec ⁻¹ toward 104°T (-1.2 to +0.4°C)
12 April-11 May	5.4 cm sec ⁻¹ toward 148°T (-1.8 to -0.1°C)	0.4 cm sec ⁻¹ toward 106°T (-1.7 to -1.5°C)	3.6 cm sec ⁻¹ toward 116°T (-1.7 to -1.4°C)	7.0 cm sec ⁻¹ toward 104°T (-1.6 to +0.6°C)
12 May-10 June	8.0 cm sec ⁻¹ toward 147°T (-1.8 to -0.6°C)	7.1 cm sec ⁻¹ toward 107°T (-1.6 to -1.5°C)	10.2 cm sec ⁻¹ toward 112°T (-1.8 to -1.5°C)	8.6 cm sec ⁻¹ toward 101°T (-1.6 to +0.5°C)
11 June-10 July	5.5 cm sec ⁻¹ toward 128°T (-1.7 to -1.0°C)	4.1 cm sec ⁻¹ toward 104°T (-1.7 to -1.5°C)	7.0 cm sec ⁻¹ toward 113°T (-1.7 to -1.5°C)	7.9 cm sec ⁻¹ toward 102°T (-1.6 to +0.2°C)
11 July-9 Aug	3.4 cm sec ⁻¹ toward 128°T (-1.6 to 0.0°C)	11.6 cm sec ⁻¹ toward 102°T (-1.6 to +3.2°C)	14.0 cm sec ⁻¹ toward 108°T (-1.6 to +2.5°C)	6.4 cm sec ⁻¹ toward 102°T (-1.4 to +0.9°C)

During each of the five months, the mean flow was easterly, but the strength of the flow varied greatly from month to month. On the whole, this long-term variability was consistent among the various meters, with low speeds during March-April and the highest during May-June, and July-August. There is no obvious seasonal cycle in the flow, and this is borne out by the record from Lonely 4, extending through the entire year (*cf.* Table 5).

Table 5

Period	Vector mean speed cm sec ⁻¹	Vector mean direction °T	Maximum speed cm sec ⁻¹
13 Nov-12 Dec 1977	12.2	144	48.1
12 Dec 1977-11 Jan 1978	3.6	143	37.7
12 Jan-10 Feb 1978	1.0	145	44.7
11 Feb-12 Mar 1978	1.8	152	44.3
13 Mar-11 April 1978	1.3	152	26.1
12 April-11 May 1978	5.4	148	35.4
12 May-10 June 1978	8.0	147	35.6
11 June-10 July 1978	5.5	128	33.2
11 July-9 Aug 1978	3.4	128	34.6
10 Aug-8 Sept 1978	7.3	142	37.7
9 Sept-8 Oct 1978	1.4	143	65.8

The same conclusion is apparent from examination of Fig. 1.

As to the direction of flow, it does indeed appear to be steered bathymetrically. Although the area is not well sounded, the best available charts indicate the isobath trend to be 150°T at Lonely 4, 120°T at Lonely 5, and 125°T at Lonely 6; which are all in reasonable agreement with the mean flow directions in Tables 3-5 and Figs. 1-3. In particular, the more southerly trend at Lonely 4 corresponds to the isobath orientation there being substantially different from that at Lonely 5 and Lonely 6.

The temperature records are particularly interesting. Note in Table 4 that while Lonely 5 and Lonely 6 upper show temperatures within a few tenths of a degree of freezing (except during the last 30-day period), Lonely 4 and Lonely 6 lower registered the presence of warm water during every period. The effect was particularly pronounced at Lonely 6 lower. Figures 4-7 show the situation in more detail.

At the two shallow meters (Lonely 5 and 6 upper), both about 65 m below the surface, the temperature remained fairly close to the freezing point until the fourth week in July, when it shot up dramatically; the increase was about 2°C over four days. This probably represents the arrival of a warm front of water from the Bering Sea (*cf.* Figs. 5 and 6). Immediately preceding and during the temperature change, the flow was in fact easterly. Subsequent to this initial advective summer warming, the temperature fluctuated in a complex pulse-like manner, with amplitudes of up to several degrees. The major pulses of warm water were preceded by easterly flow and those of cold water by westerly. The pulses were very similar at both meters, located about 4 km apart. These two meters were therefore registering a temperature regime which was advectively controlled, but until late July all the water in the region at that depth was strongly influenced by the freezing process, regardless of the origin of the water. During the summer, strong temperature gradients exist, and waters of different origin being advected past the meters caused a highly variable local temperature regime.

The temperature changes at the two lower meters (Lonely 4 and 6 lower), located 180-190 m below the surface, represent a different thermal history (*cf.* Figs. 4, 7). Nevertheless, it is again an advectively controlled one. The difference is that even during winter, temperatures $1-2^{\circ}\text{C}$ above the freezing point occurred frequently and in a pulse-like manner, with daily mean temperatures occasionally exceeding 0.5°C . This water can only represent Atlantic water moving onto the shelf, in effect upwelling from depths offshore below about 350 m.

Comparison of Figs. 4 and 7 shows the record to be highly coherent. The two meters were located about 60 km apart, so that large portions of the shelf appear to be affected simultaneously by such warm-water invasions. Evidence for even a larger scale to the phenomenon was obtained in 1976, when synoptic CTD sections spanning over 130 km of the shelf showed a similar upwelling (*cf.* Annual Report for RV 151, 1977). The events are very frequent, sometimes separated by only 4-5 days, and water warmer than 0°C can persist for over a week at a time. A preliminary inspection of the

records indicates the warm events to typically occur near the bursts of westerly flow, but firm conclusions await correlation analysis of the temperature and velocity time series.

VIII. Conclusions

An energetic current regime over the outer shelf extends landward to at least the 100 m isobath. The flow is characterized by a series of pulses, in which the water alternately moves eastward or westward along the isobaths in a reciprocating fashion. The strength of these pulses is typically about 20 cm sec^{-1} , but can on occasion exceed 65 cm sec^{-1} , and their duration varies from a day to several weeks. The eastward pulses are generally stronger and longer-lasting. The long-term mean flow is therefore eastward (along the isobaths) and in the range $5\text{--}10 \text{ cm sec}^{-1}$. There does not appear to be any seasonal cycle in the flow. These remarks apply to the motion below about 60 m; above this depth the velocity field is unknown, as the drifting ice makes moored measurements at lesser depths extremely hazardous.

The thermal regime down to at least 65 m is largely advectively controlled, with the water bearing the mark of the freezing process until mid-summer. At that time warm water is advected into the region, probably largely from the Bering Sea, and there are strong horizontal temperature differences. Under these circumstances waters of different origin being advected past a given point cause a highly variable local temperature regime. Closer to the bottom, there is a frequent invasion of warm and saline Atlantic water, occurring in a pulse-like manner and extending over large portions of the shelf. During such events the temperature increases to $1\text{--}2^\circ\text{C}$ or more above the freezing point. The pulses occur at all times of the year and have time scales similar to the reciprocating along-shelf motion discussed above. These are in effect upwelling events from 350 m or deeper offshore, and they must bring relatively large amounts of salt and sensible heat onto the shelf.

XI. Needs for further study

There are two major tasks for the future, one of analysis and one of experiment. The first is to provide a dynamic understanding of the available observations. Should the flow prove to be forced by atmospheric events, a key question may prove to be whether or not available meteorological data are adequate for model testing.

The second task is to extend the measurements further inshore. A first step in this process is being taken in FY 1979 under RV 91. However, moorings in water shallower than about 60 m involve exponentially increasing risk factors, and they require a different deployment strategy.

X. Summary of January-March Quarter

A. Field operations

See appended report.

B. Estimate of funds expended to February 28, 1979

Allocation	10/1/78 - 9/30/79		\$60,300
1. Salaries. Faculty and staff		7,246	
2. Benefits		1,087	
3. Indirect costs		3,892	
4. Supplies and other direct costs		11,807	
5. Equipment		206	
6. Travel		<u>1,912</u>	
Total expenditures		\$26,150	
Balance			\$34,150

XI. Auxiliary Material

A paper was published in the reviewed literature in 1978:

Aagaard, Knut, Clark Darnall, and Fred Karig (1978)
Measurements with moored instruments in ice-covered
waters. *Deep-Sea Res.*, 25, 127-128.

A second paper was presented at the Fall 1978 AGU meeting:

Aagaard, Knut and Richard B. Tripp (1978) Saline water
on the northern Alaskan shelves. *EOS*, 59(12), 1091.

University of Washington
Department of Oceanography
Seattle, Washington 98195

Preliminary Report

University of Washington Participation in
NOAA Recovery/Deployment Phase of Cruise W-32
Current Measurements in Possible Dispersal Regions
of the Beaufort Sea
17 February - 24 February 1979

by

Clark Darnall

NOAA Contract 03-5-022-67, TO 3

Approved by:



Knut Aagaard, Research Professor
Principal Investigator



George Anderson, Professor
Associate Chairman for Research

1. *Objectives*

To look at the time-dependent circulation and dynamics of the outer continental shelf of the Beaufort Sea, by means of long-term Eulerian time-series current studies at selected locations, where the ice cover is not seasonally removed. Cruise W-32 was a deployment phase of the current meter studies.

2. *Narrative*

Mooring deployment phase

Two moorings were deployed 40-45 mi NE of Oliktok, Alaska, and two moorings were deployed 30-35 mi north of Flaxman Island, Alaska. At each area, there was an inshore mooring deployed in 60 m (water depth) with current meters at 40 m and 50 m, and an acoustic transponder/release at 54 m, and an offshore mooring deployed in 100 m with current meters at 50 m and 90 m, and release at 94 m.

A physical description and location of the moorings is in the Appendix.

The report of events is as follows:

17 February 1979 S. Harding arrived in Deadhorse, began unpacking and setting up equipment.

18 February 1979 C. Darnall arrived in Barrow to pick up deployment equipment stored at NARL.

19 February 1979 C. Darnall flew to Deadhorse in NARL twin otter N127RL. Flight time one hour, 30 minutes. Both NOAA helicopters N56RF (pilot Lt. Laydon, mechanic Mr. Dehart) and N57RF (pilot Mr. LaBonty, mechanic Mr. Mitchell) were already at Mukluk Camp, Deadhorse, Alaska, therefore we were able to start our deployments immediately. We used N57RF (on Tundra skids) and Mr. Lloyd Lowery (who was performing seal surveys in the area) used N56RF (on floats). Mr. Lowery kindly agreed to ferry our anchors and flotation to our mooring site and then hunt seals in the general area for the rest of the day.

20 February 1979 Weather clear, winds light easterly, temperature -27°C.

- 0845 AST - Harding, Persons, Darnall departed Mukluk Camp in N57RF (LaBonty). We refueled at Deadhorse International Airport and headed for the inshore mooring NE of Oliktok (designated Oliktok #1). Lowery in N56RF followed about 45 minutes later.
- 1100 AST - After seven landing/depth soundings, we had 60 m. This position 71° 10.0' N, 148° 52.7' W was further north than we had expected. N56RF dropped off the anchors and flotation.
- 1230 AST - AMF 322 transponder/release in the water. We heard it occasionally pinging.
- 1245 AST - Lower current meter in the water.
- 1315 AST - Upper current meter in the water.
- 1321 AST - The mooring was cut loose and in place. We loaded up and returned to Mukluk Camp.
Day flight time one hour, 40 minutes.
We set up the current meters for the next day, charged the echo sounder battery, and prepared for mooring Oliktok #2.

21 February 1979 Weather high thin stratus, winds, 280°M, 8 kts., temperature -23°C.

- 0810 AST - Harding and Darnall departed Mukluk Camp in N57RF (LaBonty and Mitchell).
- 0945 AST - After several soundings we had 115 m water depth. N56RF dropped our anchors and flotation. Position 71° 11.4' N, 148° 44.3' W.
- 1047 AST - AMF 322 transponder/release in the water (occasionally pinging).
- 1104 AST - Lower current meter in the water.
- 1134 AST - Upper current meter in the water.
- 1143 AST - Mooring was in place. We headed for Mukluk.
Day flight time one hour, 50 minutes.
We prepared for next mooring (designated Flaxman #1).
Dr. Roy Overstreet from NOAA at Boulder arrived. He observed and assisted in our remaining deployments.

22 February 1979 Weather clear, wind 290°M, 8 kts., temperature -26°C.

- 0800 AST - Harding, Overstreet and Darnall departed Mukluk in N57RF (LaBonty).
- 0925 AST - We found our depth (59 m) and began our set up. N56RF delivered its load. Position 70° 42.7' N, 146° 2.6' W.

0956 AST - AMF 322 transponder/release in the water (occasionally pinging).

1005 AST - Lower current meter in the water.

1055 AST - Upper current meter in the water.

1100 AST - Mooring in place. We returned and prepared for next mooring.
Day's flight time one hour, 22 minutes.

23 February 1979 Weather clear (with clouds to the east), wind 270°M, 12 kt.,
temperature -26°C.

0810 AST - Harding, Overstreet, and Darnall departed Mukluk in N57RF (Laydon).

0935 AST - Depth was 108 m, floats and anchor delivered. Weather had deteriorated,
snowing, with limited visibility. Position 70° 51.4' N, 145° 45.0' W.

1025 AST - AMF 322 in the water.

1036 AST - Lower current meter in the water.

1126 AST - Upper current meter in the water. Before the upper flotation unit
was hooked up, our lowering line parted, and the mooring dropped
into position. There is enough buoyancy in the lower flotation
to recover the mooring, but the upper current meter will not be
functioning properly.

1128 AST - Mooring in place and we packed up. The weather was quite nasty
by this time and the visibility low.
Day's flight time one hour, 35 minutes.

24 February 1979 We packed our equipment and airshipped it to Seattle.
Harding returned to Seattle.

25 February 1979 Darnall returned to Seattle.

3. *Methods*

Deployment phase

The current meter moorings were designed and constructed at the Department of Oceanography, University of Washington. The flotation was 18 inch glass spheres distributed along the mooring. The current meters were Aanderaa Model RCM-4. The acoustic transponder/releases were AMF Model 322. The mooring line was 1/4-inch diameter Miniline using Kevlar Fibers; it was pre-measured, cut and loaded on aluminum reels with connecting links at all

instrument and flotation points. The anchor consisted of lengths of railroad rails (each approximately 70 lbs.), with galvanized chain laced through holes cut in one end.

The deployment equipment consisted of a ten-foot high A-frame which holds the mooring line reel, and is used for an anchor-first, vertical deployment mode. Hydraulic disc brakes and a stopper controlled the descent speed, and allowed for insertions of instruments and flotation. All components of the deployment system are of lightweight material and can be broken down for helicopter-borne operations.

4. *Personnel*

Stephen Harding	Research Aide	University of Washington
Clark Darnall	Oceanographer	University of Washington
Kate Persons	OCS co-ordinator	NOAA
Roy Overstreet	Project Manager	NOAA
Bob LaBonty	Pilot	NOAA
Terry Laydon	Pilot	NOAA
Roy Dehart	Mechanic	NOAA
Gary Mitchell	Mechanic	NOAA

Acknowledgments

The NOAA flight crew's performance in maintaining and operating and assisting us on the ice was essential to our operations. Ms. Persons' coordination of the OCS project at Mukluk Camp and her cheerful assistance of our deployments was greatly appreciated. I would also like to thank Dr. Roy Overstreet for his help, and hopefully he had an enjoyable and informative trip. The willingness of Mr. Lloyd Lowery to help us with our project, while setting a record of seals taken in the time span, greatly simplified and eased our job.

APPENDIX

Mooring locations:

Oliktok 1 - 71° 10.0' N, 148° 52.7' W

Oliktok 2 - 71° 4.4' N, 148° 44.3' W

Flaxman 1 - 70° 42.7' N, 146° 2.6' W

Flaxman 2 - 70° 51.4' N, 145° 45.0' W

Flight time:

NOAA Helicopter N57RF - 3 hours, 27 minutes.

FIFTH ANNUAL REPORT

Research Unit # 138

Reporting Period: 1 April 1978-
31 March 1979

Number of Pages:

NORTHWEST GULF OF ALASKA SHELF CIRCULATION

R.D. Muench
J.D. Schumacher
R. Sillcox

Pacific Marine Environmental Laboratory
3711-15th Avenue, N.E.
Seattle, Washington 98105

31 March 1979

I. Summary

Field investigations, begun in Autumn 1974, have and continue to provide data which aid our understanding of hydrographic and current regimes in the northern Gulf of Alaska. Important features identified include:

- Description of mean flow in lower Cook Inlet and verification of the flow using new field data.
- Verification of a strong southwesterly flow through Shelikof Strait related to forcing on the shelf outside of the shelf outside of the Barren Islands.
- Delineation of annual variability of baroclinic transport in the Alaskan Stream.
- Description of circulation and hydrography over the continental shelf of the northwest Gulf of Alaska during fall, winter and spring.

Further analysis of the field data collected during the past year will focus on explaining driving mechanisms for mean and fluctuating flow components and evaluating their importance relative to pollutant transport.

II. Introduction

A. General Nature and Scope of Study

The general objective of this work unit is to relate oceanic advective and diffusive processes to potential pollution problems due to OCS petroleum development. This is being accomplished through field activities including moored current measurements and water mass analysis using temperature and salinity observations. The region being considered includes the northwest Gulf of Alaska continental shelf west from about the longitude of Seward, Alaska to Unimak Pass and extends offshore to the outer boundary of the Alaskan Stream some 100 km off Kodiak Island.

B. Specific Objectives

1. Kodiak Island region

- a) Examine flow over the troughs and banks off Kodiak Island and on the shelf downstream from Shelikof Strait using current meters, drift cards and hydrographic data.
- b) Characterize temporal and spatial variability in the flow field as a function of season.
- c) Relate observed and computed geostrophic surface winds to observed currents.
- d) Determine spatial variability of tidal currents.
- e) Characterize seasonal hydrographic distributions.

2. Lower Cook Inlet

- a) Relate observed and computed over-the-water winds to observed currents.
- b) Correlate surface currents obtained by Lagrangian techniques with subsurface Eulerian observations.
- c) Relate surface currents obtained by Doppler radar techniques to Lagrangian surface current measurements.
- d) Characterize temporal and spatial variability in the flow field including flows through the Barren Islands and upper Shelikof Strait as a function of season.

3. Mitrofanina Island

- a) Examine correlations between observed currents, meteorological parameters and sealevel variations.
- b) Determine influence of bathymetry on the flow field.
- c) Examine local vs non-local forcing of shelf water motions.
- d) Relate Icy Bay results to this new area in order to test their general applicability.

C. Relevance to Problems of Petroleum Development

Two distinct environmental problems can accompany petroleum development in a marine region; catastrophic spills and chronic or long-term leakage. This research unit addresses both of these problems. The eventual effect of a catastrophic spill depends upon where the spilled oil goes, i.e., its trajectory, how long it takes to get there, and how much diffusion of oil occurs along the trajectory. This study will provide estimates of the fields of water motion which exert primary control over such trajectories and over diffusion processes along the trajectories. Oil introduced into the environment via long-term or chronic leakage is more likely to be dispersed throughout the water column and, possibly, scavenged by suspended particulate matter. The problem then becomes one of understanding net transport of suspended matter, a process related to advective and diffusive fields within the water column. Understanding of these processes requires an analysis of the velocity field and its driving mechanisms. This study addresses these latter points.

III. Current State of Knowledge

The first annual report (32 March 1975) summarized the state of knowledge prior to commencing this study. That report, subsequent reports and publications and Sections VI-VIII of this report update the initial summary.

IV. Study Area

Upon completion of the Final Report for the Northeast Gulf of Alaska Continental Shelf program (1 October 1978), this study has been concerned with the northwestern Gulf of Alaska continental shelf from Portlock Bank east of Kodiak Island (about the longitude of Seward, Alaska) westward to Unimak Pass. Detailed

physical descriptions of this region have been presented in previous annual reports, in manuscripts and in prior publications.

V. Sources, Methods and Rationale of Data Collection

Instrumentation, field and processing methods are identical to those used in the past and are documented in previous reports from this series. Where deviations from standardized methods are significant, they are discussed within the context of the appropriate subregional study.

VI - VIII. Results, Discussion and Conclusions

Many results from the past year's activities have been incorporated into manuscripts for publication either as ERL Technical Reports or in the open oceanographic literature. Four such manuscripts are appended to this annual report and represent a major portion of the productivity of the past year's efforts in analysis:

- Muench, R.D., H.O. Mofjeld & R.L. Charnell 1978. Oceanographic conditions in lower Cook Inlet: spring and summer 1973. J. Geophys. Res. 83(C10), 5090-5098.
- Schumacher, J.D., R. Sillcox, D. Dreves & R.D. Muench 1978. Winter circulation and hydrography over the continental shelf of the northwest Gulf of Alaska. NOAA Technical Report ERL 404-PMEL 31, 16 pp.
- Reed, R.K., R.D. Muench & J.D. Schumacher 1979. On baroclinic transport of the Alaskan Stream near Kodiak Island. (In preparation for submission to Deep-Sea Res.)
- Schumacher, J.D., R.K. Reed, M. Grigsby & D. Dreves 1979. Circulation and hydrography near Kodiak Island; September-November 1977. (Submitted for publication as an ERL Technical Report.)

In addition to these manuscripts, which adequately summarize the scope of analysis carried out during the past year, we discuss below some preliminary results from the lower Cook Inlet current measurement program.

Summary of Results from the lower Cook Inlet current program

Vertical taut-wire arrays of moored current meters were deployed in lower Cook Inlet for two periods of time; winter 1977-78 and summer 1978. Locations of these moorings, superposed upon bathymetry, are indicated on Figure 1. Depths of meters on each mooring and periods of deployment are listed in Table 1. Actual lengths of record did not necessarily coincide with mooring periods; in several cases malfunctions caused records to be considerably shorter than the full mooring period.

The mean currents observed can be described by the use of current roses. Winter data are presented in this format in Figures 2-8. In interpreting these figures, lengths of the lines represent the mean speed of the current which was flowing in the indicated direction. Numbers at the ends of the lines are percentage of the total number of records for which the current was flowing in that direction. For example, the C-1 record from 20 m depth showed a clear flow tendency toward the SSW as 54% of the time currents flowed in that direction

(i.e. the two lines delineated by 27% each). The zeros at the northern edge of the rose indicate that flow was in that direction less than 0.5% of the time. The other roses can be interpreted in similar fashion.

Referring to the current roses, we see a clearly defined flow to the SSW and SW in the western portion of the inlet at C-1 and the C-2 near-surface meter. The deeper meter at C-2 showed greater scatter and a tendency toward bimodal flow (SSW and NNE) which was not evident near the surface. At station C-3 currents were weaker, especially near the bottom, though there was still a tendency for westerly flow. At C-4 the westerly flow tendency was present but very weak. At mooring C-5 the pattern was dramatically different, with larger flows (20-30 cm/sec) and a clear westerly direction. The mooring at C-6 did not yield useable data, but that at C-7 indicated an extremely weak and variable flow with speeds of a few cm/sec and only a slight tendency toward northerly flow. The records from C-8 and C-10 show a strong westerly flow. Taken in concert, these records support the circulation pattern deduced from a more limited data set by Muench et al (1978) as presented in the Appendices.

Examples of u, v and time-stick plots of detided currents from lower Cook Inlet are shown in Figures 10-12. These plots indicate the large degree of variability present in the system despite relatively clear-cut mean directions in many cases. Pronounced fluctuations having time scales of 3-4 days were common; their explanation is the subject of presently ongoing analysis.

IX. Needs for Further Study

- A primary need is for continued analysis of the existing data set.
- We recommend that the synthesis report, due during FY80, be included as a chapter in a book dealing with all aspects of the Kodiak Island regional oceanography. Pertinent results of continuing analysis can then be included in this chapter. More specialized topics will be addressed, as in the past, via contributions to the general oceanographic literature.
- There is a need for additional field work in the embayments, such as Kiliuda Bay, the highly productive region off southern Kodiak Island. Oceanographic experiments should be carried out in conjunction with meteorological experiments, allowing for coupling of wind and water motions.

X. Summary of January-March Quarter

No field work was carried out in this research unit during this quarter.

XI. Auxiliary Material

- A. References Used: None
- B. Papers in preparation or print:

- Muench, R.D., H.O. Mofjeld & R.L. Charnell 1978. Oceanographic conditions in lower Cook Inlet: Spring and Summer 1973. J. Geophys. Res. 83(C10), 5090-5098. (In print)
- Schumacher, J.D., R. Sillcox, D. Dreves & R.D. Muench 1978. Winter circulation and hydrography over the continental shelf of the northwest Gulf of Alaska. NOAA Technical Report ERL 404-PMEL 31, 16 pp. (In print)
- Reed, R.K., R.D. Muench & J.D. Schumacher 1979. On baroclinic transport of the Alaskan Stream near Kodiak Island. (In preparation)
- Schumacher, J.D., R.K. Reed, M. Grigsby & D. Dreves 1979. Circulation and hydrography near Kodiak Island; September-November 1977. (In press)
- Shay, T.J. 1979. Low frequency current fluctuations in the northwest Gulf of Alaska. (In preparation)
- Several other specific topics suitable for manuscripts are also being addressed, but the work is not yet far enough along on these to narrow down to specific titles or subjects.

C. Oral Presentations

- Schumacher, J.D., R. Sillcox, D. Dreves & R.D. Muench 1978. Winter circulation and hydrography over the northwest Gulf of Alaska continental shelf. Eos, Trans, AGU 59(4), 305. (abstract of presentation at Spring 1978 AGU Meeting)
- Sillcox, R., R.D. Muench, J.D. Schumacher & D. Dreves 1978. Winter currents in Shelikof Strait. Eos, Trans, AGU 59(4), 305. (abstract of presentation at Spring/1978 AGU Meeting)
- Shay, T.J. & R.D. Muench 1978. Shelf break currents in the northwestern Gulf of Alaska. Eos, Trans. AGU 59(12), 1091. (abstract of presentation at Fall 1978 AGU Meeting)
- Muench, R.D. 1979. The northern Gulf of Alaska continental shelf- a unique northwest coastal regime. (presented at the First OCS Seminar on the California Continental Shelf and Slope Circulation and Exchange, La Jolla, CA, February 1979)

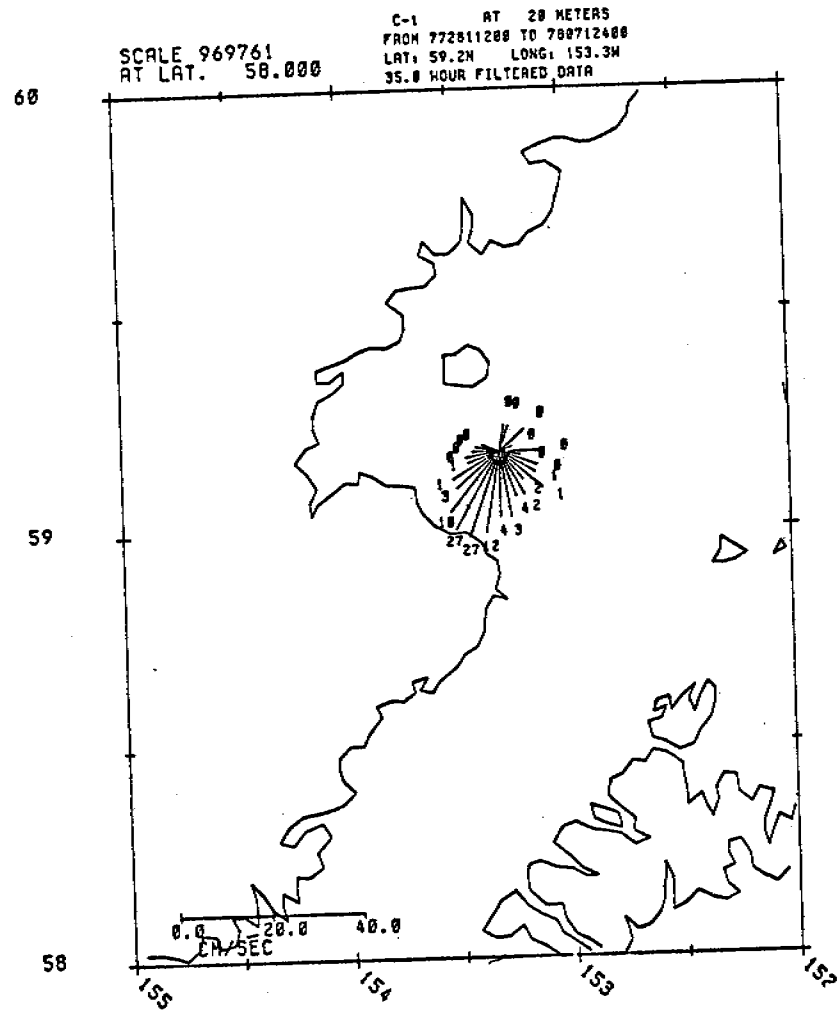
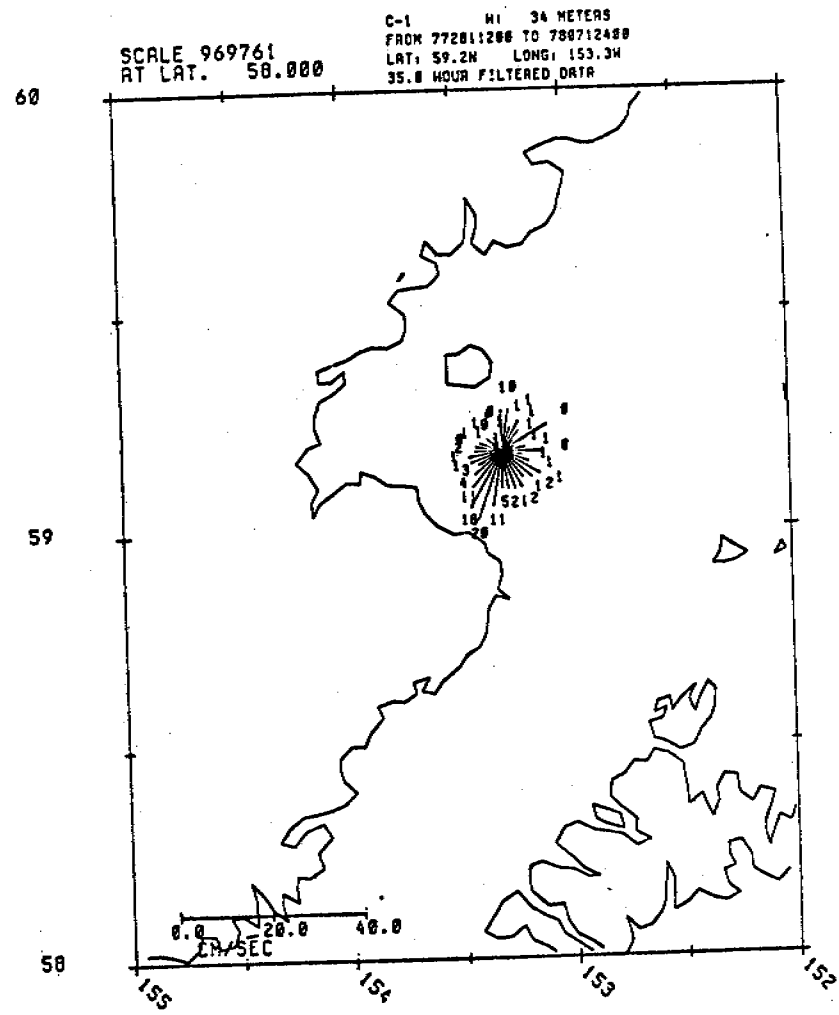


Figure 2.



240

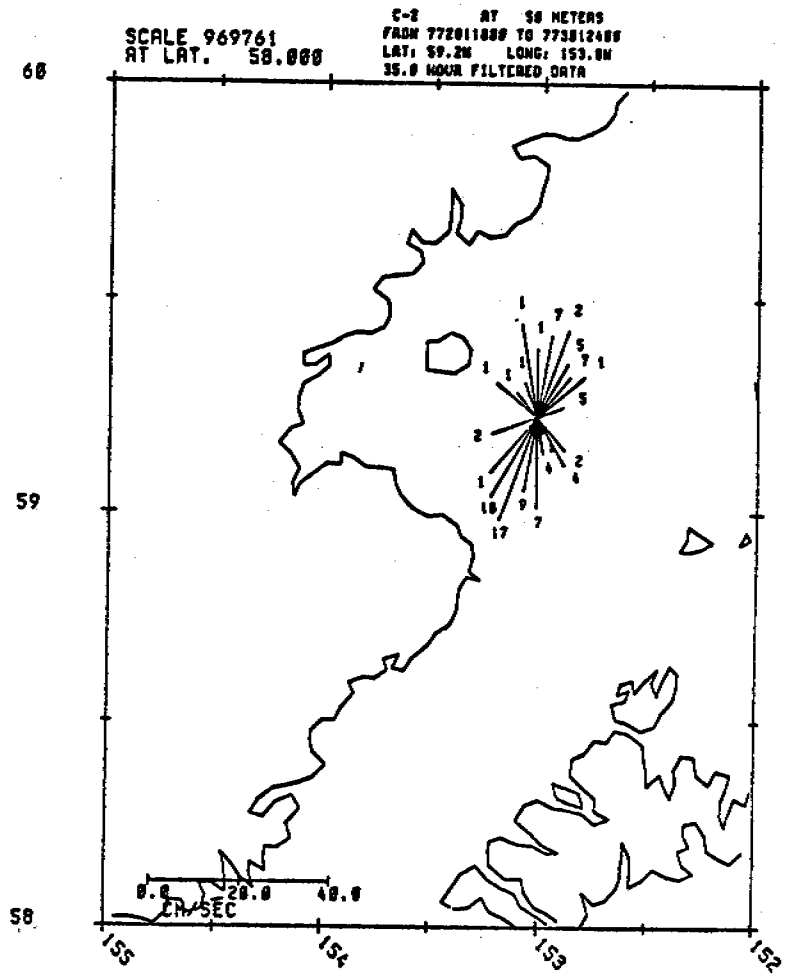
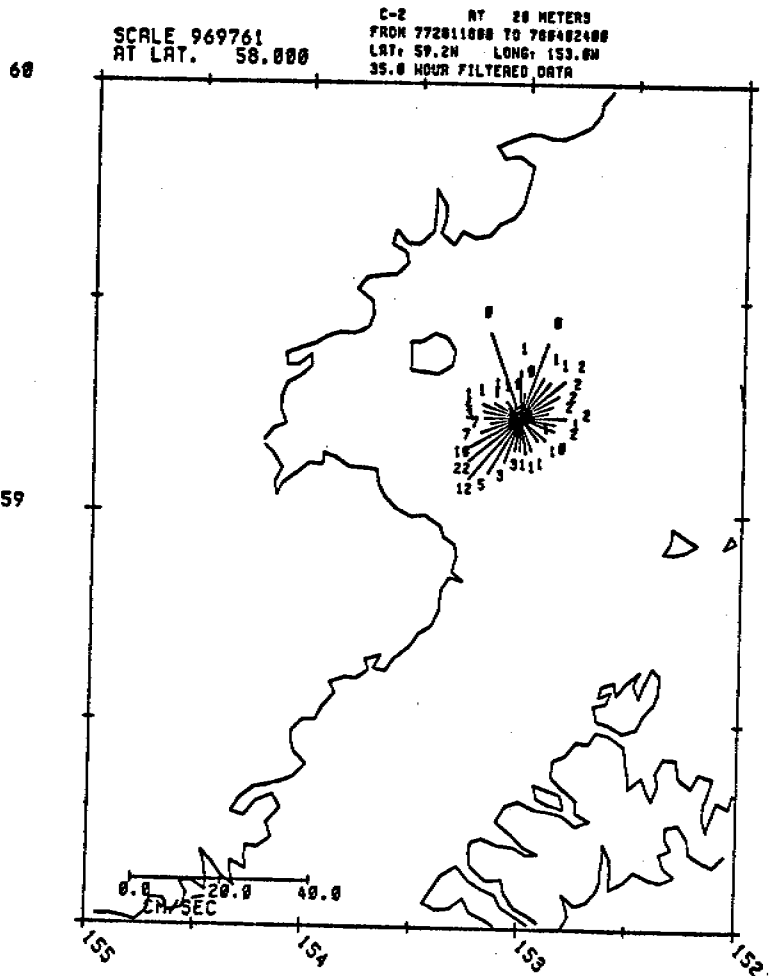


Figure 3.

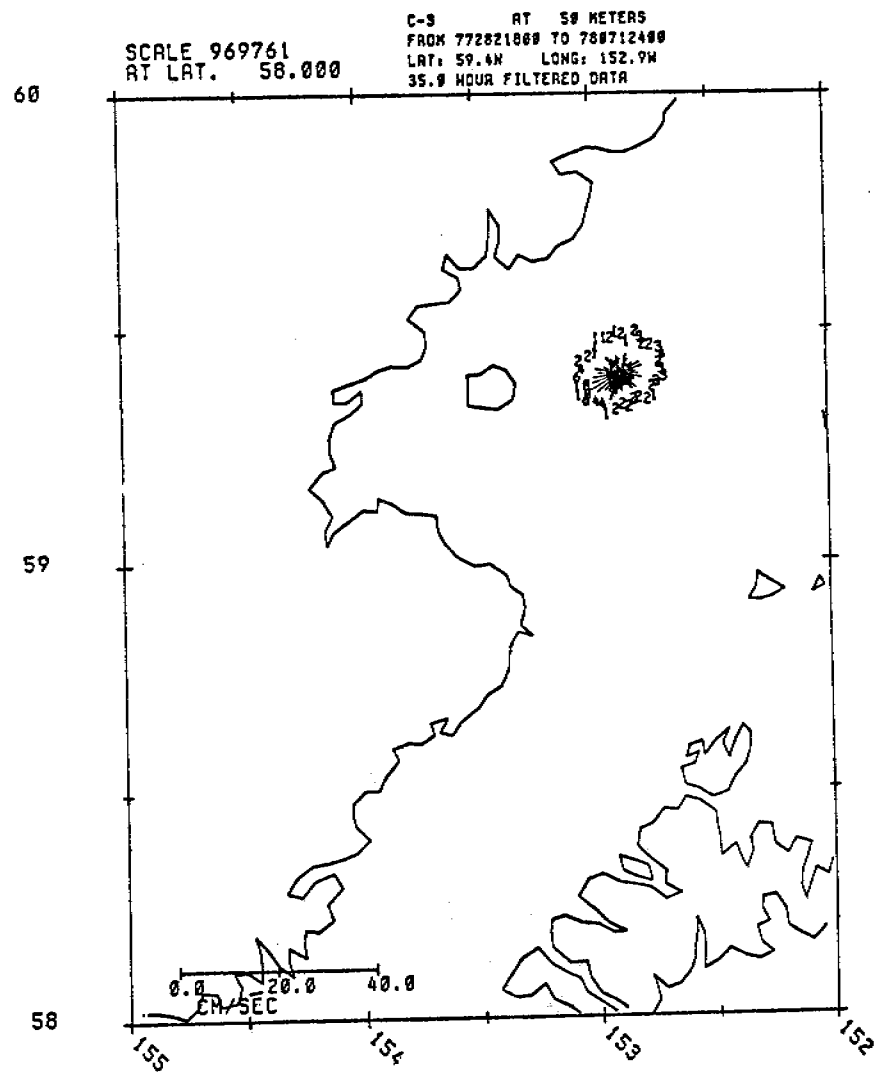
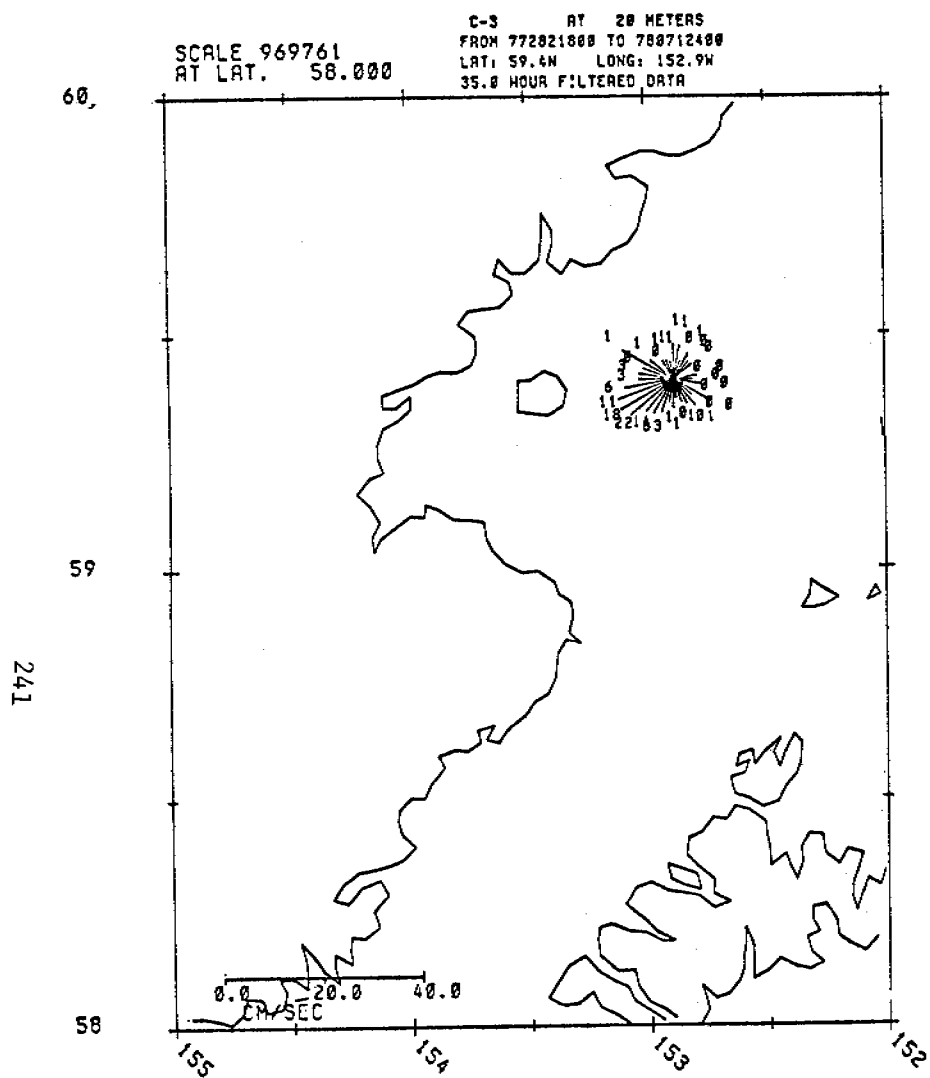


Figure 4.

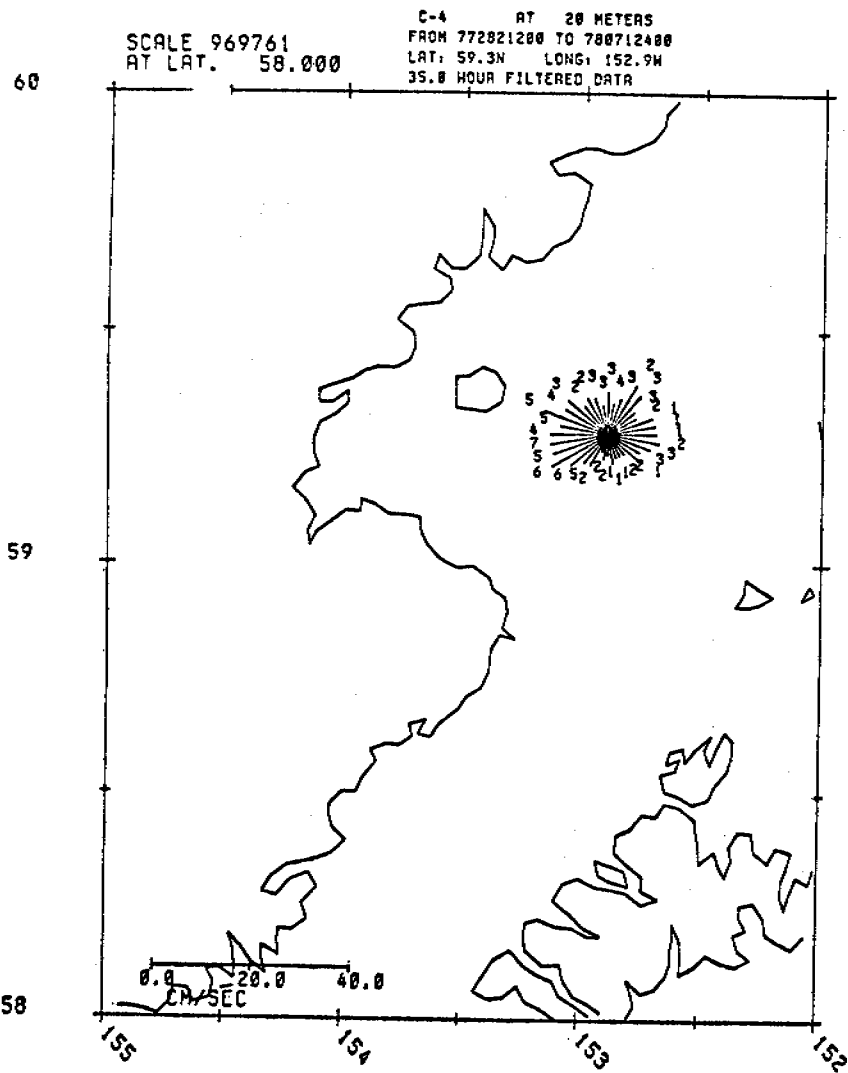
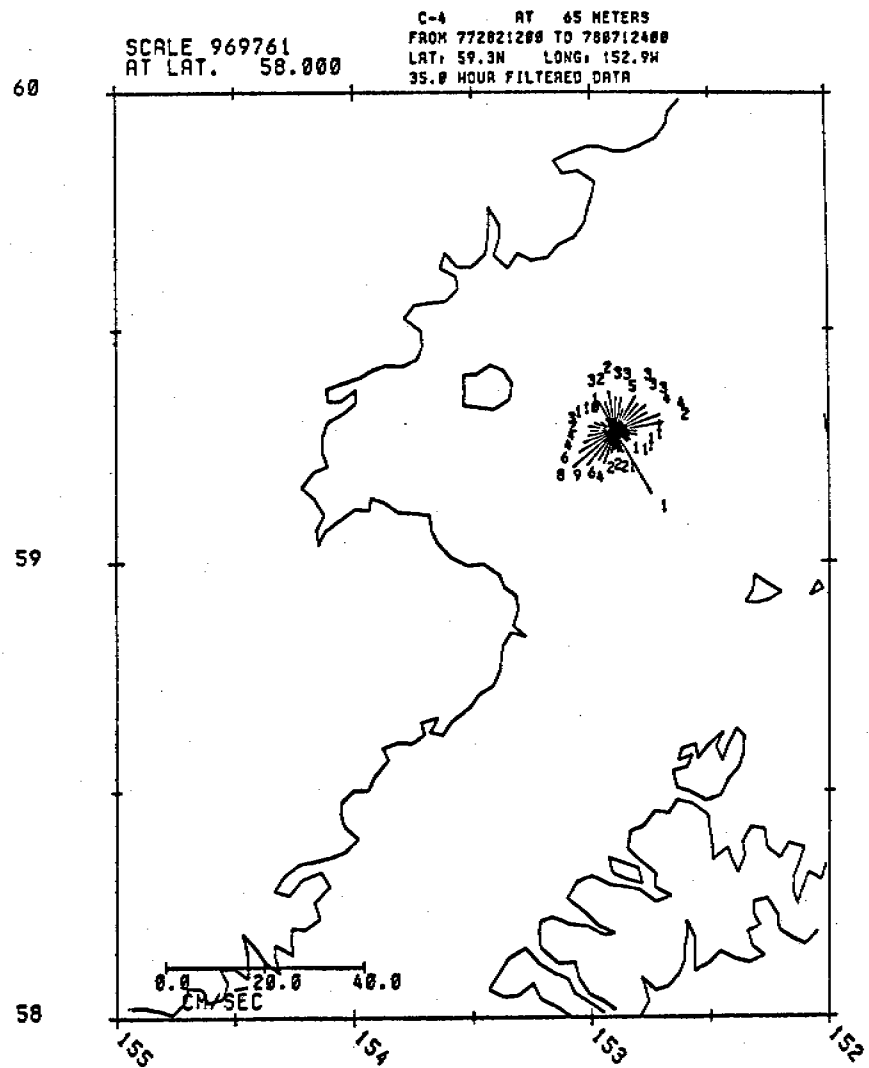


Figure 5.



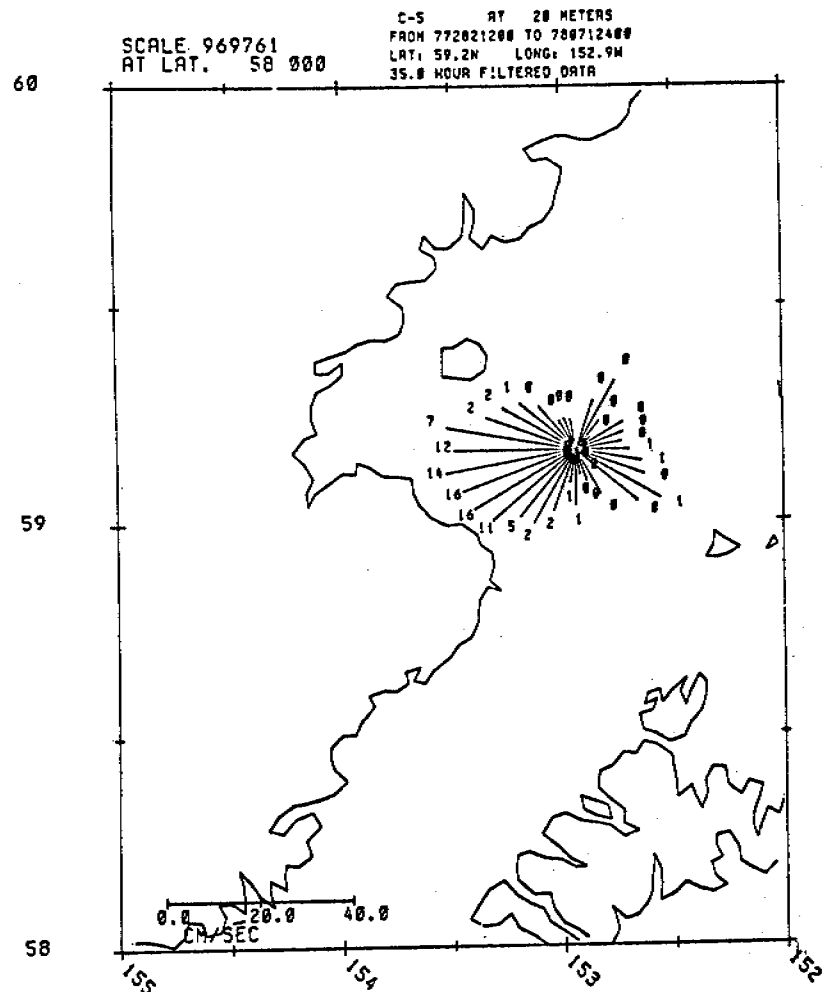
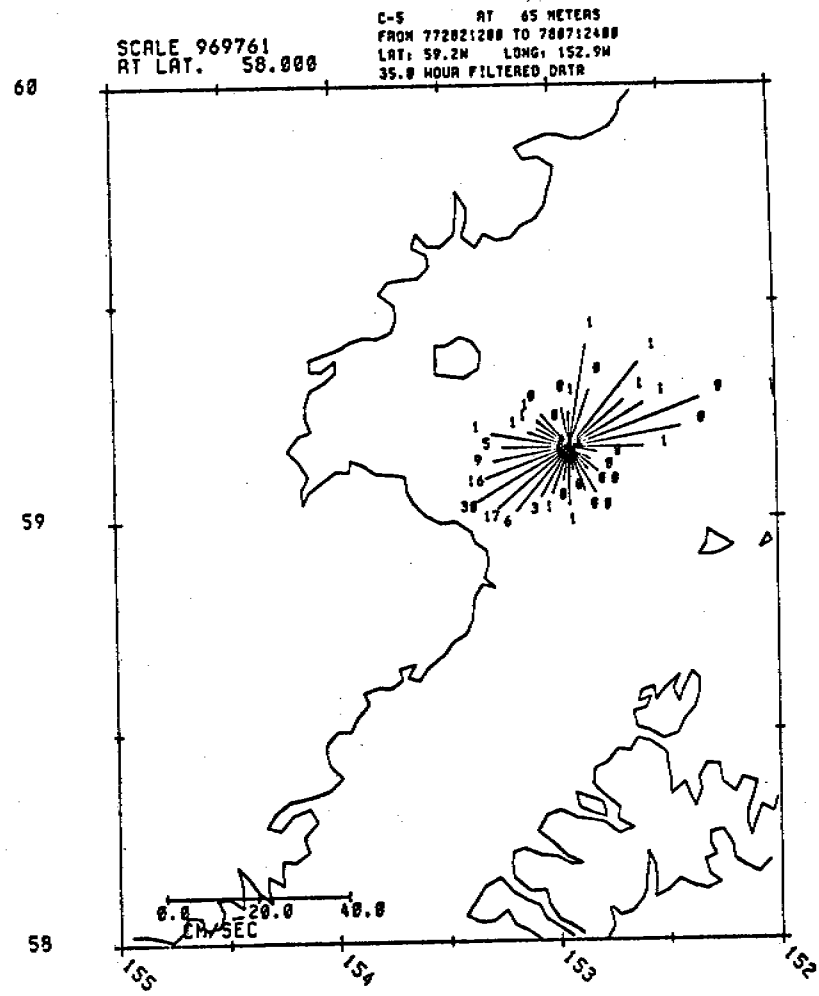


Figure 6.



SCALE 969761
AT LAT. 58.000

C-7 AT 65 METERS
FROM 772841200 TO 780311800
LAT: 59.3N LONG: 152.2W
35.0 HOUR FILTERED DATA

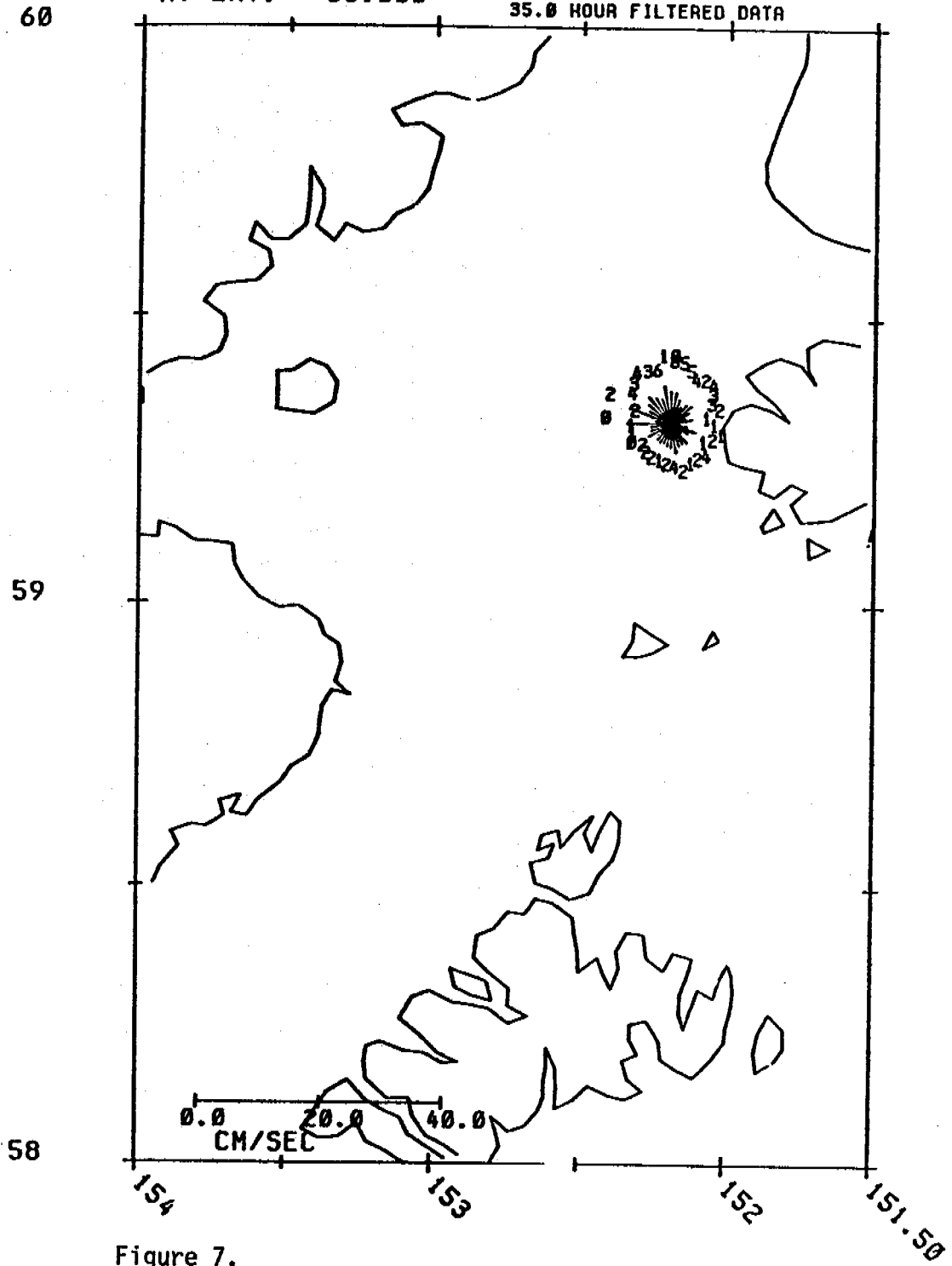


Figure 7.

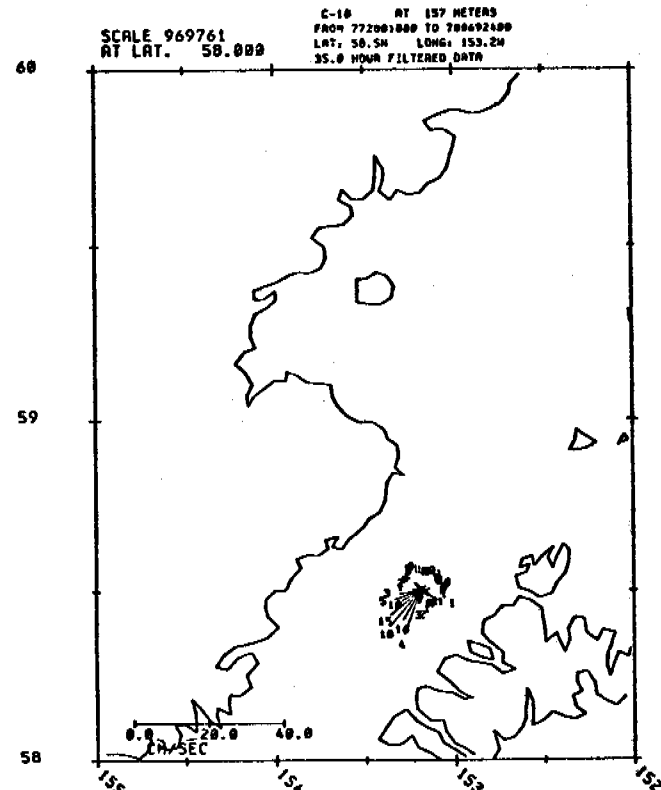
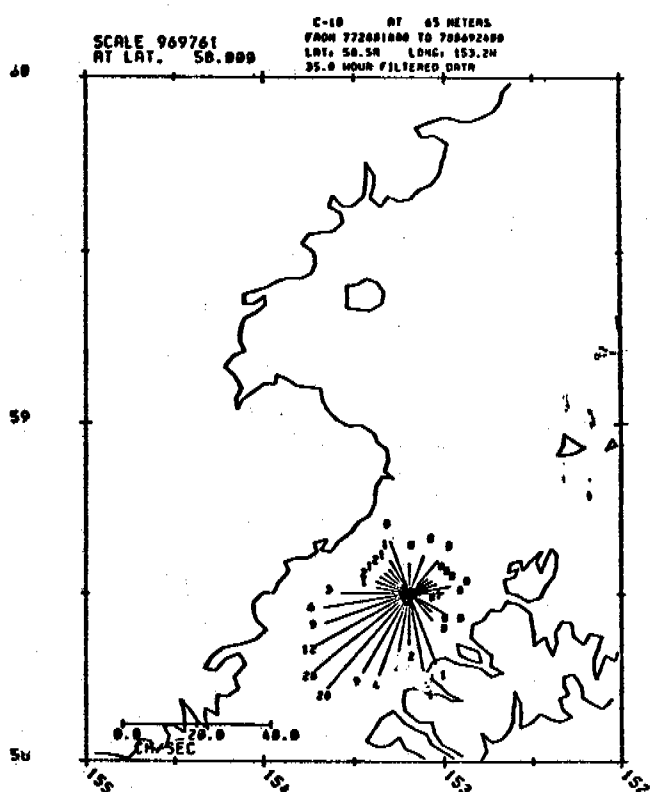
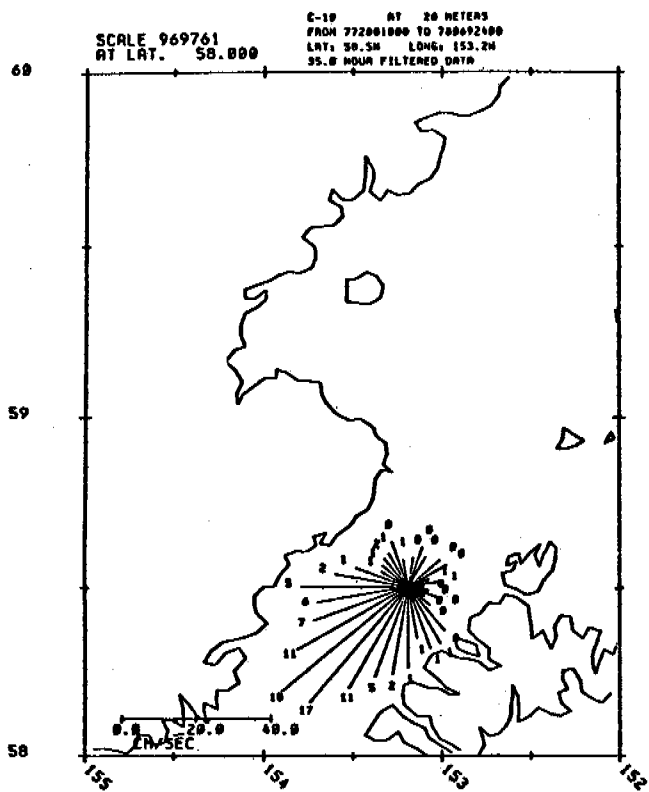


Figure 8.

Table 1. Winter 1977-78 current meter moorings in lower Cook Inlet

MOORING ID	LATITUDE	LONGITUDE	BOTTOM DEPTH (M)	METER	METER DEPTH	IN	OUT	COMMENTS
C-1	50 10.8 N	153 18.0 W	42.0	2512 1810	34.0 20.0	10/5/77 10/5/77	3/16/78 3/16/78	Sediment traps above vineys
C-2	59 13.6 N	153 01.6	64.0	2498 2355	50.0 20.0	10/5/77 10/5/77	3/16/78 3/16/78	
C-3	59 24.2 N	153 53.2 W	59.0	2359 2494	50.0 20.0	10/6/77 10/6/77	3/15/78 3/15/78	
C-4	59 16.9 N	152 54.0 W	84.0	1672 1452	65.0 20.0	10/6/77 10/6/77	3/15/78 3/15/78	PG. 229; sed. traps 10 m. above bottom, did not work
C-5	59 09.9 N	152 56.3 W	128.0	1981 1804	65.0 20.0	10/6/77 10/6/77	3/15/78 3/15/78	
C-6	59 18.0 N	152 38.3 W	7.10	1818 1817	65.0 20.0	10/7/77 10/7/77	3/18/78 3/18/78	#1817 had bad encoder
C-7	59 19.1 N	152 11.8 W	71.0	1986 2164	65.0 20.0	10/8/77 10/8/77	3/13/78 3/18/78	#2164 had bad battery
C-8	59 02.5 N	152 03.6 W	191.0	1681 1680	65.0 180.0	10/4/77 10/4/77	3/17/78 3/17/78	#1680 had lost rotor
C-9	LOST							
C-10	58 30.2 N	153 11.6 W	170.0	1824 1982 1683 PG 232	157.0 65.0 20.0 168.0	10/4/77 10/4/77 10/4/77 10/4/77	3/17/78 3/17/78 3/13/78 3/13/78	
C-11	LOST							
C-12	59 31.6 N	152 14.0 W	50.0	2358 3291	20.0 46.0	1/27/78 1/27/78	10/10/78 10/10/78	#2358 Spindel rod bent, #3291 rotor lost
C-13	59 28.2 N	152 40.0 W	68.0	3293 2356	26.0 56.6	5/27/78 5/27/78	10/16/78 10/16/78	#3293 rotor lost

Table 1 (cont'd). Summer 1978 current meter moorings in
Lower Cook Inlet

MOORING ID	LATITUDE	LONGITUDE	BOTTOM DEPTH (M)	METER	METER DEPTH	IN	OUT	COMMENTS
C-1B	59° 10.7 N	153° 18.8 W	40.2	2504	18	5/27/78	10/18/78	TG & ST entangled upon recovery
				3286	35	5/27/78	10/18/78	
				TG 205	38	5/27/78	10/18/78	
				ST	30			
C-2B	59° 13.5 N	153° 07.7	62	3136 2505	18 48	5/27/78	10/18/78	#2505, no rotor
C-3B	59° 24.4	152° 53.6	64	3180	55	5/27/78	10/18/78	#3180, probable timer failure; cycles w/external trigger only
				598	25	5/27/78	10/18/78	
C-4B	59° 16.7	152° 54.9	83	3294	19	5/27/78	10/18/78	
				3290	64	5/27/78	10/18/78	
				ST	73	5/27/78	10/18/78	
				TG 189	78	5/27/78	10/18/78	
C-5B	59° 09.9	152° 53.9	135	2156	27	1471859	291.005	#2156 does not print correctly. Red crust on wire.
				3184	72	1471853	2912010	
				1815	127	1471848	2912017	
C-6B	59° 18.7	152° 37.9	77	3173	26	1480217	2912142	Not sufficient flotation
				3295	71	1480213	2912147	
C-7B	59° 18.5	152° 10.5	68	2249	17	1480820	2910041	
				2500	62	1480832	2910047	
C-8B	59° 01.9	152° 03.5	190	3179	63	1482220	2872031	#3179, heavy algae #2252, possible error in last record (1/4 to 1 hr.) #1682, Barnacles
				2252	64	1482220	2872031	
				1682	179	1482212	2872044	
C-9B	58° 46.7	152° 16.3	124	1973	66	1481804	2872316	#2501, slight algae, rotors free
				2501	67	1481804	2872316	
				2248	114	1481756	2872320	
				TG 229	122	1481953	2872324	
C-10B	58° 30.1	153° 11.9	175	3171	25	1481711	2822133	#3171, heavy algae growth on side of rotor. #1669, encoder jammed during port recovery spin marks
				3175	70	1481706	2822138	
				1669	165	1481700	2822149	
C-11B	59° 33.4	151° 39.8	87	1451 sediment trap	82.4 77.4	1490224 1490230	2891477	#1451, vane fine broken and rotor heavily fouled. Sediment trap lost when mooring was traveled.

APPENDIX

Manuscripts Resulting from Data Analysis During Past Year

The following were submitted as part of this report:

Muench, R.D., H.O. Mofjeld, and R.L. Charnell (1978) Oceanographic Conditions in Lower Cook Inlet: Spring and Summer 1973. J. Geophys. Res. Vol. 83, No. C10, pp. 5090-5098.

Schumacher, J.D., R. Sillcox, D. Dreves, and R.D. Muench (1978) Winter Circulation and Hydrography Over the Continental Shelf of the Northwest Gulf of Alaska. NOAA Technical Report ERL 404-PMEL 31. 16 pp.

Reed, R.K., R.D. Muench, and J.D. Schumacher (1979) On Baroclinic Transport of the Alaskan Stream near Kodiak Island. (In preparation for submission to Deep-Sea Res.)

Schumacher, J.D., R.K. Reed, M. Grisby, and D. Dreves (1979) Circulation and Hydrography Near Kodiak Island, September-November 1977. (Submitted for publication as an ERL Technical Report.)

Fourth Annual Report

Bristol Bay Oceanographic Processes (B-BOP)

R.L. Charnell
J.D. Schumacher

Pacific Marine Environmental Laboratory
Environmental Research Laboratories, NOAA
3711 15th Avenue NE
Seattle, Washington 98105

L.K. Coachman
T.H. Kinder¹

Department of Oceanography
University of Washington
Seattle, Washington 98295

¹Naval Ocean Research and Development Activity
Code 331/NSTL Station MS 39429

Research Unit 549 (PMEL); 141 (UW)

Period: 1 April 1978 - 31 March 1979

Number of Pages: 70

30 March 1979

Table of Contents

I.	Summary	1
II.	Introduction	1
	A. Objectives	1
	B. Tasks	1
III.	Study Area	2
IV.	Present Status	2
	A. Introduction	2
	B. Structure fronts in the Bering Sea	5
	C. Tidal Analysis	7
	D. The deep eddy south of the Continental Shelf	8
	E. Winter hydrography	61
	F. References	65
V.	Cooperation	66
VI.	Publications	66
VII.	Needs for further study	67
VIII.	Conclusions	67
	Appendix A. Hydrographic summary	69
	Appendix B. Mooring summary	70

I. Summary

The current reporting period, April 1978 through March 1979, covers the final experiments specifically conceived to address OCSEAP objectives in Bristol Bay and includes data analysis which will lead to the formulation of a comprehensive understanding of physical oceanographic processes occurring within Bristol Bay. Field efforts during this period were directed toward two objectives; the general nature of flow in Bristol Bay and detailed experiments of the dynamics of two structural fronts and their relation to: 1) the biology of the area and 2) an examination of the velocity field across and along the front. Analysis efforts have continued toward elucidating such phenomena as: fine structure, fronts, tides and tidal currents, eddy circulation off the shelf, and the mean and low frequency flow through the area. These efforts should lead to a reasonable synthesis of the regional physical oceanography, and its influence on the petroleum development hazard assessment.

II. Introduction

A. Objectives

This work unit attempts to relate oceanic advective and diffusive processes to problems that petroleum development may cause. Specific goals are:

1. To describe and understand the general water circulation and hydrographic structure in the study area through the year; and,
2. To determine the spatial and temporal variabilities of the velocity and hydrographic fields and understand their causes.

B. Tasks

1. Hydrographic Data: The thrust of hydrographic data acquisition and analysis has been to: (1) refine the spatial and temporal resolution of structure fronts; (2) determine the hydrographic structure during winter; (3) further investigate the fine structure near the shelf break; (4) examine the hydrographic structure with respect to tidal variation; and (5) examine the deep eddy observed south of the continental slope.
2. Current Meter Data: We are using current meter data to: (1) elucidate the tides; (2) examine the velocity field details across structure fronts; (3) investigate low frequency flow; and (4) to determine vertical and spatial coherence.
3. Pressure Gauge Data: This data is being used to support current meter data in understanding the dynamic balances associate with flow components, specifically tidal and low frequency flow.
4. Meteorological Data: This data is required to correct pressure gauge data to water level data; and to examine the oceanic response to atmospheric forcing.

III. Study Area

The study area continues to be the southeastern Bering Sea, approximately bounded by the Alaskan coast from Unimak Pass to Nunivak Island, thence by a line running southwest to the Pribilof Islands and by the shelf break to Unimak Pass. Efforts of this period have extended over the shelf area to the north of this area, over the continental slope and rise to the south of this area, and in the waters surrounding the Pribilof Islands. More detailed descriptions of the area may be found in previous annual reports and publications listed.

IV. Present Status

A. Introduction

Four years of field work and analysis are beginning to congeal into a consistent view of Bristol Bay Oceanographic Processes. The character of the area is one of a broad shelf bounded on the west by the oceanic region of the Bering Sea, and on the east and south by the land mass of Alaska. To the north the area blends into a similar shelf region of the Norton Sound-Chukchi Sea investigation. Large scale influences stem from exchange with the Bering Sea, freshwater input from the land masses, precipitation, occasional summer storms, intermittent ice formation and winter storms.

A persistent hydrographic feature is the general horizontal distribution of salinity grading from the relatively fresh (<31.5 ‰) coastal water to the more saline (~ 33.0 ‰) waters along the shelf break. Nearshore salinities vary over the course of the year with freshwater input and intermittent ice formation. Even with these variations, the horizontal gradient across the shelf does not vary by more than ~ 1.5 ‰ on the average. Winter observations (February 1978), collected through the ice and in ice-free areas, reveal a similar gradation in salinity from the shelf/slope to the coastal waters. Since the distribution of salinity maintains itself over the year, there must be a net transport of salt across the shelf.

Salt and water budget considerations were examined and suggested that tidal scale diffusion controls the salt flux across the shelf (Kinder and Coachman, 1978). This model is supported by the known current regime which is dominated by tidal flow and has very low mean flows.

Three distinct hydrographic regions exist: well mixed coastal waters generally shoreward of 50 meter isobath, shelf break waters generally located seaward of the 100 meter isobath, and the central shelf waters located between 50 and 100 meter isobaths. These boundaries are well defined except in the region (near Unimak Pass) where all three meet. The various domains are separated by fronts: the coastal/central shelf waters by a front which results from the balance between buoyancy input and tidal stirring (Schumacher et al. 1979), the central shelf/shelf break by a front resulting from differential diffusion (Coachman and Charnell, 1979), and the shelf break/Bering Sea by a front resulting from differential tidal excursions (Kinder and Coachman, 1978). Within each region, variability is inter and intra seasonal, yet the average conditions yield the long-term situation discussed above. Contained within each domain are processes significant to our understanding of the physics oceanography and their relation to the immediate problem of development influence.

The coastal domain is characterized by a well mixed, vertically homogeneous water column. This domain is subject to seasonal thermal variations with a range of 10-12°C and seasonal or spatial variations in salinity of 2-3‰. Tides are sufficient to keep the water column uniformly mixed throughout the year. Horizontal variations in salinity exist, however, ranging from ~32‰ to <30‰. The low salinities result from fresh water input. The high salinities reflect a generation mechanism which is highly variable from winter to winter. The mechanism suggested consists of an outbreak of extremely cold dry air spilling off the Alaska mainland and rapidly freezing the water. This ice is subsequently blown seaward and more ice is formed. This leads to a local increase of salt through brine rejection. The resulting high salinity is then dissipated through the same horizontal diffusion mechanism which maintains the long term salt balance. The occurrence of this salt formation, however is likely dependent on the severity of the winter and the presence of offshore winds.

Separating the coastal domain and the central shelf domain is a narrow region of marked change in the vertical structure of the water column. The narrow transition zone has been classified as a structure front since the vertically averaged parameters do not change dramatically across the region. The basic change in vertical character across the front is from a vertically homogeneous structure in the coastal water to a stratified structure in the central shelf domain. The front is narrow, 5 to 10 km and its width is a function of bottom slope. The hydrographic structure across the front suggest a flow of 2 to 4 cs^{-1} along the front in a counter-clockwise sense around the bay. The baroclinic speeds are consistent with current meter measurements in the vicinity of the front.

The central shelf domain is characterized by thermal and haline stratification. Currents in this domain are dominated by tides and exhibit extremely low mean flow (generally less than 1 cs^{-1}). Bottom temperatures range from -1.7°C to 3°C, and surface temperatures range from -1.7°C to 12°C. The salinity difference seldom exceeds 0.5‰ with the bottom waters higher in salinity.

The bottom temperature for a season appears to be established during the previous winter (Coachman, 1978). Cold dry continental winds begin to spill out over Bristol Bay in September. As heat is removed from the surface layer, convective overturn occurs. Further heat removal serves to cool the entire water column during period before ice insulates the surface from vertical exchange processes. Ice generally begins to cover the central shelf domain in December-January. The ice is blown into the region from the north and to some extent is formed in the near shore reaches of the bay. As the ice melts, the heat content is further reduced and likewise so is the salt content. Thus, stratification exists over the central shelf where ice is present.

With the approach of spring (April to May) winds shift to a maritime onshore regime¹, and the ice pack begins to decrease in extent. The existing halocline is enhanced by local freshwater addition (melting ice), maintaining the stability of the water column. With the lack of ice cover, surface waters are exposed to insulation and warming ensues. This further increases stability. Stratification restricts exchange with the lower layer, thus the surface layer becomes very warm while the bottom layer remains near its winter temperature.

¹Climatic Atlas, Volume II, 1977.

The warm saline waters of the Bering Sea are separated from the colder fresher waters of the central shelf by a transition region extending from the shelf break to about the 100 meter isobath. The seaward limit of this zone is manifested by a marked increase in horizontal salinity gradient and the shoreward extent is manifested by a similar increase in horizontal salinity gradient. These manifestations represent two fronts with differing generation mechanisms. Seaward of central shelf waters, the tidally generated bottom mixed layer and the wind generated surface mixed layer no longer span the entire water column. Between the two well stirred layers is a region where the distinctly different water masses of the central shelf and the Bering Sea can mingle and exchange properties. The notable character of this zone is the multitude of micro to fine scale (less than 1 meter to 10's of meters) layers of each water type. These layers indicate a greater vertical flux of heat than of salt which can lead to statically unstable conditions (Coachman and Charnell, 1979). Fine structure exists throughout the transition zone, but decays toward the slope. The large horizontal extent of the fine structure, a few 10's of kilometers (Coachman and Charnell, 1979) indicates little vertical mixing energy is available in the transition zone. The flux across the transition zone appears to be one of an on-shelf transport of Bering Sea water along the bottom and at the surface with a transport of shelf waters seaward at mid-depths. Hydrographic properties across this region yield a baroclinic flow to the northwest (along the bathymetry) with speeds of about 5 cs^{-1} . This flow is consistent with direct current measurements and satellite tracked drifter trajectories. These low mean flows provide little energy for lateral mixing.

Although the Bering Sea is not a part of the Bristol Bay work unit, that part of the Bering Sea overlying and just seaward of the continental shelf is of importance to Bristol Bay oceanographic processes. The Bering Sea is the source for salt which maintains the salt cross shelf balance. Hydrographic data indicate a constant weak flow to the northwest along the continental slope (Kinder, Coachman and Galt, 1975), many mesoscale features seaward of the slope, and indications of flow along the Alaskan Peninsula penetrating onto the shelf. This is a weak flow along the slope which is ~ 3 to 5 cs^{-1} in magnitude. Synoptic hydrographic surveys have shown current rings (Kinder and Coachman, 1977) and cyclonic and anti-cyclonic eddies seaward of the slope (Kinder, Schumacher and Hansen, in preparation). Lagrangian drifters confirmed the existence of a cyclonic eddy approximately 80 kilometers in diameter with smaller anticyclonic eddies around its perimeter. The features elucidated by the drifters and hydrographic data was not found in a hydrographic survey conducted six months later. Flow around the eddy (~ 10 - 15 cs^{-1}), was a factor of three higher than that along the slope and shelf break. Exchange between shelf and oceanic waters may occur along the Alaska Peninsula in the vicinity of Unimak Pass. The conventional belief that waters from the Gulf of Alaska flow through Unimak Pass and/or that a strong mean flow exists along the Alaska Peninsula is indicated on various schemes of large scale circulation (see examples in Hughes, Coachman, and Aagaard, 1974). These circulation schemes have resulted in a false sense of consistency and strength of such flows. A flux is suggested in some of our data, e.g. a drifter trajectory along the Peninsula (Section D, Figure 5) and in distributions of hydrographic properties (Kinder, 1976); however, such fluxes do not require an organized mean flow either through Unimak Pass nor along the Peninsula. Further, current records from the vicinity (see Reed, 1978) do not support the concept of consistent mean flow.

Over the entire shelf area, tidal currents dominate flow. The average tidal currents range from 10 to 30 cs^{-1} , generally decreasing with depth in some fashion. The major axis of tidal flow in the southern portion of Bristol Bay are aligned parallel to the Alaska Peninsula, while tidal flow in the northern portion of the area is nearly rotary. The dominance of the tidal currents (shown below as % of total variance) is apparent in all current meter records; however, the variation in dominance appears to be correlated with the hydrographic domains:

Depth Range	Average % of Total Variance at Tidal Frequencies	Average % of total Variance at Sub Tidal Frequencies	Domain
100-150 m	80.1	19.9	Shelf break
60-100 m	96.2	3.8	Central Shelf
40-60 m	97.2	2.8	Eastern Central Shelf
less than 40 m	93.5	6.5	Coastal

The measure of sub-tidal variance reflects the presence of low frequency flow. The greatest % of sub-tidal variance is observed in current records from the shelf break zone and suggests impact from the Bering Slope current and the mesoscale circulations on shelf domain flow. Over the central shelf, tides dominate flow and (RU 435) appears to correctly model the measured currents over the available comparison. In the coastal domain, tides also account for most of the variance, but there does appear to be a weak organized flow. Along the slope and shelf break, flow parallels the bathymetry with speeds of approximately 5 cs^{-1} . Over the central shelf, mean flow is weak with randomly oriented net drifts of less than 1 cs^{-1} . Measurements from the coastal domain indicate that along the boundary between coastal/central shelf water, a cyclonic flow exists with speeds of 2 to 3 cs^{-1} . These measured mean speeds are consistent with geostrophic calculations and appear to be driven by mass distribution resulting from addition of fresh water. The contribution to the mean flow from tidal current residuals is unknown at this time. Flow due to residuals could be comparable to the flow driven by the mass field.

B. Structure Fronts in the Bering Sea - Ongoing Work

Investigations of the nature and significance of structure fronts in the Bering Sea continued through this reporting period. The major emphasis was to examine correlations between physical and biological features around the Pribilof Islands, and to examine dynamics of the front as elucidated by the summer 1978 front experiment.

Fronts have long been recognized by oceanographers, and there has been a belief that these features affect the marine biology (e.g. Uda, 1959). With the exception of upwelling fronts, however, evidence for these affects has been mostly qualitative and even anecdotal (e.g. Knauss, 1957). Recently, in addition to increased physical interest in fronts (J. Geophys. Res. 83 (C9), 1978, contains 25 papers on fronts), quantitative investigations of biological effects are appearing (Savidge, 1976; Fournier et. al., 1977; Fournier et al., 1978; Pingree et al., 1978).

Over the eastern Bering Sea there are fronts both over the slope (Kinder and Coachman, 1978) and over the 500 km wide shelf (Schumacher et al., 1979; Coachman and Charnell, 1979). During the ice-free part of the year, the structural front reported by Schumacher et al. (1979) follows the 50 m isobath over the southeastern shelf, and also surrounds the Pribilof Islands (Fig 1). The front separates two distinct vertical hydrographic structures: homogeneous and two layered. On the shallower side of the front tidal stirring mixes the water column completely. On the deeper side of the front, however, turbulence does not mix the entire column and a pycnocline develops between the upper layer, stirred by wind, and the lower layer, stirred by tide. This front, of about 10 km width, separates a vertical mixing regime where stirring overcomes buoyancy addition at the surface (primarily from insolation and melting ice) from a mixing regime where the buoyancy suppresses stirring sufficiently to form strong stratification. This process has been described for the northwest European shelf (Pingree and Griffith, 1978; Simpson et al., 1978; Simpson and Pingree, 1978), and for the Bering Sea by Schumacher et al. (1979).

Biological effects can be hypothesized for this front over the Bering Sea shelf. Since the front controls the vertical distribution of heat from insolation, it forms an effective barrier to stenothermal organisms (the late summer temperature difference across the front exceeds 5°C). Additionally, the flow pattern associated with the front (James, 1978) can influence the distribution of smaller organisms and dissolved nutrients. Surface convergence can concentrate food, attracting larger organisms, while surface divergence, or upwelling, can bring nutrients into the photic zone, promoting primary production. Finally, the division of the waters into domains of varying stability can markedly affect primary production (Sverdrup, 1953, cogently discusses stability effects on primary production). When the plankton are light-limited (presumably in early spring during frontogenesis), the stratified side of the front is favorable to high photosynthetic rates. When the plankton are nutrient-limited, however, the homogeneous side of the front favors phytoplankton growth. It is possible that during the year all these mechanisms operate, and seabirds, which are high in the trophic web, respond to several of them. Distribution of seabirds are related to oceanic-scale variations in the availability of food (Bourne, 1963; Ashmole, 1971). The relationship between seabirds and the physical oceanography includes the trophic interactions of phytoplankton, zooplankton, and nekton on many spatial and temporal scales. Quantitative relations between mesoscale (10 to 100 km or so) physical features, and seabird concentrations rarely have been established, since they require concurrent oceanographic and ornithological measurements over appropriate scales. Temporal scales of meso-scale physical features are often weeks or longer, so that they may be considered permanent compared to a life stage of seabirds (e.g. breeding or migrating). One step in understanding complex ecological relationships between physical oceanography and seabirds is to establish correlation between them. Gould (1971) successfully did this over the tropical North Pacific, relating seabird concentrations to equatorial upwelling and convergence. Following previous investigations, he assumed that physical effects on the seabirds' food supply caused this correlation. Similarly, we hypothesize that the front surrounding the Pribilof Islands, a known breeding ground for several seabird species, affects the relationship between seabirds and their prey. To test this, we examined concurrent bird observation and physical measurements, and through our understanding of the biology of the birds and the physical processes we speculate on casual relationships between birds and physics. We intend that this speculation will stimulate further investigation of this ecosystem.

A detailed study of the dynamics of the front was undertaken between Nunivak Island and the Pribilofs. Four current meter stations were deployed between July and September 1978, in a closely spaced array spanning the front. Pressure gauge data were also collected across the front. Upon deployment of the current meter arrays, a series of XBT and CTD observations were collected over a tidal cycle to examine the lateral migration of the front. Also, two anchor CTD stations were occupied in the front. A similar series of XBT, CTD sections were occupied upon recovery of the current meter arrays in September. Preliminary processing of the data is nearing completion and analysis is beginning.

C. Tidal Analysis

Apparent reductions in tidal currents were observed in summer 1976. Current meter data also indicated periods of reduced tidal amplitudes in 1977. The anomalous tidal currents result in variations of harmonic constituents over the year. The stability of harmonic constituents is the underlying principal for all tidal predictions. To investigate possible anomalous tidal currents in Bristol Bay, several theoretical models were developed by H. O. Mofjeld. These are analytic models in which the effects of friction, stratification and variable bottom topography can be estimated. The first type model used one or two water layers without rotation or variable topography, but with frictional coupling at the pycnocline and at the bottom. This model produced estimates of wave attenuation as tides propagated into Bristol Bay along the Alaska Peninsula, as well as vertically-averaged estimates of tidal currents within each layer. The second type of model considers free Kelvin waves propagating along the Alaska Peninsula in the presence of eddy viscosity, rotation and topographic variations in the offshore direction. In this case, details of the current profiles can be studied in terms of counter-rotating, bottom Ekman layers. The results of the theoretical work indicate that the observed, anomalous tidal currents in Bristol Bay probably are not real but are from instrument problems. Preliminary results were presented at the Mid-Atlantic Bight Physical Oceanography Workshop (15-16 November 1978).

D. Observation of a Baroclinic Eddy: An Example
of Meso-scale Variability in the Bering Sea¹

by

T. H. Kinder²

Department of Oceanography
University of Washington
Seattle, WA 98195

J. D. Schumacher

Pacific Marine Environmental Laboratory
Environmental Research Laboratories, NOAA
Seattle, WA 98105

D. V. Hansen
Atlantic Meteorological and Oceanographic Laboratories
Environmental Research Laboratories, NOAA
Miami, FL 33149

¹ Contribution No. , Department of Oceanography, University of Washington

² Present address: Naval Ocean Research and Development Activity,
NSTL Station, MS 39529.

ABSTRACT

Shallow (17 m) drifters, released during May 1977 and tracked by satellite, delineated an eddy in the southeastern Bering Sea. Located above complex topography (depth range: 200 m - 3000 m), the eddy had a diameter of about 150 km and had speeds of 7 to 16 cm/s at 50 km from its center. A CTD survey during July defined the eddy from 200 m to 1500 m depth in temperature and salinity distributions, but no hydrographic evidence for the eddy existed at the surface. A geostrophic calculation referenced to 1500 m agreed qualitatively with the drogue data, and accounted for all but 2 to 4 cm/s of the drogue speeds. Examination of the TS correlation showed that the water at the eddy's core was the same as that at its periphery, in contrast with a cyclonic ring observed nearby in July 1974.

The last drifter left the eddy in October, and a second CTD survey in February 1978 showed that the eddy had either dissipated or moved. An earlier STD survey of the region in summer 1971 had not shown either a ring like that seen in 1974 or an eddy like that seen in 1977. In spite of the ubiquitous inclusion of permanent eddies and steady currents in Bering Sea circulation schemes, recent evidence from synoptic data suggests that the hydrographic and velocity fields are highly variable on scales of 50 to 100 km and a few weeks to a few years.

1. Introduction

Nearly all depictions of flow over the deep Bering Sea (Figs. 1 and 2) show meso-scale features, variously interpreted as eddies, gyres, rings, Rossby waves, vortices, or "gyrals". Arsen'ev (1967) constructed dynamic topographies from 5500 hydrographic stations taken during 1874-1959, and Ohtani (1973) constructed dynamic topographies based on Japanese hydrographic data gathered from 1959-1965. Both of these mean topographies showed eddies with about 100 km diameters. Hughes et al. (1974) presented many historical schemes for the surface currents, and also proposed their own scheme (Fig. 3). These constructs used various mixtures of hydrographic data, sparse current measurements, ship drifts, and large additions of intuition, and like the topographies of Arsen'ev and Ohtani they showed eddies or gyres of about 100 km size.

More synoptic data also suggested meso-scale flow features. During 1970 Favorite and Ingraham (1972) inferred both cyclonic and anticyclonic gyres from STD (salinity-temperature-depth) data taken near Bowers Ridge (Fig. 1). Favorite and Ingraham also used 1971 STD data from an extensive survey over the southeastern Bering Sea to infer gyres there, including an anticyclonic gyre just south of Pribilof Canyon (International North Pacific Fisheries Commission, 1972). During an eleven-day STD survey during 1972 Kinder et al. (1975) found cells along the continental slope from near Unimak Pass to Cape Navarin, which they speculated were formed by Rossby waves incident and reflected off that continental slope. Similarly, an eight-day hydrographic survey over Pribilof Submarine Canyon in 1974 revealed a cyclonic current ring in the outer reaches of the canyon, occupying the position of Favorite's and Ingraham's 1971 anticyclonic gyre (Kinder and Coachman, 1977). Examination of infrared and visible satellite data by Solomon and Ahlnäs (1978) showed numerous vortices adjacent to the Kamchatka Peninsula during fall and winter.

All these features were of similar size (order 100 km), although they may have had other differences.

Some features of the circulation revealed in these studies appear permanent, but others do not. The long-term dynamic topographies, in agreement with the various current schemes, show a general cyclonic circulation about the deep basin (Fig. 3). This circulation includes the Kamchatka and Bering Slope Currents, which have also been confirmed by synoptic surveys (Reid, 1973; Hughes et al., 1974; Kinder et al., 1975). On the other hand, the many gyres or eddies that are included, and are thus by implication deemed permanent, do not seem to occupy the same positions in the various topographies and current schemes. Additionally, synoptic surveys have thus far not confirmed the permanence of these eddies, and the question arises as to whether they are recurring or perhaps transient features. Especially in the light of the vortices reported by Solomon and Ahlnas in the Kamchatka Current, the strongest current in the Bering Sea, efforts to map the mean Bering Sea circulation (e.g., Hughes et al., 1974; Kinder et al., 1975; Favorite et al., 1976) may be badly aliased. Similar misgivings have been raised by these authors, and most recently by Solomon and Ahlnas (1978). Although available data are mostly unable to resolve fully the meso-scale variability, either spatially (10 km to 200 km) or temporally (weeks to years), the data are suggestive: the eddy kinetic energy (meso-scale variability) is at least comparable to the mean kinetic energy over most of the deep Bering Sea. Thus attempts to either infer the long-term mean circulation from nearly synoptic data or to infer meso-scale structure from long-term means are likely to be frustrated. The oceanographic literature of the Bering Sea abounds with both (Hughes, 1972, gives many citations).

Another problem arises in constructing the circulation pattern in the Bering Sea because most velocities have been inferred from temperature and salinity measurements, using either the dynamic method or by the continuity of properties. Short periods of direct current measurements support some of these inferences, but direct measurements are too sparse to be convincing, particularly when complex current patterns are hypothesized. Typically weak gradients of temperature, salinity, and dynamic height exacerbate this problem. Thus, in addition to the difficulty of correctly extrapolating results temporally, there is some question whether anything can be safely inferred about the velocity field. For instance, if much of the geostrophic velocity is barotropic, as found in the high latitude West Spitsbergen Current (Greisman, 1976), then it is difficult to define meso-scale flow features based on hydrographic data alone. Clearly the resolution of a meso-scale flow feature by both current measurements and hydrographic distributions would bolster confidence in earlier work.

During summer 1977 we obtained shallow drifter and concurrent CTD (conductivity-temperature-depth) measurements which revealed a cyclonic meso-scale eddy in the southeastern Bering Sea. These data permit us to do the first comprehensive study of one of the eddies (or gyres) that have been ubiquitous in previous dynamic topographies and current schemes. We examine the structure of the eddy, and compare it to other features observed in the Bering Sea and elsewhere, and finally we reflect on the question of the general Bering Sea circulation and its meso-scale variability.

2. Setting

While the Bering Sea (Fig. 1) is mostly underlain by either featureless

continental shelf or flat abyssal plain, the bottom of the eastern Aleutian Basin (Fig. 2) is comprised of continental slope incised by large submarine canyons, a broad plateau which rises steeply from the sea floor, and the seamounts of the Aleutian Island arc (Scholl et al., 1968; Scholl et al., 1970). The boundaries of this topographically complicated region are: to the west the deep (>3400 m) and flat plain of the Aleutian Basin, to the south and east the Aleutian Islands permitting shallow (<200 m) communication with the North Pacific Ocean, and to the north a broad (>500 km) and shallow (<170 m depth) continental shelf.

Modified by the bathymetry, the circulation over the deep basin of the Bering Sea is apparently known in broad outline (Fig. 3), but not in detail (Hughes et al., 1974; Favorite et al., 1976). In agreement with the mean annual wind stress curl, flow is cyclonic with a strong western boundary current, the Kamchatka Current, flowing southward along the Kamchatka Peninsula. This current transports about $20 \times 10^6 \text{ m}^3/\text{s}$ into the North Pacific, and is partially fed by the westward flowing Bering Slope Current. Parallel-ling the shelfbreak from near Unimak Pass to near Cape Navarin (Fig. 1), this broad (~ 200 km) current transports about $5 \times 10^6 \text{ m}^3/\text{s}$ (Kinder et al., 1975). A diffuse haline front, associated with the Bering Slope Current system, overlies this continental slope, separating the oceanic regime over the Aleutian Basin from the continental shelf regime to the north (Kinder and Coachman, 1978).

Salinity variations are usually more important than temperature in controlling density variations, and vertically the salinity structure is simpler than the temperature structure (Fig. 4). Salinity increases, almost monotonically, from 33 g/kg at the surface to about 34.5 g/kg at 1500 m depth (the deepest measurements discussed here). From a surface maximum in summer

of 12°C, temperature passes through a minimum (2.9–3.5°C) at 100–300 m depth, then through a maximum (3.6°C) at 300–500 m depth and decreases to 2.2°C at 1500 m depth; the temperature minimum is much weaker here than further west (Kinder et al., 1975). The warm surface layer is a result of seasonal heating, and the temperature minimum is relict from winter cooling and convection. The warm water beneath the temperature minimum layer is advected from the North Pacific Ocean through the deeper western passes which permit free communication at all depths.

3. Measurements

A. Drifters

We deployed six Lagrangian drifting buoys on two lines across the current near the shelf break northwest of Unimak Pass on 26 and 27 May 1977. These buoys, produced by Polar Research Laboratories, are cylindrical aluminum spars about 3 meters long and constrained by flotation and ballast to float about two-thirds submerged. Each buoy was affixed by a 10 m nylon tether to a "windowshade" drogue which was 2 m wide by 10 m tall; thus the drogue extended between 12 and 22 m depth. This depth was selected as a compromise between engineering and navigation: retaining the drogue requires a long tether, while avoiding grounding requires a short tether. Drogue survival during this deployment was good as most drogues were apparently lost only after grounding (Table 1 and Fig. 5).

Slippage of drifters is a complicated function of surface wind, sea state, and current structure that is presently being researched (Vachon, 1978). In uniformly moving water the leeway of our system is estimated to be about one-half percent of the relative surface wind. For an undrogued buoy, the leeway increases to about 5% of the surface wind. For this deploy-

ment, we estimate that slippage was negligible and apply no correction.

The buoy's location was determined by Random Access Measurements System (RAMS) of the NIMBUS-6 satellite (Levanon, 1975). At the latitude of the Bering Sea RAMS provided up to five locations daily for each buoy, but at irregular times. The RMS error of each location was about 4 km, and each satellite overpass provided data for an ambiguous pair of locations. Between sequential orbits it is usually, but not always, possible to identify the proper location. Hence, in addition to the errors arising from uncertainties in the satellite's orbit, doppler measurement, etc., errors of tens or even hundreds of kilometers occur. These erroneous positions were removed by objectively comparing each position for displacement from preceding and succeeding positions, and rejecting locations implying excessive speeds. For these data, 150 cm/s was the speed limit, which resulted in retaining 80 to 90 percent of the original data. The position data were then smoothed and interpolated to a six-hour interval by a piecewise least square fit with a low order (usually cubic) polynomial. Velocity series were additionally smoothed by a simple three-point triangular filter. In the final series features with time scale of about two days or greater remain, while the tidal and inertial signals are mostly removed.

B. CTD Measurements

We took CTD (conductivity-temperature-depth) stations during July 1977 and February 1978, using a Plessey 9040 CTD profiling system. Data from these stations were compared to water samples obtained at the greatest depth on about one-half the casts, confirming an accuracy of $\pm 0.02^{\circ}\text{C}$ and ± 0.02 g/kg. We also used spring 1971 STD (salinity-temperature-depth) data taken by National Marine

Fisheries Service (Ingraham et al., 1973). They used similar calibration procedures and reported accuracies of $\pm 0.01^\circ\text{C}$ and ± 0.01 g/kg.

The July grid included 42 stations requiring six days (26-31 July 1977, Fig. 6), and the February grid included 19 stations requiring three days (20-23 February 1978). These two surveys were thus synoptic with respect to the large eddy and probably synoptic with respect to any features large enough to be resolved. The spring 1971 hydrographic data included 114 stations occupied over 19 days (23 May - 10 June 1971). This survey encompassed a much larger area than our two later surveys, but it also was synoptic with respect to an eddy like that observed in 1977.

With accuracies of $\pm 0.02^\circ\text{C}$ and ± 0.02 g/kg, density (σ_t) may be calculated within ± 0.02 kg/m³. Dynamic heights referred to 1500 db (our CTD was limited to 1500 m depth) are thus accurate to 1.0 dyn cm (10^{-1} m²/s²), and surface speeds computed from stations spaced 40 km apart are accurate to ± 4 cm/s. Examination of our data showed consistent patterns in the distributions of temperature, salinity, and speeds, so that the precision may be considerably better than this.

4. Observations

A. Drifters

Examination of field measurements taken over the southeastern shelf and slope during 1975-1977 suggested that the Bering Slope Current and the haline front extend from the Pribilof Islands (the southeastern limit of work reported by Kinder et al., 1975) almost to Unimak Pass. Thus we envisaged a northwesterly flow over the slope extending from near (not necessarily through) Unimak Pass, and separated from the shelf regime by the front. We found no evidence for water exchange across the shelfbreak, with the exception of the region just

north of Unimak Pass along the Alaska Peninsula. In order to test this assumption that the southeastern shelf and oceanic regimes were thus isolated, we deployed six shallow drifters near the shelfbreak during May 1977 (Table 1). We anticipated that they would move generally northwestward, paralleling the bathymetric contours and that they would not cross between the shelf and oceanic regimes.

The drifter tracks realized our expectations, although they also showed complex details (Fig. 5 and Table 1). Generally the drift was northwestward, paralleling the isobaths at mean speeds ~ 5 cm/s. Over the shelf, away from the shelf edge, speeds were even lower, often < 1 cm/s. Only drifter 56 crossed between oceanic and shelf regimes, and this occurred just north of the Alaska Peninsula where hydrographic distributions had already led us to suggest a weak or intermittent eastward flow (Kinder et al., 1978). The apparent crossing of two drifters at 175 W, one originating in the oceanic and one in the shelf regime, was separated by 100 days and may show a shift of the front that separates these regimes. Three of the drifters (56, 544, and 503) defined an eddy centered near 55-00 N and 169-30 W.

Drifter 56 made two loops around the eddy (Fig. 5B), the first during summer (June-July) at a radius of 50 km, and completing the second in mid-October at a radius of 80 km. During the second circuit the drifter made two large (20 to 50 km radius) anticyclonic loops west of the eddy but still nearly completed a second revolution. Drifter 503 completed one and one-half loops at a radius of 50 km before transmissions stopped on 14 August (Fig. 5C). As with the track of drifter 56, there is variability at scales smaller than the eddy. Drifter 544 also made one and one-half loops around the eddy at a radius of 60 km (Fig. 5D)

Table 1. Drifter Data¹

<u>Buoy Number</u>	<u>Deployed</u>	<u>Last Transmission</u>	<u>Drogue Lost</u>	<u>Comments</u> ²
11	shelf 152 m 26 May 1977	5 Jan. 1978	5 Jan. 1978	Drifted northwestward and wandered near the Pribilof Islands before drifting farther westward over the slope.
27	shelf 154 m 26 May 1977	25 Dec. 1977	23 Oct. 1977	Drifted northwestward and grounded on St. Paul Island.
56	shelfbreak 298 m 26 May 1977	14 Nov. 1977	31 Oct. 1977	Drifted northwestward over slope, then around eddy twice, then onto shelf near Alaska Peninsula.
268 535	shelfbreak 269 m 26 May 1977	20 Sep. 1977	16 Sep. 1977	Drifted northwestward over slope, then grounded on St. George Island
544	Bristol Canyon ³ 411 m 26 May 1977	3 Oct. 1977	2 Oct. 1977	Drifted northwestward over slope, then around eddy, thence northwestward over the basin and lower slope.
503	mid-slope 2205 m 27 May 1977	16 Nov. 1977	25 Oct. 1977	Drifted northwestward over slope, then around eddy.

- NOTES: 1. See Fig. 5.
 2. St. Paul is the northernmost and St. George the southernmost of the Pribilofs (Fig. 1).
 3. Bristol Submarine Canyon trends east-west, seaward of and paralleling the shelfbreak southeast of the Pribilofs.

before exiting to the west in mid-August. Like drifter 503, it began with a 15 km radius anticyclonic circle, and like drifter 56 it executed a large (25 km radius) anticyclonic circle to the west of the large eddy. The track of drifter 544 when it left the eddy is similar to drifter 56's track in the same area, but drifter 544 executed a large anticyclonic meander, while drifter 56 executed an anticyclonic circle tangent to the large main eddy.

Overlaying the tracks of all drifters (Fig. 5A) showed spatial coherence or temporal persistence for many small features. Many other small features, however, appeared in only one drifter track so that judging the coherence or persistence of these features is difficult. The anticyclonic feature southwest of the eddy defined by drifters 56 and 544 apparently existed for at least one month: drifter 544 entered the meander about 10 August and left (at 55-40 N) on about 29 August, while drifter 56 entered the small eddy on 31 August and crossed its own track heading eastward on 18 September.

B. July 1977 Hydrography

Horizontal plots of temperature and salinity (Figs. 7 and 8) from the July survey revealed a thick cell with a cold and salty core. This cell was centered on station 4 ($54^{\circ}54.7'N$, $169^{\circ}24.8'W$), and thus was coincident with the eddy delineated by the drifter tracks (Fig. 5). We show distributions at 10 m because this depth is comfortably within the shallow isothermal and isohaline layer (Fig. 4). Distributions at 500 m, 1000 m, and 1500 m depth are shown because of the cell's clear signature at these depths. Because of its vertical structure (Fig. 4), horizontal plots of temperature at depths near the seasonal thermocline or near temperature extrema can be confusing.

Surprisingly, the shallow distributions (Figs. 7A and 8A) give no hint of the eddy. A cool and salty area near the Aleutian Island arc (here at $168^{\circ}W$), also

seen in other surveys, is probably caused by tidal stirring along the islands and in the passes; upwelling may also play a role (Swift and Aagaard, 1976). Near the shelfbreak the isohalines delineated the front overlaying the slope, and the isotherms there probably reflected varying distributions of the heat from insolation caused by differing stabilities in the upper water columns. It is difficult to detect the eddy from these distributions.

In the deeper distributions, however, a cooler and saltier cell was manifest. It was possible to discern the cell in the temperature and salinity distributions below 200 m depth, and deeper than 500 m (Figs. 7 and 8) the cell dominated the distributions. At 500 m depth the core was 0.20°C cooler (<3.30°C) and 0.10 g/kg more saline (>34.10 g/kg) than the periphery. Even at 1500 m depth the cell was well defined: 0.10°C cooler (<2.15°C) and 0.02 g/kg saltier (>34.54 g/kg) at the core than adjacent waters. At both depths these differences equate to isotherms and isohalines vertically displaced about 100 m.

Although the core of the eddy was saltier and cooler, the temperature-salinity correlation demonstrated that the water within the core of the eddy had TS properties similar to that on the periphery. The range of temperature and salinity at each depth (Figs. 7 and 8) was not caused by a water mass difference. Temperature-salinity properties define a relationship conforming with the general Bering Sea TS curve (e.g., Kinder et al., 1975). We also demonstrate this quantitatively by comparing the salinity at 3°C (for depths below the temperature maximum, Fig. 4) between stations near the core of the eddy and those on the periphery (Table 2). There was no difference in salinity (i.e., the TS relationship was preserved), but the depth of the 3°C isotherm showed about a 100 m vertical displacement.

This uniformity of the TS correlation was found for the cells in 1972

Table 2. Salinity at 3°C

The salinity of the deep 3°C isotherm (below the temperature maximum, see Fig. 4) is shown with the depth of the isotherm: mean \pm one standard deviation.

	Number	Salinity (g/kg)	Depth (m)
All stations	25	34.30 \pm .02	853 \pm 61
Core stations ¹	7	34.30 \pm .01	787 \pm 58
Periphery stations ²	18	34.30 \pm .02	879 \pm 39

¹ Stations 4.1, 5.1, 5, 4, 3, 10, 11

² Stations 7, 1, 2.1, 3.1, 3.2, 4.3, 4.2, 5.2, 5.3, 6.1, 17.1, 17, 6, 2, 9, 12, 13, 22

See Fig. 6 for station numbers.

(Kinder et al., 1975), but not for the ring in 1974 (Kinder and Coachman, 1977). Water in the cells along the continental slope in 1972 showed TS differences, amounting to about 0.10 g/kg at 3°C, but these were uncorrelated with the cells' structure. In contrast, the ring observed in 1974 showed a difference of 0.06 g/kg at 3°C which correlated strongly with the ring's structure. This implies that the 1977 eddy is similar to the cells seen in 1972, and that it was not formed by an entrainment mechanism along a water mass boundary, which is characteristic of ring formation (e.g., Fuglister, 1972).

C. Geostrophic Comparison

The shallow dynamic topography (10/100 db, Fig. 9) had a broadly cyclonic flow, with several smaller features that also appeared in temperature or salinity distribution (Figs. 7A and 8A). Deeper dynamic topographies (100/1500, 500/1500, 1000/1500 db; Figs. 9B-D), however, clearly illustrated the cyclonic eddy centered on station 4. Because of the contribution from depths below 100 m, the 10/1500 db topography (not shown) also clearly displayed the eddy. Maximum speeds were about 16 cm/s at 10 db referenced to 1500 db; Kinder et al. (1975) found 1500 db a reasonable reference level based on comparing velocity inferred from density (STD) casts and velocities measured by parachute drogues, and we discuss this choice further in this section. As with the temperature and salinity measurements, the distributions above the seasonal influence (about 200 m depth, see Fig. 4) appear complex and do not reveal an eddy. Deeper distributions, however, manifest a cyclonic eddy congruent with the drifter tracks.

We calculated speeds geostrophically (the Rossby number $\approx .04$: centrifugal force is small) from CTD station pairs that were adjacent to segments of drifter trajectories (Fig. 10 illustrates a section). Assuming that the velocity field

did not change during the period early June to mid-September from which we selected segments of tracks, we grouped all segments passing between a CTD station pair together. The results (Table 3) show agreement between mean speeds, but only within broad scatter. Drifter tracks and dynamic topographies both showed greater speeds over the northwestern half of the eddy than in the southeastern half, and the agreement between the two methods was better where more drifter segments were averaged. The drifter speeds were consistently higher than the calculated speeds, and when station pairs having three or more segments were used (the first four entries in Table 3), the difference was about 2 cm/s.

This speed difference probably results either because the eddy had a small barotropic component, or because the 1500 m reference level was too shallow. Distributions at 1500 m depth corresponded to isopycnal displacements of about 100 m (section 4B), thus the 1500 m reference level misses some of the baroclinicity. At many of the stations the data extended throughout most of the water column; at only eleven stations did bottom depth exceed 2000 m. At station 4, the center of the eddy, the depth was 2700 m and at station 6, the deepest station, depth was 3150 m. It is likely that if our data had extended farther down at the deeper stations we could have reduced the 2 cm/s speed difference. At the same time, much of the bottom beneath and nearby the eddy lies at depths less than 1500 m (Fig. 2). Clearly the eddy extended to the bottom at some locations, and perhaps throughout its extent.

D. Permanence

It seemed possible that the eddy observed in summer 1977 could be permanent. Mean dynamic topographies and synoptic surveys have shown a generally cyclonic circulation in the eastern corner of the deep basin: eastward flow north of the Aleutian Arc and westward flow south of the Pribilof Islands (e.g. Fig. 11B).

Table 3.

Speeds Inferred from Density Measurements and from Drifter Tracks

CTD Station Pair ⁴	Geostrophic Speed Relative to 1500 db ¹ (cm/s)	Speed from Drifter Tracks ² (cm/s)	Number of Segments of Track and Duration ³ (days)
11, 19	10 (8-12)	14.2 ± 3.0	4 (30)
6, 5	14 (12-16)	16.2 ± 6.5	4 (21)
4.3, 4.1	14 (12-16)	16.2 ± 4.7	5 (24)
3, 2	7 (6-8)	6.7 ± 2.3	3 (45)
4, 3	3 (0-6)	10.0	1 (9)
4, 11	7 (4-10)	14.5 ± 10.6	2 (12)

¹ Geostrophic speed was subjectively analyzed from a cross section (e.g. Fig. 10). The mean and the range are given.

² The mean and standard deviation are given.

³ Duration is the total number of days for all segments.

⁴ Figure 6 has station positions.

Large changes in bottom depth added credence to this possibility, because a permanent eddy requires permanent forcing, and bottom topography is an obvious candidate. For these reasons, and because of the many permanent gyres of appropriate size in the circulation schemes and dynamic topographies (some of which match the eddy well), we examined additional data. During 23 May to 10 June 1971 the National Marine Fisheries Service occupied 114 STD stations over the region (Ingraham et al., 1973), and we took 19 CTD stations within a 100 km radius of station 4 during February 1978. The drifters had shown the eddy in place for four months (June-September), and the 1971 and 1978 data offered the opportunity to confirm a permanent meso-scale gyre in the Bering Sea for the first time.

Temperature, salinity, density, and dynamic heights at various depths for the 1971 data did not indicate an eddy located near $55^{\circ}00'N$ and $169^{\circ}30'W$. The distributions were horizontally more uniform in 1971 compared with 1977, and the circulation was generally cyclonic similar to 1977 (Fig. 11). One feature that does stand out is the anticyclonic eddy south of Pribilof Canyon where Kinder and Coachman (1977) observed a cyclonic ring in 1974. The water below 200 m near the position of the 1977 eddy was more saline and cooler than the surrounding water in 1971. The temperature at 1000 m and the dynamic topography (500/1000 db) emphasize this difference (Fig. 11), but such closed isopleths were atypical of plots at other depths. If we did not know of the eddy in 1977, we would not be impressed with the weak cyclonic cell southeast of the 1977 eddy's core. In fact, one could as easily claim association between this position and an anticyclonic cell. Thus a cyclonic eddy was not present in 1971.

During 20-23 February 1978 we took CTD stations encompassing the entire

eddy defined by the July 1977 data. There was no eddy, and the variation in the distributions of temperature, salinity, and geopotential at different levels was less than in 1977. There was a suggestion that the eddy had moved to the west about 100 km since July 1977 (speed ~ 0.5 cm/s); the western edge of our 1978 grid could have included the eastern periphery of a cyclonic eddy. Our coverage was too limited to define this, and we cannot distinguish between a translation of the eddy (necessarily to the west or southwest because of the bottom topography) or a decay in place. Seven months after the eddy was first observed centered on $55^{\circ}00'N$ and $169^{\circ}30'W$, it was no longer present there.

5. Discussion

A similar study by Cresswell et al. (1978) west of Australia revealed a similar eddy: it was not visible in surface hydrographic distributions, but it dominated surface velocity. Their 20 m drogues, tracked by satellite, conformed to an eddy which was prominent hydrographically at 1000 m depth. Voorhis et al. (1976) found a similar situation in the MODE region. Inferring subsurface velocity from the changing pattern of surface temperature, they concluded that while the surface temperature pattern did not reveal mesoscale eddies directly, advection at the surface by deep mesoscale eddies dominated the evolution of the surface temperature field. Deep eddies can dominate the surface velocity field in the southeastern Bering Sea, but the surface salinity and temperature signatures of these eddies is masked by other processes.

Early studies of the Bering Sea circulation espousing permanent gyres lacked both spatial and temporal resolution, so that their results did not reveal the small spatial and short time scale variability which probably existed. More recent studies (Table 4 and Section 1) were reasonably synoptic and had

Table 4.
Recent Synoptic Surveys

Date	Features ¹	Method	Reference
1. September 1970	Eddies near Bowers Ridge	STD	Favorite and Ingraham (1972)
2. May-June 1971	Eddy in Southeastern Aleutian Basin	STD (some parachute drogue)	International North Pacific Fisheries Commission (1972)
3. August 1972	Eddies along continental slope (Bering Slope Current System)	STD (some parachute drogue)	Kinder et al. (1975)
4. July 1974	Current ring near Pribilof Canyon	Hydrocast (some current meter)	Kinder and Coachman (1977)
5. January 1976 - June 1977	Vortices east of Kamchatka (Kamchatka Current)	Infrared and visible satellite imagery	Solomon and Ahlnäs (1978)

¹ See Figures 1 and 2.

sufficient spatial resolution to define one realization of an eddy like that seen in summer 1977. Before the 1977 work, however, concurrent velocity measurements were inadequate and the surveys were not repeated. Thus the velocity field could only be inferred from geostrophic calculation, and an eddy's existence was often dependent on one or two hydrographic stations. Additionally, from a single survey it was difficult to evaluate the permanence of such features. Our study of the 1977 eddy suggests that even the eddies that were defined by only a few hydrographic stations were real: a broad areal survey of the region, with typical spacing of 100 km, would have defined the 1977 eddy by only two or three stations. Conversely, our hydrographic survey was inadequate to resolve the small anticyclonic loop to the west of the eddy that drifters 56 and 544 revealed (Figs. 5B and 5D). The February 1978 survey, demonstrating the absence of the eddy, suggests that many of the permanent gyres attributed to the Bering Sea may have been mistaken inferences from observations of transient eddies. Richman et al. (1977) concluded that eddies occupy the MODE site only "occasionally", and our analysis suggests a similar situation in the eastern Bering Sea. Because of the large variation in bottom depth, it is reasonable to think that some mesoscale flow features are recurring. The observational evidence, however, suggests that most mesoscale features are not permanent.

The various circulation schemes showing permanent mesoscale features vary. Small permanent gyres on one scheme disappear or change rotation in another. Some of the gyres appear to have been invoked to alleviate contouring problems; such problems are not surprising if the hydrographic field is undersampled. The current ring observed near Pribilof Canyon in 1974 was absent in 1971 and 1977,

and the eddy observed in 1977 was absent in 1971 and 1978. Whenever mesoscale features have been clearly identified and a second data set exists that permits checking their permanence, the features have been found temporary. There is no reason to assume that such permanent mesoscale gyres exist until observations demonstrate otherwise. It is perhaps more important now to learn more of the dynamics of such eddies: how they are born, and how they decay or propagate away.

This impermanence does not apply to two features of the Bering Sea circulation: the Kamchatka Current and the Bering Slope Current. Both these components of the circulation appear in long-term mean topographies and current schemes (e.g., Arsen'ev, 1967; Hughes et al., 1974; Favorite et al., 1976), and both have been confirmed by synoptic surveys (Reid, 1973; Hughes et al., 1974; Kinder et al., 1975). What is now clear is that even these currents are highly variable (Solomon and Ahlnäs, 1978; Kinder et al., 1975). Some of these depictions of permanent gyres have found their way into non-physical studies (e.g. Ray et al., 1978), where they may deceive the user and subvert his intent.¹ Previously current schemes were not only the most convenient, but often best current information for such studies. With our present knowledge such current schemes should be used cautiously, for it is clear that our concept of even the mean circulation is imprecise.

¹ Ray and his colleagues face the difficult task of finding appropriate current descriptions for ecosystem studies. In some parts of the Bering Sea, data are inadequate to confidently construct such descriptions.

Acknowledgments

The crew of NOAA ships Miller Freeman and Surveyor launched the drifters and did the CTD casts. D. Pashinski coordinated drifter logistics. M. Sayles commented usefully on our manuscript, and F. Favorite contributed his experience and insight to our interpretations. R. Charnell was chief scientist during deployment of the drifters, and P. Laird supervised CTD data processing: both were lost at sea in December 1978.

This work was funded by the Outer Continental Shelf Environmental Assessment Program (OCSEAP) which is managed by the National Oceanic and Atmospheric Administration (NOAA) for the Bureau of Land Management (BLM).

References

- Arsen'ev, V. S. 1967. *Currents and Water Masses of the Bering Sea*. Izd. Nauka Moscow (in Russian) (Translation 1969, National Marine Fisheries Service, Biological Laboratory, Seattle), 146 pp.
- Cresswell, G. R., T. J. Golding, and F. B. Boland. 1978. Buoy and ship examination of the subtropical convergence south of Western Australia. *J. Phys. Oceanogr.* 8(2):315-320.
- Favorite, F., A. J. Dodimead, and K. Nasu. 1976. Oceanography of the Subarctic Pacific Region, 1960-71. Bulletin Number 33, International North Pacific Fisheries Commission, Vancouver, 187 pp.
- Favorite, F. and W. J. Ingraham, Jr. 1972. Influence of Bowers Ridge on circulation in the Bering Sea and influence of Amchitka Branch, Alaska Stream, on migration paths of sockeye salmon. In *Biological Oceanography of the Northern North Pacific Ocean*, A. Y. Takenouti, ed. Idemitsu Shoten, Tokyo. pp. 13-29.
- Fuglister, F. C. 1972. Cyclonic rings formed by the Gulf Stream, 1965-66. *Studies in Physical Oceanography: A Tribute to George Wüst on his 80th Birthday*. A. Gordon, ed., Gordon and Breach, pp. 136-178.
- Greisman, P. E. 1976. *Current Measurements in the eastern Greenland Sea*. Ph.D. thesis, University of Washington, Seattle, WA. 145 pp.
- Hughes, F. W. 1972. *Circulation and transport in the western Bering Sea*. Ph.D. thesis, University of Washington, Seattle, WA. 162 pp.
- Hughes, F. W., L. K. Coachman, and K. Aagaard. 1974. Circulation, transport and water exchange in the western Bering Sea. Chapter 3 in *Oceanography of the Bering Sea*, D. W. Hood and E. J. Kelley, eds., Institute of Marine Science, University of Alaska, Fairbanks.

- Ingraham, W. J., D. M. Fisk, C. J. Bartlett, and S. E. Turner. 1973. Physical-chemical oceanographic data from the North Pacific Ocean and Bering Sea, 1971. National Marine Fisheries Service Data Report 75. 169 pp.
- International North Pacific Fisheries Commission, 1972. *Annual Report, 1971*. Vancouver, B.C. pp. 95-96.
- Kinder, T. H. and L. K. Coachman. 1977. Observation of a bathymetrically trapped current ring. *J. Phys. Oceanogr.* 7(6):946-952.
- Kinder, T. H. and L. K. Coachman. 1978. The front overlaying the continental slope of the eastern Bering Sea. *J. Geophys. Res.*, 83(C9):4551-4559.
- Kinder, T. H., L. K. Coachman, and J. A. Galt. 1975. The Bering Slope Current System. *J. Phys. Oceanogr.* 5(2):231-244.
- Kinder, T. H., J. D. Schumacher, R. B. Tripp, and J. C. Haslett. 1978. *The evolution of the hydrographic structure over the continental shelf near Bristol Bay Alaska, During summer 1976*. University of Washington, Department of Oceanography Technical Report Ref: M78-16. 72 pp.
- Levanon, N. 1975. Special issue on data collection from multiple earth platforms. *IEEE Transactions on Geoscience Electronics.* GE 13(1).
- Ohtani, K. 1973. Oceanographic structure in the Bering Sea. *Memoirs of the Faculty of Fisheries, Hokkaido University* 21(1):65-106.
- Ray, G. C., J. A. Dobbin, and R. B. Salm. 1978. Strategies for protecting marine mammal habitats. *Oceanus* 21(4):55-67.
- Reid, J. L. 1973. *Northwest Pacific Ocean Waters in Winter*. John Hopkins University Press, Baltimore. 96 pp.
- Richman, J. G., C. Wunsch, and N. G. Hogg. 1977. Space and time scales of mesoscale motion in the western North Atlantic. *Rev. Geophys. Space Phys.* 15(4):385-420.

- Scholl, D. W., E. C. Buffington, and D. M. Hopkins. 1968. Geological history of the continental margin of North America in the Bering Sea. *Marine Geol.* 6:297-330.
- Scholl, D. W., E. C. Buffington, D. M. Hopkins, and T. R. Alpha. 1970. The structure and origin of the large submarine canyons of the Bering Sea. *Marine Geol.* 8:187-210.
- Solomon, H. and K. Ahlnäs. 1978. Eddies in the Kamchatka Current. *Deep-Sea Res.* 25(4):403-410.
- Swift, J. H. and K. Aagaard. 1976. Upwelling near Samalga Pass. *Limnol. Oceanogr.* 21(3):399-408.
- Vachon, W. A. 1978. Instrumented Full-scale Tests on a Drifting Buoy and Drogue. Charles Stark Draper Laboratory Inc., Rep. 947, 180 pp.
- Voorhis, A. D., E. H. Schroeder, and A. Leetma. 1976. The influence of deep mesoscale eddies on the sea surface temperature in the North Atlantic subtropical convergence. *J. Phys. Oceanogr.* 6(6):953-961.

FIGURE LEGENDS

1. The Bering Sea. The 1000 m and 3000 m isobaths delineate the continental slope.
2. The bathymetry of the Aleutian Basin. Isobaths from 200 m (approximating the shelfbreak) to 3400 m depth are shown with an interval of 400 m. (After Scholl et al., 1970.)
3. Surface current scheme for the deep basin. The western boundary current, the Kamchatka Current, and the northwestward flow paralleling the shelfbreak, the Bering Slope Current, are common to all reasonable current schemes and mean dynamic topographies. The existence of the permanent meso-scale eddies in the scheme is unproven. Dotted arrows represent "less certain" features, and the numbers are measured speeds in cm/s (from Hughes, 1972).
4. Temperature ($^{\circ}\text{C}$) and salinity (g/kg) profiles. In summer, there is a shallow isothermal layer overlaying the seasonal thermocline. A temperature minimum, at 100 m depth, overlies a maximum ($\sim 3.6^{\circ}\text{C}$). Below about 500 m depth temperature decreases with depth. Salinity increases with depth throughout the water column. (See Fig. 6 for station locations.)
5. Drifter tracks. (A) Composite of six tracks, showing general northwestward drift and the large eddy near 55-00 N and 169-30 W. Note the similarity of the two tracks southwest of the eddy. (B) Buoy 56. (C) Buoy 503. (D) Buoy 544.
6. Station positions, NOAA ship Surveyor, 26-30 July 1977. Station 4 was selected to lie at the center of the circle defined by the drifter tracks (see Fig. 5A).
7. Temperature ($^{\circ}\text{C}$). (A) 10 m. (B) 500 m. (C) 1000 m. (D) 1500 m. The eddy clearly shows as cooler water at 500 m depth and below, but not at 10 m depth (cf. Fig. 8). Station 4 is circled and the dashed line delineates the shelfbreak (~ 170 m depth). (See Fig. 6 for station numbers.)
8. Salinity (g/kg). (A) 10 m. (B) 500 m. (C) 1000 m. (D) 1500 m. The haline front overlaying the continental slope shows at 10 m. but there is no clue to the presence of the eddy. At 500 m and below, however, the eddy shows clearly as saltier water (cf. Fig. 7). Station 4 is circled and the dashed line delineates the shelfbreak (170 m depth). (See Fig. 6 for station locations.)
9. Dynamic topographies ($10^{-1} \frac{\text{m}^2}{\text{s}^2} = 1$ dynamic cm). (A) 10/100. (B) 100/1500. (C) 500/1500. (D) 1000/1500. The shallowest distribution (A) shows the general cyclonic circulation of the eastern deep basin, but not the eddy. The deeper distributions (B, C, and D) show the eddy clearly. The 10/1500 topography (not shown; superpose A and B) is dominated by the eddy (cf. Fig. 5, 7, and 8). Station 4 is circled and the dashed line delineates the shelfbreak (~ 170 m). (See Fig. 6 for station locations.)

10. Cross section of speed inferred from hydrography (cm/s). Speeds calculated by the dynamic method are contoured for a northwest-southeast section (Fig. 6 has station locations). These speeds agreed with mean drifter speeds, although there was considerable scatter (Table 3). Note the scale change at 200 m depth.
11. Summer 1971 data. (A) Temperature ($^{\circ}\text{C}$) at 1000 m depth. (B) Geopotential 500/1000 ($10 \text{ m}^2/\text{s}^2 = 1 \text{ dynamic cm}$). The distributions are flatter than in 1977 (cf. Fig. 7 and 9). Depending on one's biases, it is possible to find excellent agreement or complete disagreement between the surveys of 1971 and 1977. The truly permanent features are the general cyclonic tendency of the flow, and the presence of several meso-scale features. Individual meso-scale features (e.g. the 1977 eddy) are transient.

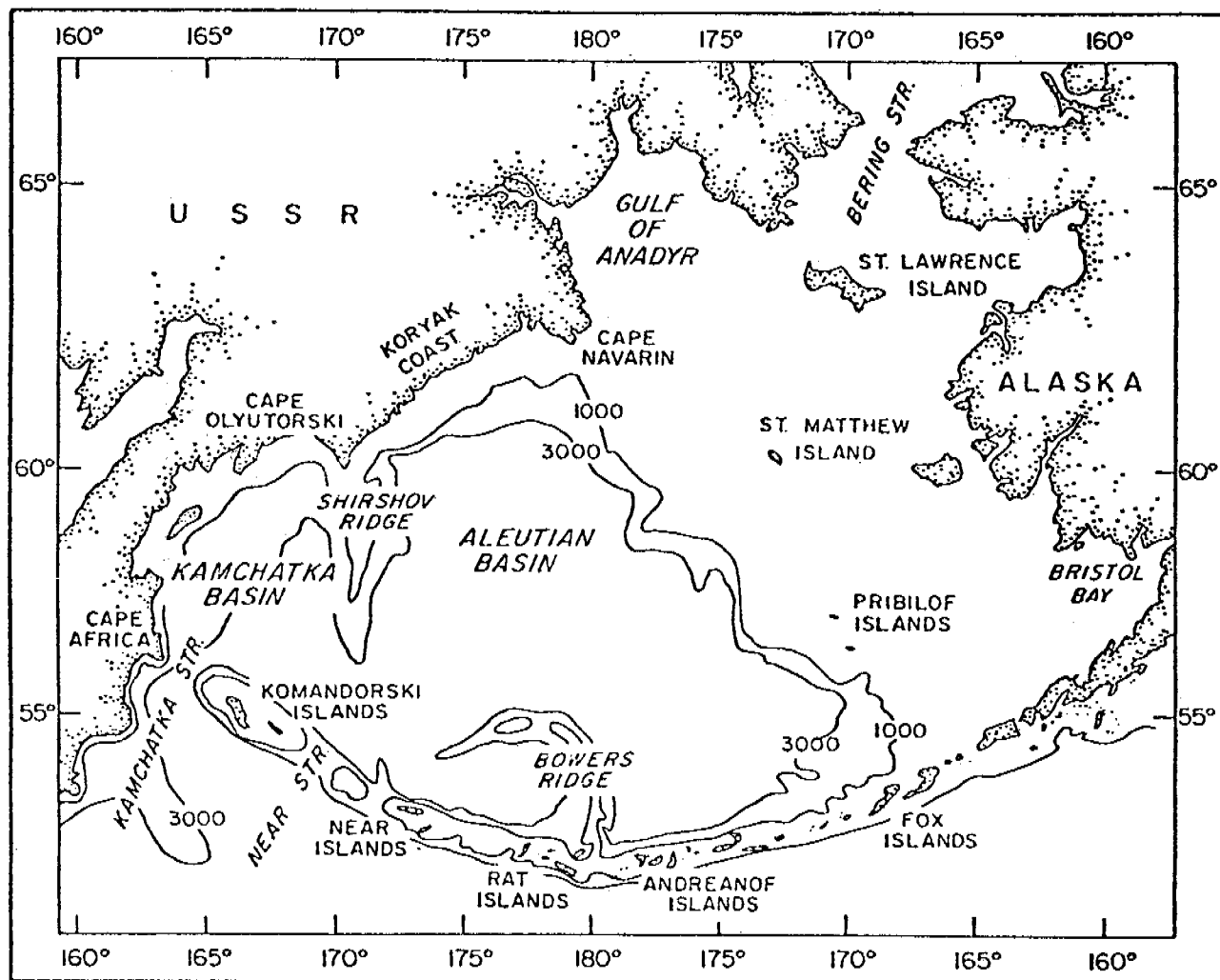


Figure 1. The Bering Sea. The 1000 m and 3000 m isobaths delineate the continental slope.

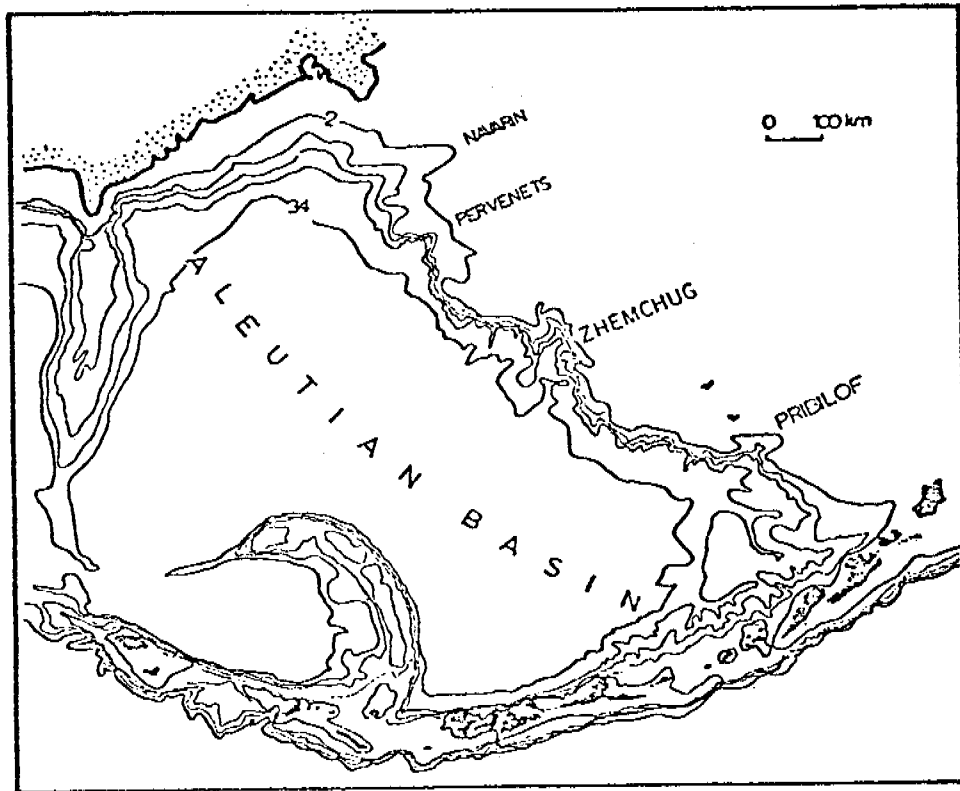


Figure 2. The bathymetry of the Aleutian Basin. Isobaths from 200 m (approximating the shelfbreak to 3400 m depth are shown with an interval of 400 m. (After School et al., 1970.)

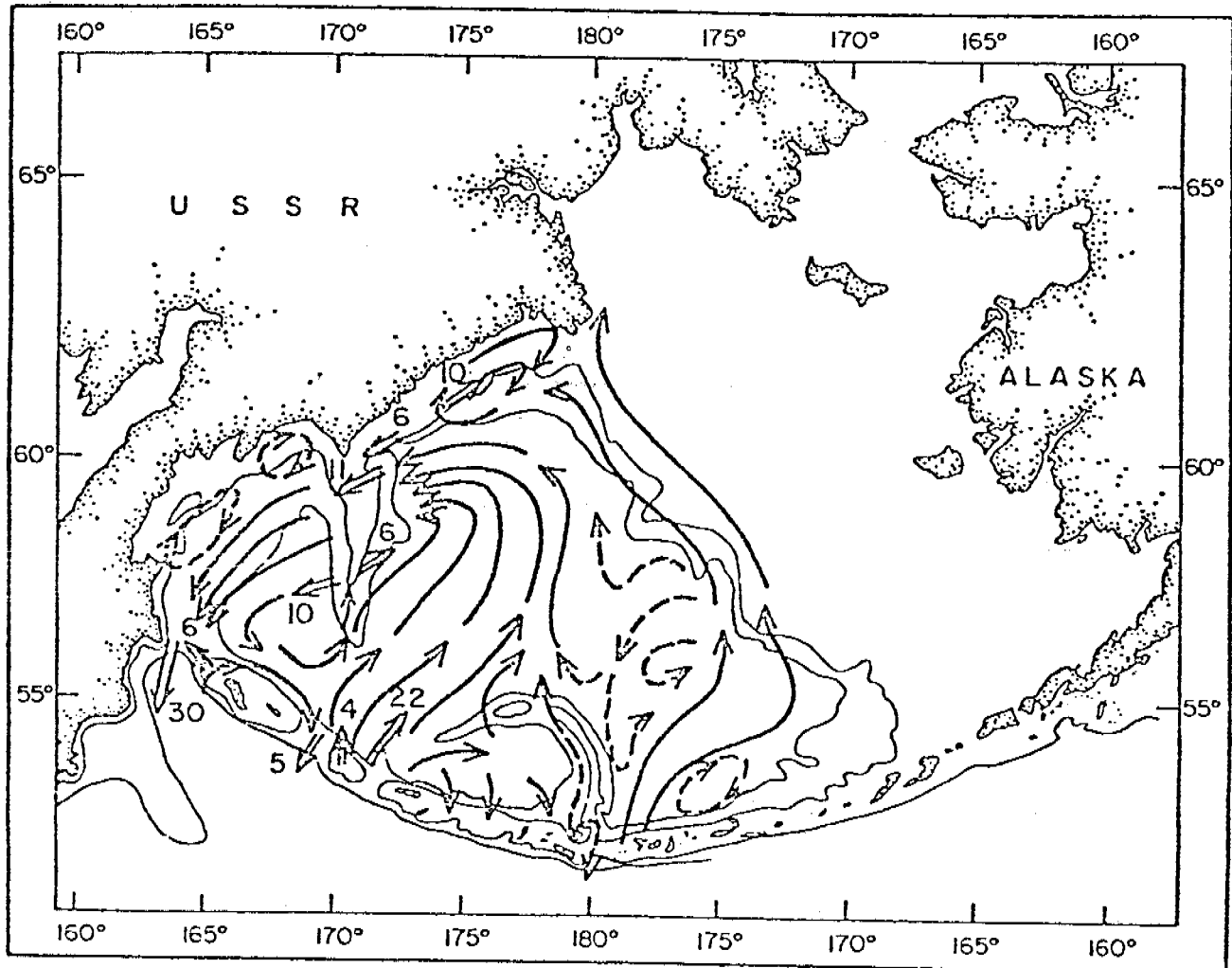


Figure 3. Surface current scheme for the deep basin. The western boundary current, the Kamchatka Current, and the northwestward flow paralleling the shelfbreak, the Bering Slope Current, are common to all reasonable current schemes and mean dynamic topographies. The existence of the permanent meso-scale eddies in the scheme is unproven. Dotted arrows represent "less certain" features, and the numbers are measured speeds in cm/s (from Hughes, 1972).

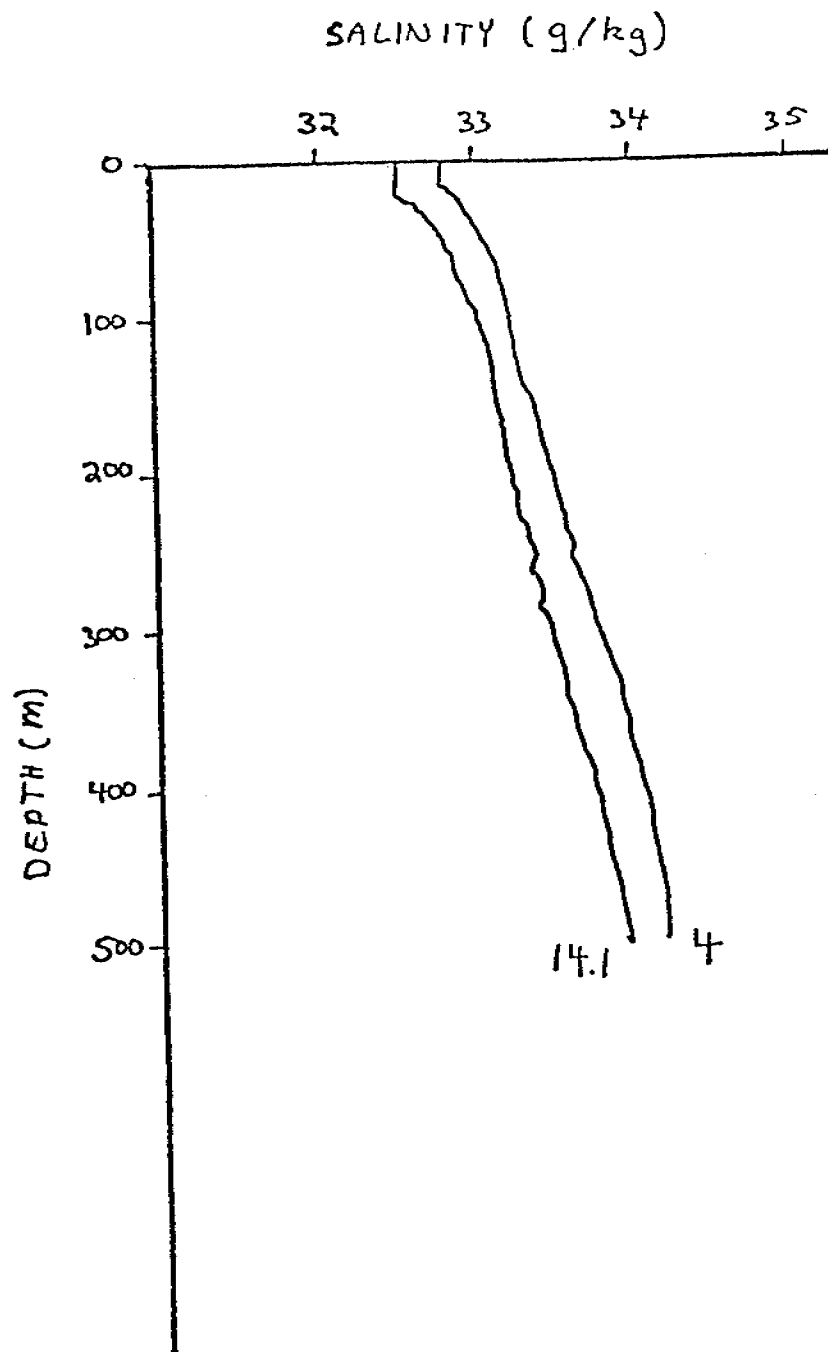
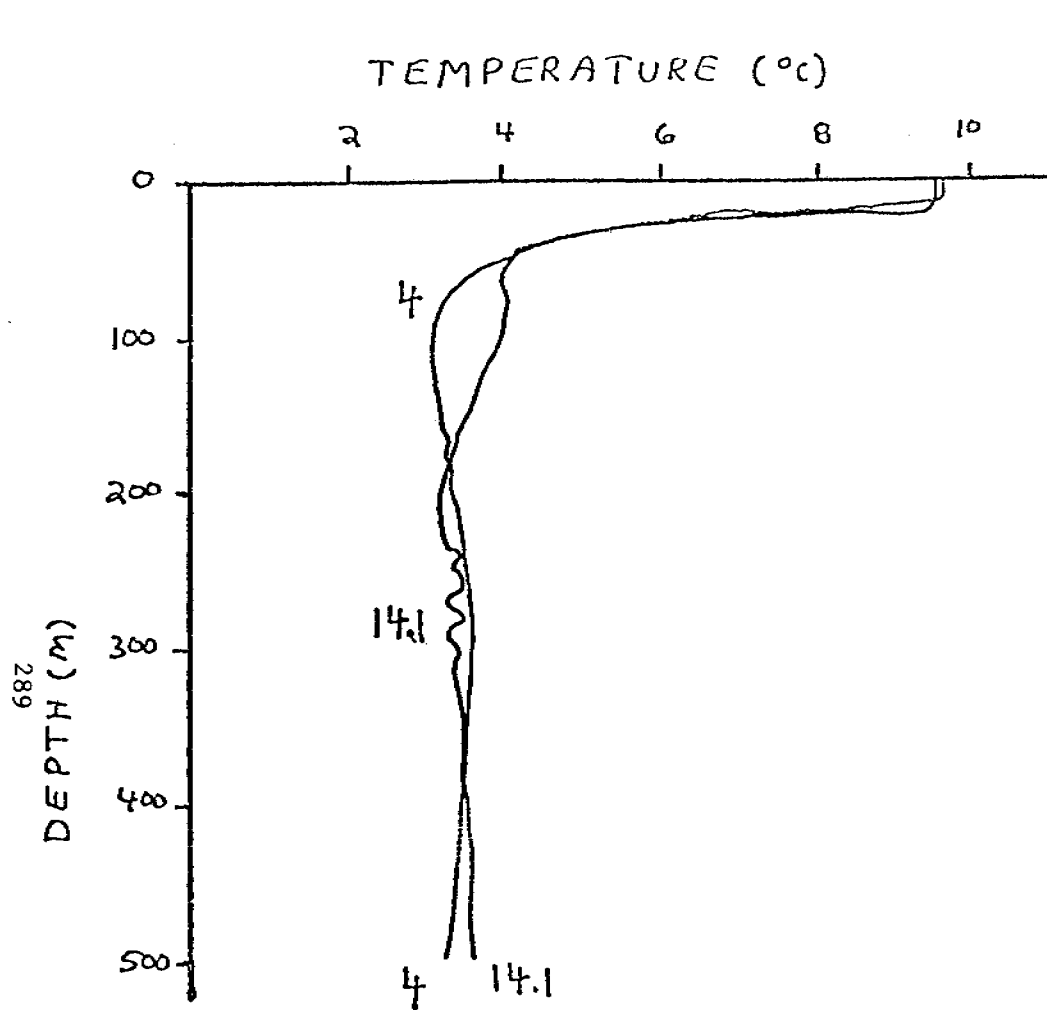


Figure 4. Temperature ($^{\circ}\text{C}$) and salinity (g/kg) profiles. In summer, there is a shallow isothermal layer overlaying the seasonal thermocline. A temperature minimum, at 100 m depth, overlies a maximum ($T \approx 3.6^{\circ}\text{C}$). Below about 500 m depth temperature decreases with depth. Salinity increases with depth throughout the water column. (See Fig. 6 for station locations.)

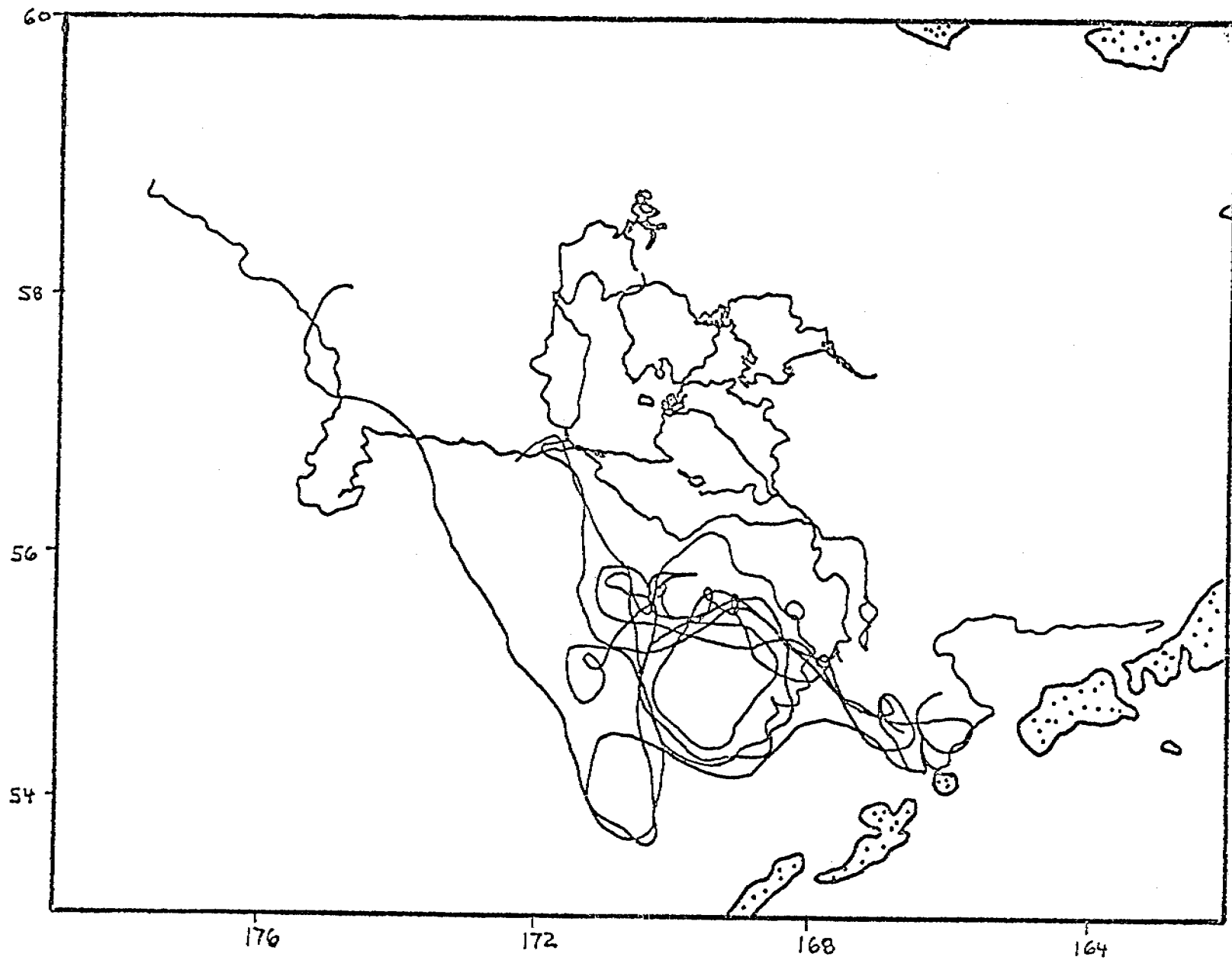


Figure 5A. Drifter tracks. (A) Composite of six tracks, showing general northwestward drift and the large eddy near 55-00 N and 169-30 W. Note the similarity of the two tracks southwest of the eddy.

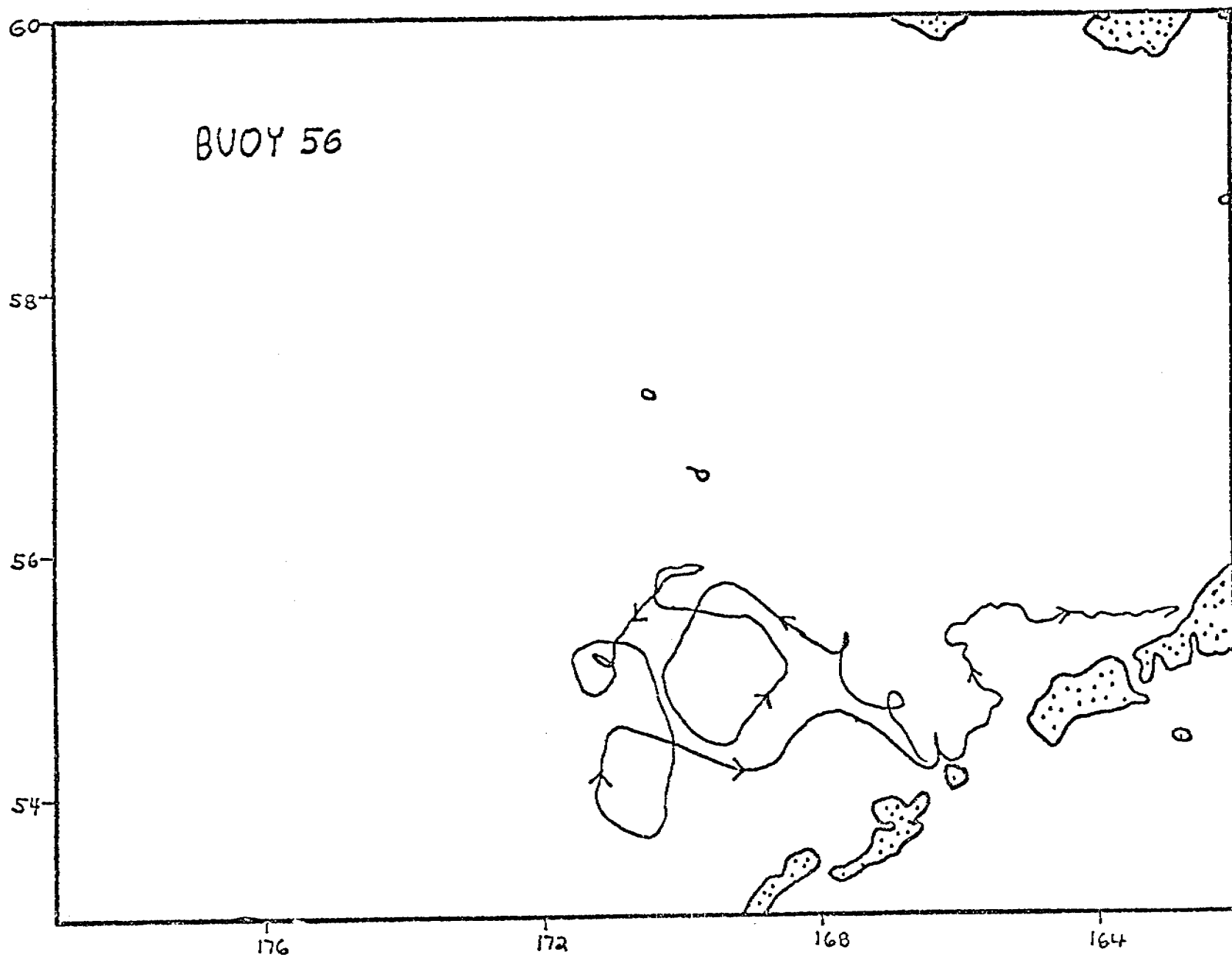


Figure 5B. Drifter tracks. (B) Buoy 56.

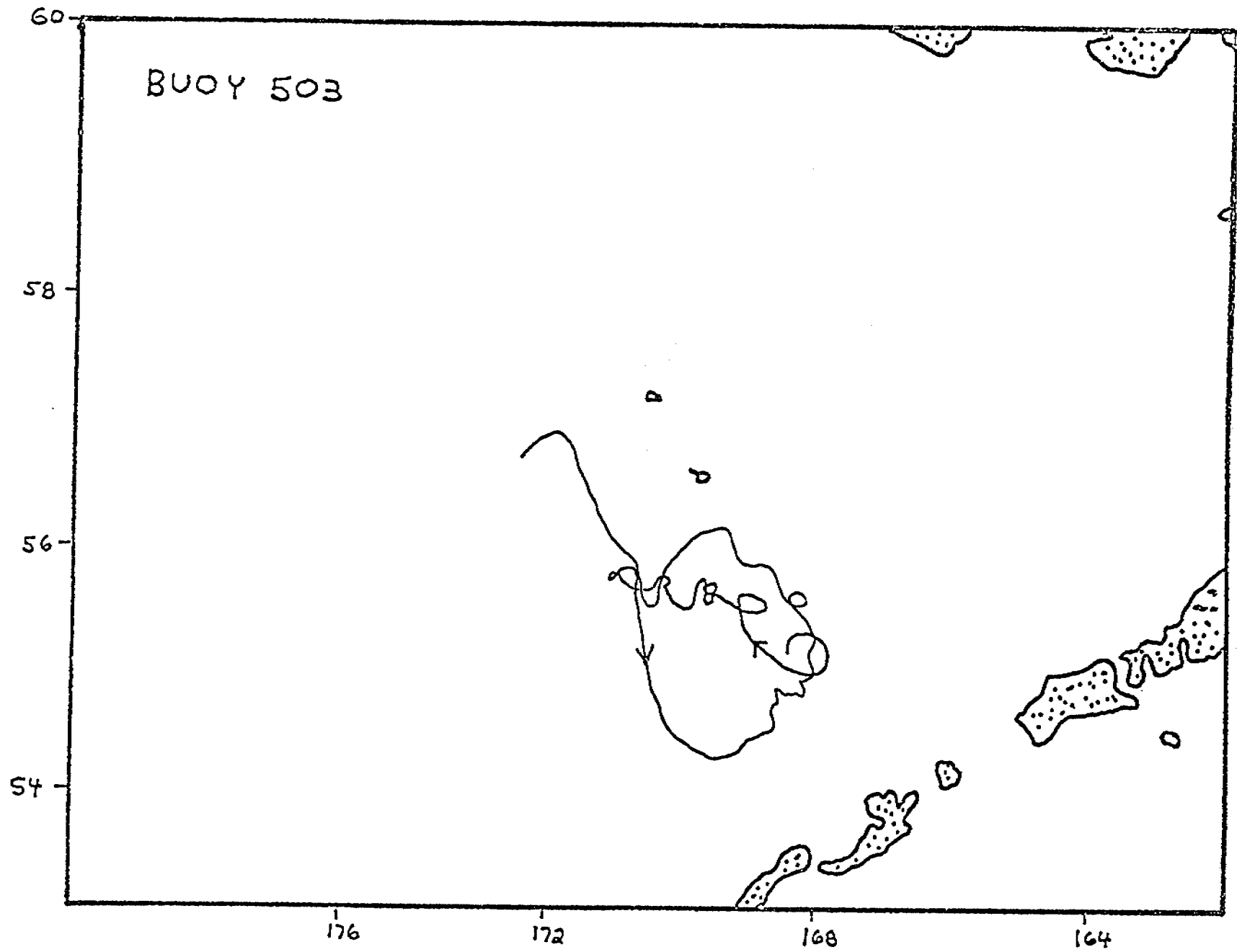


Figure 5C. Drifter tracks. (C) Buoy 503.

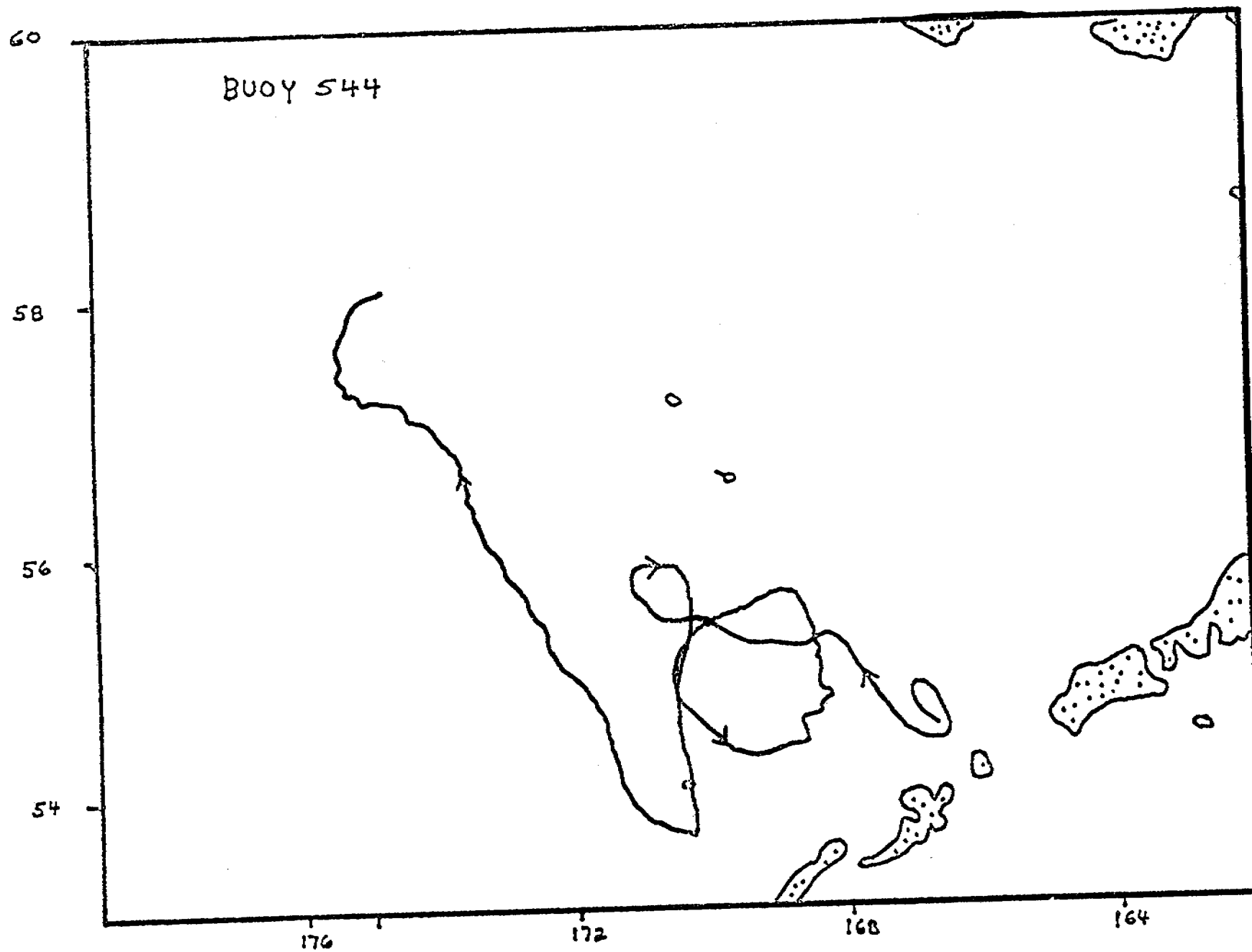


Figure 5D. Drifter tracks. (D) Buoy 544.

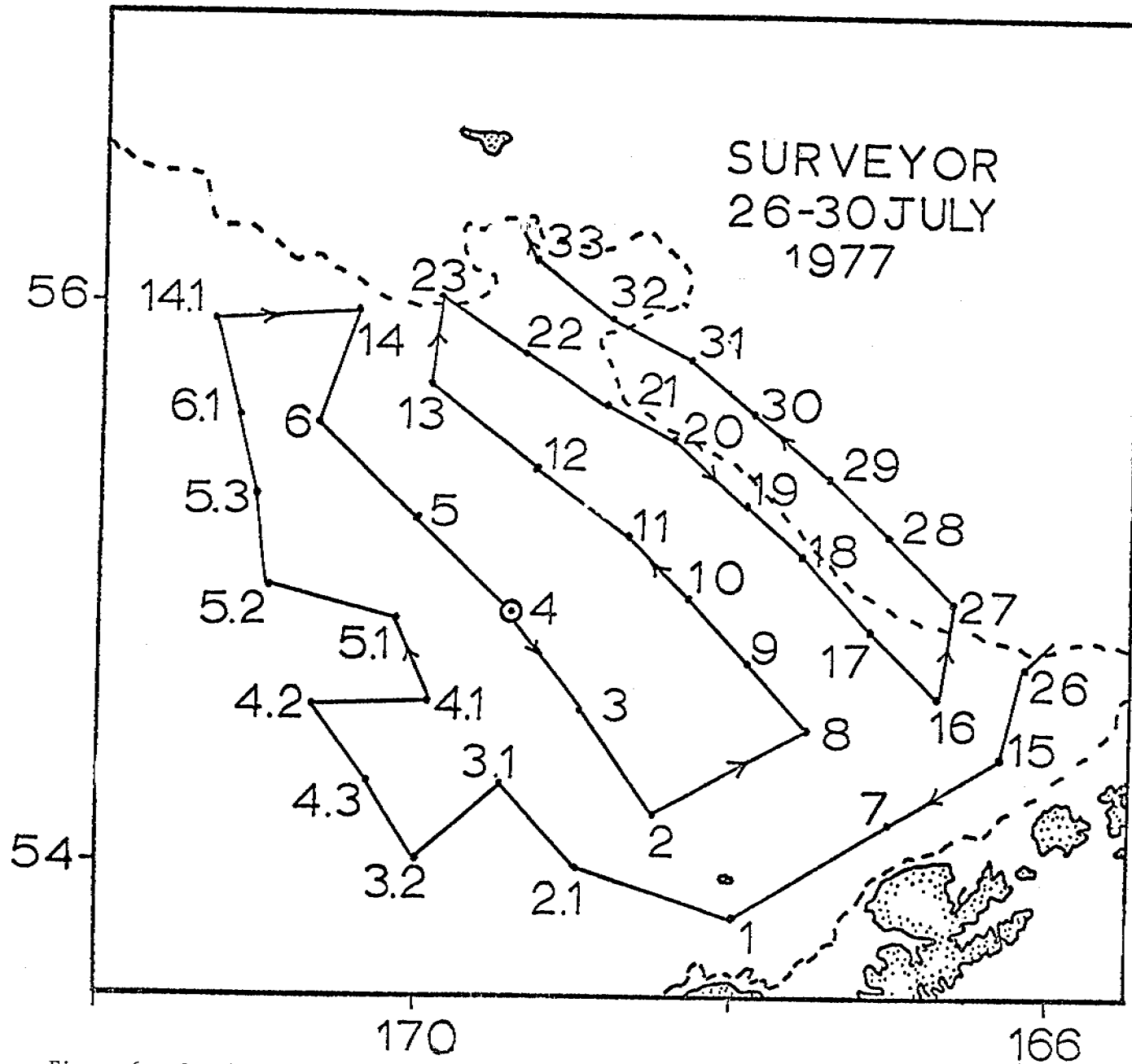


Figure 6. Station positions, NOAA ship Surveyor, 26-30 July 1977. Station 4 was selected to lie at the center of the circle defined by the drifter tracks (see Fig. 5A).

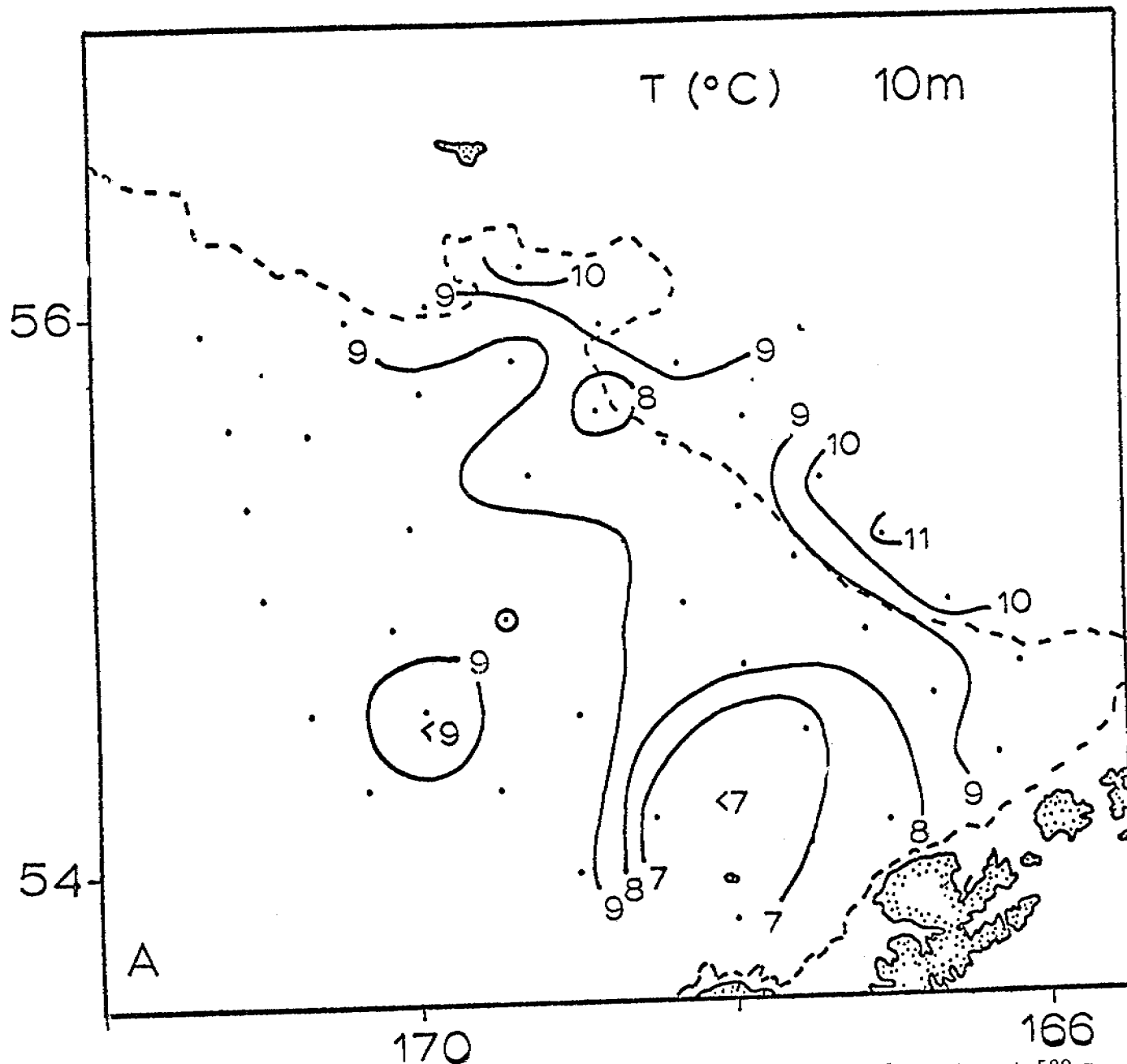


Figure 7A. Temperature ($^{\circ}\text{C}$). (A) 10 m. The eddy clearly shows as cooler water at 500 m depth and below, but not at 10 m depth (cf. Fig. 8). Station 4 is circled and the dashed line delineates the shelfbreak ($\sim 170^{\circ}$ m depth). (See Fig. 6 for station numbers.)

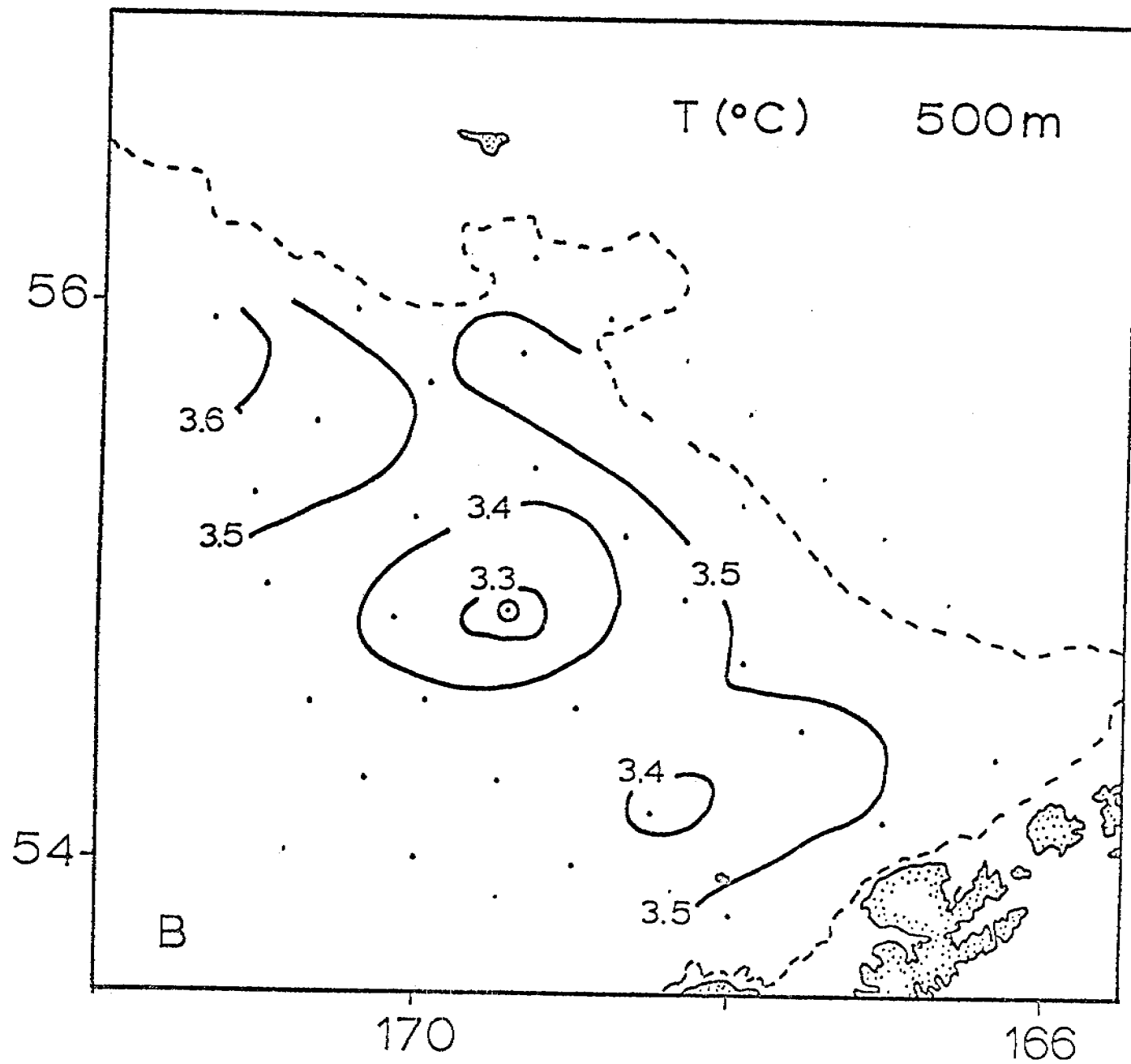


Figure 7B. Temperature ($^{\circ}$ C). (B) 500 m.

T(°C) 1000 m

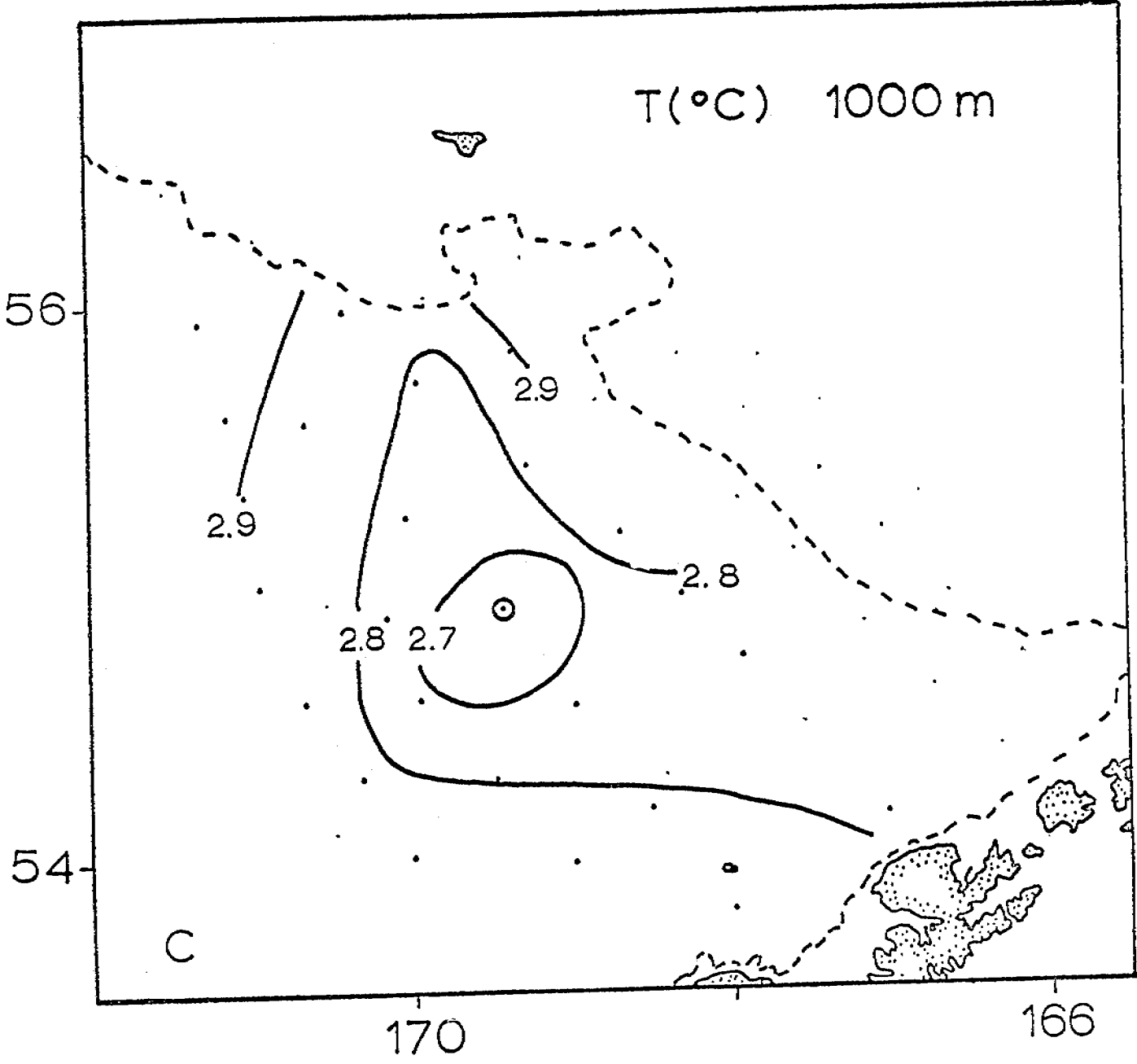


Figure 7C. Temperature (°C). (C) 1000 m.

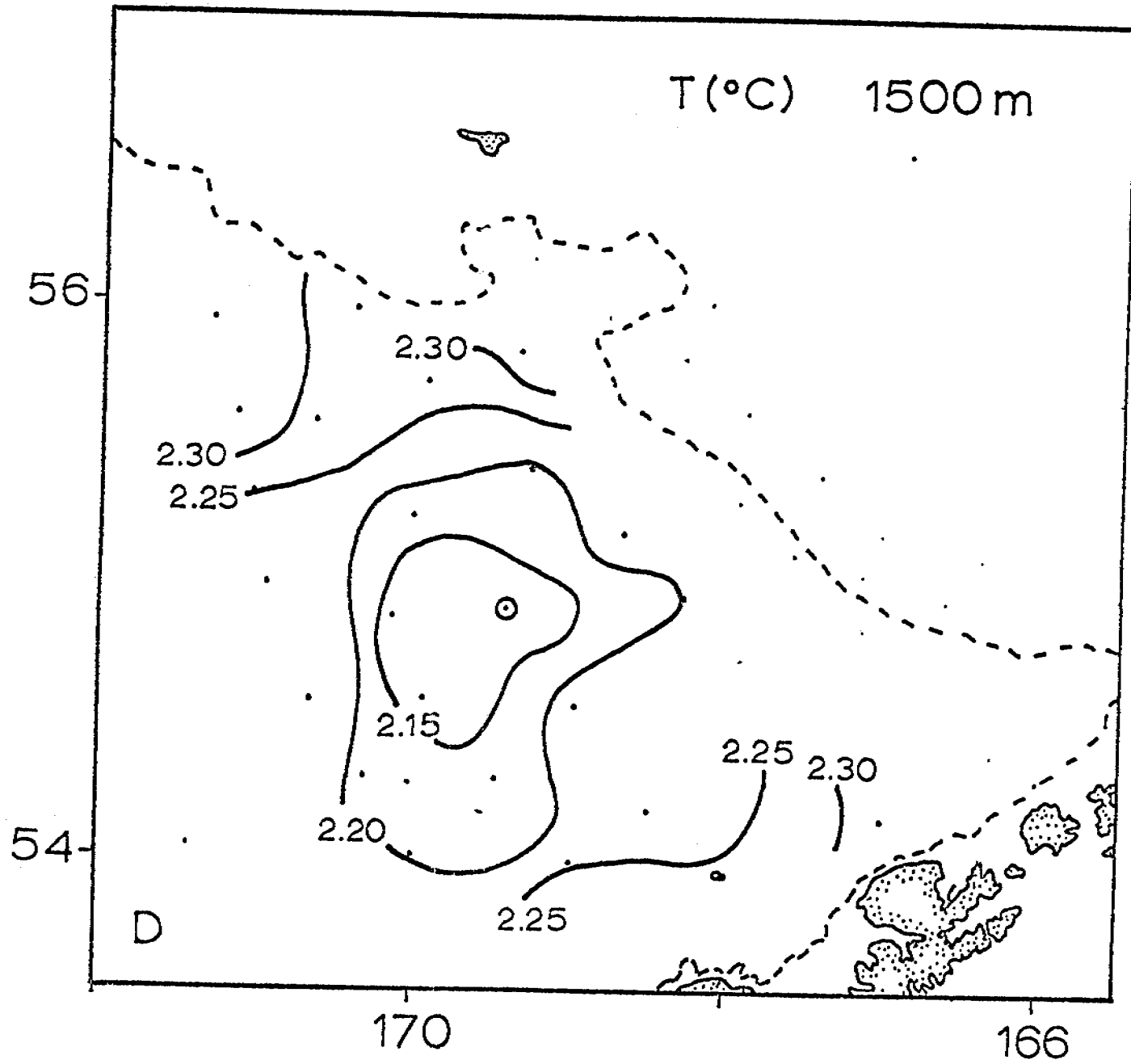


Figure 7D. Temperature (°C). (D) 1500 m.

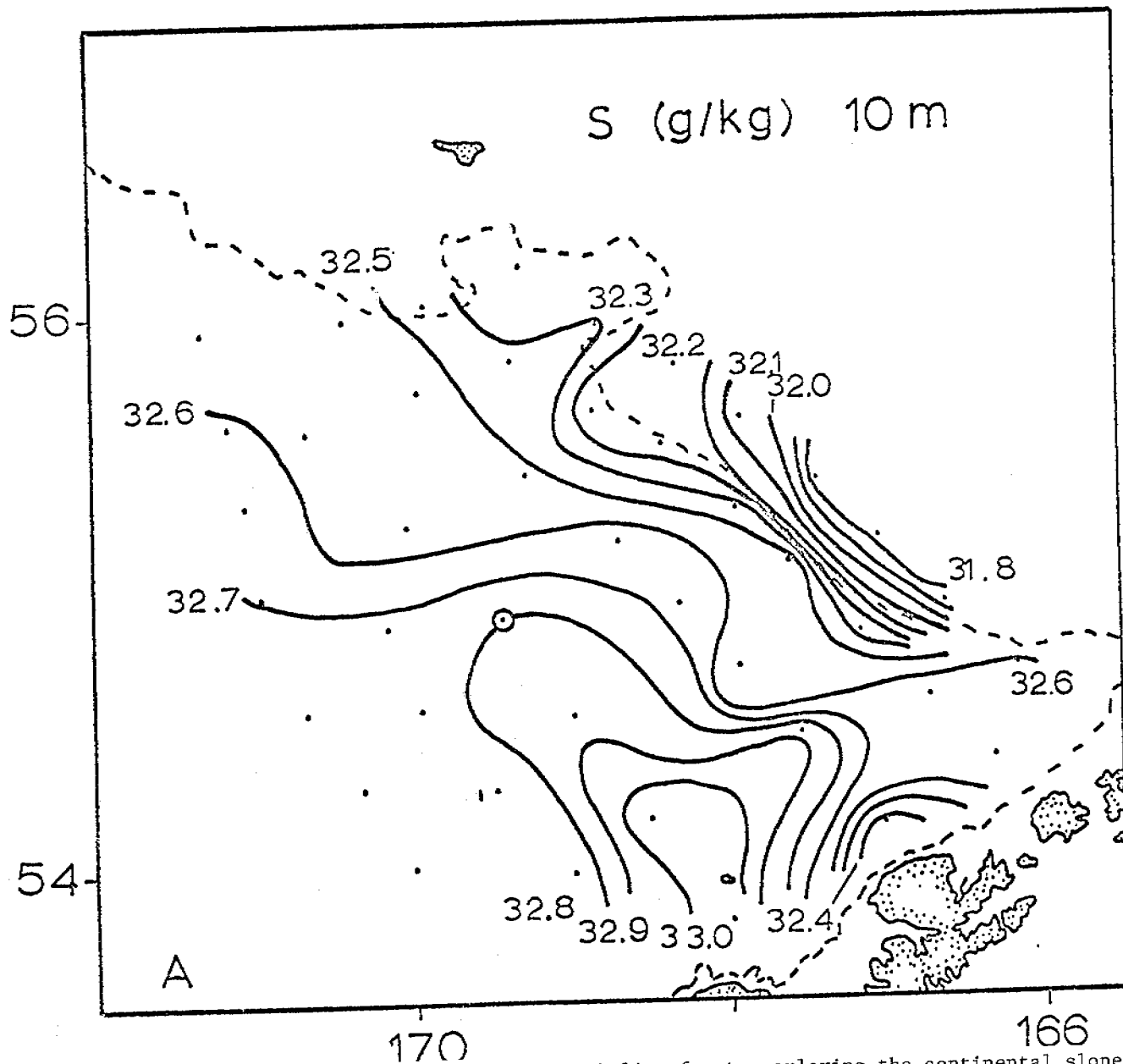


Figure 8A. Salinity (g/kg). (A) 10 m. The haline front overlaying the continental slope shows at 10 m, but there is no clue to the presence of the eddy. At 500 m and below, however, the eddy shows clearly as saltier water (cf. Fig. 7). Station 4 is circled and the dashed line delineates the shelfbreak (170 m depth). (See Fig. 6 for station locations.)

300

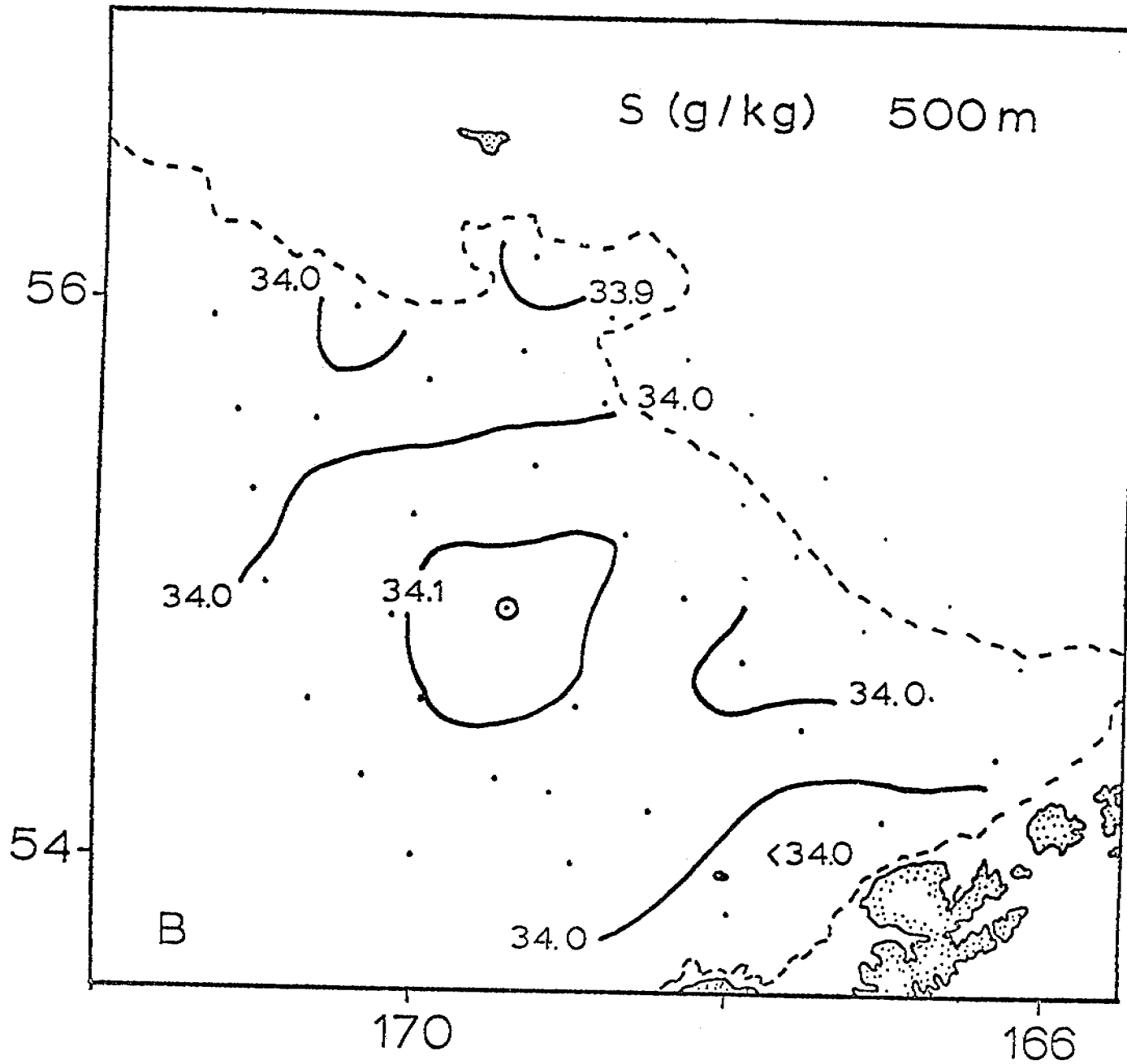


Figure 8B. Salinity (g/kg). (B) 500 m.

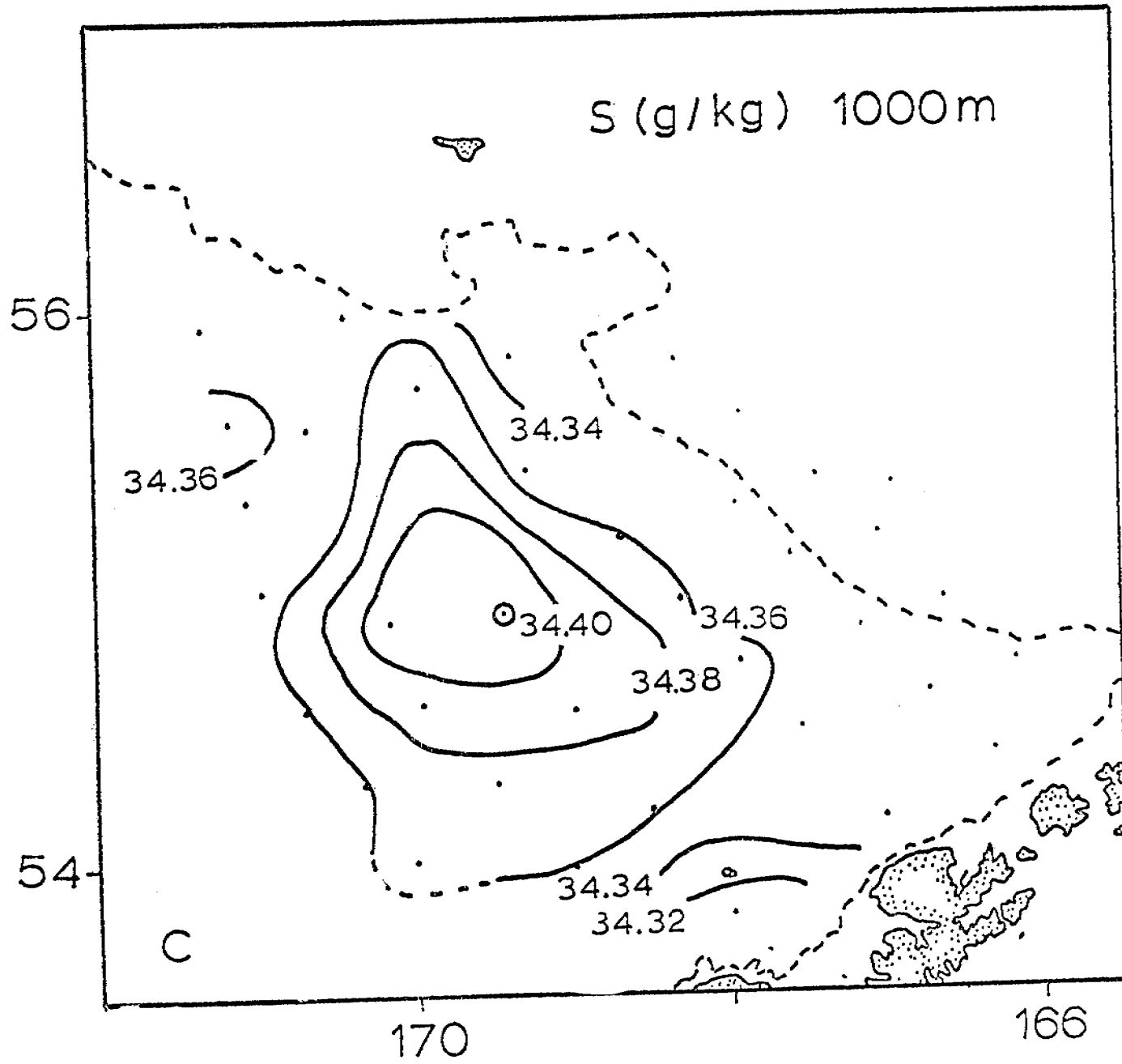


Figure 8C. Salinity (g/kg). (C) 1000 m.

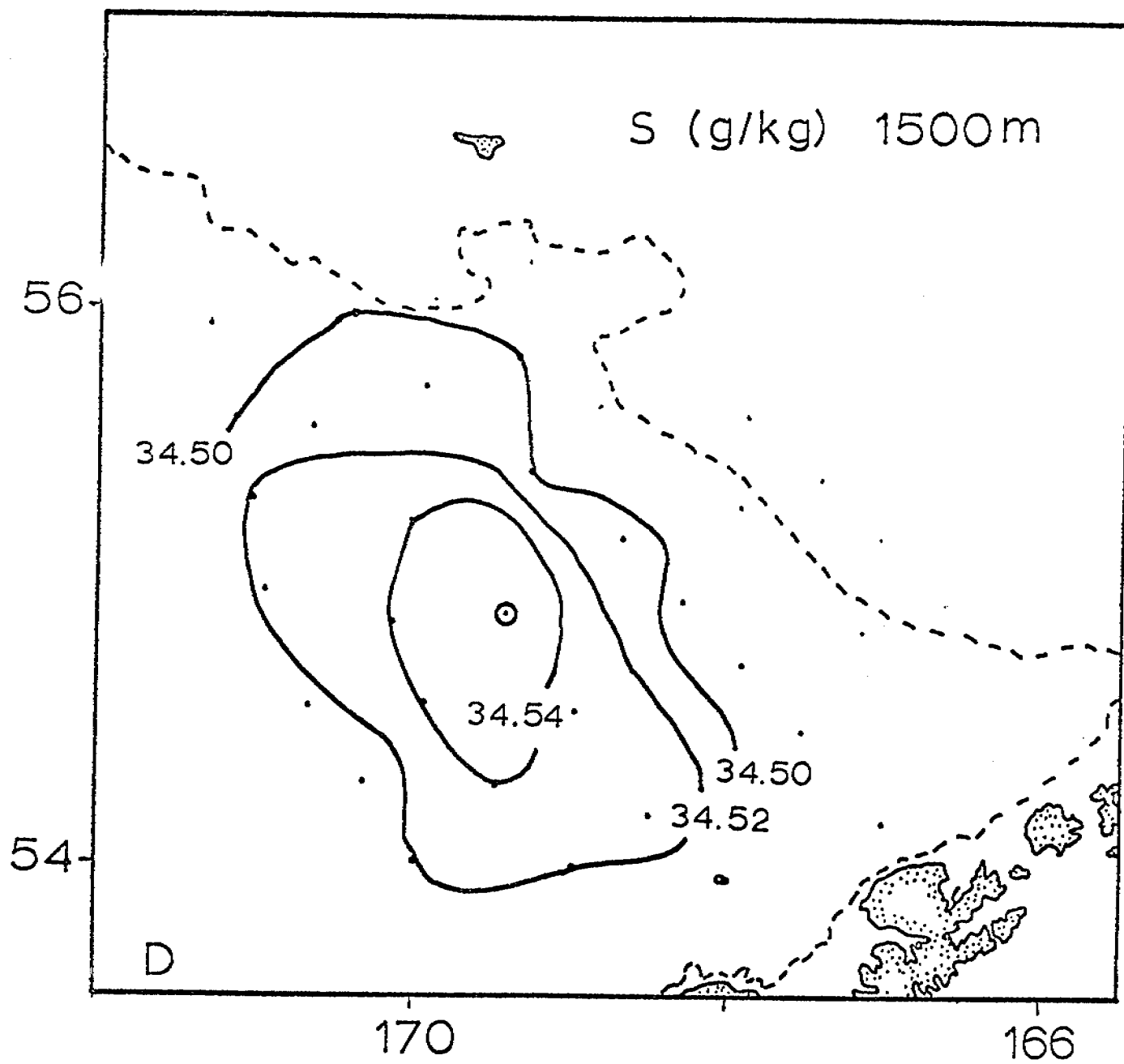


Figure 8D. Salinity (g/kg). (D) 1500 m.

GEOPOTENTIAL
($10 \text{ m}^2/\text{s}^2$)

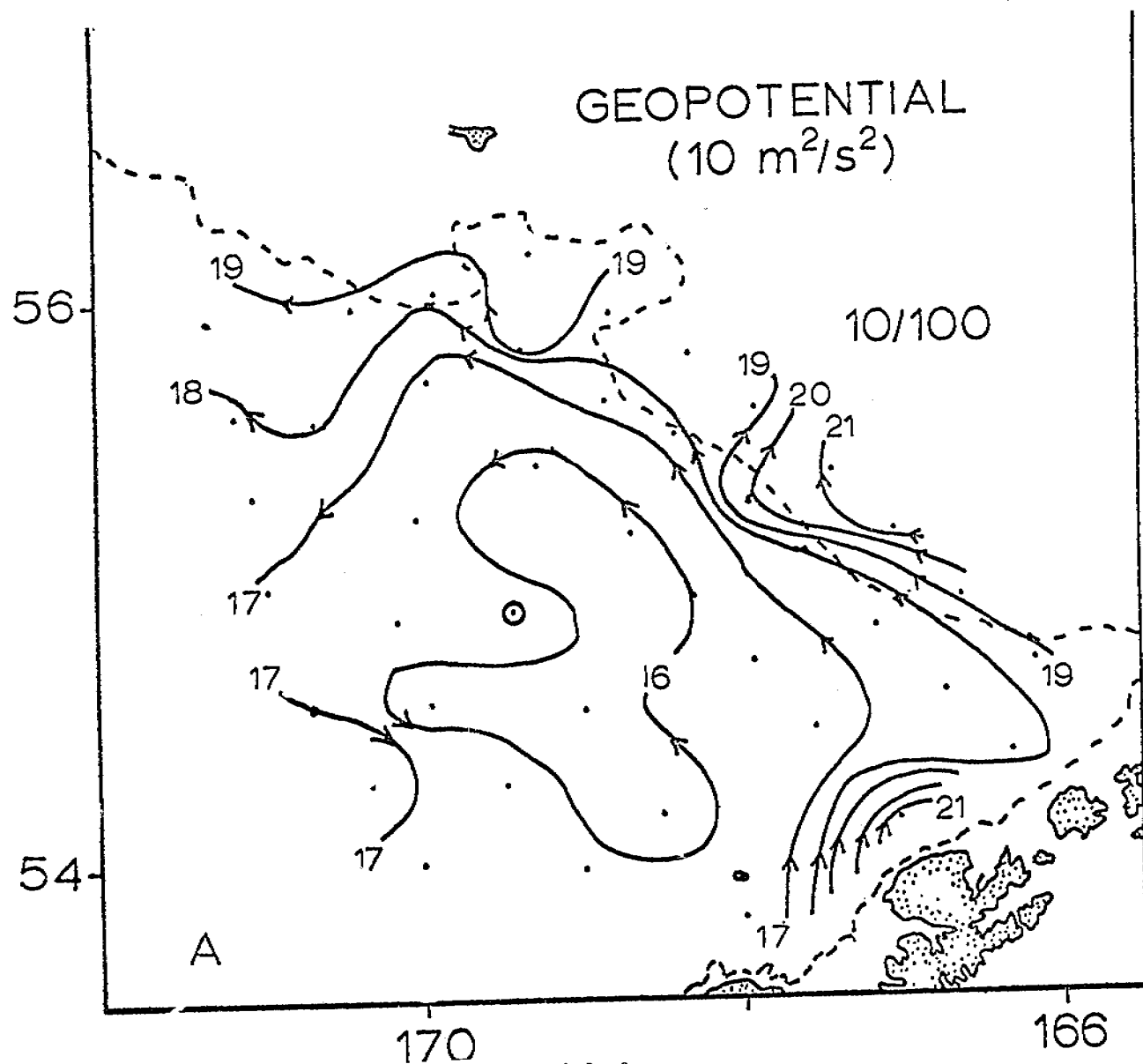


Figure 9A. Dynamic topographies ($10^{-1} \text{ m}^2/\text{s}^2 = 1$ dynamic cm). (A) 10/100. The shallowest distribution (A) shows the general cyclonic circulation of the eastern deep basin, but not the eddy. The deeper distributions (B, C and D) show the eddy clearly. The 10/1500 topograph (not shown; superpose A and B) is dominated by the eddy (cf. Fig. 5, 7 and 8). Station 4 is circled and the dashed line delineates the shelfbreak (~ 170 m). (See Fig. 6 for station locations.)

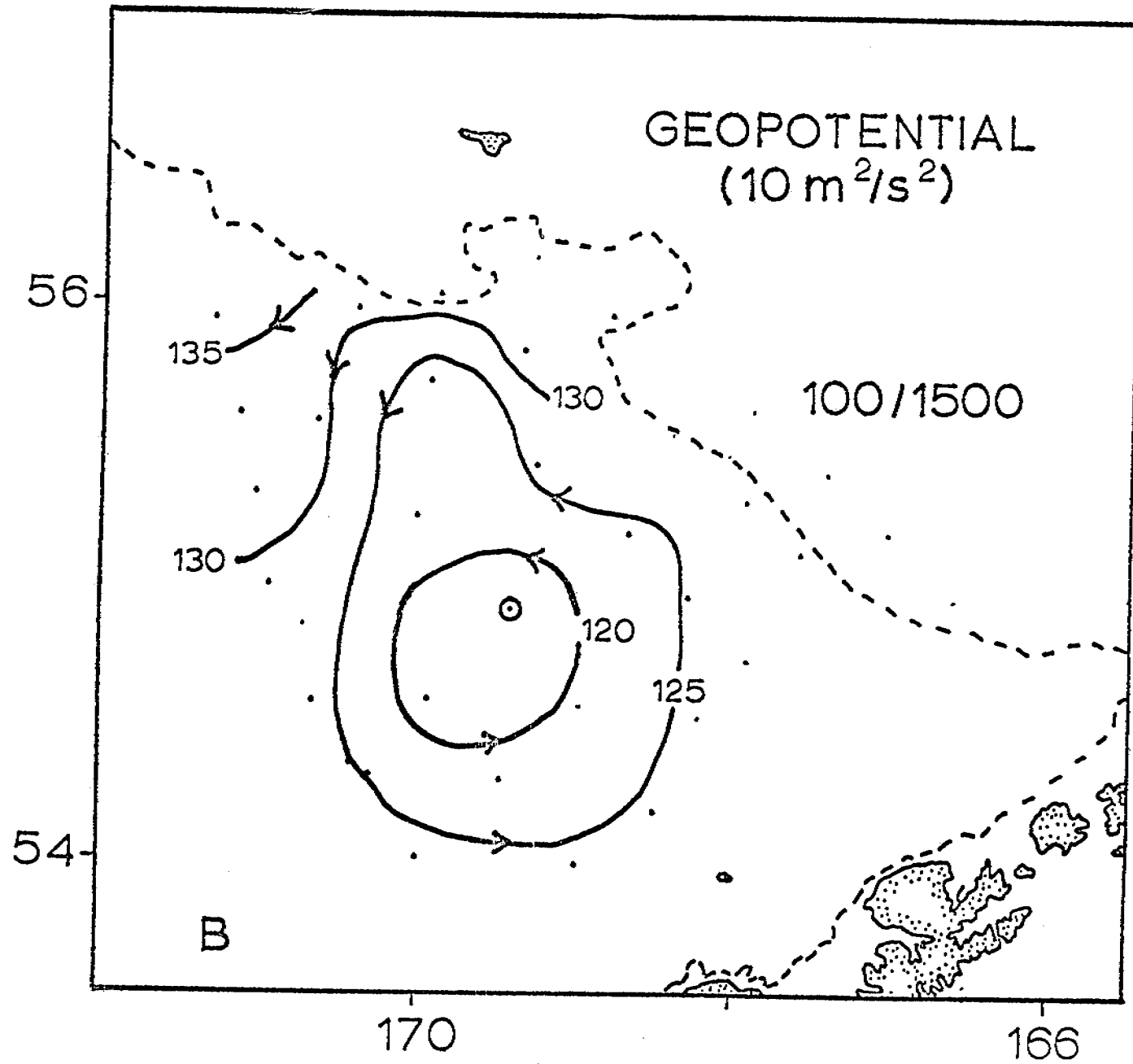


Figure 9B. Dynamic topographies ($10^{-1} \text{ m}^2/\text{s}^2 = 1$ dynamic cm).
(B) 100/1500.

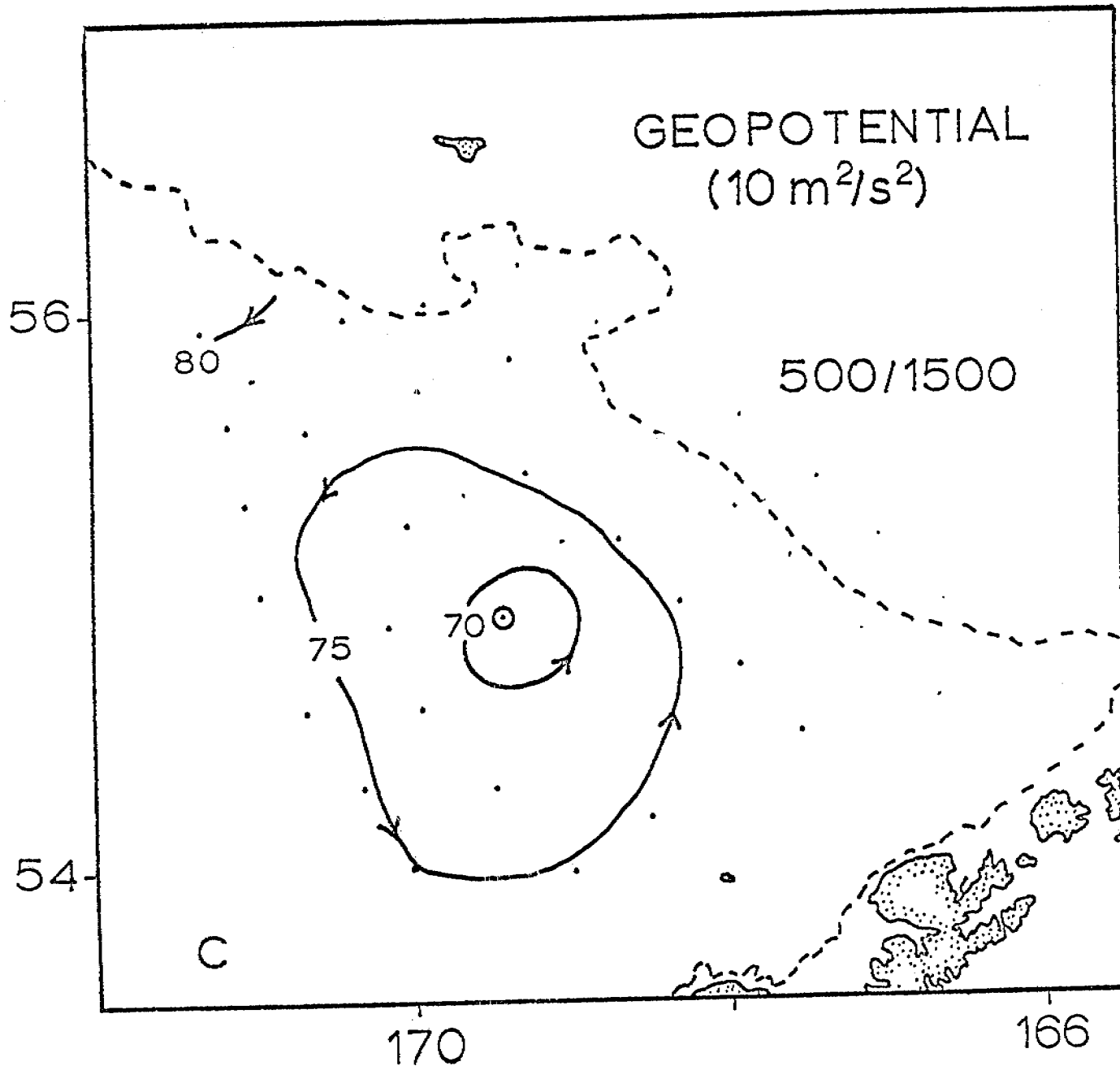


Figure 9C. Dynamic topographies ($10^{-1} \text{ m}^2/\text{s}^2 = 1 \text{ dynamic cm}$).
(C) 500/1500.

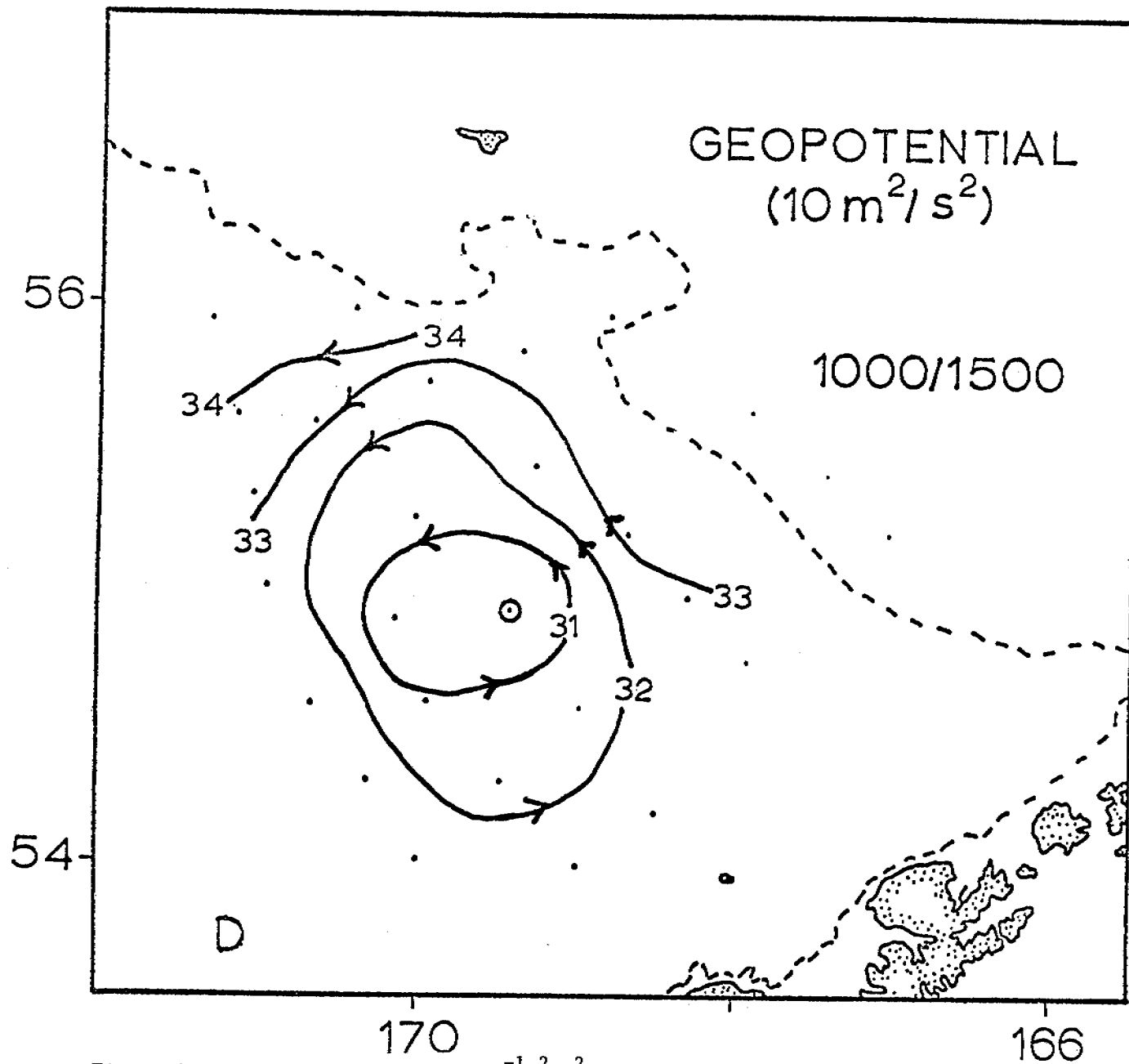


Figure 9D. Dynamic topographies ($10^{-1} \text{ m}^2/\text{s}^2 = 1$ dynamic cm).
(D) 1000/1500.

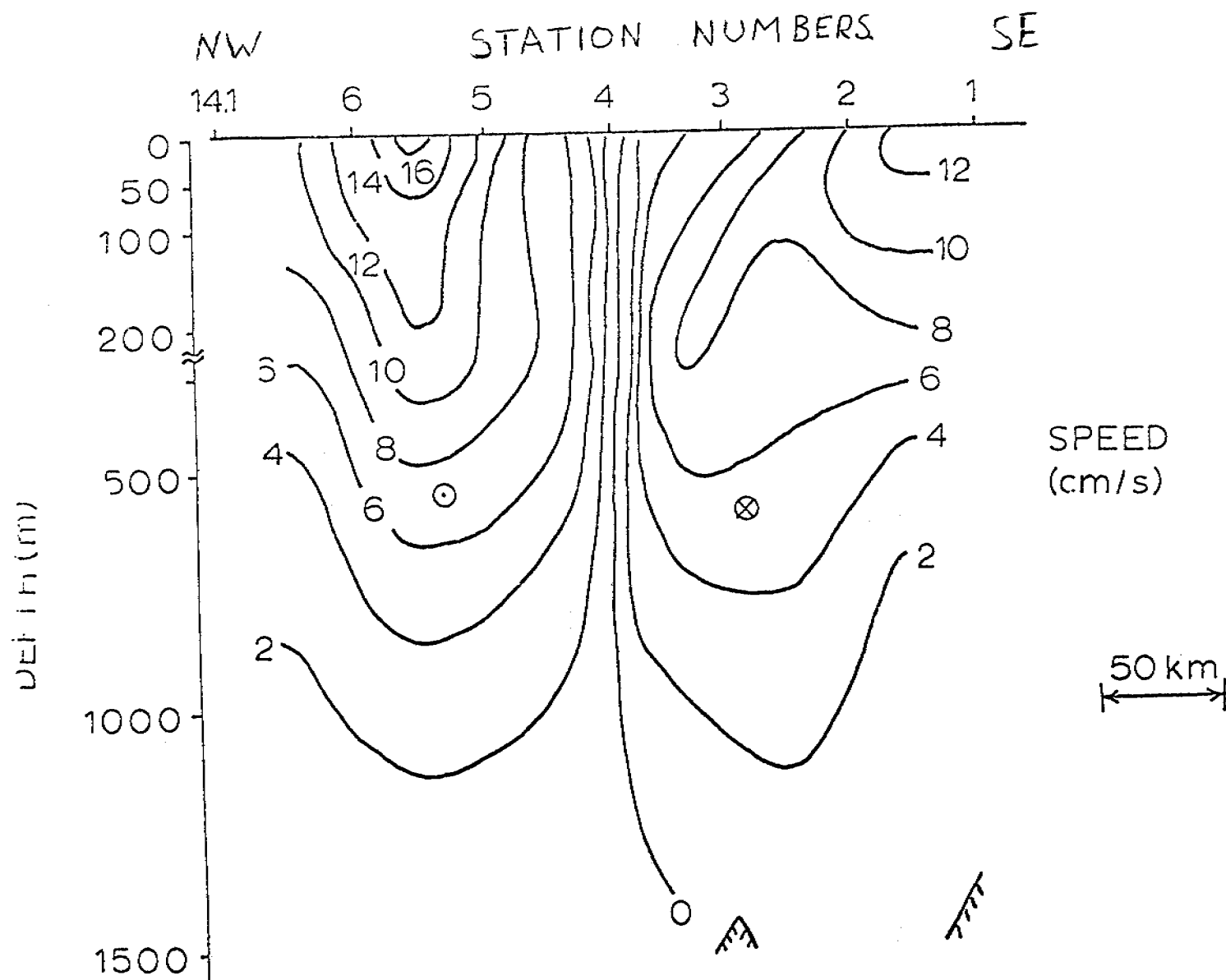


Figure 10. Cross section of speed inferred from hydrography (cm/s). Speeds calculated by the dynamic method are contoured for a northwest-southeast section (Fig. 6 has station locations). These speeds agreed with mean drifter speeds, although there was considerable scatter (Table 3). Note the scale change at 200 m depth.

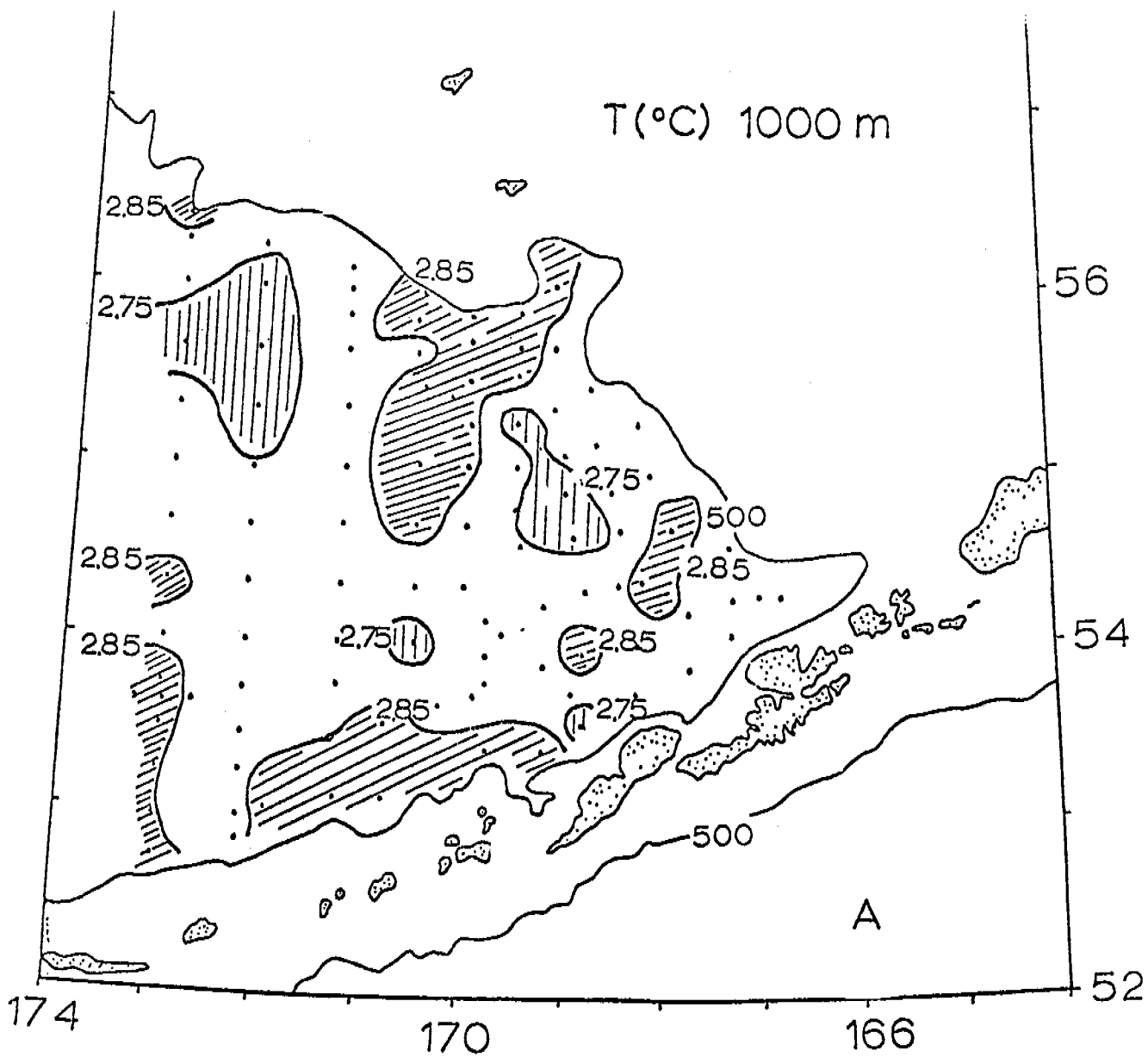


Figure 11 A. Summer 1971 data. (A) Temperature ($^{\circ}\text{C}$) at 1000 m depth. The distributions are flatter than in 1977 (cf. Fig. 7 and 9). Depending on one's biases, it is possible to find excellent agreement or complete disagreement between the surveys of 1971 and 1977. The truly permanent features are the general cyclonic tendency of the flow, and the presence of several meso-scale features. Individual meso-scale features (e.g. the 1977 eddy) are transient.

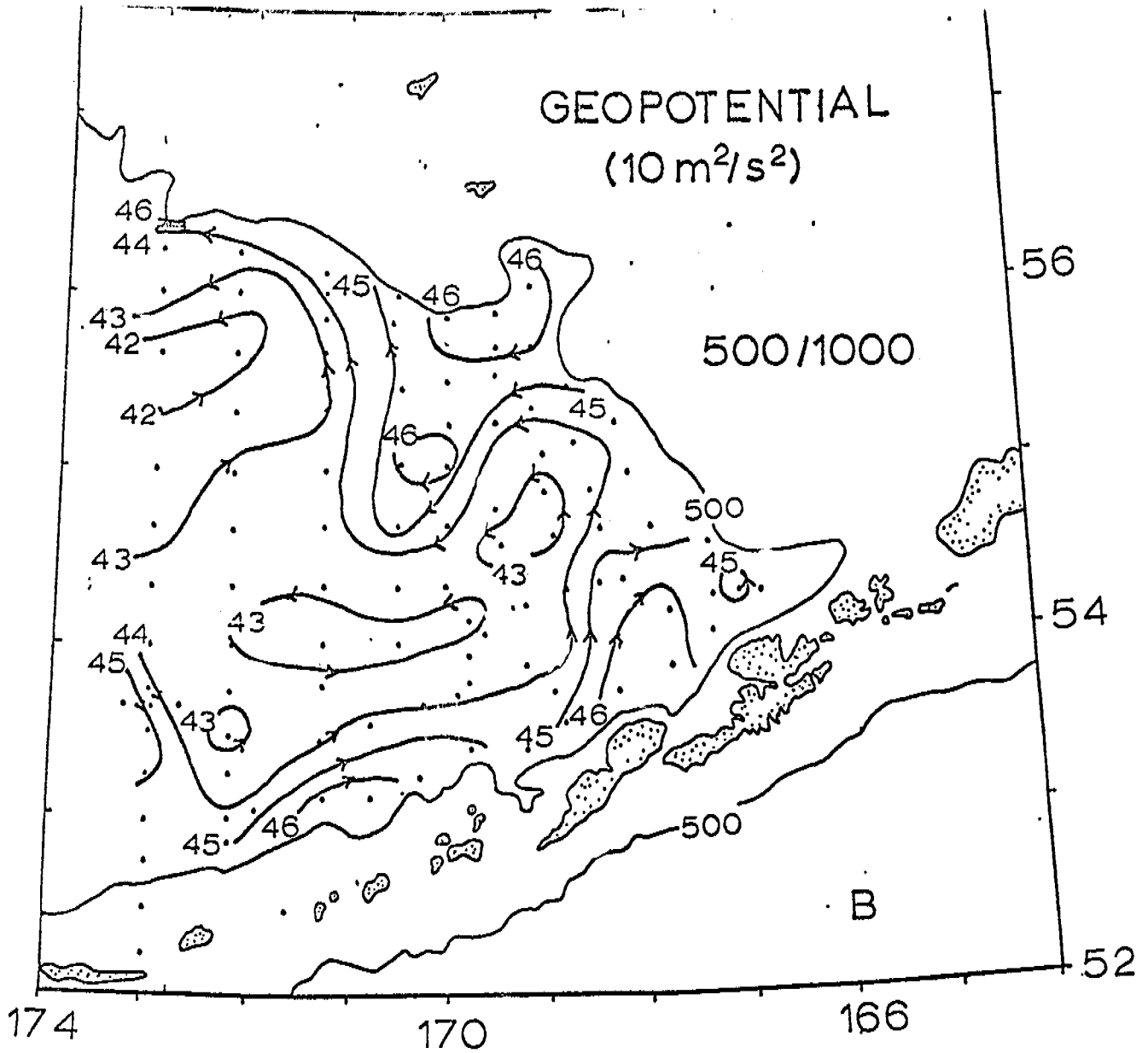


Figure 11B. Summer 1971 data. (B) Geopotential 500/1000 ($10 \text{ m}^2/\text{s}^2 = 1 \text{ dynamic cm}$).

E. Winter Hydrography

Winter hydrographic conditions in Bristol Bay were examined in February 1978. The NOAA Ship SURVEYOR collected CTD observations in ice free areas and along the ice edge while a helicopter, operating from Nunivak Island, collected CTD observations through the ice. The helicopter occupied 23 stations, on both sides of the 50 meter isobath. For data collection through the ice, an ODEC portable CTD was used, while the Ship used a Grundy model 9040 CTD.

The three hydrographic domains which obtain during summer exist during winter months. The coastal domain remained well mixed, while central shelf waters were stratified when ice covered and well mixed when ice free. The outer shelf domain existed in a somewhat modified form, the inner front was less distinct and the outer front bounded an apparently more energetic current regime.

Throughout the year, tidal stirring is sufficient to mix the entire water column (≤ 50 m) in the coastal domain. During winter, surface cooling and brine rejection add negative buoyancy and tidal stirring maintains a vertically uniform distribution of mass. Over the central shelf, convective cooling and increased wind mixing overcome the stratification extant during summer and result in a well mixed water column (Fig. 1). When ice is present, however, further cooling by exchange with the atmosphere is inhibited. Cooling due to the presence of ice occurs, but as ice melts the upper layer becomes less saline. Similar to conditions in summer, tidal mixing is not sufficient to stir the entire water column and stratification occurs (Fig. 1). Because salinity has dominant affect on density, stratification will tend to persist even after ice is removed, either by advection or melting.

The increased horizontal salinity gradient between the central shelf-outer shelf domains is less distinct in winter than summer. There is little suggestion of a front in either surface temperature or salinity distributions (Fig. 2); however, horizontal gradients are stronger near the bottom. Apparently vertical processes (surface cooling and wind stirring) become more important and the gradient in the horizontal salinity flux which is suggested as the formation mechanism (Coachman and Charnell, 1979) is obscured. Although fine structure still exists (at station 52), the outer shelf domain has the appearance of a two rather than a three layered structure.

Dynamic topography, combining data from ice covered and ice free regions, is shown in Figure 3. Assuming a baroclinic geostrophic balance, we calculated surface speeds of $3-4 \text{ cs}^{-1}$ relative to a 40 dB reference level over the shelf parallel to the 50 m isobath. These speeds and their direction are consistent with direct current observations during winter. Over the slope, the July 1977 baroclinic eddy was not evident and the dynamic topography (01400dB) indicates a sinuous flow generally along bathymetric contours toward the northwest. Along the slope, baroclinic speeds were calculated to be up to $\sim 40 \text{ cs}^{-1}$, with values generally about 20 cs^{-1} . Thus, geostrophic speeds were at least a factor of two greater than summer speeds.

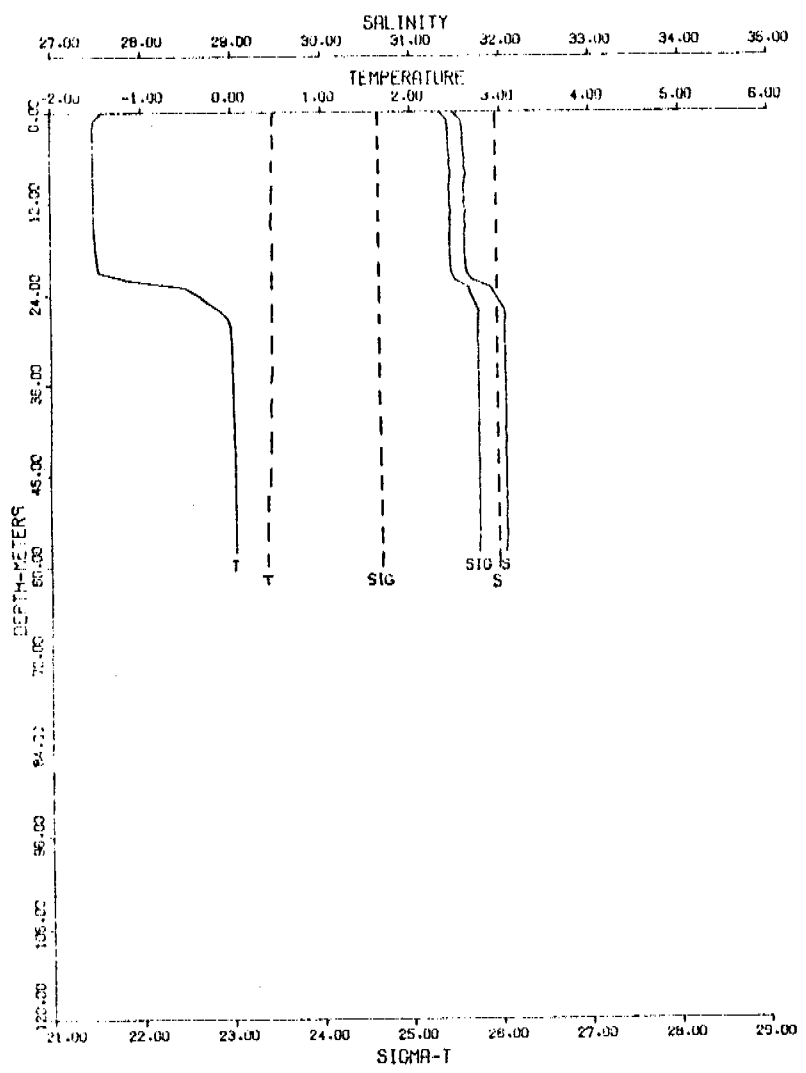


Figure 1. Vertical structure observed over the central shelf during February 1978. The dashed profiles represent conditions seaward of ice cover and the solid profile is typical of stratification under ice cover.

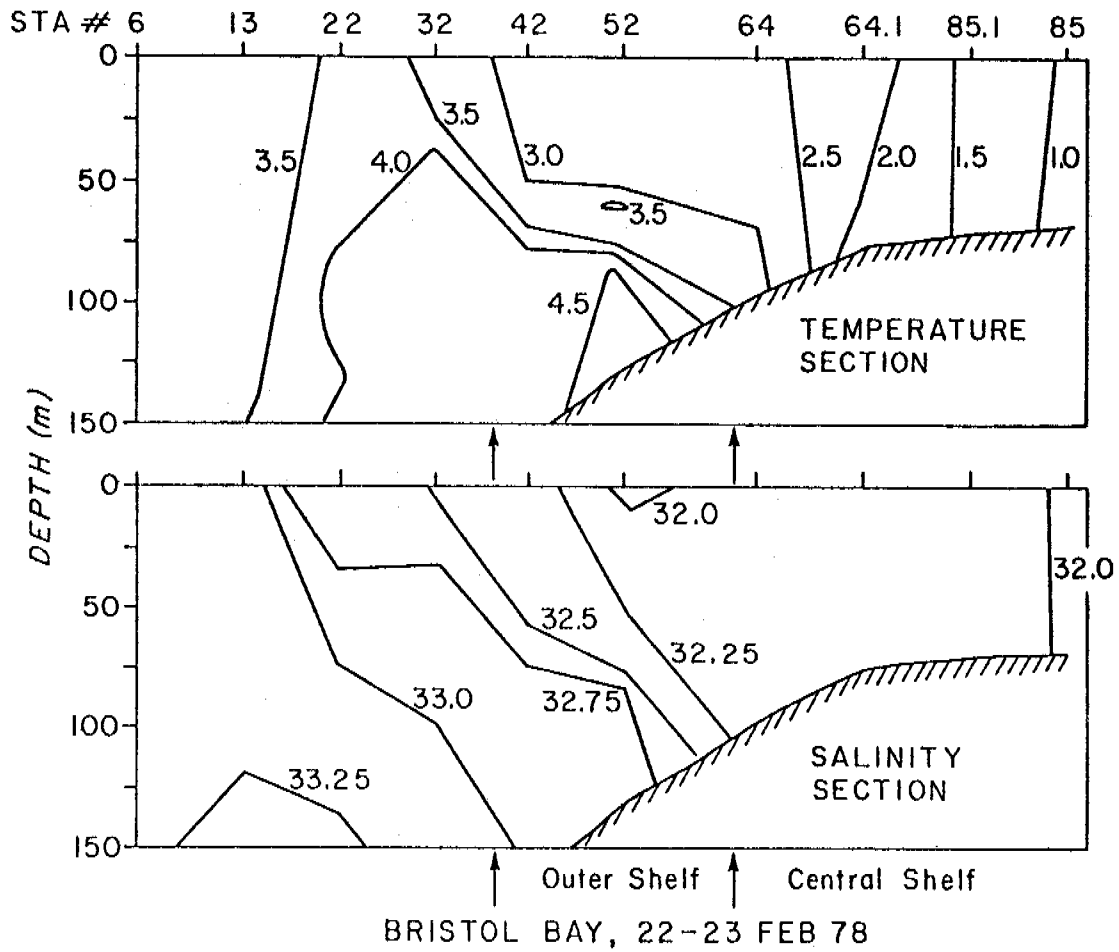


Figure 2. Temperature and salinity sections during winter 1978. For station locations see Figure 3.

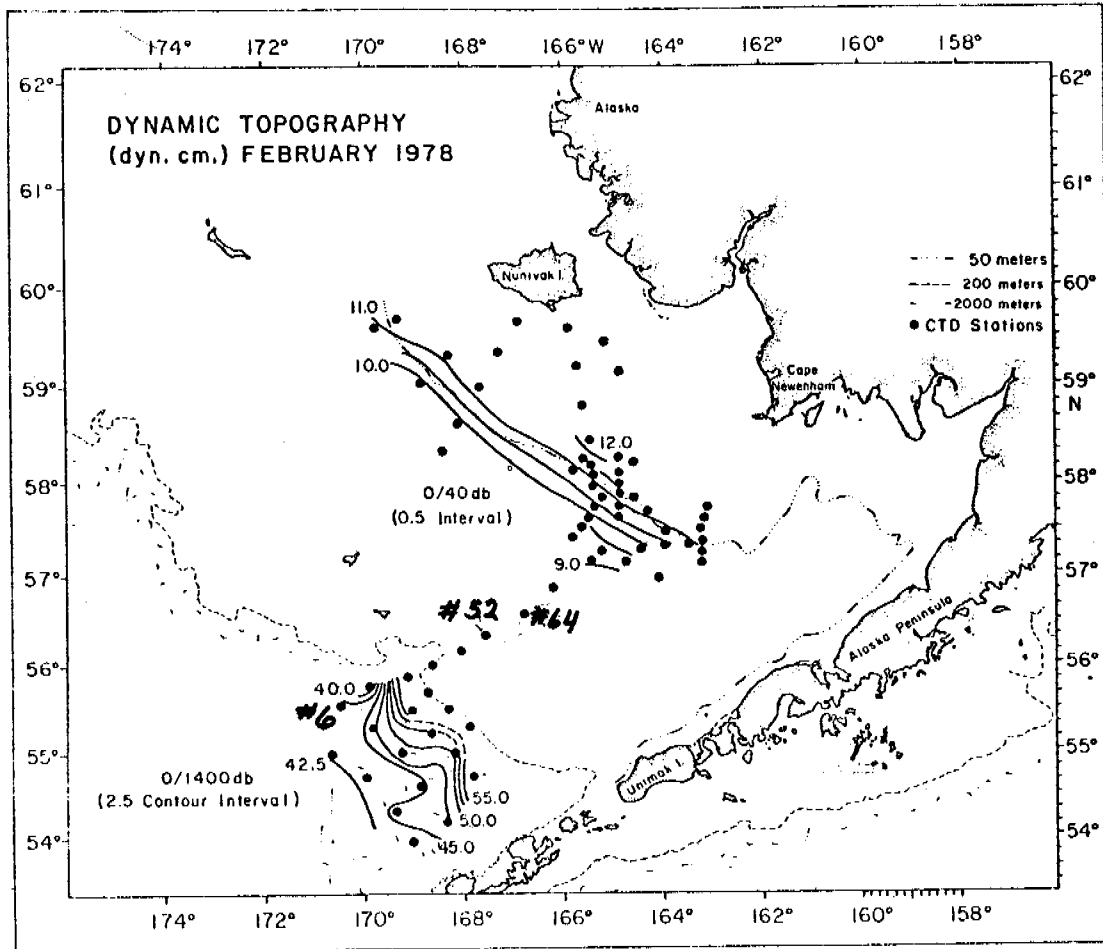


Figure 3. Dynamic topography for winter 1978: note the change in reference level for coastal and deep basin contours.

F. References

This subsection includes all cited works in Section IV. Present Status except those referenced in Section IV. D. and/or Section VI. Publications.

- Ashmole, N.P., 1971. Seabird ecology and the marine environment. In D.S. Farmer and J.R. King, eds. Avian Biology Vol. I, Academic Press, New York. pp.233-286.
- Bourne, W.R.P., 1963. A review of oceanic studies of the biology of seabirds. Proc. 13th Int. Ornithol. Congr. 1962. pp. 831-854.
- Coachman, L.K. 1979. Water circulation and mixing in the southeast Bering Sea. In Progress Report Probes Phase I, 1971-1978.
- Fournier, R.O., M. Van Det, S. Wilson and N.B. Hargreaves, 1978. The influence of the shelf break front off Nova Scotia on phytoplakton standing stock in late winter. Unpublished manuscript.
- Fournier, R.O., J. Mara, R. Bohrer, and M. Van Det, 1977. Plankton dynamics and nutrient enrichment of the Scotian shelf. J. Fish.Res. Bd. Can.34(7): 1004-1018.
- Gould, P., 1971. Interactions of Seabirds over the Open Ocean. Ph.D. Thesis, University of Arizona.
- James, I. 1978. A note on the circulation induced by a shallow-sea front. Estuarine And Coastal Marine Sciences 7: 786-789.
- Knauss, J.A., 1957. An observation of an oceanic front. Tellus, 9: 234-237.
- Pingree, R.D. and D.K. Griffiths, 1978. Tidal fronts on the shelf seas around the British Isles. J. Geophys. Res. 83 (C9):4615-4622.
- Pingree, R.D., P.M. Holligan, and G.T. Mardell, 1978. The effects of vertical stability on phytoplankton distributions in the summer on the northwest European shelf. Deep Sea Res. 25(11):1011-1028.
- Savidge, G., 1976. A preliminary study of the distribution of chlorophyll in the vicinity of fronts in the Celtic and western Irish Seas. Estuarine and Coastal Mar. Sci. 4:617-625.
- Simpson, J.H., C.M. Allen, and N.C.G. Morris, 1978. Fronts on the continental shelf. J. Geophys. Res. 83(C9):4607-4614.
- Simpson, J.H. and R.D. Pingree, 1978. Shallow fronts produced by tidal stirring. In Oceanic Fronts in Coastal Processes, M.J. Bowman and W.E. Esaias, eds. Springer-Verlag, New York. pp. 29-42.
- Sverdrup, H.V., 1953. On conditions for the vernal blooming of phytoplankton. J. Conseil, Conseil Perm. Intern. Exploration Mer. 18. 287-295.
- Uda, M., 1959. Water Mass Boundaries - "Siome." Frontal Theory in Oceanography. Fish Res. Bd. Canada Manuscript Report Series, No. 51, Seminar 2, pp. 10-20.

V. Cooperation

We are cooperating with other research units as follows:

- 289 (Royer) Satellite imagery usefully delineates the structural front and the seasonal ice cover.
- 435 (Leendertse) We provide hydrographic, current and pressure data. Together we attempt to understand the tidal regime.
- 217 (Hansen) We are trying to understand the deep eddy, initially revealed by drifters, and to compare current meter and drifter records where appropriate.
- 206 (Vallier and Gardner) We are exchanging thoughts and data on the St. George Basin regime.
- 83 (Hunt) We are attempting to relate the bird distribution to the structural front near the Pribilof Islands.
- 367 (Reynolds) We are exchanging ideas and data on the effects of local meteorology on the oceanography.

VI. Publications resulting from Bristol Bay work

- Coachman, L.K. and R.L. Charnell, 1977. Finestructure in Outer Bristol Bay, Alaska. Deep Sea Res. 24 (10): 869-889.
- Coachman, L.K. and R.L. Charnell. Lateral water mass interactions - a case study, Bristol Bay, Alaska. J. Phys. Oceanogr., Vol. 9 (No. 2)
- Kinder, T.H., 1977. The hydrographic structure over the continental shelf near Bristol Bay, Alaska, June 1976. University of Washington, Department of Oceanography, Technical Report M77-3, 61 pp.
- Kinder, T.H. and L.K. Coachman, 1978. The front overlaying the continental slope of the Eastern Bering Sea. J. of Geophys. Res., 83 (C9): 4551-4560.
- Kinder, T.H., J.D. Schumacher, R.B. Tripp and J.C. Haslett, 1978. The evolution of the hydrographic structure over the continental shelf near Bristol Bay, Alaska, during summer 1976. University of Washington, Department of Oceanography Technical Report. Ref. No. M78-16, April 1978, 72 pp.
- Kinder, T.H., J.D. Schumacher and D.V. Hansen. Observations of a baroclinic eddy in the southeastern Bering Sea. Submitted to J. Phys. Oceanogr.
- Muench, R.D. and R.L. Charnell, 1977. Observations of medium scale features along the seasonal ice edge in the Bering Sea. J. Phys. Oceanogr. 7 (4): 602-606.
- Reed, R.K., 1978. Heat budget in the eastern Bering Sea. J. Geophys. Res., 83(C7): 3635-3645.
- Schumacher, J.D., T.H. Kinder, D.J. Pashinski and R.L. Charnell. A structural front over the continental shelf of the Eastern Bering Sea. J. Phys. Oceanogr. Vol. 9 (No. 1).

Schumacher, J.D., T.H. Kinder and D.J. Pashinski. Observations of Advective and Diffusive Processes over the Continental Shelf of the southeastern Bering Sea. In preparation.

VII. Needs for Further Study

We believe that the continued study of Bristol Bay should emphasize analysis of data already obtained, and selected field work directed at specific objectives. The remaining tasks to be undertaken are:

1. A synthesis of all the accumulated information into a single document reflecting the Physical Oceanography of Bristol Bay.
2. Continued efforts to resolve the apparent presence of anomalous tidal currents exhibited in a number of current meter records. This includes: analysis of current meter operating characteristics to evaluate possible instrument problems such as rotor fouling, theoretical investigations into physical processes which might lead to such records, and a field experiment during Summer 1979.
3. Continued elucidation of the meteorological environment and its impact on physical processes

VIII. Conclusions

Field work in the Bristol Bay region has yielded more complete understanding of the physical oceanography. This understanding is reflected in Section IV of this report (present status), in previous reports, and in the publications listed in Section VI.

Major elements include:

1. the shelf exhibits low mean flow and the kinetic energy is tidally dominated;
2. the hydrographic structure in summer separates into three distinct domains: coastal, central shelf and shelf break;
3. melting ice in winter can re-establish vertical structure locally in the central shelf domain;
4. finestructure is ubiquitous in the shelfbreak domain, and is evidence of lateral water mass interaction;
5. the central shelf and coastal domains are separated by a structural front which results from a varying balance between buoyancy input and tidal mixing;
6. a similar front exists near the Pribilof Islands and has biological implications;
7. tidal currents show anomalous diminution and amplification at some locations while tidal heights do not, reflecting possible instrument malfunction;
8. flow over the deep basin is spatially and temporally complex with occurrences of current rings and eddies;

9. the heat balance over the central shelf during summer primarily involves atmospheric exchange;

10. certain ice-edge features are associated with the wind; and,

11. low frequency (less than diurnal) flow is episodic or quasi-periodic,

12. the three domain character of the shelf hydrographically is also exhibited in the velocity field.

Many of these elements receive amplification and discussion of their implication in papers, while others are the subject of preliminary reports. Thus far, many interesting features have been identified and these need to be more fully understood. Further analysis of data in hand, numerical and analytical investigation, and selected field work are required, with the emphasis on data analysis. As these salient features are understood, a reasonable synthesis of the regional physical oceanography will be possible.

APPENDIX A

Hydrographic Summary

The following cruises collected hydrographic data included in this reporting period:

<u>Cruise</u>	<u>Designation</u>	<u>Dates</u>	<u>Casts</u>	<u>XBTs</u>
<u>Surveyor</u>	RP4-SU-78A Leg 1	13 February to 1 March	64	-
<u>UHTH</u>	BBICE	17 February to 28 February	19	-
<u>Surveyor</u>	RP4-SU-78A Leg 5	27 April to 16 May	85	-
<u>Surveyor</u>	RP4-SU-78A Leg 6	26 May to 12 June	46	-
<u>Discoverer</u>	RP4-DI-78B Leg 1	10 July to 3 August	269	107
<u>Discoverer</u>	RP4-DI-78B Leg 3	10 September to 22 September	109	196

APPENDIX B
MOORING SUMMARY

MOORING	POSITION	DEPLOYMENT PERIOD	INSTRUMENTATION
BC-2F	57-02.4N 163-26.5W	10 September 1977 Not Recovered	2cm - 19m, 53m
BC-3D	57-17.7N 165-29.7W	9 September 1977 16 July 1978	2cm - 19m, 97m
BC-4F	58-37.2N 168-22.0W	13 September 1977 Not Recovered	2cm - 18m, 46m 1 PG - 51m
BC-4G	58-37.0N 168-21.6W	19 July 1978 20 September 1978	2cm - 18m, 46m 1 PG - 52m
BC-20A	60-25.7N 171-05.2W	17 September 1977 21 July 1978	1cm - 22m 1 PG - 52m
BC-20B	60-25.6N 171-05.1W	21 July 1978 13 September 1978	2cm - 19m, 32m
BC-21A	60-23.4N 169-11.2W	16 September 1977 20 July 1978	1cm - 28m 1 PG - 40m
BC-21B	60-23.9N 169-10.4W	20 July 1978 13 September 1978	2cm - 20m, 32m
FX-1A	58-42.8N 168-09.5W	20 July 1978 20 September 1978	2cm - 16m, 38m
FX-2A	58-52.0N 167-56.5W	19 July 1978 21 September 1978	1cm - 20m 1 PG - 42m
FX-3A	58-47.4N 168-13.1W	20 July 1978 20 September 1978	2cm - 14m, 36m

ANNUAL REPORT

Contract: #03-5-022-56
Research Unit: #289
Task Order: #19
Reporting Period: 4/1/78-3/31/79
Number of Pages: 62

CIRCULATION AND WATER MASSES IN THE GULF OF ALASKA

Thomas C. Royer

Institute of Marine Science
University of Alaska
Fairbanks, Alaska 99701

March 1979

TABLE OF CONTENTS

LIST OF TABLES

LIST OF FIGURES.

I. SUMMARY.

II. INTRODUCTION

III. CURRENT STATE OF KNOWLEDGE

IV. STUDY AREA

V. SERVICES, METHODS, AND RATIONAL OF DATA COLLECTION

VI. RESULTS AND DISCUSSION

 A. Coastal Current Response to Hydrology.

 B. Coastal Currents as defined with Satellite-tracked Drifting Buoys

 C. Analysis of Winds at Middleton Island.

 D. Rotary Spectra Techniques.

 E. Currents at IMS 9 (58°41.1'N, 148°21.6'W) from April 1976 through March 1977.

 F. Prince William Sound Study

 G. Transport Variations in the Alaska Current

 H. Remote Sensing Activities.

 I. Synthesis Report

VII. CONCLUSIONS.

VIII. NEEDS FOR FURTHER STUDIES.

IX. SUMMARY OF FOURTH QUARTER OPERATIONS

 A. Task Objectives.

 B. Field Activities

 C. Results.

 D. Problems Encountered

REFERENCES

APPENDIX I - Abstracts of Papers Submitted or Presented. .

LIST OF TABLES

Table I. Fitted Annual Transports

LIST OF FIGURES

- Figure 1. Comparison of annual precipitation cycles for Gulf of Alaska
- Figure 2. Annual temperature cycle for southcoast Alaska
- Figure 3. Mean monthly fresh water flow rates, southcoast Alaska for two watershed areas 600 km long by 1) 100 km and 2) 150 km wide
- Figure 4. Month to month changes in freshwater influx as calculated from dynamic height changes and predicted from hydrologic models
- Figure 5. Dynamic topography (0-100 db) for April 1976
- Figure 6. Dynamic topography (0-100 db) for September 1976
- Figure 7. Drifter 1174 trajectory, released 6 June 1976.
- Figure 8. Drifter 1203 trajectory, released 26 July 1976
- Figure 9. Cross-section of salinity, ‰, for September 1976 for the Cape Suckling line. Approximate position that drifter intersected the line is indicated.
- Figure 10. Monthly statistics of the MDO longshore wind component over a composite year.
- Figure 11. Vector-averaged monthly mean wind vectors at MDO, EB33 and EB03 (1972 - 1977)
- Figure 12. Vector-averaged monthly mean MDO Ekman transport vectors over a composite year.
- Figure 13. Monthly statistics of onshore Ekman transport over a composite year at MDO according to the present study (A), and at 60° N 146° W according to Bakun (1975) (B).
- Figure 14. Daily mean onshore Ekman transport during 1973 based (a) on observed MDO winds and (b) on indices calculated by Bakun (1975) for 60° N 146° W.
- Figure 15. Reconstructed density at 75 meters (upper panel) and current vectors at 55 m as a stick diagram at IMS 9, April 1976 - March 1977

LIST OF FIGURES

CONTINUED

- Figure 16. Progressive vector diagram for Hinchinbrook
Entrance at 30 m, beginning November 1977.
- Figure 17. Progressive vector diagram for Montague Strait
at 30 m, beginning November 1977
- Figure 18. Composite year Alaska Stream transports with
least squares fitted curves.
- Figure 19. Fitted curves of baroclinic transports for Seward
Line, Composite Year

I. SUMMARY

The understanding and interpretation of the data acquired during the past four years in the Gulf of Alaska has continued in the past year along with the acquisition of data from a few selected sites. The analysis is allowing us to return to our previously acquired data and refine our interpretations. For example, we have concluded that small or mesoscale eddies are frequently located over the outer shelf near the continental slope. Returning to some of our previous hydrographic data, we can see vague patterns that can now be identified as eddies in those sections.

The focus has been on mesoscale driving mechanisms in the past year's research. The mechanisms for driving the shelf circulation, such as wind stress, precipitation, runoff, and offshore circulation have been more clearly identified. This has lead to a detailed treatment of winds at Middleton Island and the hydrology for the southcoast region.

An initial synthesis of the physical oceanography for the Northeast Gulf of Alaska (NEGOA) has been completed. A revision of this preliminary work is in progress. Development of an interdisciplinary synthesis for NEGOA should be the next step in advancing the scientific knowledge of the region.

II. INTRODUCTION

The emphasis of RU #289 this year has been on the analysis of data gathered in previous years under OCSEAP support. Gradual transition has occurred from data gathering to data analysis and interpretation. Limited field work under OCSEAP support has continued with project personnel participating in five cruises and have maintained current meter moorings at two locations throughout the year. The primary purpose of the continuing field effort is to better define the circulation and its driving mechanisms in a few localized regions, such as Prince William Sound.

The progression of ideas on the circulation of the shelf area of the Gulf of Alaska has lead us from an initial concept of generalized cyclonic flow to highly localized flow patterns. We have identified flow regimes and have speculated on their driving mechanisms. We now have the annual cycle in the baroclinic circulation quite well-defined and attention is now being directed to the smaller scale temporal and spatial perturbations. At the same time we are able to adjust our focus and address processes which influence the circulation over the continental shelf of the entire Gulf of Alaska. This latter aspect is important to identify the similarities between the local shelf circulation over the Alaskan coastline. For example, what common driving mechanisms occur in the NEGOA and Kodiak lease areas?

III. CURRENT STATE OF KNOWLEDGE

Since the inception of the OCSEAP-NEGOA program, the knowledge of the physical oceanography, in particular circulation and water masses, has evolved from the point where the annual cycle was marginally described to where we now understand some of the physical mechanisms which control the annual cycle. This progress follows the traditional scientific method where initial observations lead to the development of hypothesis after which these hypotheses must be tested. After these tests, the hypothesis will probably be modified and retested until a satisfactory refinement is attained. The work of this research unit hovers somewhere between the development and initial testing of hypothesis. The practical implications of this evolution are obvious in the case of OCSEAP: we will be better able to predict the shelf circulation and hence the possible trajectories that oil spills would follow. The improved understanding of the physical mechanisms which control the circulation allow predictions to be made from our observational periods. Therefore, from measureable or easily predicted parameters, such as the meteorological parameters, we can imply the response of those parameters which are more difficult to measure in real time, such as currents.

The development of hypothesis must come from the individual principal investigators. Incorporation of these hypotheses into an improved understanding of the physical oceanography of the region must be carried out jointly in some type of synthesis. In order not to invert the thought process, a scientific synthesis should be carried out prior to a more practical or pragmatic synthesis. (Details of these recommendations can be found in Section VII, Needs for Further Studies.)

IV. STUDY AREA

Field work under this research unit has ranged over the continental shelf of the southern Alaska coastline from Yakutat to Unimak Pass from the coastline to tens of kilometers beyond the shelf break. The satellite data archived for OSCEAP by this unit covers the entire Alaskan coastline from the Beaufort Sea to Southeast. The analysis portion of the past years work has been addressing the entire Gulf of Alaska region, whereas field work in the past year has been limited to that portion from Prince William Sound to Kodiak Island. The study area represents a combination of the NEGOA and Kodiak lease areas. This is because the two regions are connected through the shelf circulation along with the larger scale circulation of the region.

V. SERVICES, METHODS AND RATIONALE OF DATA COLLECTION

As in previous years, the primary data collection method used by this research unit is the CTD/STD (salinity - temperature - depth) profile. Some current meter and bottom pressure gauge deployments have also been undertaken to supplement the hydrographic data. From the CTD/STD data, contour maps of salinity, temperature, density and dynamic height are constructed. These contours provide information on the direction and intensity of the flow. The current meter measurements provide a means of "calibrating" the currents obtained from the density fields. The sea level as measured at the coastline by NOS (National Ocean Survey) stations is used in conjunction with the bottom pressure data to determine changes in the slope of sea level between the two positions and hence a measure of current changes.

The CTD/STD station positions are determined by 1) a knowledge of the spatial scales of the features to be measured and 2) requirements to continue a time history of oceanographic parameters at a particular location. The objective of both of these criteria is an improved understanding of changes in the parameters, spatially and temporally.

VI. RESULTS AND DISCUSSION

A. COASTAL CURRENT RESPONSE TO HYDROLOGY

The hypothesis boldly expressed in last year's annual report, has been revealed by a journal reviewer as not being entirely correct. That hypothesis stated that the coastal currents in the Gulf of Alaska respond seasonally to precipitation and wind stress. While the conclusions are correct, the actual mechanisms are not as simple as was originally believed. Indeed, wind stress does have a significant influence on the coastal circulation through the convergence and divergence of low density surface water at the coast. Precipitation influxes fresh water into the coastal system, but the amount of change in dynamic height at the coast cannot be accounted for by precipitation. Precipitation adds, at most, two to three meters of water over a twelve month period. The changes observed in the coastal area require about five meters of fresh water to enter within a brief period of time, on the order of one month.

A simple hydrology model was developed to account for this difference in the amount of fresh water entering the system. The model begins with the annual cycle in precipitation over southcoast Alaska as available from the National Weather Service (Fig. 1). The precipitation in winter is snow and thus does not generally contribute to the coastal fresh water except where

Mean Monthly Precipitation
Coastal Alaska, Northeast
Pacific, 1970-1976

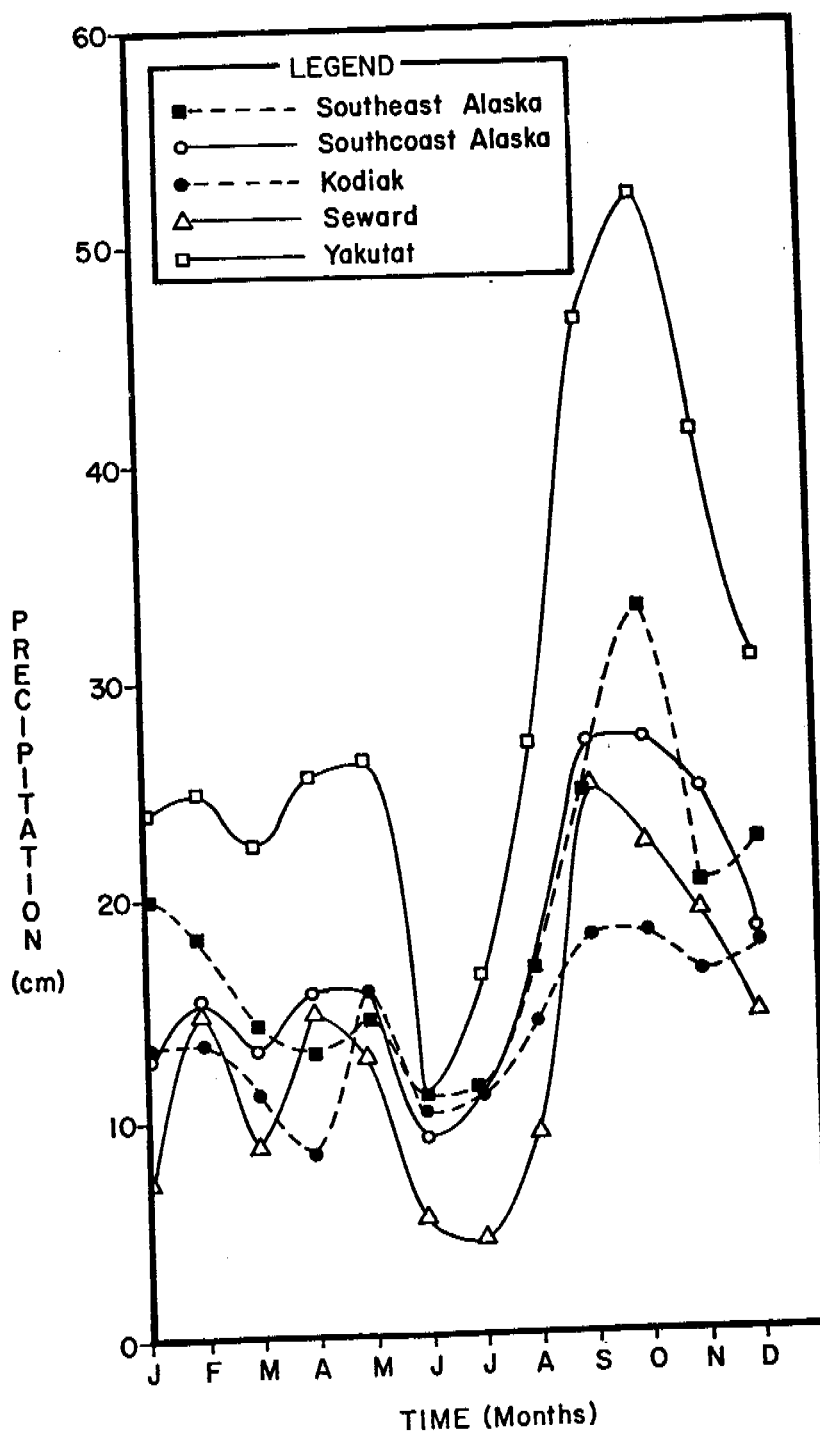


Figure 1. Comparison of annual precipitation cycles for Gulf of Alaska.

the snow falls directly on the water. The air temperature for southcoast Alaska must be used to determine the form of precipitation (Fig. 2). Assuming freezing temperatures from mid-October to mid-April, 50% of the precipitation is in the form of rain in those months. During the remainder of the year, all precipitation is assumed to be rain. The snow is assumed to be released in a linear manner, patterned after the flow in the Resurrection River near Seward (Fig. 3). The contribution of fresh water from the Copper River is estimated from historical flow measurements. This flow differs from that of the Resurrection River because the Copper River drains interior rather than coastal regions. The Copper River flow is therefore more in phase with the annual temperature cycle and not as dependent on the fall coastal precipitation. Two sizes of watershed areas were used, both 600 km long with one 100 km wide and the other 150 km wide. The runoff from the watershed is assumed to be limited to a 10 km wide band (based on hydrographic section data). The contribution of this fresh water influx to the observed month to month changes in dynamic height reveals excellent agreement from about April through September (Fig. 4). In winter, the fresh water discharge decreases to very small values and the wind stress becomes increasingly important causing coastal convergences. Thus, the hydrological cycle predicts a rapid drop in dynamic height in the fall, but the greater wind stress in winter forces lower density water to the coast, keeping the dynamic height high. This relatively high dynamic height might also be due to the advection of fresh water from southern Alaska.

B. COASTAL CURRENTS AS DEFINED WITH SATELLITE-TRACKED DRIFTING BUOYS

In a joint effort with Don Hansen at AOML, analysis of the coastal hydrography and drifting buoys was carried out in the past year. The

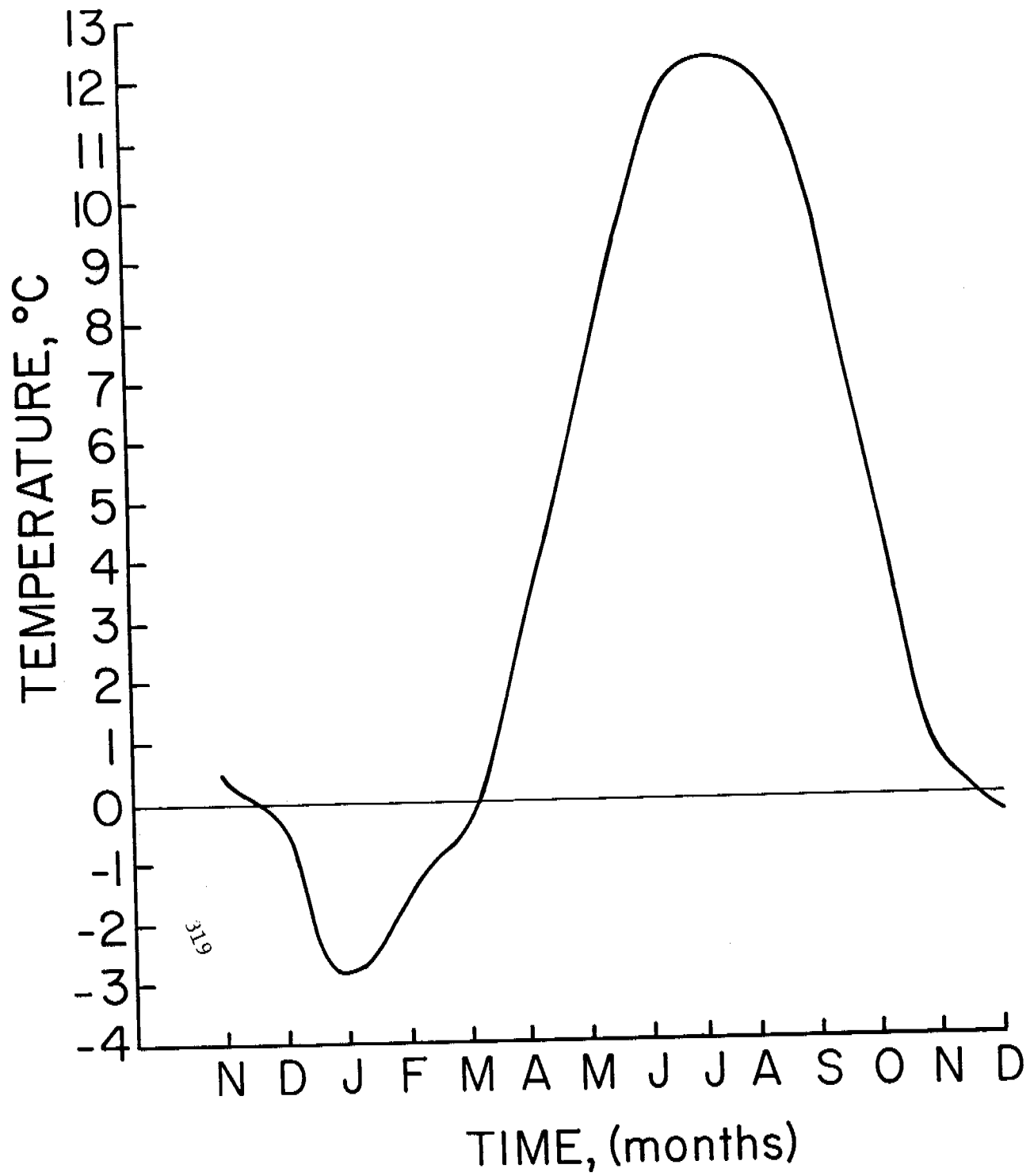


Figure 2. Annual temperature cycle for southcoast Alaska.

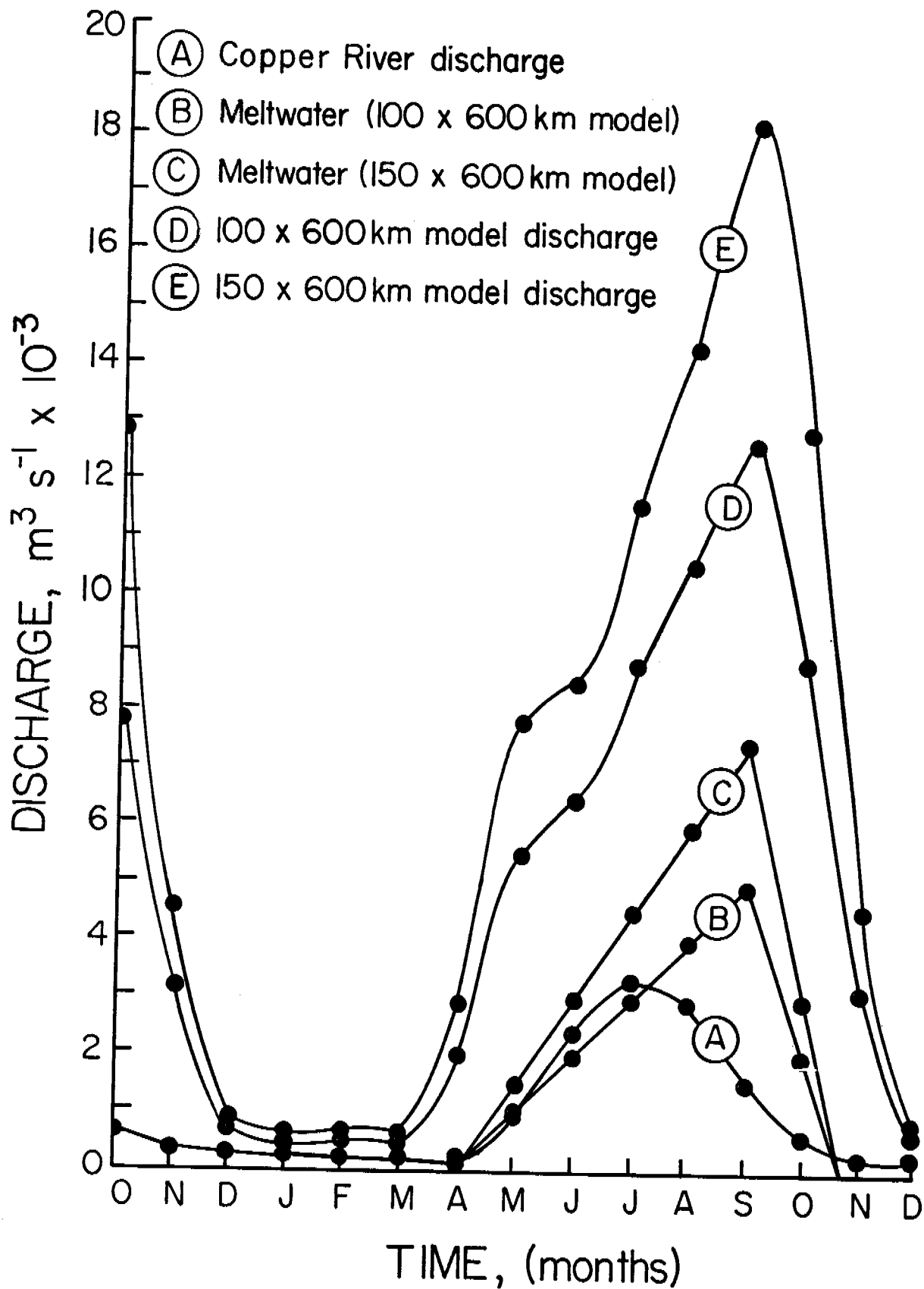


Figure 3. Mean monthly fresh water flow rates, southcoast Alaska for two watershed areas 600 km long by 1) 100 km and 2) 150 km wide.

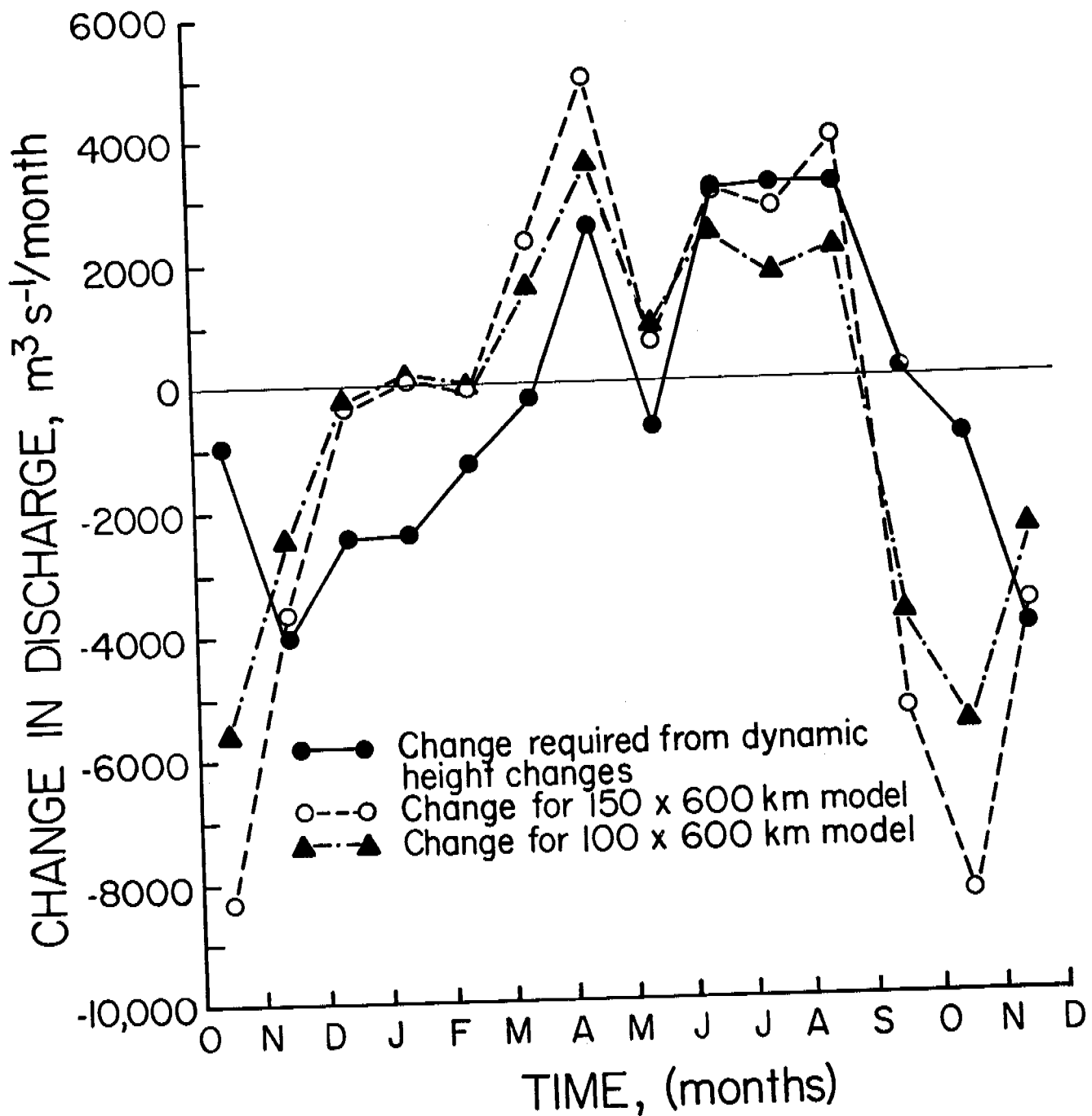


Figure 4. Month to month changes in freshwater influx as calculated from dynamic height changes and predicted from hydrologic models.

drifting buoys were released in the northeastern Gulf of Alaska during September 1975 and May, June and July 1976. Hydrographic surveys of the area were made in April 1976 before most of the buoys were released and in September after the drifters had grounded. (No drifters exited the NEGOA region).

The dynamic topography for the upper 100 meters for April 1976 (Fig. 5) illustrates a general cyclonic flow in the offshelf region. Several meanders or eddies are evident in the region near to the shelf break. The first meander (progressing from southeast to northwest) is also present in the deeper dynamic topography (300-1000 db). In September 1976 (Fig. 6), the offshelf eddy is no longer present in the upper layers but remains in the deeper regions. Note that the permanent eddy located to the west of Kayak Island has intensified in September in comparison with April.

The trajectory of drifter 1174, released 6 June 1976 shows a similar pattern to that represented by the dynamic topography for the first week to ten days (Fig. 7). Afterward it seems to retain a shoreward component that is not present in the dynamic topography. Upon approaching to within 10 km of shore, the northward or shoreward motion ceases and the drifter moves parallel to the coast until west of Kayak Island. At that point it becomes involved with "permanent" eddy until it ejected on the shoreward side and continues toward Prince William Sound. It ran aground on Montague Island a short time later. The trajectories of the drifters released in July 1976 (Fig. 8) were quite similar in most aspects to the trajectories of the earlier drifters except all (three) of those released later entered Prince William Sound before then ran aground.

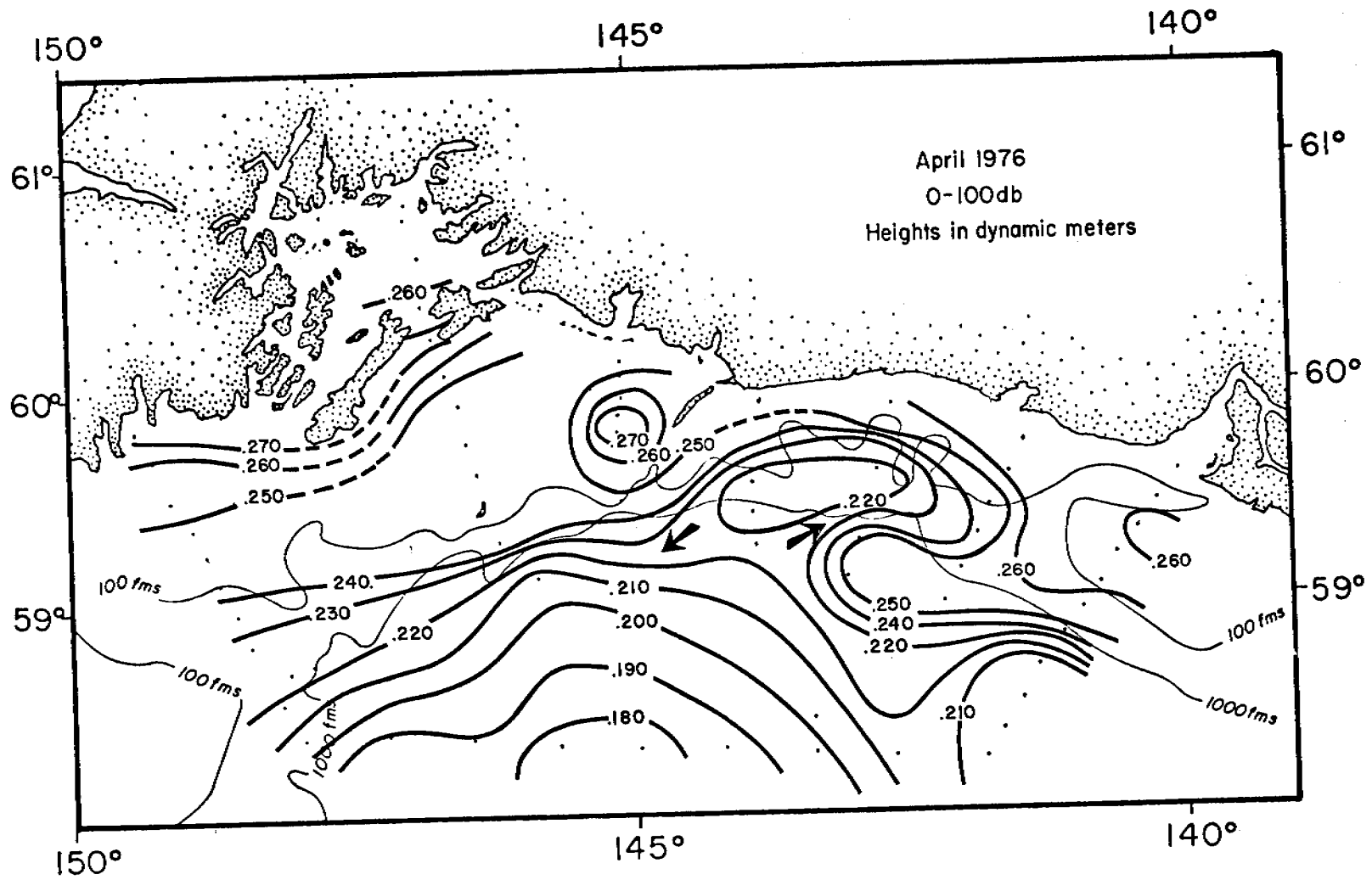


Figure 5. Dynamic topography (0-100 db) for April 1976.

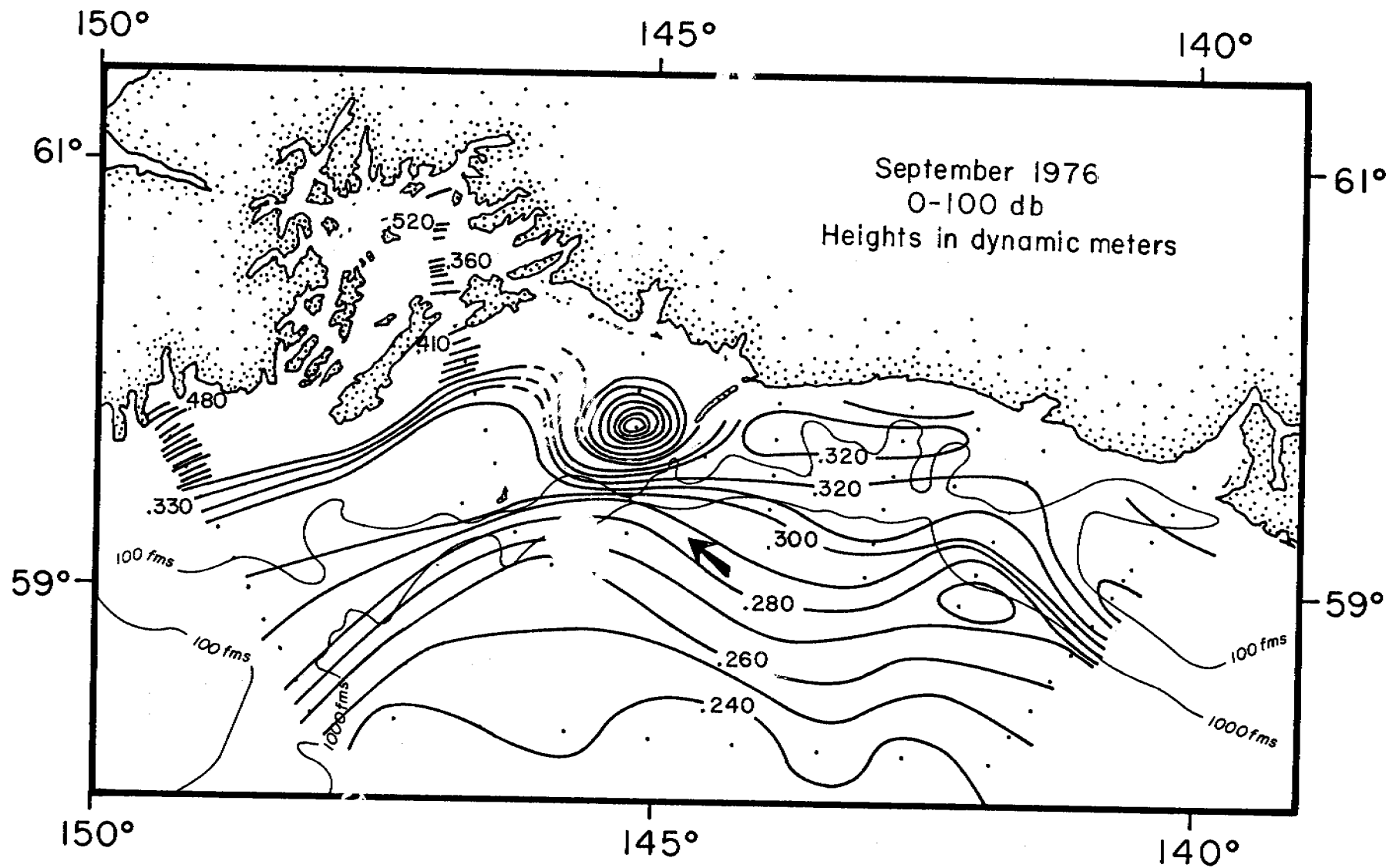


Figure 6. Dynamic topography (0-100 db) for September 1976.

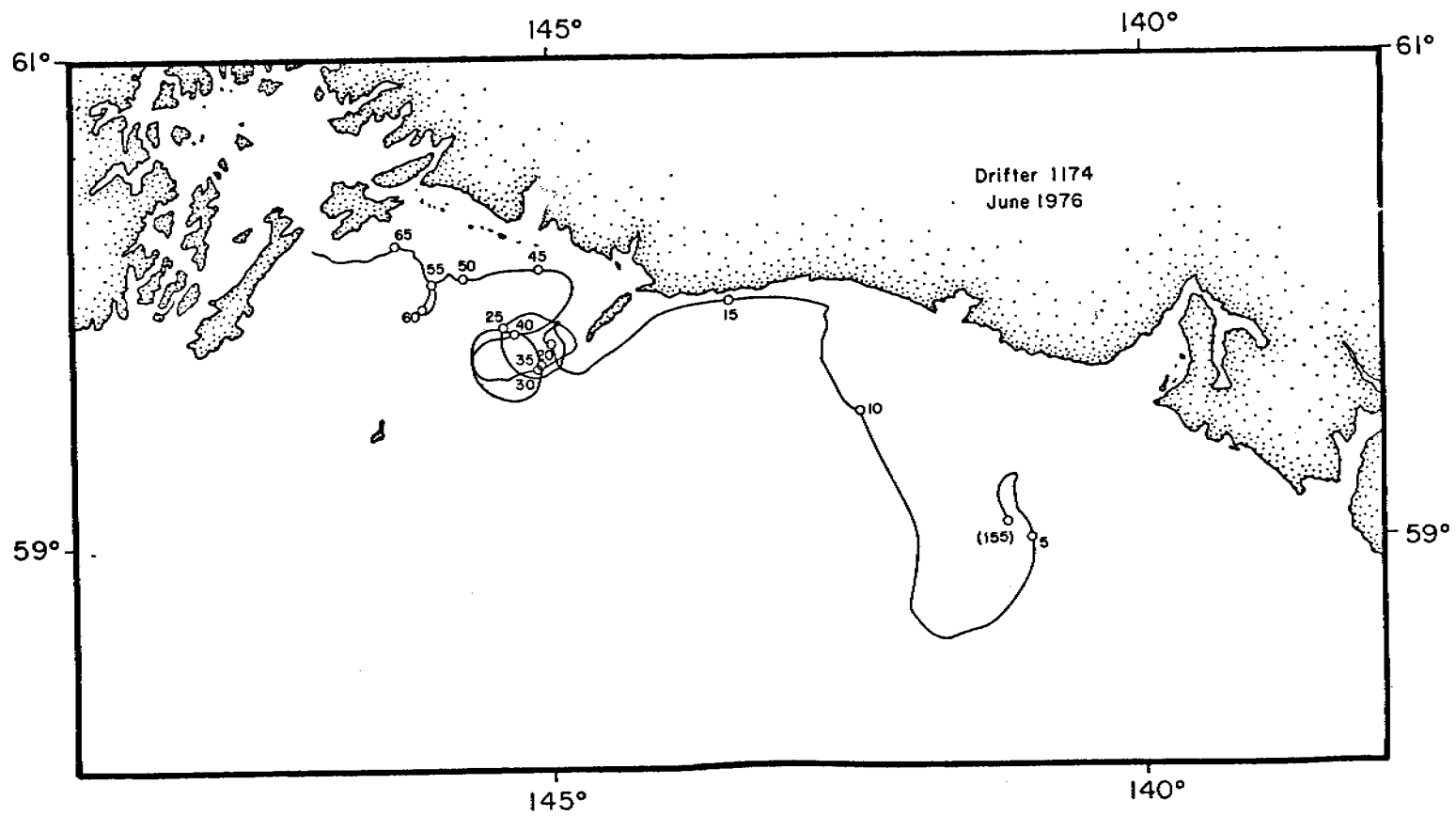


Figure 7. Drifter 1174 trajectory, released 6 June 1976.

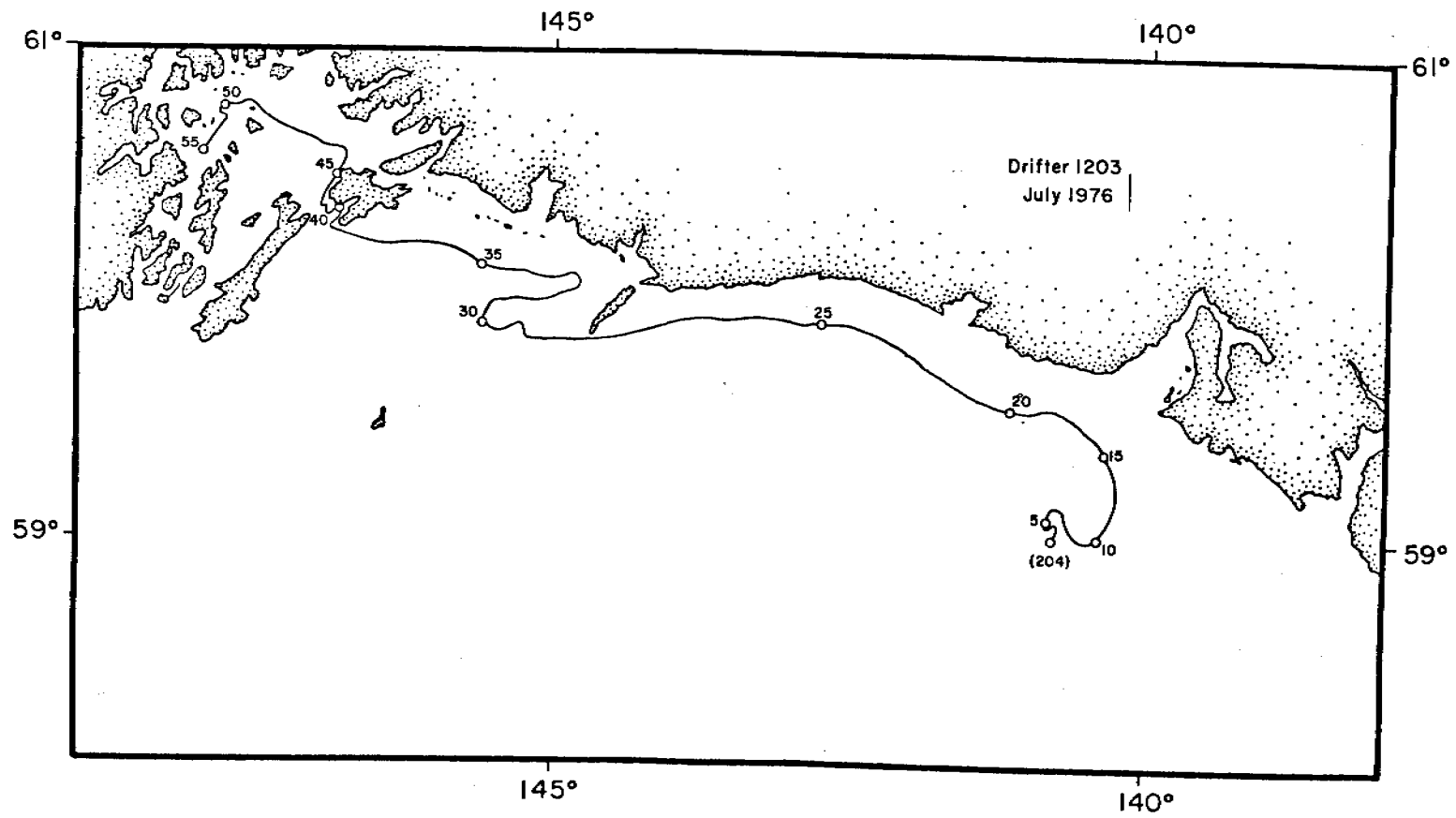


Figure 8. Drifter 1203 trajectory, released 26 July 1976.

A hypothesis was developed to explain the drifter's behavior. Assuming that a large amount of fresh water enters the system from the coastal rains and runoff, especially in fall, this fresh water will move along and offshore. As it moves offshore, frictional coupling between the upper and lower layers will cause some water from the lower layer to be carried offshore, too. This water from the lower layer must be replaced. This is accomplished by an onshore flow in the lower layer.

It is assumed that initially the drifters, which were drogued at about 35 m, had their drogues in the lower layers. Thus they progressed shoreward. They continued to move shoreward until they entered the fresh, offshore moving upper layer. As can be seen in the upward, offshore slope in the isohalines (and isopycnals), the fresh water layer is deepest at the coast (Fig. 9). As the drogue encounters the upper layer it begins to move offshore where it enters the onshore moving lower layer. In this manner the drogue stabilizes on that surface where there is no motion on or offshore. After that point, the drogue will only move parallel to the coast until the interface is destroyed, it encounters the bottom, or other forces on the drifter remove it from the interface. Given the above hypothesis, it can be concluded that the drifters followed an interface from east of Kayak Island into Prince William Sound.

C. ANALYSIS OF WINDS AT MIDDLETON ISLAND

A statistical study of the wind observations at Middleton Island has been completed. These observations are important to the OCSEAP-NEGOA work because they are the only long term marine weather observations available in the NEG OA region. Other reporting stations in the region, such as Cordova or Yakutat are located in sheltered areas and are not truly marine

Salinity, Cape Suckling Line September 1976

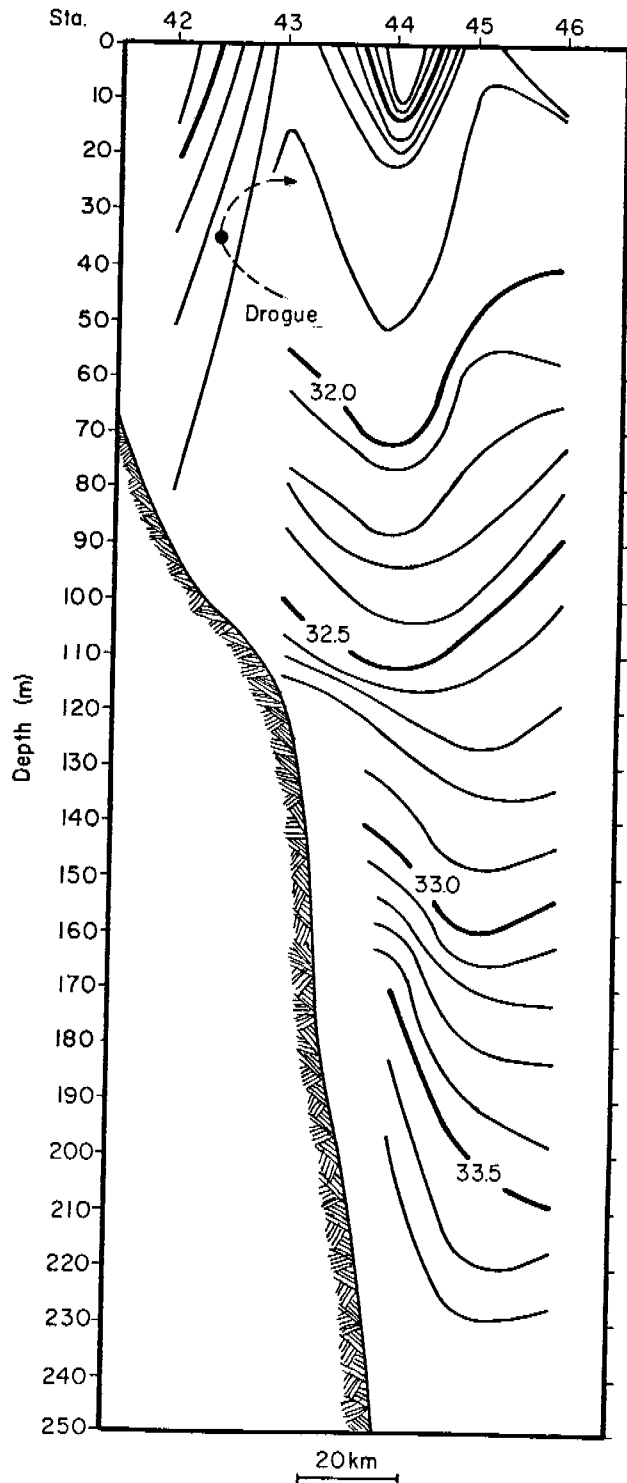


Figure 9. Cross-section of salinity, ‰, for September 1976 for the Cape Suckling line. Approximate position that drifter intersected the line is indicated.

observations. We do have buoy observations offshore, but these have been installed recently and do not have a long record. However, in this study some comparisons are made between the observations at Middleton Island and at the buoys. The wind data at Middleton Island covered the period from May 1972 to January 1977.

Over the period of the observations, the longshore component of the wind vector of the composite year is always westward. That is, on a monthly average, there is always a westward wind (Fig. 10). With the exception of January, there is always an onshore component, too. However, this does not mean that there cannot exist occasional months with eastward winds (averaged over the month) as can be seen in Figure 11. This same figure illustrates the similarity between Middleton Island winds (MDO) and those from buoys; EB33, near Yakutat and EB03, near Kodiak. While MDO and EB33 are quite similar, EB03 shows much more variability in the wind direction. The difference is because EB03 is located at a position where the low pressure systems pass over it, in contrast to positions in the northern Gulf of Alaska where only the upper limbs of these storms are generally seen as they stagnate and fill. The storms are stalled here by the coastal mountains and therefore do not pass over these stations.

The observed winds have application to the shelf circulation through the Ekman transport (Fig. 12). On the average, there is an onshore transport throughout the year; it is also slightly eastward. There is approximately an order of magnitude difference between the summer and winter onshore transports. It is important to note that the Ekman transport is onshore throughout the year. There is no period of offshore transport, which is necessary for upwelling. This does not agree with the results of Bakun (1975). His estimates of the Ekman transport are based on geostrophic

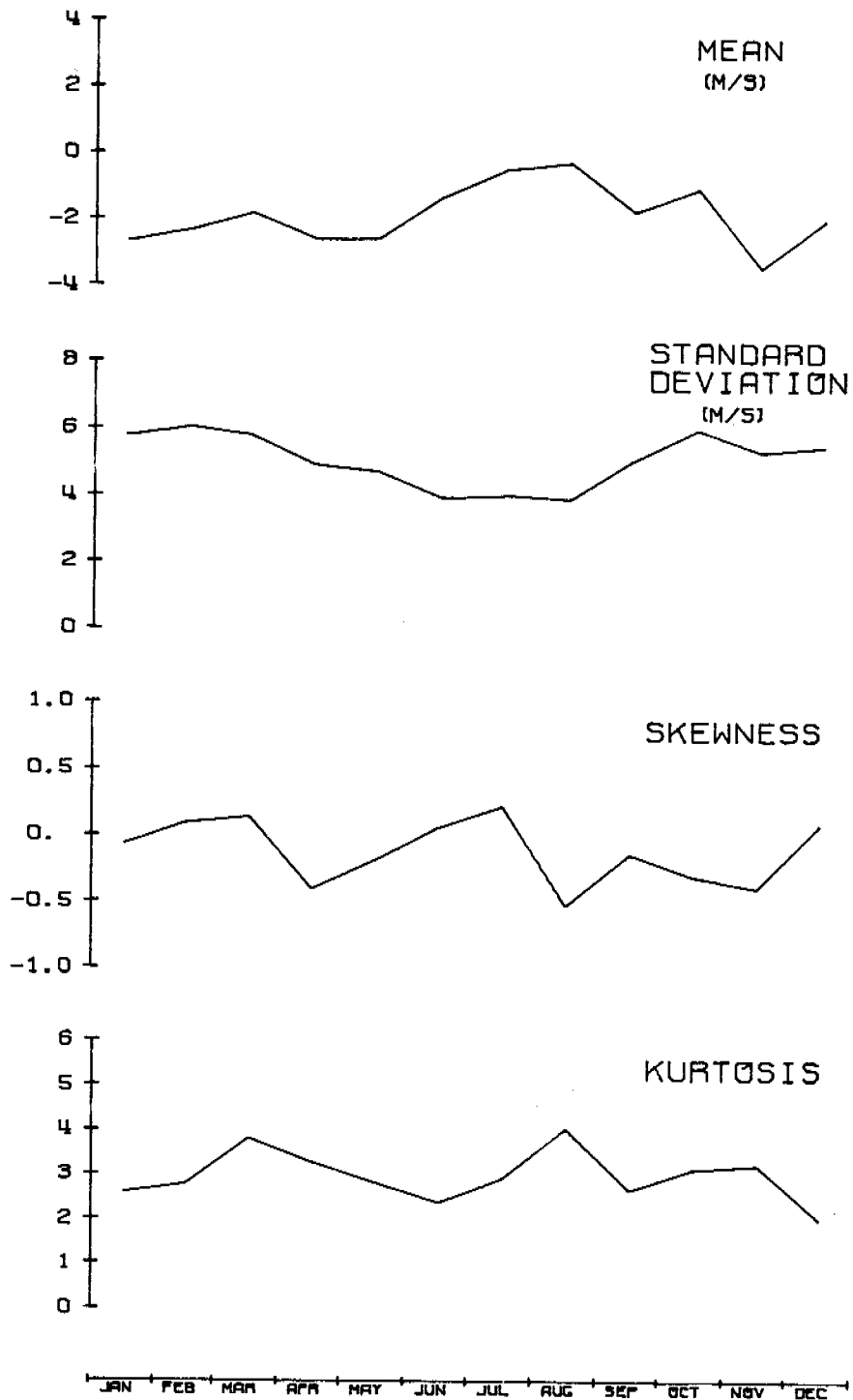


Figure 10. Monthly statistics of the MDO longshore wind component over a composite year.

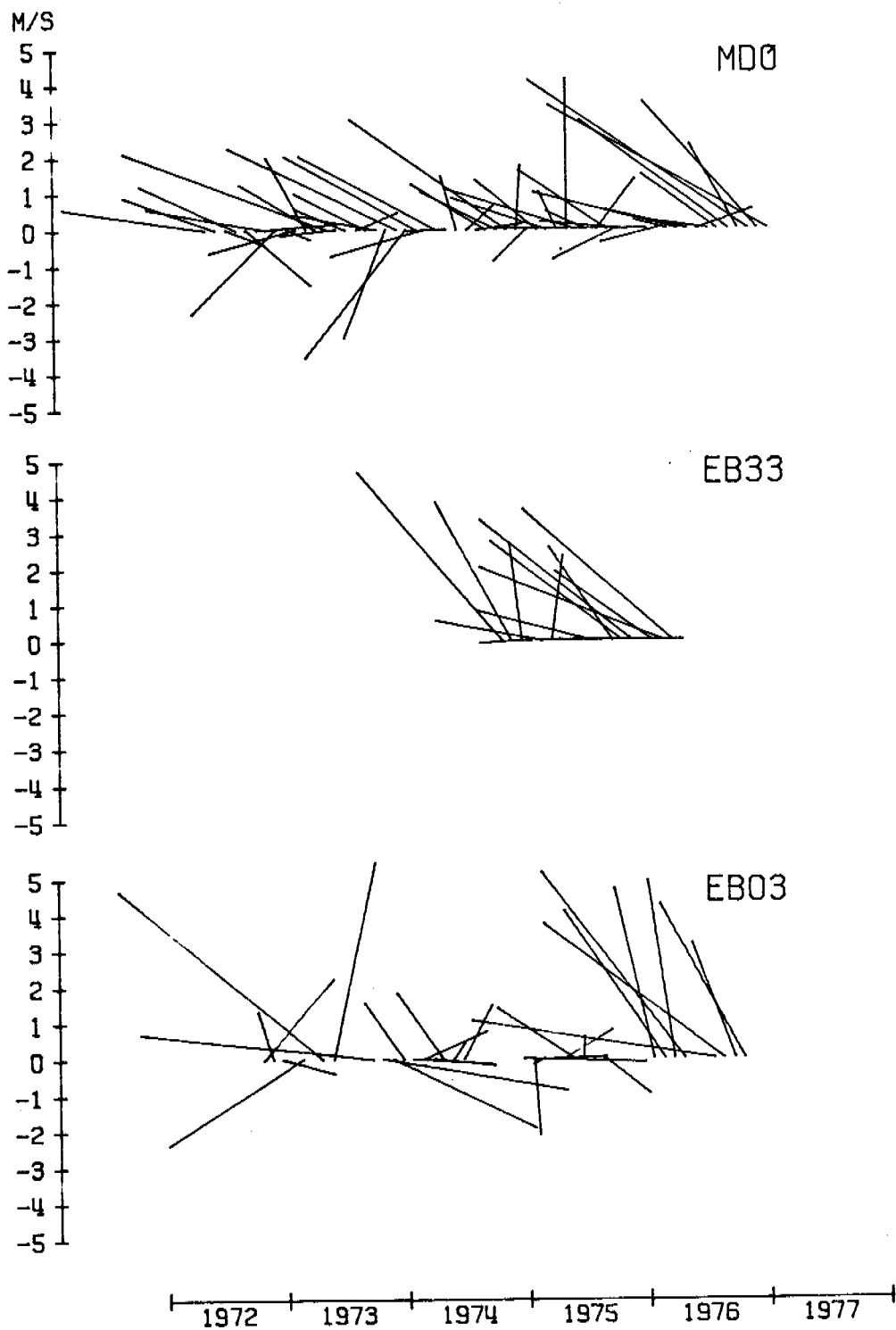


Figure 11. Vector-averaged monthly mean wind vectors at MDO, EB33 and EB03 (1972 - 1977).

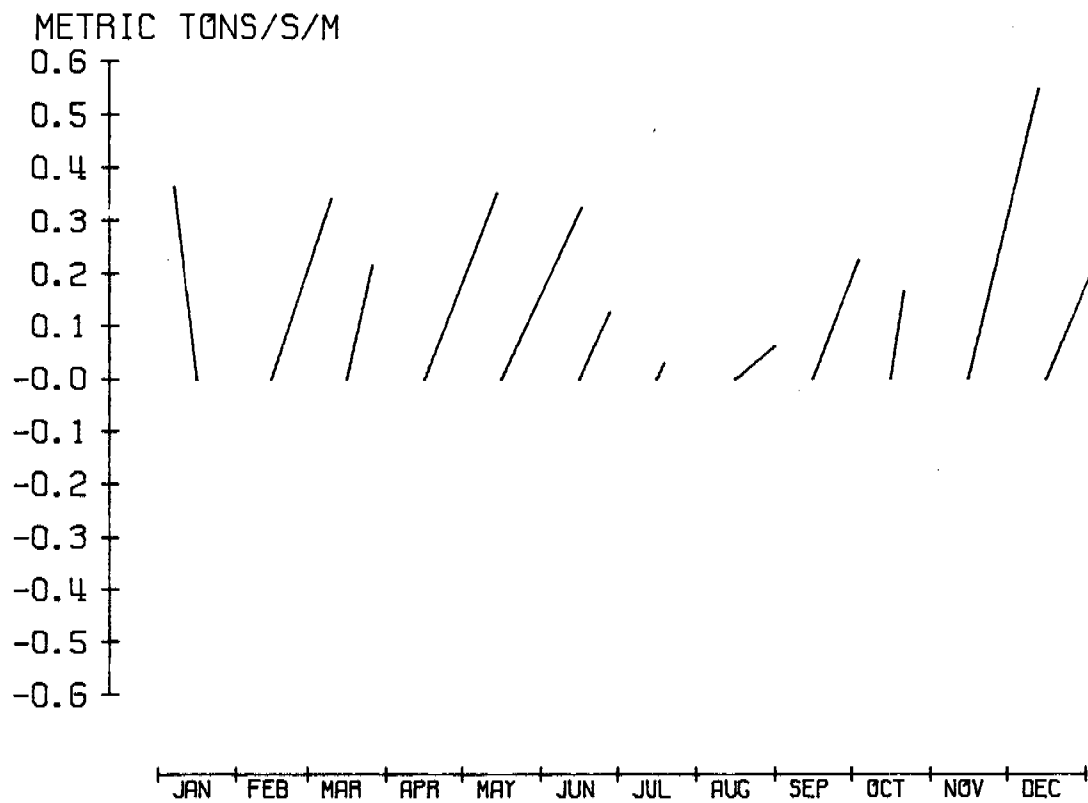


Figure 12. Vector-averaged monthly mean MDO Ekman transport vectors over a composite year.

winds determined from a large scale ($3^{\circ} \times 3^{\circ}$) sea level atmospheric pressure grid. As can be observed in Figure 13, Bakun tends to overestimate the onshore transport in winter and underestimate it in summer. Bakun also tends to overestimate extreme events and not predict short term transport reversals that are often found within a month. The daily mean Ekman transports for 1973 for the two data sets show a vague agreement, but serious differences (Fig. 14). The autocorrelation functions for the two sets show that the autocorrelation for the actual observations drop off much more rapidly than does the function for Bakun's data. This implies that short period, perhaps local, transport reversals are not well represented by Bakun (Fig. 14). These short term events are important. The autocorrelation function for MDO falls approximately to zero after about two weeks, indicating that the dominant event time scale must lie between one day and about two weeks. There is no evidence of any persistence on the seasonal time scale, as there is in the case of Bakun indices. The observed annual cycle in sea level at Seward of 17.4 cm, conforms with the MDO winds rather than those of Bakun. The conclusion is that the direct role of wind stress in the Gulf of Alaska on the baroclinic and barotropic circulation has been overemphasized.

D. ROTARY SPECTRA TECHNIQUES

In the analysis of winds at Middleton Island, rotary spectra were determined for the wind observations. Rotary spectra gives a measure of the rotation of the wind vector; both its sense and rate of rotation. It was determined that some of the intermediate products (the inner and outer rotary cross-spectra) can be used to characterize the movement of rotating systems past the observation point. For instance, the speed and direction

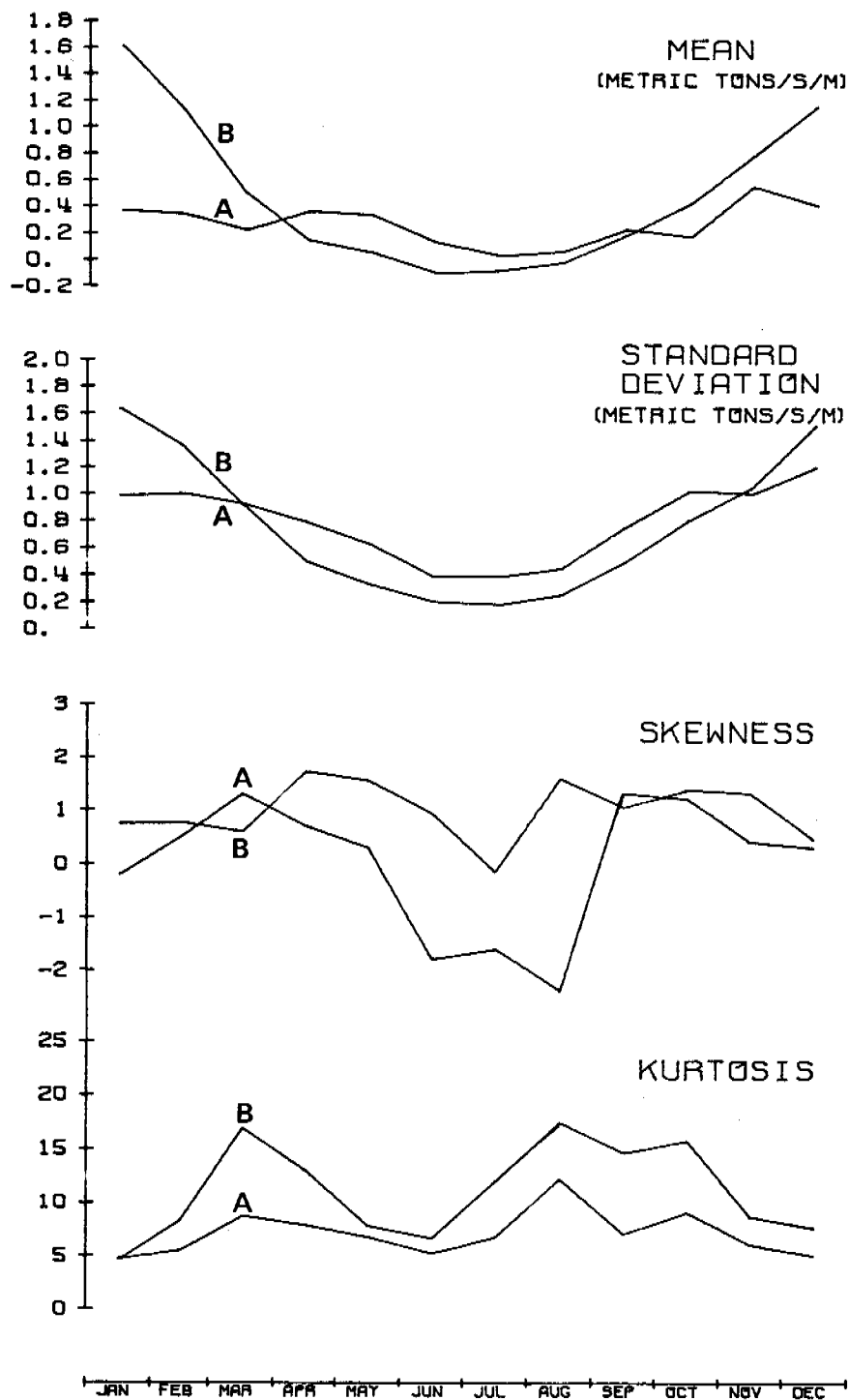


Figure 13. Monthly statistics of onshore Ekman transport over a composite year at MDO according to the present study (A), and at 60° N 146° W according to Bakun (1975) (B).

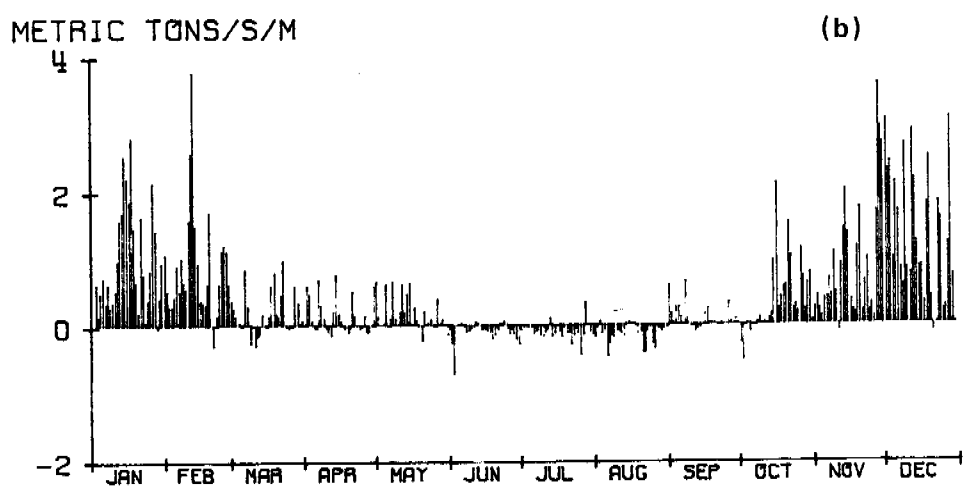
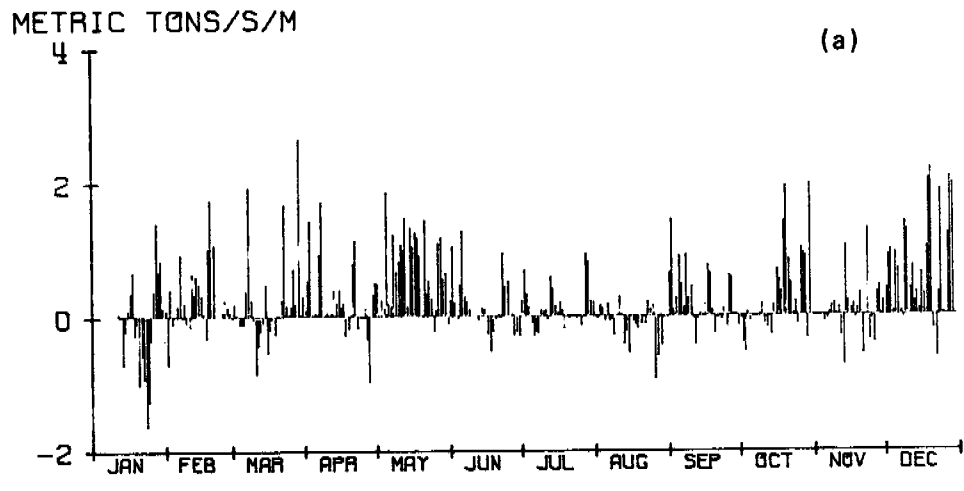


Figure 14. Daily mean onshore Ekman transport during 1973 based (a) on observed MDO winds and (b) on indices calculated by Bakun (1975) for 60° N 146° W.

of the mean eddy path between two stations can be determined along with a qualitative measure of the deviations of the rotating system from this path.

This technique was applied to atmospheric storm systems between Middleton Island, Yakutat and Kodiak. Its correctness was verified through the use of synoptic pressure maps. However, the technique probably has little application to meteorological parameters, since these synoptic pressure maps are readily available. In oceanography, such a network of reporting stations is not available, nor do they appear to be in the near future. Therefore, the greatest application of this technique should be in oceanography. For example, the characteristics of propagation of an eddy past two current meter arrays separated in space can be determined. The use of three current meter arrays would even give a more accurate picture.

E. CURRENTS AT IMS 9 ($58^{\circ}41.1'N$, $148^{\circ}21.6'W$) FROM APRIL 1976 THROUGH MARCH 1977

Analysis of current meter measurements at IMS Station 9 and the hydrographic section running out of Seward has continued this past year. The stick diagram for the 55 m depth is shown in Figure 15. There is a general southwestward flow (nearly parallel to the local isobath) throughout the year with irregular reversals superimposed on this flow. The reversals predominate from July through September. The lower panel of Figure 15 is the density at 75 m for the same mooring. A long period density decrease is evident from the time of the mooring installation until November, when it increases for a short period. A large, rapid density decrease takes place in mid-December. The hydrographic sections

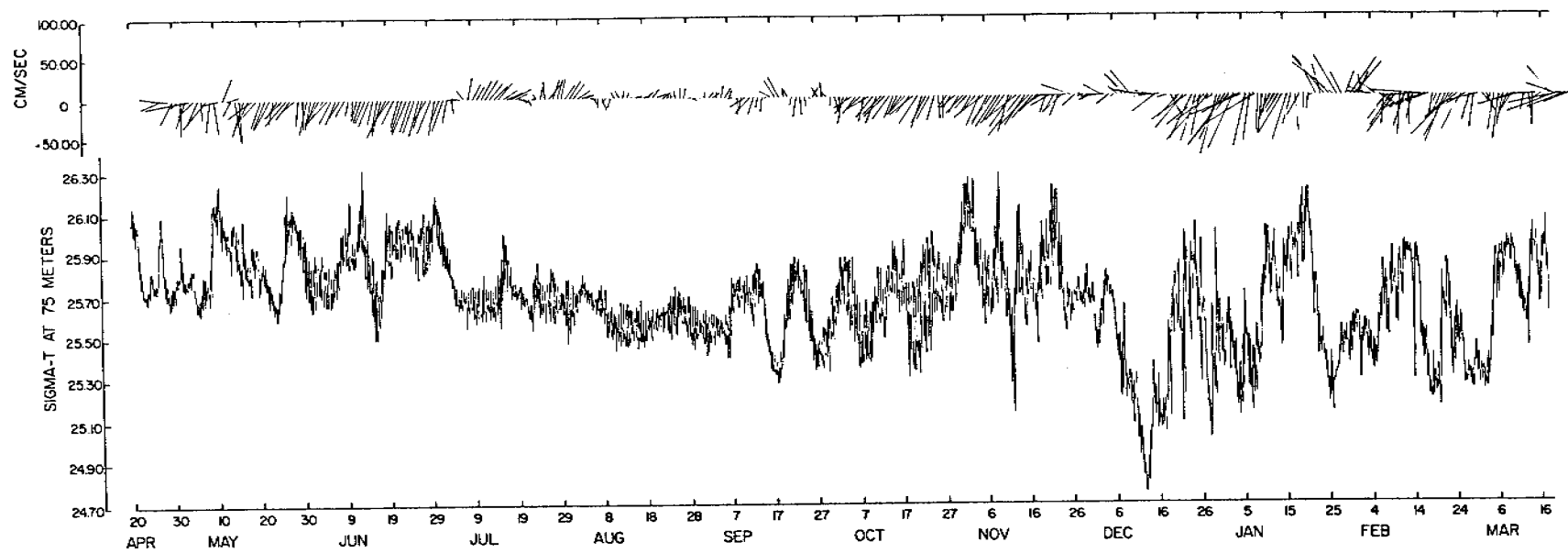


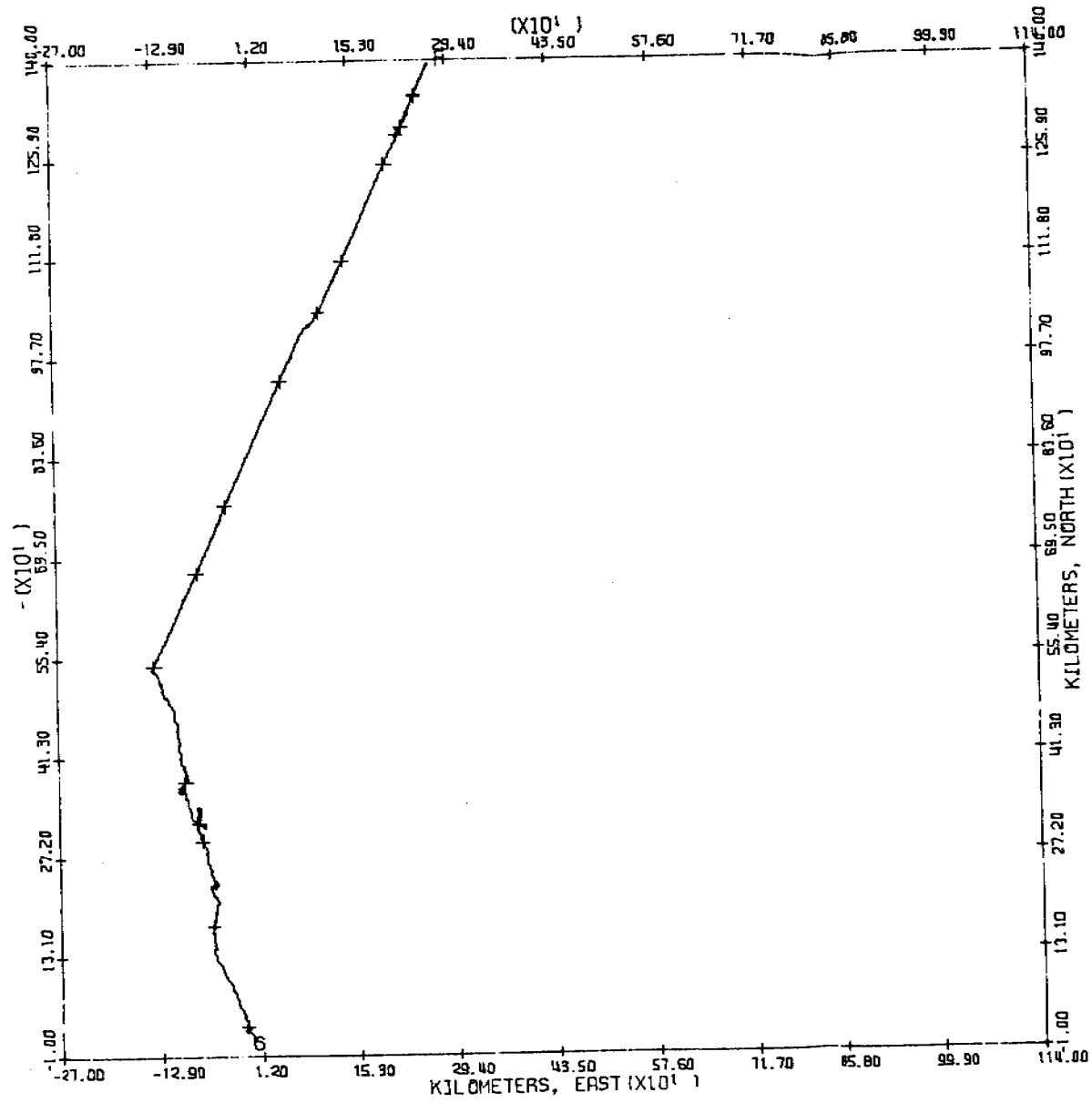
Figure 15. Reconstructed density at 75 meters (lower panel) and current vectors at 55 m as a stick diagram at IMS 9, April 1976 - March 1977.

taken while the mooring was in place, indicate that the area is infested with eddies. The reversals apparently are associated with the propagation of eddies across the section line and through the array. These eddies or rings are moving against the mean westward flow. The high frequency of eddies in summer could be a result of the repositioning of the Alaska Current over the continental shelf break at that time of year. A detailed analysis of these data is in progress with a paper expected in a short period of time. (It is important to note that although it was attempted to place this current meter array within the Alaska Current it was apparently are shoreward of it. It is not known if accelerations observed are due to changes in intensity of the flow or changes in the position of the flow.)

F. PRINCE WILLIAM SOUND STUDY

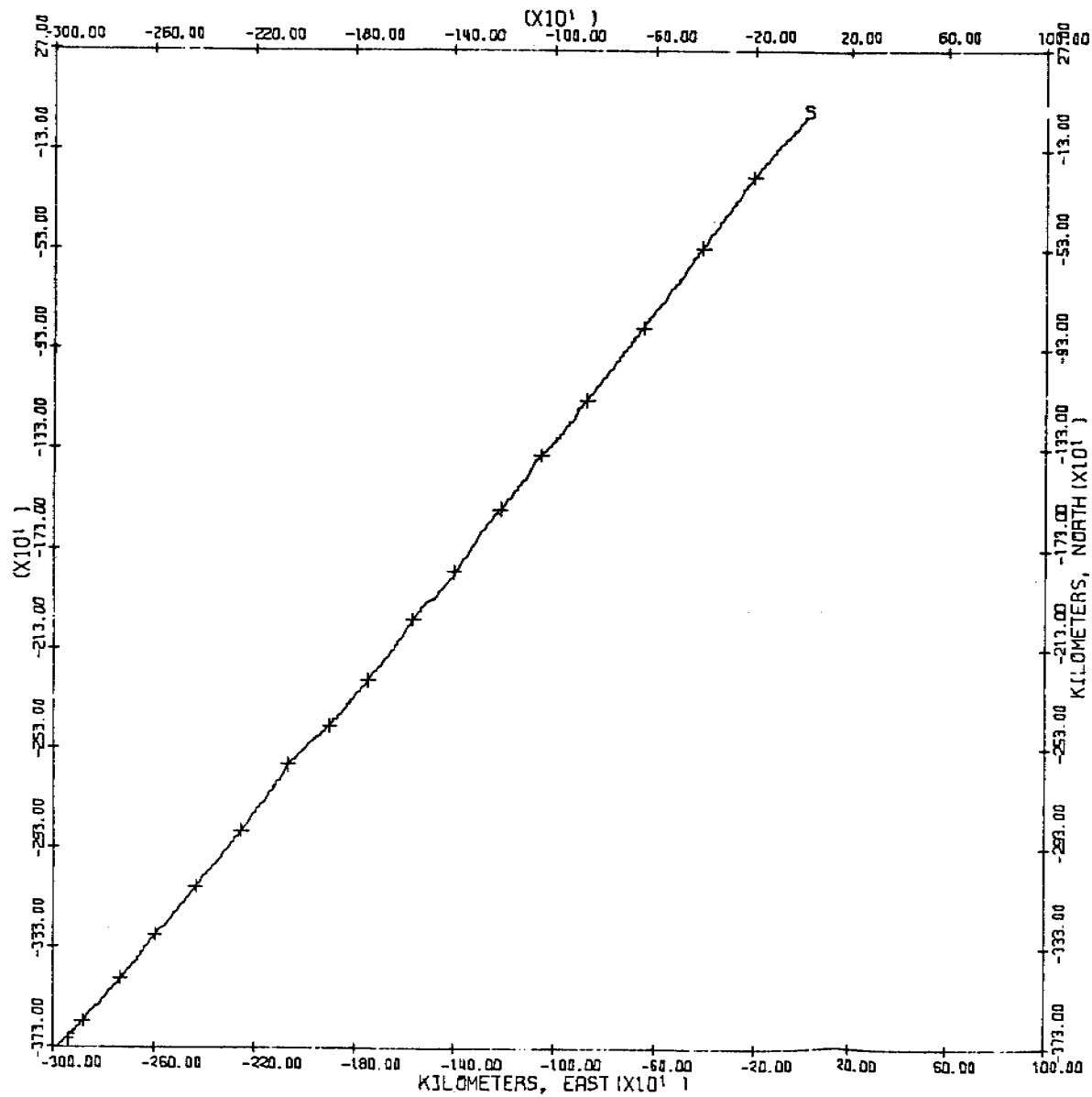
With evidence from the drifter studies that coastal flow might be into Prince William Sound, an effort to better define the flow into and out of the sound was started. This began with a hydrographic survey of the sound and installation of current meters at Hinchinbrook Entrance and Montague Strait in November 1977. Current meter arrays have been maintained in these positions until the present time.

A progressive vector diagram from the Hinchinbrook mooring (HEA) (Fig. 16) show an inward flow at 30 m beginning in November 1977 for about 140 days. (Hinchinbrook Entrance is therefore a more appropriate term than Exit.) In a similar fashion, the progressive vector diagram for Montague Strait (MSA) (Fig. 17) shows a general outward flow for the same time period. These results are in accord with the drifter results. The hydrographic surveys indicate a general cyclonic, baroclinic flow



HEA
 30 M
 FIRST RECORD AT 2017 UT 15 NOV 77
 10 DAYS BETWEEN TJC MARKS

Figure 16. Progressive vector diagram for Hinchinbrook Entrance at 30 m, beginning November 1977.



MSA
 30 M
 FIRST RECORD AT 230 UT 12 NOV 77
 10 DAYS BETWEEN TIC MARKS

Figure 17. Progressive vector diagram for Montague Strait at 30 m, beginning November 1977.

within Prince William Sound. Current meter data available for Valdez Harbor (Courtesy of J. Colonell working under support of Alyeska Pipeline Company) indicate that unusual current events occur almost simultaneously over Prince William Sound. This points to some sort of large scale forcing, probably atmospheric.

Data gathering, reduction and analysis are continuing on Prince William Sound to determine the seasonal fluctuations in the circulation there. At this time it appears that the most appropriate classification of the sound is as an enclosed sea.

G. TRANSPORT VARIATIONS IN THE ALASKA CURRENT

The Alaska Current acts as the offshore boundary of the study region, and its fluctuations are important to any investigation of shelf circulation in the Gulf of Alaska. We now have approximately the same number of transects off the shelf in the central Gulf of Alaska as we do for the shelf area. However, because the Alaska Current can change its position, unlike the coastal jet, the estimates of its transport have a considerable amount of scatter in them. Also, the major axis of the flow is not necessarily in the same direction at all times unlike the coastal flow and the section might not be orthogonal to the current. Accepting these shortcomings, an attempt has been made to estimate the annual cycle in the Alaska Current and over the shelf at Seward.

Prior tabulation of the Alaska Current has been done by Favorite, Dodimead and Nasu (1976). These data are to be compared with the OCSEAP data which have been gathered in a quasi-seasonal manner since 1974. Because the techniques used in obtaining this latter data set are more consistent, its noise level or sampling errors should be less. Favorite,

Dodimead and Nasu (1976) have 24 transport estimates while there are 19 estimates from the OCSEAP data.

A sinusoidal curve was fit to each set of transport estimates by a least squares method. The period of the sinusoidal curve was one year. Its phase and amplitude are determined from the data.

TABLE I
Fitted Annual Transports

Source	Mean $\times 10^6 \text{ m}^3 \text{ s}^{-1}$	Annual Amplitude $\times 10^6 \text{ m}^3 \text{ s}^{-1}$	Month of Maximum	Month of Minimum	Error $\times 10^6 \text{ m}^3 \text{ s}^{-1}$
Favorite, Dodimead, and Nasu(1976)	9.3	1.2	2	8	1.8
OCSEAP	9.6	1.4	6	12	.8
Combined	9.5	1.4	3	9	1.4

The means of the two data sets are quite similar (Table I). (It should be also noted that the Favorite data covers 1965-1970 whereas the OCSEAP is from 1974-1977). The overall mean of $9.5 \times 10^6 \text{ m}^3 \text{ s}^{-1}$ is somewhat higher than prior estimates. The amplitude of the annual cycle in the transport is $1.2 - 1.4 \times 10^6 \text{ m}^3 \text{ s}^{-1}$, fairly consistent for both data sets. Where the two sets differ, however, is on their estimates of the time of the maximum transport. The OCSEAP data indicate a maximum in June, whereas the other data have a maximum in February. Both estimates differ considerably from the previously assumed transport maximum in December-January (Fig. 18). If the transport variation is considered a response to wind stress changes, the maximum in

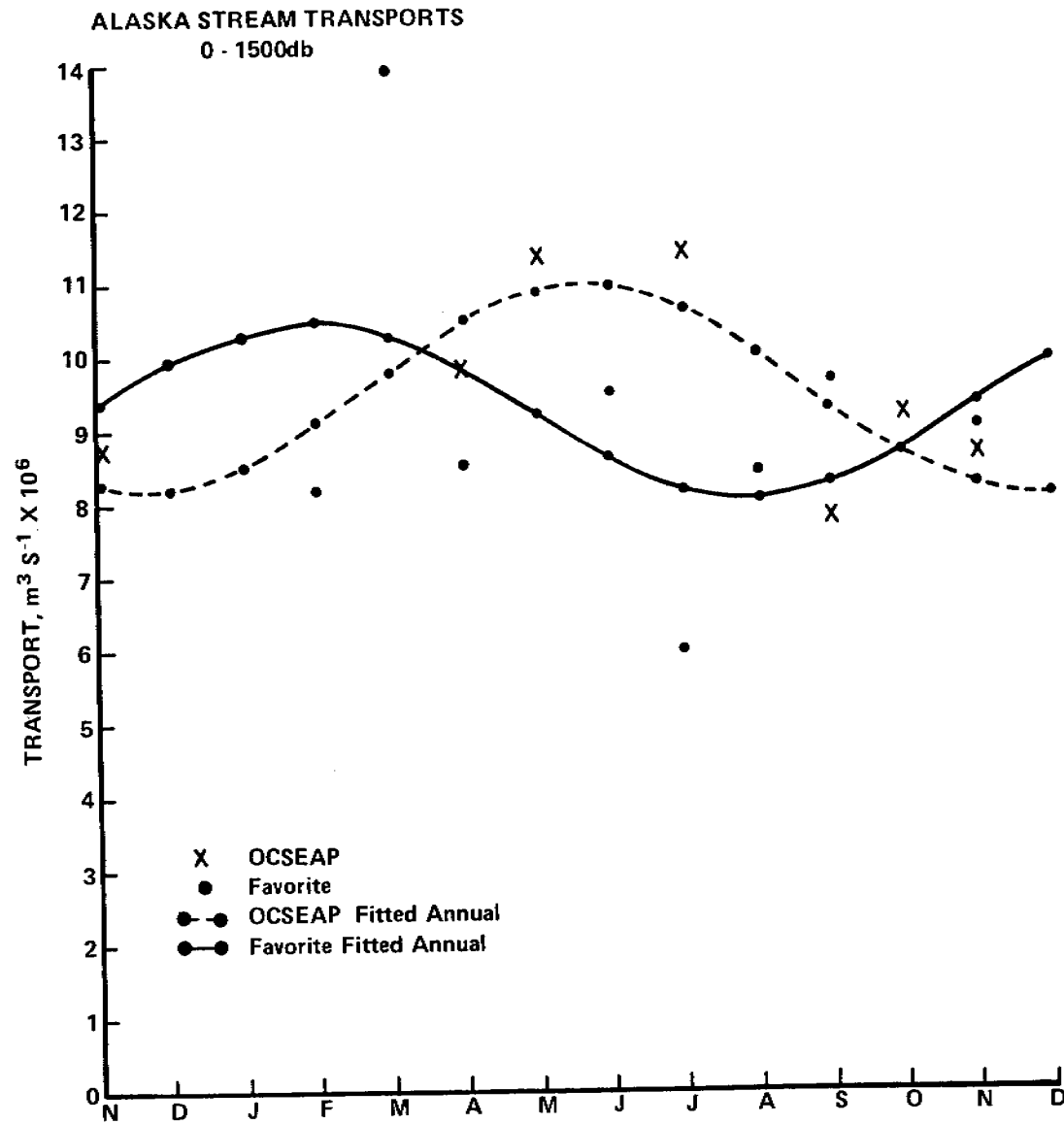


Figure 18. Composite year Alaska Stream transports with least squares fitted curves.

spring or early summer is reasonable. The effect of wind stress on the baroclinic flow requires a certain amount of delay in the response since the effect requires the transport of water across the shelf to form new density distributions. Note that within this annual cycle, there are also large deviations from the fitted curves (Fig. 18).

A similar transport analysis for the hydrographic section over the shelf terminating at Seward (the Seward Line) demonstrates changes in the baroclinic transport across the shelf (Fig. 19). Between stations 1 and 2, there is a maximum transport in January coincident with the maximum wind stress. Moving offshore, 2-3 has a maximum in fall, coincident with maximum fresh water influx. Progressing offshore, the maximum shifts to November and the amplitude diminishes. At 6-7 there is a phase shift and increase in the amplitude of the annual signal. This shift is believed to be a result of flow around Kayak Island moving along the shelf break. The peak is approximately 180° out of phase with the 1-2 transport, indicating that it could be the inner side of a shelf break jet. The 180° reversal of phase for 7-8 supports this conjecture. The next two transport estimates indicate very small annual signals. As mentioned in Section VI E., this area has much eddy activity. Accordingly it was found, that the standard deviation of the flow estimates at this location was much higher than nearby station-pair estimates. For 10-11, the dominance of the Alaska Current gives a maximum flow in May-June.

H. REMOTE SENSING ACTIVITIES

Incoming NOAA-VHRR satellite data has been monitored as in years past with support of the NOAA-CDA satellite station at Gilmore Creek and the Remote Sensing Library at the Geophysical Institute.

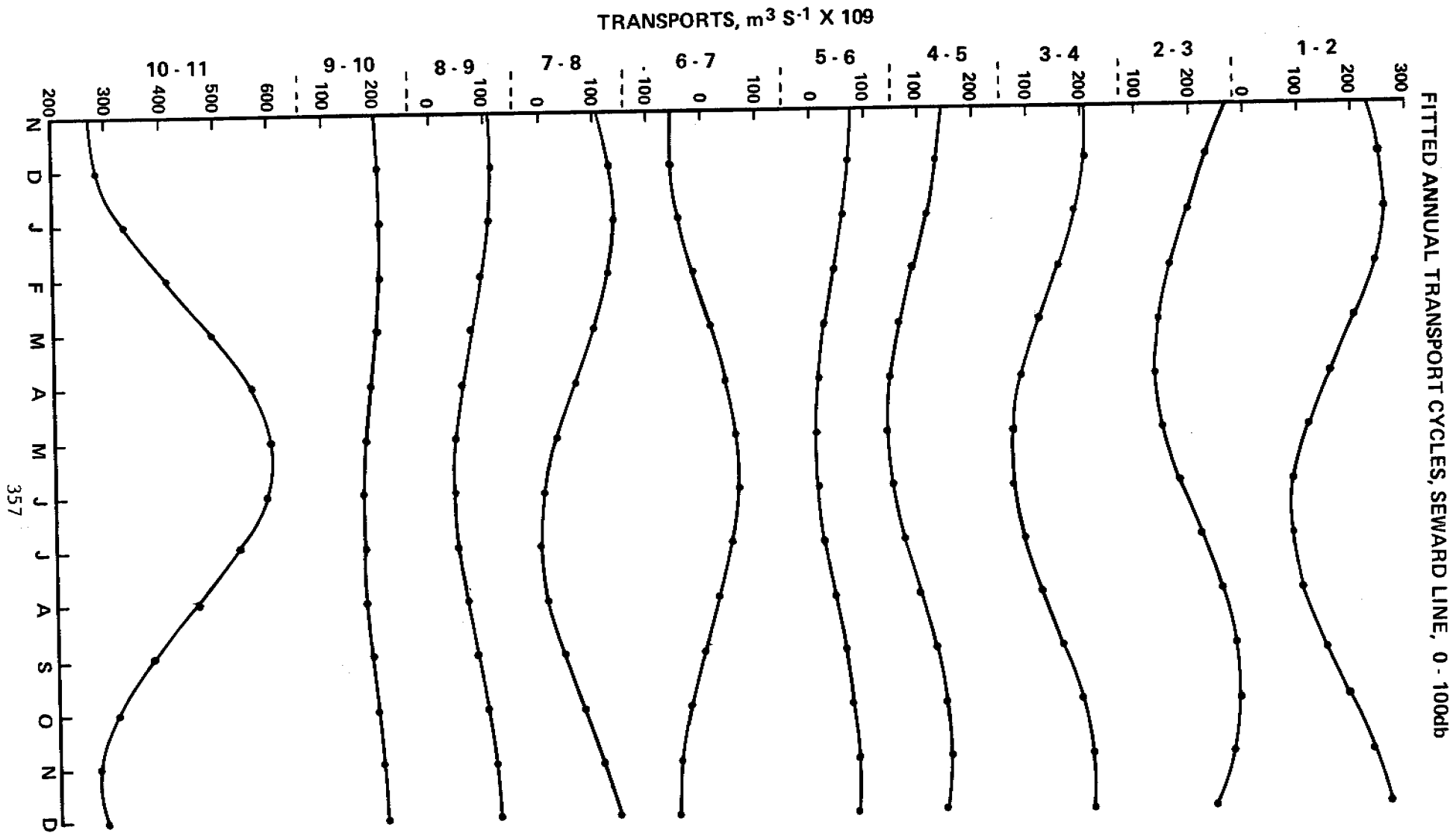


Figure 19. Fitted curves of baroclinic transports for Seward Line, Composite Year.

During the past year, from January 1978 through February 1979, a total of 2,000 photographic prints of satellite scenes were produced for us at the satellite tracking station. These prints include 600 enlargements and 90 gray tone enhancements for IR surface temperature structure. Three digital magnetic tapes of special interest have been copied for permanent retention and future study. The new satellite imagery for 1978 is contained in 9 ringbinders, increasing the total number of the collection to 28 ringbinders. Each binder is catalogued with a list of contents. As the binders are filled and the cataloging completed, the lists are distributed to the Remote Sensing Library and to PMEL in Seattle.

Requests for satellite imagery support from other investigators has increased. Of the total 2,000 pictures generated, 540 were submitted to others. Most requests have been made in support of field activities such as cruises and have been made prior to these activities. During the field experiment, the satellite data are monitored for the area of interest and appropriate copies are made. The major users have been PMEL and University of Washington in Seattle (Muench, Kinder, Schumacher). Some investigators also have requests for continuous monitoring of certain areas. However, the cloud cover over the Bering Sea was very uncooperative last summer. To give some investigators the most up to date information, e.g. on the exact location of the ice edge in preparation for a cruise (S. Martin), a close cooperation has been maintained with the NWS ice forecaster. Due to limited storage time (1 month) of satellite negatives at the tracking station, some old imagery, 80 prints, have been ordered from the Climatic Center where the negatives are permanently stored. In the past, imagery for overdue requests were rephotographed from the catalogued print to save time. However, an improvement in

quality and a substantial saving in money has been gained by ordering them from the Climatic Center.

In addition to the above customer service related work, the following have been accomplished:

1. Found one satellite print to summarize the NEGOA circulation for OCSEAP:
1 March 1978 N5 7181 IR (-20 to 28) + (29 to 41)°F.
2. Special invited report: "Arctic Sea Ice" by Kristina Ahlnäs and Gerd Wendler for the "1978 Arctic Directory", Proceedings of 7th Northern Libraries Colloquy, Paris, September 1978.
3. Replied to inquiry on marine remote sensing from "Economist Intelligence Unit Limited", London.
4. "Eddies in the Kamchatka Current" by Harold Solomon and Kristina Ahlnäs published in Deep-Sea Research, 1978, Vol. 25 pp. 403-410.
5. "Eddy-like features in the Kamchatka Current" by Kristina Ahlnäs and Harold Solomon, Polydome News No. 60 January 1979.

As a result of the above, an invitation was extended from Moscow to present a report on the eddies at the 14th Pacific Science Congress in Khabarovsk, USSR in August 1979.

6. Attended ONR sponsored workshop on "The Seasonal Sea-Ice Zone" in Monterey 25 February-1 March.
7. Abstract: "IR enhancement techniques to delineate surface temperature and sea-ice distribution" by Kristina Ahlnäs. Accepted for presentation at 13th International Symposium on Remote Sensing of Environment, 23-27 1979, Ann Arbor, Michigan.

The paper will be presented in a poster session. The accompanying paper will explain temperature enhancements in an easy to understand

way through graphs and examples. A paper like that will be useful in the customer service.

8. "Ocean Abstracts", Vol. 15 No. 1, February 1978, cited paper presented at POAC 75 in Fairbanks: "Sea-ice conditions in the Chukchi, Beaufort, East Siberian and Northern Bering Seas during March 1973, 1974, and 1975 as seen from the NOAA 2, 3, and 4 Satellites" by K. Ahlnäs and G. Wendler.
9. Abstract for POAC 79: "Sea-ice observations by satellite in the Bering, Chukchi, and Beaufort Seas" by K. Ahlnäs and G. Wendler accepted for representation in Trondheim, Norway August 1979.

I. SYNTHESIS REPORT

The first draft of a synthesis of the physical oceanography of the NEGOA region was assembled in October 1978. The synthesis had the inputs of most of the OCSEAP investigators working in the region. It was presented at the Fall OCSEAP physical oceanographers meeting and copies are available upon request. At that meeting, OCSEAP officials decided that the second draft of this report should take a new direction in that it should contain more detail than the brief (?) thirty page initial draft. A plan, procedure timetable and work assignments have yet to be established on this second draft.

VII. CONCLUSIONS

Good estimates of the mean physical oceanographic parameters for the northern Gulf of Alaska are now available through the OCSEAP work. In certain regions, such as the coastal jet, reasonable estimates of the annual fluctuations in physical conditions can now be made. We are now beginning to understand the mechanisms which cause these physical characteristics to vary. It is important to continue to address forcing mechanisms since that is the only method by which we will be able to use our observations to predict conditions for those periods with no observations.

We now know that the coastal jet responds to fresh water influxes which are controlled by precipitation and runoff. We also know that wind stress plays an important role, though its importance is not necessarily as great as was previously assumed. Our observations are plagued by eddies especially near the shelf break. Technology is presently unable to treat these eddies in a predictive sense except statistically. These features will limit

our results in that region, but remote sensing could provide the means to monitor them.

Analysis has begun on the data addressing the problem of exchange between the Gulf of Alaska and Prince William Sound. Data acquired by the conclusion of this fiscal year should be sufficient to describe mean flow and annual variations. At this preliminary stage, it appears that the general circulation is in through Hinchinbrook Entrance and out through Montague Strait. Some major reversals occasionally occur in Hinchinbrook Entrance, though none are evident in the Montague Strait data.

Our weakest information on circulation for the region is in the upper twenty meters where our current meters cannot be deployed. Drifter measurements have been shown here, not to represent onshore-offshore flow. This component is most important to pollution transport studies, but now must be inferred indirectly from hydrography, current meter and drifter data.

VIII. NEEDS FOR FURTHER STUDIES

While a change in the water density distribution due to the influx of fresh water has been identified, direct current measurements in this coastal jet have not been made. The baroclinic currents are calculated to increase with a fresh water influx, but the actual current response is unknown. Current meters should be placed in the coastal jet and its offshore boundary for at least one year. This offshore boundary is approximately 20-40 km offshore at Seward.

As mentioned in the previous section, some attention needs to be directed to the circulation in the upper twenty meters over the continental shelf. A practical solution to this problem is not presently available.

The role that the Alaska Current plays in determining the shelf circulation and/or shelf break eddy activity needs to be further investigated. This requires the direct measurement of Alaska Current transport over at least one year. The current is the major boundary of the NEGOA region that does not have good estimates.

Analysis of the data for Prince William Sound should continue. This will incorporate the meteorological forcing; wind stress, atmospheric pressure, and fresh water influx, with current meter measurements and hydrography into a description of the circulation and its causes. A numerical model of the circulation should also be included. This is the same model that we have been using for the coastal jet work. A detailed treatment of the regional hydrology is in progress and is necessary to better define the forcing mechanisms of the coastal circulation.

Some type of real time monitoring of eddies such as remote sensing needs to be continued if reliable real-time circulation predictions are necessary. Such a capability would be very helpful in assisting with a real-time pollution clean-up.

Analysis of the existing hydrographic and current meter data should continue with emphasis on better defining conditions on the other boundary (Alaska Current) and addressing the year to year variations, that is, the interannual fluctuations. For example, the wind stress anomalies have been very small since the inception of the NEGOA work. Are the conditions which we have observed typical for this region in the future? Further refinement of the forcing mechanisms needs to be carried out. A better understanding of the changes in forcing mechanisms from one lease area to another needs to be emphasized. For example, mechanisms which apply near Yakutat appear not to be important near Kodiak and certainly not at all in the Bering Sea.

The synthesis of physical oceanographic data for the northeastern Gulf of Alaska should also continue. The next stage should be an investigator meeting of all PI's to discuss recent findings and to summarize conclusions. This should be a meeting with a minimum of "observers" and therefore would differ considerably from the recent PI meetings. Instructions for the synthesis products should be outlined in detail prior to such a meeting. A requirement also exists to put together interdisciplinary NEGOA meetings once again. These gatherings should now be of great scientific value and therefore of great value to OCSEAP. They will also pave the way for an interdisciplinary synthesis.

IX. SUMMARY OF FOURTH QUARTER OPERATIONS

A. TASK OBJECTIVES

To gather and analyze hydrographic and current meter data in the northern Gulf of Alaska for the purpose of describing possible flow trajectories. To describe the physical environment and to understand its driving mechanisms. To continue to monitor NOAA satellite data for use by this project and other OCSEAP investigators. To organize and lead to synthesis of physical oceanographic data for NEGOA.

B. FIELD OPERATIONS

Cruise, 12-17 February, R/V *Acona*

Scientific Party

T. Royer
W. Kopplin
J. Shives
P. Shoemaker
M. Sweeny
L. Ernst

Methods

STD and current meter deployment and recovery

Location

Prince William Sound and adjacent waters

Data Collected

34 STD stations, two current meter arrays recovered,
one current meter array deployed

Cruise, 8-21 February, *Surveyor*

Scientific Party

D. Nebert

Methods

CTD measurements

Location

Prince William Sound, Hinchinbrook, Seward and Cook
Inlet Lines, deep water and shelf areas

Data Collected

133 CTD stations

C. RESULTS

Analysis is continuing on IMS 9 current meter data. Eddies have been identified as they moved past the array for a reconstructed density time series. This conclusion agrees with the hydrographic data and the findings of other studies which identify the shelf break as a region with many eddies and meanders.

Current meters were recovered from Hinchinbrook Entrance and Montague Strait which had been deployed in September 1978. In both cases, the upper floatation was missing. Both moorings had been snagged by some means. Both upper floats were missing from the Hinchinbrook mooring causing the array to sink to the bottom whereupon the VINY floats imploded. The fishing floats near the acoustic release remained intact and were sufficient to bring the entire array to the surface. Since additional non-defective plank-on-edge

floats were not available due to these losses, another array was not deployed at the Hinchinbrook site.

D. PROBLEMS ENCOUNTERED

The snagging of our current meter arrays has caused a loss of one meter and one pressure gauge plus a loss of data which has yet to be determined. We will continue to place an announcement in the Notice to Mariners describing these arrays. We are also considering notifying local fishermen that they will not be held at fault if they snag a mooring but that we would like to have the equipment returned.

REFERENCES

- Bakun, A. 1975. Daily and weekly upwelling indices, west coast of North America, 1967-73. U.S. Dept. Comm. Natl. Oceanic Atmos. Admin. Tech. Rept. MFS SSRF-693, 114 p.
- Favorite, F., A. J. Dodimead, and K. Nasu. 1976. Oceanography of the subarctic Pacific region, 1960-71. *International North Pacific Fish. Comm. Bull.* No. 33. 187 p.

APPENDIX I

Abstracts of Papers Submitted, Presented or Published

ON THE EFFECT OF PRECIPITATION AND RUNOFF ON COASTAL
CIRCULATION IN THE GULF OF ALASKA

by

Thomas C. Royer

ABSTRACT

Surface waters in the Gulf of Alaska undergo a net dilution throughout most of the year since the regional precipitation exceeds evaporation. Recent hydrographic data give evidence that seasonal dynamic height fluctuations in the upper layers (<100 m) are well-correlated with the seasonal changes in precipitation and runoff. The precipitation effect is magnified by coastal mountain ranges which enhance the rainfall at or near the coast, contributing fresh water at the coast through runoff. Previous estimates of the offshore precipitation gradient appear to be smaller than those measured recently. Precipitation and runoff alter the dynamic height through salinity changes. This dependence of dynamic height on salinity is possible here because of the high precipitation ($>130 \text{ cm yr}^{-1}$), runoff, longshore accumulation of fresh water around the gyre, and the low water temperatures.

The coastal sea level is in phase and has nearly the same amplitude as the local dynamic height, though not in phase with heating and cooling. Both the seasonal cycle of sea level and precipitation and their anomalies are well-correlated. The majority of the seasonal sea level variations can be accounted for by the local steric property changes. The small difference between the dynamic height and sea level implies that the barotropic effects on sea level are small.

The dynamic height and longshore flow responds to the annual hydrologic cycle for southcoast Alaska. This provides an important mechanism through which the atmosphere can affect the local ocean circulation. The dynamic height beneath 100 m responds to wind stress changes through Ekman pumping and coastal divergences and convergences. Thus precipitation, runoff and wind stress are all important to the coastal dynamics here.

COASTAL FLOW IN THE NORTHERN GULF OF ALASKA AS OBSERVED BY DYNAMIC
TOPOGRAPHY AND SATELLITE-TRACKED DROGUED DRIFT BUOYS

by

Thomas C. Royer

Donald V. Hansen

and

David J. Pashinski

ABSTRACT

Drifting buoys and dynamic topography over the continental shelf in the northern Gulf of Alaska are used to describe the coastal circulation and flow in the offshelf Alaska Current. One permanent anticyclonic eddy is detailed along with several shorter period features. In general, the buoys progressed shoreward and to the west from a release point near the continental shelf break. There was a tendency for the drifters to determine their trajectories near or inside Prince William Sound.

Precipitation, runoff, and wind stress suggest that the buoys' drogues are affected by entrainment. It is hypothesized that drifters move shoreward until their drogues encounter the offshore moving, ageostrophic, upper layer. Their position stabilizes between the onshore and offshore flow, and their subsequent movement is parallel to this interface. Though drifters might not be monitoring surface flow, it can be inferred that the surface flow is offshore here.

The behavior of drogued, drifting buoys enables them to be especially valuable in measuring flow along frontal regions.

AN ANALYSIS OF OBSERVED SURFACE WINDS AT MIDDLETON ISLAND, GULF OF ALASKA

by

David Livingstone and Thomas C. Royer

Institute of Marine Science, University of Alaska

Fairbanks, Alaska 99701

ABSTRACT

An analysis of observed surface winds at Middleton Island in the central part of the northern Gulf of Alaska reveals that the monthly mean and standard deviation of the scalar wind speed exhibit a strong annual periodicity with a winter maximum and a summer minimum. The monthly mean wind is always directed approximately towards the west-northwest, and so the mean longshore wind is in all months westwardly directed.

Monthly mean Ekman transport in the northern gulf has a component onshore in all months, which leads to sea surface set-up and downwelling, creating westward barotropic and baroclinic longshore currents. Standard deviations of onshore Ekman transport are at least twice as great as the mean. Therefore during any month, although downwelling situations predominate, shorter period reversals always occur, leading to a rapid alternation between downwelling and upwelling situations. Over a full year the longshore wind is Gaussian. Because of the westward mean wind, the onshore Ekman transport is not Gaussian, but is skewed onshore. Extreme transport events therefore tend to be onshore, and hence be downwelling events.

A comparison of onshore Ekman transport calculated from observed winds with *Bakun's* [1973, 1975a, 1975b] "upwelling indices" (computed from synoptic

surface pressure maps) for a nearby location reveals important differences between the two estimates. Onshore Ekman transport from the upwelling indices has a strong seasonal periodicity with strong downwelling in winter and weak upwelling in summer. Onshore Ekman transport also exhibits a high degree of persistence. The observed wind data indicate, however, that seasonal variations in onshore transport are not nearly as great as the indices would suggest. Winter onshore Ekman transport from observed winds is less than that predicted by the upwelling indices by a factor of three or four, and there is no summer upwelling season. Scatterplots reveal no strong functional relationship between the two series.

THE USE OF ROTARY SPECTRA TO DETERMINE EDDY PROPAGATION
AS APPLIED TO SURFACE WINDS OVER THE GULF OF ALASKA

by

David Livingstone and Thomas C. Royer

ABSTRACT

Rotary cross-spectra for wind vectors from stations located in a region where there is frequent cyclonic activity contains information on the propagation characteristics of the passing storms. Both the rate and direction of propagation of the low pressure centers can be ascertained from the intermediate products of the rotary cross-spectra. The techniques are applied to the surface winds at three locations over the Gulf of Alaska where cyclonic atmospheric systems are frequent in winter. The method involves the use of a change of phase angle with frequency of the rotary cross-spectra for vectors with high coherence.

The rates and directions of these cyclonic eddies are verified through the use of synoptic pressure charts. The application of this technique to current vectors from two or more arrays in the ocean can provide similar information on the rate and direction of movement of eddies in the ocean where synoptic pressure charts are not available.

ON THE SEASONAL VARIATIONS OF THE BAROCLINIC
TRANSPORT OF THE ALASKA CURRENT

by

Thomas C. Royer

ABSTRACT

Hydrographic sections through the Alaska Current from 1974 to 1978 allow estimates to be made of the seasonal fluctuations in the baroclinic transport. The average amplitude of the annual fluctuation is $1.4 \times 10^6 \text{ m}^3 \text{ s}^{-1}$ on a mean of $9.6 \times 10^6 \text{ m}^3 \text{ s}^{-1}$ for this period. The amplitude and mean are similar to those determined from historical data (1965-1970) obtained under less uniform sampling. However, the phasing and error estimates for the annual signal are very different for the two observation periods, with larger errors for the 1965-1970 data. The earlier data indicate a maximum transport for the upper 1500 m in February whereas the more recent transport measurements peak in June. Both differ from the previously assumed maximum transport in December-January, but are more consistent with an expected spin-up from the annual wind stress peak in January. The upper layer (< 100 m) transport of the Alaska Current is out of phase with the annual fluctuations in the coastal current, which has a maximum transport in fall. This coastal current is hypothesized to be primarily driven by fresh water influx. There is no discernible depth dependence to the phasing of the annual transport cycle in the Alaska Current. The current's position offshore remains fairly constant throughout the year.

EDDIES IN THE KAMCHATKA CURRENT

by

Harold Solomon and Kristina Ahlnäs

Institute of Marine Science and Geophysical Institute

University of Alaska

Fairbanks, Alaska

ABSTRACT

Visible images from the National Oceanic and Atmospheric Administration (NOAA) satellites show intense vortices, which we believe to be oceanic eddies, in the Kamchatka Current in winter. Infra-red images from the same satellites show eddies in the Kamchatka Current, and trains of eddies covering much of the western Bering Sea, in autumn. Such thermal features, which were not explicitly taken into account in previous oceanographic studies of this region, might cause the exceptionally high space and time variability in computed geostrophic transports and indicate a need for a new approach in attempts to clarify the nature of the net circulation and its seasonal and year-to-year variability.

Some of the observed eddies show a distinct spiral arm structure. This is the first instance of which we are aware of published evidence of such structure in oceanic eddies.

SEA-ICE OBSERVATIONS BY SATELLITE IN
THE BERING-, CHUKCHI-, AND BEAUFORT SEAS

by

K. Ahlnäs and G. Wendler

Institute of Marine Science and Geophysical Institute

University of Alaska

Fairbanks, Alaska

ABSTRACT

The interest in sea-ice conditions of the waters surrounding Alaska has increased substantially over the last years, mainly as a consequence of oil and gas exploration in the offshore areas and the supply needs for the Prudhoe oil fields. During the same time, new series of satellites were launched, which facilitated the task of surveying ice conditions from space. We used the civilian, NOAA - VHRR satellites, while the DMPS-series are military. Both have very similar characteristics. The ground resolution of the NOAA - VHRR is 1 km at nadir and imagery is obtained simultaneously in the visible and infrared region, hence making it possible to obtain data also during the night time in the absence of clouds. Furthermore, we were able to produce IR "enhancements" of any specific scene for surface temperature studies, as we had access to the original digital data tapes of the NOAA - VHRR satellites.

Our study concentrated on three areas:

a) The sea-ice edge in the Bering Sea was studied for a 5-year period, 1974-1978. For this time period, the location of the ice edge at

selected geographical positions was compiled. The general process during the freeze-up and break-up cycle is described and the paths of ice movement and stagnation areas are discussed. Interesting to note are the large variations in the ice extent which occur from year to year. For example, in the spring of 1976, at the time of maximum ice extent, the ice reached much further to the south than in the following year. This could be explained by differences in the general atmospheric circulation during these two years.

b) The transport of ice through the Bering Strait can be either north or south, depending on the wind direction. With a northerly wind, cold ice from the Chukchi Sea is imported into the Bering Sea. The velocity of the moving ice averages about 0.5 km/hr. However, under strong northerly wind conditions, large amounts of ice can be moved through the Bering Strait. Two cases are well documented (around 31 January 1977 and around 20 March 1978). Using infrared imagery, the total amount of ice exported could be measured, and the velocities of the ice movement during these storm events could be estimated and related to the surface wind speed and general synoptic situation.

c) For the five-year period, 1974-1978, the ice decay during summer time along the northern coast of Alaska was investigated. Similar to the ice conditions in the Bering Sea, large changes do occur from year to year. For example, in 1975 the ice hardly retreated at all and supply barges did not reach the Prudhoe Bay oil fields until October with emergency ice breaker assistance. The following years the ice retreated much earlier and further. Differences in the year to year ice conditions are documented and explained. For example, for all three months of 1975 (July, August, and September), when

the ice is normally retreating in the Beaufort Sea, a deviation in the wind velocity, adding a north-westerly wind vector to the general mean circulation was found.

EDDY-LIKE FEATURES IN THE KAMCHATKA CURRENT

by Kristina Ahlnäs and Harold Solomon

Visual and infrared images obtained from the National Oceanic and Atmospheric Administration (NOAA) series of satellites have recently been showing evidence of large and intense eddy-like features off the eastern coast of the Kamchatka Peninsula in the northwestern North Pacific Ocean. The existence of these features (winter ice features only) was first reported in the literature by Motoki (1977). A more detailed analysis, including justification for regarding the winter features as ice rather than low clouds, and a discussion of some broader oceanographic implications, has been given by the present authors (Solomon and Ahlnäs, 1978).

These features do not occur uniformly at all times of the year. Open-water features, which show up most clearly on the infrared images, seem to occur mainly in September (Figure 1). The temperature of the sea surface varies from about 3°C at the center of the feature to 8°C outside. Using the oceanographic structure reported by Ohtani (1973), we deduced upwelling from a depth of about 50 m at the center of the features. The coverage of at least the northern half of the image region by trains of these eddy-like features should be of interest to POLYMODE News readers. The spiral arm structure of these features constitutes the first reported occurrence of such structure in the ocean.

Both Motoki (1977) and Solomon and Ahlnäs (1978) referred to these features as "eddies." They may well be eddies, but a cursory examination of the scales involved fails to reveal an obvious consistent dynamical structure. The shape of the spirals seems to indicate anticyclonic rotation, by analogy with atmospheric storms showing similar structure (though wound in the opposite sense), but the cold core would be associated with cyclonic rotation if the features are baroclinic and in geostrophic balance. The observed scales make it difficult to conclude that the motion is ageostrophic. At a

latitude of 52°N, and length scale of perhaps 20 km across only the central core of the "eddy," the advective Rossby number is $\frac{U}{fL} = 0.14U$. A scale velocity of at least about 5 m/sec would be necessary to give a Rossby number close to 1. Even this would only break the rotational constraint to permit significant motion directly down the pressure gradient, and would not necessarily cause rotation in the opposite direction. This is also the approximate condition for cyclostrophic effects to become comparable to geostrophic effects. Consequently, we think that these features should be regarded as paradoxes and interesting objects of further research, rather than as proven eddies.

"Eddies" made visible by floating ice on the surface are shown in Figure 2 and Figure 3 (three days later). These are visual band images. Note that the "eddies" persist for three days, while the cloud cover changes completely. These eddies seem to occur mainly in March and April, and only when the Bering Sea ice pack reaches this far south as evidenced by satellite imagery.

(The authors agree to have this article quoted provided that credit is given.)

Mr. E. Kendall and his competent crew at Gilmore Creek NOAA-NESS CDA Station produced the satellite imagery. We wish to thank Prof. T. Royer for helping to arrange Solomon's visit to the University of Alaska and for making the data available for this study, Michio Kishi for comments on the problems in interpreting the satellite data, and Takashi Murakami and Nobuyuki Shikama for discussion of the nature of the eddies.

References

- Motoki, Toshihiro (1977) Kamchatka Hanto togan ni hassei shita kaijo no uzu (in Japanese). Tenki, 24, 605-606.
- Ohtani, Kiyotaka (1973) Oceanographic structure in the Bering Sea. Mem. Fac. Fish., Hokkaido Univ., 21, 65-106.
- Solomon, Harold and Kristina Ahlnäs (1978) Eddies in the Kamchatka Current. Deep-Sea Res., 25, 403-410.

IR ENHANCEMENT TECHNIQUES TO DELINEATE SURFACE
TEMPERATURE AND SEA-ICE DISTRIBUTIONS

K. Ahlnäs
Institute of Marine Science
University of Alaska, Fairbanks, Alaska 99701

The VHRR (Very High Resolution Radiometer) IR sensor on the NOAA series of near-polar orbiting environmental satellites is capable of recording scene temperatures from -90 to 40°C . Normally a more narrow range is used for better gray scale contrast. The spatial resolution for both simultaneous channels, the VIS (0.6 to 0.7μ) and the IR (10.5 to 12.5μ), is 0.9 km.

When ocean areas are cloudfree, possible surface temperature structure can be enhanced on the IR scene. A preselected temperature range is programmed into a minicomputer that works on the original satellite tape, thus avoiding any deterioration in image quality.

The exact location of coastlines is at times difficult to distinguish on visual imagery. On the IR imagery it can often be delineated in great detail by using a split level temperature enhancement. This is particularly effective in fall, during the time of freeze-up, when the ocean water still is relatively warm and the land areas cold. A good "look-up" table to use for this case would be -10 to -2°C for the land areas and -2 to 6°C for the water. Both scales would utilize the whole 32-shade gray scale from white for the coldest to black for the warmest temperature entry. With a temperature span of 8°C in both scales, one degree centigrade would correspond to 4 gray shades. The scale split, -2°C , is shared by both scales. Since it corresponds to black in the lower scale and white in the higher it constitutes a very pronounced division line coinciding with the delineation of the coastline at the time of freeze-up.

The coastline in the Arctic Ocean is obscured for most of the year due to the existence of shore fast ice that blends in with the land. After snow melt the land gets considerably warmer than the ocean. Running a split level enhancement with the coast temperature as the division gives a good contrast.

For instance, on 12 July 1977 the temperature of the Arctic coast was 11°C and an excellent coastline definition was obtained with a "look-up" table of $(-2$ to $11) + (11$ to $21)^{\circ}\text{C}$. On this enhancement the coast line around Barrow is black while the barrier reef along NW Seward Peninsula is white.

In August the Arctic coast is usually ice free with a narrow band of relatively warm water along the coast, especially in the shallow barrier island area west of Prudhoe Bay. A split at 7°C on 14 August 1977 brings out the fine temperature structure of the near coastal water.

Ice formation and melting is advantageously studied with a modified split scale temperature enhancement. A look-up table like (-40 to -4) + (-4 to -2) black + (-2 to 5) $^{\circ}$ C will give a wide transition area in black for sea ice that is just ready to melt or slush that is freezing. In addition, the table delineates the sea ice in the lower scale and the open ocean water in the higher scale. A good example for this was seen around the Pribilof Islands in the Bering Sea on 29 March 1977.

Oceanic eddies can be temperature enhanced in a spectacular way on satellite infrared imagery. Some of the more pronounced eddies in the Bering Sea have been observed in the waters east of the Kamchatka Peninsula in the fall of both 1976 and 1977. They are all anticyclonic with cold cores and diameters approaching 100 km. Some of the eddies show a very distinct spiral structure, with the spiral arms decreasing in temperature as they wind inward in an anticyclonic sense. On 26 September 1977 the eddies were pronounced enough to show up even on the standard IR. A single scale temperature enhancement from 2 to 11 $^{\circ}$ C defined them in detail to be studied. Temperatures measured by photographic densitometer decrease from 6 $^{\circ}$ C in the outside spiral to 3 $^{\circ}$ C in the core. A temperature of 3 $^{\circ}$ C indicates upwelling from a depth of 50 m. Anticyclonic eddies with divergent cold core centers suggest that the eddies may not be in dynamical balance.

To check on the accuracy of the densitometer reading the same "look-up" table, 2 to 11 $^{\circ}$ C, was rerun while asking the minicomputer to identify temperatures of 3 $^{\circ}$ C in black and 6 $^{\circ}$ C in white. This made the eddies north of the Commander Islands show up with black centers surrounded by white.

OCS COORDINATION OFFICE

University of Alaska

ENVIRONMENTAL DATA SUBMISSION SCHEDULE

DATE: March 31, 1979

CONTRACT NUMBER: 03-5-022-56

T/O NUMBER: 19

R.U. NUMBER: 289

PRINCIPAL INVESTIGATOR: Dr. T. C. Royer

Submission dates are estimated only and will be updated, if necessary, each quarter. Data batches refer to data as identified in the data management plan.

<u>Cruise/Field Operation</u>	<u>Collection Dates</u>		<u>Estimated Submission Dates</u> ¹		
	<u>From</u>	<u>To</u>	<u>Batch 1</u>	<u>2</u>	<u>3</u>
Acona #193	7/1/74	7/9/74	submitted	None	None
Acona #200	10/8/74	10/14/74	submitted	None	None
Acona #202	11/18/74	11/20/74	submitted	None	None
Acona #205	2/12/75	2/14/75	submitted	None	None
Acona #207	3/21/75	3/27/75	submitted	None	None
Acona #212	6/3/75	6/13/75	submitted		
Oceangrapher #805	2/1/75	2/13/75	submitted	None	None
Silas Bent #811	8/31/75	9/28/75	Submitted		
Discoverer #812	10/3/75	10/16/75	(a)		
Surveyor #814	10/28/75	11/17/75	submitted		
Discoverer #816	11/23/75	12/2/75	(b)	None	None
Station 60	7/2/74	10/08/74	None	Submitted	None
Station 64	4/28/75	5/20/75	None	(c)	None
Station 9A	-	-	-	Lost	
Station 9B	4/20	7/24/76	-	submitted	submitted
Moana Wave MW 001	2/21/76	3/5/76	submitted		
Moana Wave MW 003/004	4/20/76	5/21/76	submitted		
Moana Wave MW005	7/22/76	8/1/76	submitted		
Moana Wave 006	9/13	9/19/76	submitted		

<u>Cruise/Field Operation</u>	<u>Collection Dates</u>		<u>Estimated Submission Dates</u> ¹		
	<u>From</u>	<u>To</u>	<u>Batch 1</u>	<u>2</u>	<u>3</u>
Surveyor SU 003	9/7/76	9/17/76	submitted		
Surveyor	9/20/76	10/2/76	submitted		
Miller Freeman	11/1/76	11/19/76	submitted		
Moana Wave	10/7/76	11/16/76	submitted		
Miller Freeman	3/9/77	4/2/77	submitted		
Station 9C	7/22/76	11/2/76	submitted		
Acona 248	8/11/77	8/14/77	submitted		
Discoverer	11/8/77	11/16/77	submitted		
Acona 253	11/10/77	11/17/77	submitted		
Hinchinbrook	11/10/77	9/19/78	None	Submitted	Submitted
Montegue	11/10/77	9/19/78	None	Submitted	Submitted
Station 9D	11/3/76	3/29/77	None	Submitted	Submitted
Acona 256	2/16/78	2/25/78	submitted		
Acona 260	4/22/78	5/8/78	submitted		
Acona 264	7/31	8/12/78	1/15/79		
Acona 266	9/17	9/30/78	1/15/79		
Hinchinbrook	9/19/78	2/15/79	None	6/30/79	lost
Montegue	9/19/78	2/13/79	None	6/30/79	6/30/79
Acona 271	2/12/79	2/17/79	6/30/79		
Surveyor	2/8/79	2/21/79	6/30/79		
Montegue	2/13/79	Current			

- Note: ¹ Data Management Plan and Data Formats have been approved and are considered contractual.
- (a) Parent tapes were coded in PODAS format, tapes were submitted to F. Cava as requested.
 - (b) Data useless due to malfunction of shipboard data logger.
 - (c) In edit process. Development of computer editing program has held up data.
- Data Batch 1 = STD/CTD
2 = Current meter
3 = Pressure guage

ANNUAL REPORT

**Contract #R7120848
Research Unit: 367
Reporting Period;
April 1, 1978 to
April 1, 1979**

NEAR-SHORE METEOROLOGY

**R. Michael Reynolds
S.A. Macklin
B.A. Walter**

Pacific Marine Environmental Laboratory
Seattle, WA 98105

April 1, 1979

CONTENTS

Page

1. Summary of Objectives
2. Introduction
 - A. General Nature and Scope of Study
 - B. Specific Objectives
 - C. Relevance to Problems of Petroleum Development
3. Current State of the Knowledge
4. Study Area
5. Rationale, Sources, and Methods of Data Collection
6. Results

Appendices

- A. Observations of Mesoscale Winds in Lower Cook Inlet, Alaska - March 1978
- B. Preliminary Results From a Mesoscale Net in the Lower Cook Inlet, Alaska.
- C. Winds Over the Albatross Banks - A Comparison of Measurements from EB46008, FNWC, and Kodiak.
- D. The Response of Coastal Winds at Albatross Banks, Lower Cook Inlet, and Hinchinbrook Entrance to a Passing Synoptic Disturbance - Preliminary Analysis

1. SUMMARY OF OBJECTIVES

The objective of this study is to define the dominant mesoscale features in four specific coastal regions, Albatross Banks, Kiliuda Bay, lower Cook Inlet (LCI), and Hinchinbrook Entrance (Figure 1). A variety of data sources are being coalesced into an accessible data base for this task. These sources include land based weather stations, data buoys, oil drilling platforms, NOAA ships, ships of opportunity, ferries, AMOS stations, and remote installations which were deployed as a part of this study (Table 1.). Also included in the data base are synoptic data from the Navy Fleet Numerical Weather Central (FNWC) analysis. It is hoped that not only will important, local, mesoscale processes be identified, but that some means for predicting their occurrence and extent can be developed. Any predictive scheme must rely on ready sources of information such as a numerical forecast or concurrent land based measurements, and we will investigate which of these seems best.

With the above-stated general goal in mind, we are pursuing the following specific objectives.

1. We will provide graphic presentations of the data from each area for typical seasonal or synoptic conditions. The presentations will include time series plots, progressive vector diagrams, and fabric diagrams.
2. We will establish the relationship (or lack of relationship) between over-the-water winds and numerically-derived (FNWC) synoptic scale winds. The term 'over-the-water' in this instance means data from environmental buoys 46007, 46008, 46009 (Figure 1).
3. We will compare 'over-the-water' winds with winds from nearby land-based stations. With respect to the data

buoys listed above, the land stations to be used will be Homer, Kodiak, and Middleton Island. These were selected for comparison because they are close to the respective buoys, and are fairly reliable.

4. We will select two synoptic sequences involving the presence of strong storm conditions, and evaluate the response of each of the study areas to the sequences. Storms in the Gulf of Alaska are not static patterns, but kinetic ensembles. As such, it is felt that some consideration must be given to the evolution of the local wind fields in response to the changing synoptic field, and not to patterns alone.

5. We will make measurements of the winds in Kiliuda Bay and relate them to winds measured in Kodiak and offshore from data buoy EB 46008.

2. INTRODUCTION

A. General Nature and Scope of Study

Many mesoscale meteorological processes modify the surface winds in the coastal regions of Alaska, often seriously enough to obfuscate any attempts at relating synoptic weather maps to surface conditions. A typical example is the case of a predicted zephyr which, in actuality is strong and offshore near the coast, a result of mountain drainage from the interior. Away from shore, the continental boundary layer is rapidly modified by momentum and heat transfer through the sea surface with entrainment of the air aloft. Modification is manifested as a variation in temperature, wind speed, and/or direction. A thorough knowledge of coastal wind conditions is an important ingredient to responsible offshore industrial development. Surface winds strongly affect both mean water circulations and the trajectories of surface contaminants.

The work under R.U. 367 is aimed at defining which processes are active in modifying the wind field along the coast of Alaska, how prevalent they are, and how far offshore they act. All available meteorological data will be utilized in developing as complete a description as possible for four regions, Albatross Banks, Kiliuda Bay, lower Cook Inlet, and Hinchinbrook Entrance (Figure 1).

The work is principally a comparison of the observed flow field and larger scale forcing, with some consideration to the energetics of the planetary boundary layer. Both ends of the spectrum are important in such a study due to the juxtaposition of different modifying processes.

There appear to be three dominant processes which modify the coastal wind field. First, the mountainous terrain produces a complex wind field which is evident on land and which often extends a significant distance offshore.

A study of coastal processes in the vicinity of Icy Bay (see the 1978 annual report) shows that the mountain effect is seen at least 100 km offshore. Second, the downhill movement of a stable boundary layer, termed a 'fall wind' or 'katabatic wind', can cause significant winds along the coast. The fall winds are especially pronounced in the winter; they are focused into jets at the mouths of estuaries, and extend to approximately 20 km offshore. Third, a strong land-sea temperature difference in the boundary layer produces a local force which acts to enhance the westerly component of the mixed layer in a rather complicated way; one manifestation of this force is the sea breeze circulation.

The study areas are all meteorologically complicated, unpredictable, and vulnerable to industrial development. In all regions data is sparse and intermittent. For example, the entire western coast of LCI is without a single village, not to mention an airport or weather facility. Hence, if some comparison of actual versus predicted winds is to include this area, remote meteorological stations must be erected. We have deployed three remote stations which are shown on Figure 2. Aside from these stations, all meteorological data which can be considered representative has been collected in a data base. We have included in our data base information from a wide variety of sources including data buoys, oil platforms, ferries, ships of opportunity, NOAA research ships, AMOS stations, NWS stations, and even numerically determined analyses (Figure 2). The details of the data base and how we plan to use it are discussed in Section 5.

B. Specific Objectives

Specific objectives have been discussed in detail in Section 1.

C. Relevance to Problems of Petroleum Development

Lower Cook Inlet has just endured a major lease sale in which oil companies promised record breaking sums for the opportunity to drill. At present we receive data from two oil platforms operating in LCI, and there is speculation that as many as eight rigs will soon be active there. If oil is indeed discovered, many more operations will be initiated with the concomitant increased probability of an accident. Furthermore, research into the oceanic circulations in this enclosed region reveals a chaotic unpredictable pattern, to a large extent controlled by wind stress history over the water. This ability of the wind to control the current field, especially the near-surface currents, together with the frictional coupling of the wind and surface oil confirms the importance of a knowledge of the wind field.

In addition, knowledge of the predictability of the winds in various regions is important for any shipping, platform operations, or aircraft operations. Thus, any areas which do not yield to existing forecast procedures, must be delineated. Either new forecasting techniques or direct telemetering measurements must be developed to properly specify the winds in these regions.

3. CURRENT STATE OF THE KNOWLEDGE

Last year, we presented a thorough assessment of the knowledge of the local wind fields in the Gulf of Alaska in our annual report. Large scale synoptic patterns and certain coastal wind patterns were discussed, notably LCI and Icy Bay regions. This year we have added to that knowledge by analysis of data which has been collected over the past year. Much of that analysis is covered in the four appendices at the end of this report.

4. STUDY AREA

A map of the study area is shown in Figure 1, while Figure 2 gives the locations of the various sources of data for the research. Mountains dominate both sides of the nearly parallel coastline of LCI. Based on the studies of mountain steering in the Icy Bay region one would expect the winds in the upper region of LCI to be almost always either up or down the channel, a fact which is confirmed by the wind study in our 1978 annual report, Appendix B. However, south of the forelands, the general broadening of the channel results in a reduction of the wind speeds in LCI compared to those in the upper Cook Inlet. Further south the mountain trend is broken on each side; to the west by the Kamishak Gap, and by Kennedy Entrance to the east. The presence of these gaps allows winds in the area of Augustine Island to be easterly or westerly. Westerly winds are especially strong in the winter when a pronounced low occupies the Gulf of Alaska to the east of LCI. Then winds flow down gradient, funneling through the Kamishak Gap and spreading across the open water. Exactly how often this occurs, and what the seaward extent of it is, is one of the prime objects of this study.

The region to the east of Kodiak Island, in the vicinity of the Albatross Banks, is less complicated than the LCI region, as it faces the open sea and hence is similar, in general features, to the Icy Bay region. In such areas, we expect to see katabatic funneling near the mouths of the estuaries producing offshore flow components extending out to 20 km, and some mountain steering further offshore. The extent of the mountain steering can be of the order of 100 km, and analysis of the data from environmental buoy EB-46008 indicates such is the case here.

Finally, the region of Hinchinbrook Entrance is of importance, and a data buoy has been placed there. As discussed above, and elaborated on below, measured winds in this region will be compared to those predicted by a variety of sources to establish some measure of the predictability of those winds.

5. RATIONALE, SOURCES, AND METHODS OF DATA COLLECTION

As any experienced field scientist knows, direct measurement of over the water winds is difficult and expensive. Thus, any direct measurements of the winds are terribly important, and every means possible to utilize these measurements must be expended. In making comparisons of over-water winds to other measurements, all possible sources of land measurements must be explored also. Finally, computer-derived winds and synoptic patterns such as those by Putnins (1966) must also be included in a rather large and elaborate data base. Little conclusive results are possible without ready access to all available data in short order, and it is one of the goals of this study to create such a data base. Because of the need to incorporate data of widely varying format, the R2D2 data base already in use at PMEL was not entirely suitable. Instead, a newly developed, state-of-the-art system called SIR (Scientific Information Retrieval) has been adapted. The SIR system promises to provide us with the needed flexibility to launch a wide variety of comparisons, incorporating all possible data.

In SIR, data from each unique source are grouped together in a "case." In our usage, "case," for the most part, refers to a particular weather reporting facility, i.e., Kodiak NWS, EB-46009, NOAA Ship DISCOVERER (see Table 1). For each case, we have defined two different information packets or "records." Record type 1 contains general case information such as station name, location, elevation, observing agency, reported variables, frequency of data collection, data forwarding agency, and miscellaneous comments concerning instrumentation, etc. Only one type 1 record is required for each case. Record type 2 contains specific meteorological surface data for each station.

Included are station pressure, sea level pressure, wind speed, wind direction, air temperature, mixing ratio, sea surface temperature, synoptic weather designator, latitude, longitude, date and time. A separate type 2 record is required for each observation time. Other record types can be defined as necessary in order to expand the data base, i.e., record type 3 could be used to store atmospheric vertical profiles.

Within SIR an allowable range for each variable can be defined. As data are entered into the data base each variable is examined; any value outside of the defined bounds results in the expulsion from the data base of that record containing the variable. Redundant entries are similarly rejected. All rejected data are saved in an external file for examination. Clearly this built-in procedure promotes a high degree of quality control in the data base.

To date two methods of data retrieval have been investigated. One retrieval procedure extracts from the data base all available observations for a given time and a given geographic area. The other retrieval algorithm produces a time series for a given station over a given time window. This routine can also be used to retrieve ship tracklines and observations. In house computer routines are being adapted to accept data from these retrievals. Additionally a plotting procedure has been designed wherein data from the data base are displayed on a coastline map of the study area (Fig.3).

An up-to-date summary of the data base is contained in Table 2. Data status is reported in three modes; data at PMEL, data in intermediate format, and data within SIR data base. In the future we plan to use SIR's internal report generating capabilities to produce data base status reports.

6. RESULTS

As the proposed data base is now in good working order, we expect that the most ambitious analysis will be completed during the last half of this fiscal year. However, at this time we can begin to assess some of the more obvious features of the local meteorology.

In Appendix A and Appendix B, we examine the processes and wind fields which dominate the lower Cook Inlet region. As expected, this region is strongly controlled by the mountainous topography. In particular, three dominant geographic features appear to control almost all the wind flow in the central portion of the area. These are flow from the NNE-SSW directions, the main inlet axis, flow from the WNW-ESE directions through the 'Kamishak Gap', and wake flow around Augustine Island. Within approximately 20 km of the coasts, katabatic winds and local embayments can produce offshore winds.

When the wind is blowing from the WNW, through the Kamishak Gap, the wake behind Augustine Island extends well downstream of the island, and the WNW winds are seen as far as 200 km into the Gulf of Alaska. The center of the LCI during these conditions is highly confused, and no consistent pattern has as yet emerged.

Appendix C compares winds on the Albatross Banks to concurrent measurements at Kodiak. The comparison indicates little useable direct applicability of the land measurements to the offshore waters. This result was certainly expected, and is one of the reasons for this study. Although the winds produced by the Navy's Fleet Numerical Weather Central facility compare exceptionally well with the measured winds, they are not completely independent as the data buoy measurements were included by FNWC in producing their analysis. However, the FNWC analysis represents a geostrophic approximation over a large (391 km) grid spacing. Therefore, we can state that

the winds at the position of EB46008 were little, if any, affected by the land mass of Kodiak Island.

Finally, Appendix D is a preliminary description of the response of the coastal winds of the western Gulf of Alaska to typical strong synoptic systems. In this analysis, we analyze the winds which were measured during a typical storm passage by the various stations in our three study regions. A storm which passed from the north Pacific Ocean across the Aleutian Islands and into the Bering Sea generating strong easterly winds in the Gulf of Alaska produced synoptic winds only over Albatross Banks. In lower Cook Inlet and Hinchinbrook Entrance local orography played a strong role in modifying air motions. We plan to look at these modifications in more detail and to study wind response to other strong disturbances with varying tracklines.

TABLE 1. List of Meteorological Stations Shown in Figure 2.

1. Anchorage	NWS
2. King Salmon	NWS
3. Kodiak	NWS
4. Homer	NWS
5. Kenai	NWS
6. Iliamna	NWS (part time AMOS)
7. Whittier	NWS
8. Seward	NWS
9. Valdez	NWS
10. Cordova	NWS
11. Johnston Point	NWS (Air Force)
12. Big River Lake	NWS (contract)
13. Dolly Varden	Oil Rig
14. Phillips	Oil Rig
15. Shuyak	NWS (remote wind)
16. Cape Hinchinbrook	NWS (AMOS)
17. Middleton Island	NWS (AMOS)
18. EB-346007	NDBO
19. EB-46008	NDBO
20. EB-46009	NDBO
21. TUSTUMENA	Alaskan Ferry
22. Contact Point	PMEL
23. Augustine Island	PMEL
24. SURVEYOR	NOAA Ship
25. DISCOVERER	NOAA Ship
26. Kiliuda Bay	PMEL
27. Copper River	PMEL
28. Ships of Opportunity	Misc.
29. Diamond M. Dragon	Oil Platform
30. Ocean Bounty	Oil Platform
31. FNWC	Navy (computer)

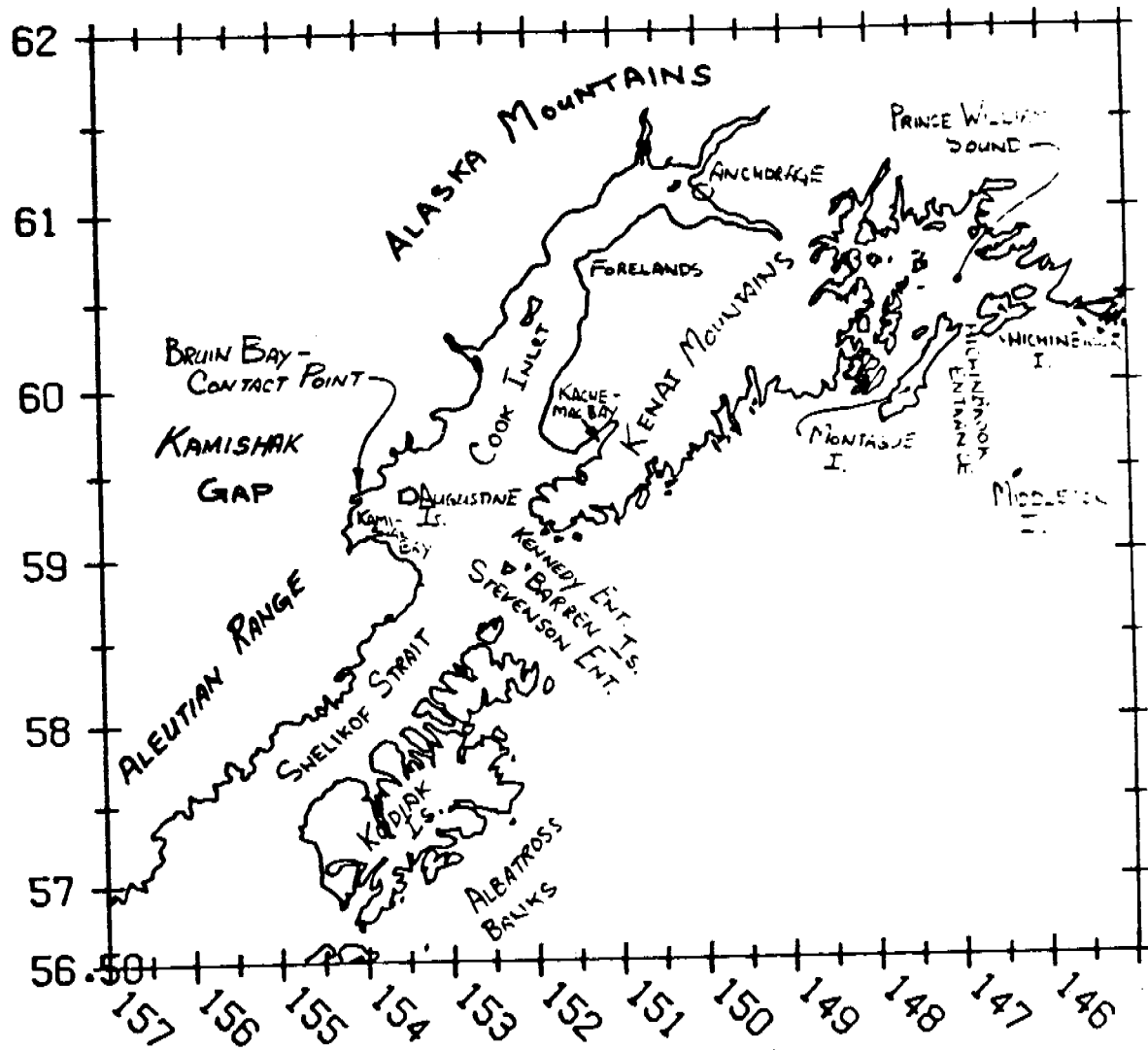


Figure 1. Map of the study area showing main geographic features considered in this study.

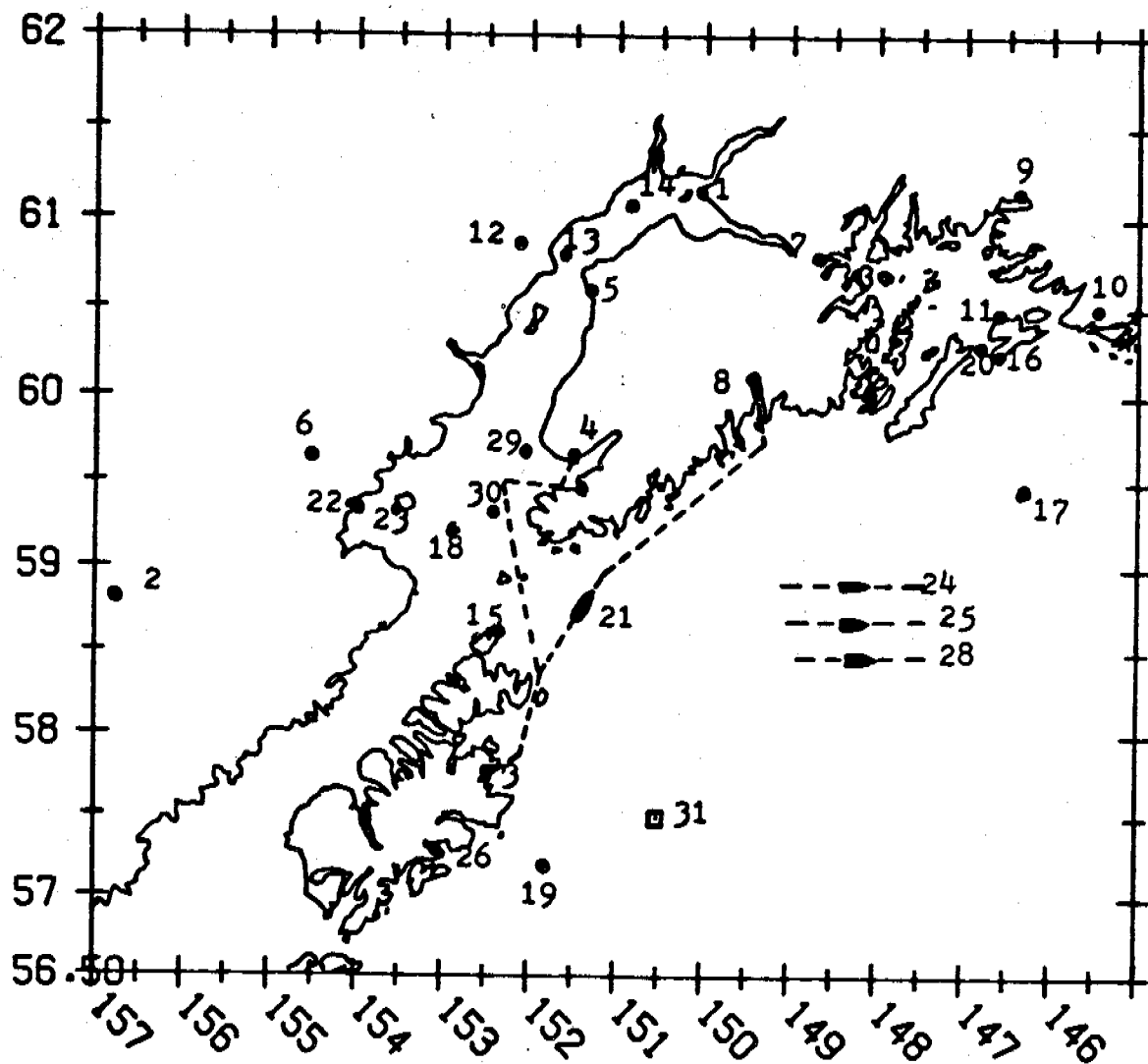


Figure 2. Map of the study area showing sources of data which are included in this study.

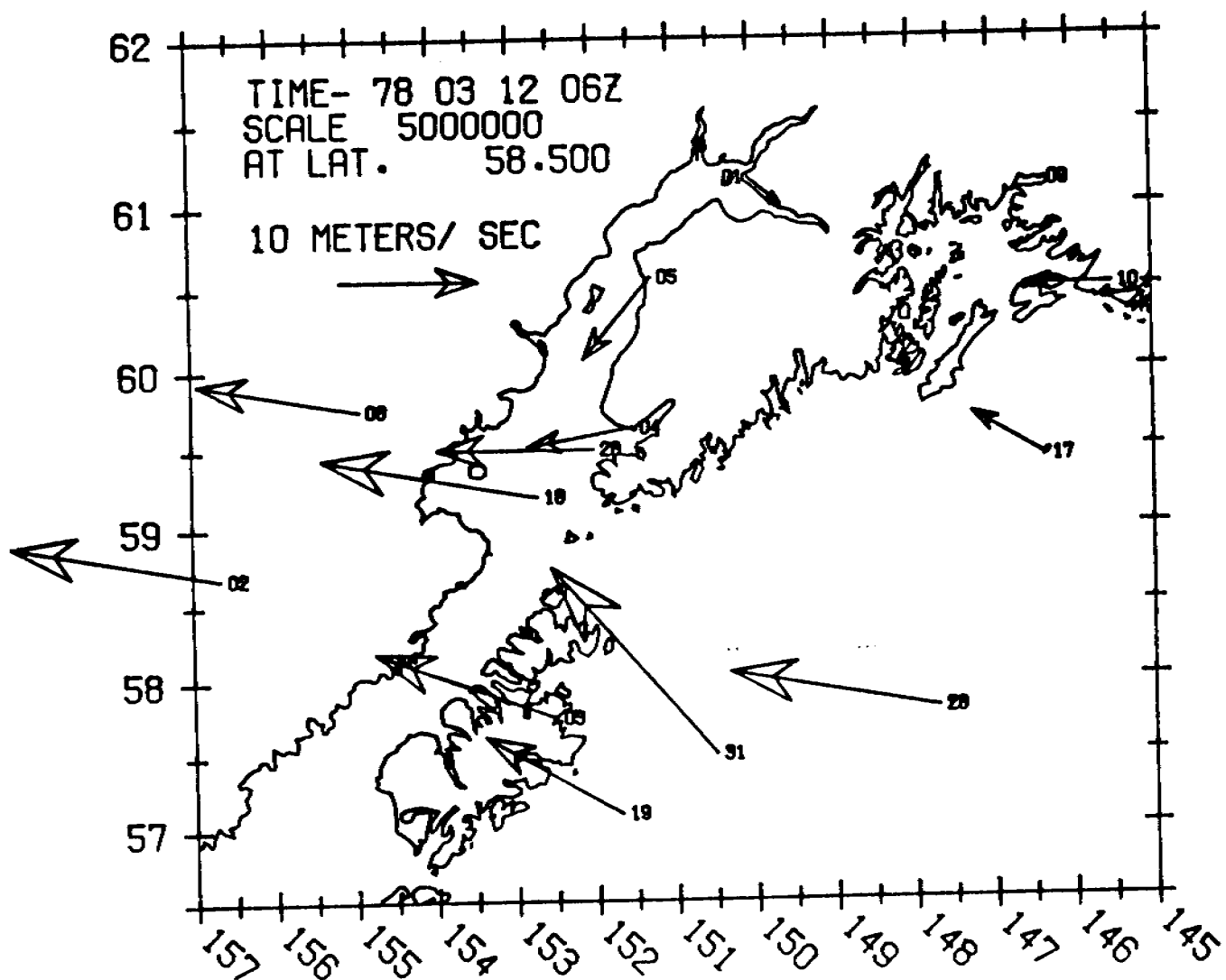


Figure 3. Map showing simultaneous winds measured at various sites in the western Gulf of Alaska. Figure 2 and Table 1 document the various station which are reporting.

APPENDIX A

OBSERVATIONS OF MESOSCALE WINDS IN LOWER COOK
INLET, ALASKA - MARCH 1978

S. Allen Macklin
Pacific Marine Environmental Laboratory

CONTENTS

	Page
Abstract	
1. Introduction	A1
1.1 Geographical Setting	A1
1.2 Physical Processes	A2
2. Data Acquisition and Reduction	A3
3. Climatic and Synoptic Background	A5
3.1 Climatic Summary - March	A5
3.2 Synoptic Summary - March 1978	A6
4. Discussion	A7
4.1 Orographic Channeling	A7
4.2 Drainage Winds	A10
4.3 Wake Winds	A11
5. Summary	A12
6. Acknowledgements	A13
7. References	A14
8. List of figures	A17

ABSTRACT

Surface wind data were collected and analyzed for the lower Cook Inlet region in March 1978. The dominant surface air circulation is due to pressure gradient forcing along two nearly orthogonal orographic channels. As much as 84% of surface air movement observed in lower Cook Inlet can be explained in terms of this flow. Additional meso-scale flows of katabatic and lee wave nature were identified at Kachemak Bay, Cape Douglas and Augustine Island.

1. Introduction

With the advent of oil exploration in lower Cook Inlet and the accompanying hazard of oil spills, it is important to gain a more complete understanding of the regional surface wind circulation. The local economic base is predominantly dependent upon the abundant fishing and crabbing industry of lower Cook Inlet. If this industry is to be protected, accurate assessment of oil spill movement must be a real capability. A precursor of this capability is the knowledge of Cook Inlet air movement in response to large and small scale meteorological forcing. An accurate knowledge of coastal winds is also important in determining shallow water circulations in estuaries and on the continental shelf (Csanady, 1976; Schumacher et al., 1978; Muench et al., 1978), in charting the distribution of marine larval species, and in providing accurate wind information to both aeronautical and marine navigators.

1.1 Geographical Setting

Cook Inlet (Fig. 1) lies in south central Alaska; the city of Anchorage and the Talkeetna plain are situated to the north, the Kenai peninsula borders Cook Inlet on the east. These areas are among the most populated and developed in the state. However, the western side of the Inlet is quite remote and unpopulated. The Inlet is connected to the Gulf of Alaska by Kennedy and Stevenson Entrances (separated by the Barren Islands) to the southeast, and by Shelikof Strait (situated west of the Kodiak archipelago) to the south. Major estuaries include Knik and Turnagain Arms in upper Cook Inlet and Kamishak and Kachemak Bays in lower Cook Inlet. Water depths in the Inlet are less than 100 m, except in the southern portion where the depth ranges between 100 and 200 m. Winter ice conditions on Cook Inlet occur over the period late October

to mid May. The most severe ice buildup is found in January when ice thicknesses may approach 80 cm and extend as far south as Anchor Point. Kachemak and Kamishak Bays also experience ice cover (Hutcheon, 1972a, 1972b, 1973).

Much of Cook Inlet is bordered by mountains. To the north lies the formidable Alaska Range. To the east the Talkeetna and Kenai Mountains flank a 40 km wide coastal plain extending from Turnagain Arm south to Kachemak Bay. To the west lie the Chigmit Mountains and the Aleutian Range. Augustine Island, an active volcano, rises to a height of 1300 m in Kamishak Bay; the Barren Islands range from 400 to 600 m in elevation. The Kodiak Island archipelago is also mountainous ranging in elevation from 750 to 1400 m.

The elevation contours of figure 1 indicate that a major axis extends from the Talkeetna plain north of Anchorage south-southwestward down the Inlet into Shelikof Strait. This channel is bounded on the east by the Talkeetna and Kenai Mountains, Afognak and Kodiak Islands and on the west by the Alaska and Aleutian Ranges. The only breaks in the mountain barrier occur at Kennedy and Stevenson Entrances (north and south of the Barren Islands, respectively) where Cook Inlet and the Gulf of Alaska meet, and at the Kamishak Gap, a region of relatively low elevation between Iliamna Lake and Kamishak Bay. This cross Inlet channel constitutes a minor orographic axis.

1.2 Physical Processes

This report focuses on meteorological phenomena produced by the interaction of the atmosphere with its underlying surface. Some of these events stem from the change in terrain elevation and roughness, others result from thermal variations of the terrain. Because of the

A3.

small spatial scales over which these flows occur (Cook Inlet extends about 250 km in its longest dimension) they are generally unpredictable by the synoptic mesh currently employed by the National Weather Service and thus definable as mesoscale events.

Two dominant processes are suggested by initial assessment of the region and first-hand interviews with local weather forecasters, mariners and aviators. Because of the rugged terrain, wind fields produced by orographic channeling, deflection or blockage of synoptic air motions are prevalent in the region. Due to the nature of forcing, this flow is strongly dependent on the magnitude and orientation of the local pressure gradient (Weber). Strong accelerations can be encountered which may persist some distance offshore. The second process, drainage or katabatic flow, results from the strong atmospheric heat sink afforded by the permanently cold underlying glacial surfaces or radiatively-cooled surfaces of the mountains. The resulting dense air adjacent to the surface flows downhill and is often focused into local jets by the orography. Velocities can exceed 50 m/s and extend for some tens of kilometers off the coast (Reynolds et al., 1978).

2. Data Acquisition and Reduction

Several agencies of the National Oceanic and Atmospheric Administration supplied data for this study. The National Weather Service, Alaska Region, furnished hourly surface meteorological observations from stations at King Salmon, Anchorage, Kenai, Homer and Iliamna for the month of March 1978. Additionally, NWS provided hand-drawn sea-level pressure analyses of the Alaskan region at six hour intervals for most of the month. Environmental buoy EB-46007 (Fig. 1), installed by NOAA's Data Buoy Office, sampled marine surface meteorological data every three hours over the period March 6

through March 31. Hourly surface marine weather data were also routinely observed and logged by the NOAA research vessels DISCOVERER and SURVEYOR which were carrying out oceanographic operations in March.

For this study, NWS data were used directly from the reporting logs. Observed sea level atmospheric pressure was utilized as input to a fifth-order polynomial isobaric algorithm to produce sea-level pressure patterns and geostrophic wind distributions over lower Cook Inlet (Fig. 4). A linear interpolation scheme was employed to fill missing data points in the environmental buoy data. The time series was then smoothed by a three point triangular filter. A wind vector diagram (Fig. 5) (Davis and Ekern, 1977) and time series (Fig. 6) were constructed from the filtered time series.

Supplementary observations of surface weather parameters and low-level atmospheric profiles of temperature and humidity were conducted from the SURVEYOR from March 17 to March 19. Fig. 7 describes the cruise track, open circles designate low-level profiling instrument launch sites. Profiling was accomplished with an Airsondetm system designed and manufactured by A.I.R., Inc., Boulder, CO. Ascent rates were nominally 150 to 200 meters/minute. A complete data frame (time, pressure, temperature, wet bulb-temperature) was produced every 6 to 8 seconds. During post analysis, data were averaged over several points (a function of ascent and data transmittal rates) to produce data at about 30 meter increments. A time series of observed surface winds at fifteen minute intervals was generated by subtracting the ship's horizontal motion vector from the relative wind vector recorded by the ship's aerovane. This series was used to investigate the flow events documented in Figs. 8, 9, and 11.

3. Climatic and Synoptic Background

In order to fully comprehend the ensuing discussion of mesoscale processes in Cook Inlet, some feeling for the large scale flow must be generated. The climate of the south Alaska coast can roughly be divided into two regimes: winter, characterized by an inland high pressure cell and frequent storm progressions from the west along the Aleutian Islands, and summer with lower pressure over the continent and reduced storm activity. Fall and spring constitute transition periods between these two climatic states.

3.1 Climate Summary - March

The month of March may be representative either of late winter or reflect a springtime transitional state. Weather improvement is delayed by the wide expanse of ocean and lingering winter climate over Siberia. As a matter of fact, the greatest frequency of cyclogenesis in the Northern Hemisphere takes place during March in the East China Sea. (Wilson, 1978a). Many of these storms or their progeny directly affect the Alaskan region, albeit they arrive in an acclimated state.

Primary and secondary storm tracks (Fig. 3a) in the Alaska region run northeastward to the western Aleutians and into the eastern Bering Sea or parallel to the Aleutians into the Gulf of Alaska. Monthly mean wind vectors closely reflect the monthly mean sea level pressure pattern pictured in Fig. 2. Of course, caution must be exercised in interpreting such figures as the climatic mean pattern need never be realized in nature. In the mean, Cook Inlet lies in the northwestern quadrant of an elongated closed low pressure cell centered over the west central Gulf of Alaska. A second closed low pressure cell occurs further to the west.

These two centers comprise the Aleutian Low. Climatologically, average surface winds are generally channelled down the Inlet in upper Cook Inlet, but blow southeastward in lower Cook Inlet.

3.2 Synoptic Summary - March 1978

In March 1978, storm centers closely followed the western Pacific climatological paths, but varied in the eastern Pacific. The secondary track extending from central Gulf of Alaska northward to the coast (Fig. 3a) became a primary one with more travel. At the steering level a broader trough than usual occurred off the coast of Asia accompanied by a sharper trough in the Gulf of Alaska and eastern Pacific Ocean and a ridge over the mountains of western North America. The overall mean sea level pressure pattern closely paralleled climatology, although central pressures were 8 mb lower than the mean.

A blocking high, part of a warm ridge that extended across western North America, strengthened over northeastern Siberia. Warm air accompanying this ridge brought record high mean temperatures to stations near the ridge axis. Anchorage reported a $+2.8^{\circ}\text{C}$ departure from the 30 year mean for March. Lighter than normal precipitation prevailed in Alaska as a result of the ridging. Kodiak reported 92% and Anchorage 83% of normal monthly precipitation (Wilson, 1978b; Taubensee, 1978). Lower Cook Inlet was relatively ice free.

Cook Inlet came under the meteorological influence of seven cyclones during March. The storm tracks are presented in Fig. 3b. These storms arrived in two waves--the first spanning the period March 8 through March 21, the second from March 27 through March 31. Only one of these storms followed the primary track of Fig. 3a. The other six were equally divided between the northern tracks leading

into the north Gulf of Alaska and into the Bering Sea across the Alaskan Peninsula.

The regional sea level pressure and geostrophic wind distribution during the SURVEYOR cruise is shown in Fig. 4a and 4b. This was a quasi-stationary period with northeasterly surface winds. A complex low pressure pattern blanketed south Alaska with closed low cells in the Gulf of Alaska and south of the Aleutians (Fig. 3b).

4. Discussion

4.1 Orographic Channeling

It is apparent from Fig. 1 that the low level wind flow in Cook Inlet is orographically constrained. The atmospheric boundary layer is confined to an elongated basin about 1 km in depth and 100 km in width extending some 400 km from the NNE to the SSW. Near the southern terminus of the basin, a cross-channel some 75 km wide runs WNW-ESE from Iliamna Lake across Kamishak Bay to Kennedy and Stevenson Entrances.

The wind vector diagram for EB-46007 for March 1978 is shown in Fig. 5. As indicated by the contours, winds from three basic directions appear more frequently than others. These events represent flow down the Cook Inlet basin and bi-directional cross-channel flow at the southern end of the basin. Slight warping of the down-basin contours in the diagram suggests the possibility of some winds from Kachemak Bay.

In order to assess the amount of orographically channeled flow during the month, observed wind directions (to the nearest 10°) from the data buoy were categorized into five wind direction sectors: down-channel winds from 000° to 040° , cross-channel winds from 090° to 140° and from 270° to 310° , Kachemak Bay winds from 050° to 070° ,

A8.

and all other winds (Table 1). During March then, as much as 84% of the flow can be explained in terms of orographic channeling. About 10% of the observations stem from winds blowing out of Kachemak Bay and another 7% may be due to other mesoscale effects.

Time series of meteorological variables sampled during the month of March 1978 by the data buoy are presented in Fig. 6. The wind direction series also indicates three prevalent surface wind directions for the period: down the basin from 030° and cross-channel from 110° and 290° . These flow directions correspond to the two orographic wind axes mentioned above. The transition between directions appears to be very rapid, often less than six hours. On March 13 there is evidence of flow up the basin. This should be a rare wintertime event because of the climatic pressure distribution noted in Section 3. During the summer, however, the prevailing wind would likely be southerly (from about 200°) and flow from 030° would be the exception.

Surface wind direction is visually correlated with surface atmospheric pressure observed at the buoy. The four instances of persistent westerly flow through the Kamishak Gap (March 10, 16-17, 21-23, 29) occur when pressure is increasing. Assuming an easterly mid-latitude synoptic weather progression, this corresponds to an easterly pressure gradient. Counter flow through Kennedy and Stevenson Entrances into Cook Inlet generally occurs under a strong westerly pressure gradient, i.e. with a low pressure cell in eastern Bristol Bay. Down-basin winds occur under a relaxed gradient and during periods of continental high pressure.

Since the pressure gradient in the south coastal Alaskan region is strongly dictated by the relative positions of the many migratory cyclonic disturbances, it is a worthwhile exercise to attempt to explain the orographically-channelled surface wind in terms of storm center location.

A9.

Between 12 Z March 9 and 00Z March 10 a storm tracked eastward across lower Cook Inlet (Fig. 3b). At that time the data buoy wind direction shifted from easterly cross-channel flow to down-basin to westerly cross-channel flow. As this storm moved inland, another disturbance progressed across the Alaskan Peninsula into Bristol Bay. This caused an abrupt wind reversal at the data buoy. Easterlies persisted until this storm retrograded far enough westward to lose influence. This retrograding Bristol Bay system later generated southerly geostrophic wind as reflected in the up-basin wind observed at the data buoy. Much of the remaining flow in Cook Inlet similarly can be explained in terms of the storm center locations of Fig. 3b.

An estimate of the regional variability of the surface wind field was determined by comparing wind directions from the data buoy with those from five local observatories within a 300 km radius of the buoy. Sample periods are restricted to the four occasions of westerly flow through the Kamishak Gap. These periods comprise a total of five days or 16% of the monthly winds. Results are summarized in Table 2. The large number of samples from EB-46007 results from a sample rate twice that of the other stations.

The high degree of orographic control of westerly flow at EB-46007 is evidenced by the extremely small standard deviation in wind direction. Winds remain essentially uni-directional although they are 70 km downstream from the Kamishak Gap. In comparison, the closest station, Homer, although agreeing well in the mean, has the largest variance of any of the five stations. This is probably due to local orographic effects at Homer and the frequent occurrence of drainage winds blowing out of Kachemak Bay. Of all the stations, Iliamna agrees best with the buoy. This is not surprising, as Iliamna lies near the western end of the Kamishak Gap. It is thus likely that observed Iliamna winds are an important indicator of westerly flow in lower Cook Inlet.

4.2 Drainage Winds

Superimposed upon the orographically-channeled winds are small scale features such as drainage winds and wake flow. Drainage winds can be expected along most of the mountainous southeastern and western coasts of Cook Inlet. The magnitude of these winds is dependent upon the cold air reservoir, the local slope, and the degree of orographic funneling of the seaward flowing air. The distance of protrusion into the Inlet is a function of the external pressure gradient and the intensity of mixing generated by the air-sea temperature gradient (Reynolds et al., 1978). Drainage winds also affect the eastern side of lower Cook Inlet. These winds, however, must first transit the 40 km of Kachemak Bay or the coastal plain to the north.

Kachemak Bay often exhibits pronounced outflow winds since several glaciers terminate at its eastern end. In fact, during strong westerly winds observed at EB-46007, Homer has on occasion reported ENE winds. When the SURVEYOR occupied station at the mouth of Kachemak Bay at about 1000 Z on March 18, 1978 (Fig. 8), the overall surface wind field was down channel. For about an hour as the ship steamed out of the Bay, winds blew directly out of Kachemak Bay. These winds seemed confined to the southern portion of the Bay's mouth and ceased as the SURVEYOR moved out of the lee of Anchor Point to the north.

Some twelve hours earlier as the ship took station about 10 km from shore near Cape Douglas (Fig. 9), a strong katabatic wind was encountered. This wind originated from Mt. Douglas (2100 m) and funneled out the valley portrayed in the figure. The width of the valley mouth at the coast and the width of the flow at the ship station are on the order of 2 km. A comparison of vertical potential temperature profiles at this station and over open water at the

north end of Shelikof Strait is presented in Fig. 10. The two soundings are similar in structure from about 300 or 400 m upward. From about 200 to 300 m the Cape Douglas sounding exhibits a strong stable layer indicative of katabatic flow. This layer has been eroded from the surface to 200 m in the 10 km passage from the coast to the station by the upward surface heat flux. EB-46007 is only 40 km from this valley. It is probable that conditions exist under which the katabatic flow would persist as far as the data buoy.

4.3 Wake Winds

Augustine Island rises some 1300 m above sea level at the eastern edge of Kamishak Bay presenting a conic-shaped obstacle to local air flow. From theoretical and laboratory studies of flow around a circular cylinder (Hinze, 1959; Batchelor, 1967), it has been shown that the imposed pressure and velocity distributions generate vortical flow in the lee of the cylinder. Flow behind an isolated mountain must show similar characteristics. Lettau (1967) reports that at high velocities, wind speeds at mountain summits tend to average about one half of the free atmosphere speeds. This suggests that expected accelerations due to narrowing of the streamlines are overcompensated by frictional effects. According to Scorer (1967), the arc sector defining the wake in which lee effects are noticed may vary from 10° to as much as 70° in typical cases. The disturbance amplitude decreases rapidly in height (like $Z^{-\frac{1}{2}}$) and in downstream distance (like X^{-1}).

During the period in which the SURVEYOR steamed in the vicinity of Augustine Island (Fig. 11), the free stream wind ranged in direction from 320° to 020° with speeds from 3 to 8ms^{-1} . Assuming a meteorologically disturbed arc sector of 70° in the lee of the summit and considering the range in free stream wind direction, all the

observed winds to 03Z in Fig. 11 could be categorized as wake flow. No confused flow is encountered until a station occupation at about 02Z some 4 km offshore (8 summit heights downstream of the peak). Here, in an hour's time and within an area of two square km, wind direction was observed to vary over nearly 360° thereby suggesting vortical flow induced by the mountain. No further indications of wake flow were encountered as the SURVEYOR left the lee of the island.

5. Summary

Observations from regional National Weather Service facilities, from Environmental Buoy 46007, and from NOAA research vessels were gathered and analyzed for the month of March 1978 in an attempt to describe the surface wind field of lower Cook Inlet. The climatic and synoptic state during the observation period was assessed to facilitate a more complete comprehension of the acting mesoscale processes.

The topography of Cook Inlet forms two nearly orthogonal wind axes which cross in lower Cook Inlet. The major axis extends from Anchorage in the NNE into Shelikof Strait in the SSW. The cross-channel axis begins at Iliamna Lake on the west, passing through the Kamishak Gap, across lower Cook Inlet and through Kennedy and Stevenson Entrances.

Pressure gradient driven flow in these orographic channels may explain as much as 84% of the surface wind measured in lower Cook Inlet by the data buoy. A regional analysis of surface winds during westerly outbreaks in lower Cook Inlet indicated the persistence of wind direction from the Kamishak Gap and the difficulty in predicting this flow from surface wind observations at nearby NWS stations. Several smaller-scale meteorological flows were observed during an investigatory cruise of lower Cook Inlet. These flow features were

superimposed on the larger-scale orographically-channelled winds. Katabatic winds were found blowing from Mt. Douglas and from Kachemak Bay; eddy lee flow was present in the wake of Augustine Island.

Future research will bear on correlation of the local pressure gradient with observed wind velocity and extension of the regional wind variability analysis to include winds from all directions. In order to discern the integrated effect that these mesoscale processes have on the wind circulation of lower Cook Inlet, additional observations must be made with a much more dense observational network or with the aid of research aircraft.

6. Acknowledgements

I wish to thank all who have assisted in field operations, data processing, and typing. In particular, I appreciate the efforts of E. Diemer and his staff at the Anchorage NWS Forecast Office, Captain Grunwell and the complement of the NOAA Ship SURVEYOR, and D. Wrenn for typing. I am especially thankful for the counsel and encouragement furnished by my colleagues, M. Reynolds, B. Walter and J. Schumacher.

This study was supported in part by the Bureau of Land Management through interagency agreement with the National Oceanic and Atmospheric Administration, under which a multi-year program responding to needs of petroleum development of the Alaskan Continental Shelf is managed by the Outer Continental Shelf Environmental Assessment Program (OCSEAP) Office.

7. REFERENCES

- Batchelor, G.K. (1967): An Introduction to Fluid Dynamics. University Press, New York, N.Y., 615 pp.
- Brower, William A. Jr., H.F. Diaz, A.S. Prechtel, Harold W. Searby and James L. Wise (1977): Climatic Atlas of the Outer Continental Shelf Waters and Coastal Regions of Alaska, Volume 1 Gulf of Alaska. Arctic Environmental Information and Data Center, Anchorage Alaska, Publication B-77, 439 pp.
- Csanady, G.T. (1976): Mean circulation in shallow seas. J. Geophys. Res., 81, 30: 5389-5399.
- Davis, Briant L. and Michael W. Ekern (1977): Wind fabric diagrams and their application to wind energy analysis. J. Appl. Meteor., 16, 5: 522-531.
- Hinze, J.O. (1959): Turbulence, McGraw-Hill Book Company, New York, New York, 586 pp.
- Hutcheon, Richard J. (1972a): Forecasting ice in Cook Inlet, Alaska. NOAA Tech. Memo. AR-5, 14 pp.
- _____ (1972b): Sea ice conditions in the Cook Inlet, Alaska during the 1969-70 winter. NOAA Tech. Memo. AR6, 11pp.
- _____ (1973): Sea ice conditions in the Cook Inlet, Alaska during the 1971-1972 winter. NOAA Tech. Memo., NWS AR-8, 18pp.
- Lettau, Heinz H. (1967): Small to large-scale features of boundary layer structure over mountain slopes. Proceedings of the Symposium on Mountain Meteorology, Atmospheric Science Paper 122, Colorado State University, Fort Collins, Colorado, p. 1-74.
- Muench, R.D., H.O. Mofjeld and R.L. Charnell (1978): Oceanographic conditions in lower Cook Inlet - spring and summer 1973. J. Geophys. Res., 83, C10: 5090-5098.
- Reynolds, R. Michael, Thomas R. Heister and S. Allen Macklin (1978): Coastal meteorology of the Gulf of Alaska, Icy Bay to Yakutat Bay. Contribution 383

from the NOAA/ERL Pacific Marine Environmental Laboratory, Seattle, Washington (in publication as NOAA Tech. Rpt.)

- Schumacher, J.D., R. Sillcox, D. Dreves and R.D. Muench (1978): Winter circulation and hydrography over the continental shelf of the northwest Gulf of Alaska. NOAA Tech. Rpt. ERL-404-PMEL, 31, 16 pp.
- Scorer, R.S. (1967): Causes and consequences of standing waves. Proceedings of the Symposium on Mountain Meteorology, Atmospheric Science Paper 122, Colorado State University, Fort Collins, Colorado, p. 75-101.
- Taubensee, Robert E. (1978): Weather and circulation of March 1978. Monthly Weather Review 106, 6: 909-915.
- Weber, G. Philip: Surface winds in some Alaskan coastal passes. Unpublished. Available from NWS Forecast Office, 701 C Street, Box 23, Anchorage, Alaska 99513, 15 pp.
- Wilson, Elwyn, E., Editor (1978a): Marine weather diary. Mariners Weather Log 22, 1:69-70.
- _____ (1978b): Smooth log, north Pacific weather, March and April 1978. Mariners Weather Log 22,5: 356-359.

A16.

Table 1.

CATEGORIZATION OF WIND DIRECTIONS FROM EB-46007,
MARCH 6 THROUGH MARCH 31, 1978.

FLOW TYPE	COMPASS SECTOR	NUMBER OF OBSERVATIONS	PERCENTAGE OF OBSERVATIONS
DOWN CHANNEL	000-040	74	38
EASTERLY CROSS CHANNEL	090-140	39	20
WESTERLY CROSS CHANNEL	270-310	51	26
KACHEMAK BAY	050-070	17	9
OTHER	150-260 320-350, 080	15	7
TOTAL		196	100

Table 2.

WIND DIRECTION STATISTICS FOR SIX REGIONAL STATIONS DURING
WESTERLY FLOW IN LOWER COOK INLET, MARCH 1978.

STATION	EB-46007	ILIAMNA	KING SALMON	KODIAK	HOMER	ANCHORAGE
DISTANCE FROM EB-46007	-	140	225	155	90	290
MEAN WIND DIRECTION (DEG)	285	289	327	317	297	298
STANDARD DEVIATION (DEG)	10	56	71	51	91	81
NUMBER OF SAMPLES	44	18	19	20	15	17

8. List of Figures

Figure	Caption
1	Topographic map of Cook Inlet, Alaska showing features discussed in this study.
2	Mean March sea level pressure (mb) and surface wind vectors (ms^{-1}) based on 15 or more years of data. Surface air movement is down Cook Inlet due to the presence of a low pressure cell in the Gulf of Alaska (adapted from Brower et al., 1977).
3	Storm tracks in the Alaska region: a) mean March primary (solid line) and secondary (dashed line) tracks based on 9 years of data (adapted from Brower et al., 1977); b) March 1978 storm tracks - figures indicate day of month, open circles designate the 12 Z position of the storm center, dark circles the 00 Z position, dark squares indicate stationary periods of twelve or more hours (adapted from Wilson, 1978b).
4	Computed sea level pressure (mb-1000) and geostrophic wind velocity (ms^{-1}) over the Cook Inlet region on March 18, 1978 at a) 00 Z and b) 12Z. Input data locations are indicated by diamonds in the figure.
5	Wind vector diagram constructed from EB-46007 data collected over the period March 6 - 31, 1978. Three dominant wind directions are indicated by the contours (percent observations per percent of the area of the circle).
6	Time series of wind speed, wind direction, wind vector velocity, and atmospheric pressure constructed from EB-46007 data collected over the period March 6 - 31, 1978. Three dominant wind directions are evident and are visually correlated with atmospheric pressure.
7	Cruise track of the NOAA Ship SURVEYOR over the period March 17 - 19, 1978. Open circles indicate upper air sounding stations.

A18.

- 8 Observations of surface wind velocity in the vicinity of Kachemak Bay, March 18, 1978. Surface air outflow occurs along the southern coast. A full flag on the vector shaft designates a 5 ms^{-1} wind speed, a half flag designates a 2.5 ms^{-1} wind speed.
- 9 Observations of surface wind velocity in the vicinity of Cape Douglas, March 17 - 18, 1978. Katabatic flow extends offshore from a mountain valley. Elevation contours are in feet above mean sea level.
- 10 Comparison of vertical potential profiles from airsonde ascents near Cape Douglas and in north Shelikof Strait. A remnant katabatic layer is evident below 300 m in the Cape Douglas sounding.
- 11 Observations of surface wind velocity in the vicinity of Augustine Island, March 18, 1978. Variable winds at about 02 Z suggest the presence of vortical flow in the lee of the mountain. A quarter flag on the vector shaft designates wind speed less than 1.5 ms^{-1} .

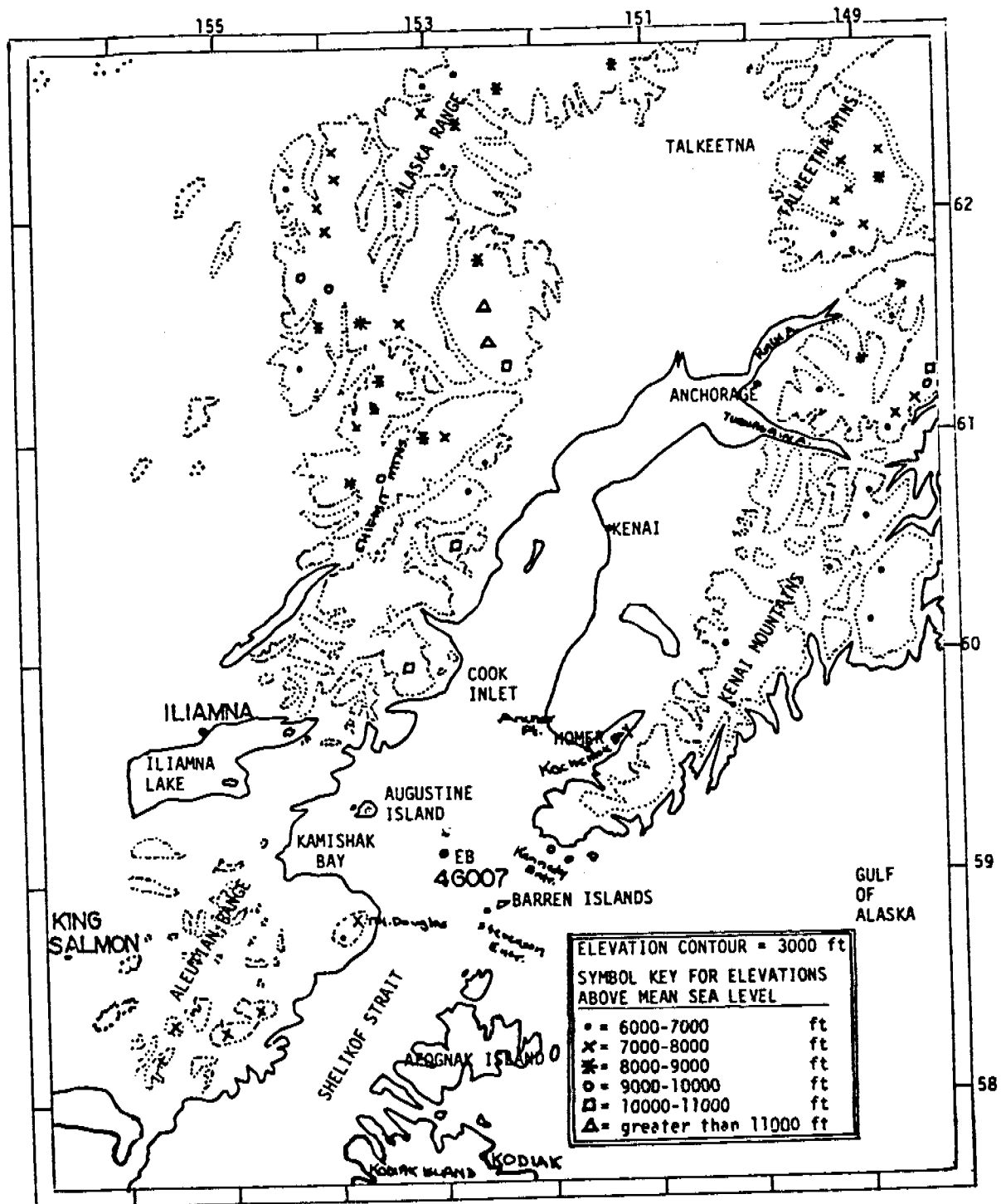


Figure 1. Topographic map of Cook Inlet, Alaska showing features discussed in this study.

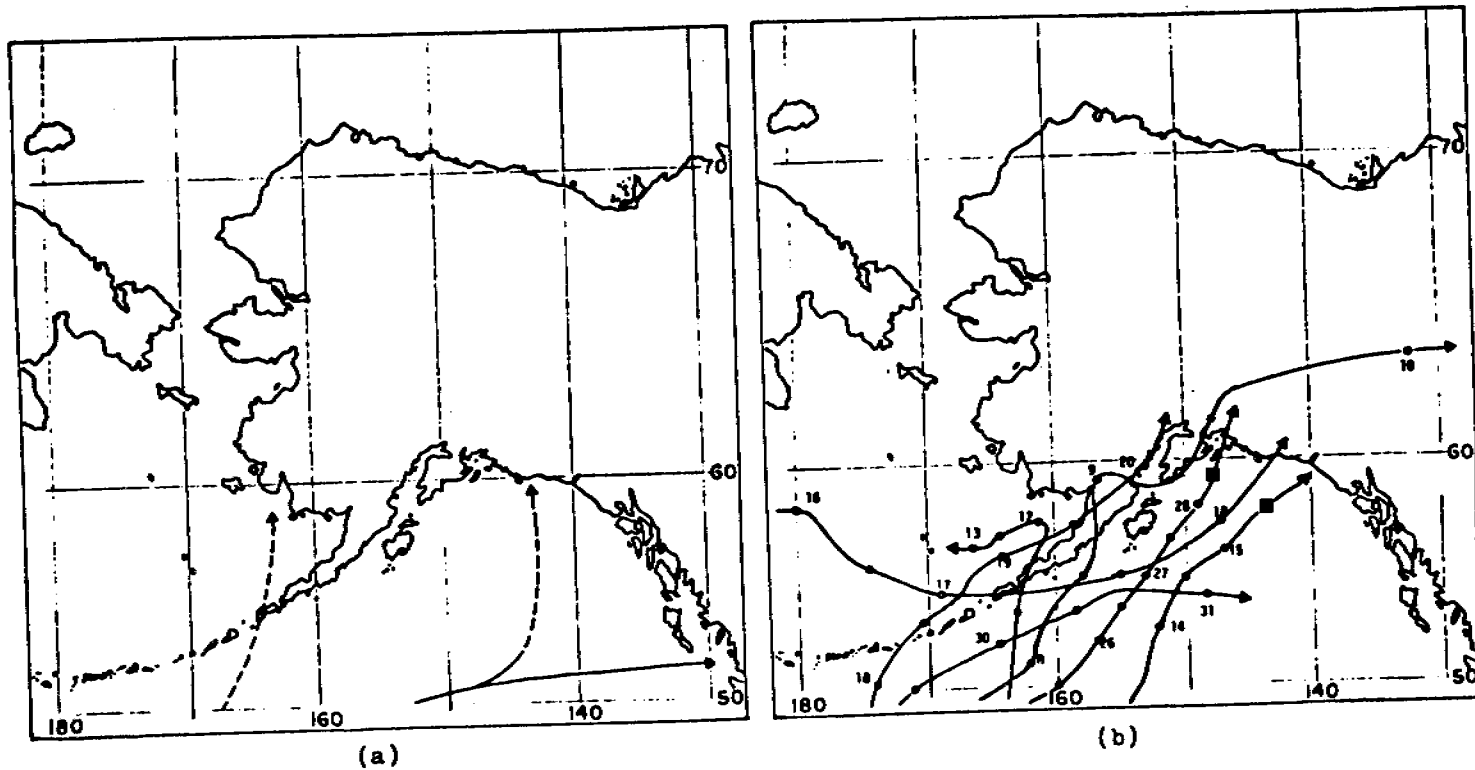
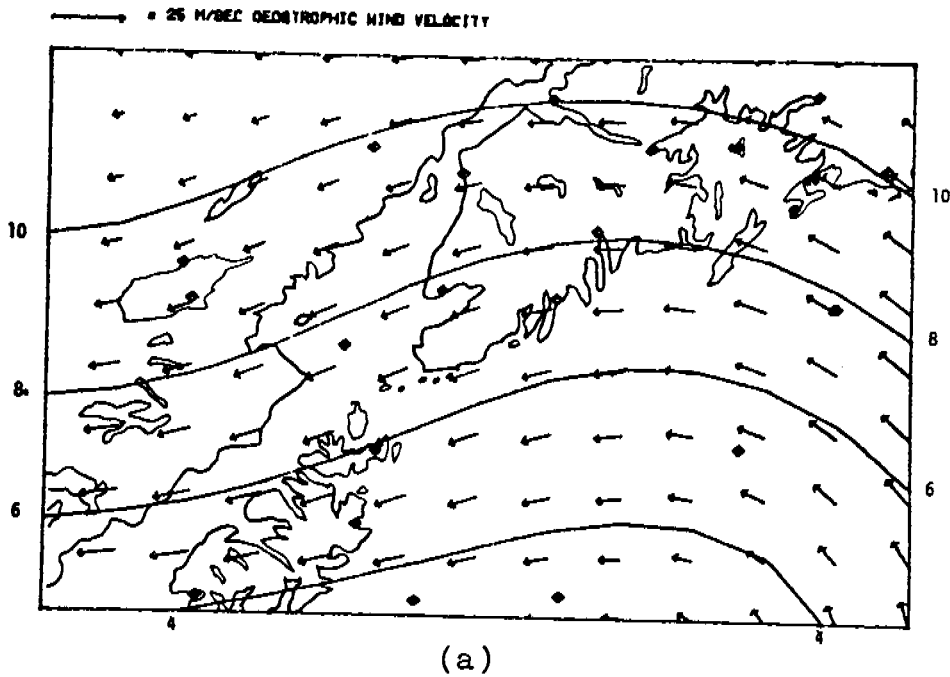


Figure 3. Storm tracks in the Alaska region: a) mean March primary (solid line) and secondary (dashed line) tracks based on 9 years of data (adapted from Brower et al., 1977); b) March 1978 storm tracks - figures indicate day of month, open circles designate the 12 Z position of the storm center, dark circles the 00 Z position, dark squares indicate stationary periods of twelve or more hours (adapted from Wilson, 1978b).

SEA LEVEL PRESSURE (MB) 5TH ORDER FIT MARCH 18, 1978 00 GMT



SEA LEVEL PRESSURE (MB) 5TH ORDER FIT MARCH 18, 1978 12 GMT

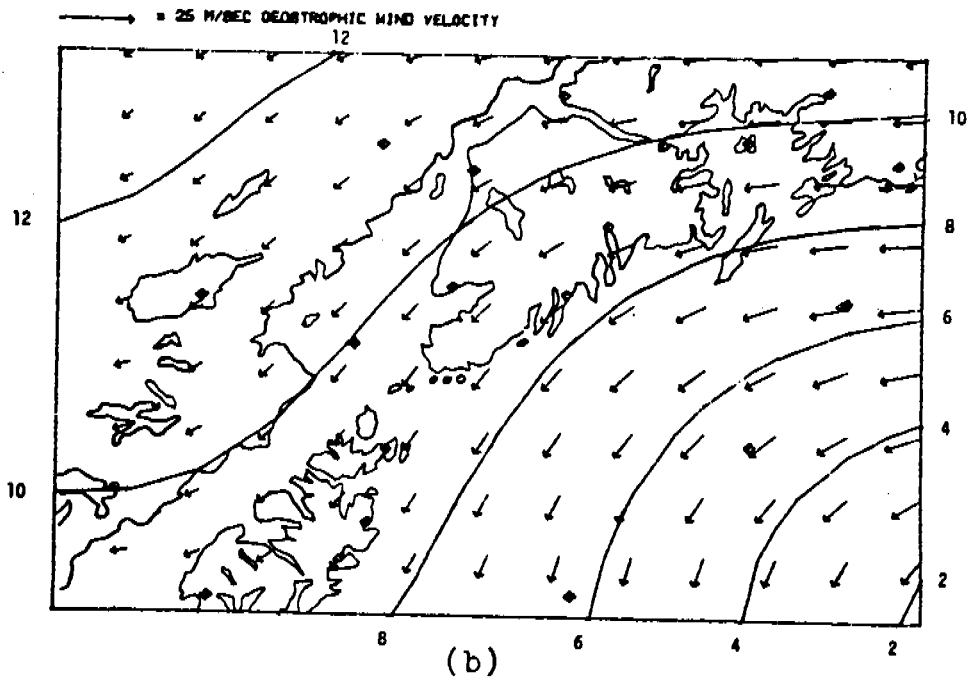


Figure 4. Computed sea level pressure (mb-1000) and geostrophic wind velocity over the Cook Inlet region on 18 March 1978 at a) 00 Z and b) 12 Z. Input data locations are indicated by \diamond .

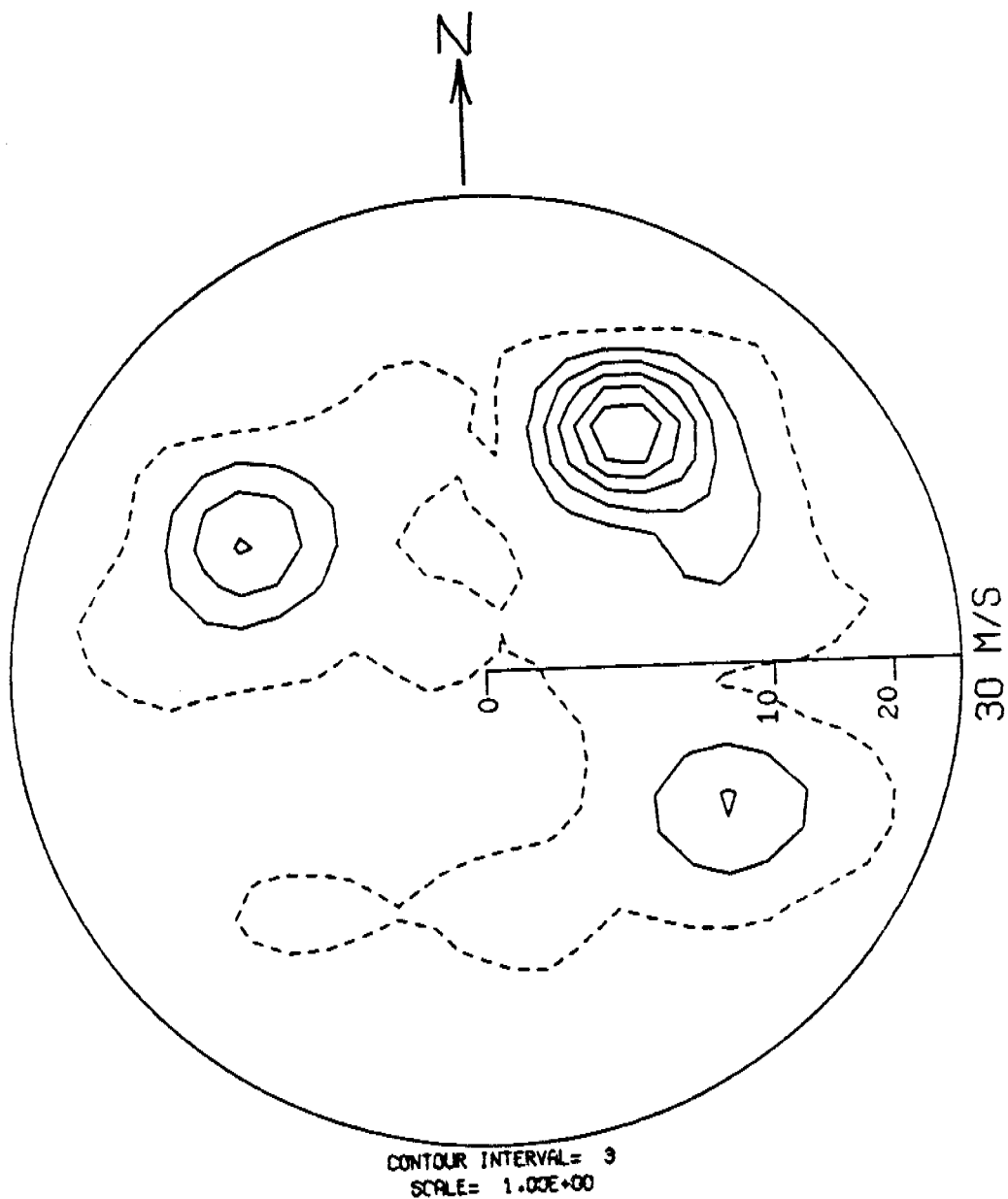


Figure 5. Wind vector diagram constructed from EB 46007 data collected over the period 6 - 31 March 1978. Three dominant wind directions are indicated by the contours (percent observations per percent of the area of the circle).

EB
46007

6 MAR THROUGH 31 MAR 1978
TIME SERIES OF 3 HOURLY DATA

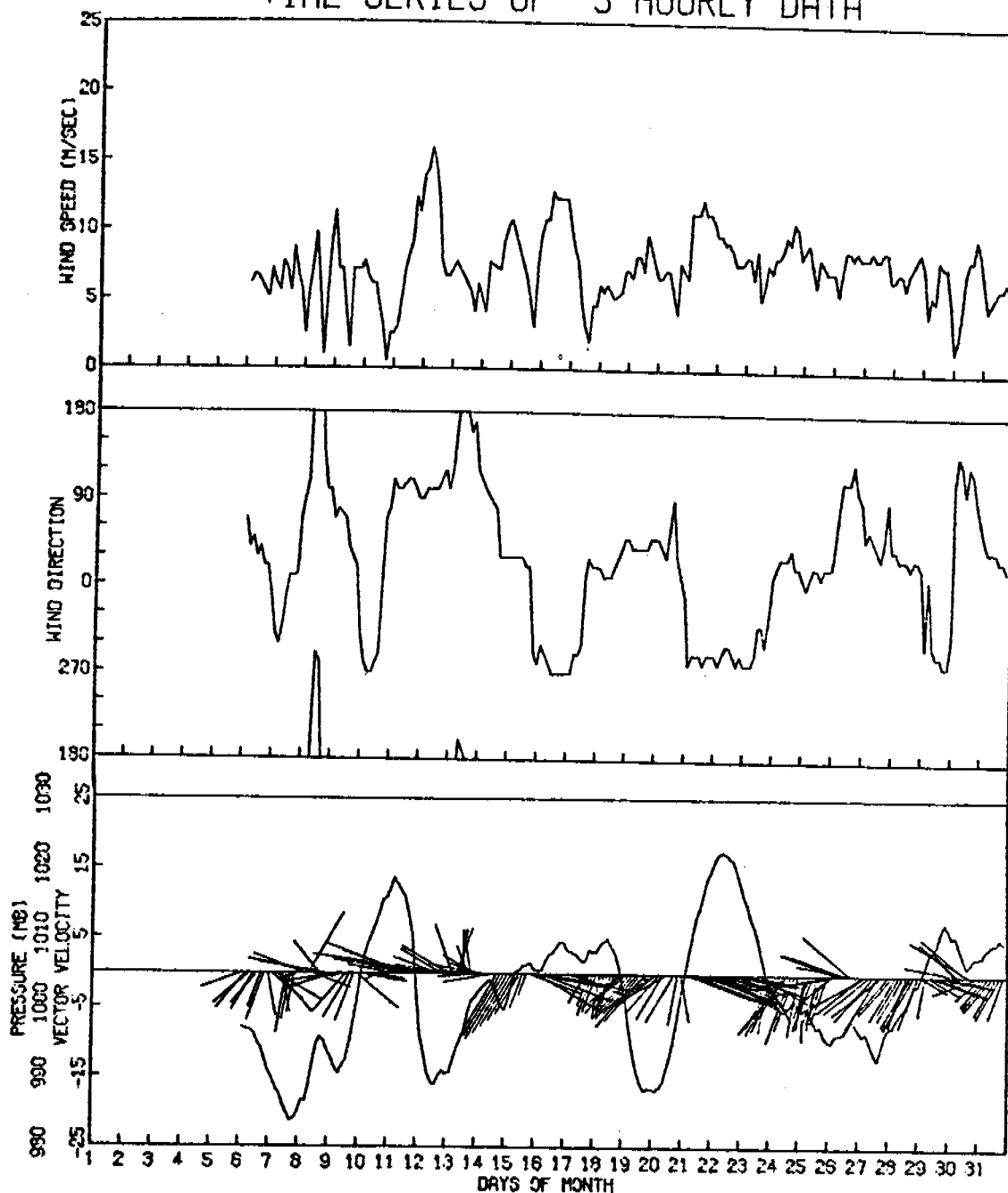


Figure 6. Time series of wind speed, wind direction, wind vector velocity, and atmospheric pressure constructed from EB 46007 data collected over the period 6 - 31 March 1978. Three dominant wind directions are evident and are visually correlated with atmospheric pressure.

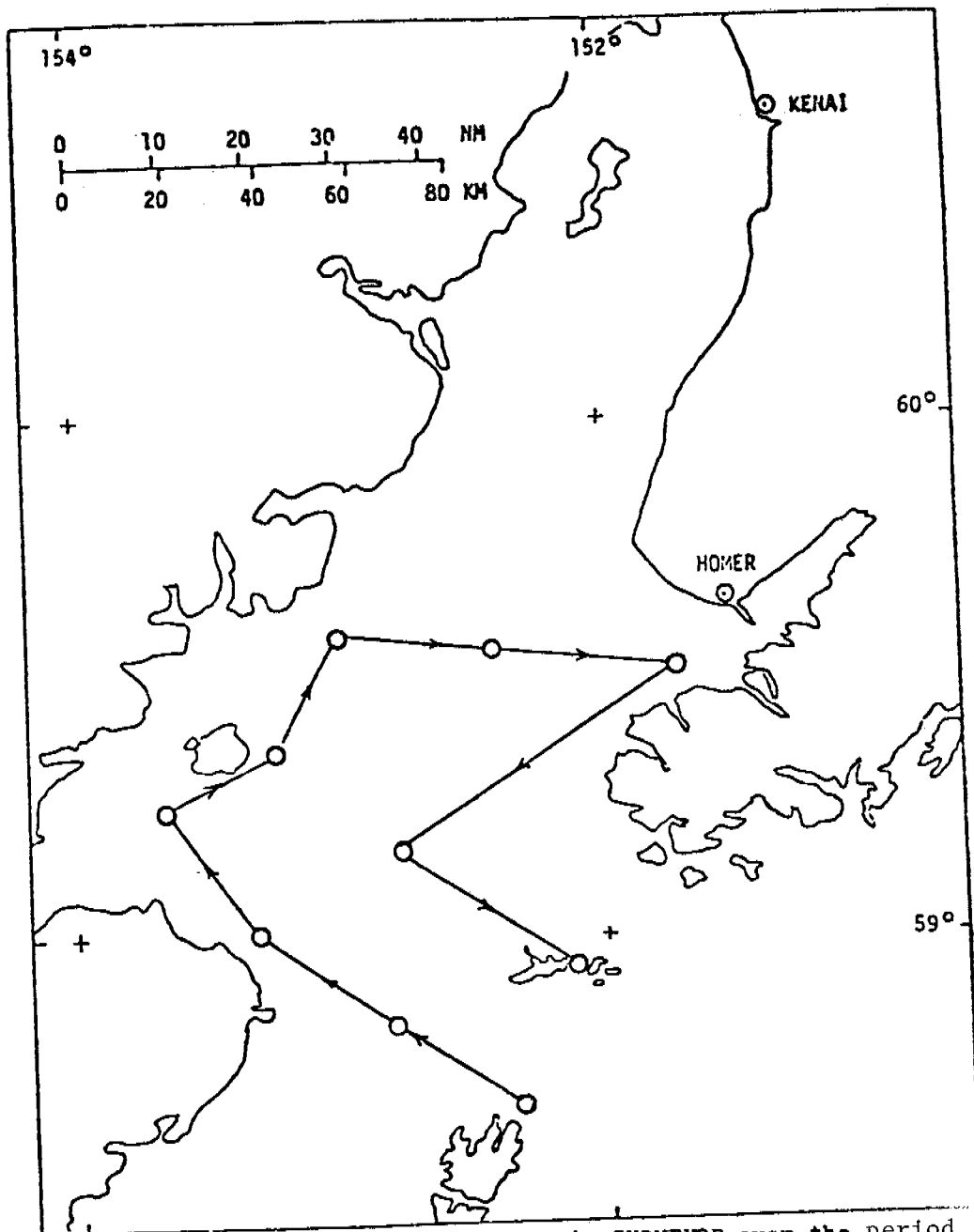


Figure 7. Cruise track of the NOAA Ship SURVEYOR over the period 17 - 19 March 1978. Open circles indicate upper air sounding stations.

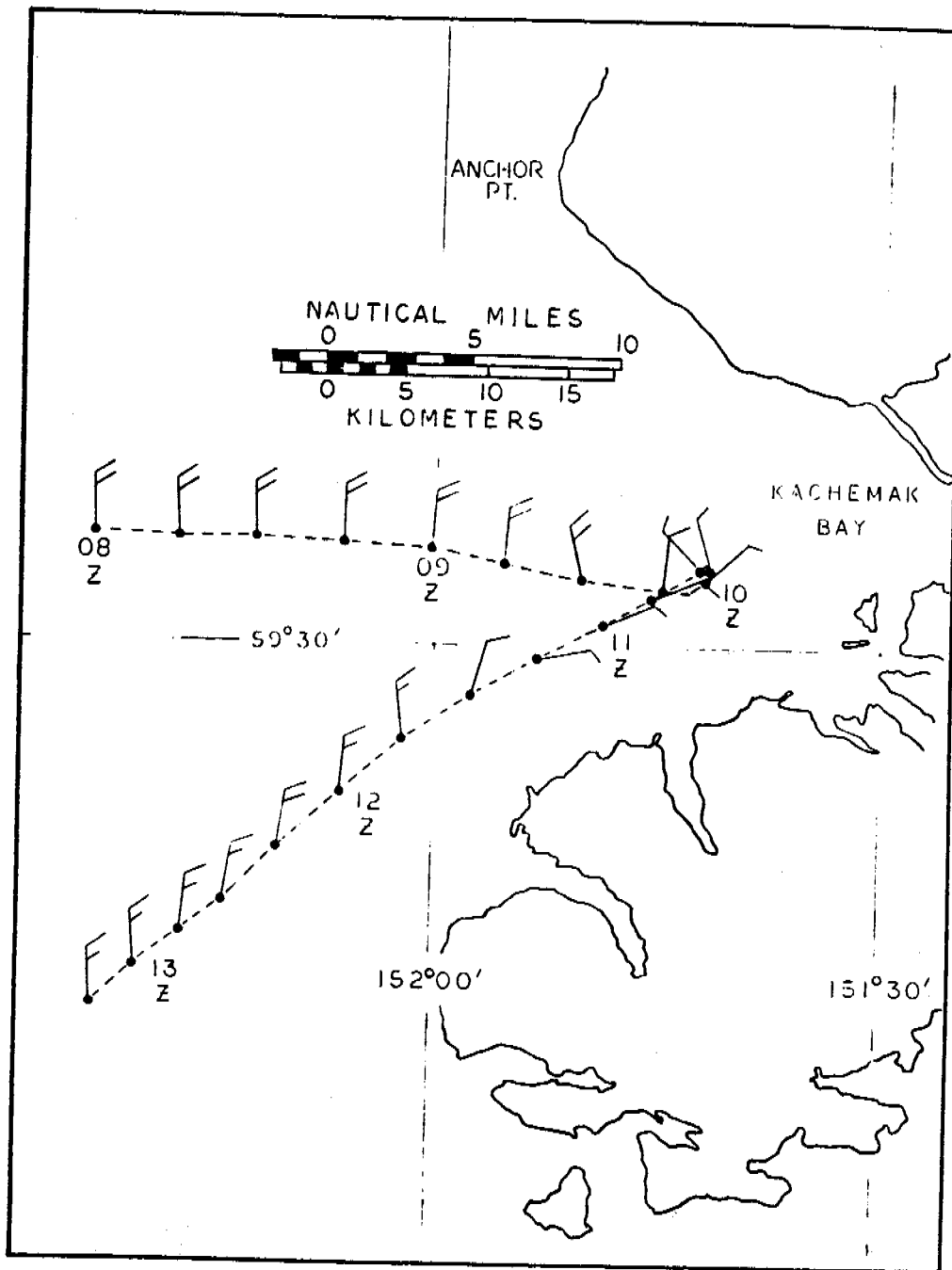


Figure 8. Observations of surface wind velocity in the vicinity of Kachemak Bay, 18 March 1978. Surface air outflow occurs along the south coast. A full flag on the vector shaft designates 5 m s^{-1} wind speed, a half flag designates 2.5 m s^{-1} wind speed.

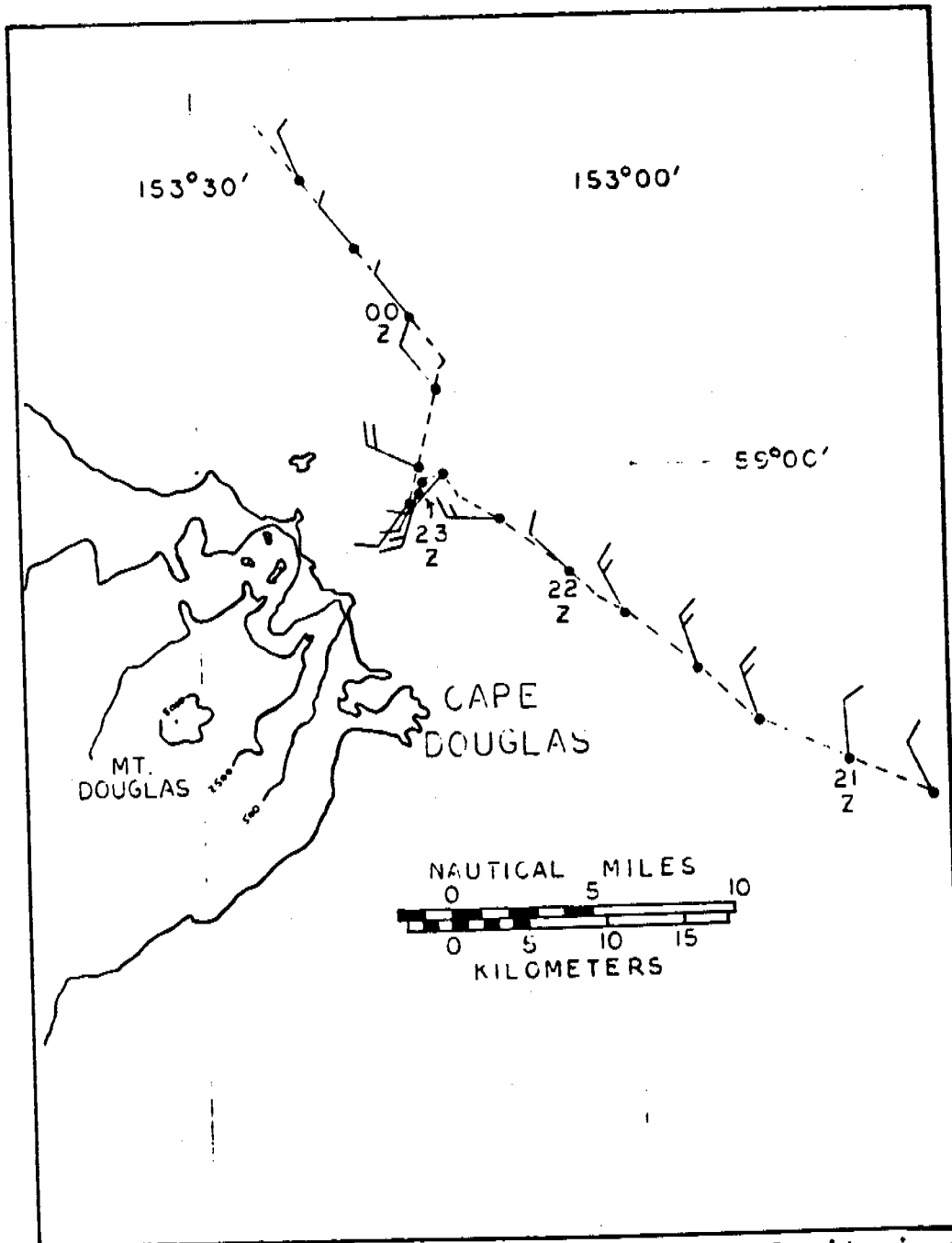


Figure 9. Observations of surface wind velocity in the vicinity of Cape Douglas, 17 - 18 March 1978. Katabatic flow extends offshore from a mountain valley. Elevation contours are in feet above mean sea level.

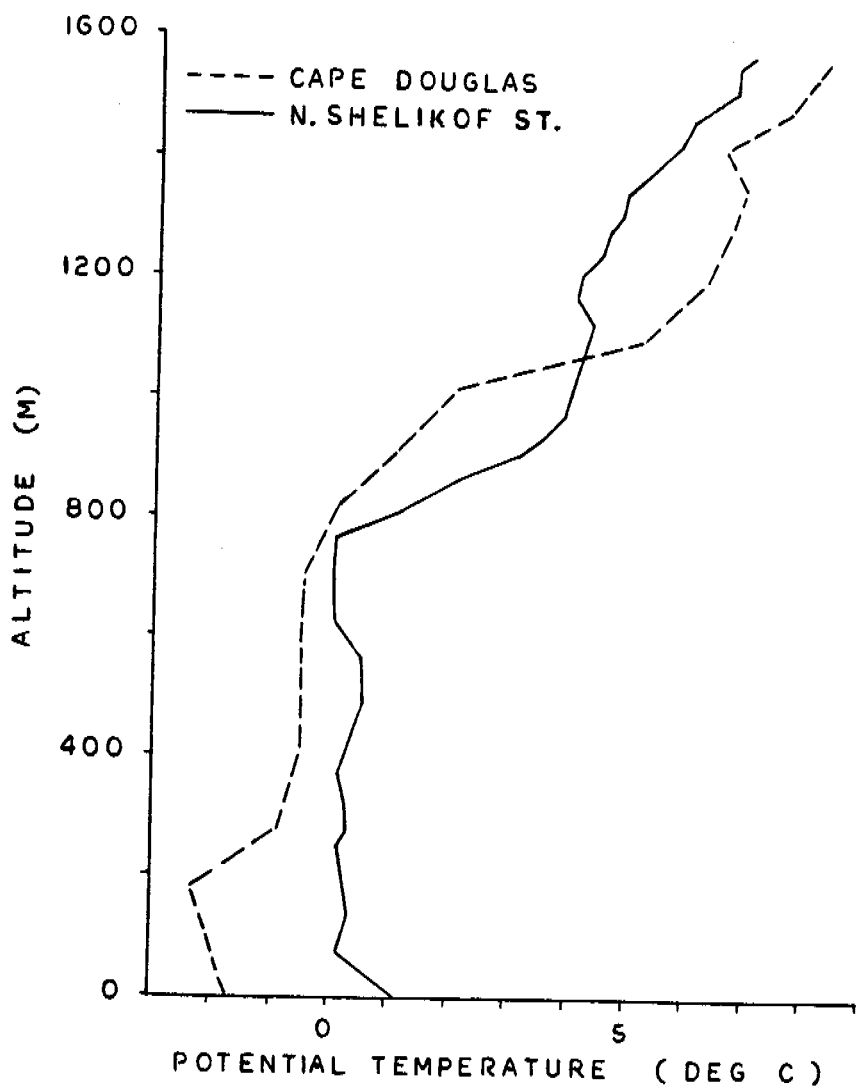


Figure 10. Comparison of vertical potential temperature profiles from airsonde ascents near Cape Douglas and in north Shelikof Strait. A remnant katabatic layer is evident below 300 m in the Cape Douglas sounding.

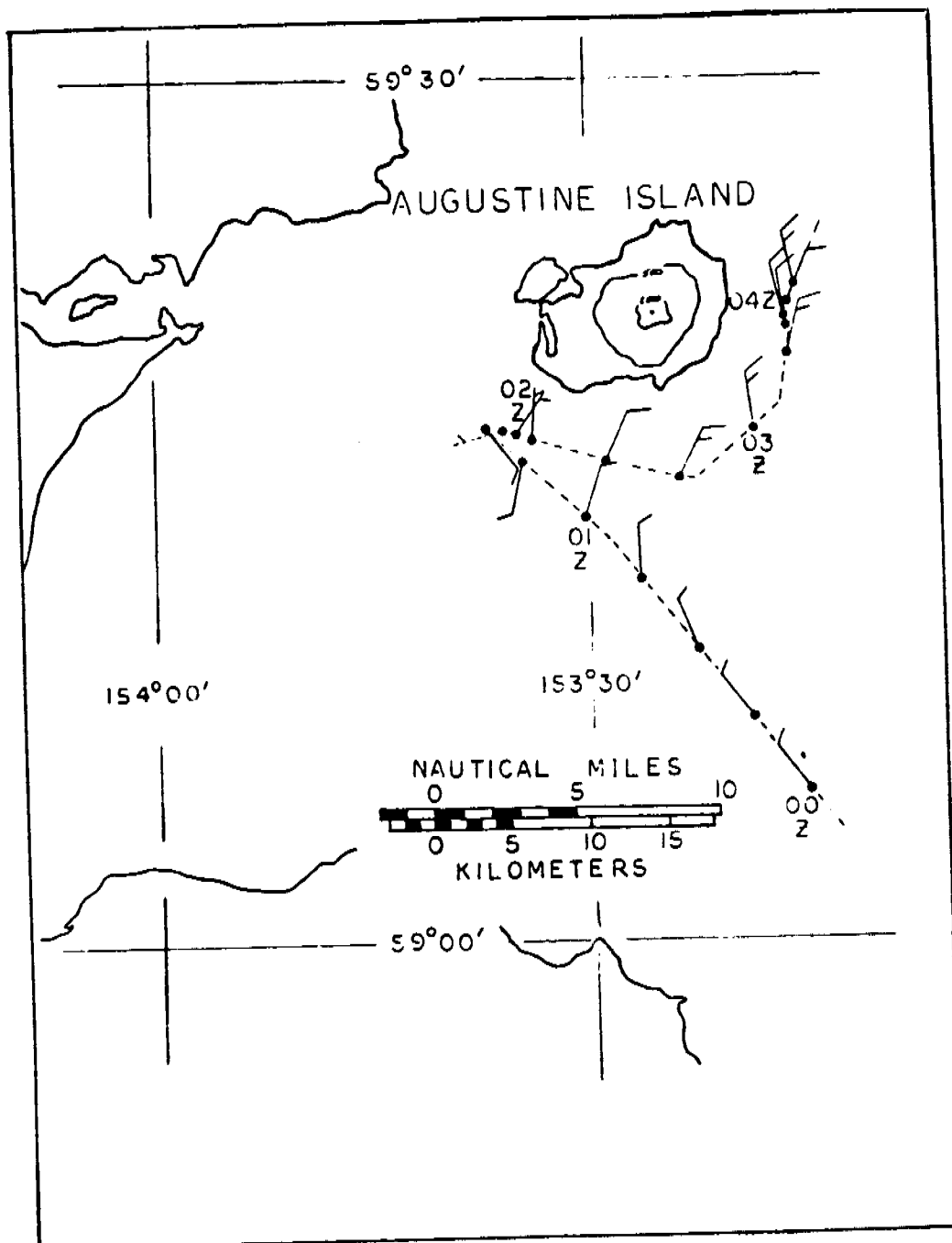


Figure 11. Observations of surface wind velocity in the vicinity of Augustine Island, 18 March 1978. Variable winds at about 02 Z suggest the presence of vortical flow in the lee of the mountain. A quarter flag on the vector shaft designates wind speed less than 1.5 m s^{-1} .

APPENDIX B
PRELIMINARY RESULTS FROM A MESOSCALE NET IN
THE LOWER COOK INLET, ALASKA

R. Michael Reynolds
Pacific Marine Environmental Laboratory

B1.
Preliminary Analysis From a Mesoscale Net in
Lower Cook Inlet, Alaska

This note is a very preliminary examination of the wind fields in lower Cook Inlet as interpreted from several recently installed weather observation facilities. Field meteorology is always a frustrating game in that it is often difficult to find any times when all instrumentation was operating together. It seems as though one or the other crucial measurement was missing at just the time when it would have been most helpful in interpreting the field.

A summary of wind conditions for lower Cook Inlet, as known to that time, was prepared by Thomas R. Hiester and S.A. Macklin and included in last year's annual report. In that report, the wind field was characterized as topographically dominated by two orographic channels, the Shelikof Strait-Inlet channel and an orthogonal channel comprised of the 'Kamishak-Iliamna Gap' to the NW and Kennedy and Stevenson entrances to the SE (hereafter referred to as the entrances). It was shown that while winds at Kenai and Homer strongly reflected the axis of the mountains along the Kenai Peninsula, those in the center of LCI were much more variable, and favored the NW-SE orientation, especially during periods of strong winds. That report also outlined several mesoscale processes which have been further considered by S.A. Macklin in Appendix A of this report.

Since that time, we have obtained more sources of data in the LCI region, data which will allow a better definition of the wind fields. At present, two oil platforms are operating in LCI, the Diamond M Dragon and the Ocean Bounty (Fig. 1). NOAA ships have made several expeditions into these waters. Winds are measured both at Homer and at the end of the Homer Spit. We have installed two meteorological stations along the west side of the inlet, at Augustine Island and Contact Point. The data buoy EB46007 has operated reliably except for a crucial period during the winter of 1977-1978. The ferry Tustumena makes

weekly tracks into LCI, and records meteorological data every four hours and at every course change. The NWS operates a remote weather station at Shuyak Island which operated rather desultorily. At present, all these sources of data are being collected and entered into the PMEL meteorological data base. A summary of the available data for this region is given in Fig. 2. Coverage is seen to be improving rapidly, and it seems that the fall and winter of 1978 are particularly well covered. Processing such a vast set of data, including some form of quality control, and finally incorporating it into the data base is an imposing task, one on which we are laboring.

We will look at only one month of data from which we have several key stations reporting, June 1978 (dashed lines in Fig. 2). Stations considered here will be Homer, EB46007, Shuyak, Augustine, Island and the ship SURVEYOR. The intent here is to whet the appetite, and the comparisons, while generally striking, must be considered only preliminary. Until more data is entered into the data base, we cannot produce analysis with consistent statistical procedures.

At the time of this writing, we are in an exciting phase of the work. We are able now to recall and plot data from the data base. As the figures in this appendix show, each new recall capability leads to an expanded understanding of the wind fields in the confused central portion of LCI.

Because of satellite failure, only the first 22 days of the month are available from the buoy. We have analyzed both Shuyak and Homer for 22 days and the entire month, and found no striking differences in the statistics. Therefore in the comparisons to follow, all stations have been analyzed over the same period of time, from the beginning of the month to 1500 on the 22nd day.

A time series analysis of EB 46007 is given in Fig. 3a-e. Winds during the month were generally light and tended to come from three of the directions outlined above. The

B3.

dominant directions in the order of their importance to surface stress were: 130° , from Stevenson Entrance; 220° , from Shelikof Strait region; and 310° , from Contact Point and the Iliamna Gap. The air-sea temperature differences are at all times small, hence thermodynamic processes play a small role in boundary layer adjustment. The progressive vector diagram (Fig. 3c) indicates a flow predominantly up the channel, from the south. This southerly flow was interrupted only occasionally by the cross channel flows out of the Kamishak Gap. There were two high wind periods during the 22 days which we consider here. One occurred from the 7th to the 9th, and the other from the 14th to the 16th. The pressure was dropping during these periods while winds were backing, indicative of a low pressure disturbance passing to the north. These were storms which tracked into the Bering Sea, the major summer storm track direction. A rapid shift in wind direction on the 8th implies a frontal passage. Fabric diagrams of the wind observations and energy (Figs. 3d-e) show that at the data buoy winds tended to come from the directions of Shelikof Strait and the entrances. Both fabric diagrams show a strongly bimodal distribution with peaks at about 5 ms^{-1} .

Augustine Island is out of the Shelikof-LCI axis and apparently did not see the SW winds from the Shelikof region. The fabric diagram for Augustine (Fig. 4b) shows only one major lobe at 135° , the direction of Stevenson Entrance. The PVD for Augustine data (Fig. 4a) thus shows a mean wind from the SE. During the wind events of the 8th and 14th the winds at Augustine were quite similar to those measured at the buoy. The implications of this correlation will be discussed in the concluding remarks of this appendix.

The wind station located on the tip of Shuyak Island sees winds from either the open sea, or SW winds from the Shelikof Straits. The fabric diagram (Fig. 5b) thus has a lobe pattern

which is somewhat different from that of EB46007. In many ways the distribution of winds resembles that of the open sea as depicted by the FNWC winds which are shown in Appendix C of this report. The winds at Shuyak appear to be much stronger than those measured in the interior of LCI, a ramification of its more exposed location. Its total wind energy (the sum of the square of the wind speeds) was approximately $3 \times 10^3 \text{ m}^2 \text{ s}^{-2}$ compared to values of about 2×10^3 for the previously mentioned locations. Aside from the two wind events which have been discussed, Shuyak shows an additional period of strong winds on the first of the month. The PVD (Fig. 5a) shows that these were northerly with a tendency for a cyclonic (CCW) rotation with time. North winds were observed over the Albatross Banks at this time although they were much weaker. However, neither EB46007 nor Augustine Island observed such winds. One implication of such a discrepancy is that some synoptic systems are of such a size or configuration that they do not penetrate into the LCI. During the wind event of the 8th, Shuyak recorded strong winds from the southwest which suddenly shifted to a northeast direction. The NE direction is different from that recorded at the same time in LCI, where SE winds were observed. The same differences were observed on the 14th which leads to speculation of a flow pattern into LCI from the east.

As we expected, Homer is a most poor indicator of the winds in LCI. During June winds were predominantly up the Kachemak Bay and had a large diurnal variation (Fig. 6a). The winds obtained an average maximum of about 5 ms^{-1} from the SW at about 00Z, or late afternoon, indicating a summertime sea breeze regime. At night the winds decreased considerably and shifted to a NE direction out of the bay. The PVD (Fig. 6b) and fabric diagram (Fig. 6c) for Homer indicate that none of the wind events observed over the water were apparent in Homer

where land-sea temperature variations dominated. It is of interest to note that such diurnal variations were all but non-existent at the position of the data buoy.

During the last few days of the analysis period, the SURVEYOR paid a visit to LCI. One of the capabilities of our data base is the incorporation of ship observations into the study. Fig. 7 shows the trackline of the ship SURVEYOR as it left Kodiak on the 19th of June, steamed to the vicinity of Montague Island, then sailed into LCI and down Shelikof Strait. Wind vectors are shown along the trackline. The length of the vectors is proportional to the wind speed, and the dot on the end of the vectors is the ship position. The vectors point in the direction toward which the wind is flowing. One of the most obvious features of this figure is the indication of winds flowing out of LCI through Kennedy and Stevenson Entrances. However, EB46007 (Fig. 3a) observed southerly winds at this time indicating this air was not from the Kamishak Gap, hence must be from Shelikof Straits. Winds at Shuyak (Fig. 5a) confirm this fact. They were relatively strong from the SW.

When comparing ships measurements to fixed site observations one must keep in mind the mixture of temporal and spatial variability which a ship trackline represents. The lengthy time required for a ship to cover an area even as small as LCI makes analysis somewhat more complicated. (We have long exhorted research aircraft as important tools in mesoscale studies.)

As the ship entered LCI the winds shifted to a southeast direction. Figs. 8a to 8d represent the comparison of the ship winds to winds observed locally at fixed sites. As the ship sailed into the inlet on 22 June, winds at Shuyak shifted in direction from SE to a SW direction out of Shelikof Strait. Winds at Augustine Island reflect the shelter provided by Mount Douglas which forms the south end of Kamishak Bay.

We will now attempt to derive hypothetical wind patterns for LCI based on the information considered thus far. The reader should bear in mind that we have considered one month only, and have only examined the most salient features of the data available for the month. Fig. 9a-c are wind patterns which we feel best represent the winds observed during the month of June 1978. They will provide us with a working hypothesis against which to test future analysis.

When winds flow through the Kamishak Gap, indicative of a low center in the Gulf of Ak., the flow is observed all the way across the LCI and well into the Gulf of Alaska (Fig. 9a). Meanwhile, winds are strong and up the Shelikof Strait turning out the entrances and enhancing the gap winds in the vicinity of the Barren Islands. Gap winds generally turn up the Cook Inlet during these conditions a feature which has been observed in several satellite photographs.

With a different synoptic forcing, gap winds are not evident even though strong winds blow up Shelikof Strait. During these conditions, winds can be strong in the Barren Islands region, yet light and variable in LCI (Fig. 9b). LCI winds are generally SW up the axis, but turn around Cape Douglas yielding SE winds in the vicinity of Augustine.

With a low center in the Aleutian Island region winds will often flow in to LCI from the SE, through the entrances. At Shuyak, these winds will be easterly turning to flow down the Shelikof Strait. During these conditions the flow is apparently divergent in the vicinity of EB46007 producing weak and variable winds in the central regions.

Land stations such as Homer and Kenai are severely affected by land-sea temperature differences and orographic channeling. The observed directions at these sites bears little if any correlation with the offshore observations.

In summary, the wind patterns proposed above appear to

B6.

accurately describe the observed winds during June 1978. Future analysis will determine if these wind patterns can be associated with particular synoptic scale patterns, and how seasonal they might be. It should be noted that they differ significantly from the wind patterns suggested by Dames and Moore, Inc., and thus if substantiated, lead to significantly different oil spill trajectories and surface stress.

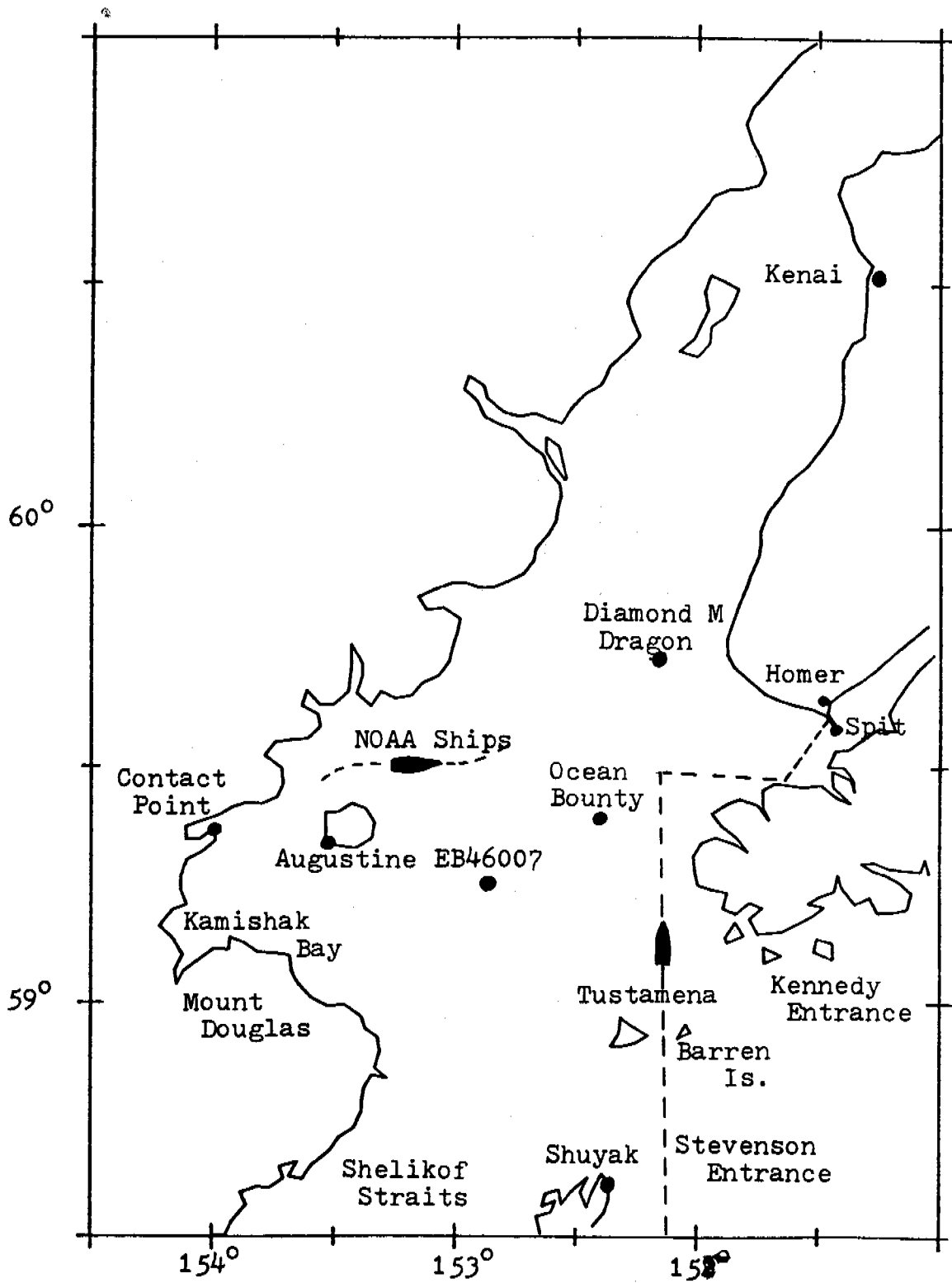
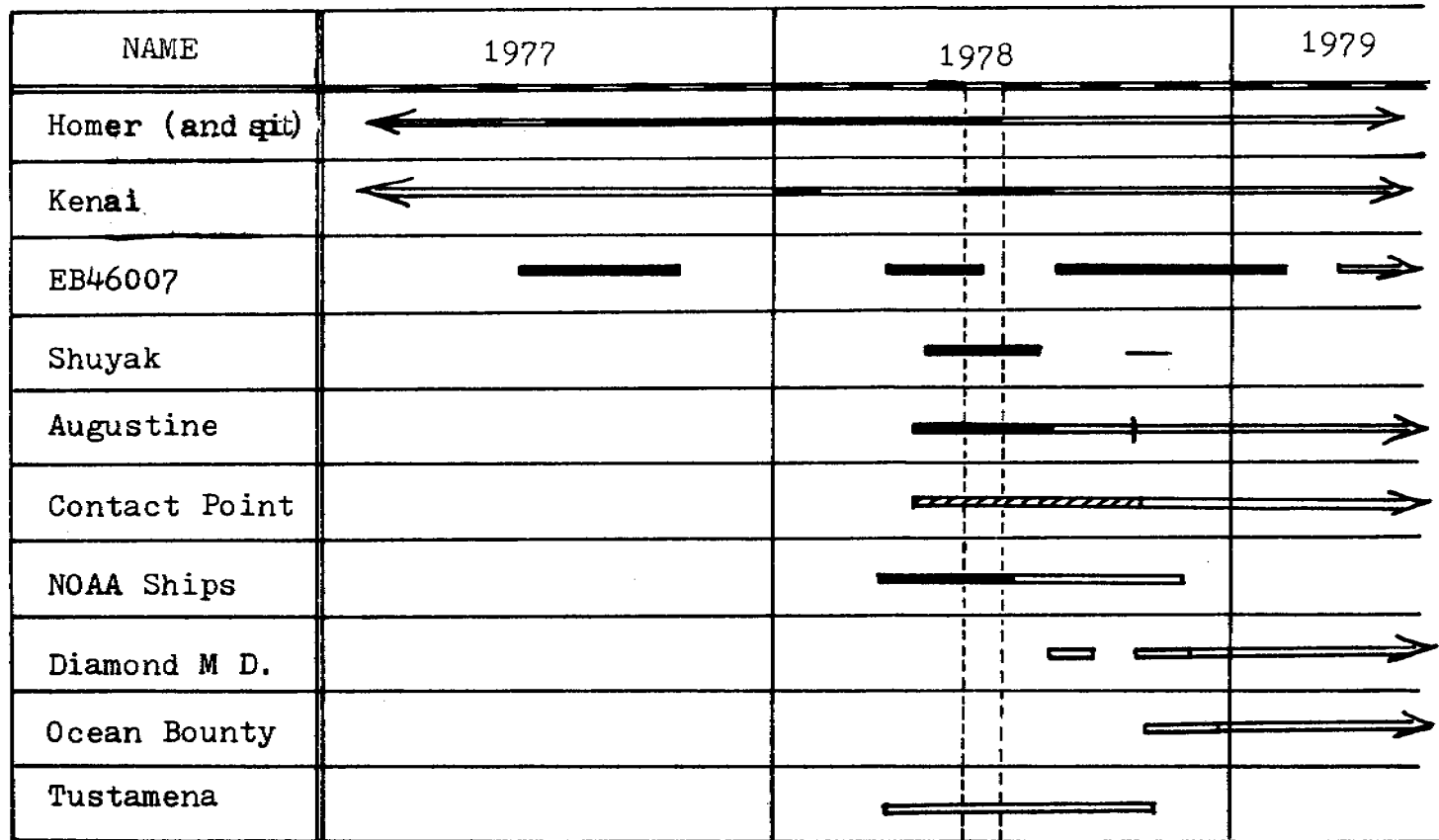


Figure 1. Map of Lower Cook Inlet showing geographic locations and sources of meteorological data.



————— Data Available
 ————— Data in Data Base
 / / / / / Problems in data

Figure 2. Chart showing sources of data for LCI and their status.

TIME SERIES OF 6 HOURLY DATA

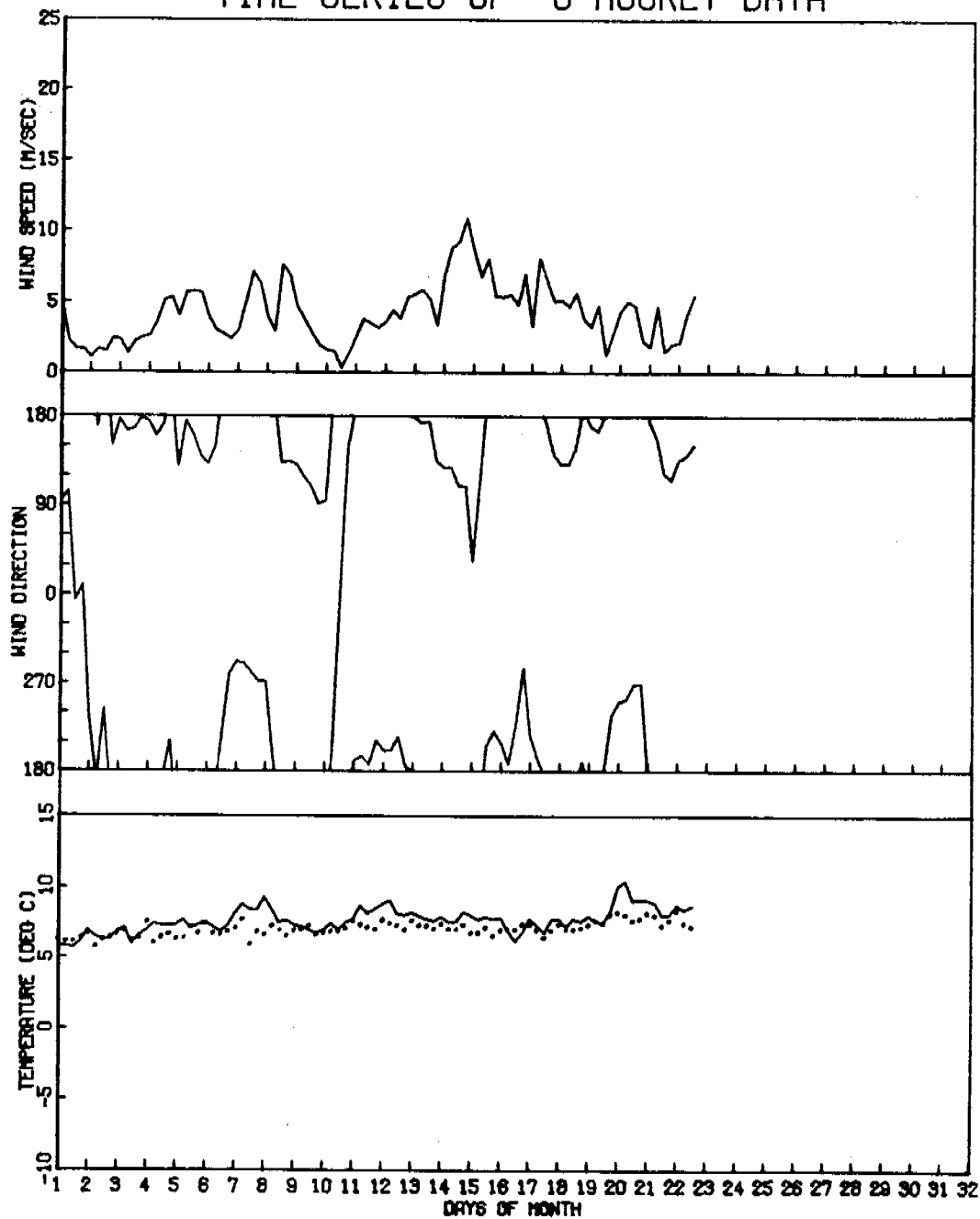


Figure 3a. Time series plot for EB46007 located in central lower Cook Inlet. Shown above are wind speed, direction, air temperature, and water bulk temperature. Data has been smoothed with a simple triangular kernel with a six hour time constant.

18

1 JUN THROUGH 22 JUN 78

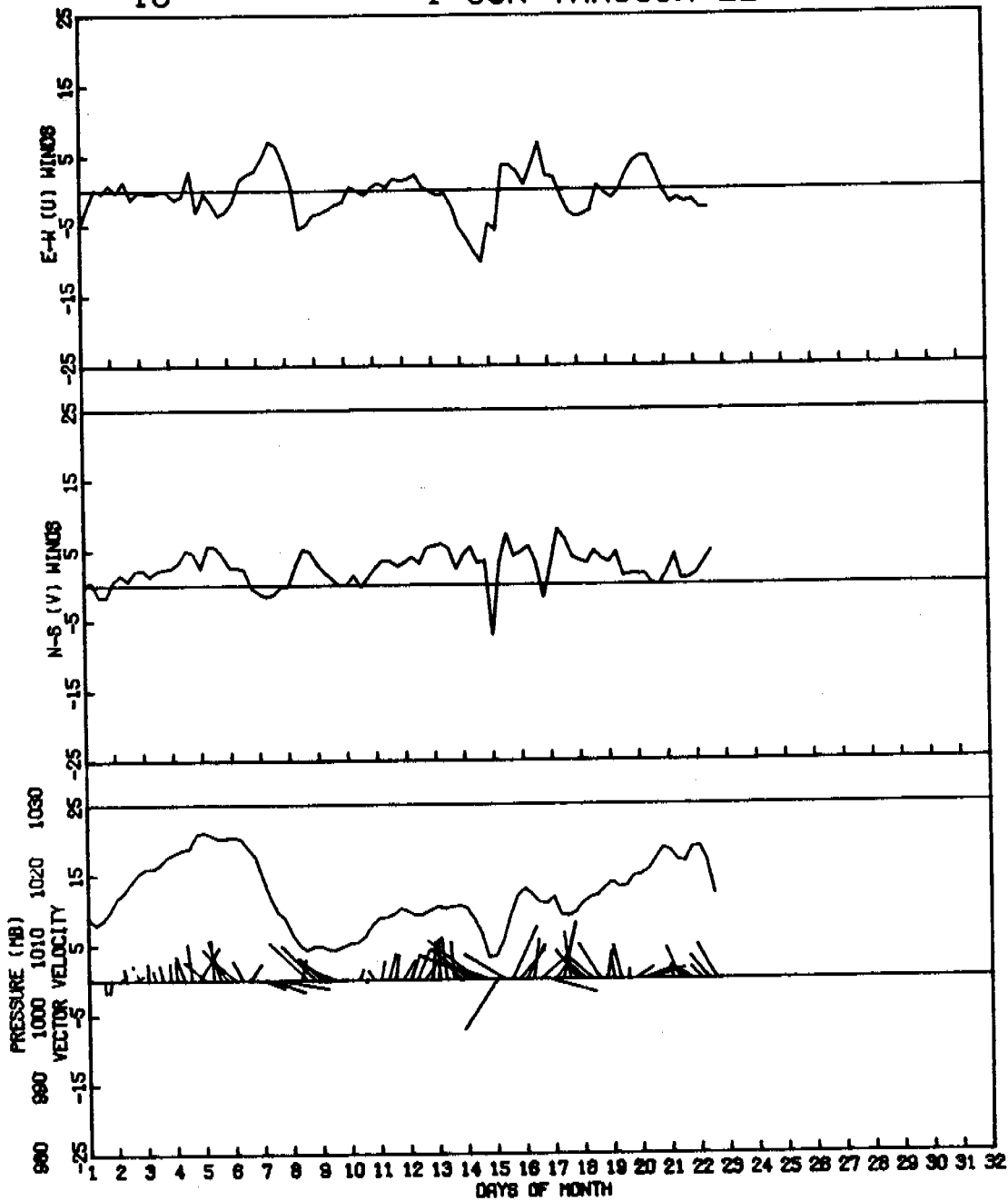


Figure 3b. Time series plot for EB46007 located in lower Cook Inlet. Vector U and V components, vector sticks, and measured pressure are shown.

MEAN V= 2.50 M/S

MEAN U= -.37 M/S

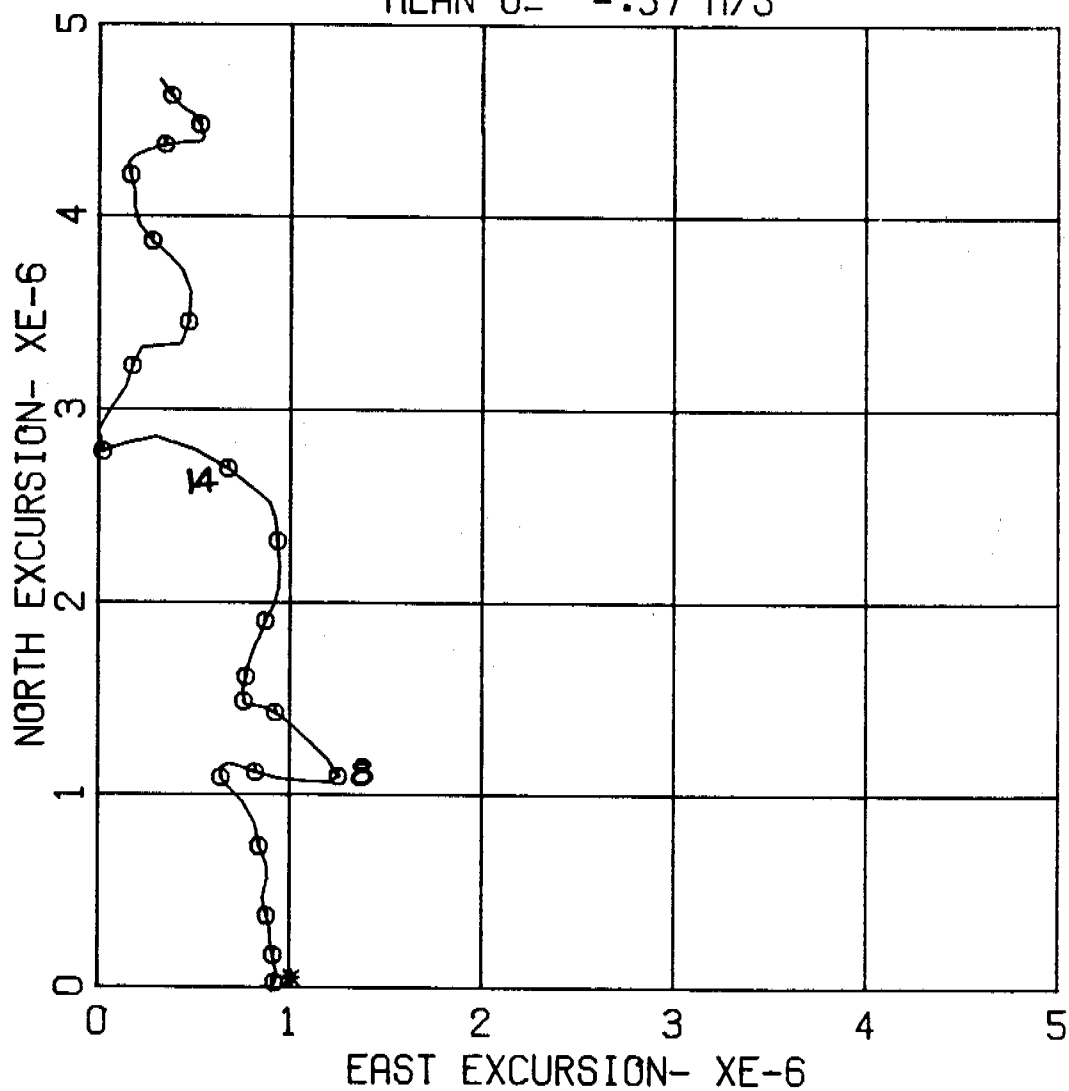


Figure 3c. A Progressive Vector Diagram for the data shown in Fig. 3a. Open circles represent the days, the line begins with the star. Distances are in meters.

WIND FABRIC DIAGRAM FOR 87 POINTS.

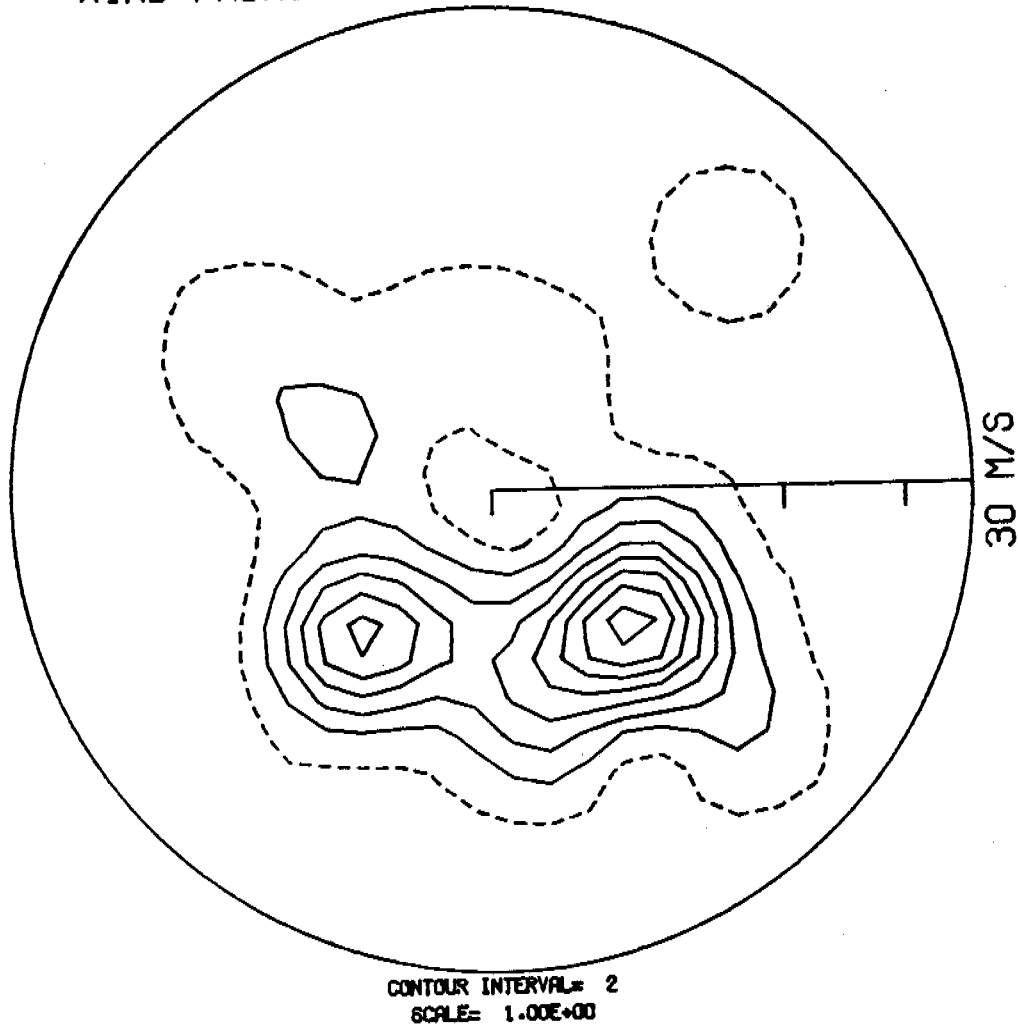


Figure 3d. Fabric diagram of the frequency of wind observations. Contours are dimensioned in units of percent observations per percent of the area of the circle. Speed is proportional to the square of the radius to account for radial spreading. The dashed lines delineate regions of no observed winds.

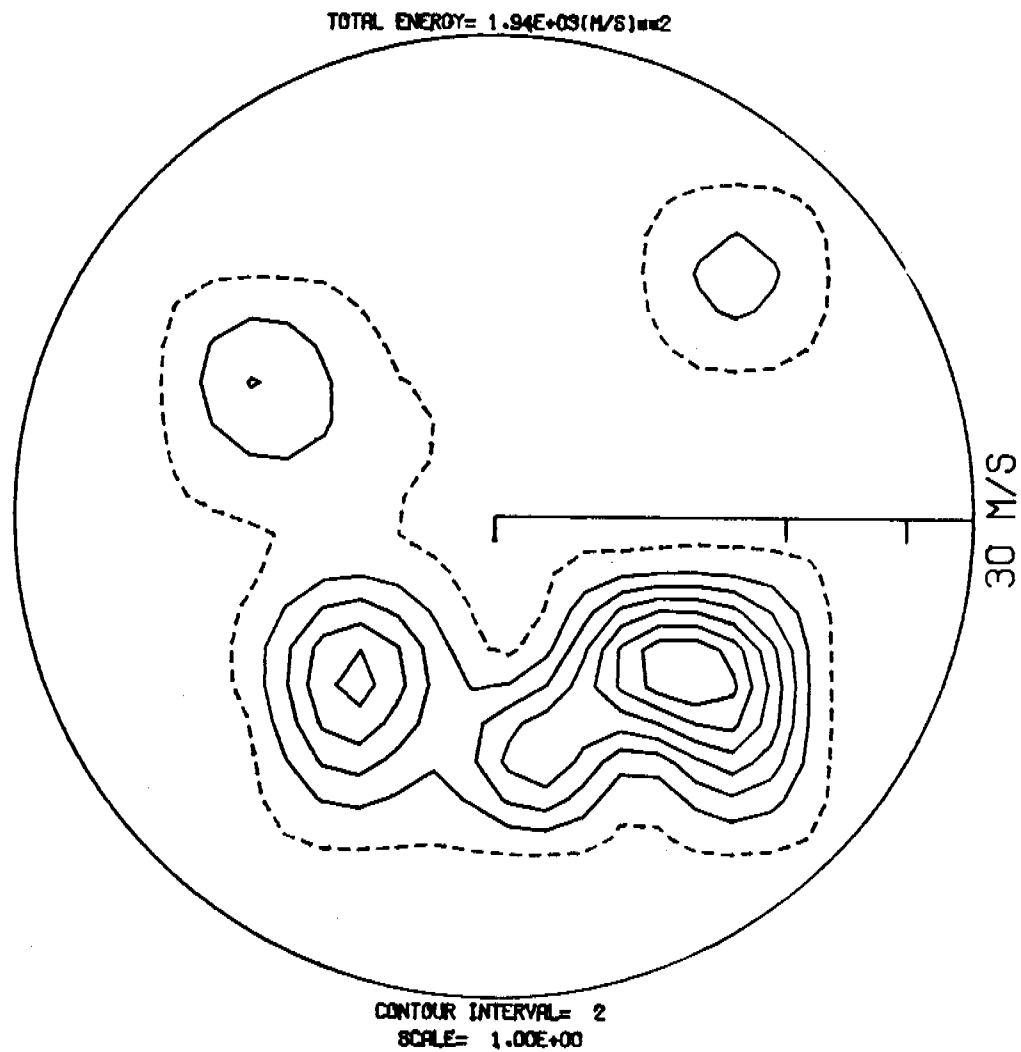


Figure 3e. Fabric diagram of the observed energy (square of the wind speed). Contours represent percent of the total energy per percent of the area of the circle.

23

1 JUN THROUGH 25 JUN 78

MEAN V= 1.30 M/S

MEAN U= -1.17 M/S

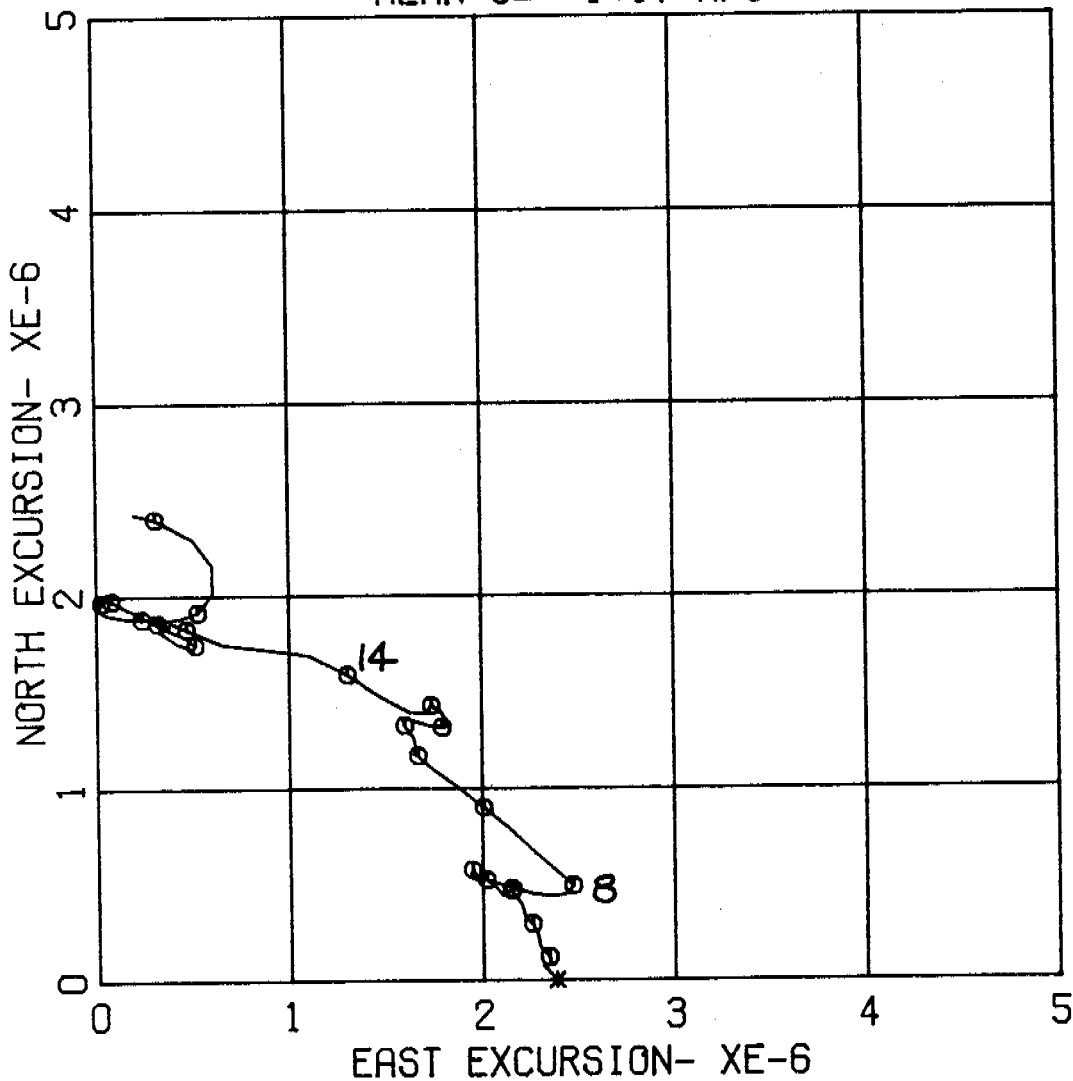


Figure 4a. Progressive vector diagram for winds measured at Augustine Island from 1-22 June 1978. Circles mark the time of days, the star represents the start. The 8th and 14th are marked.

WIND FABRIC DIAGRAM FOR 87 POINTS.

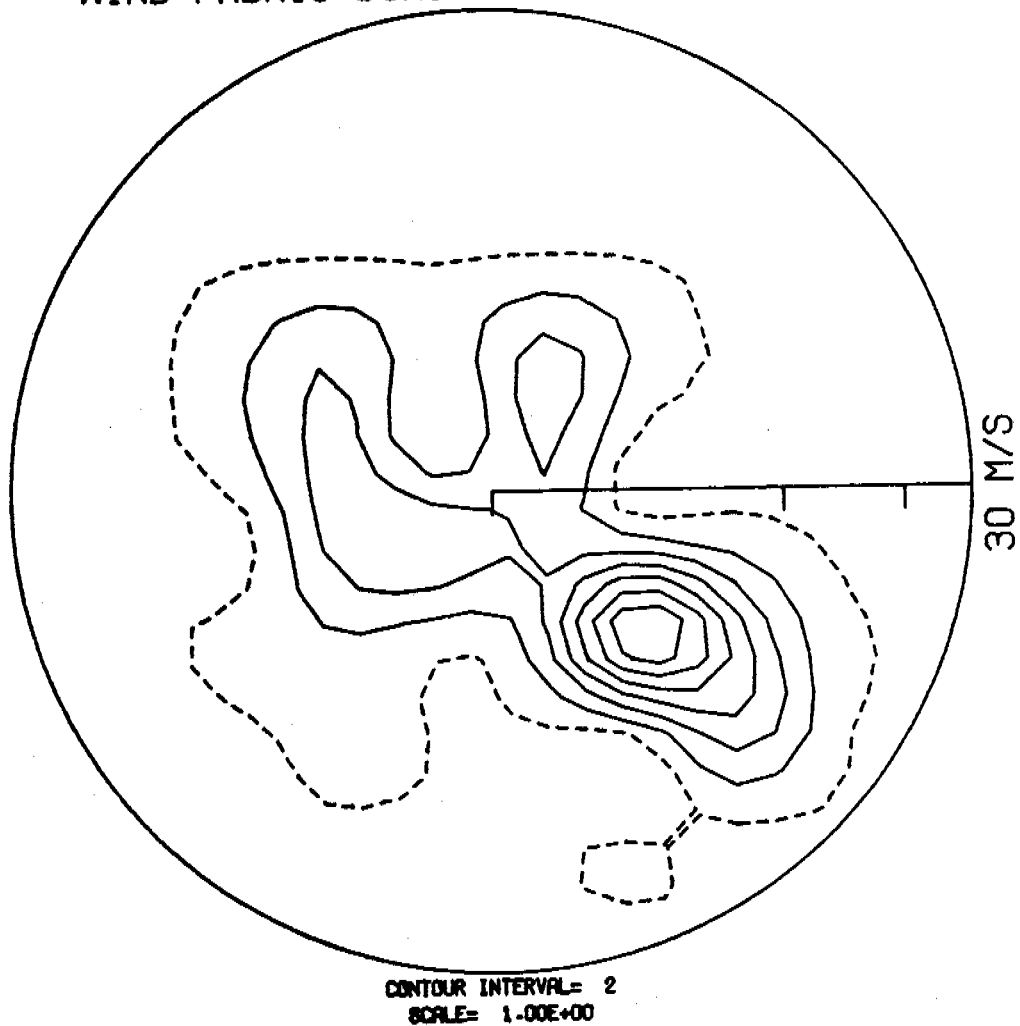


Figure 4b. Fabric diagram of wind observations for 1-22 June 1978 at Augustine Island. See Fig. 3d for explanation of this figure.

15

1 JUN THROUGH 30 JUN 78

MEAN V= .86 M/S

MEAN U= -.80 M/S

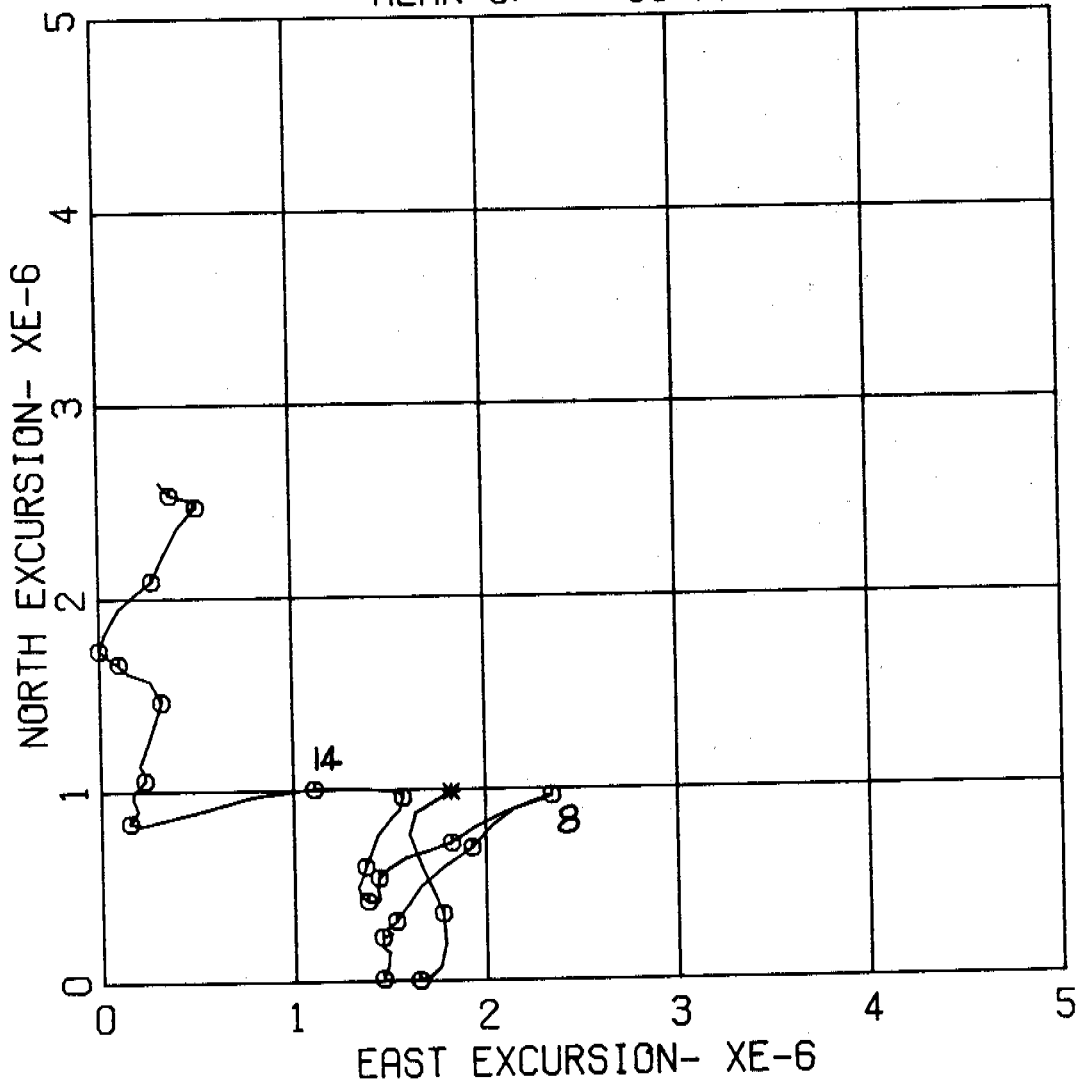


Figure 5a. Progressive Vector Diagram for winds measured at Shuyak Island from 1-22 June 1978. Circles mark beginning of days and the star marks the start. Wind events of the 8th and 14th are shown.

WIND FABRIC DIAGRAM FOR 87 POINTS.

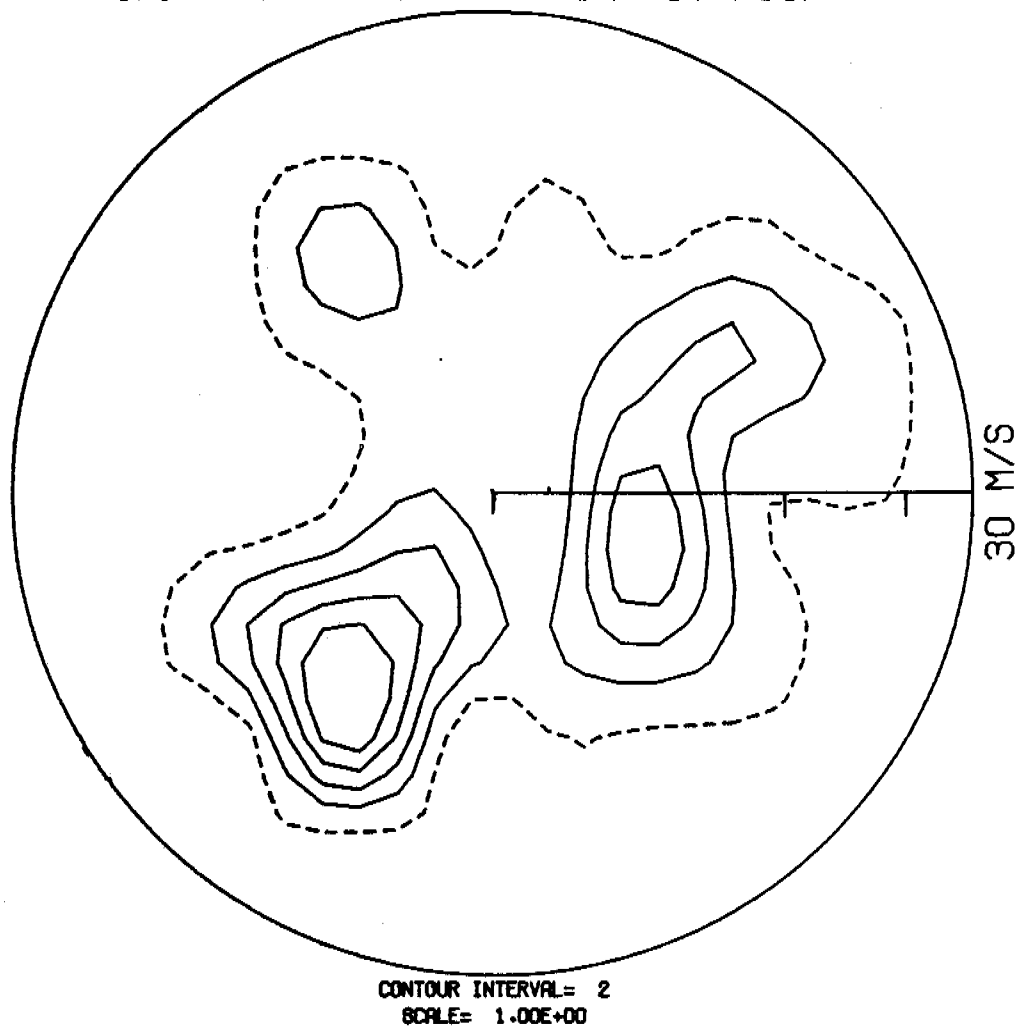


Figure 5b. Fabric diagram of wind observations measured at Shuyak Island from 1-22 June 1978. See Fig. 3d for explanation of this figure.

4

1 JUN THROUGH 22 JUN 78
TIME SERIES OF 6 HOURLY DATA

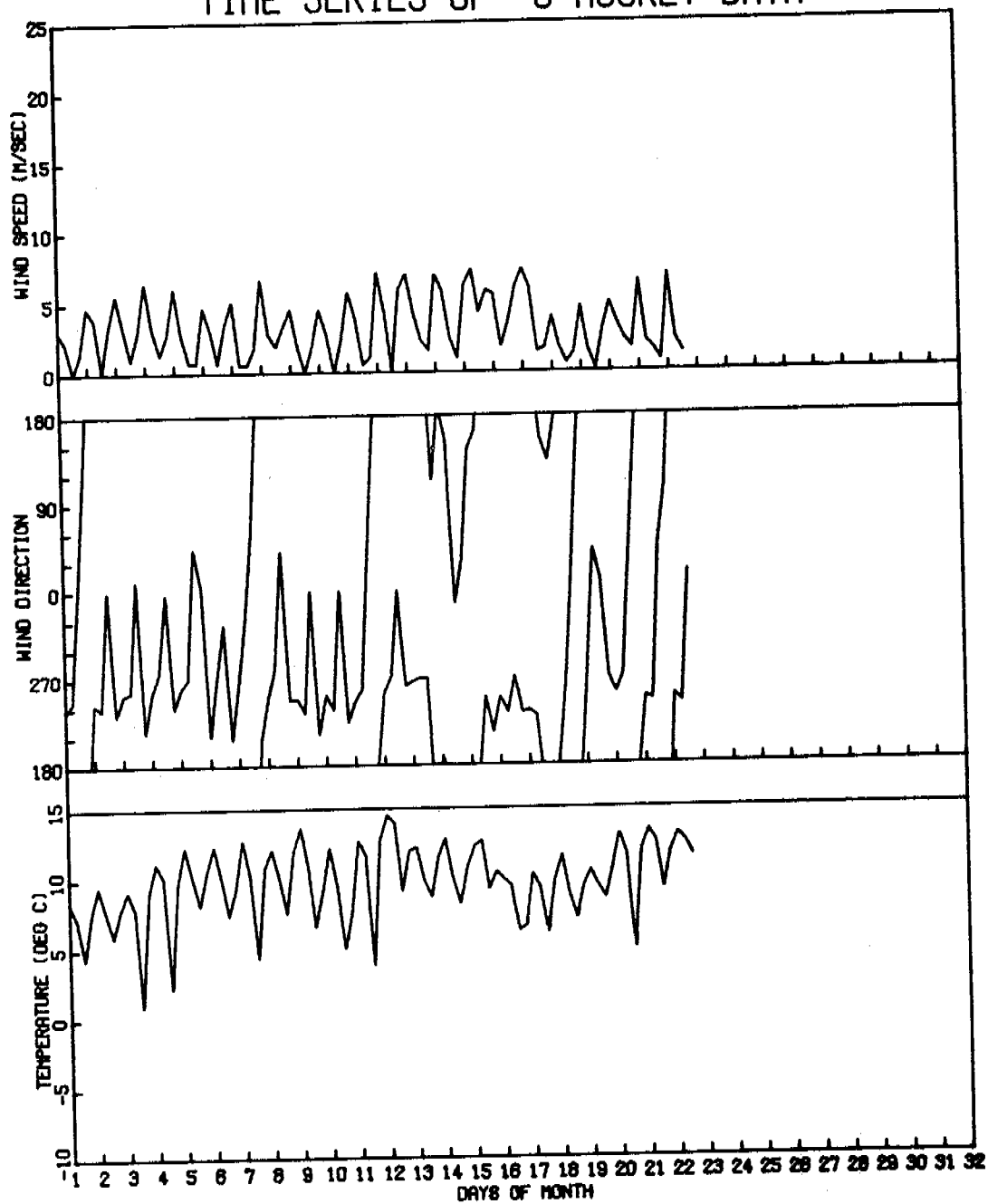


Figure 6a. Time series plot for Homer airport June 1978.
Note strong diurnal character of the air.

4

1 JUN THROUGH 22 JUN 78

MEAN V= 1.06 M/S

MEAN U= 1.97 M/S

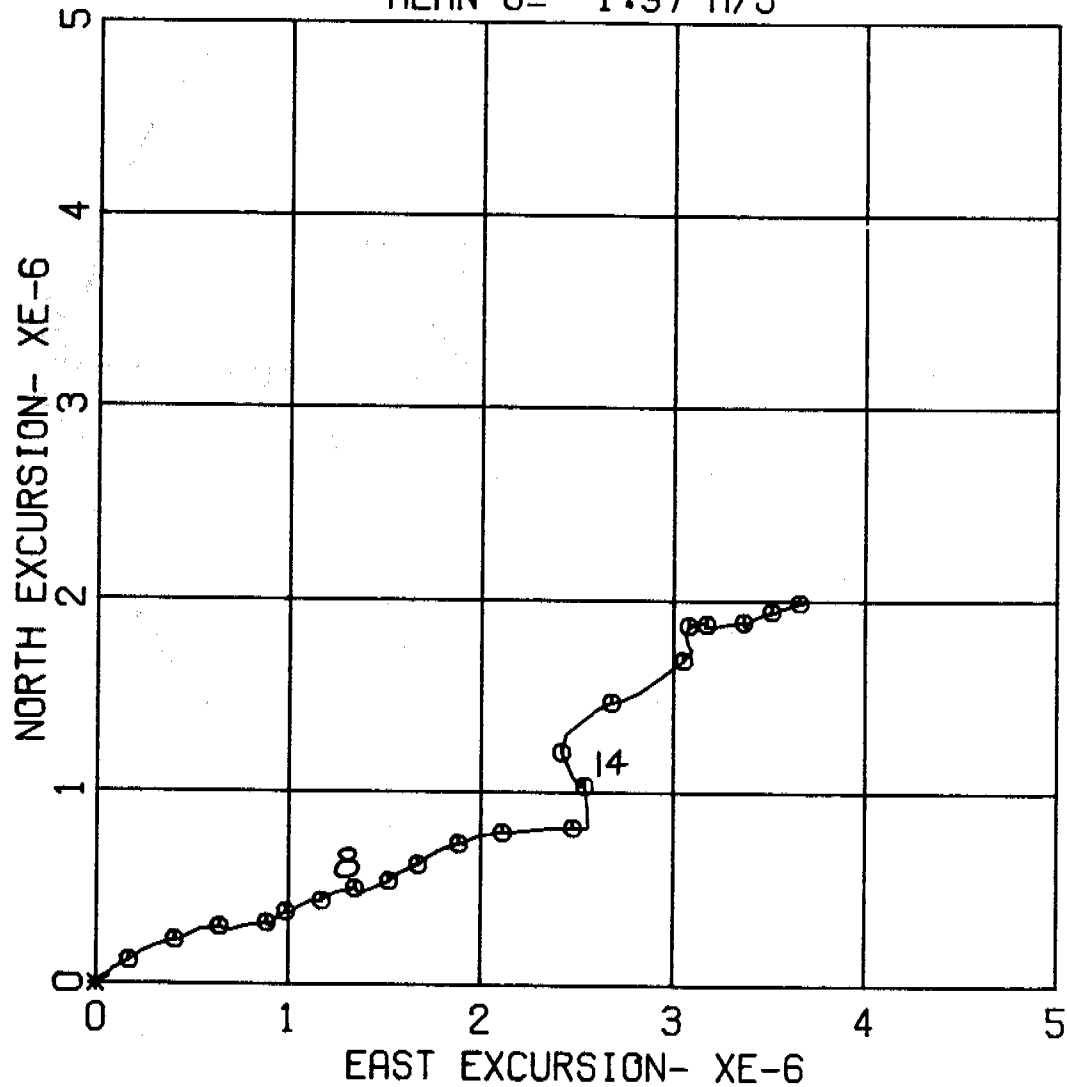


Fig. 6b. Progressive Vector Diagram for winds measured at Homer Alaska, 1-22 June 1978. Circles mark the beginning of days and the star marks the start. Wind events of the 8th and 14th are marked.

WIND FABRIC DIAGRAM FOR 87 POINTS.

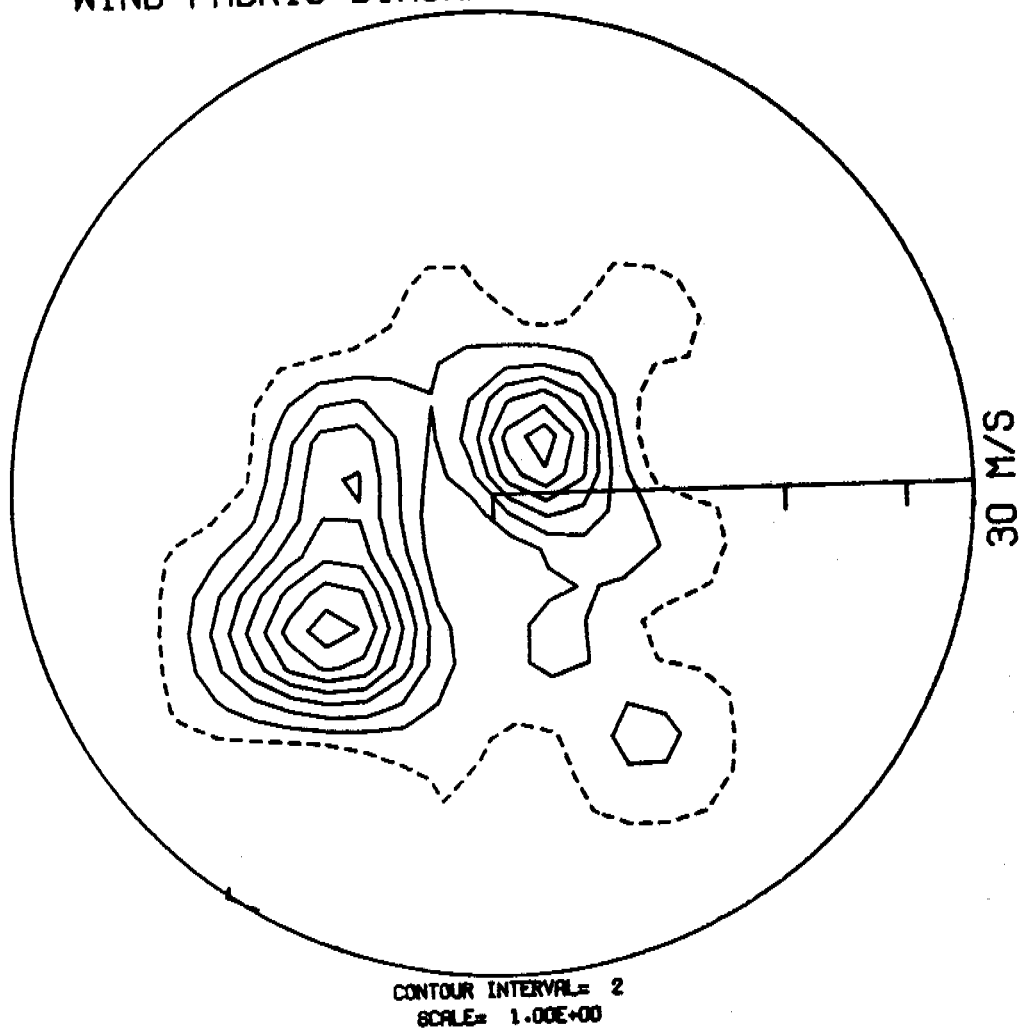


Figure 6c. Fabric diagram of wind wind observations measured at Homer from 1-22 June 1978. See Fig. 3d for details of this plot.

OBSERVATIONS FROM SHIP 24

FROM 78 06 19 13Z TO 78 06 25 19Z

SCALE 5000000

10 METERS/ SEC

AT LAT. 58.500

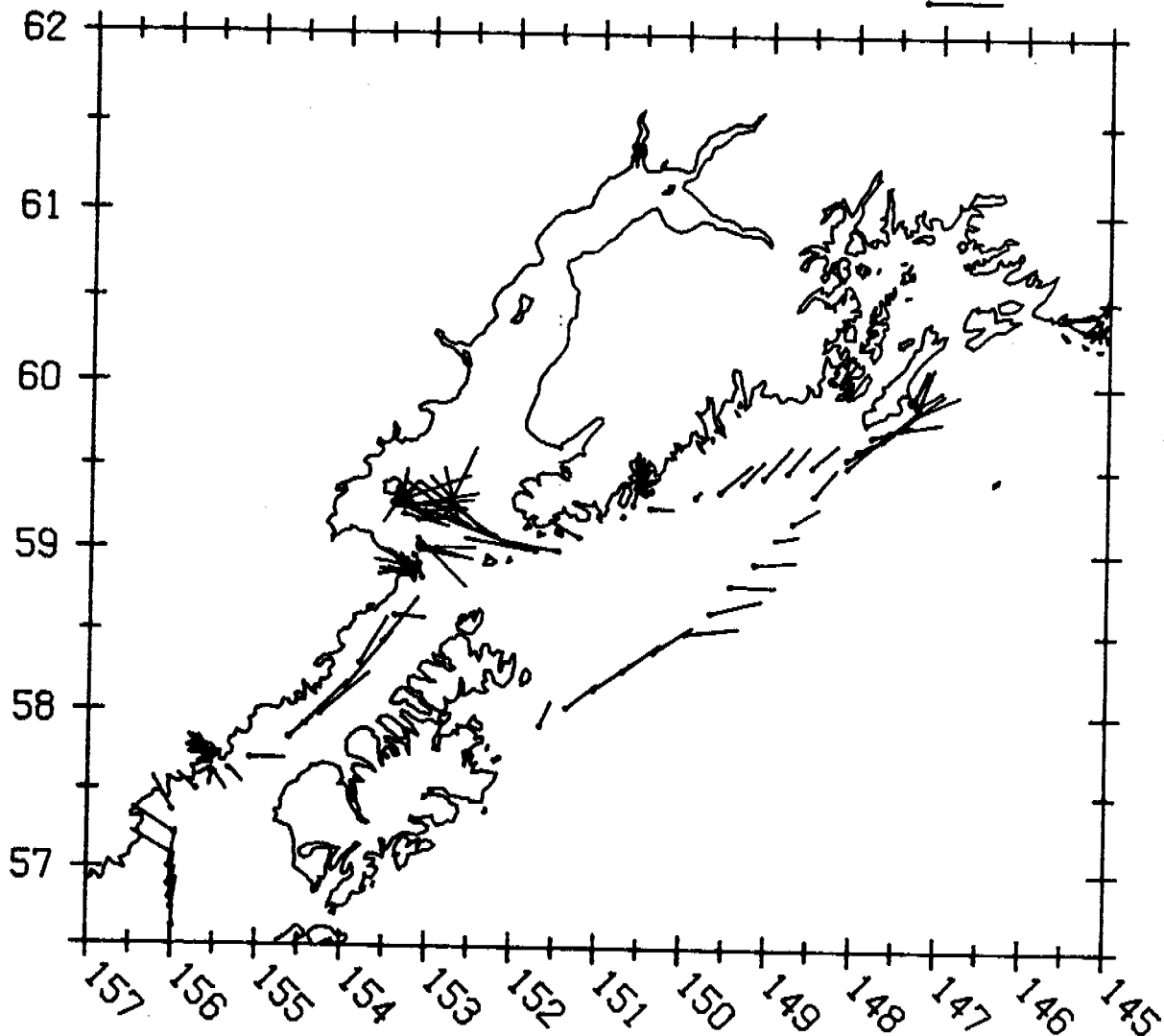


Figure 7. Trackline of the ship SURVEYOR from 19 to 25 June 1978. Sticks point in the direction of the air flow, position is marked by a dot at the end of the stick. The ship left Kodiak, sailed to Montague I. then into lower Cook Inlet and out Shelikof Strait.

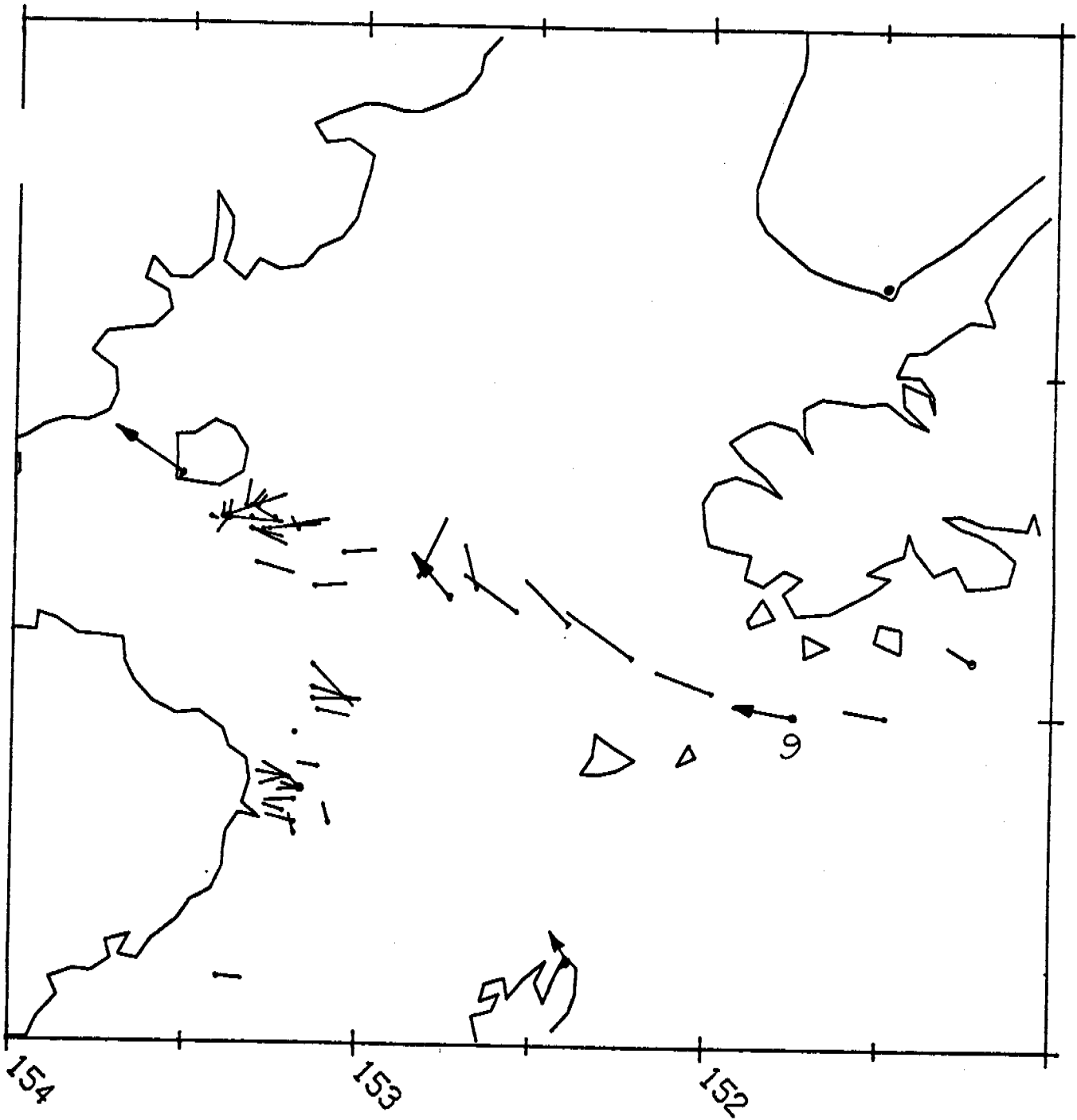


Figure 8b. Higher scale diagram of the SURVEYOR track of Fig. 7.
 Arrows represent simultaneous observations taken at 0900
 on 22 June 1978.

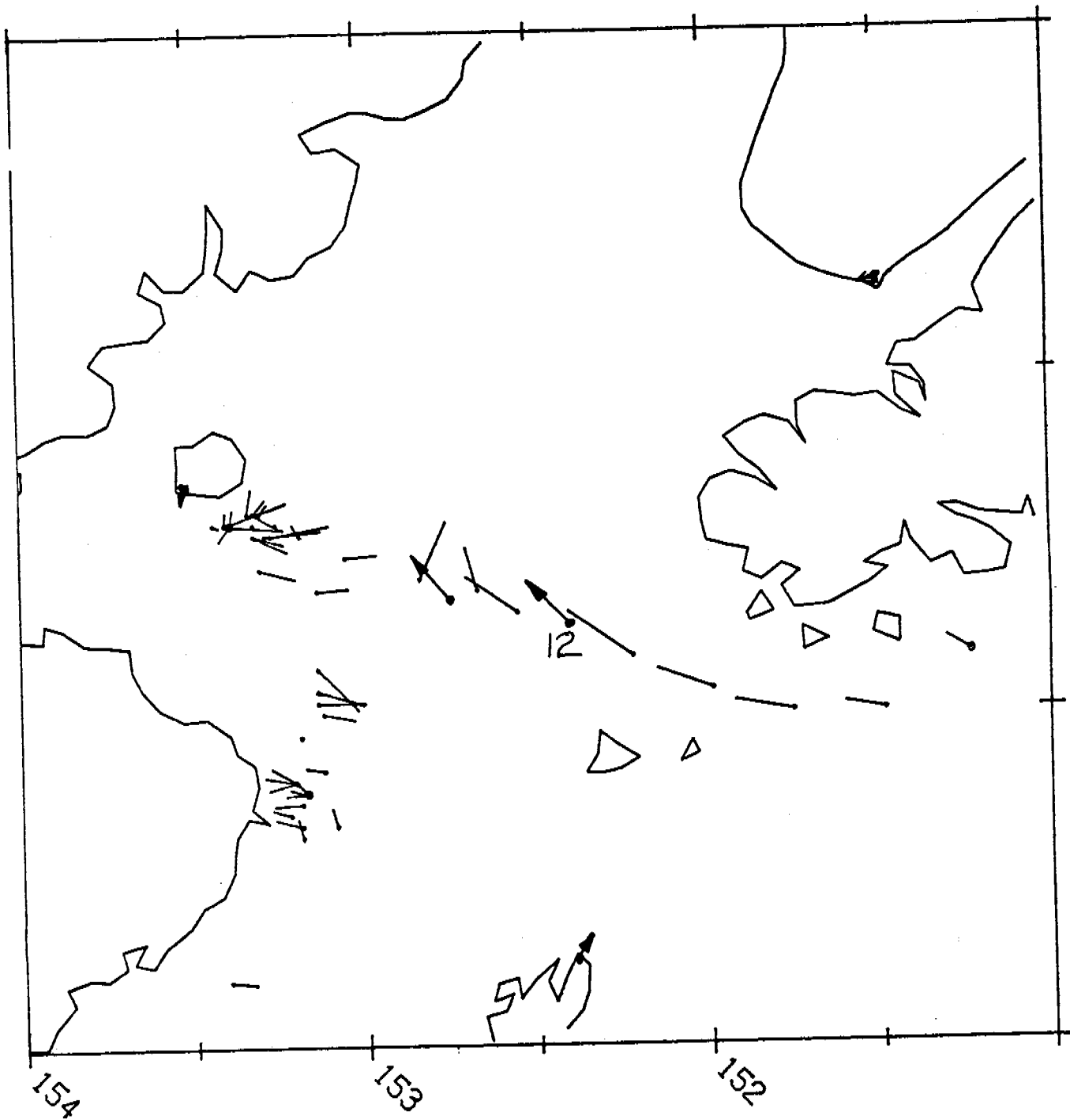


Figure 8c. Same as Fig. 8a for 1200 on 22 June 1978.

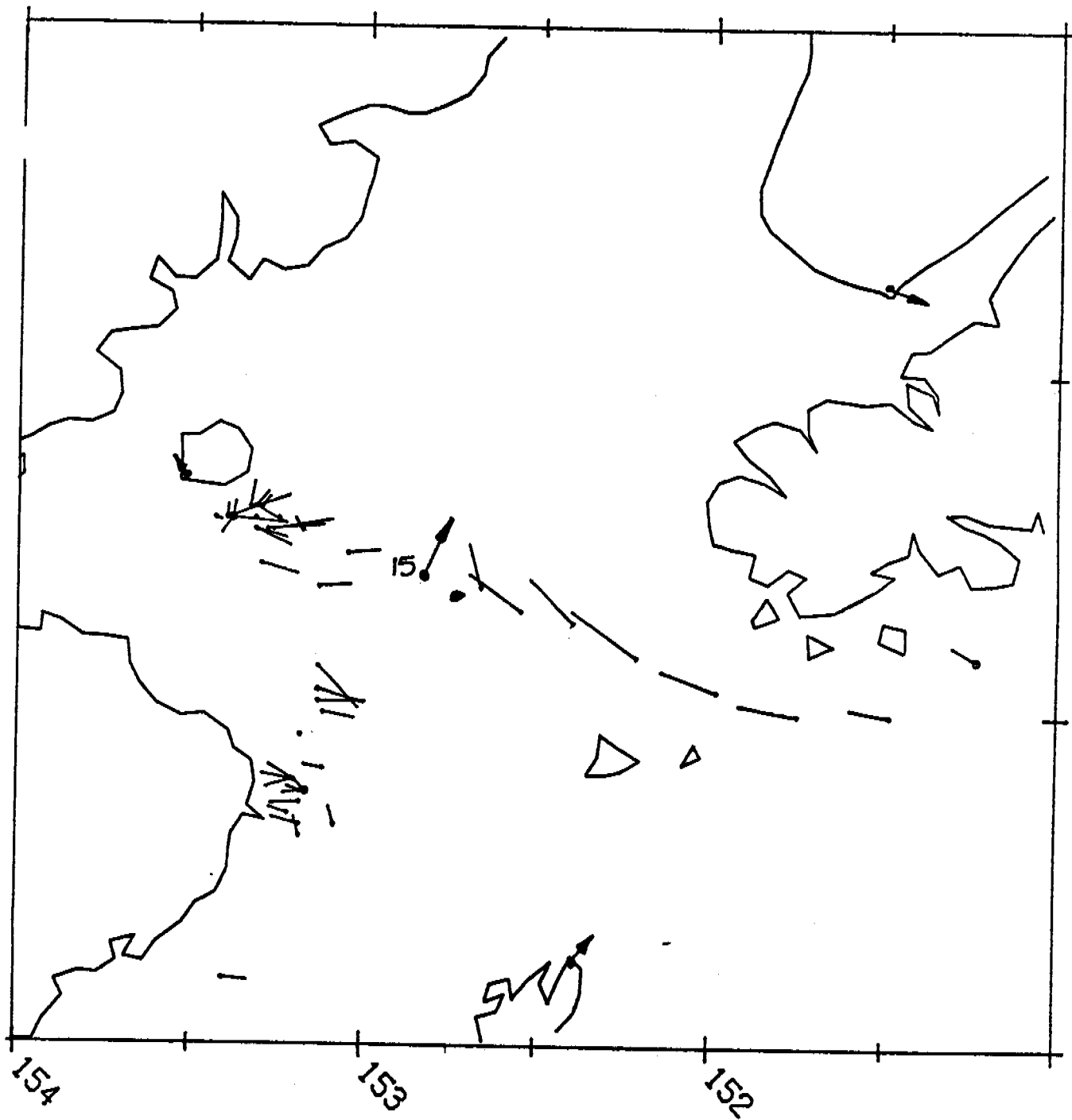


Fig. 8d. Same as Fig. 8a for 1500 on 22 June 1978.

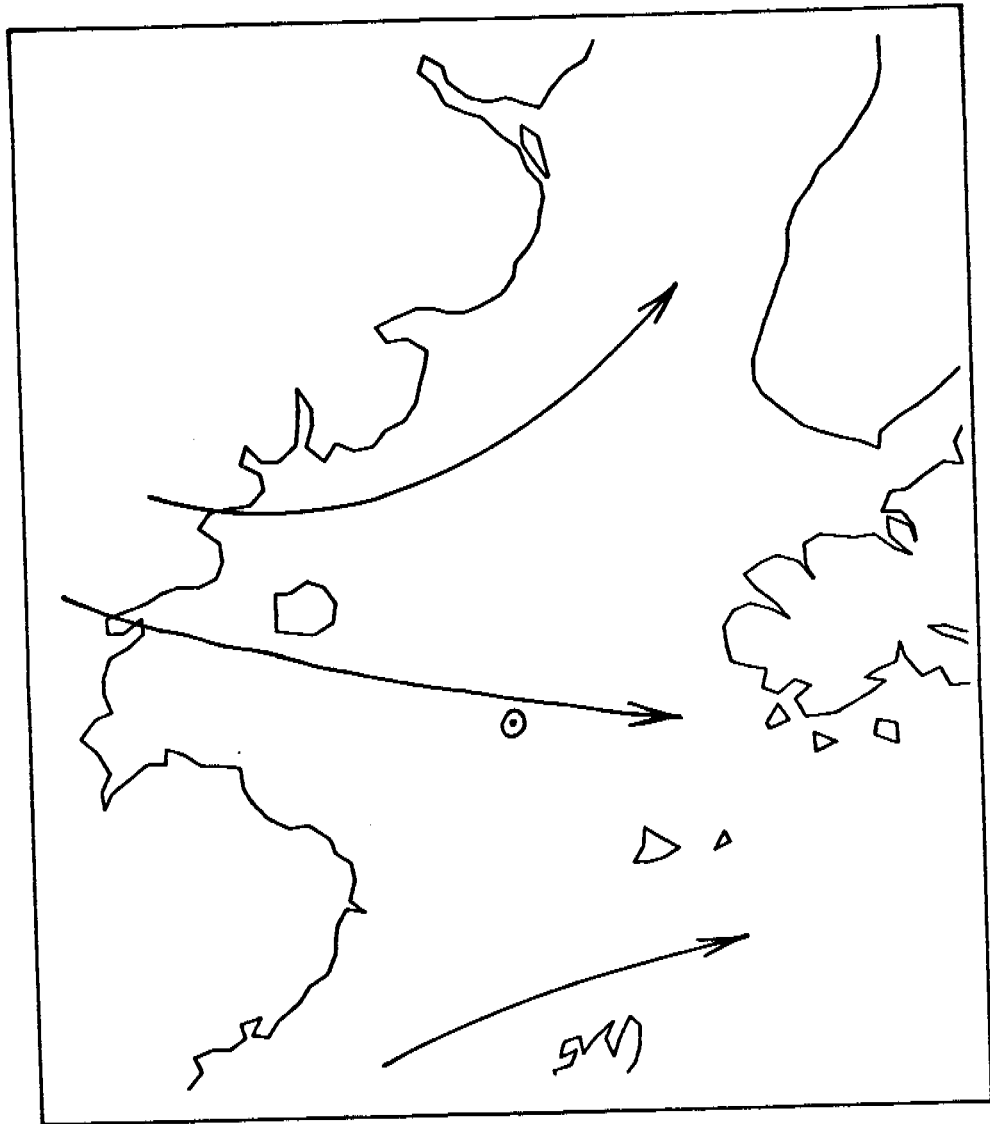


Figure 9a. Hypothetical wind field for lower Cook Inlet during periods of flow through the Kamishak Gap, indicative of a low center in the Gulf of Alaska.

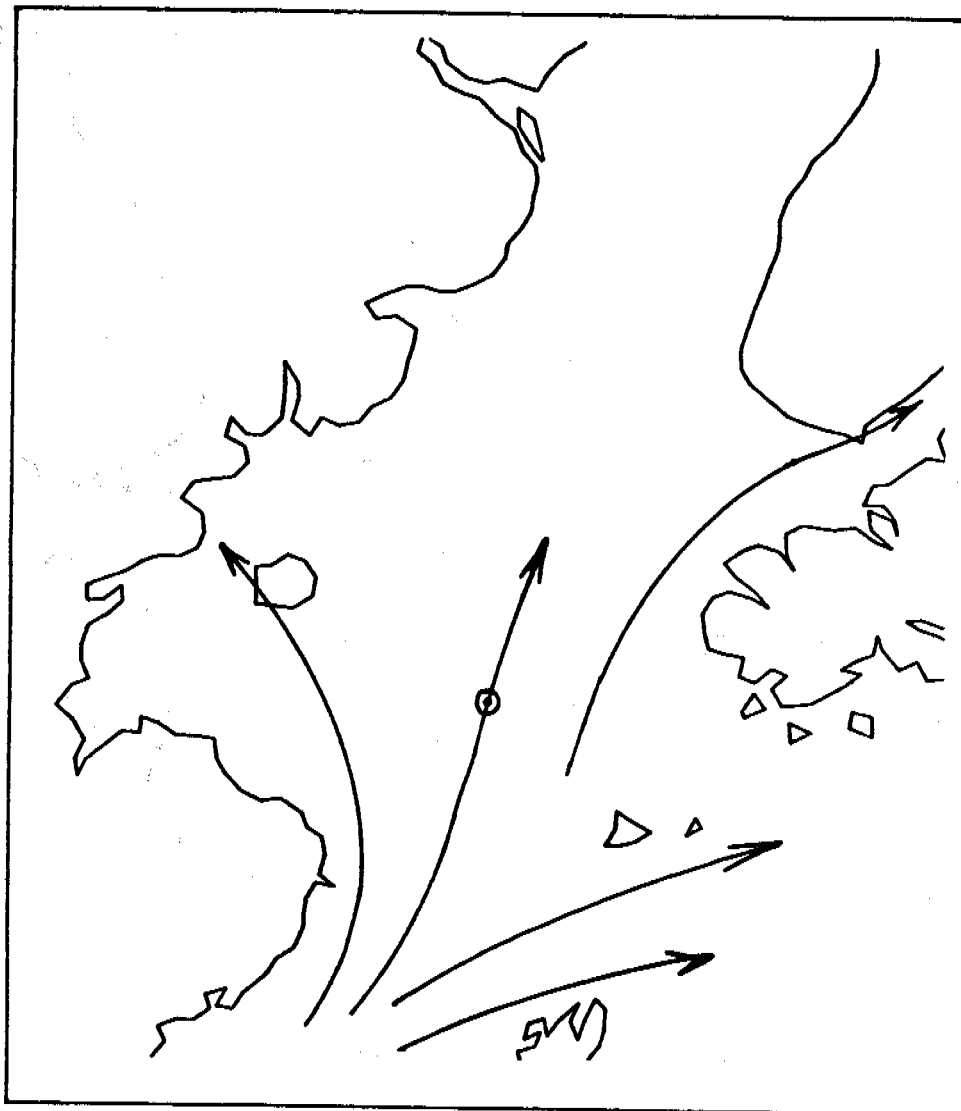


Figure 9b. Hypothetical wind field for lower Cook Inlet during period of strong flow up Shelikof Strait.

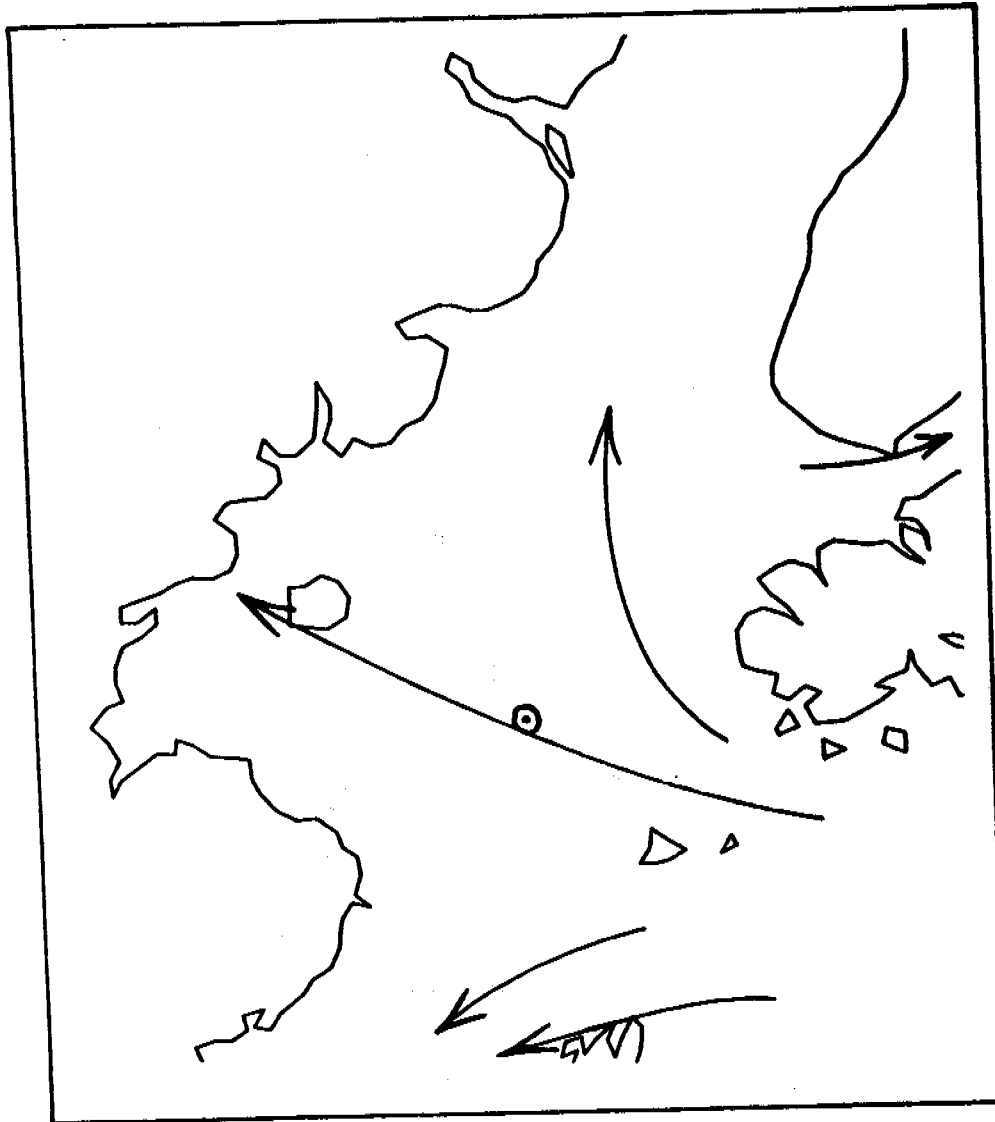


Figure 9c. Hypothetical wind field for lower Cook Inlet during period of flow from east in the Stevenson and Kennedy Entrances indicating a low center in the region of the Aleutian Islands.

APPENDIX C

WINDS OVER THE ALBATROSS BANKS - A COMPARISON OF
MEASUREMENTS FROM EB46008, FNWC, AND KODIAK

Appendix C

Winds over the Albatross Banks - A Comparison of Measurements from EB46008, FNWC, and Kodiak

This note examines meteorological data produced by two sources in the vicinity of the Albatross Banks (Fig. 1) and compares these data with direct measurements taken by EB-46008. The main intent of this study is to establish whether winds at the data buoy are severely affected by the mountains of Kodiak Island. In addition, we explore the possibility of using either the routinely collected data from Kodiak or the routinely calculated winds from a large scale numerical model as predictors of flow over Albatross Banks.

Kodiak Island is a mountainous island approximately 130 miles long (including Afognak Island) and 30 miles wide. The island is oriented approximately NE-SW but the mountains tend to run in an orthogonal direction producing many small estuaries with a NW-SE orientation. Albatross Banks lies to the east of Kodiak Island. Mountains along the east side of Kodiak range from 600 m to 1341 m (Fig. 1). The mountains extend to the coast yielding the sort of rugged coastline for which this part of Alaska is noted.

In recent studies in the vicinity of the Malaspina Glacier (Reynolds, et al., 1979) we have found that the winds within 100 km of the coast are severely affected by the mountainous coastline. Katabatic flows pour down the mountains into the estuaries of Icy Bay and Yakutat. All along that coast the winds are directed offshore with jets often appearing as the katabatic flows are focused into the estuary mouths. Offshore these winds are quickly modified by the warmer water. They are seldom seen further than 50 km offshore, and generally they are fully dissipated by 25-35 km. However, the blocking effect of the massive mountain range distorts the pressure field and produces winds which align with the mountain

range. This distortion is much further offshore. The mountains of Kodiak are smaller than those of the Alaska Range, and there is not the extensive snow field here to provide a reservoir of cold mountain air with which to feed the katabatic flows. We wonder therefore if the winds measured at an offshore station here reflect the presence of the land to the same degree.

Direct measurement of the winds on Albatross Banks was provided by National Data Buoy EB-46008 (formally EB-72). The buoy was located at a position of $51^{\circ} 7'N$, and $151^{\circ} 45'W$ (Fig. 1). In that position, it was approximately 60 km offshore and thus most likely out of range of all but the most intense katabatic flows. This buoy was installed in August 1977, and ran almost continuously until February 1979. It was a modified NOMAD buoy, 6 m in length, 3 m wide with keel depth of approximately 2.5 m from the deck. Meteorological sensors included wind speed and direction, barometric pressure, air temperature, and sea surface bulk temperature. These sensors were mounted approximately 5 m from the sea surface. Data was provided in standard archival format with speed to nearest knot, direction to nearest ten degrees, and temperatures to nearest tenth degree Celsius. The buoy was sampled every three hours by satellite transmission link. All variables were averaged for eight minutes before transmission.

The Kodiak National Weather Service facility is located at the Kodiak Coast Guard Station. The mountains are not quite as high in the vicinity of the town of Kodiak although the terrain could not be called flat. This study uses the hourly recorded surface data from the NWS facility. During March and June 1978, data was provided by the National Climatic Center in their standard surface archival format TD-1440. The roundoff and units are the same as described above for the data buoys, and only three-hourly data was archived. During the month of January 1978 we used surface data provided

C3.

directly from the NWS, thereby retaining the full hourly data set. In checking the two sets, and comparing time series with one and three hour sampling, we believe the errors resulting from the edited NCC data sets to be negligible.

Finally, we examined data provided by the Fleet Numerical Weather Central as a source of winds provided by a large scale numerical model. These winds were computed from the FNWC sea-level pressure analysis for their polar stereographic model which has a mesh length of 381 km at 60° N. A geostrophic wind was computed (Bakun, 1973) by a simple computation of pressure gradient using a 5 point array centered on $57^{\circ} 30'N$ and $150^{\circ} 30'W$. A reduction of speed by 30% and a rotation by 15° produced an estimate of the surface winds at that location.

Unfortunately, the FNWC analyses are not independent of the measurements by the data buoy. The analysis is produced by a technique called Fields by Information Blending-Sea Level Pressure version (FIBSLP). The FIBSLP technique is designed to generate the best possible pressure pattern with which to initiate the FNWC prognostic model. FIB analyzes a scalar distribution by weighting and blending information in the value, in the gradient, and in the Laplacian of the field. It accepts spot (e.g. station) values of these properties with purported individual or class estimates of reliability. In the data-starved Gulf of Alaska, a data buoy ranks high as a source of reliable data, and no doubt ranks highly in the FIB procedure. Therefore, any numerical procedures, be they analyses or prognoses which were initialized by these analyses, will reflect the buoy measurements to differing and unknown degrees. In the comparisons to follow, this lack of independence shows up as a surprisingly high correlation between the buoy and the FNWC analysis.

Time series analysis for each of the three stations was accomplished in the following manner. All the data from each source is read into an array of 744 elements, one for each hour of the month. We then used linear interpolation to fill the entire hourly array, smoothed the data with a simple triangular kernel whose time constant was approximately six hours, then resampled the data at a six-hourly rate. None of the series suffered from long intervals of missing data, and this technique produced roughly equivalent series, regardless of the original sampling rate. Having created a smoothed time series, we plotted the various wind, temperature, and pressure data on simple time plots for initial comparison. In addition, progressive vector diagrams (PVD) provided information on the mean wind properties.

Another statistical tool is the fabric diagram. The fabric diagram (Davis, et al., 1977) provides an informative display of wind statistics. A wind vector frequency diagram was designed to be a contour map of the wind velocity probability distribution, given in percent of the total observations per 1% of the area of the circle. Meteorological tradition prevails--the compass direction on the diagram is the direction from which the wind was blowing. Qualitative interpretation is facilitated by mapping velocity on the diagram as proportional to the square of the radius, in order to compensate for the spreading of the radial line segments. In this way, contours enclosing equal areas anywhere on the map represent areas of equally probable wind occurrence. The concept of such a diagram can easily be expanded to other properties of the observations. For instance, the energy of the wind (square of the wind speed) can be calculated for each observation, and an energy map will result where the contours represent percent of the total energy per 1% of the enclosed area. These energy fabric diagrams delineate

those wind directions which contribute most significantly to the total energy (and thus to the total sea surface stress).

With the above geography and analysis in mind, we now examine three months of data. The months selected for comparison were January 1978, March 1978, and June 1978. These provide typical conditions for winter, spring, and summer.

The Climatic Atlas for the Gulf of Alaska (Brower et al., 1977) provides climatic mean conditions with which to compare our observations. The atlas contains climatic means for each month for Kodiak and an offshore area which is labeled 'Area B' (Fig. 2), from which offshore reports are collected. Area B is a large area, but includes Albatross Banks. Climatic information for January, March, and June, summarized in Fig. 3, indicates a strong degree of orographic control on the surface observations taken by Kodiak. The polar plots are wind roses in which the frequency of observation is plotted as the radial length for any given wind direction. Buskin Pass is a long mountain pass which extends NW from the Kodiak airport. The influence of this pass is apparent in the January and March wind roses. The persistence of the winds (i.e., their unidirectionality) is related to the ratio of the vector mean wind speed to the mean speed, denoted by r , and both the wind roses and mean speeds given indicate much more variability in the offshore winds. For instance, the value of r for January is .47 for Kodiak, and .16 for Area B.

During the month of January, all three data sources were well correlated (Figs. 4a-e), especially wind speeds. In general, FNWC winds agree almost exactly with the winds measured at the data buoy. While Kodiak also correlates with the data buoy, the winds it measures are always smaller than those offshore. As is evident by the PVD, the vector mean wind speeds for the data buoy, Kodiak, and FNWC were

6.0, 3.4, and 6.7 ms^{-1} respectively while the total energy was 1.07×10^4 , $.557 \times 10^4$, and $1.01 \times 10^4 \text{ m}^2 \text{ s}^{-2}$. The wind directions also agreed well with the exception of two periods of time around the 16th and 25th of the month when Kodiak registered NW winds while both the data buoy and FNWC showed NE winds. There appears to be some orographic channeling of the winds from the NW direction in the Kodiak region; we will discuss this effect in greater detail later in this report. Westerly flow in the Kodiak data is apparent in examination of the U-component of the wind (positive to the east). In many more cases, Kodiak shows westerly winds when the other sources indicated slightly negative values of U.

The pressure trace indicates the passage of two cyclonic systems during this month, and the rotation of the wind direction in a cyclonic direction (CCW) suggests that the system passed just to the south of the area.

Wind fabric diagrams for the three sources (Fig. 4d) agree quite well with the exception of the NW winds at Kodiak. However, these winds are light, and hardly are discernable in the energy diagram. Hence, these winds contribute very little to the stress and it is doubtful if they are capable of producing any surface currents of note. There is a tendency for FNWC to emphasize winds and wind stress from the SE while the measured winds at the data buoy show more occurrences of winds from the NE.

In March, conditions in Kodiak were much more in keeping with the climatic mean conditions (Figs. 5a-e). Winds at Kodiak were predominantly from the NW as indicated by the frequency fabric diagram (Fig. 5d). However, one strong storm on the 12th of the month produced high easterly winds at Kodiak which distorted its energy fabric diagram and the PVD yielding a vector mean wind of 1.38 ms^{-1} from the north. The effect of a strong wind on the surface stress is evident

here, as a significant lobe appears in the energy diagram from the SW direction. Kodiak also showed much more diurnal variation in the wind speed and temperature signals. Again, the data buoy and numerical data are in good agreement, most likely for reasons outlined above. Wind directions were much more variable offshore, and velocities were much higher than Kodiak. Because of the offshore variability in comparison with the relative persistence at Kodiak, the vector mean wind speeds at buoy, Kodiak, and FNWC were 2.36, 1.38 and 2.12 ms^{-1} which were relatively close, while the energies were 8.41×10^3 , 4.18×10^3 , and $6.36 \times 10^3 \text{ m}^2 \text{ s}^{-2}$. The diurnal variability at EB46008 was much less than Kodiak, though perceptibly more than the January case.

EB46008 did not function for the latter quarter of June 1978; the last week of the month was not recorded due to electronic problems. As a result, the statistics must be less representative of the climatic mean. However, the pressure trace (Fig. 6b) and the direction record (Fig. 6a) indicate the passage of two storm systems. Nonetheless, the winds at the data buoy were surprisingly consistent from the SW. The PVD for the buoy shows this very well (Fig. 6c). The FNWC analysis also produced persistent southwest winds for the entire month, and the vector mean winds for these two sources were quite close. The climatic mean wind for June and offshore regions (Fig. 3) is consistent with this direction, but is somewhat weaker. Kodiak on the other hand showed a large variation in the wind speed and direction. The winds tended to be light and variable thus the vector mean wind speed was only $.47 \text{ ms}^{-1}$ compared to values of 3.41 and 4.50 ms^{-1} for the buoy and analysis respectively. Fabric diagrams for this month (Fig. 6d) indicate a preference for SW and NW winds at Kodiak with most of the energy coming from the SW. Kodiak was very much under the influence of diurnal forcing, i.e., sea-land breeze or katabatic flow. The time

C8.

series of speed and direction (Fig. 6a) implies that in the early morning hours winds at Kodiak generally reached a maximum and came from the NW direction typical of both land breezes and katabatic flows. At the time of this writing, it is difficult to sort out the nature of this flow. Most likely the upper air profiles will be required. Diurnal variability was evident in the buoy measurements, but was significantly smaller than that at Kodiak.

The three sources of information considered in this report reveal the following facts. The FNWC analysis is in such good agreement with the data buoy observations that we cannot consider it to be an effective independent source of data. The fact that the data buoy is certainly one of the prime sources of observational data with which the analysis is created draws into question the usefulness of that analysis if the buoy is removed.

As suspected initially, Kodiak is at no time a representative indicator of offshore conditions. Channeling of winds through Buskin Pass near the Kodiak airport creates a very persistent NW wind in the winter. A combination of katabatic flow and sea-land breeze flow produce strong diurnal variability in the summertime. However, the measurements of EB46008 indicate that the region 60 km offshore is beyond strong land contamination. Hence, an accurate synoptic model would probably be a sufficient predictor of surface winds over Albatross Banks.

Future study of this problem will include 12 hr prognoses as another more independent data source, although these are initialized by the aforementioned analyses. It seems that in this data poor region, any measurements are immediately scooped up by various weather services making it most difficult to make effective intercomparisons with numerical forecasts.

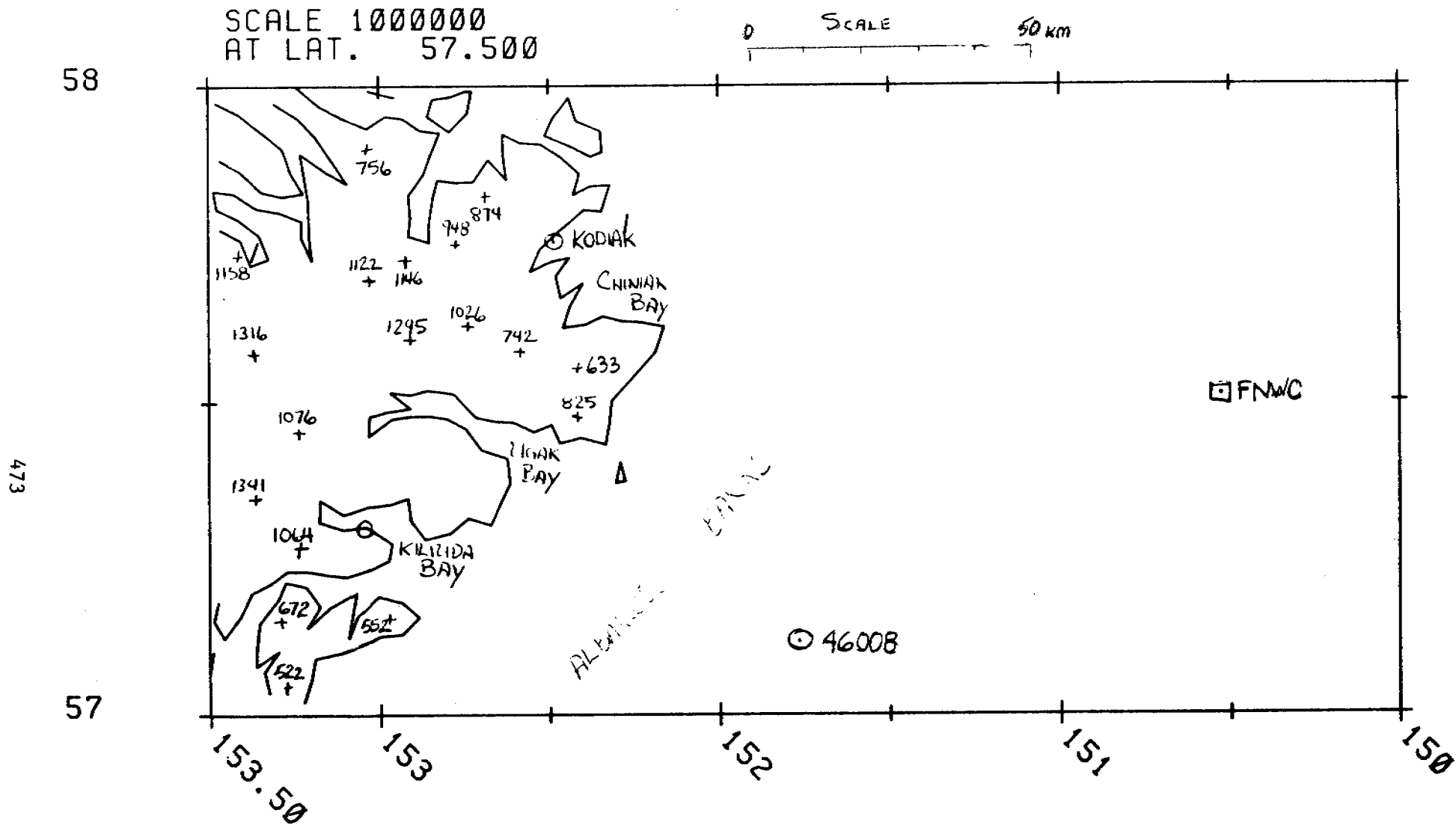


Figure 1. Map of the Albatross Banks region and the east Kodiak coast. Mountain heights are given in meters. Observations in the region are denoted by the open circle, and the position of the wind estimate by FNWC is shown by the square.

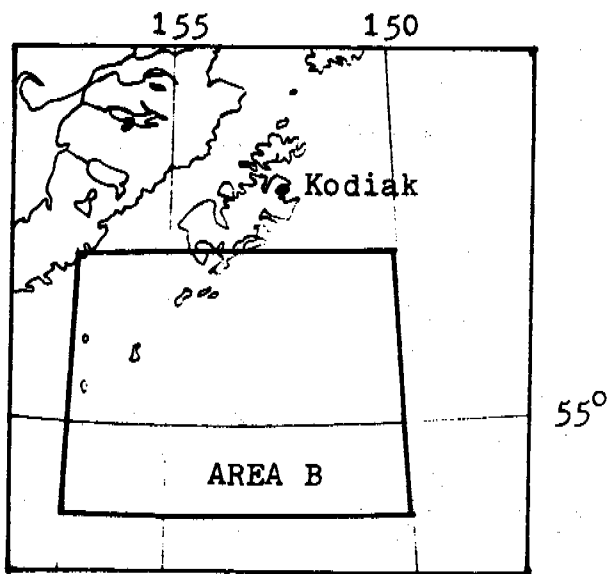
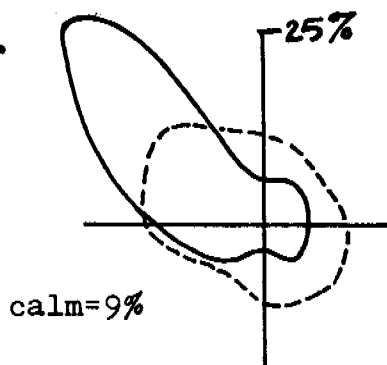


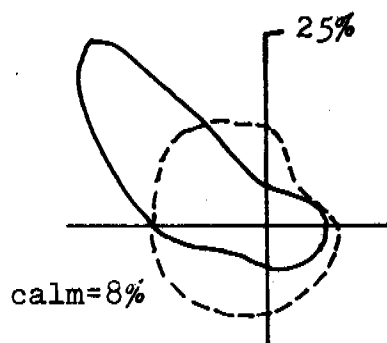
Figure 2. Map showing Kodiak Island and the Area B from which climatic data was compiled.

JANUARY



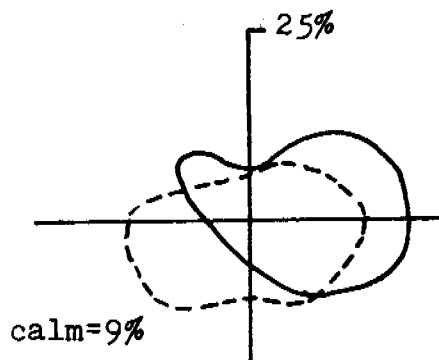
	<u>KODIAK</u>	<u>AREA B</u>
Mean Temp-C	-1.6	2.0
Std Dev-C	4.8	3.3
Mean Speed-kts	10.7	19.2
Vec Mean-kts	NW@5	NW@3
Mean P-mb	1006.7	1004
Std Dev-mb	15.8	16.5
No. Obs	7056	680

MARCH



Mean Temp-C	-.5	3
Std Dev-C	4.4	3.0
Mean Speed-kts	10.0	18.3
Vec Mean-kts	NW@4.3	WNW@3.8
Mean P-mb	1007.0	1008
Std Dev-mb	12.5	14.5
No. Obs	7184	735

JUNE



Mean Temp-C	10	9
Std Dev-C	3.3	2.0
Mean Speed-kts	7.2	12.4
Vec Mean-kts	NE@2.2	SW@1.8
Mean P-mb	1212	1212
Std Dev-mb	7.3	7.8
No. Obs	6958	1109

—— KODIAK
 - - - - AREA B

Figure 3. Climatic data for Kodiak and for an area offshore entitled Area B (see Brower et. al., 1977).

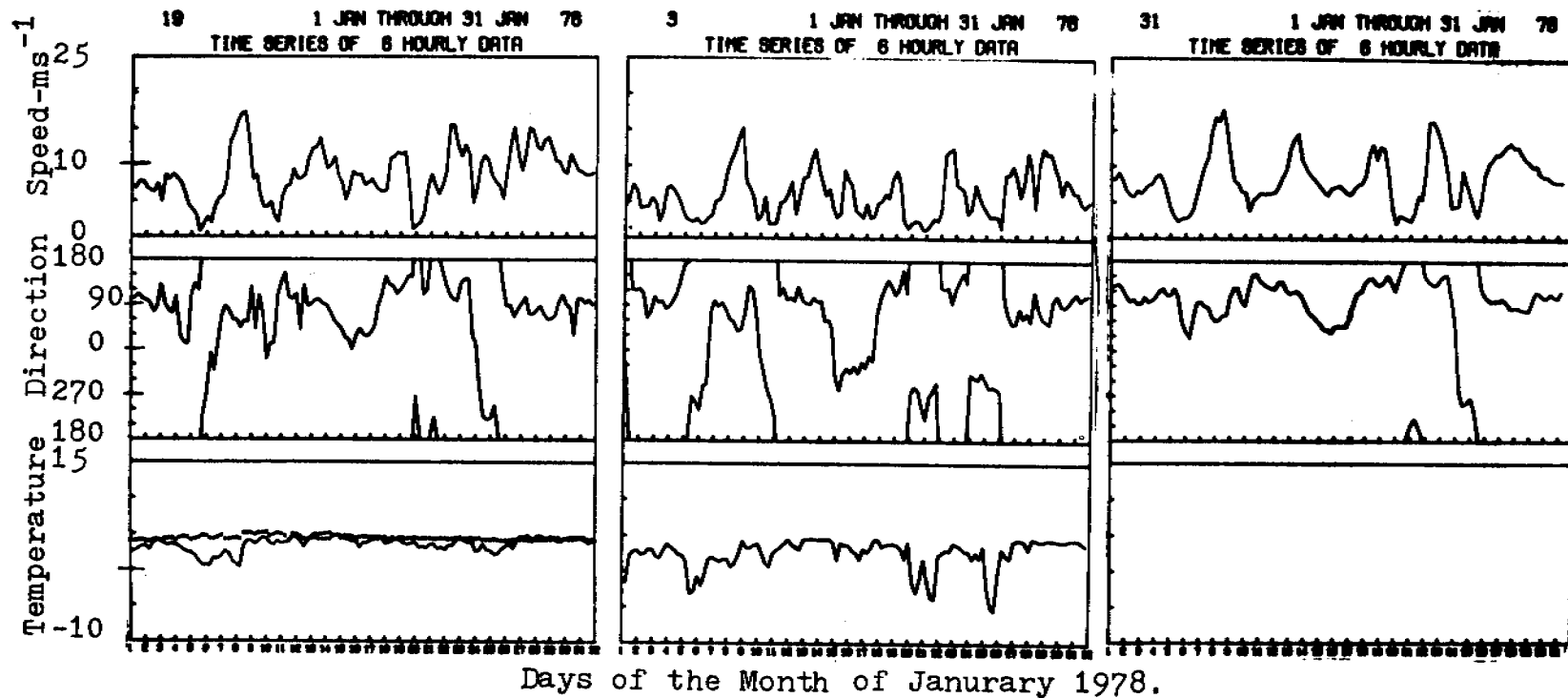


Figure 4a. Comparison of data observed by EB46008, Kodiak, and computed by the Navy's Fleet Numerical Weather Central. Station codes are 19, 3, 31 respectively. Time series plots here are observed wind speeds, directions, temperature (solid line), and sea surface temperature (solid line). Time is in GMT.

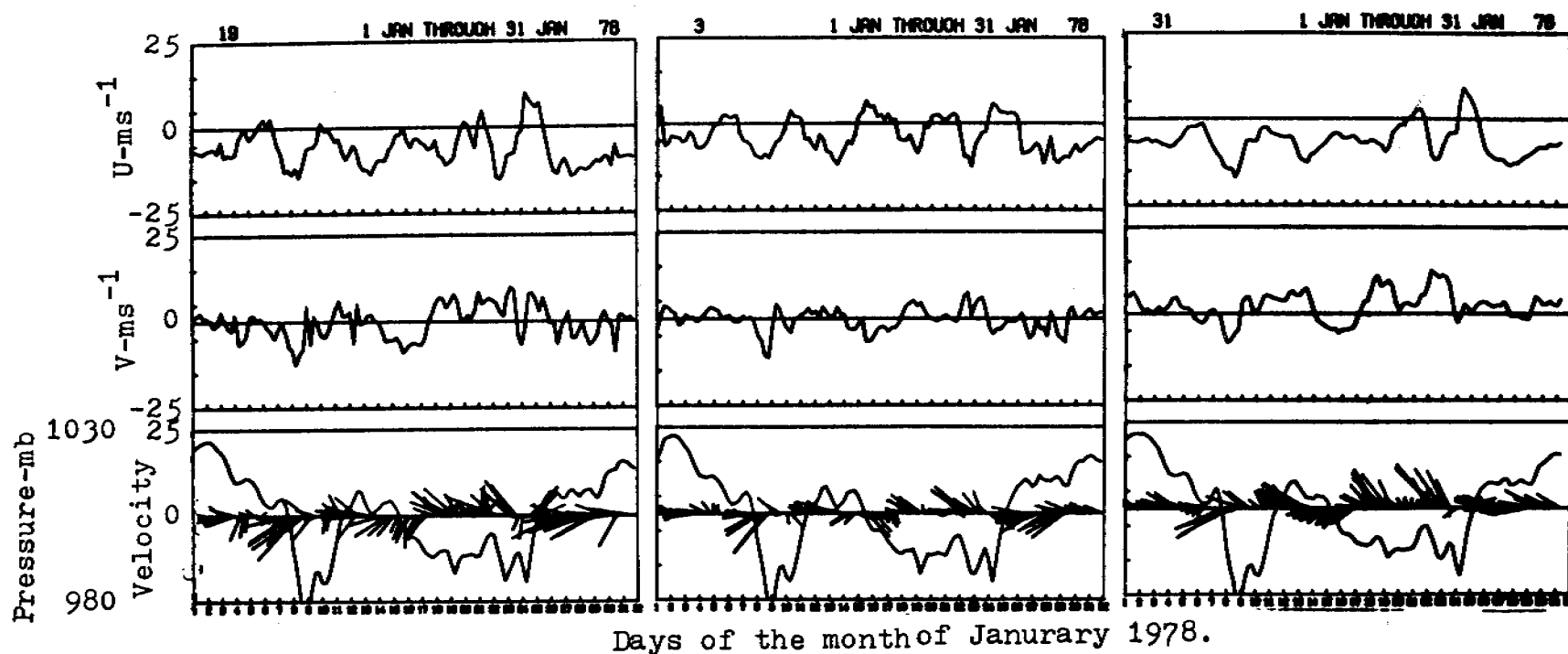


Figure 4b. Same as Fig. 4a. Curves shown are U (E-W) and V (N-S) components, and sea level pressures. The stick diagram shown points in the vector direction of the wind.

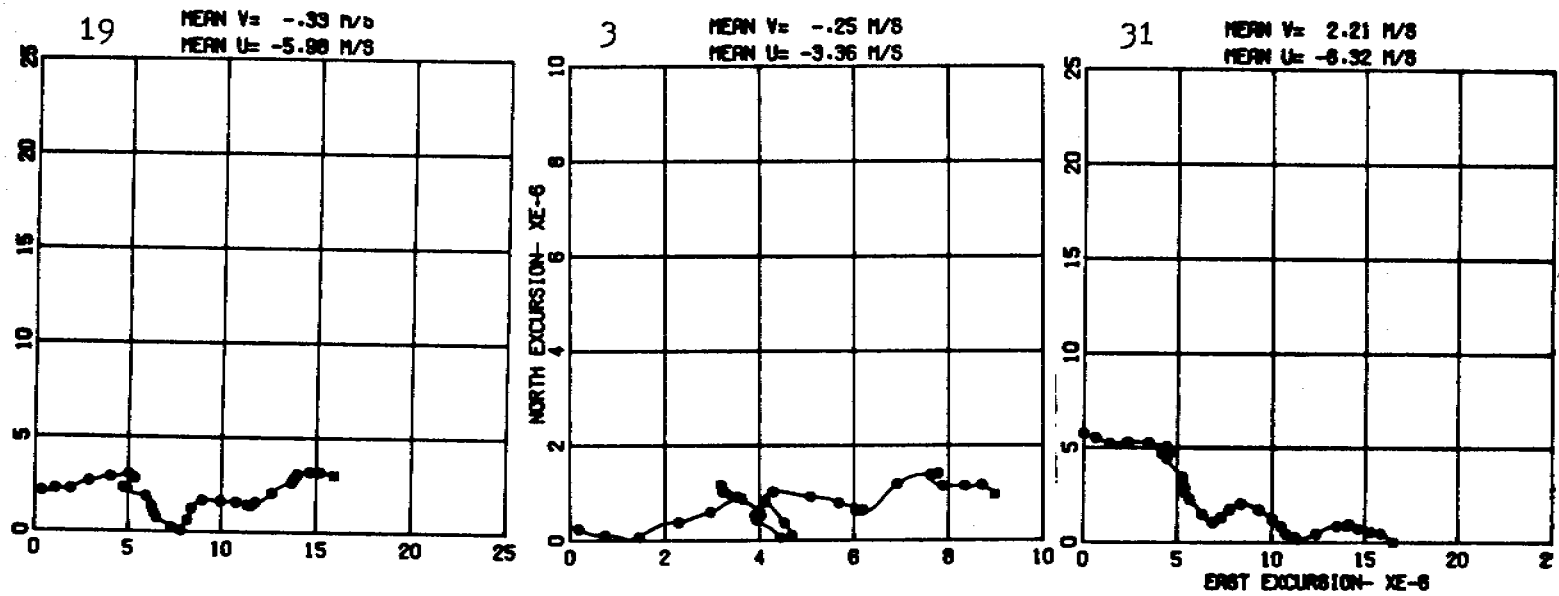


Figure 4c. Same as Fig. 4a. Progressive vector diagrams are shown here.

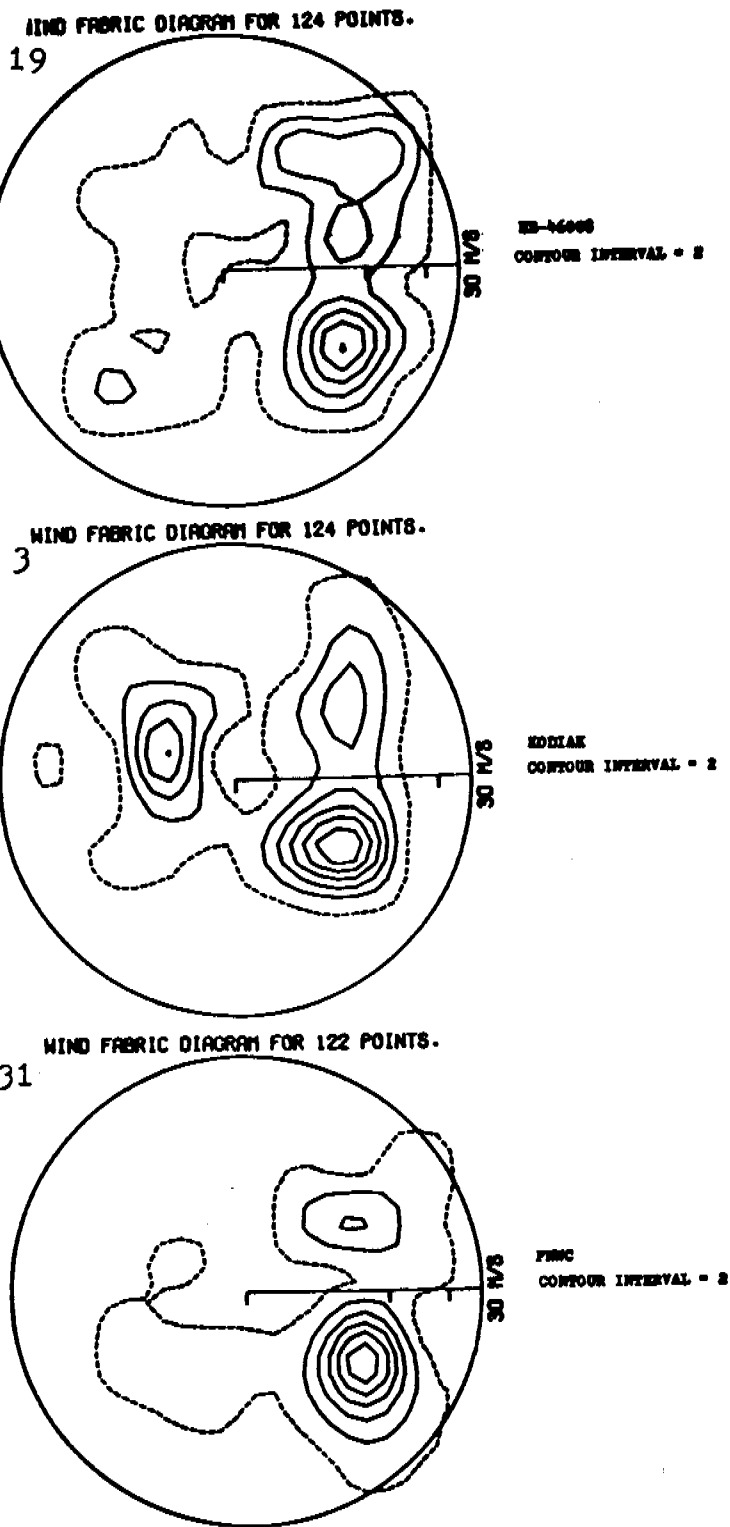


Figure 4d. Same as Fig. 4a. Shown here are the fabric diagrams of observations for the month of Jan.

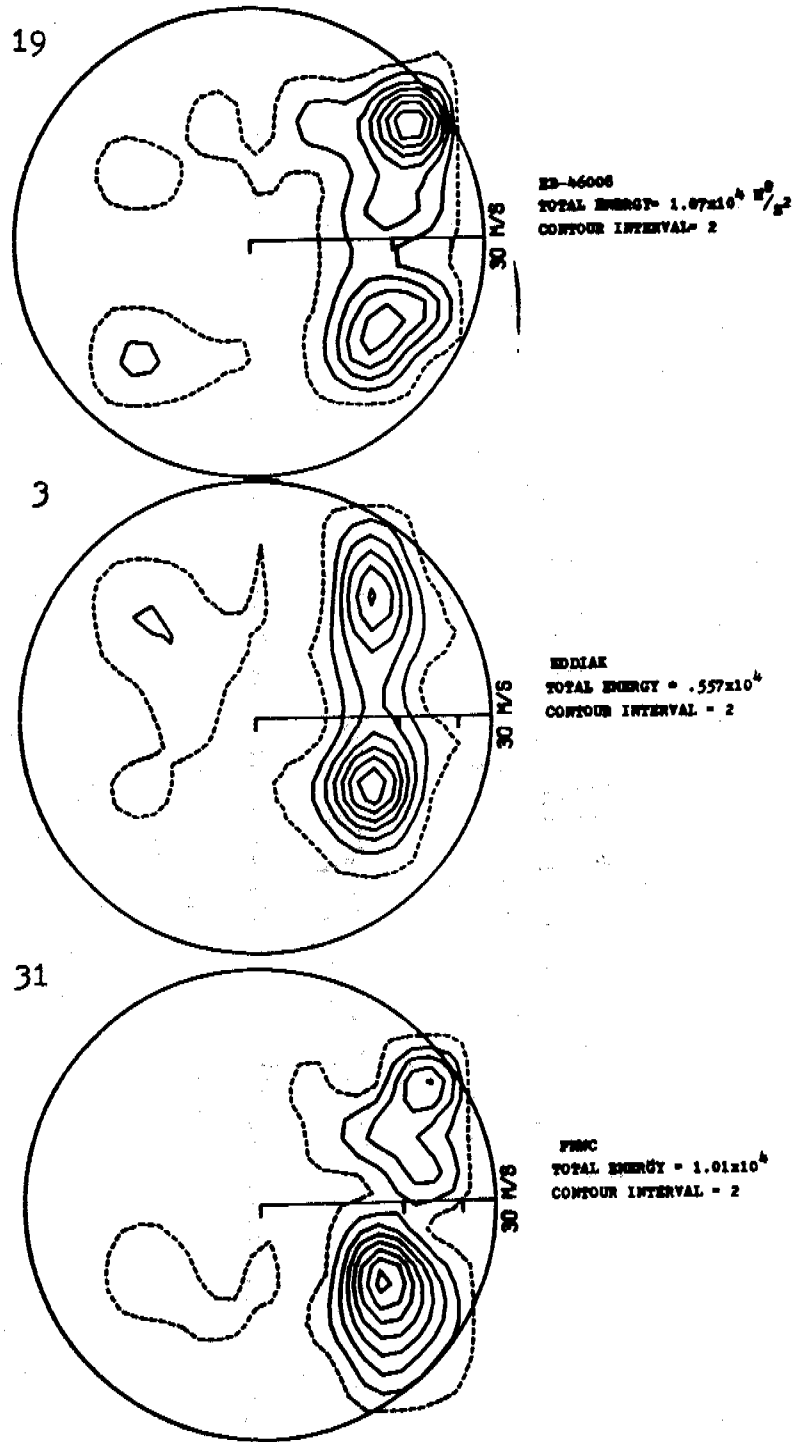


Figure 4e. Same as Fig. 4a. Fabric diagrams of wind energy are shown here.

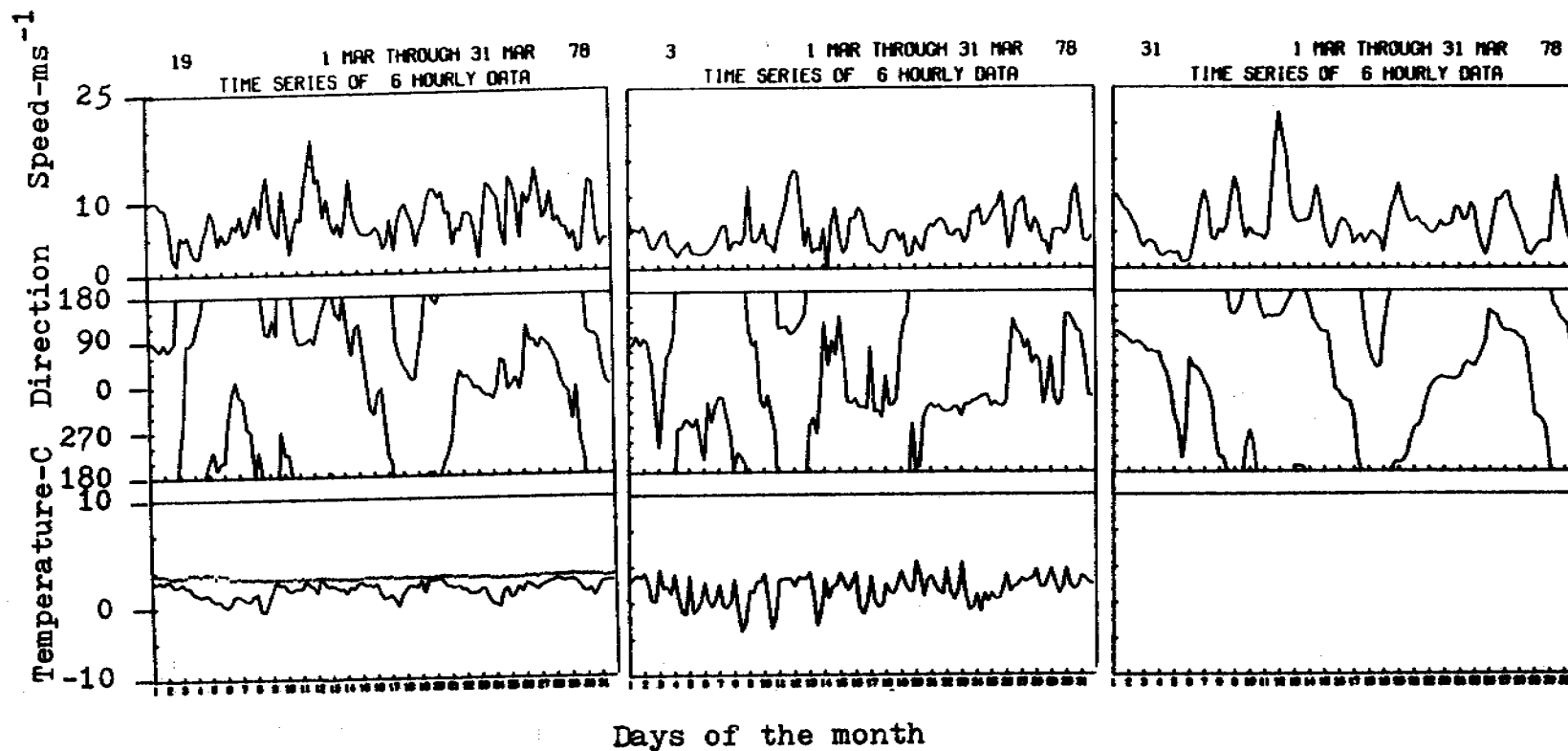


Figure 5a. Comparison of data observed at EB46008 and Kodiak, and winds computed by the Navy's Fleet Numerical Weather Central. Station codes are 19, 3, and 31 respectively. Time series plots shown here wind speed, direction, air temperature (solid line), and sea temperature (dashed line). Times shown are in GMT.

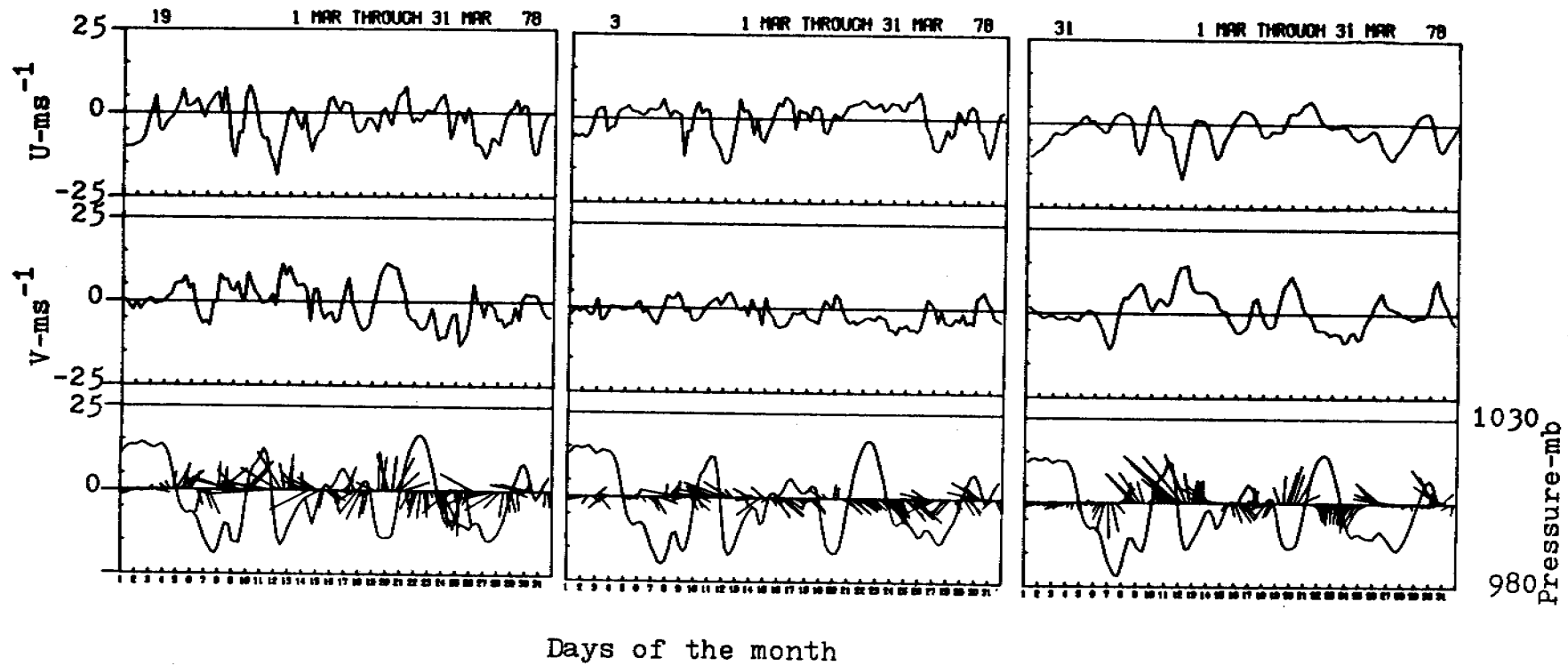


Figure 5b. Same as Fig. 5a. Curves shown are U (E-W) and V (N-S) wind components, and sea level pressure. The stick vectors point in the direction of the wind.

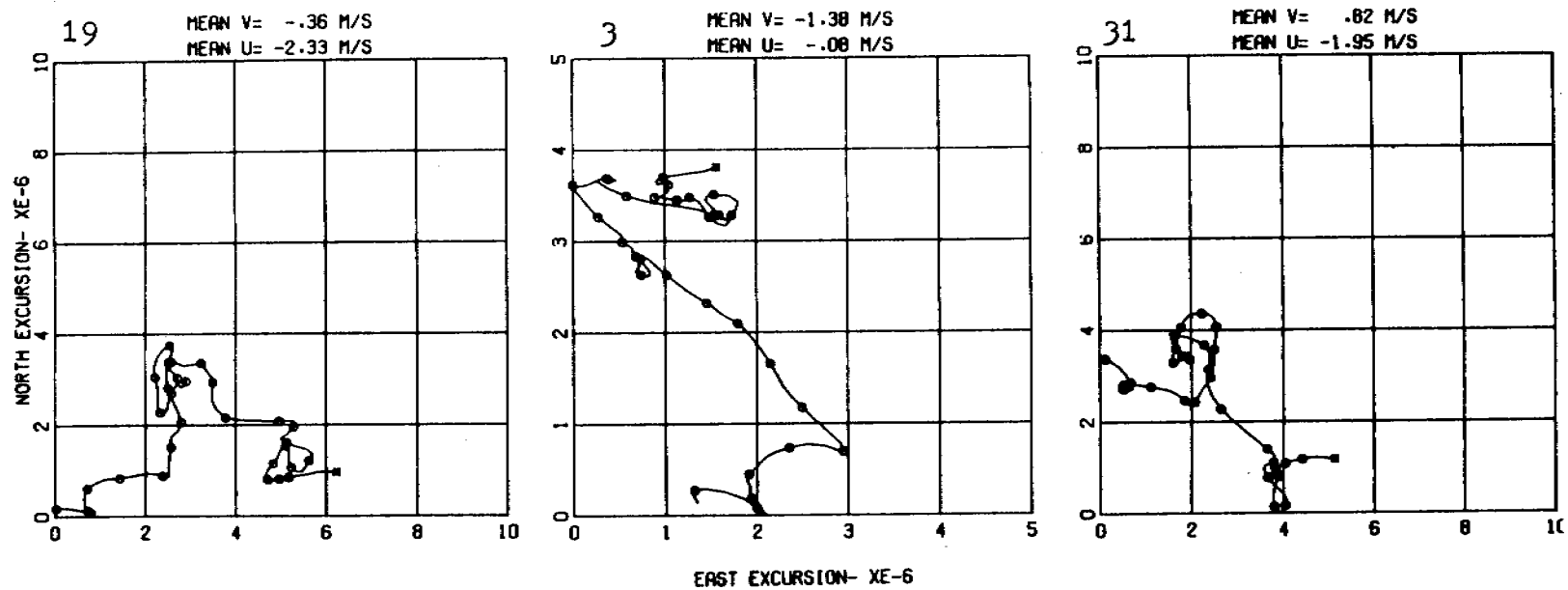
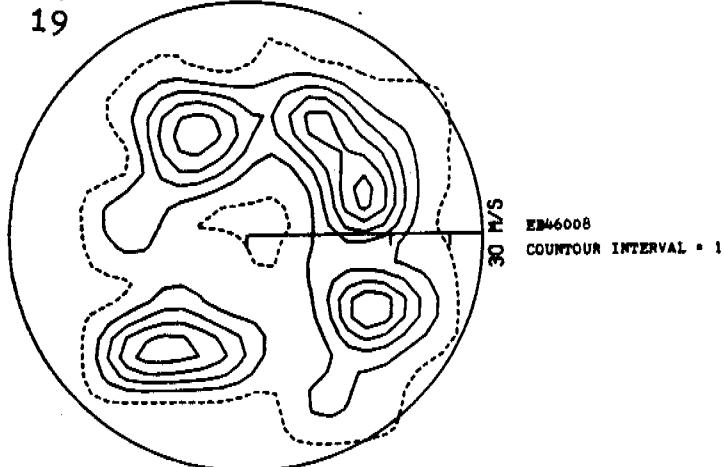


Figure 5c. Same as Fig. 5a. Curves shown are Progressive Vector Diagrams which start with the asteric.

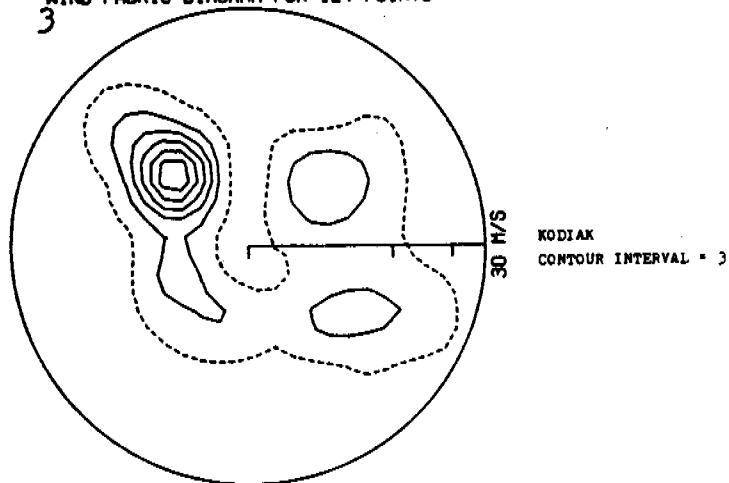
WIND FABRIC DIAGRAM FOR 124 POINTS.

19



WIND FABRIC DIAGRAM FOR 124 POINTS.

3



WIND FABRIC DIAGRAM FOR 123 POINTS.

31

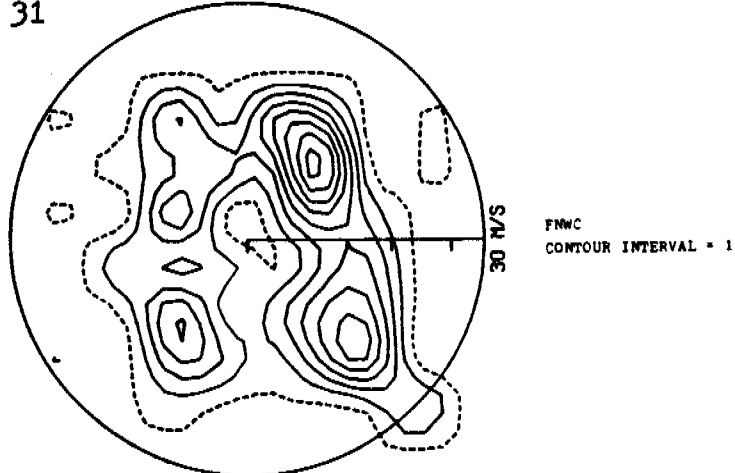


Figure 5d. Same as Fig. 5a. Fabric diagrams of the wind observations are shown here.

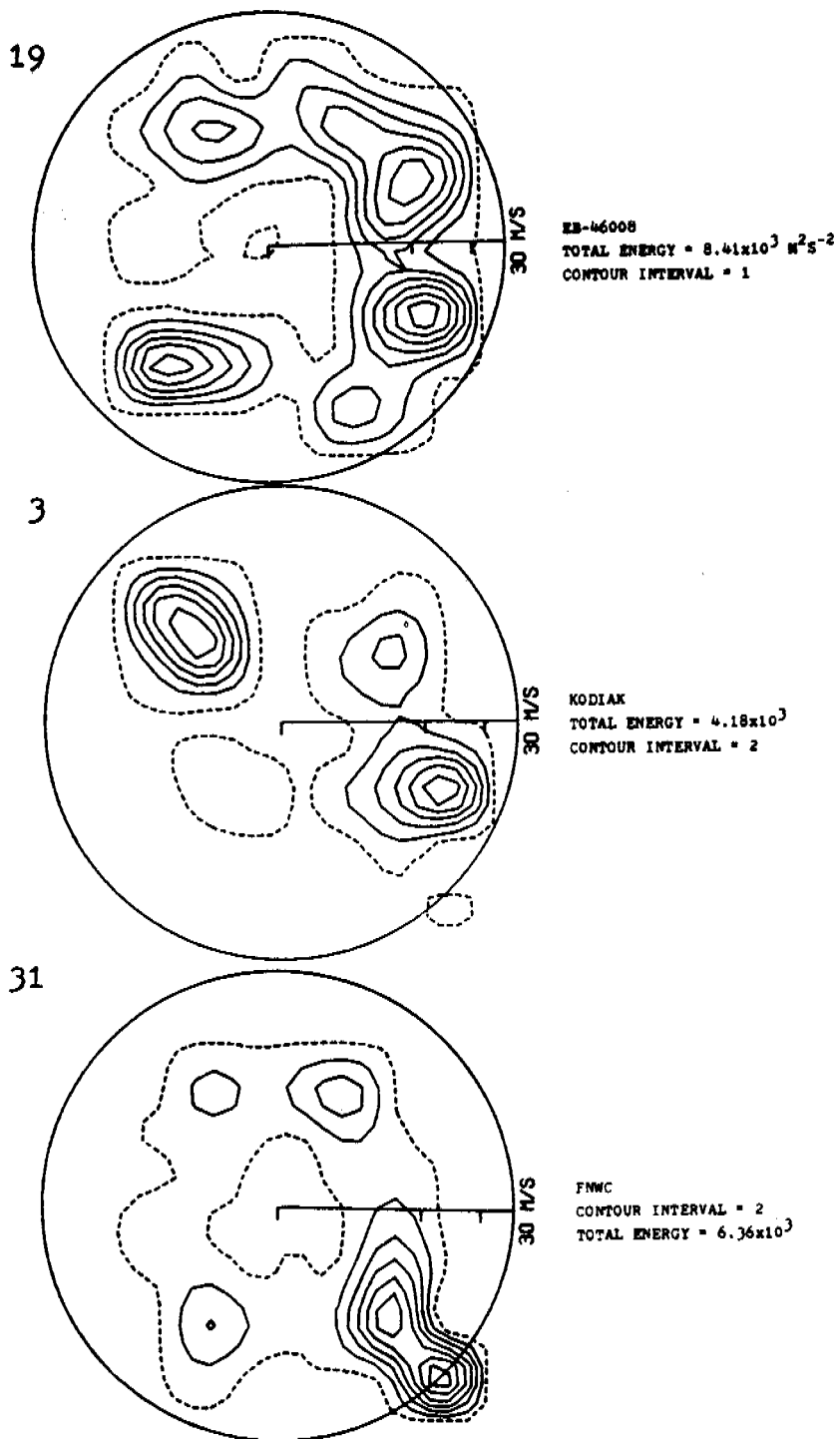


Figure 5e. Same as Fig. 5a. Fabric diagrams of wind energy are shown here.

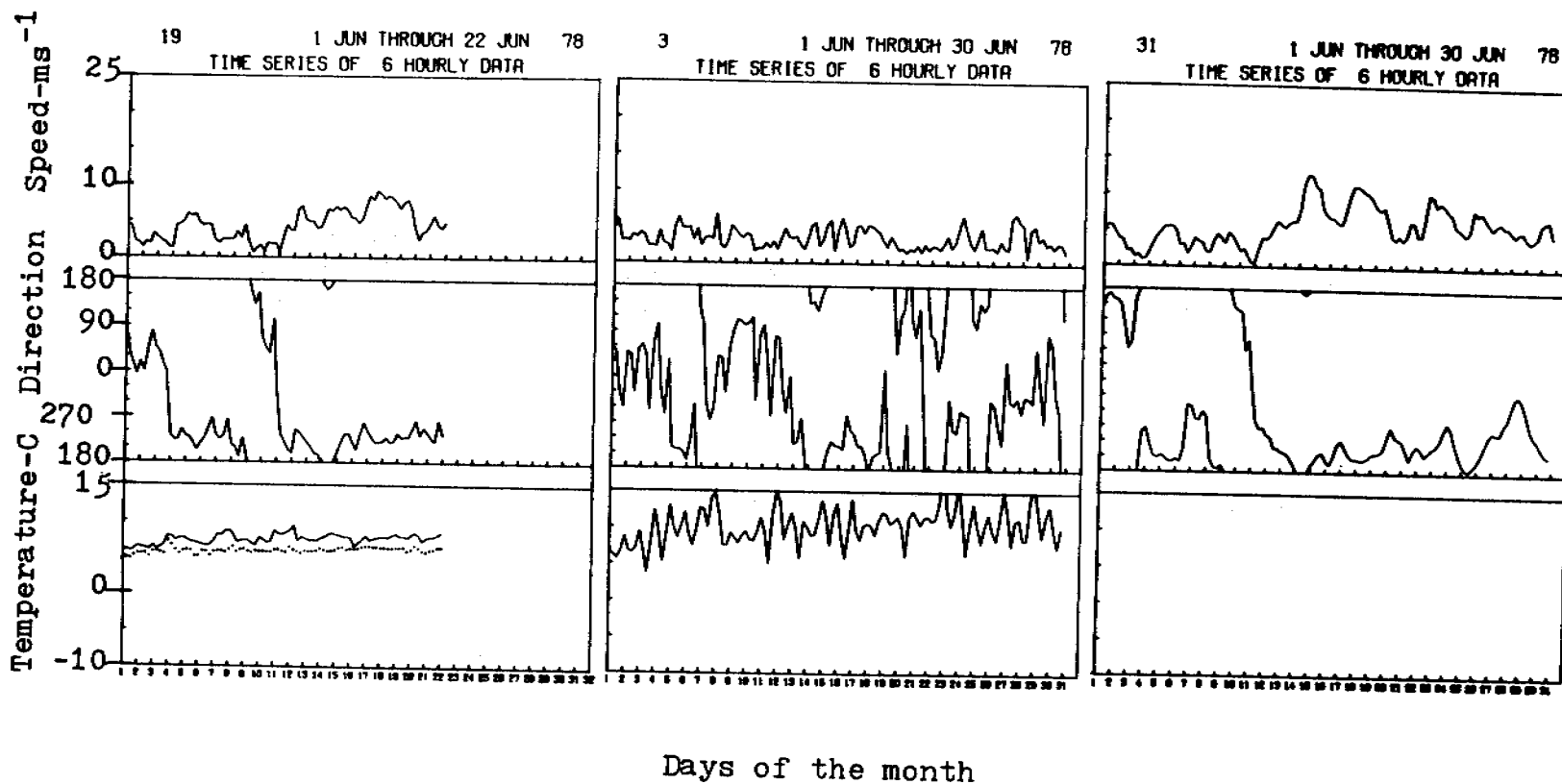


Figure 6a. Comparison of data observed at EB46008 and Kodiak, and winds computed by the Navy's Fleet Numerical Weather Central. Station codes are 19, 3, and 31 respectively. Time series plots shown here are wind speed, direction, air temperature (solid line), and sea temperature (dashed line).

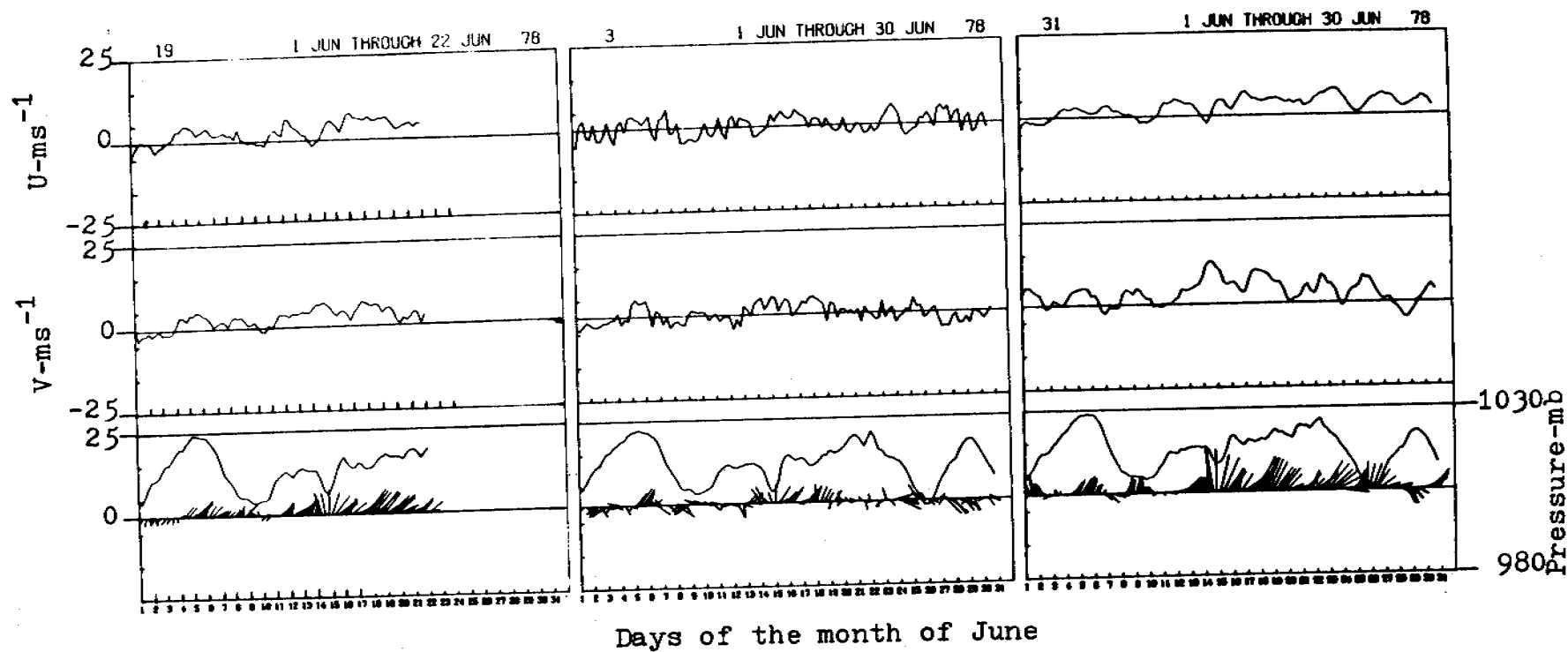


Figure 6b. Same as Fig. 6a. Curves shown are U (E-W) and V (N-S) wind components, and sea level pressure. The stick vectors point in the direction of the wind.

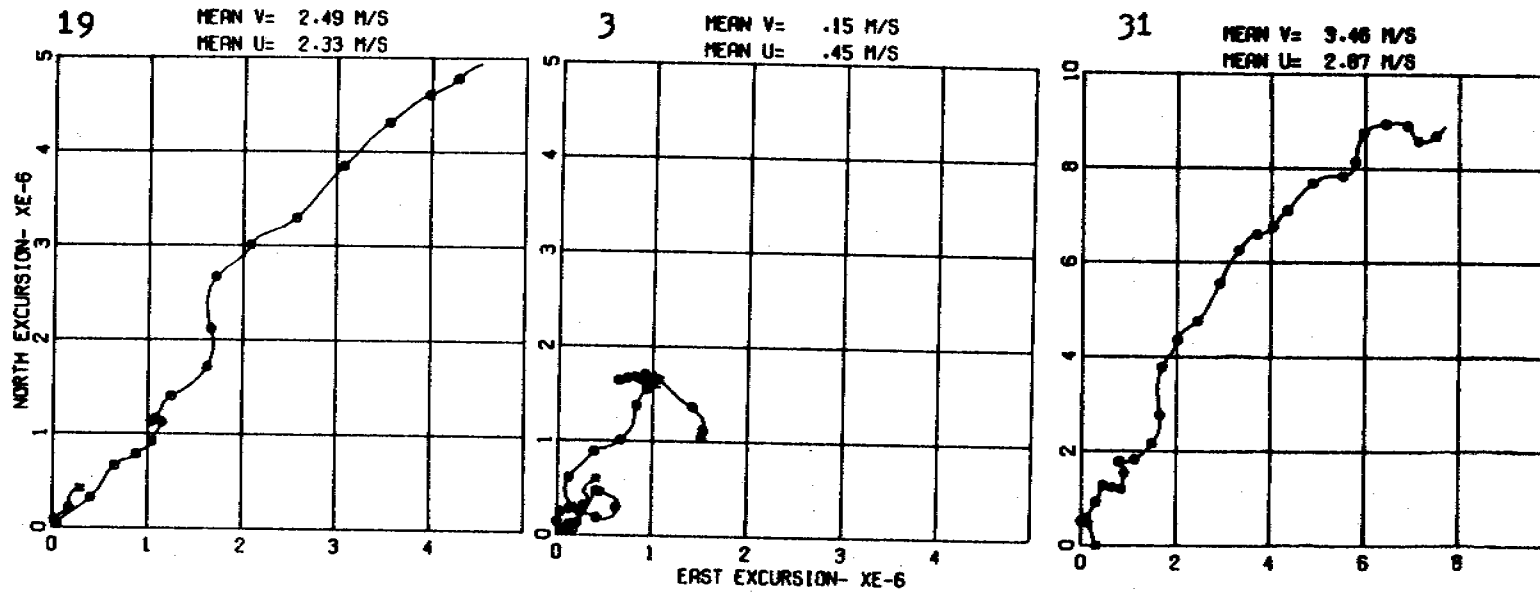
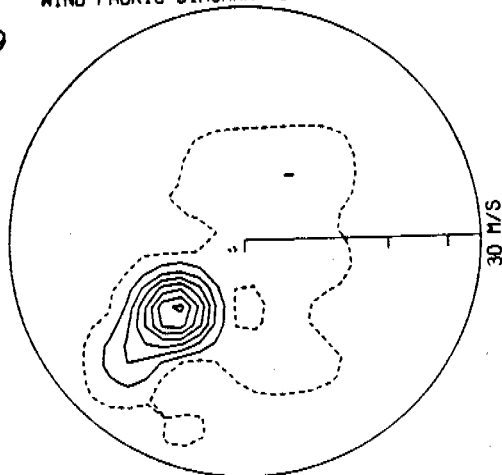


Figure 6c. Same as Fig. 6a. Curves shown are Progressive Vector Diagrams which start with the asterisk.

WIND FABRIC DIAGRAM FOR 85 POINTS.

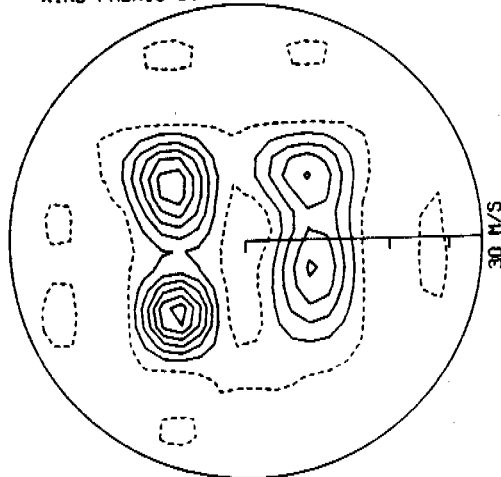
19



EB-46008
CONTOUR INTERVAL = 4

WIND FABRIC DIAGRAM FOR 120 POINTS.

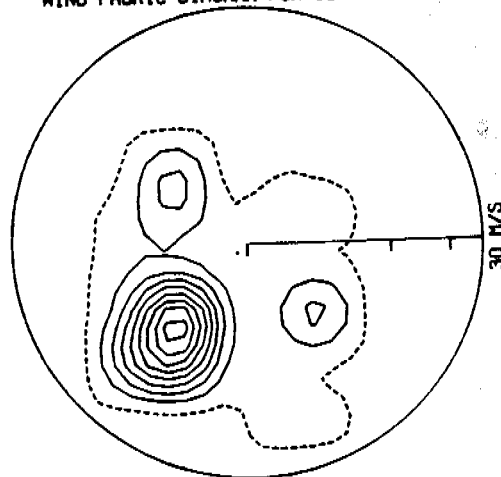
3



KODIAK
CONTOUR INTERVAL = 2

WIND FABRIC DIAGRAM FOR 120 POINTS.

31



FNWC
CONTOUR INTERVAL = 2

Figure 6d. Same as Fig. 6a. Fabric diagrams of the wind observations are shown here.

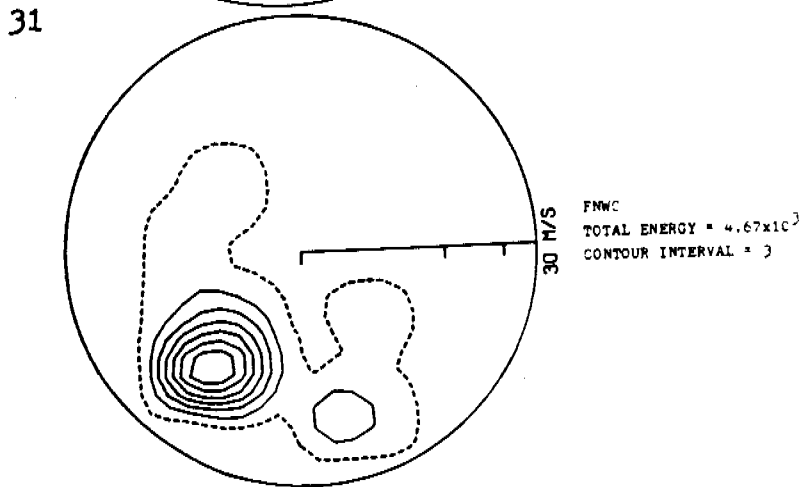
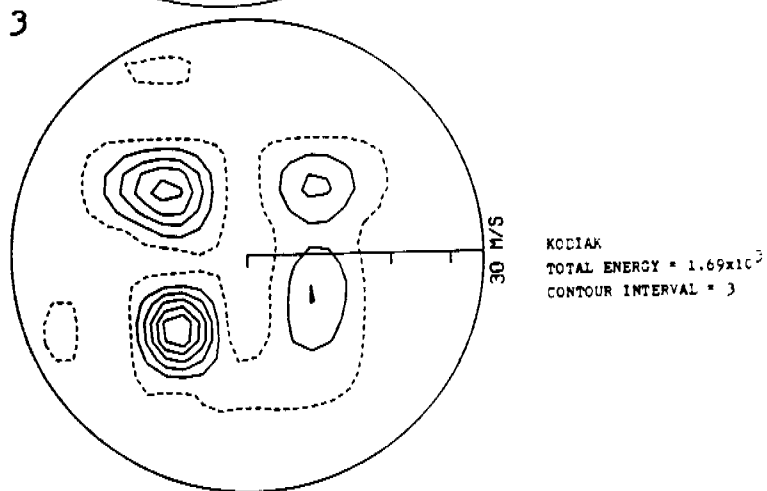
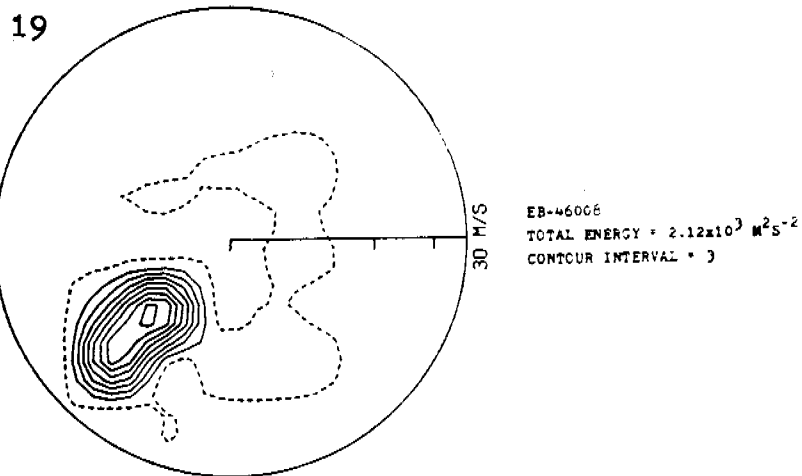


Figure 6e. Same as Fig. 6a. Fabric diagrams of wind energy are shown here.

APPENDIX D

THE RESPONSE OF COASTAL WINDS AT ALBATROSS BANKS,
LOWER COOK INLET, AND HINCHINBROOK ENTRANCE TO A
PASSING SYNOPTIC DISTURBANCE -
PRELIMINARY ANALYSIS

S. Allen Macklin

Pacific Marine Environmental Laboratory

CONTENTS

1. Introduction
2. Data Acquisition and Reduction
3. Discussion
 - 3.1 Synoptic Weather
 - 3.2 Coastal Winds
4. Summary
5. References
6. List of Figures

THE RESPONSE OF COASTAL WINDS AT ALBATROSS BANKS,
LOWER COOK INLET, AND HINCHINBROOK ENTRANCE TO A
PASSING SYNOPTIC DISTURBANCE -
PRELIMINARY ANALYSIS

1. Introduction

The continental shelf waters of Alaska are currently the site of prodigious petroleum exploration by private industry. Consequently the environmental hazard associated with off-shore development has been magnified greatly. The effective assessment and combat of spilled pollutants requires the knowledge of many factors, among which must be included the local wind field.

This study relates coastal wind fields in three proposed oil lease and transport areas - lower Cook Inlet, Albatross Banks, and Hinchinbrook Entrance (Fig. 1) - to the passage of a typical extratropical cyclone. Since the Alaskan coast is regularly affected by migrating storms, we investigate the possibility of inferring winds during an oil spill with such a synoptic scenario.

Extratropical cyclonic disturbances are thoroughly documented in basic meteorological literature (see, for example, Wallace and Hobbs, 1977). A mid-latitude cyclone originates at the crest of a wave occurring along the boundary or "front" between a cold polar air mass and a warm tropical one. The ensuing counter-clockwise circulation around the deepening low pressure center causes cold air to retreat poleward at the warm front in advance of the surface low and blow equatorward at the cold front behind the storm. Large vertical motions induced by lifting of warm air at the fronts result in precipitation. As the storm center deepens and moves farther back into the cold air mass, it dissociates itself from the juncture of the warm and cold fronts forming an occluded front. Occlusion results in the eventual decay of the cyclone; spin-off storms often generate at the old warm and cold front junction.

Individual cyclones vary in horizontal and vertical extent, in absolute pressure and pressure gradient, in temperature, in path, and in stage of development. Because of these variations it is difficult to speak either of a "typical" mid-latitude cyclone or of a major storm track in any but broad terms. Most disturbances reach Alaska in a mature, occluded state having either transited a large portion of the north Pacific Ocean or formed as spin-off lows south of the Aleutian Islands from older decaying storms. Because of the steering effect of the semi-permanent Aleutian Low, migrating cyclones tend to skirt the Aleutian Island chain and then either turn north into the Bering Sea or continue northeast into the Gulf of Alaska eventually making landfall on the southeast Alaska coast (Brower et al., 1977). This paper addresses coastal winds resulting from a spin-off storm which tracked across the east end of the Aleutian archipelago into the Bering Sea (Fig. 2).

2. Data Acquisition and Reduction

The Alaskan Regional Office of the National Weather Service furnished synoptic charts of sea level pressure over the north Pacific Ocean and hourly surface winds from stations at Homer, Kenai, Kodiak, Cordova, and Middleton Island (Fig. 1). Three hourly surface wind data collected by environmental buoys EB 46006, EB 46008, and EB 46009 were provided by the NOAA Data Buoy Office. The Fleet Numerical Weather Center (FNWC) of the United States Navy supplied a numerically-generated wind record (Bakun, 1973) for a location on Albatross Banks designated FNWC in Fig. 1. Additional synoptic information was obtained from Wilson (1978).

The synoptic charts, segments of which are reproduced in Fig. 3 a-h, were used to define the storm track of Fig. 2. Wind vector time series (Fig. 4) were produced from the surface wind data in the three oil lease regions. Estimates of synoptic

pressure gradient in mb km^{-1} were obtained by dividing the pressure difference between a point at 58°N , 150°W (Fig. 1) and the storm center by the distance between them.

3. Discussion

3.1 Synoptic Weather

Figure 3 a-h documents the synoptic field from 12Z 11 March 1978 every six hours to 06Z 13 March 1978. During this period the winds in the study areas were under the influence of the depicted cyclone which developed in the far south circulation of a storm which decayed March 10 in the Bering Sea. The storm track is shown in Fig. 2.

By 12Z on the 11th, the low had deepened to 959 mb and occluded (Fig. 3a). Cook Inlet and Albatross Banks some 1300 km northeast of the storm center were already experiencing east winds. Hinchinbrook Entrance lay beneath an extended high pressure ridge blanketing the mountains of western North America. An occluded front extended ESE from the low center. At this time the synoptic pressure gradient was determined to be $.039 \text{ mb km}^{-1}$. In the next six hours the storm moved 270 km to the NNE (Fig. 3b); its tightened gradient ($.045 \text{ mb km}^{-1}$) was reflected in increasing wind speed over the oil lease regions. Hinchinbrook Entrance reported easterlies but remained on the ridge border.

At 00Z on the 12th (Fig. 3c) the pressure gradient reached its highest value of $.049$ and Albatross Banks experienced 20 m s^{-1} winds as the front approached. To the north the storm began to flow across the central Alaskan plateau between the Alaskan and Brooks mountain ranges as the ridge steered it northward. The low pressure center receded farther into the cold air. By 06Z (Fig. 3d) the front passed Albatross Banks and was positioned over Cook Inlet; the storm center crossed the Aleutian Islands and the gradient relaxed to $.039$. In the

next six hours the cyclone rotated about 30° counter-clockwise and retrograded 150 km bringing southeasterlies to Albatross Banks. The gradient diminished to $.029 \text{ mb km}^{-1}$ but wind speed picked up at Hinchinbrook Entrance as the front approached. At 18Z the low was filling rapidly (Fig. 3f) and the front had still not reached Hinchinbrook Entrance. Although the synoptic gradient further decreased to $.019$, the local Hinchinbrook gradient was sufficient to maintain high winds. Wind speeds in the other areas were significantly reduced.

No definable front existed at 00Z on the 13th (Fig. 3g) and the storm continued to fill until it was absorbed into a new system in the Pacific Ocean after 06Z. At these times winds were moderate over the region with a synoptic pressure gradient of $.016 \text{ mb km}^{-1}$.

3.2 Coastal Winds

In discussing the regional manifestations of cyclone passage on coastal winds, frequent mention will be made to the wind vector time series presented in Fig. 4. These data are grouped by region and span the same time period covered by the synoptic weather discourse of Section 3.1. Wind direction is plotted in the meteorological sense, i.e. in the direction from which the wind is blowing; a shaft length of one centimeter is equivalent to a 10 m s^{-1} wind.

Orography plays a dominant role in the wind patterns of Cook Inlet (see Appendix A, OCSEAP 1979 Annual Report, R.U. 367). Two nearly orthogonal wind channels, one oriented N-S along the Cook Inlet basin the other stretching E-W across lower Cook Inlet, intersect in the vicinity of EB 46007. Throughout the synoptic episode this data buoy measured easterly winds along the latter channel. Maximum winds of 16 m s^{-1} were recorded at 06Z 12 March, which was also the time that the occluded front was in the area. Veering (clockwise rotation of the wind), normally accompanying frontal passage, was restricted by the topography. Homer winds generally reflected light flow down the

Inlet axis or drainage winds out of Kachemak Bay. Only during the period of frontal passage did Homer register strong easterly winds. Kenai, situated on the N-S orographic wind channel recorded down-channel winds throughout the cyclone's history! Again, the highest wind speed (10 ms^{-1}) corresponded with frontal passage at about 12Z on the 12th.

Environmental buoy EB 46008 on Albatross Banks recorded typical over-the-water wind response to the passing storm. With the low pressure center far to the southwest on March 11, winds at the buoy were from the east. The wind peaked in magnitude (20 m s^{-1}) and veered as the occluded front transited Albatross Banks at about 00Z on the 12th. As the storm retrograded into the Bering Sea, surface winds moderated to light southerlies. The FNWC computed winds (not independent of any of these wind observations) tended to overestimate the wind speed and, in the period prior to frontal passage, indicated flow with too great a southerly component. Kodiak's wind observations mirrored EB 46008 values except for a speed reduction due to friction of about 24% before the front passed and a 36% post-frontal reduction.

Middleton Island, south of Hinchinbrook Entrance, first reported easterly wind associated with the cyclone at 15Z on 11 March. For most of the storm's duration, wind direction remained essentially ESE; highest speeds occurred in a 6 hour period following 11Z on 12 March. EB 46009, some 90 km to the north, reported NE to ENE winds of near-constant magnitude over the entire observation period. Cordova, a land station 75 km east of the buoy exhibited strong northeasterly flow at the time that Middleton Island experienced its strongest ESE winds. Such coastal anomalies are assumed to be a product of orographic channeling and drainage winds. Recalling that Hinchinbrook Entrance lay at the edge of a high pressure ridge which overlay the mountainous coastal region to the north and east, Cordova winds can be explained in terms of drainage winds exiting the numerous glacial estuaries of the region under the influence



of a favorable pressure gradient. Data buoy winds at Hinchinbrook Entrance were apparently channeled by mountainous islands to the east and west. Whether the channeled air was of maritime or drainage origin remains to be determined.

4. Summary

Surface winds in three Alaskan coastal areas were explained in terms of synoptic characteristics of a mid-latitude cyclone. This storm influenced the study regions over the period 11 March to 13 March 1978 as it moved north out of the Pacific Ocean across the Aleutian Islands and into the Bering Sea. Maximum observed surface winds coincided with passage of an occluded front associated with the storm. Coastal winds in lower Cook Inlet and Hinchinbrook Entrance were dominated by orography. Winds over the Albatross Banks were observed to be a direct result of synoptic forcing alone.

Future work must address more completely the complex air flow in the Hinchinbrook Entrance region. It is likely that environmental buoy EB 46009 is exposed to a very local wind pattern and is not representative of the region in general. Finally, the complete synoptic study is to be repeated for a cyclone which tracks into the Gulf of Alaska exposing the study areas to northerly and westerly winds in its wake.

6. List of Figures

- | Figure | Caption |
|--------|---|
| 1 | Map showing lower Cook Inlet, Albatross Banks Hinchinbrook Entrance, and data sources for this study. |
| 2 | Track of an occluded Alaskan storm. Circles indicate position of the surface low pressure center at the designated times. |
| 3 | Sea level pressure, frontal position, and observed winds at a) 12Z and b) 18Z 11 March 1978, c) 00Z, d) 06Z, e) 12Z, and f) 18Z 12 March 1978, and g) 00Z and h) 06Z 13 March 1978; pressure contours are in meteorological convention (00=1000 mb),  , and designate cold, warm, and occluded fronts, respectively; full, half, and quarter flags on wind vector shafts indicate 5, 2.5, and 1 m s ⁻¹ , accordingly. |
| 4 | Surface wind vector time series for regional data sources;  indicates a 10 m s ⁻¹ wind from the east. |

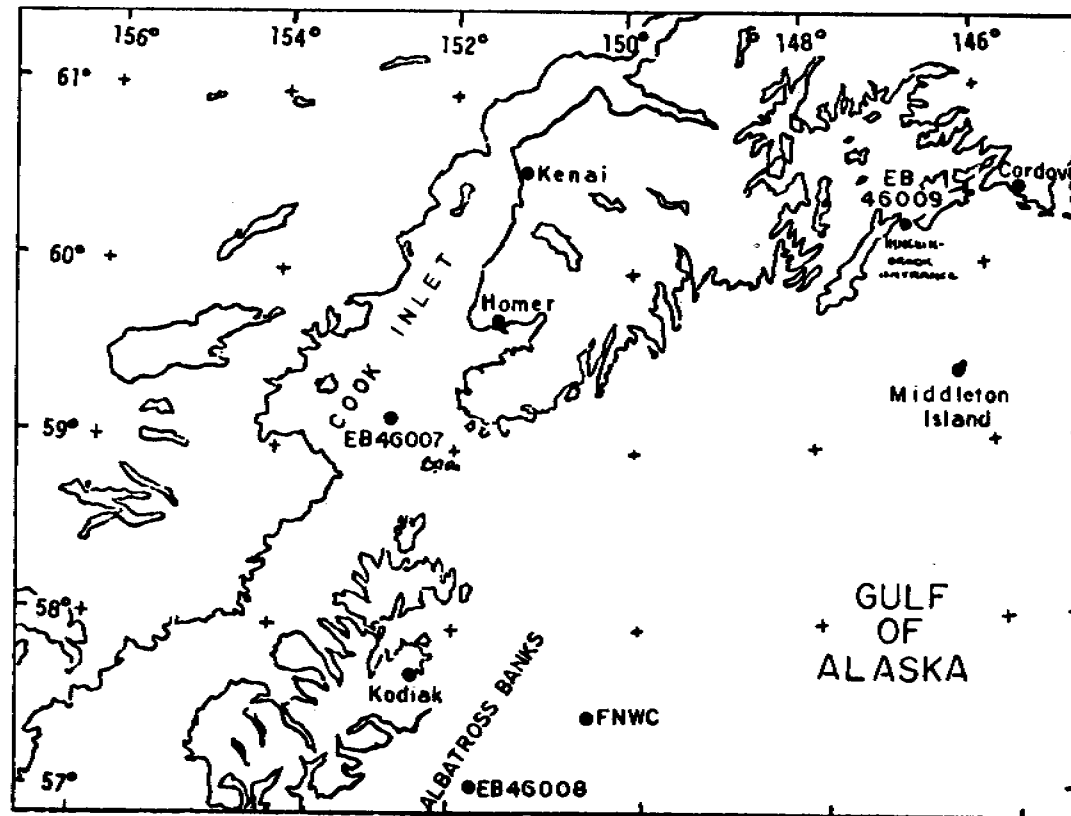


Figure 1. Map showing lower Cook Inlet, Albatross Banks, Hinchinbrook Entrance, and data sources for this study.

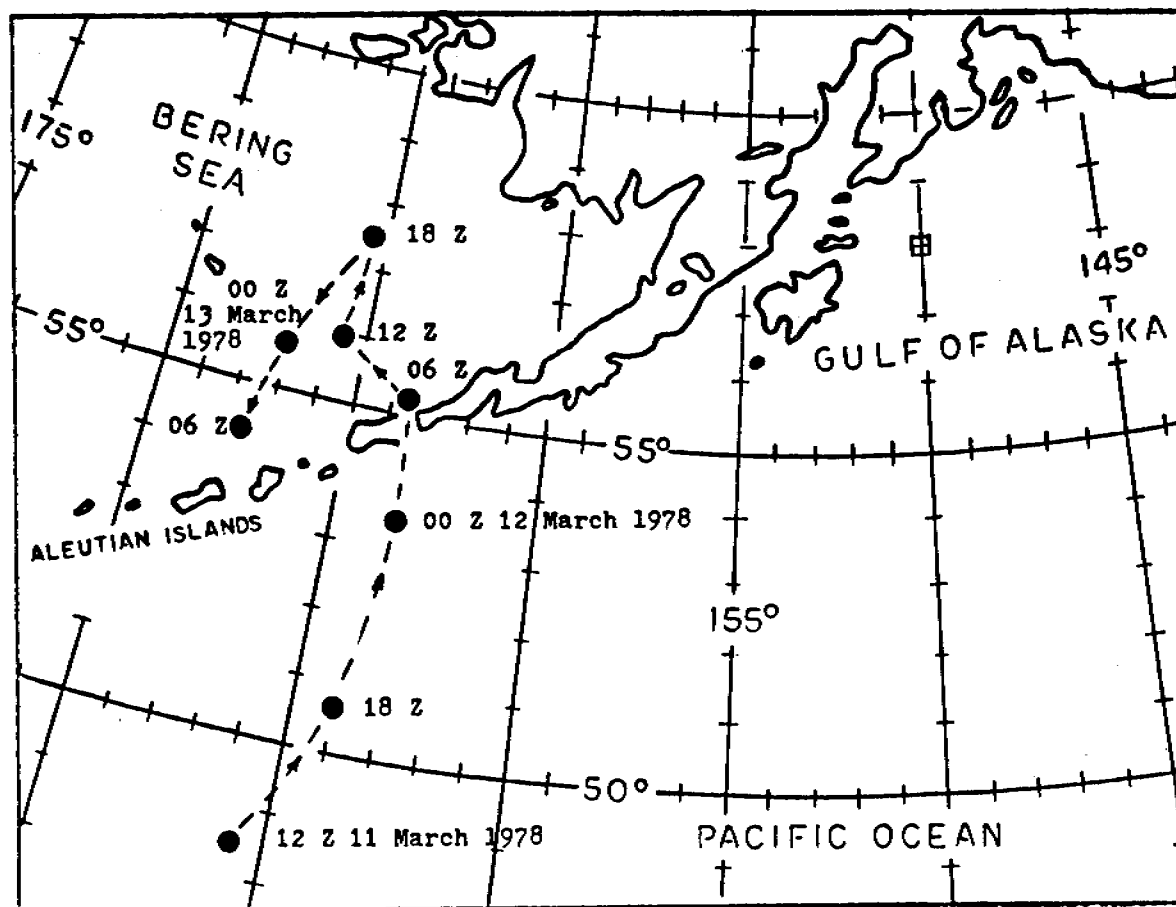


Figure 2. Track of an occluded Alaskan storm. Circles indicate position of the surface low pressure center at the designated times.

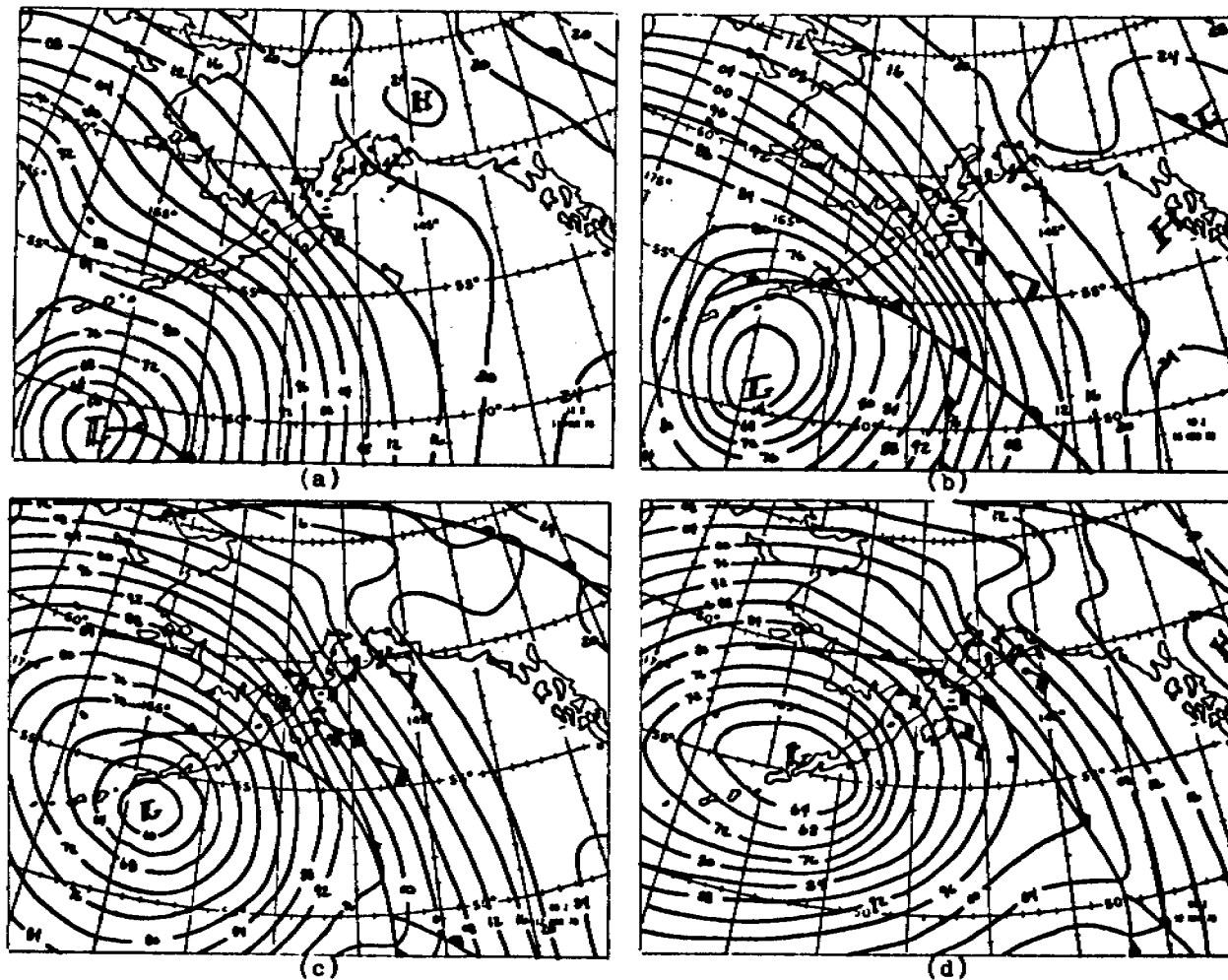
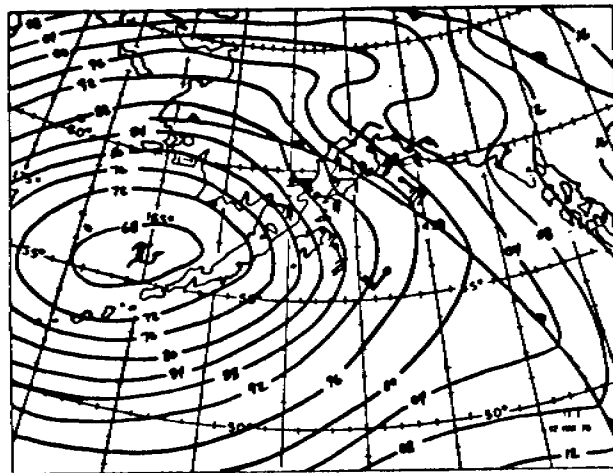
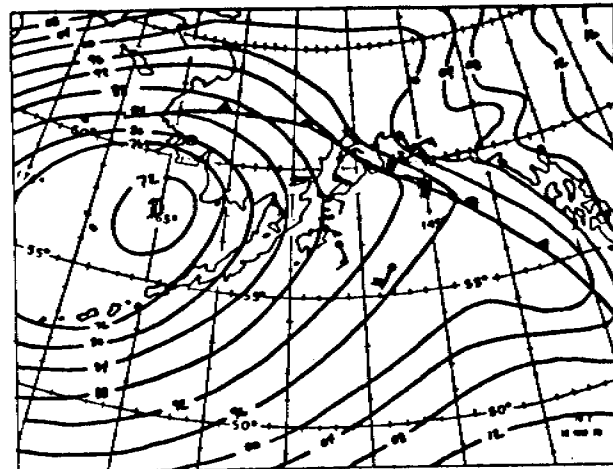


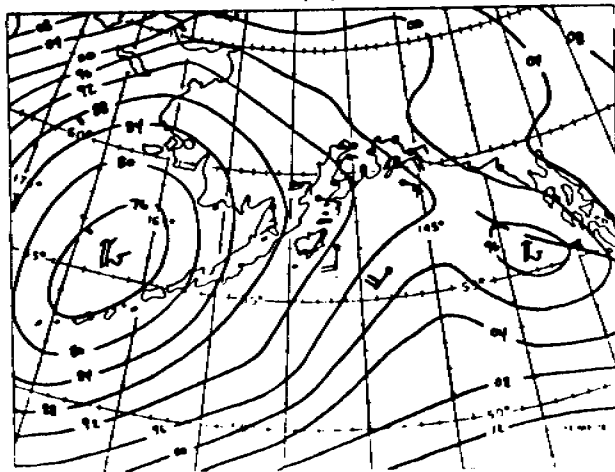
Figure 3. Sea level pressure, frontal position, and observed winds at a) 12Z and b) 18Z 11 March 1978, c) 00Z, d) 06Z, e) 12Z, and f) 18Z 12 March 1978, and g) 00Z and h) 06Z 13 March 1978; pressure contours are in meteorological convention (00=1000 mb), \blacktriangle , \blacktriangle , and \blacktriangle designate cold, warm, and occluded fronts, respectively; full, half, and quarter flags on vector shafts indicate 5, 2.5, and 1 m s^{-1} , accordingly.



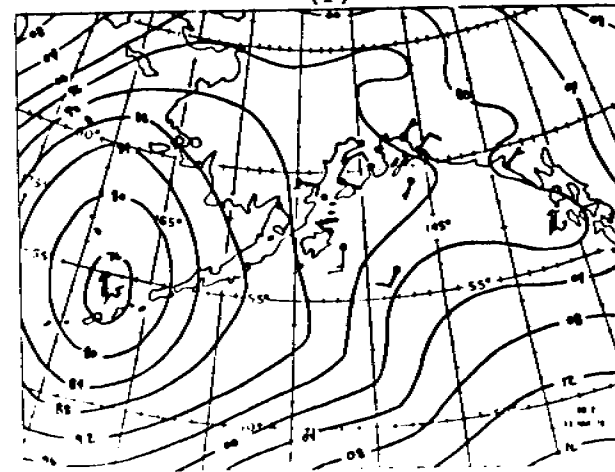
(e)



(f)



(g)



(h)

Figure 3 (cont).

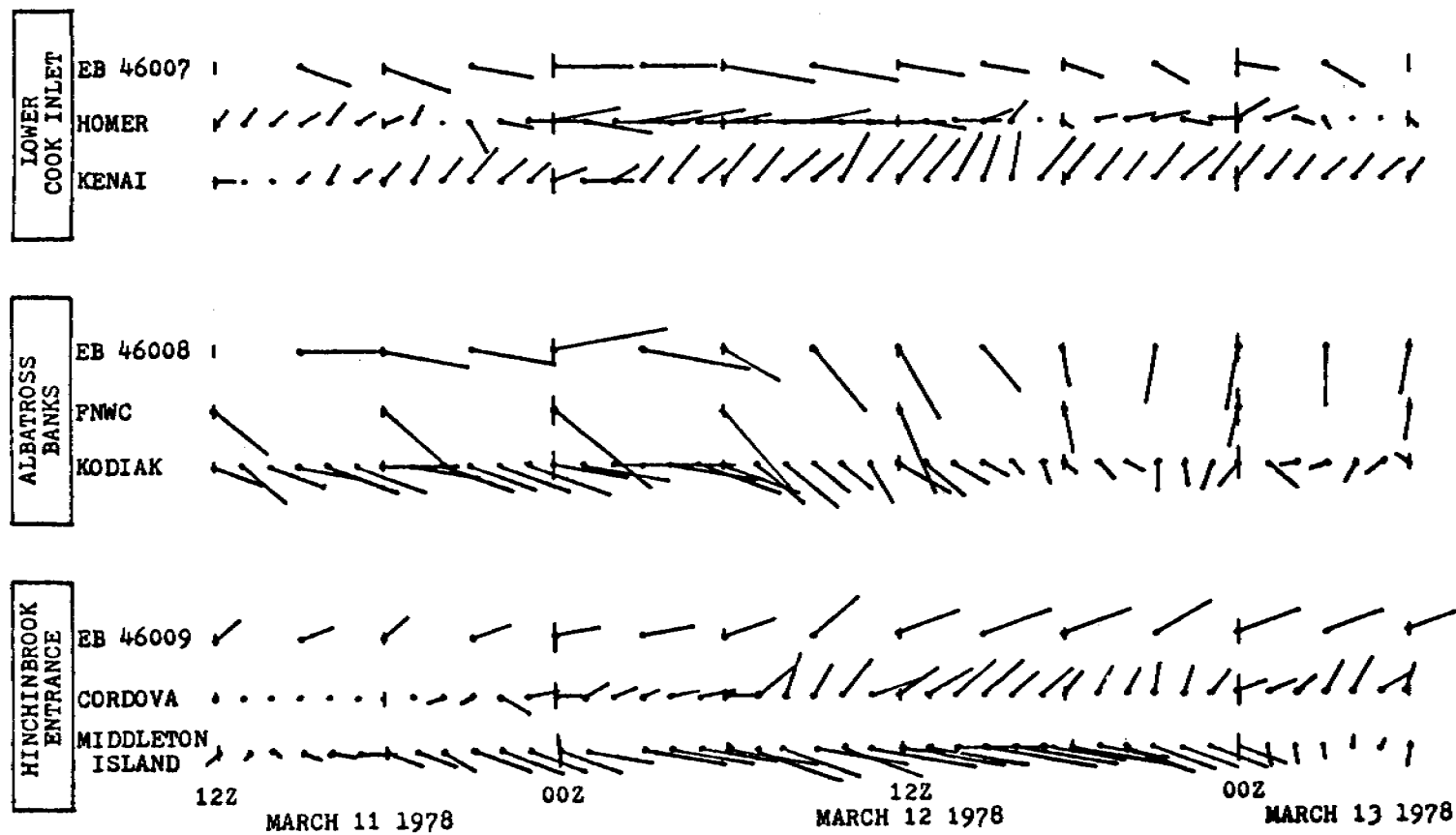


Figure 4. Surface wind vector time series for regional data sources; —•— indicates a 10 m s⁻¹ wind from the east.

ANNUAL REPORT

Research Unit: 430
Reporting Period:
31 March 1978 -
1 April 1979

BOTTOM AND NEAR-BOTTOM SEDIMENT DYNAMICS
IN LOWER COOK INLET

Principal Investigators

David A. Cacchione
David E. Drake

Pacific-Arctic Branch of Marine Geology
U.S. Geological Survey
345 Middlefield Road
Menlo Park, California 94025

1 April 1979

I. Summary

In 1978 we carried out an intensive field investigation of near-bottom and bottom sediment movement within a small area of lower Cook Inlet that contains bedforms of multiple scales. This research effort focuses on the mechanisms which control the transport of sediments, the temporal variability of this transport, and the contrasts in transport at trough and crest locations of the largest bed features. Our major objective, to provide a spatial and temporal description of bottom sediment movement in this highly complex sand wave environment, was motivated by the need to assess the potential environmental hazards posed by excessive erosion and sand wave migration.

Bouma and Hampton (RU 327) had previously described the bottom morphology of this area based on their earlier cruise data. Their results showed that the medium-scale sand waves (1-3 m heights) and the larger scale bed features (5-10 m heights) had morphologic characteristics that suggested active maintenance and/or migration. Our work was designed to provide additional information on the mobility of the bottom sediment in these areas, and to increase our understanding of the relationships between bottom flow and sediment dynamics there.

Thus far, we have found that active transport of bottom sediments occurs during fair weather and normal tidal stages. The dominant fluid stresses causing this transport are the reversing tidal currents, but large turbulent eddies, probably generated by the interaction of the tidal currents with the large sand waves also add significantly to the total stress field. The most active transport occurs near large sand wave crests, a result of flow intensification (streamline convergence) over the topographic highs. Sediment ripples (~1-3 cm heights) reverse orientation with successive ebb-flood cycles, and also migrate slowly in response to slightly excessive ebb currents. These ripple movements are active in both trough and crest locations.

Owing to a leak in one of the power cables on the long-term Geoprobe system, our hopes to examine long-term variations in bottom stress and sediment movement will be limited to analysis of effects lasting over a few weeks (~15 days). This additional data will be extremely useful in understanding spring-neap tidal variations and their effects on sediment movement, and in providing additional information on the turbulent eddies and their role in sediment dynamics.

At this point in our analysis we conclude that, although active movement of bed materials is caused by tidal currents, no evidence for migration of the largest bed forms has been found. Our analyzed data is limited to several days; further analysis of the longer term record is in progress. We cannot eliminate the possibility that very intense bottom stresses ($u_* > 10$ cm/s) might occur during highest spring tides, particularly if storm effects are superimposed.

II. Introduction

A. General Nature and Scope of Study

This research involves a field investigation of near-bottom and bottom sediment transport at selected sites in Lower Cook Inlet. Of particular interest are the temporal and spatial variations in sediment movement within the area of large sand waves in the central portion of the inlet (Bouma and Hampton, RU 327). In this study we hope to increase our understanding of the fluid mechanisms which control the transport process, and the changes in the sediment surface that occur in response to the fluid stresses.

Estimates of the quantities and rates of materials transported along and above the seafloor in areas of energetic currents are necessary to make quantitative

assessments of potential environmental hazards due to erosion and sediment instability. This work hopefully will provide sufficient direct and indirect data on the sediment movement and bottom fluid stresses at the experimental sites to aid in this assessment. The presence of large-scale bed forms and other smaller bed features, together with previous data that show strong tidal currents near the sea floor, strongly motivated initiation of this work.

Bouma and Hampton (RU 327) have reported on the geological and geophysical characteristics of lower Cook Inlet, and have documented the existence of several scales of bed forms in the region (RU 327). This work provides an excellent background to support our topical investigation of sediment dynamics. Their previous bathymetric charts, morphologic descriptions and sediment analyses were used to guide our experimental design and the selection of the instrument deployment sites. In addition, we were fortunate to have both A. Bouma and M. Hampton actively assist us in our field program on the R/V SEA SOUNDER.

This investigation complements similar work which we have previously undertaken in the northern Bering Sea under BLM/NOAA (OCSEAP) support, and on the continental shelf west of Los Angeles harbor under BLM support. In each of these experiments, our principal focus has been the response of the bottom and near bottom sediments to fluid stress. In particular we are attempting to estimate the relative importance of the various physical mechanisms; for example, surface waves, internal waves, tides, mean flow, etc., in causing or controlling the movement of these materials in each of the study areas. By carrying out these experiments in distinctly different geological and oceanographic settings, we eventually hope to compare the sediment response (initiation of motion, bed form production and migration, resuspension, etc.) in these regions and to develop a semi-quantitative model for sediment transport in different continental shelf environments.

B. Specific Objectives

The major focus of this work is to provide quantitative estimates of bottom sediment transport within an area of large bed forms in lower Cook Inlet. Specific objectives of this work are:

- (1) To provide a spatial and temporal description of bottom sediment transport.
- (2) To develop estimates of bottom sediment flux related to high energy events such as storms and tides.
- (3) To relate the magnitude of bedshear to the initiation of bottom sediment movement for each sedimentary environment.
- (4) To provide detailed descriptions of sea floor physiography and surface sediment characteristics in selected areas of observation.
- (5) To describe changes in the surface character of the sea floor over relatively long duration (at least one month).

C. Relevance to Problems of Petroleum Development

High rates of sediment transport and erosion are potentially hazardous to sea floor installations like oil well completion structures and pipelines. The presence of the large sand waves (\approx 5-8 m heights) in central lower Cook Inlet raises several questions regarding their origin, present mobility, and interaction with the bottom currents. This work is intended to provide data on the intensity of bottom flow and sediment movement within the region of large sand waves previously described by Bouma and Hampton (RU 327). These data will hopefully aid in the determination of mobility of bed forms in Cook Inlet, and the potential hazard that excessive sediment transport might create.

Additionally, waste materials introduced into the bottom environment by drilling operations (e.g., drill muds) and oil spilled during recovery accidents will be in part be transported by the bottom currents. This work will assess the magnitude and direction of this transport and also provide indications of the extent of vertical mixing above the sea floor at the study sites. If oil-contaminated sediments are effectively transported large distances along the bottom, and resuspended well up into the overlying water column, the spatial extent of harmful effects from these pollutants could be considerably greater than otherwise anticipated. For example, the strong tidal currents in Cook Inlet can be effective in moving oil and trace metals over large distances. A tidal current with mean speed of 20 cm/s over 6 hours will produce transport of near-bottom suspended matter over distances of about 4 km. If these near-bottom materials are contaminated with oil or other pollutants, the impact on the local ecology will have a length scale of at least that distance.

The ability to predict accurately the movements of pollutants in the sea is strongly dependent on our knowledge of local transport processes. Specific regions, particularly those with complex bottom topography like Cook Inlet, will have unique aspects to the mechanisms which control the paths and amounts of material that are moved. This study will hopefully provide insights into this transport process, and provide engineers, scientists and others a quantitative basis for understanding and prediction.

III. Current State of Knowledge

Bouma and Hampton (RU 327) and Hayes et al. (RU 138) have provided detailed discussion of the geological setting and physical oceanographic conditions, respectively, in lower Cook Inlet. Lower Cook Inlet is defined as the southern portion of the inlet between Kalgin Island (about 60°17'N) and the Barren Islands (about 59°00'N). Our work in this project is limited to a small section within central lower Cook Inlet (Figure 1) where large sand waves are typical bottom features.

A. General geological setting

Cook Inlet is a tidal estuary about 350 km long and 100 km wide at the mouth, oriented in a N-NE direction. Bouma and Hampton (RU 327) point out that large glaciers during the Pleistocene period eroded previously deformed bedrock and deposited unconsolidated sediments throughout Cook Inlet. Much of the present near-surface sediments that are actively transported by the currents are these relict materials. No major rivers presently discharge into the lower inlet, and the present supply of sediments to the system is thought to be minimal (Bouma and Hampton, RU 327).

A bathymetric chart, Figure 1, shows several embayments cut into the lower Cook Inlet coastline, and the presence of the volcano, Augustine Island, on the western side. The contours show an elongate trough extending from about 60°N to about 59°20'N parallel to the major north-northeasterly orientation of the inlet. The maximum water depth in this trough is about 75 m. The water depths in our study area (A in Figure 1) were 55-64 m. The inlet terminates in a gently sloping ($\approx 1/3^\circ$) ramp where water depths gradually deepen to about 200 m west of Barren Islands.

Bouma and Hampton (RU 327) have described the distribution of sediments and bed forms throughout lower Cook Inlet. They and Sharma and Burrell (1970) show that the surface sediments become finer toward the mouth of the lower inlet, with mean sizes of about 0.4 mm in the north-central area decreasing to about 0.15 mm

near the ramp. The sediments are generally well to moderately-well sorted, with poorer sorting in and near embayments. Excellent summaries of bed form types and distributions found in lower Cook Inlet are given by Bouma et al. (1977) and Bouma et al. (1978). They report that bed features of most scales and slopes are present, including ripples, sand waves, dunes, mega-ripples, sand ribbons, and sand ridges.

In the area of our experiment, site A in Figure 1, three major bed features were present:

- (1) ripples with heights of 1-4 cm, wavelengths of 10-30 cm;
- (2) medium sand waves with heights of 10 cm-1 m, wavelengths of 5 - 100 m; and
- (3) large sand waves with heights of 3 - 8 m, wavelengths of 300-1000 m.

B. General physical oceanography

The general oceanographic conditions in lower Cook Inlet for the summer period of 1973 are reported by Muench et al. (1978). Physical oceanographic data show that currents are highly variable in space and time. Reversing M_2 tidal currents with near-surface speeds of 3-5 knots, are most energetic along the eastern side. Muench et al. (1978) show that low to nil tidal currents are found east of Augustine Island and toward the southern boundary (ramp). In the area of our work (Figure 1), the tidal current ellipse has its major axis in a north-northeasterly (flood) to south-southwesterly (ebb) orientation, with surface current speeds of 1 to 2 knots.

The summer mean flow regime (Muench et al., 1978) has relatively strong southerly flow along western portion of the inlet, which transports less saline water diluted by river discharge from the upper inlet. A weaker northerly return flow in the upper layers moves into the inlet along the eastern border, mixing with the more intense southerly flow in a confused mean flow pattern near central lower Cook Inlet. The data shown by Muench et al., 1978, indicate that along the ramp, the mean flow at about 104 m depth on the eastern side of the ramp was southerly and persistent with speeds less than 10 cm/s.

A third important factor for which little published information is available is the storm effect. Increased near-bottom currents due to strong storm winds in fall and winter and upwelling/downwelling currents are probably very significant throughout lower Cook Inlet. Hopefully the latest field data taken by PMEL oceanographic instrumentation will provide new information on these flows.

IV. Study Area

Figure 1 shows the study area and general bathymetry. Area A in Figure 1 outlines the deployment sites of three Geoprobe tripods and the location of our most intensive shipboard sampling program. Large sand waves (\approx 5-8 m heights) previously surveyed and reported by Bouma and Hampton (RU 327) are the major bathymetric features in area A. Smaller sand waves and sediment ripples are also abundant in that area.

In addition to our intensive shipboard survey in area A, Figure 1, we also conducted a survey of bed forms, currents, and suspended sediments within area B. This particular survey was undertaken to assess the feasibility and desirability for long-term Geoprobe deployment within an area of medium- to small-scale sand waves.

Based on the evaluation of shipboard data collected during the cruise, and after consultations with Bouma and Hampton (who participated in the field work) we opted to deploy the long-term Geoprobe within area A. One of the overriding considerations in this decision was the need for data on potential hazards to OCS petroleum develop-

ment. The quantity of sediment transported as large sand waves and the time history of this transport are critical factors in assessment of the potential hazard to bottom structures in lower Cook Inlet.

In addition, we have estimated that current speeds in excess of 150 cm/s at 2 m above the sea floor will possibly damage the Geoprobe tripod instruments or topple the structure. Therefore, we wanted to obtain near-bottom current speed data at the possible deployment sites before making a final selection. Our shipboard measurements indicated that maximum speeds at about 2 m above the bottom in area A, were less than 100 cm/s during peak tidal flow. Therefore, we decided to use area A for the deployment of the long-term Geoprobe.

V. Sources, Methods, and Rationale of Data Collection

During our field work we obtained two basic types of data: (1) shipboard data collected from the R/V SEA SOUNDER, and (2) time-series data taken and recorded with Geoprobe tripods. We were fortunate to have considerable background data and discussions provided by Bouma and Hampton (RU 327) and Charnell, Muench et al. (PMEL, personal communications) regarding the geological framework and physical oceanography, respectively, of this region. Our plan was to concentrate on shipboard measurements in the area of largest sand waves ($\approx 5 - 8$ m heights), and to deploy our Geoprobe tripods at sites within that region.

Our shipboard work was carried out during the period 24 July - 31 July, 1978, prior to the Bouma (RU 327) cruise in the same general area. A list of cruise personnel and dates, together with a summary of the various shipboard data taken on that cruise are given in Appendix A. We obtained geological data using shipboard sampling devices and an underwater television/70 mm camera system; geophysical data using side scan sonar, 12 kHz echo-sounder and other seismic equipment on the R/V SEA SOUNDER (Appendix A); and oceanographic data using profiling systems including C-T-D, current meter, transmissometer, and a surface temperature/salinity system. We also took water samples for suspended sediment analysis. We covered approximately 280 km of trackline using side-scan sonar (excellent quality records) and about 510 km of trackline using the 12 kHz echo sounder. Most of these lines were run within areas A and B in Figure 1. Eight anchor stations were occupied for shipboard sampling. Three stations were occupied (two in area A, one in area B) for extended periods to provide time-series measurements of current profiles, light transmission profiles, C-T-D profiles, near-bottom suspended sediment concentrations, and bottom photographs/videotapes. Data at these stations were collected every two hours. A summary of the station data is given in Table 1. The time series anchor stations taken at stations 2 and 7 were within area A, Figure 1; the time series at station 3 was in area B.

The anchor station data were collected to supplement the time-series data acquired with the Geoprobe tripods. The shipboard data provide measurement of physical parameters and suspended sediments within the water column, and can be used to compare with similar data collected near the sea floor.

The size analysis data from the cores will be used for textural sediment analysis, with particular attention on the mean sizes of surface material. In estimating the likelihood of sediment transport at the Geoprobe sites, a critical parameter is the mean grain size.

The side scan sonar records and other geophysical data will be used in conjunction with the data of Bouma and Hampton (RU 327) to map the bed form features in areas A and B. Bouma and Hampton have been provided with these data and with the underwater television tapes and 70 mm bottom photographs to add to their spatial coverage. Some of these data are discussed below in the results section.

TABLE 1. Anchor station data - Lower Cook Inlet
7/24/78 - 7/31/78 - R/V Sea Sounder

<u>Station</u>	<u>Lat(N)</u>	<u>Long(W)</u>	<u>Start</u>	<u>End</u>	<u>Data Type*</u>
1	59°-27.6'	152°-38.6'	1200-7/25	1910-7/25	TV, CAM, CM, G1
2	59P-27.4'	152°-37.9'	2025-7/25	1830-7/26	Time Series, G2
3	59°-32.1'	152°-15.9'	0750-7/27	0100-7/28	Time Series
4	59°-27.5'	152°-38.2'	0730-7/28	0735-7/28	Core
5	59°-27.6'	152°-38.4'	0759-7/28	0810-7/28	Core
6	59°-27.6'	152°-38.4'	0830-7/28	0835-7/28	Core
7	59°-27.6'	152°-38.3'	1800-7/28	2115-7/28	Time Series
8	59°-27.5'	152°-37.1'	1907-7/30	2038-7/30	Core, TV, CAM, G3

*Key: TV = video tape; CAM = 70 mm bottom camera; G1, G2, G3 = geoprobes
Time Series = current meter, C-T-D, transmissometer profiles;
water samples; TV, CAM

Two Geoprobe tripods were deployed in the area of large sand waves (area A, Figure 1), one tripod (G1) in a trough and one (G2) near the crest. Each of these tripods recorded data for about 3 days; Table 2 summarizes their operations and sampling scheme.

The deployment scheme that enabled precise placement of the tripods at the desired trough (G1) and near-crest (G2) locations, respectively, required considerable planning and timely execution. After conducting a detailed side scan sonar and echo-sounding survey of the desired sites, two surface marker buoys were deployed about 300 meters apart. The ship then navigated for deployments relative to the marker buoys. The precise timing of the launch of the Geoprobe tripods was conducted by careful observation of the 12 kHz record as the ship slowly moved over the large bed forms. After recovery of G1 (Table 2), the system was checked, batteries and cassette tape replaced, and then redeployed at site G3.

The recovery of both G1 and G2 did not proceed smoothly. In both instances, the tripod recovery packages failed to surface when acoustically released. This necessitated dragging for each tripod, consuming a total of about 14 hours. Fortunately, we were able to recover both tripods by dragging without damaging either system. The back-up recovery system, a bottom drag line, and the acoustic ranging transponder on the tripods proved valuable aids in these recoveries. We have determined that the electrolytic acoustic release mechanism on G1 failed to corrode completely due to a low voltage supply in the releasing section of the underwater unit. This malfunction effectively prevented the recovery floats from surfacing. On G2 we determined that the acoustic release performed satisfactorily, but infer that the recovery floats were fouled by the bottom line.

Tripod G3 was recovered during the October, 1978 recovery cruise on the R/V SEA SOUNDER. The primary recovery package on the Geoprobe tripod functioned properly during this recovery.

VI. Results

Some of our results have been incorporated in a paper recently presented by Bouma et al. (1979). A copy of this paper is included in the annual report of Bouma and Hampton (RU 327) and is not presented here. The detailed characteristics of the sedimentary bed forms and the regional geological framework of lower Cook Inlet are discussed in detail by Bouma and Hampton (RU 327), and these results will not be repeated here.

Figure 2 is a detailed bathymetric map of area A (Figure 1), showing the complicated bottom contours caused by the large sand waves. The map was drawn by computer analysis of echo-sounding records obtained during our cruise and the subsequent Bouma-Hampton cruise of 1978 (M. Rapoport, personal communication). Figure 2 shows the locations of the two short term Geoprobe deployments (GP1=G1, GP2=G2). Note that GP1 is situated in a trough, and GP2 is near a crest of the large sand waves.

Figure 3 contains three transects (see Figure 2 for locations) within the large sand wave area. Approximate locations of G1 and G2 along the transit line and line 320, respectively, illustrate the trough and near-crest positions of the two tripods. Figure 4 is a reproduction of a 12 kHz echo-sounding profile taken while slowly drifting in a southerly direction close to the site of G1. The large sand waves appear extremely regular in cross-section; however, as Figure 3 indicates, their lateral distribution is actually more complex. The average slopes of these large features as determined from the 12 kHz records is about 0.5 degrees and 4 degrees on their back sides and stoss sides, respectively.

The spatial distribution (and aesthetic appeal) of these sand waves, including the medium scale bed forms whose heights are about 1-2 meters and wavelengths of

TABLE 2: Geoprobe operational summary
(all times local)

<u>Geoprobe No.</u>	<u>Time/Date on Bottom</u>	<u>Time/Date Recovered</u>	<u>Lat(N)</u>	<u>Long(W)</u>	<u>Mean Depth(M)</u>	<u>Basic Interval</u>	<u>Burst Samples</u>	<u>Burst Rate</u>
G1	1800/7-25	1825/7-28	59°-27.5'	152°-38.3'	65.5	7.5 min	180	1 sec
G2	1546/7-26	2008/7-29	59°-27.4'	152°-37.9'	58.6	7.5 min	180	1 sec
G3	1907/7-30	2000/10-21	59°-27.5'	152°-37.0'	56.8	1 hour	128	2 sec

10-100 meters, are illustrated in the side-scan sonar records (Figure 5). As discussed by Bouma et al. (1978, 1979), the crests of the medium-scale bed forms are often oblique to the larger sand wave crests; the angular relationships change as a function of position on the larger features. It is also worth noting here that the angular relationships between the small sand ripples and the medium-scale sand waves also vary as a function of position along the medium-scale features. The acoustic return from one Geoprobe, G1, can be seen on the side-scan sonar record in Figure 5a. This interpretation was confirmed by acoustic ranging with the transponder located on the tripod.

A summary of the Geoprobe data recorded in the basic mode (Cacchione and Drake, 1979) from G1 and G2 are shown in Table 3. We have not yet completed our analysis of the data from G3, mostly owing to difficulties encountered in the transcription of the cassette to computer tape. We have recently discovered that a pinhole leak developed in one of the G3 tripod connectors, causing progressive failure of the G3 pressure sensor and, most unfortunately, the G3 tape recorder while the system was in operation. We presently estimate that about 15 consecutive days of data will be usable, with nearly 70 days of data only partially useful, at best. A complete analysis of this system failure is in progress, and will be reported later. Another problem occurred in the speed sensor (Savonius rotor) on G1. The magnetic reed switch which senses the rotor spins failed shortly after deployment; this failure caused zero values for rotor speed on tripod G1 (Table 3). This failure does not obstruct the data analysis, however, since the electromagnetic current meters on G1 performed satisfactorily for most of the experiment.

The other Geoprobe sensors performed satisfactorily. Temperatures, light scattering and light transmission data have very low variance at both locations (Table 3). The absolute differences in temperatures between G1 and G2 are marginally significant, since each sensor is only rated to an accuracy of $\pm 0.1^\circ\text{C}$. Similarly, the absolute differences in light transmission values between G1 and G2 are not significant, since the values shown are relative units that depend on the individual instrument calibrations. However, the consistently high values of light transmission and low values of light scattering at each site are significant. This result is in agreement with the transmissometer profiles (Figure 6) taken during the July cruise. The two profiles in Figure 6 show that at each site, the mid- to bottom-water is relatively clear and uniform. These transmission profiles are typical of other transmission data collected during our July cruise. The low (nearly 0) light scattering values at each tripod also indicate that very low turbidity is found at 2 m above the sea floor.

Histograms for pressure, temperature and light transmission are provided in Figure 7. These plots clearly show the variability in temperature and light transmission.

Pressure and electromagnetic current meter data for both G1 (GP1 in Figure 2) and G2 (GP2 in Figure 2) are shown in Figure 8. The pressure values represent unfiltered, integrated measurements over each 7.5 minutes (basic interval, Table 2) taken at 2 meters above the bottom. Data from the electromagnetic current sensor, located at 1 meter above the bottom, were used for the current plots in Figure 2. Averages of each current component in north-south (v) and east-west (u) directions were computed from which average speed, s , and average current direction, θ , were estimated for each burst.

$$s = (u^2 + v^2)^{1/2}; \theta = \tan^{-1} \frac{v}{u} \quad (1)$$

Eight consecutive values of s and θ were then used to derive hourly averages which are plotted as "stick" vectors in Figure 8.

The pressure values have a range of about 4 meters (also see Table 3), a figure

Table 3. Geoprobe tripod data statistical summary

	<u>G1</u>						
	pressure	rotor	vane	temp 1	temp 2	light transmission	light scattering
mean	63.54	0.00	161.54	9.35	9.45	0.60	0.05
maximum	65.64	0.79	359.75	9.41	9.52	0.64	0.10
minimum	61.65	0.00	0.52	9.29	9.38	0.46	0.04
variance	1.23	0.00	-	0.00	0.00	0.00	0.00
stand dev	1.11	0.03	-	0.04	0.04	0.03	0.00

	<u>G2</u>						
mean	56.65	19.95	150.26	9.16	9.24	0.89	0.05
maximum	58.66	50.05	359.88	9.24	9.41	0.93	0.09
minimum	54.91	2.02	0.00	9.09	9.18	0.78	0.03
variance	1.15	87.51	-	0.00	0.00	0.00	0.00
stand dev	1.07	9.35	-	0.05	0.04	0.02	0.00

typical for tides in central Cook Inlet. The pressure records in Figure 8 show a slightly mixed tide, but the semi-diurnal (M_2) component is clearly dominant. The diurnal inequality for this period is about 0.8 meters. Comparison with tidal tables for Seldovia, about 50 km east of the measurement sites, indicates that these data were taken during the waning stages of a spring tidal period. The difference between mean pressures at sites G1 and G2 for this period is 6.9 meters (also see Table 3) suggesting that G1 and G2 were vertically separated by that distance. That measurement indicates the vertical scale of the large sand waves is at least 7 meters.

Maximum hourly-averaged current speeds occur about 0300 local on 7/27/78 during ebb tide (Figure 8). The speeds at G1 and G2 are 36 cm/s and 48 cm/s, respectively, for that period. The highest flow speeds in both cases are in the ebb (southerly) direction; however, the dominance of ebb appears to be greatest at the near-crest (G2) site. Not shown clearly in Figure 8 are rapid current reversals and accelerations during ebb tide, when typically less than 1 hour elapses between slack high water and slack low water. The flood tidal current accelerates less, taking several hours from slack low water to maximum flood current.

Figure 9 contains plots of the average current speed (see equation (1)) for each burst (s in equation (1)) recorded by the four electromagnetic current meters on G1. These data (Figure 9) show the higher speeds and rapid accelerations of ebb flow.

Figure 10 contains examples of the burst current speed data taken by the electromagnetic current meters. The data were sampled once per second; the irregular fluctuations in the speeds are probably due to turbulent eddies. As discussed later, the turbulence level increases with the tidal current speed, and is higher at the crest (G2) location.

Geoprobe bottom photographs that illustrate the effects of the moderately intense tidal currents on the bottom sediment are shown in Figure 11. Figures 11a and 11b portray reversals of sand ripple orientations during one flood-ebb cycle at G1 and G2, respectively. Figure 11c illustrates the same effect at G3, and additionally documents the long-term net changes that occur at that site over a one-month period. The ripples have wavelengths of about 15-20 cm and heights of about 1-2 cm. The ripples are better developed at the near-crest site; organisms (sand dollars) are apparent at G1. The photographs in Figure 11a show a mottled pattern that is thus far unexplained. Since the anomalous "spots" also cover the bottom organisms (sand dollars), we suspect that the cause is either due to photographic processing or due to material in suspension above the bottom. No evidence to aid in the determination of these "spots" has been found in box cores or in the suspended sediment samples.

VII. Discussion

We have carried out a field program to provide data on sediment movement within an area of large sand waves in lower Cook Inlet. In section VI we presented our available results, and indicated that problems with the long term Geoprobe (G3) data tape prevents us from discussion of most of that data here (except for the photographs). What we have not presented are the other data collected during our 1978 cruise, including over 7 hours of underwater television tapes, several hundred 70 mm photographs, and numerous geophysical records. We feel that these data are best considered in the analysis and discussions given by Bouma and Hampton (RU 327), and we are working with them to interpret those results.

Currents over large-scale bed forms are difficult to analyze because of the nonuniformity induced in the flows near the bed by the topography (Smith and McLean, 1978). The basic problem involves the divergence (convergence) of the streamlines

as the flow moves from the crest to trough (trough to crest) region. Horizontal gradients in the local bottom shear stress, τ_0 , develop because of the accelerative effects, which then make it difficult to relate a site-specific, or local, measurement of τ_0 to the generation and migration of the large bed forms. Ideally, we would have a large number of stress-measurement devices, like Geoprobos, deployed in a transect across one or more of the larger bed features. A spatial average of τ_0 , obtained by averaging the local measurements, would then be the appropriate stress related to the development and movement of the large scale bed forms. The local measurements of τ_0 , nevertheless, are important to understanding local incipient movement and resuspension of sediments, as well as relating small-scale bed form movements (ripples) to the fluid motion.

In the sense of the above argument, our measurements are very limited in trying to relate the migration rates of the largest sand waves (\approx 500 meter wavelengths) to our Geoprobe shear measurements (2 sites). However, some approximations can be made based on the two data sets.

Our tidal current data (Figure 8) agrees with the general concept that ebb flow is greater than flood in the central and western parts of lower Cook Inlet. We also showed that peak ebb currents generally exceeded peak floods currents over the 2.5 day record, and that current speeds were generally greater at the crest (G2) site. The latter result agrees with the concept of streamline convergence over the topographic highs, creating higher flow speeds above the sand wave crests relative to above the troughs.

The current meter records for the electromagnetic (e-m) current sensors (Figures 9 and 10) show several other interesting features. The current reversal and acceleration effects discussed above will complicate the boundary layer flow near the bed, probably causing non-logarithmic flow profiles over part of the tidal cycle. Another significant and obvious feature in the e-m current speed data is the variation in the nature of the speed curve from one tidal cycle to the next. Although the pressure and hourly-averaged currents (Figure 8) show well-behaved tidal variations, the 7.5 minute burst averages of current speed (Figure 9) are considerably more irregular. We have reason to believe that the data in Figure 9 after hour 60 is probably erroneous due to low battery power to the e-m current meters. Up to that time, however, we feel that the data is of excellent quality. In fact, the rotor speeds and the e-m current speeds at the uppermost sensor (1 m) on G2 (not shown) agree very well. The persistently lower speeds during hours 30-42 in Figure 9 occur during the lowest tidal stage (see pressure in Figure 8). The irregularity in the record suggests that other processes like turbulence and topographic effects are locally significant.

A third important feature in the current records are the relatively high frequency fluctuations superimposed on the tidal oscillations (Figures 9 and 10). These irregular, higher frequency fluctuations are very coherent in the vertical, and also occur in the rotor speed data (not shown in Figure 9) at G2. The peak-to-peak magnitudes of these fluctuations are typically about 5 cm/s, and represent very energetic flow events. We attribute these current fluctuations to large turbulent eddies probably generated by interaction of the tidal flow and the large to medium scale bed forms. This interpretation implies that the vertical eddy scale is greater than 1 meter, since the horizontal eddy currents are coherent over all current meter levels.

Figure 12 shows the variance in the e-m speed data computed by transforming the individual samples of Cartesian speed components to polar representation (r, θ) . The variance of speed for each burst of N samples is then

$$\text{Var}(r) = \frac{\sum_{i=1}^N (r_i - \bar{r})^2}{N-1}$$

with \bar{v} the mean speed of each burst. In our data, $N = 180$ samples. The variance of the burst speed data is proportional to the horizontal kinetic energy in the fluctuating velocity field at each level; i.e., proportional to the horizontal eddy kinetic energy. This eddy motion would both add to the instantaneous stress imparted to the surface sediments by the local flow, and also induce a randomness to the total stress field. These eddies might be a mechanism for the "bursting" phenomenon at the sea floor that has been described by Heathershaw (1974) and Gordon (1974).

The local shear stress at Geoprobe site G1 can be estimated from the "burst"-averaged horizontal currents measured at four levels. In the usual manner, we define

$$\tau_0 = \rho u_*^2 \quad (2)$$

u_* is shear velocity, and ρ is fluid density. u_* is computed from the Karman-Prandtl relationship for turbulent boundary layer flow:

$$\frac{u}{u_*} = \frac{1}{k} \ln \frac{z}{z_0} \quad (3)$$

u is horizontal speed measured at a level z above the bottom; and z_0 is a roughness scale. k is von Karman's constant (≈ 0.4). u_* can be computed for two or more measures of u and z using a technique described by Sternberg (1972).

Estimates of u_* (and z_0) were computed for each burst, then averaged to produce hourly values which are plotted in Figure 13. The pressure data is also shown in Figure 13 to relate the fluctuations in u_* to the tidal cycles.

Based on box core data collected by Bouma and Hampton (RU 327), mean sizes of surface sediments at site G1 are about 0.35 to 0.4 mm. Critical flow speed at 1 meter above the bottom, u_{100}^c , and a critical shear velocity, u_{*c} , can be inferred for these sizes (Sternberg, 1972). In this case $u_{100}^c \sim 20$ cm/s; $u_{*c} \sim 1.6$ cm/s. Actual flow speeds at 1 meter that exceed u_{100}^c and shear velocities greater than u_{*c} would cause incipient motion of the bed particles. The sediment analyses for several cores taken near the tripod sites indicate that the surface sediments are well- to moderately-well sorted.

The uppermost current speed record in Figure 9 gives a burst-averaged measure of u_{100} for G1. It is apparent that $u_{100} > u_{100}^c$ ($=20$ cm/s) occurred a substantial percentage of the total record (about 35%). Similarly, inspection of Figure 12 shows that $u_* > u_{*c}$ ($=1.6$ cm/s) occurred often, suggesting that during maximum ebb and, less frequently, at maximum flood movement of the bed materials occurred.

These results are correlated with the bottom photographs (Figure 11) which show sand ripple reversals and ripple migration during ebb and flood tides. The migration rates and estimate of net transport as ripples will be made in subsequent analyses.

Concentrations of suspended matter measured from filtered water samples and as inferred from the transmissometer data from the Geoprobe tripods and shipboard profiles (Figure 6) were very low (<1 mg/l). Samples collected near G1 and G2 from 1 m above the bottom (see sec LC3 and LC9 in Figure 2) had 0.65 mg/l and 2.1 mg/l of suspended matter, respectively. Microscopic examination of the suspended matter showed that this difference in concentration was caused by an abundance of sand-size grain aggregates in the samples from station LC3 (crest). All samples collected in the sand wave trough were devoid of these aggregates and were predominantly composed of siliceous biogenic detritus and discrete particles of fine silt. In addition, samples obtained from 30 cm above bottom at station LC3 during peak ebb-tidal flow contained a small number ($\sim 5-10$ grains/l) of fine to very-fine sand-size quartz particles. These grains were not found in samples from 100 cm above bottom, although the grain aggregates were present in approximately equal amounts at both levels.

The suspended sediment data correlate well with the higher currents measured during ebb flow at the crest site as discussed above. Figure 12 shows that even at

the trough site, bottom stress is high enough to resuspend materials during ebb and flood conditions. The bottom photographs show active ripple movements caused by both ebb and flood at G1 and G2, with the more active transport occurring near the crest. The presence of organisms and burrows in photographs at G1 also correlate with the presence of biogenic material found in suspension near the bottom there.

VIII. Conclusions

1. Tidal currents during fair weather and low to moderate tidal stages are strong enough to transport sediment as bed load within the region of large sand waves in lower Cook Inlet.
2. Current measurements and bottom stress computations from the current profiles show that the sediments in the troughs of the large sand waves are resuspended by both ebb and flood tidal currents. Bottom photographs of reversing sediment ripples corroborate this result.
3. Higher currents and bottom stress near the crests of the large sand waves create a zone of very active sediment movement, predominantly in the form of small sediment ripples. Streamline convergence over the crests is a major cause of the increased transport in those areas.
4. Energetic turbulent eddies are common features at all measurements sites. These eddies create random, large stresses at the sea floor, adding to the sediment entrainment and transport. Their origin is undetermined, but we suspect that large tidal currents passing over an irregular bottom are a primary source for the turbulence.
5. No evidence for movement of the medium-scale (~1 m heights) or large-scale (~5-10 m heights) sand waves was found. We infer, however, that since relatively low tidal stages produce bed load transport, maximum tides coupled with storm effects will be sufficient to cause migration of the medium-scale sand waves.

IX. Needs for Further Study

1. Long-term (3 month) measurements of bottom currents (and stress) and bottom photographs at several (about 4) locations across a single large sand wave. This should be repeated for summer (fair weather) and winter (stormy) conditions. The data could lead to an understanding of the migration rates of the large scale (and medium scale) bed forms. This experiment should be done in conjunction with precision (+ 3 meter) acoustic surveys of the bed forms using shipboard and rotating (fixed) side-scan sonar records.
2. Time-series sampling of the near-bottom suspended load in repeated transects over the large sand waves will also help develop our estimates of resuspension and bed mobility.

X. Summary of January - March Quarter

A. Ship or Laboratory Activities

No ship or field operations were conducted.

B. Data Analysis

We are continuing to analyze our Geoprobe data collected during the 1978 experiment. In particular we plan to:

- (1) produce completed plots of all data for G1 and G2;
- (2) remove errors from the G3 data and produce plots of useable measurements;
- (3) derive u_* values for G2 and G3 current data;
- (4) estimate transport rates at all sites.

XI. Auxiliary Material

A. References

- Bouma, A. H., Hampton, M. A., Wennekens, M. P., and Dygas, J. A., 1977, Large dunes and other bedforms in lower Cook Inlet, Alaska, Proc. 9th Ann. Offshore Tech. Conf., Houston, p. 79-85.
- Bouma, A. H., Hampton, M. A., Rapoport, M. L., Whitney, J. A., Teleki, P. G., Orlando, R. C., and Torresan, M. E., 1978, Movement of sand waves in lower Cook Inlet, Alaska, Proc. 10th Ann. Offshore Tech. Conf., Houston, p. 2273-2276.
- Bouma, A. H., Rapoport, M. L., Orlando, R. C., Cacchione, D. A., Drake, D. E., Garrison, L. E., and Hampton, M. A., 1979, Bedform characteristics and sand transport in a region of large sand waves, lower Cook Inlet, Alaska, Proc. 11th Ann. Offshore Tech. Conf., Houston, in press.
- Cacchione, D. A. and Drake, D. E., 1979, A new instrument system to investigate sediment dynamics on continental shelves, Mar. Geol., in press.
- Gordon, C. M., 1974, Intermittent momentum transport in a geophysical boundary layer, Nature, 248(5447), p. 392-394.
- Hampton, M. A., Bouma, A. H., Torresan, M. E., and Colburn, I. P., Analysis of microtextures on quartz sand grains from lower Cook Inlet, Alaska, Geology, 6, p. 105-110.
- Heathershaw, A. D., 1974, "Bursting" phenomena in the sea, Nature, 248(5447), p. 394-395.
- Muench, R. D., Mofjeld, H. O., and Charnell, R. L., 1978, Oceanographic conditions in lower Cook Inlet: Spring and Summer, 1973, J. Geophys. Res., 83(C10), p. 5090-5098.
- Sharma, G. D. and Burrell, D. C., 1970, Sedimentary environment and sediments of Cook Inlet, Alaska: Am. Assoc. Petroleum Geologists Bull., 54, p. 647-654.
- Smith, J. D. and McLean, S. P., 1978, Spatially averaged flow over a wavy surface, J. Geophys. Res., 82(12), p. 1735-1746.
- Sternberg, R. W., 1972, Predicting initial motion and bedload transport of sediment particles in the shallow marine environment, In: Shelf Sediment Transport, Process and Pattern, eds. D. J. P. Swift, D. B. Duane, and O. H. Pilkey, Dowden, Hutchinson, and Ross, Stroudsburg, Pa., p. 61-82.

B. Papers

1. Bouma, A. H., Rapoport, M. L., Orlando, R. C., Cacchione, D. A., Drake, D. E., Garrison, L. E. and Hampton, M. A., 1979, Bedform characteristics and sand transport in a region of large sand waves, lower Cook Inlet, Alaska, Proc. 11th Ann. Offshore Tech., Conf. Houston, in press.
2. Cacchione, D. A., Drake, D. E., Rapoport, M. L., and Bouma, A. H., Local stress and ripple migration in a large sand wave field, in preparation.

C. Oral Presentation

1. Rapoport, M. L., Cacchione, D. A., Bouma, A. H., and Drake, D. E., Seafloor microtopography, tidal current characteristics and bottom boundary layer time-series measurements, July-August, 1978, Lower Cook Inlet, Alaska, Amer. Geophys. Union, 1979 Spring meeting - to be delivered.

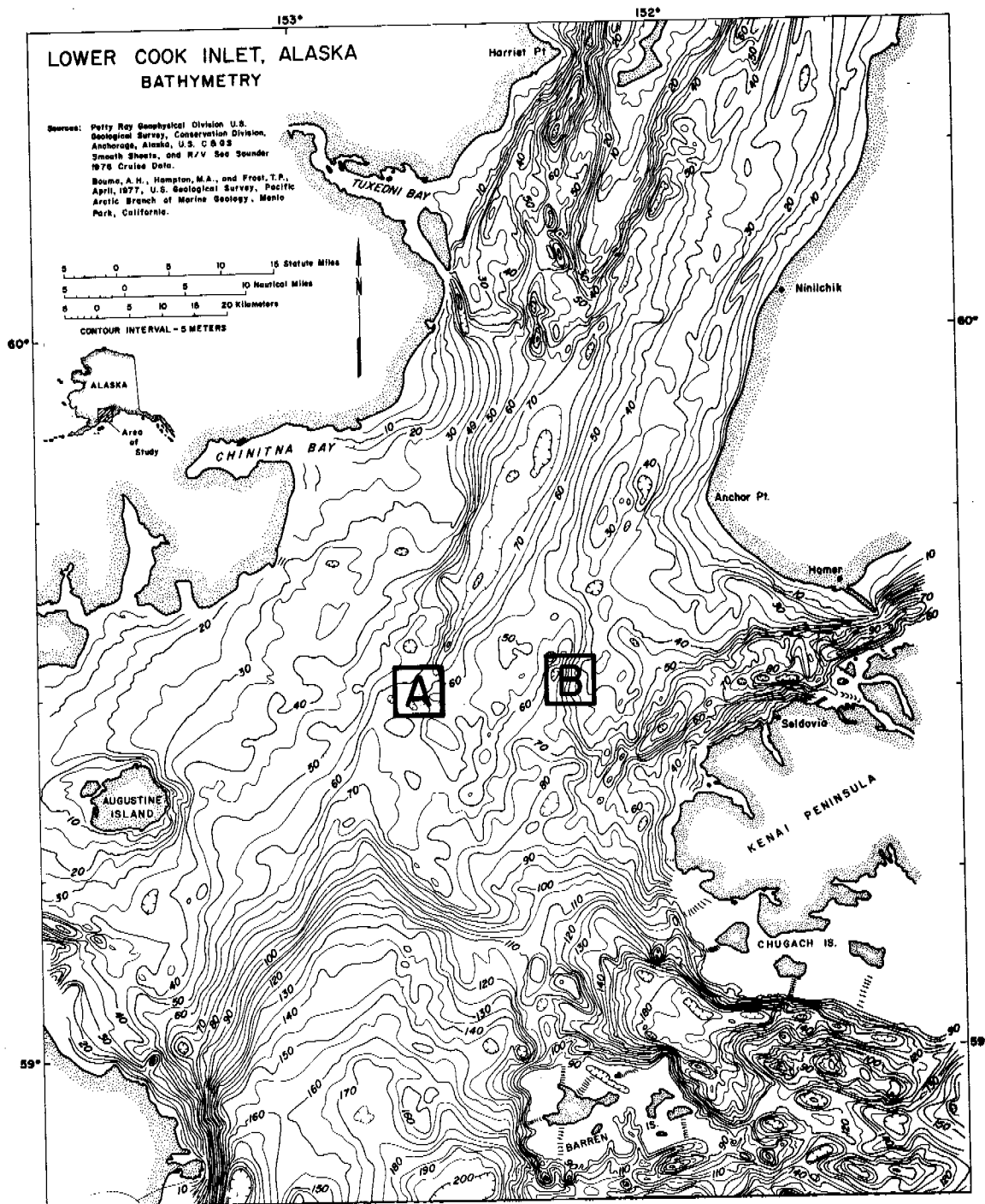


Figure 1. Bathymetric chart of lower Cook Inlet showing areas of study (A and B) during July, 1978.

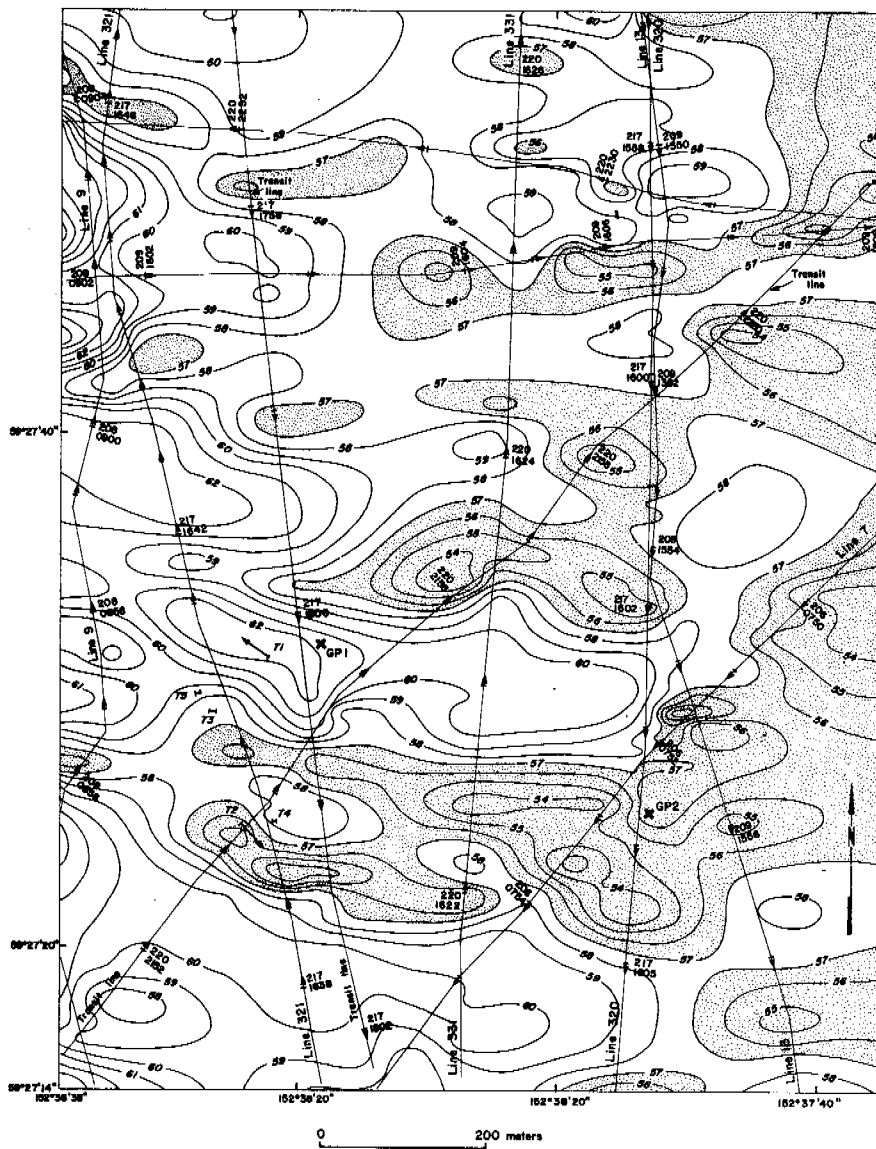


Figure 2. Detailed bathymetry showing large sand waves and Geoprobe sites GP1 and GP2 in lower Cook Inlet. Track lines were made during two cruises by R/V SEA SOUNDER in 1978.

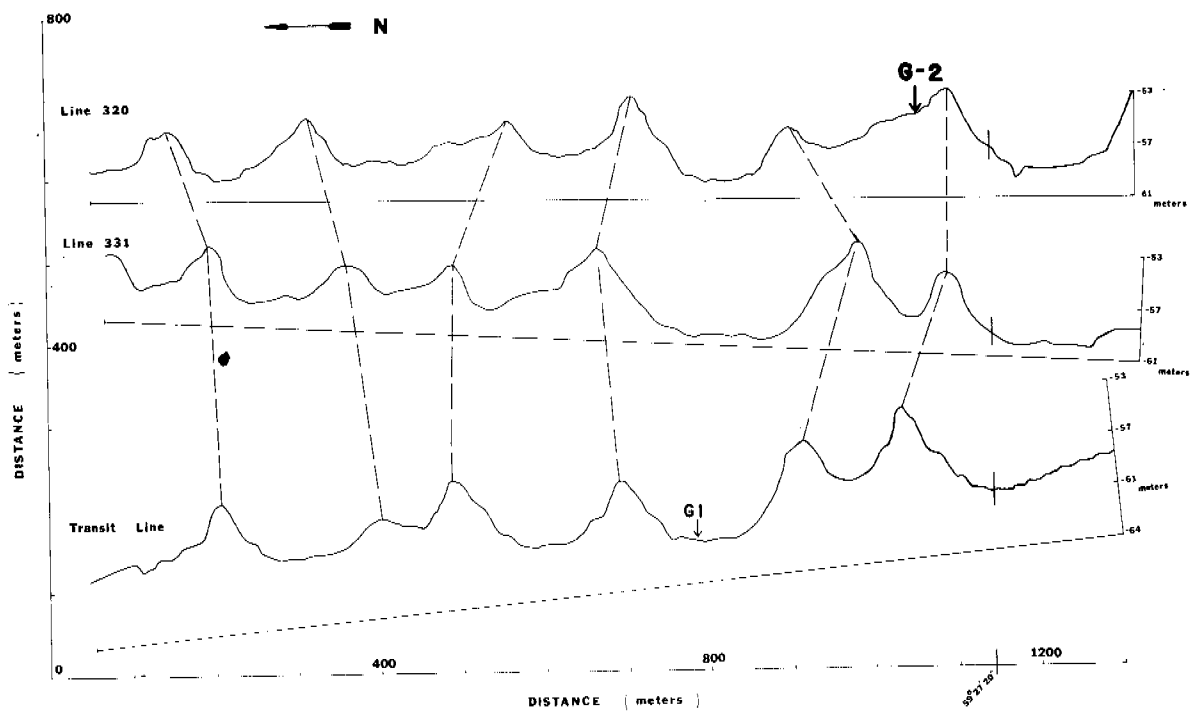


Figure 3. Bathymetric cross-sections of three 12 kHz lines that show approximate positions of Geoprobegs G1(=GP1) and G2(=GP2). Vertical scale is greatly exaggerated. The locations of the lines are shown in Figure 2.

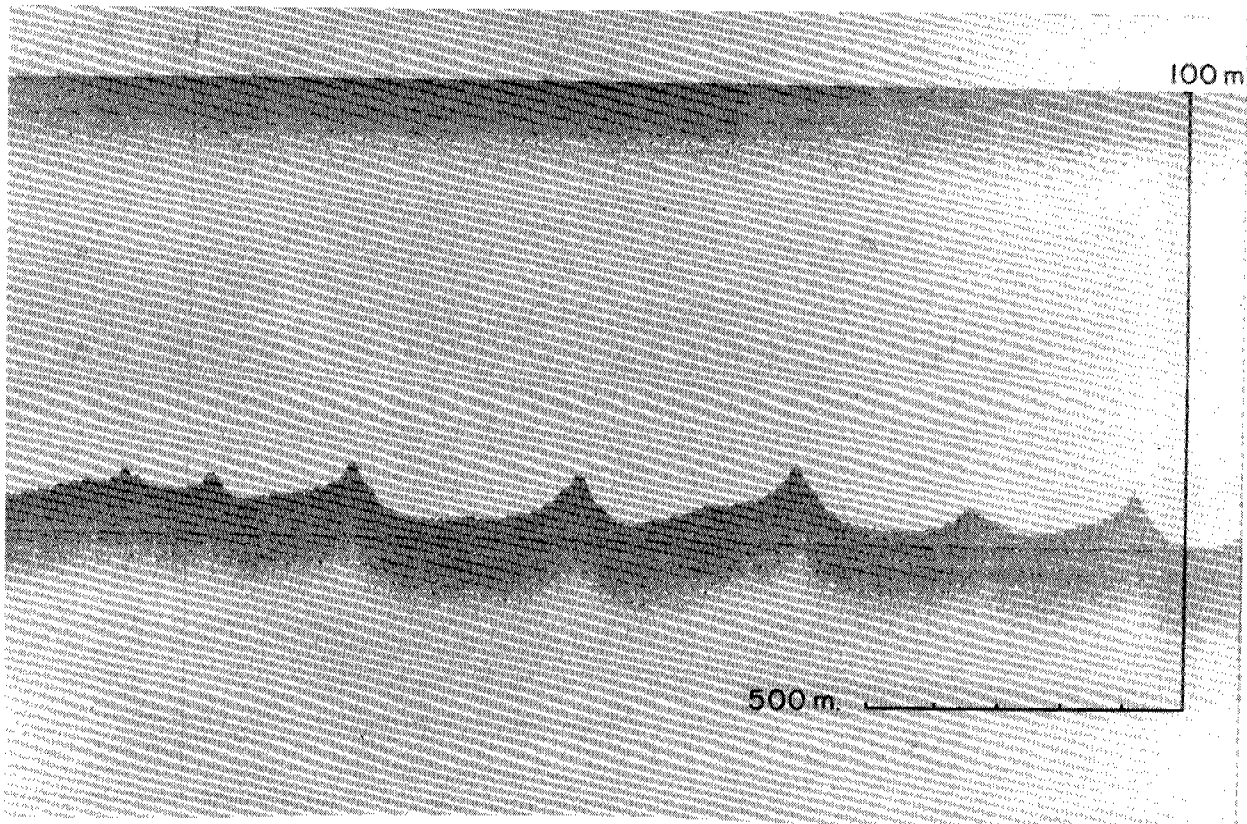


Figure 4. Example of 12 kHz echo-sounding profile taken near G1 prior to deployment. Ship was drifting slowly (~1 knot) in a southerly direction.

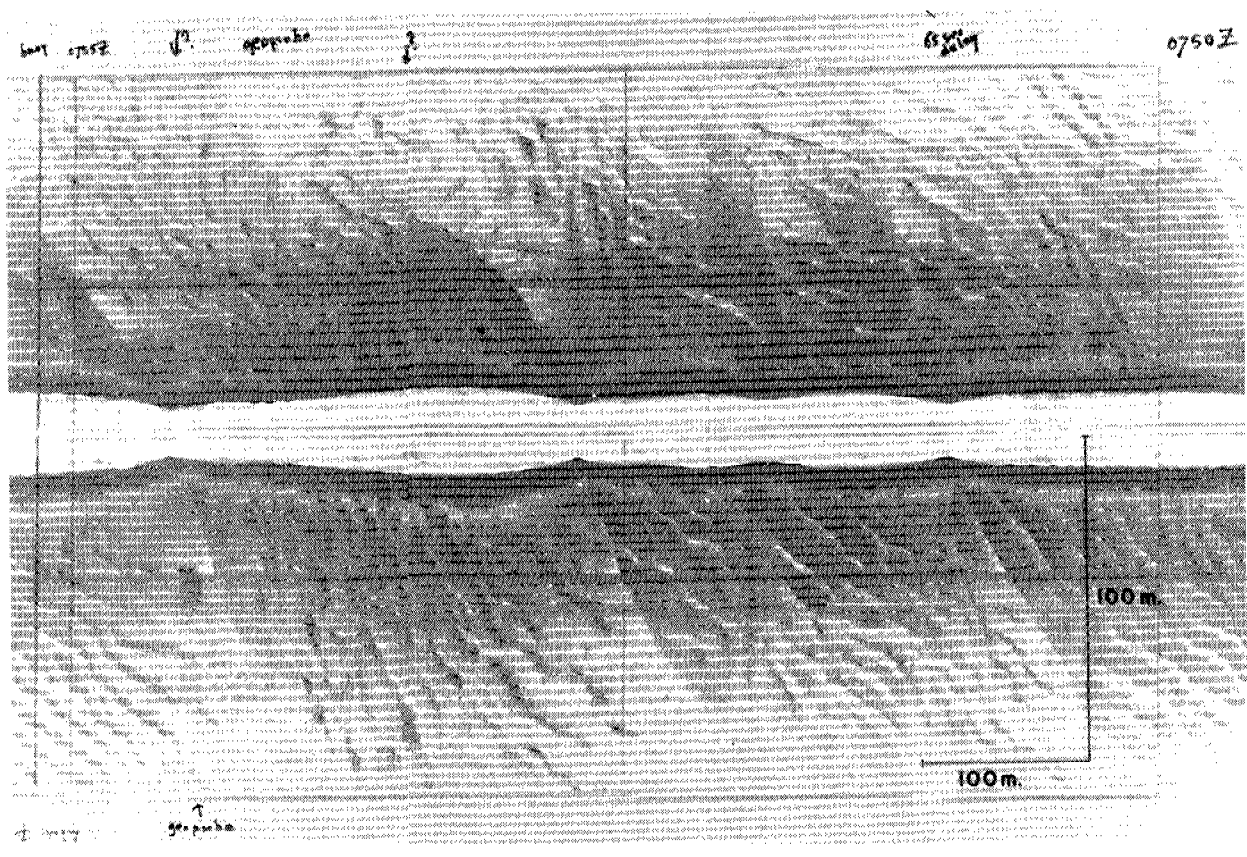


Figure 5a. Side-scan sonar records taken during the July, 1978 cruise to lower Cook Inlet. Records were taken along line 7 (Figure 2) near Geoprobe G2. Record (a) has side scan echo interpreted as Geoprobe tripod (G2). Large sand wave crests are about 250-300 meters apart. Smaller sand wave crests are generally oblique to the larger waves.

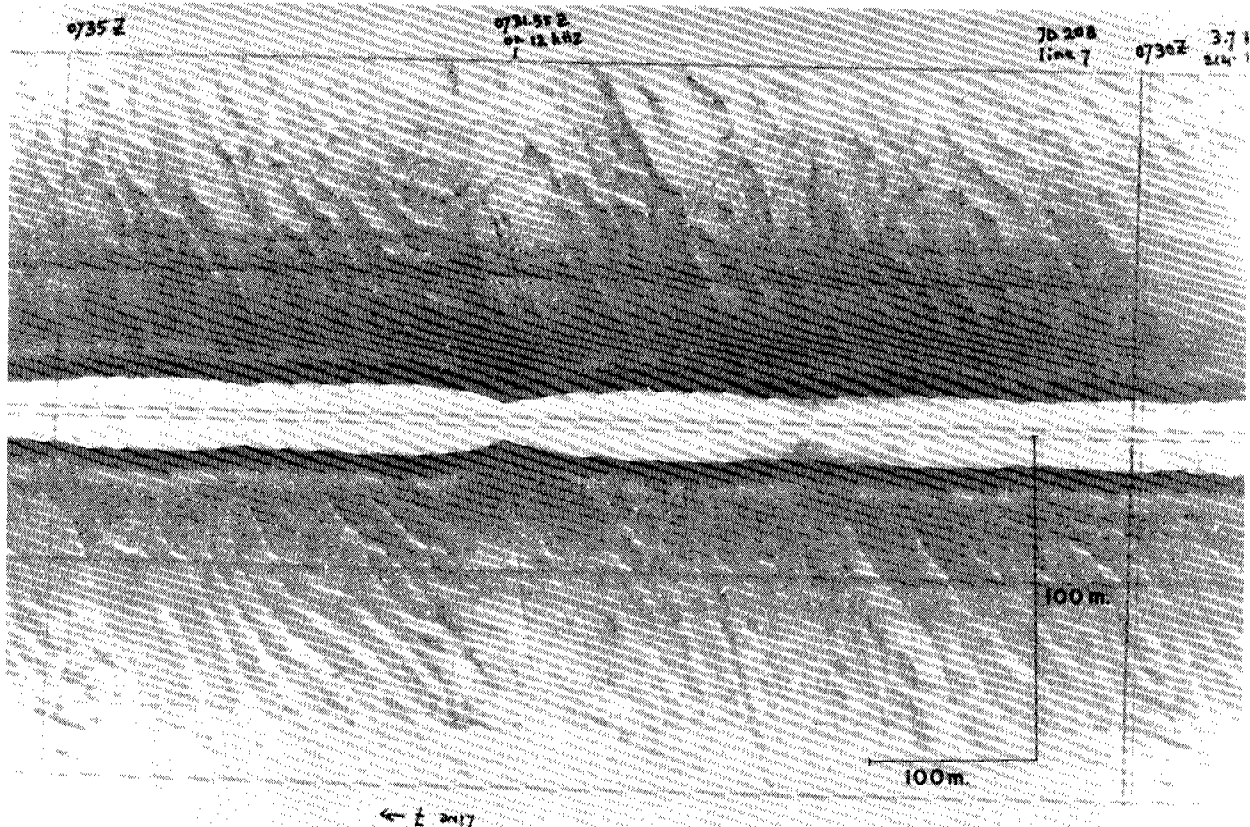


Figure 5b. Side-scan sonar record taken about 1 km north of record shown in Figure 5a.

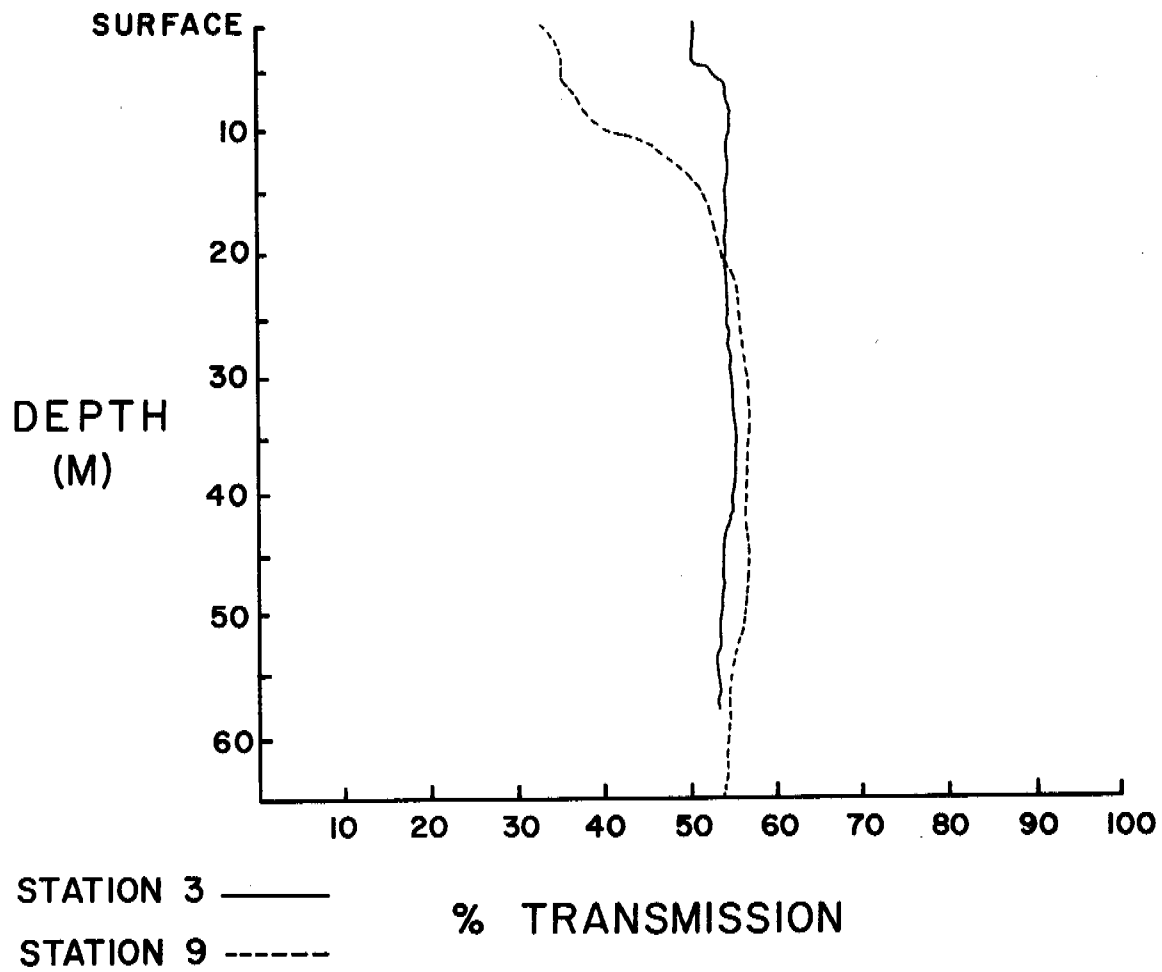


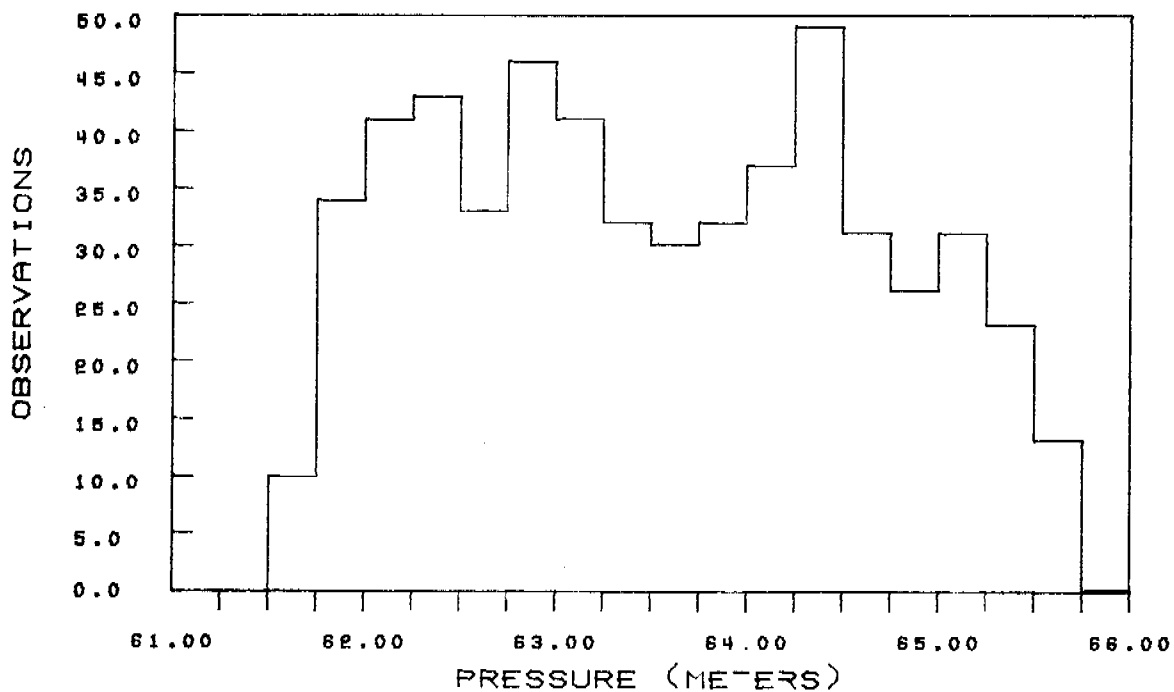
Figure 6. Transmissometer profiles taken during July, 1978 cruise on R/V SEA SOUNDER. Station 3 is LC-3 (crest), and station 9 is LC-9 in Figure 2.

Figure 7a. Pressure histogram - G1

PRESSURE - G1, LOCO 78

OBSERVATION PERIOD IS 7/25/78 2000 L -

NUMBER OF POINTS = 552 DT = 7.50



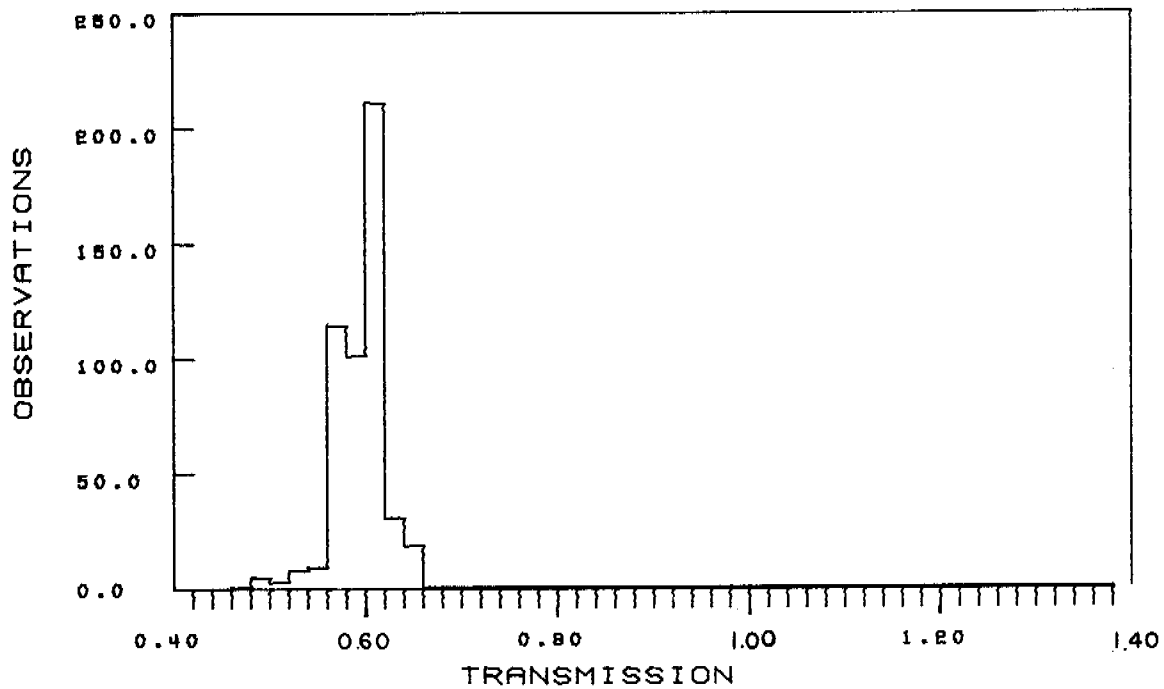
MAX = 65.64 MEAN = 63.54 VAR = 1.22
MIN = 61.65 SDEV = 1.10 SKEW = -0.21

Figure 7b. Light transmission histogram - G1

TRANSMISSOMETER - LOCO G1

OBSERVATION PERIOD IS 7/25/78 2000L-

NUMBER OF POINTS = 500 DT = 7.50



MAX = 0.64

MEAN = 0.59

VAR = 0.00

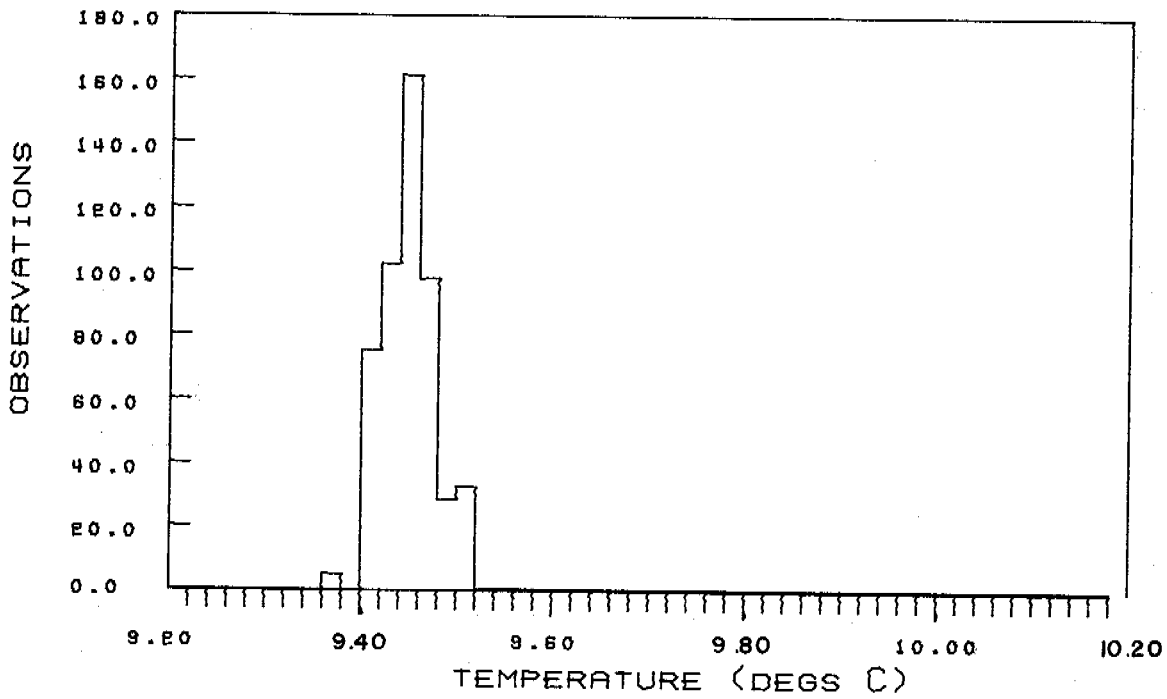
MIN = 0.46

SDEV = 0.03

SKEW = -1.25

Figure 7c. Temperature histogram - G1

TEMPERATURE (2) - LOCO G1
OBSERVATION PERIOD IS 7/25/78 2000L -
NUMBER OF POINTS = 500 DT = 7.50



MAX = 9.52

MEAN = 9.45

VAR = 0.00

MIN = 9.38

SDEV = 0.03

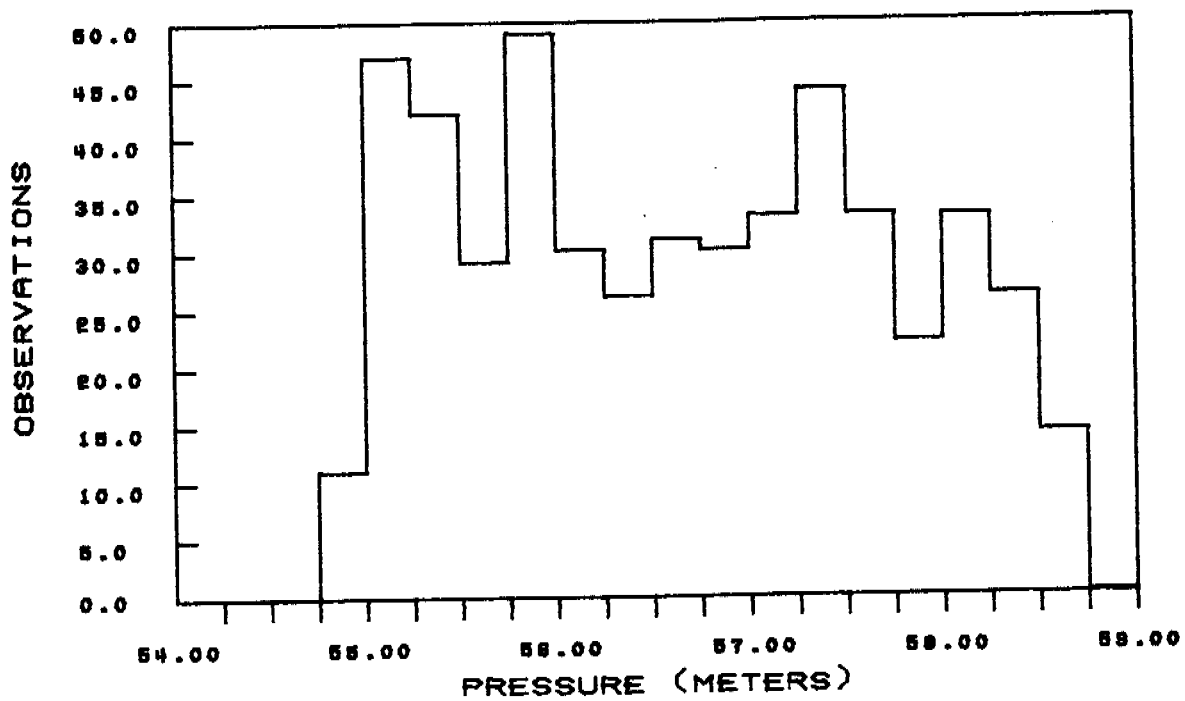
SKREW = -50.08

Figure 7d. Pressure histogram - G2

PRESSURE - LOCO G2

OBSERVATION PERIOD IS 7/26/78 1630 L -

NUMBER OF POINTS = 500 DT = 7.50



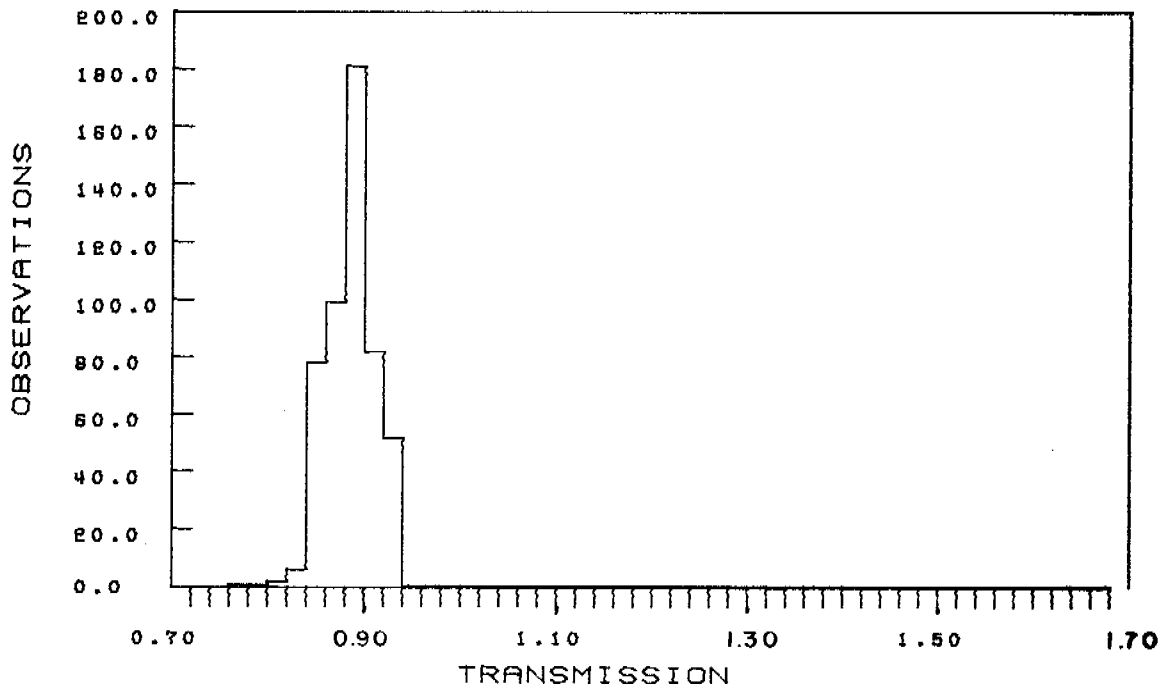
MAX = 58.66 MEAN = 56.65 VAR = 1.16
MIN = 54.91 SDEV = 1.08 SKEW = -0.08

Figure 7e. Light transmission histogram - G2

TRANSMISSOMETER - LOCO G2

OBSERVATION PERIOD IS 7/26/78 1630 L -

NUMBER OF POINTS = 500 DT = 7.50



MAX = 0.93

MEAN = 0.89

VAR = 0.00

MIN = 0.78

SDEV = 0.03

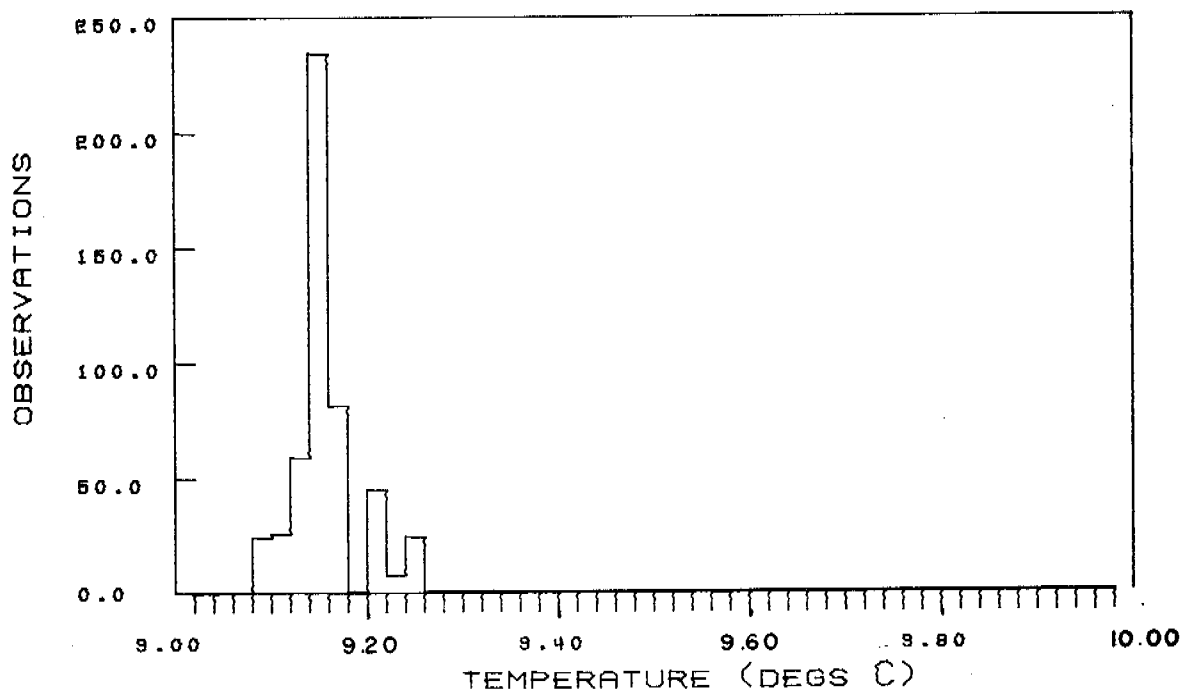
SKEW = -0.50

Figure 7f. Temperature histogram - G2

TEMPERATURE (2) - LOCO G2

OBSERVATION PERIOD IS 7/26/78 1630L -

NUMBER OF POINTS = 500 DT = 7.50



MAX = 9.24

MEAN = 9.16

VAR = 0.00

MIN = 9.09

SDEV = 0.03

SKEW = -19.11

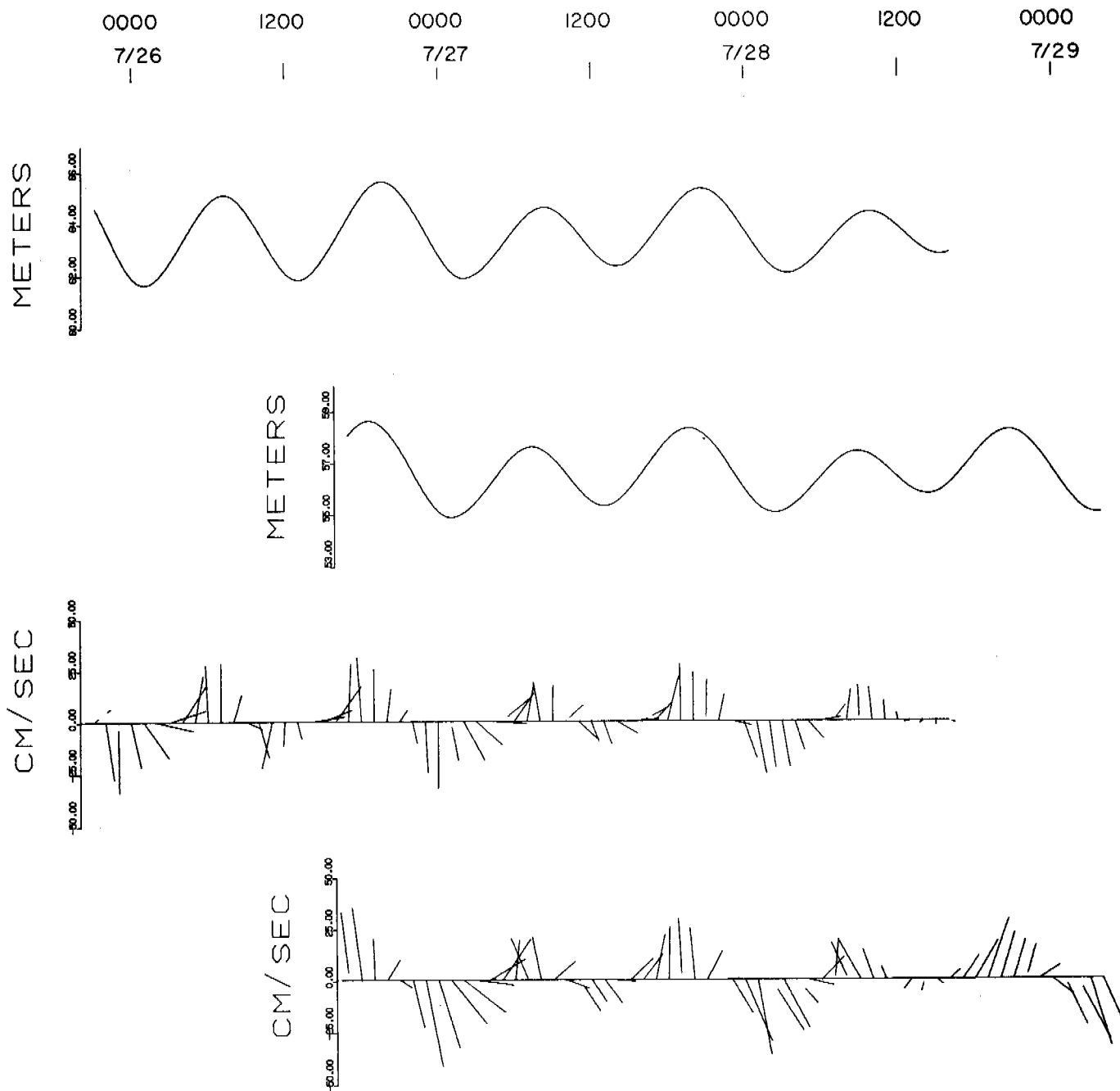


Figure 8. Pressure in meters of water and current vectors ("sticks") in cm/s from Geoprobe sites G1 (upper) and G2 (lower). Numbers at top are local times and days.

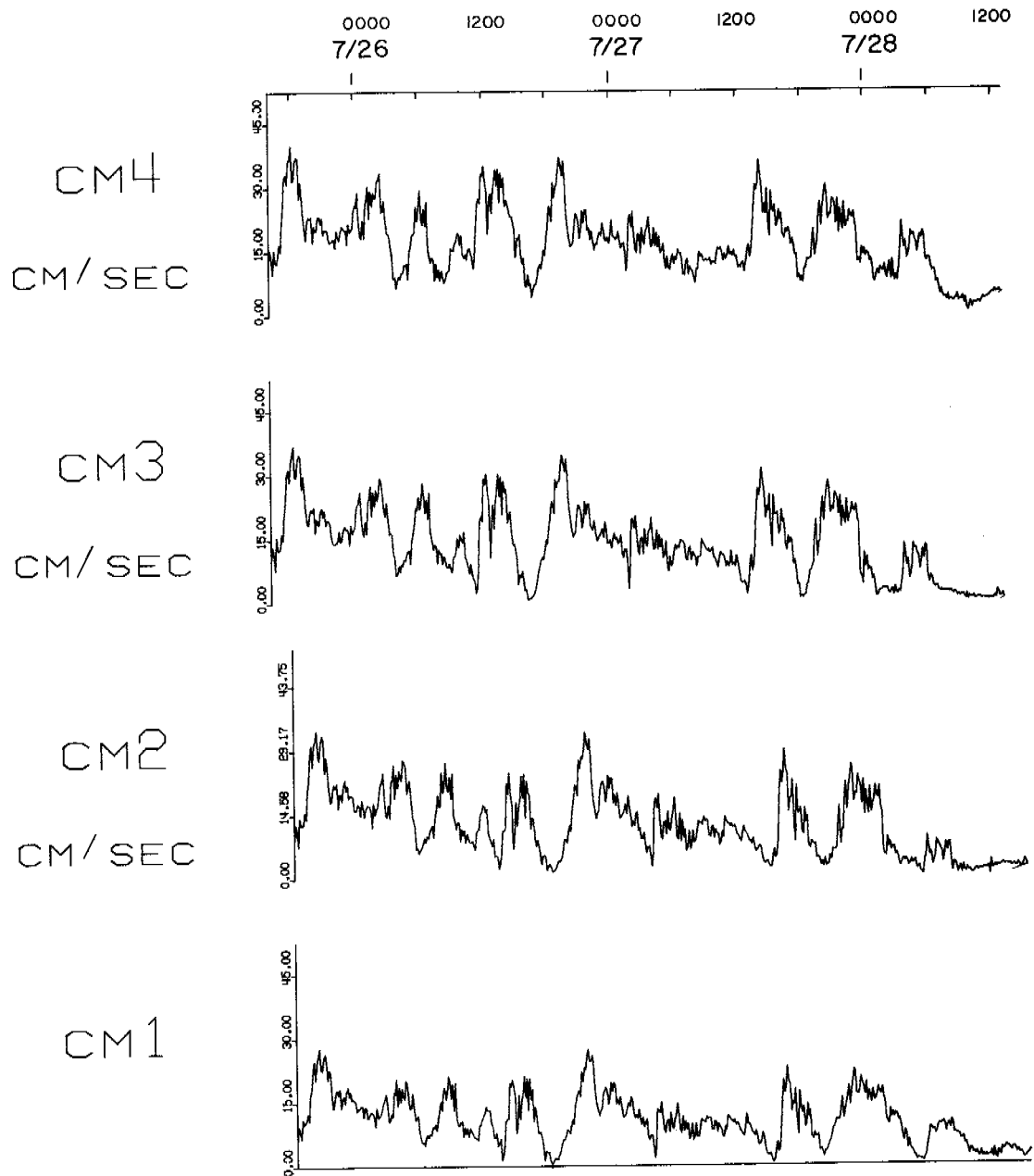


Figure 9. Burst-average current speeds measured at four levels above the bottom at site G1 with Geoprobe electromagnetic current meters. Levels are 20 cm (CM1), 50 cm (CM2), 70 cm (CM3), and 100 cm (CM4) above the bottom. Numbers on top are local times and days.

COOK 78 G1A BURST

7/26/78 0000L

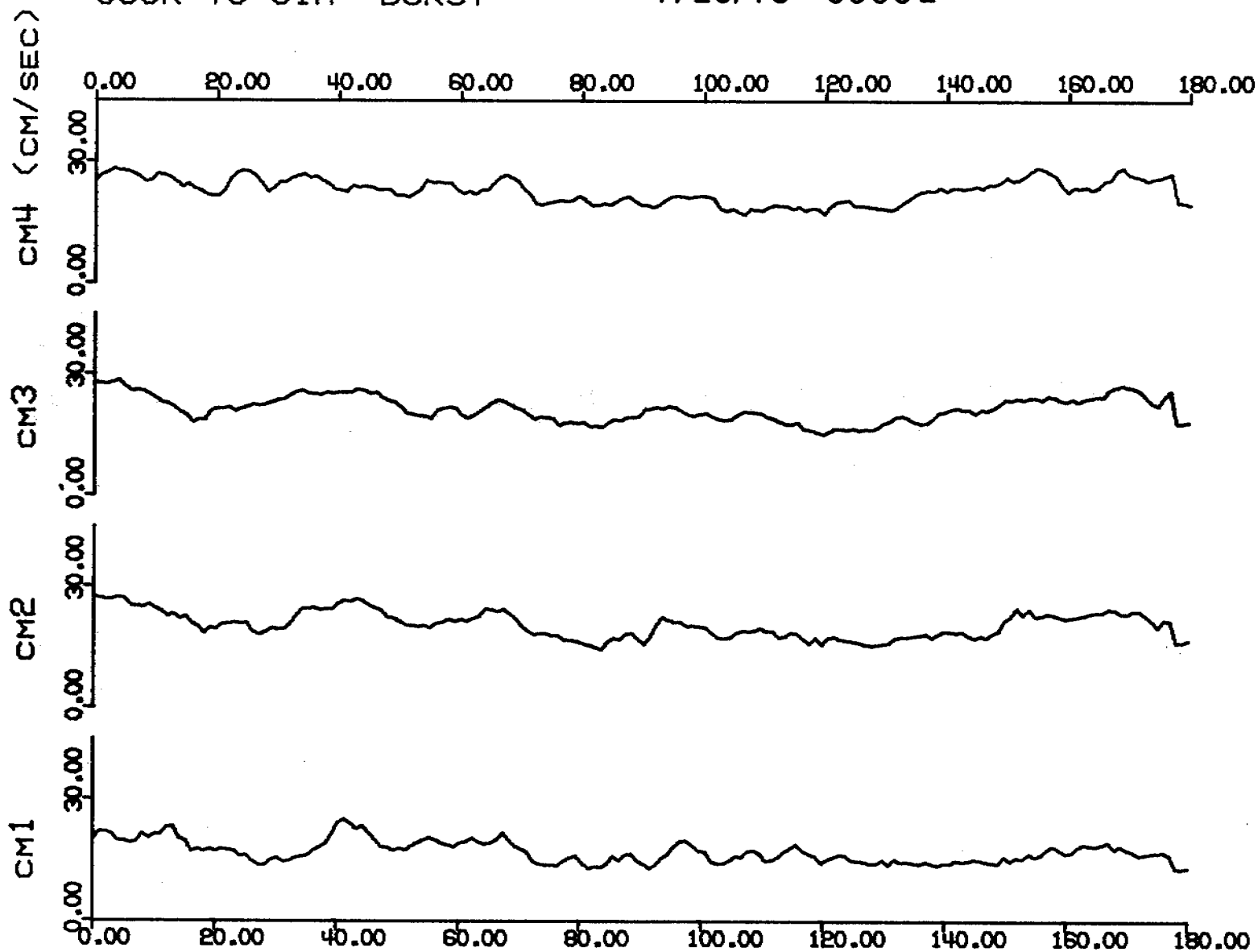


Figure 10a. Burst current speed data taken with the electromagnetic current meters at G1. Sampling rate was 1/second. Distances above sea floor: CM1 at 20 cm, CM2 at 50 cm, CM3 at 70 cm, CM4 at 100 cm.

COOK 78 G2A BURST

7/27/78 0030L

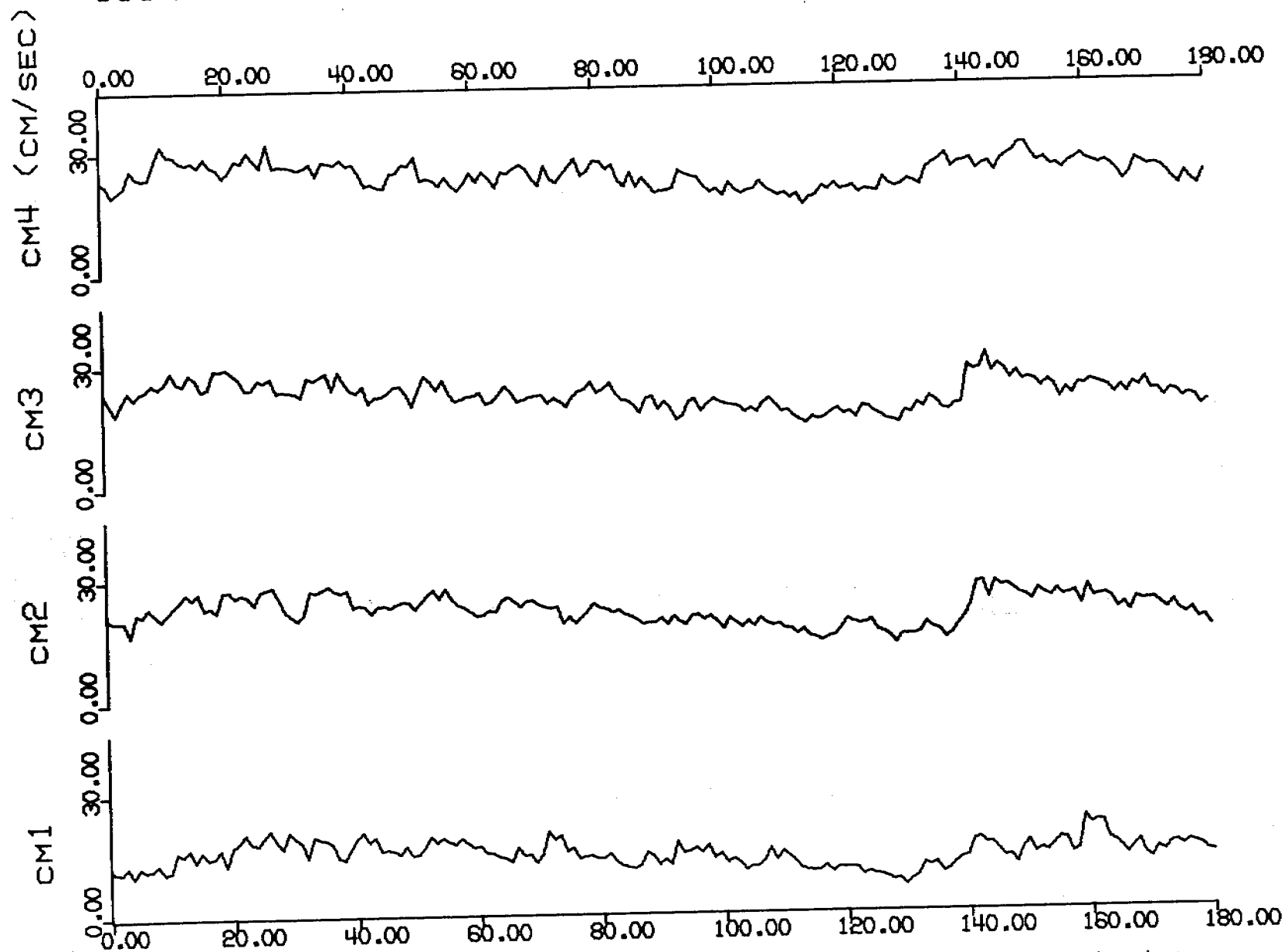


Figure 10b. Burst current speed data taken with the electromagnetic current meters at G2. Sampling rate was 1/second. Distances above sea floor: CM1 at 20 cm, CM2 at 50 cm, CM3 at 70 cm, CM4 at 100 cm.

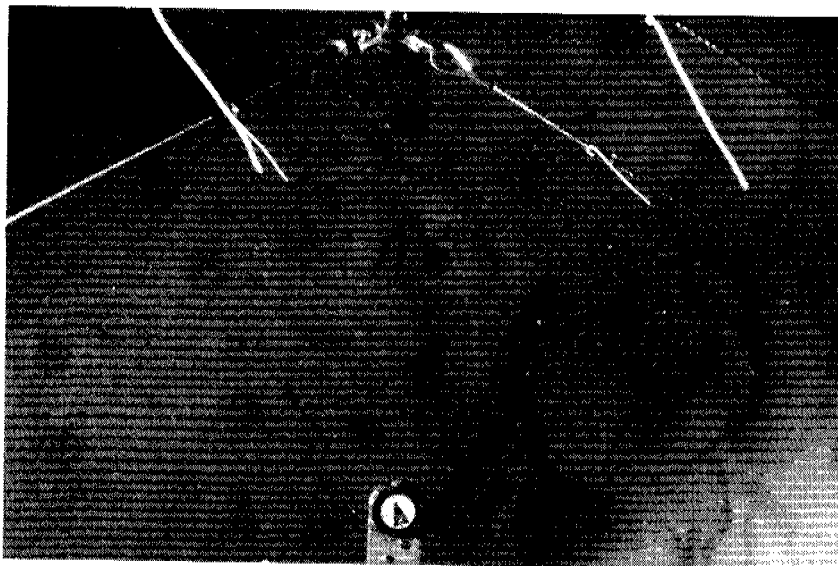
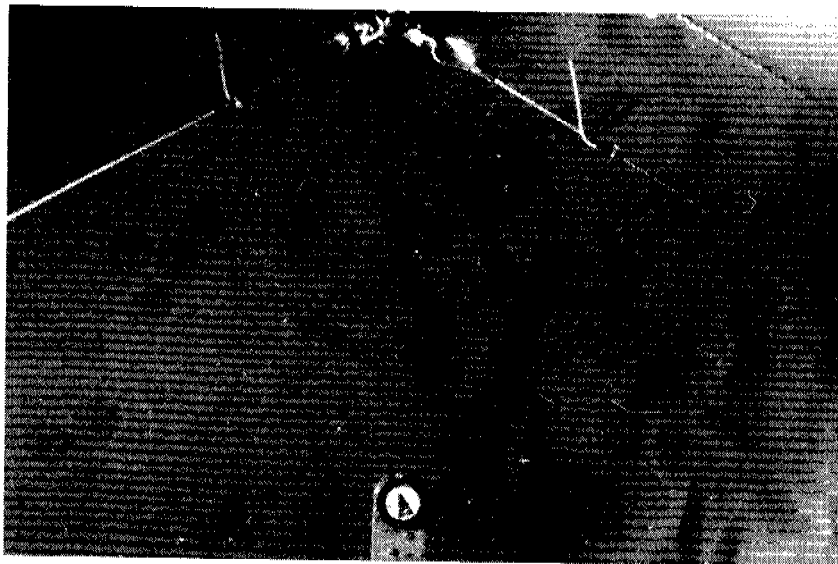


Figure 11a Photographs taken with the 35 mm camera systems on Geoprobe tripod. Flood (upper) and successive ebb (lower) at G1. Compass dial in lower part of photograph is about 7.5 cm in diameter. Nylon strings attached to e-m support cables indicate flow direction.

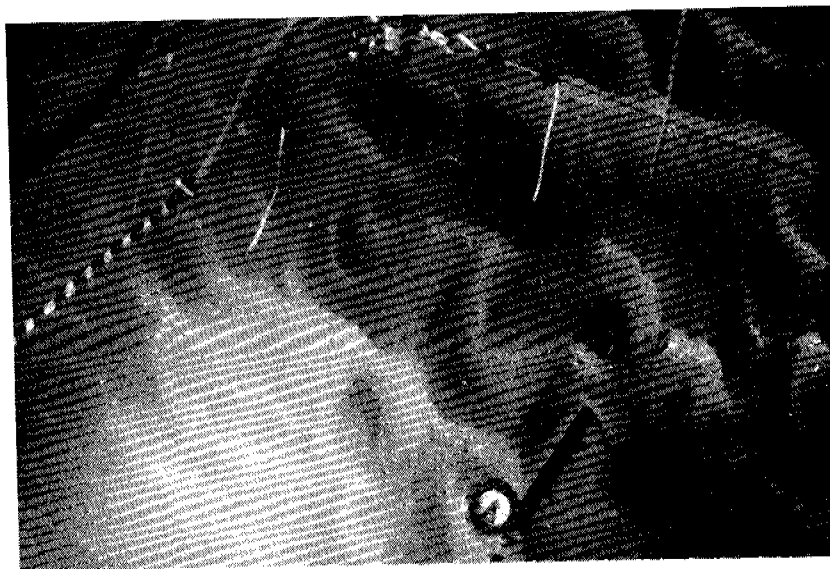
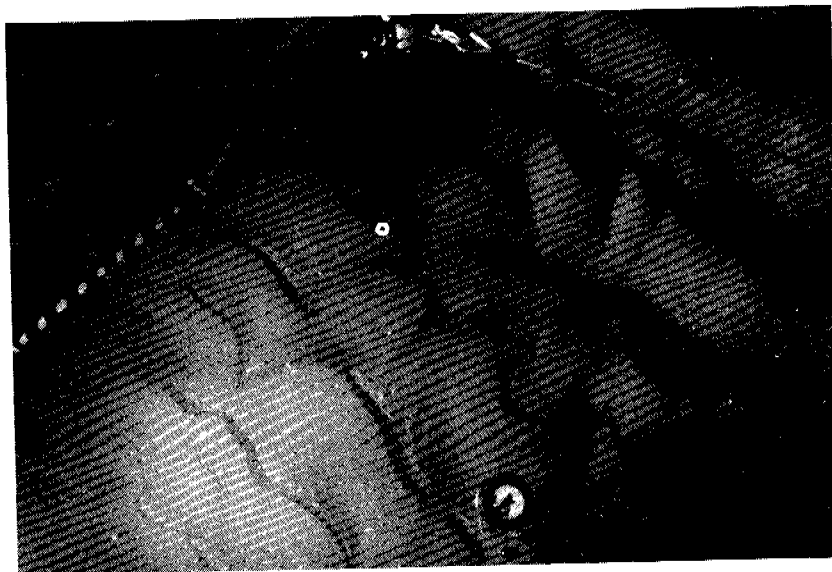


Figure 11b Photographs taken with the 35 mm camera systems on each Geoprobe tripod. Flood (upper) and successive ebb (lower) at G2. Compass dial in lower part of photograph is about 7.5 cm in diameter. Nylon strings attached to e-m support cables indicate flow direction.

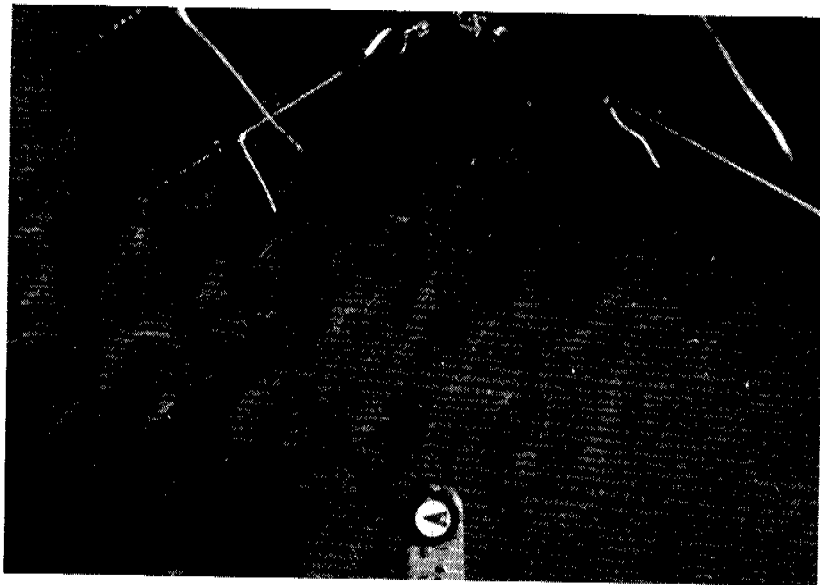
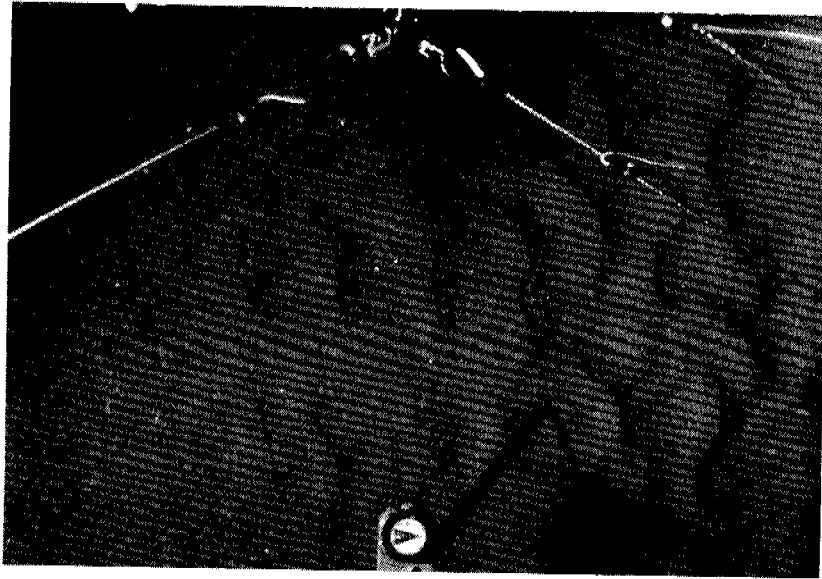


Figure 11c Photographs from G3. Flood (upper) and ebb (lower) sequence.
Compass dial in lower part of photograph is 7.5 cm in diameter.

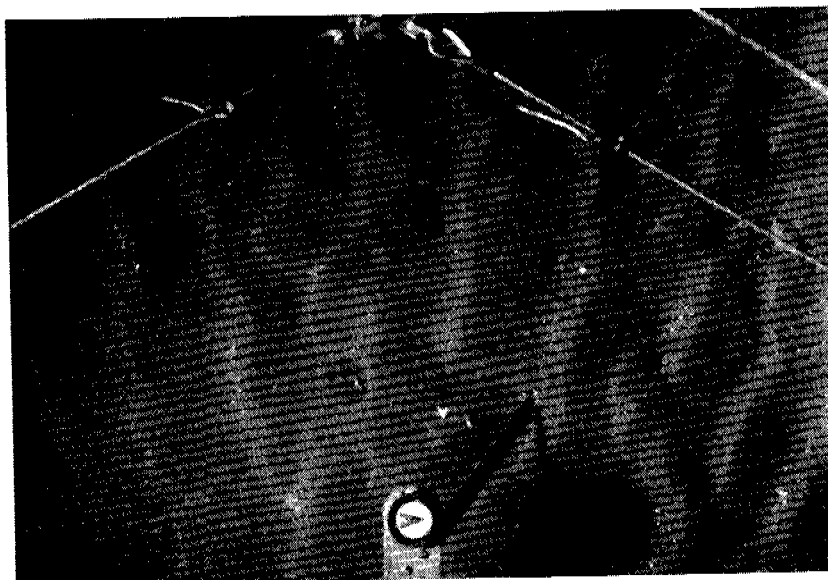
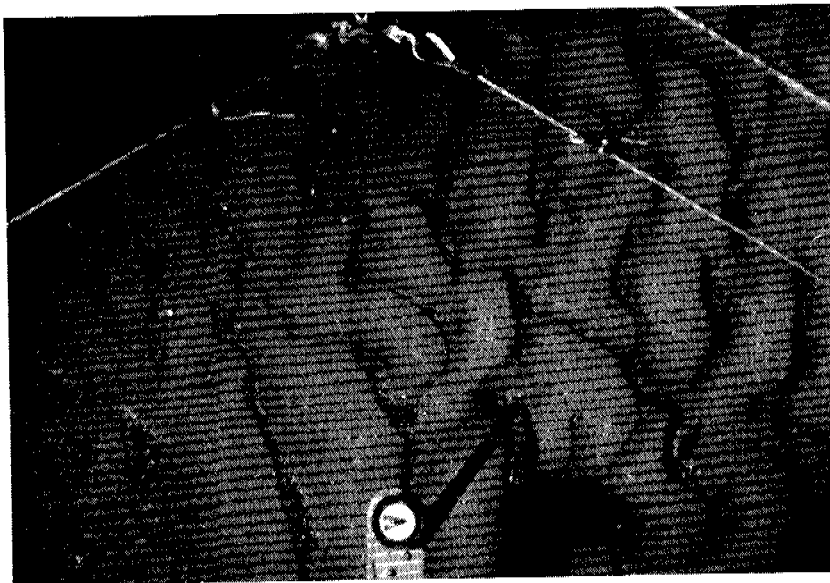


Figure 11d Photographs from G3 taken one month after those in Figure 11c.
Flood (upper) and ebb (lower) sequence.

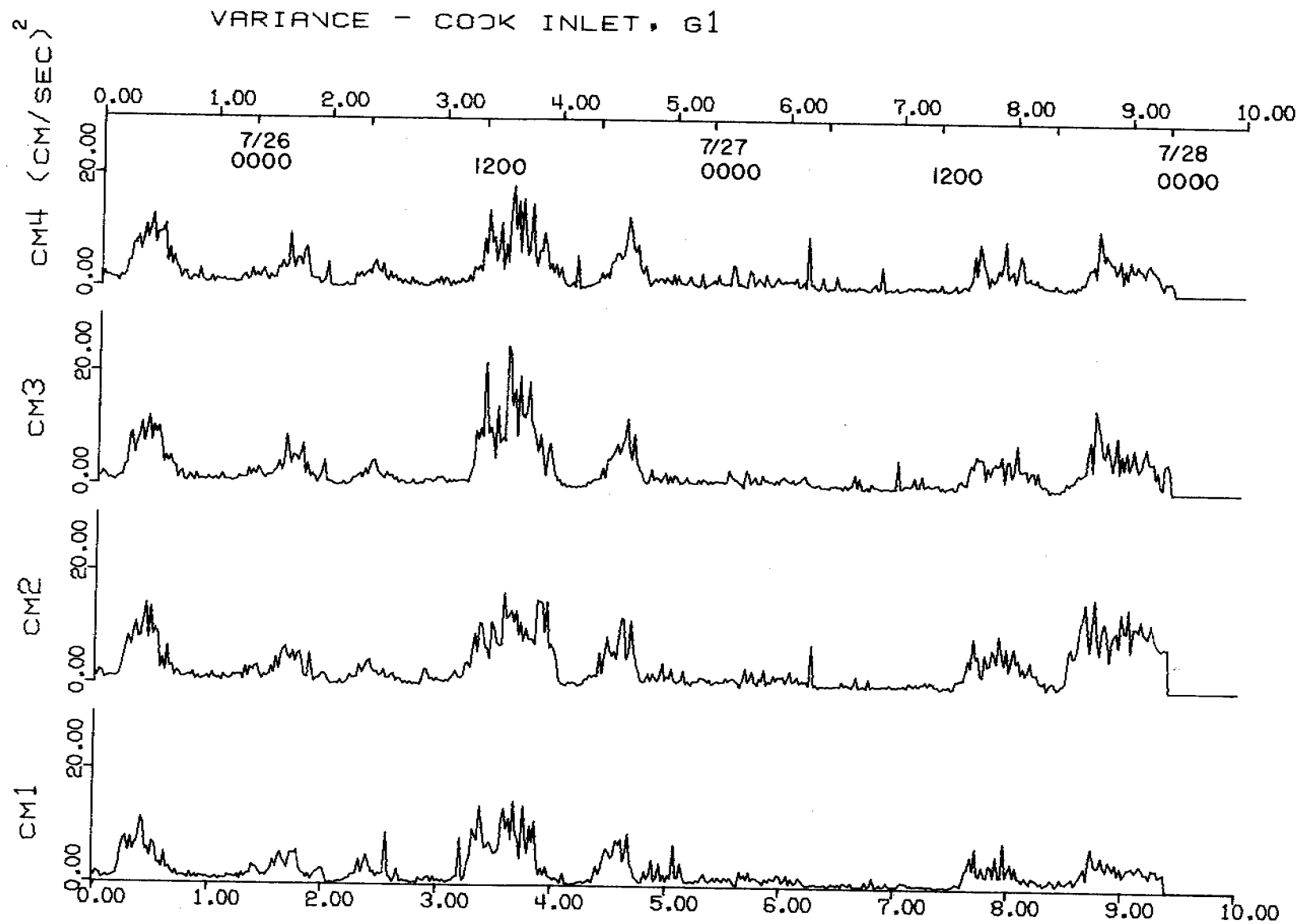
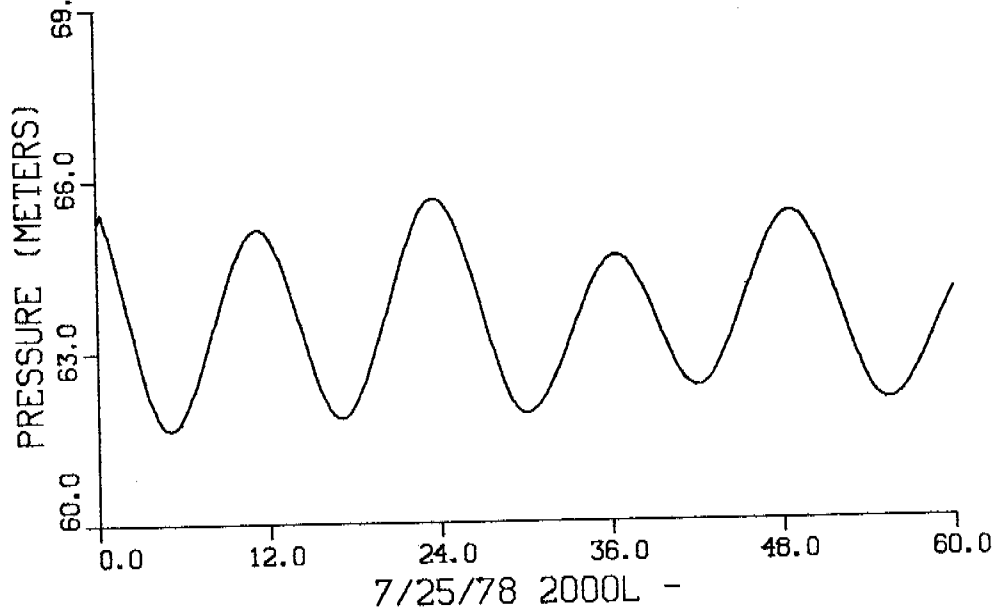


Figure 12. Variance of current speeds at each level for G1. Data taken by electromagnetic current meters at 20 cm (CM1), 50 cm (CM2), 70 cm (CM3), 100 cm (CM4) above sea floor.

HOURLY VALUES OF PRESSURE



HOURLY AVGS OF U-STAR

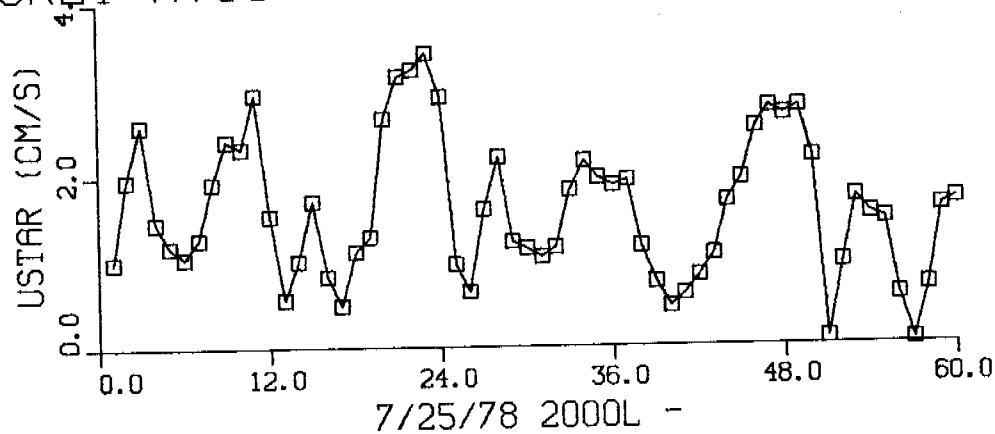


Figure 13. Shear velocity (u_*) in cm/sec and pressure (p) in m of water for G1 data. Time is along horizontal axis in hours. u_* values are hourly-averages.

Appendix A

CRUISE REPORT
OF THE
BRANCH OF MARINE GEOLOGY
U.S. GEOLOGICAL SURVEY, MENLO PARK, CA
FOR
CRUISE -S7-78-WG-

GENERAL CRUISE INFORMATION

AREA: W. GULF OF ALASKA / Lower Cook Inlet Geoprobe sites

SHIP: R/V SEA SOUNDER

CHIEF SCIENTIST(S): Dave Cacchione / Dave Drake

TYPE OF DATA

COLLECTED: GEOPHYSICAL , GEOLOGICAL , HYDROGRAPHIC

CRUISE DATES:	LOCAL DATE/TIME*	TIME (JD/GMT)	PORT
START CRUISE:	24 JUL 9 7 HRS	205/19 7	Leave Seward, AK St Cruz
END CRUISE:	31 JUL 8 10 HRS	212/18 10	End Cruz, Ar Homer, AK

* EXPRESSED IN LOCAL STANDARD TIME.

INITIAL UNDERWAY TIME:	HOURS	DAYS & HOURS
	167	6 DAYS 23 HRS

PERSONNEL LIST

NAME	AFFIL	DUTIES	ABOARD	ASHORE
CACCHIONE, D.		CHIEF SCIENTIST	202/ 0 0	214/ 0 0
DRAKE, D.		CHIEF SCIENTIST	202/ 0 0	214/ 0 0
WIBERG, P.		DAVE CURATOR	202/ 0 0	214/ 0 0
GARDNER, J.		GEOLOGIST	202/ 0 0	214/ 0 0
BOUMA, A.		GEOLOGIST	202/ 0 0	
HAMPTON, M.		GEOLOGIST	202/ 0 0	
PATRICK, R.		ELECTRONICS T	202/ 0 0	
NICHOLSON, J.		ELECTRONICS T	202/ 0 0	214/ 0 0
WILSON, R.		MECHANICAL T		214/ 0 0
TATE, G.		WATCH STANDER	202/ 0 0	214/ 0 0
TOTMAN, C.		WATCH STANDER	202/ 0 0	213/ 0 0
SCHWAB, B.		WATCH STANDER		
CLUKEY, E.		WATCH STANDER	203/ 0 0	214/ 0 0
RAPPAPORT, M.		NAVIGATOR		

MADISON/C.
MADISON/C

NAVIGATOR
NAVIGATOR

205/ 0 0

214/ 0 0

EQUIPMENT SYSTEMS USED

---NAVIGATIONAL---	---GEOPHYSICAL---	---GEOLOGICAL---	---HYDROGRAPHICAL---
	SIDE SCAN SONAR 3.5KH BATHYMETRY 12KH BATHYMETRY SNGL CHANL ARCFR UNIBOOM	TELEVISION SEAFLOOR CAMERA SCUTAR GRAB	GEOPROBE HYD CURRENT METR TRANSMISSOMETER CTD METER VAN DORN BOTTLE TEMP/SALINOMETER

DATA COLLECTED

GEOPHYSICAL

DATA TYPE OR SYSTEM	RECORDING MEDIUM	TRACKLINE KILOMETERS	TRACKLINE N. MILES	RECORDING TIME(HRS)	ROLL REEL LIST-RIJ
SNGL CHANL ARCFR	ANL PAPER ROLL	57.2	30.9	4.3	1
UNIBOOM	ANL PAPER ROLL	82.2	44.4	7.3	1
SIDE SCAN SONAR	ANL PAPER ROLL	281.7	152.1	37.6	7
3.5KH BATHYMETRY	ANL PAPER ROLL	172.1	92.9	19.8	2
12KH BATHYMETRY	ANL PAPER ROLL	517.8	279.6	83.5	7

GEOLOGICAL/HYDROLOGICAL SAMPLES

SAMPLING DEVICE	SAMPLING ATTEMPTS	SAMPLES RECOVERED	NUMBER OF SAMPLES FROM A GIVEN WATER DEPTH INTERVAL		
			0-1003	100-30003	>30003
GRAVITY CORE	1	1	0	1	0
VAN VEEN GRAB	1	0	0	0	0
SCUTAR GRAB	5	5	5	0	0
VAN DORN BOTTLE	20	20	20	0	0
	-----	-----	-----	-----	-----
TOTALS	27	26	25	1	0

GEOLOGICAL/HYDROLOGICAL (ANALOG)

DATA TYPE ---OR-SYSTEM---	RECORDING ----MEDIUM----	RECORDING TIME(HRS)	NUMBER OF TAPES, ROLLS,LISIS,EIC.
TELEVISION	ANLOG MAG TAPE	7.2	7
SEAFLOOR CAMERA	PHOTOGRAPH	5.2	14

NUMERICAL OBSERVATION

DATA TYPE ---OR-SYSTEM---	NUMBER OF READINGS	TAKEN OVER HOW MANY STATIONS
HYD CURRENT METR	22	6

OPERATIONS INFORMATION

STATION DATA STATIONS OCCUPIED: 8, TOTAL TIME ON STATION: 64.7 HRS,
 TRACKLINES TRACKLINES RUN: 37, TOTAL TRACKLINE TIME: 60.6 HRS,
 CUMULATIVE TRACKLINE DISTANCE: 655.1 KM / 353.7 N. MILES

DEPLOYMENTS

GEOPROBE 4 / CTD METER 23 / TRANSMISSOMETER 20

Annual Report
April 1, 1978 - April 1, 1979
Research Unit #435

MODELING OF TIDES AND CIRCULATIONS OF THE BERING SEA

National Oceanic and Atmospheric Administration

J. J. Leendertse and S. K. Liu, Principal Investigators
The Rand Corporation
Santa Monica, CA

April 1, 1979

MODELING OF TIDES AND CIRCULATIONS OF THE BERING SEA

J. J. Leendertse and S. K. Liu

During the reporting period our effort has been in carrying out modeling investigations for the Bristol Bay - St. George Basin area and for Norton Sound (Fig. 1). For the first study area, we have completed the final prediction and verification run of the three-dimensional turbulent energy model and are preparing a report describing the setup, adjustment and verification of this model (Ref. 1).

BRISTOL BAY INVESTIGATION AREA

After the model's adjustment phase, which was reported in the previous progress report, the period between 16-19 July 1976 was selected for verifying the predictability of the model and the establishment of a set of predictive parameters.

During the model's verification period, observed currents at four locations have been compared to the computed values, located nearest to those current meter deployments. Details of the comparison and analysis are presented in our final report (Ref. 1). To demonstrate the model's predictability, comparisons made at four stations are presented in Figs. 2 through 5. Figure 2 contains four graphs. Graph A gives the water level at grid point (14,14) from dynamic computation. Graph B illustrates the computed east/west current components at four depths at this grid location, plotted together with the hourly observed east/west current component at station BC-2 (see insert map) measured at a 20-meter depth. Graph C gives similar comparisons, but for the north/south velocity components. These computed values agree quite well with the reported average values. Some uncertainties still exist. These uncertainties include the true horizontal location of the station. Depth values in the model are schematized according to the published navigation chart, which may not represent the true local depth. Local depth of the mixed layer may also be slightly different from the modeled value. Finally, the predicted water level at the model's open boundary also contains certain random and systematic errors which would affect the computed results. Graph D contains six curves representing the computed vertical velocity components at six selected layers. The vertical velocity of these layers not only reveals tide-induced vertical displacements, but also contains instabilities induced by the vertical stratification. The dynamic behavior of each layer is closely related to the local vertical densimetric Froude number and the Brunt-Väisälä frequency. A more detailed discussion on the vertical dynamic behavior is presented in Ref. 1. Figure 3 gives similar comparison graphs for station BC-5. In this figure, the currents are plotted as magnitudes and direction. The computed currents in the lower layers agree quite well with the observed values, whereas surface currents are in general higher than the computed magnitudes--particularly at their maximum range. The predicted current directions are excellent (Graph C). Some of the

underestimates in the surface currents at this particular location may be traced to the low turbulent energy content. This is indicated by the dichotomic velocity distribution in the vertical (Graph D). Notice the lack of vertical velocity gradients in the bottom layers as compared to the similar graph in Fig. 2.

The next figure (4) represents the comparison at station BC-14, which is located very close to the Alaskan Peninsula. The computed currents agree well with the observed values, particularly for the east-west component. The vertical motions due to wind and tides increase the turbulence intensity close to the southern boundary and the salinity and temperature distributions are nearly homogeneous. Vertical displacements are very large, resulting in a vertically near-homogeneous structure.

Good agreement is also found at station BC-15 (Fig. 5). This station is shallower than the previous three stations. Vertical displacements of water columns show pronounced instabilities (Graph D), yet the magnitude is only about one-third of that at station BC-14.

In the simulation, the computed vertical velocity component also gives a convenient indication of the vertical displacement by means of frequency-domain analysis. To illustrate the vertical instabilities, we analyzed the vertical velocity component for selected layers at several locations by the spectral method. For example, in the surface layer at station BC-2, the computed vertical velocity component contains not only tide-generated vertical displacements, but also oscillations induced by the stratification effect (Fig. 6). These spectra all possess a similar shape; they fall approximately as f^{-2} at the lower frequencies and then flatten out to around f^{-1} above 0.5 cycles per hour. This characteristic shape agrees with the observed spectra of the first mode internal waves (Ref. 2).

The tidal propagation within the modeled area may be illustrated by a set of three-dimensional plots from the results of the hydrodynamic computation. A period of 12 hours of the verification period, from 0200 hour to 1400 hour June 18, 1976, is selected to demonstrate the movement of the water surface in the modeled area. Figure 7 illustrates the rising and falling of the water surfaces in the modeled area at three-hour intervals as they would be seen by a spectator looking from the north toward the Alaska Peninsula. Higher tidal harmonics superimposed on the principal lunar and solar components are also evident. It should be pointed out that the result would be different if the computation were to be carried out assuming a homogeneous density structure. This is due primarily to the different vertical shear structures induced by the vertical density gradient and the modification of the horizontal pressure gradient caused by the variations in the horizontal density distribution.

The computed co-tidal charts for the diurnal and semidiurnal components are presented in Figs. 8 and 9. These results are derived from 51 hours of computed results by means of 2-D Fourier transformation.

They are compared to the observed charts for the K1 and M2 components derived from long-term data compiled by NOAA. Both the phase and the location of amphidromic points agree well with the observed chart. It seems our bottom friction coefficient is still somewhat on the high side.

During the course of modeling Bristol Bay, the following conclusions have been reached:

1. Bristol Bay is primarily a tide- and wind-driven system with distinctive nonhomogeneous hydrodynamic behavior. Therefore a three-dimensional model is required to characterize its response to these driving forces.
2. Vertical resolution is essential for good representation of the vertical fine structures.
3. The bay system is not very dissipative. Because of the three-dimensional representation, where interlayer stress interacts with local density gradient and turbulence level, the required bottom stress coefficient is much smaller than that required in shallow estuaries.
4. The model's boundary is selected in a location which is not sensitive to the general wind setup in the Bering Sea as a whole. Due to this consideration, the predicted water level at the open boundary which drives the model requires no further wind adjustment for the prediction of current field in the modeled area.
5. To model the nonhomogeneous structure of the bay, the computation of subgridscale turbulent energy is necessary for a good representation of the vertical dynamic behavior. This approach also enables us to reduce from a large number of temporal-spatial varying diffusion coefficients to a few closure constants by which the model is adjusted. Therefore these adjusted closure constants represent a set of efficient predictors of the system's behavior under future conditions.
6. The computed current field from predicted tides at the open boundary agrees very well with the observed values in the modeled area.
7. Because of the sensitive interactions between density gradient, vertical shear structure and the vertical momentum exchange processes, it is very difficult to separate the wind and tide effects on the circulation. As a consequence, accuracy in tidal current prediction is a prerequisite in predicting surface drift and the pathways of pollutant discharges.
8. The model developed in the study forms a good basis for establishing a predicting method for response of the Bristol Bay system under forces induced by wind, tide and local density variations.

MODELING OF ICE MOVEMENT AND OIL SPILL TRAJECTORY SIMULATION

An ice movement model has recently been added to the basic three-dimensional model. The computational scheme and coding for machine computation has been completed. The code is presently being tested under various hypothetical conditions. Preliminary results indicate that the computational scheme is workable. Further tests will be performed using Norton Sound as soon as boundary data becomes available. The tidal data collected in October 1978 is being analyzed at PMEL.

For oil-spill trajectory simulation, extensive computation and graphic programs are under development. In order to provide wind input for the simulation, weather statistics from the Norton Sound area are being analyzed. A suitable method will be selected for generating random wind fields according to the local weather statistics. Trade-offs between several possible methods are being studied at the present time.

References

1. *A Three-Dimensional Model for Estuaries and Coastal Seas: Vol. VI, Bristol Bay Simulation*, S. K. Liu and J. J. Leendertse, The Rand Corporation, R-2405-NOAA, April 1979 (in preparation).
2. Gordon, R. L., "Internal Wave Climate Near the Coast of Northwest Africa During JOINT-1," *Deep-Sea Research*, Vol. 25, 1978, pp. 625-643.

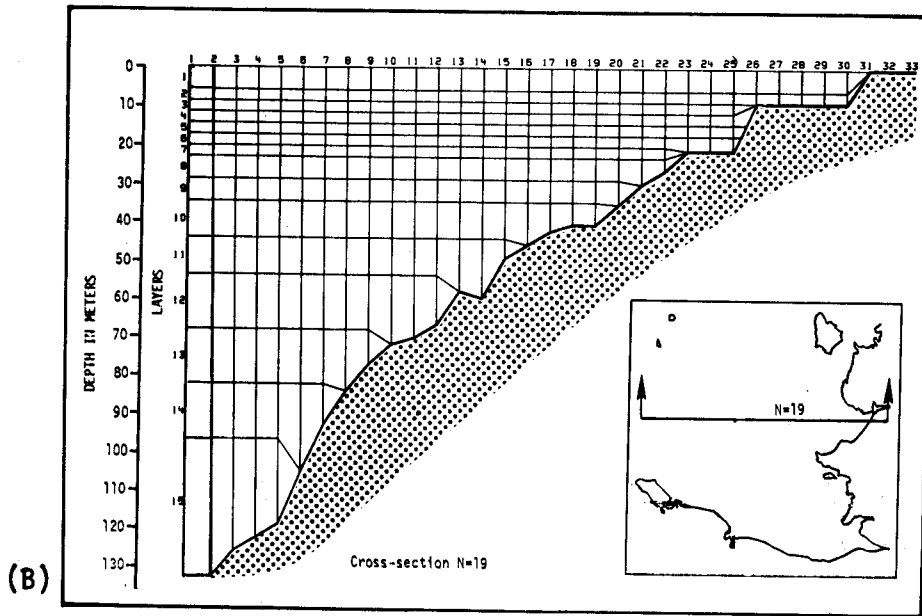
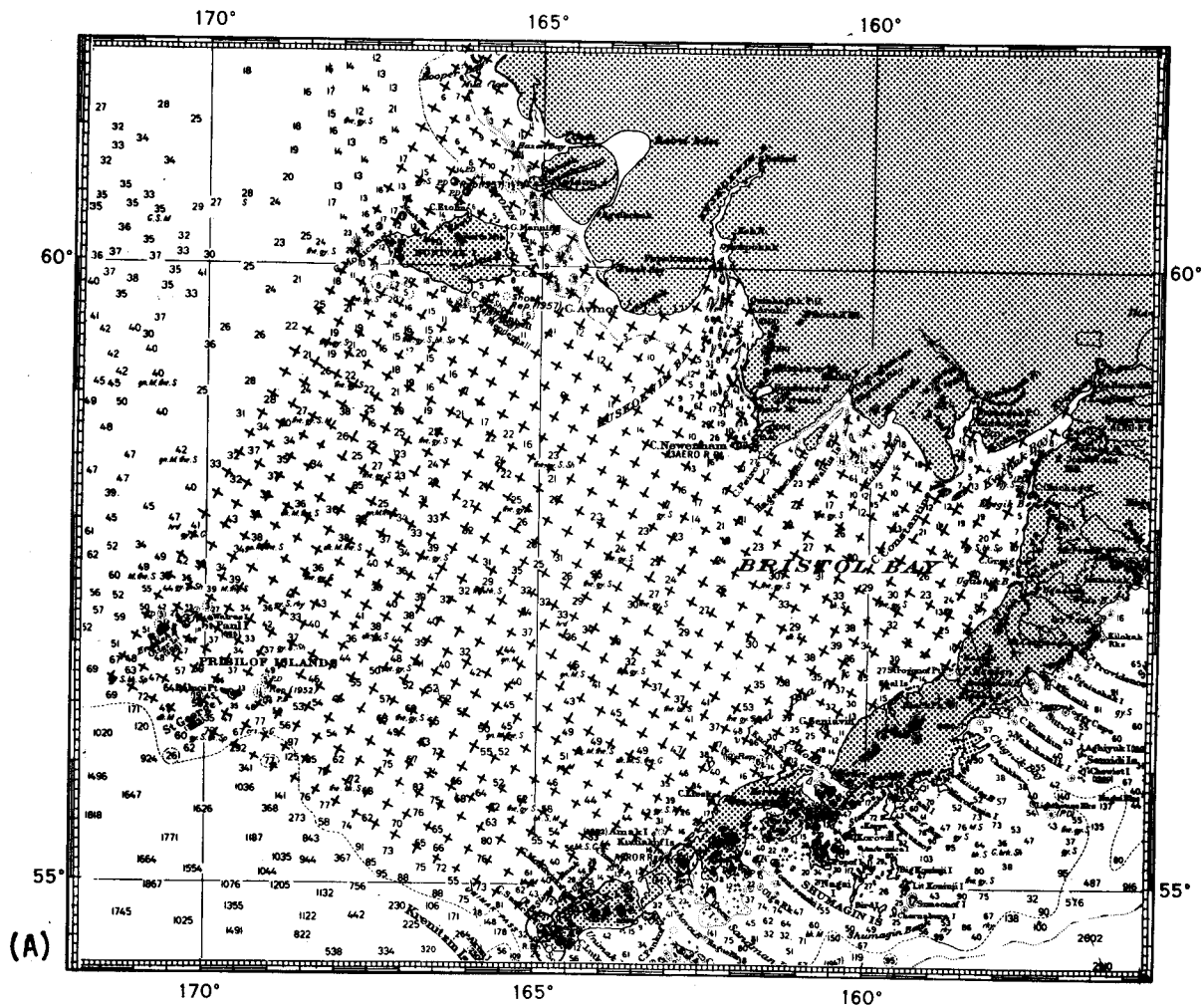


Fig. 1--Horizontal (A) and vertical (B) distribution of grid dimensions, showing the arrangement of layer thickness in the Bristol Bay model, as illustrated by the cross-section through Kuskokwim Bay (N=19).

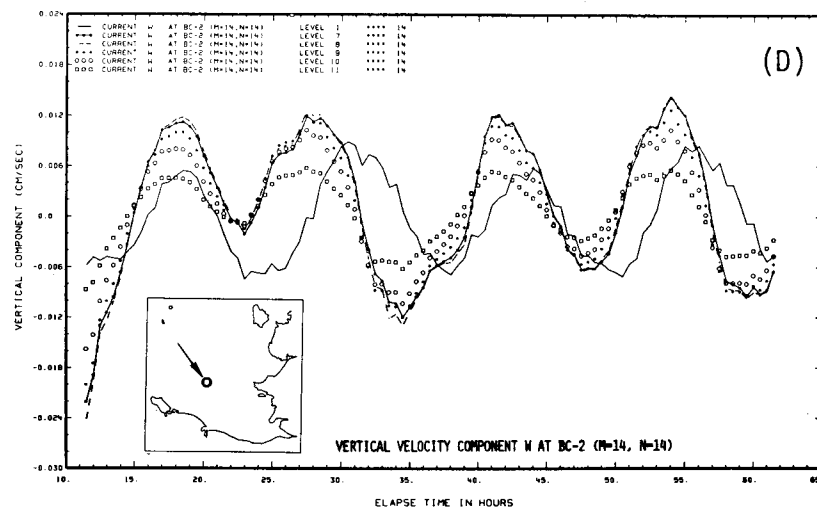
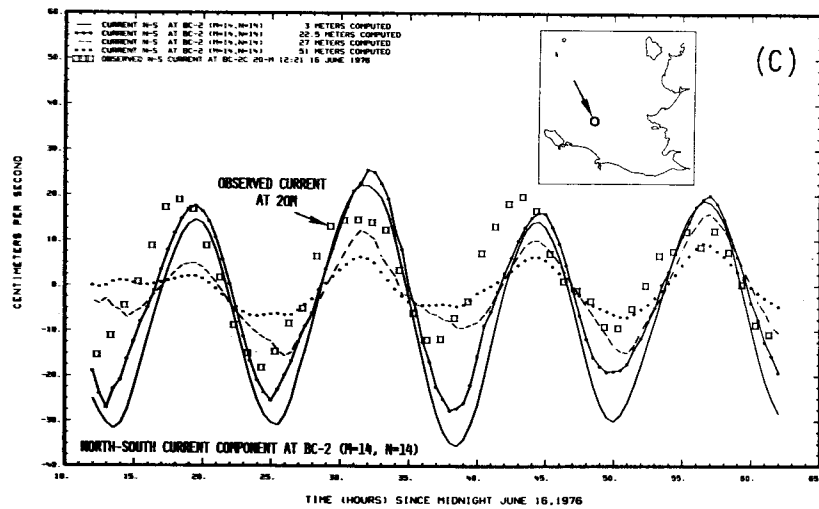
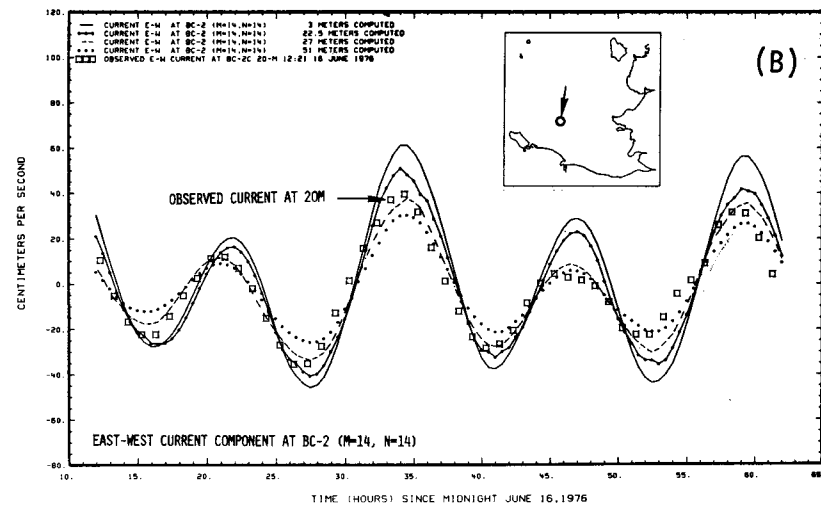
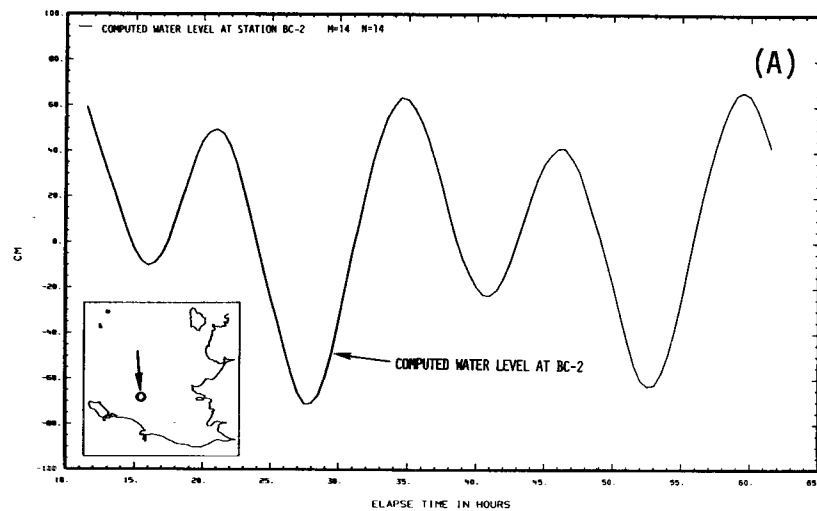


Fig. 2 -- Comparison between the computed and the observed current component at a given location (B and C) together with the local water level (A) and vertical velocity component at six selected levels (D) during the period 0000 16 June through 1400 18 June 1976.

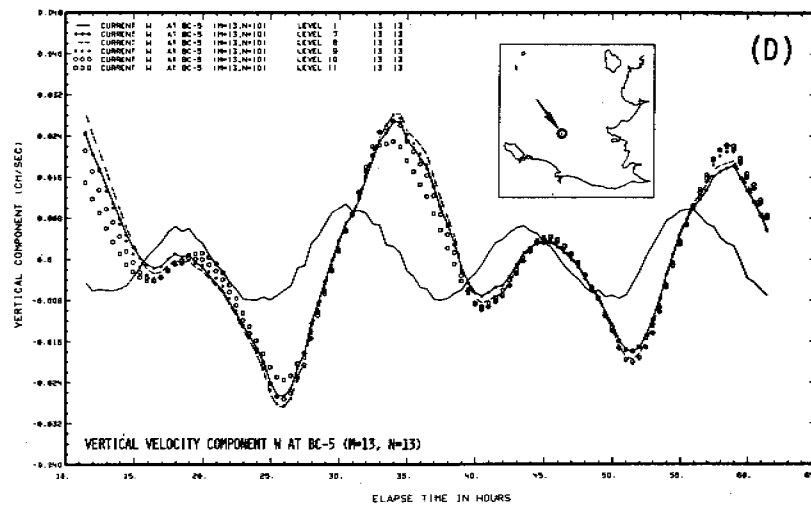
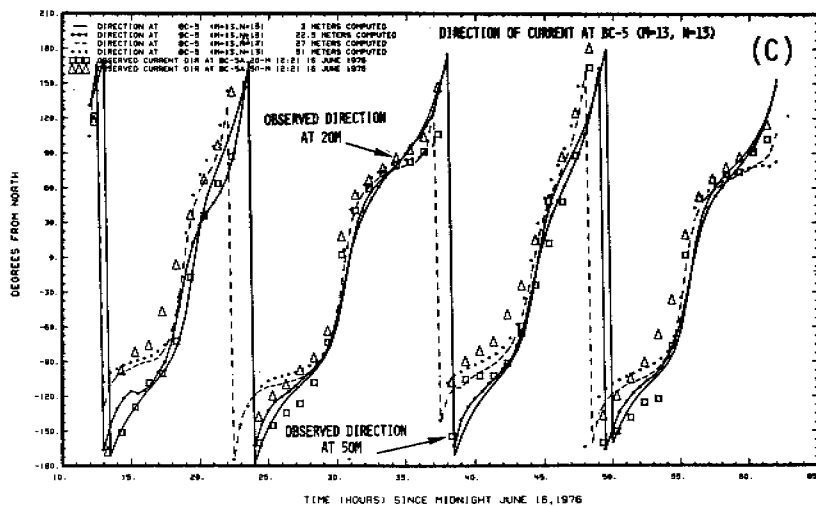
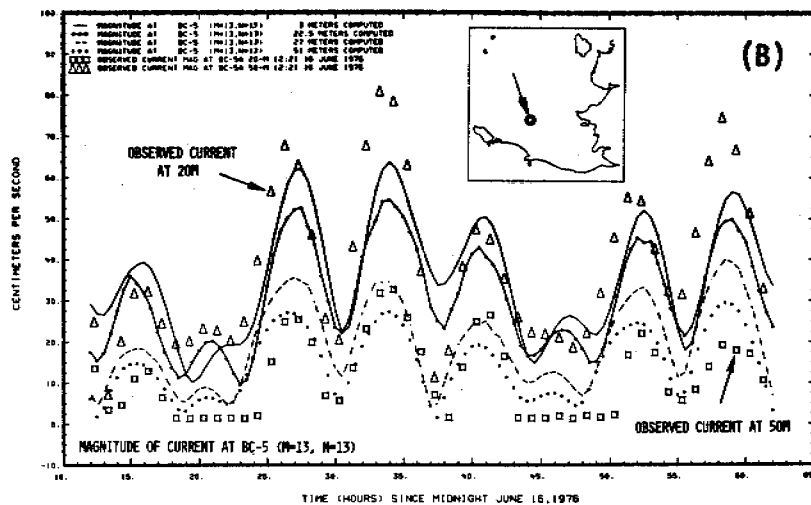
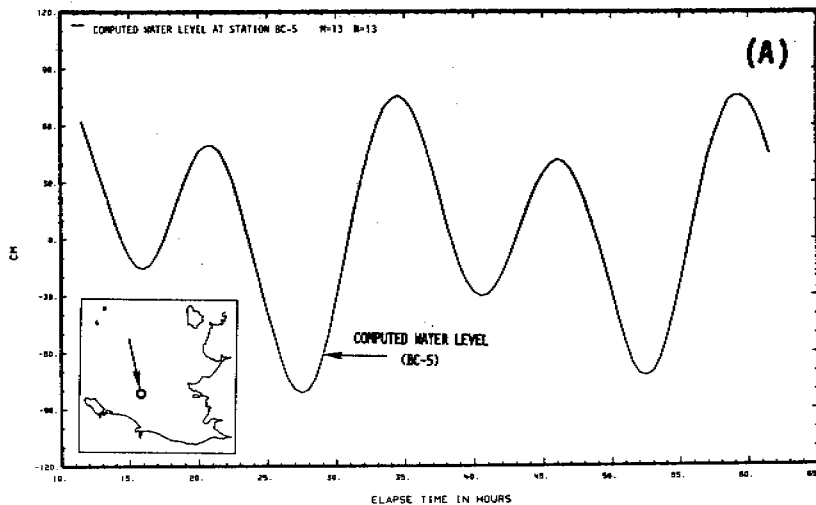


Fig. 3 --Comparison between the computed and the observed current speed and direction (B and C) together with the local water level (A) and vertical velocity component at six selected levels (D) during the period 0000 16 June through 1400 18 June 1976

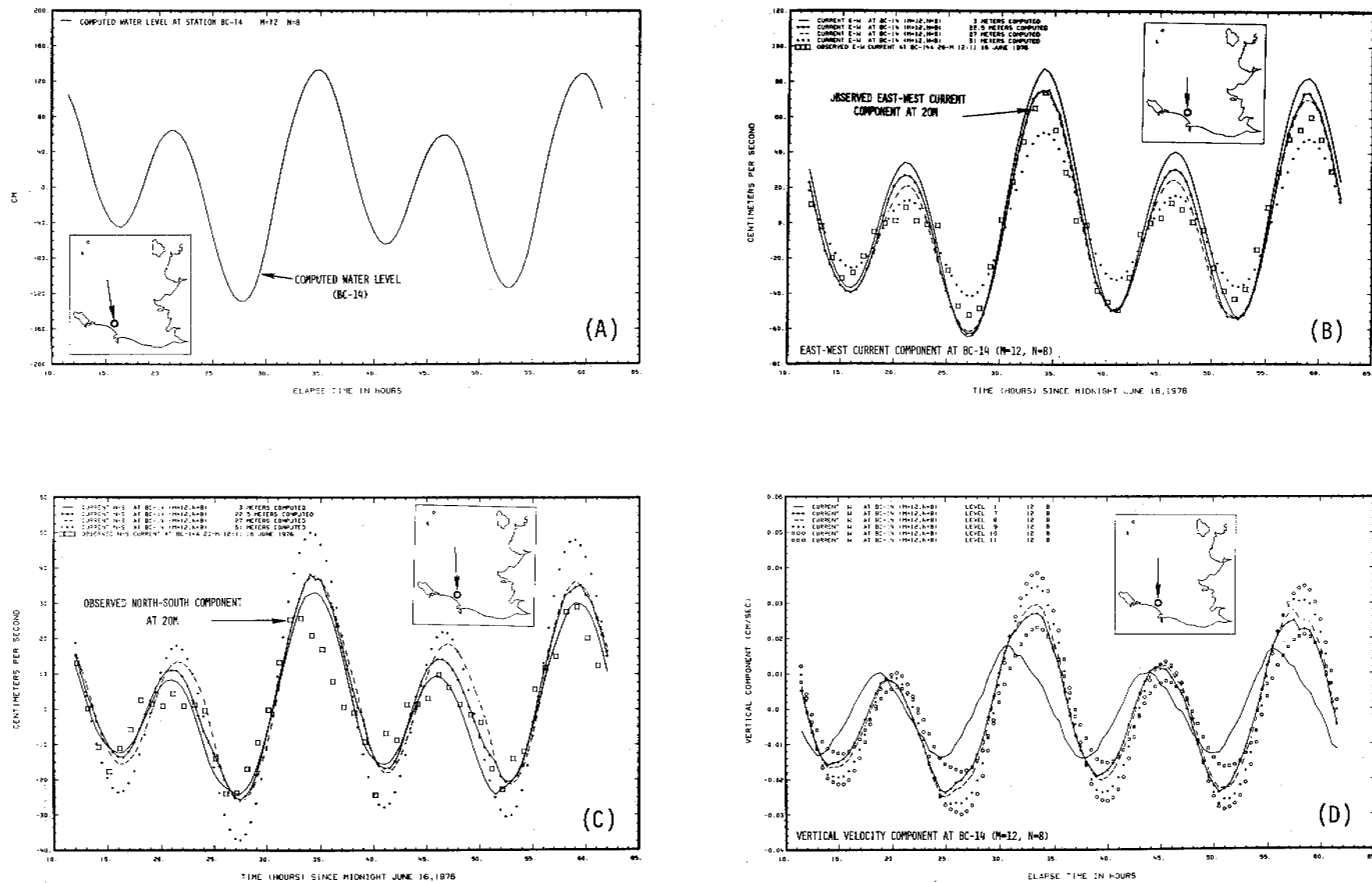


Fig. 4 -- Comparison between the computed and the observed current components at a given location (B and C) together with the local water level (A) and vertical velocity component at six selected levels (D) during the period 0000 hr 16 June through 1400 18 June 1976.

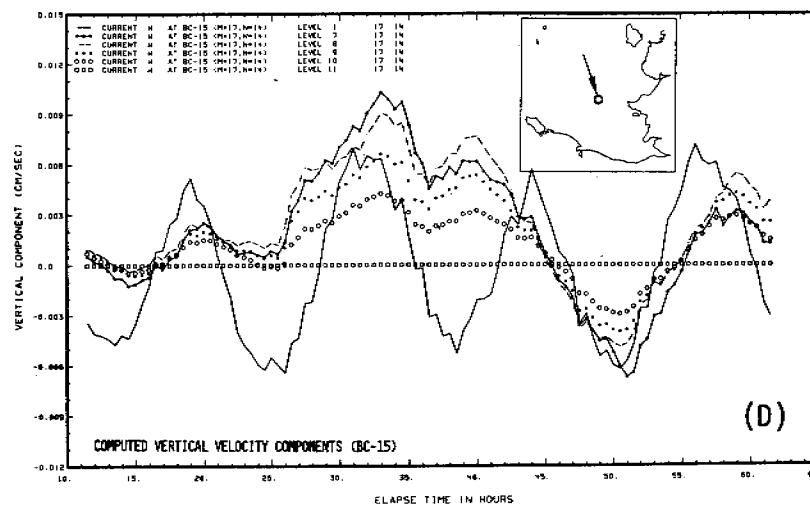
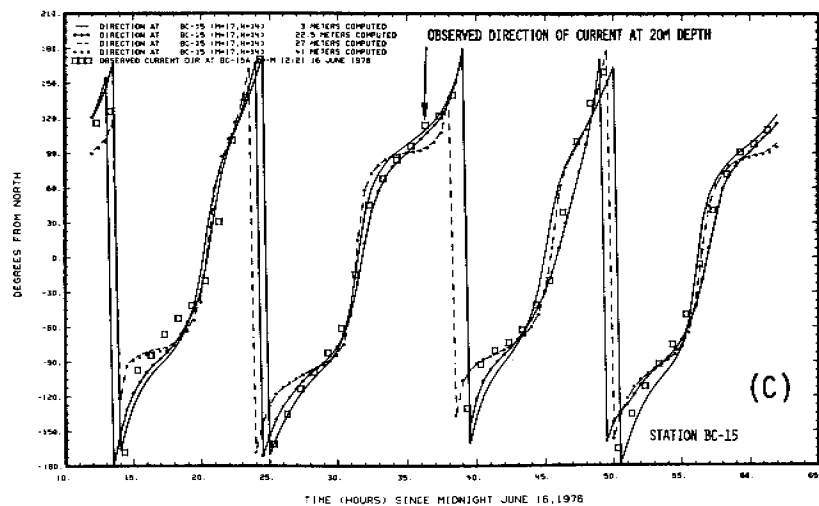
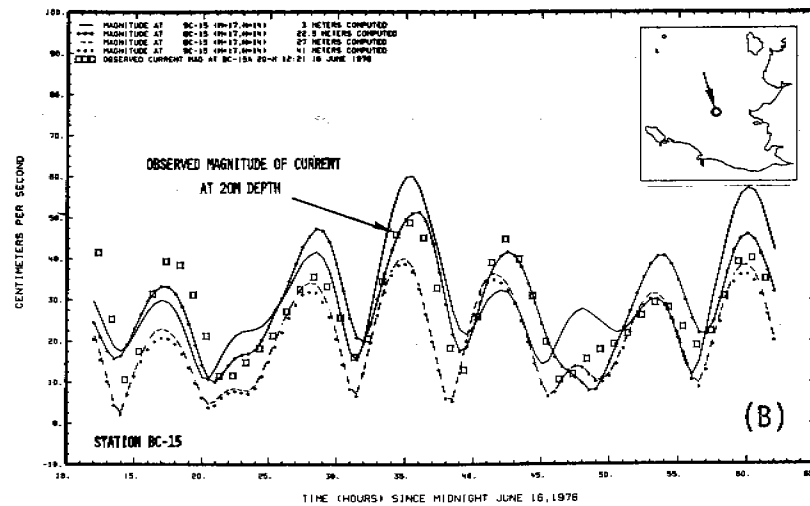
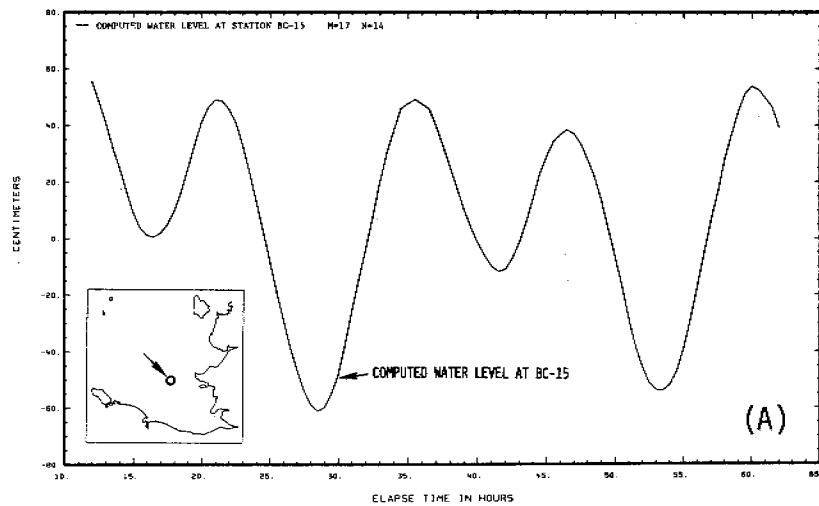


Fig. 5--Comparison between the computed and the observed current speed and direction (B and C) together with the local water level (A) and vertical velocity component at six selected levels (D) during the period 0000 16 June through 1400 18 June 1976.

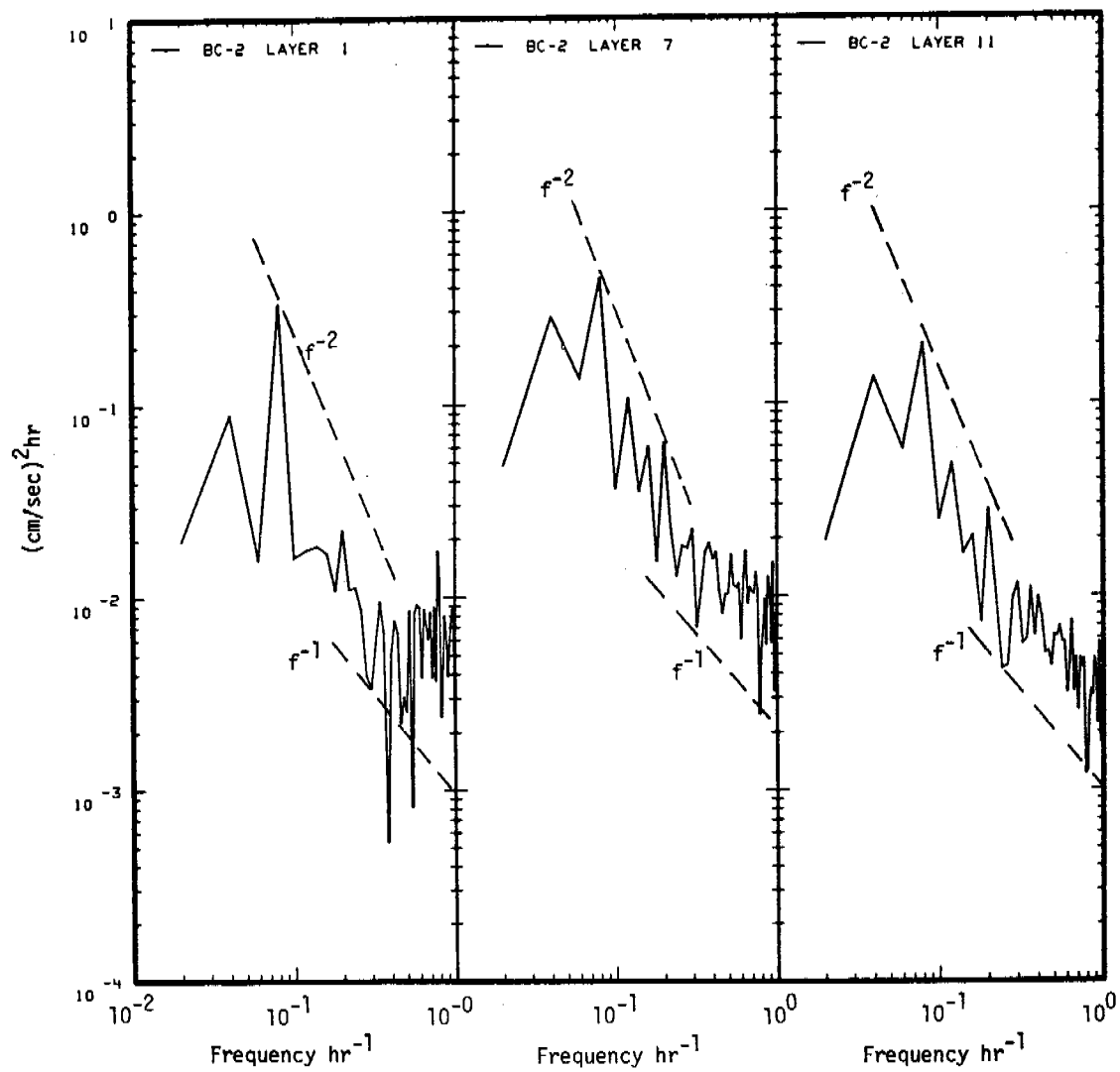
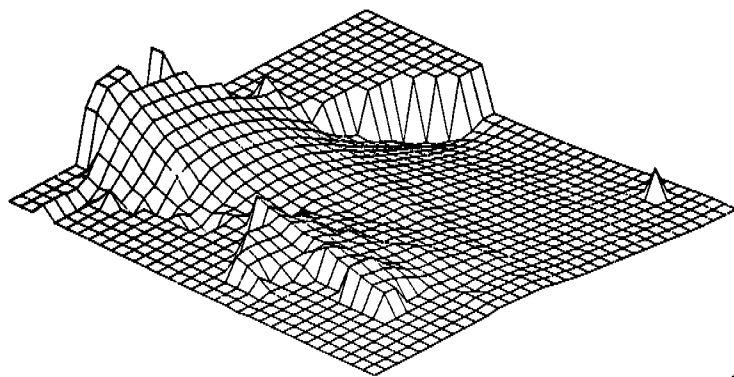
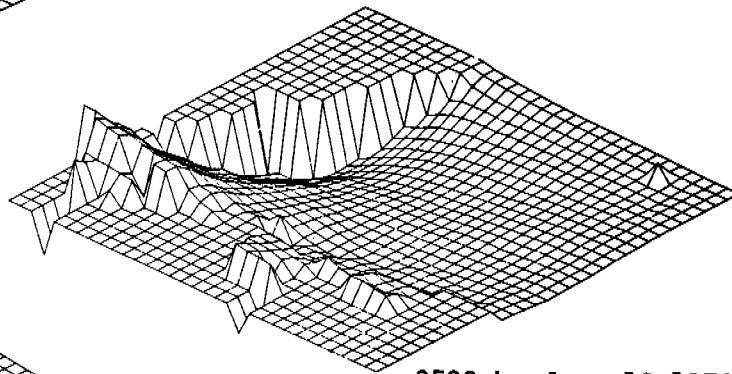


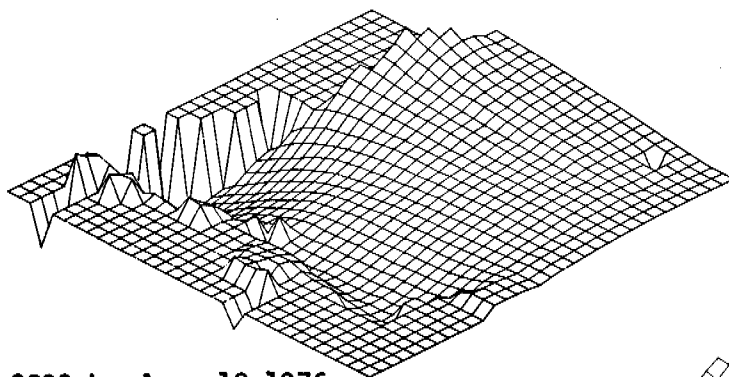
Fig. 6 --The spectra of vertical displacements in three layers (surface, within pycnocline and near bottom) at station BC-2. The slope falls approximately as f^{-2} at the lower frequencies and then flattens out to f^{-1} .



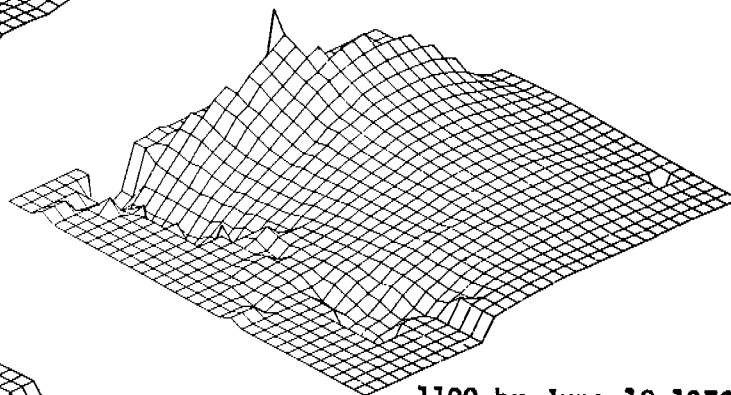
0200 hr June 18 1976



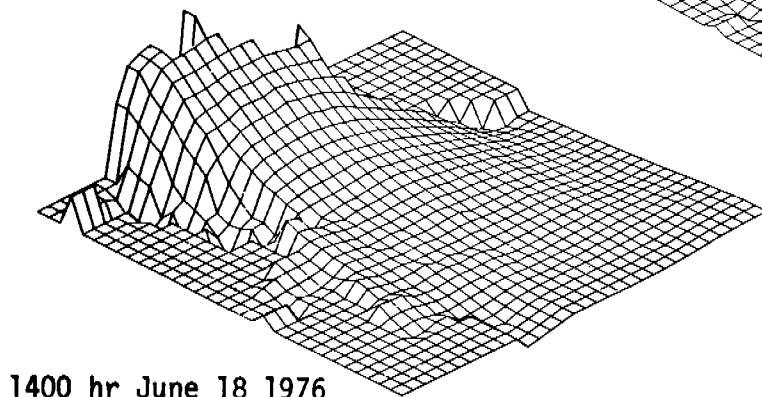
0500 hr June 18 1976



0800 hr June 18 1976



1100 hr June 18 1976



1400 hr June 18 1976

Fig. 7 --Three-dimensional plots of the computed water surface movement in the modeled area during a 12-hour period in the verification run. Higher tidal harmonics superimposed on the principal lunar and solar components are evident.

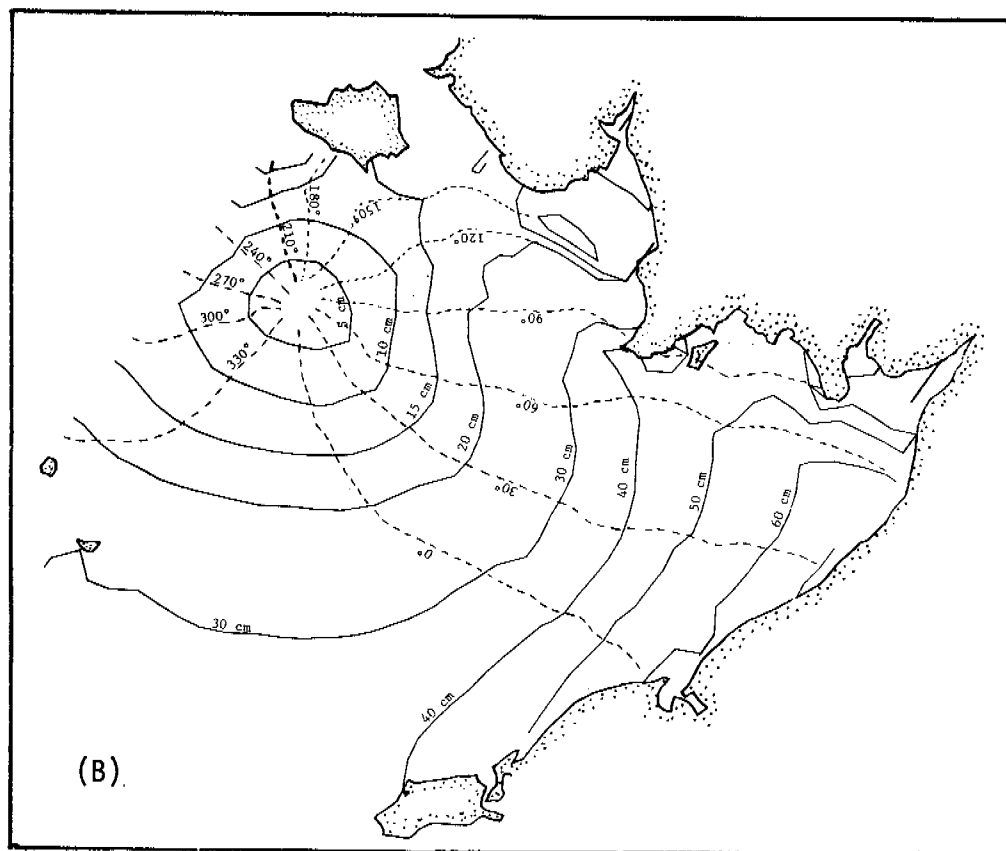
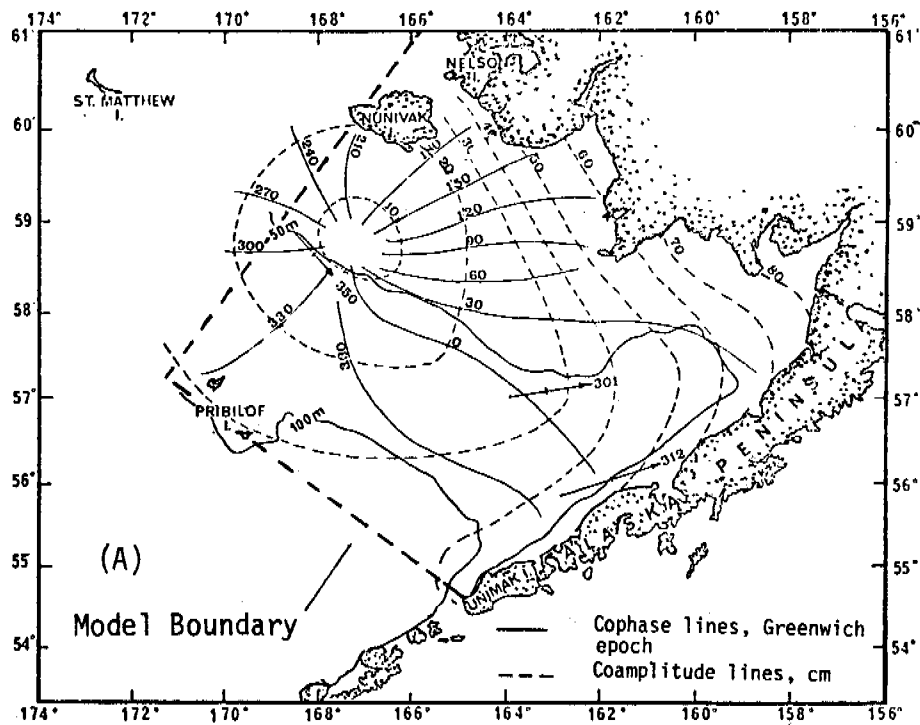


Fig. 8 --Comparison between the computed (B) amplitude and phase of the diurnal tide and a similar chart (A) derived from field data as compiled by the Pacific Marine Environmental Laboratory, National Oceanic and Atmospheric Administration

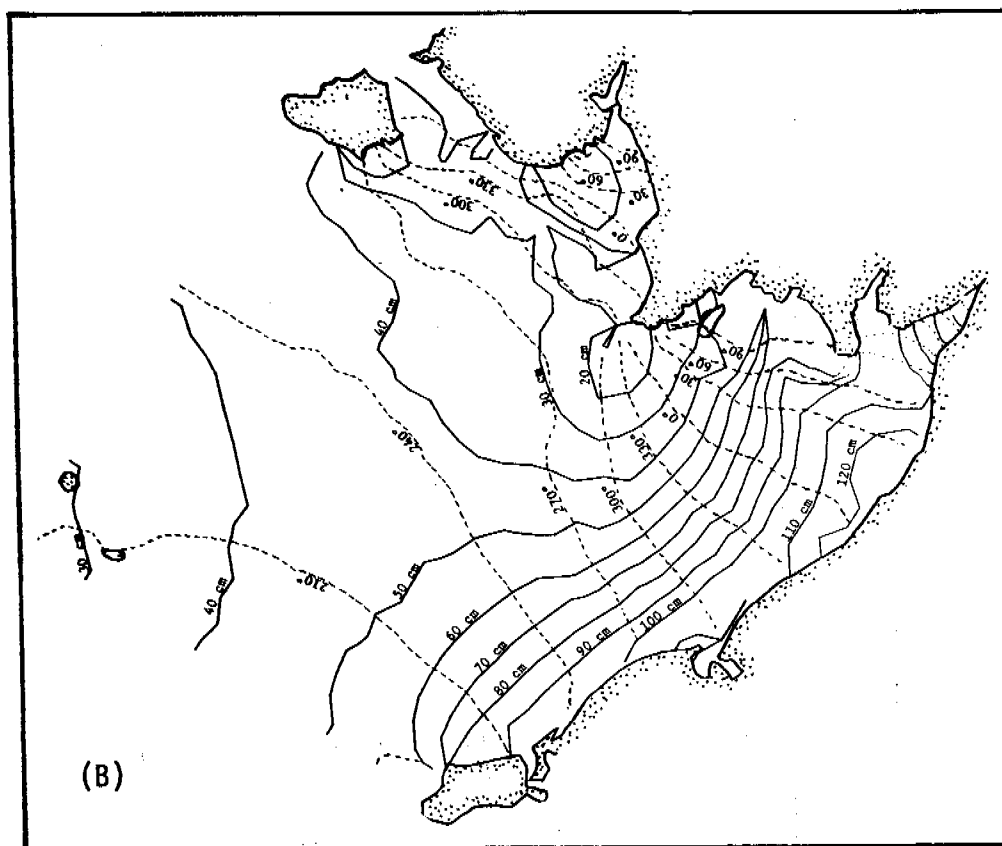
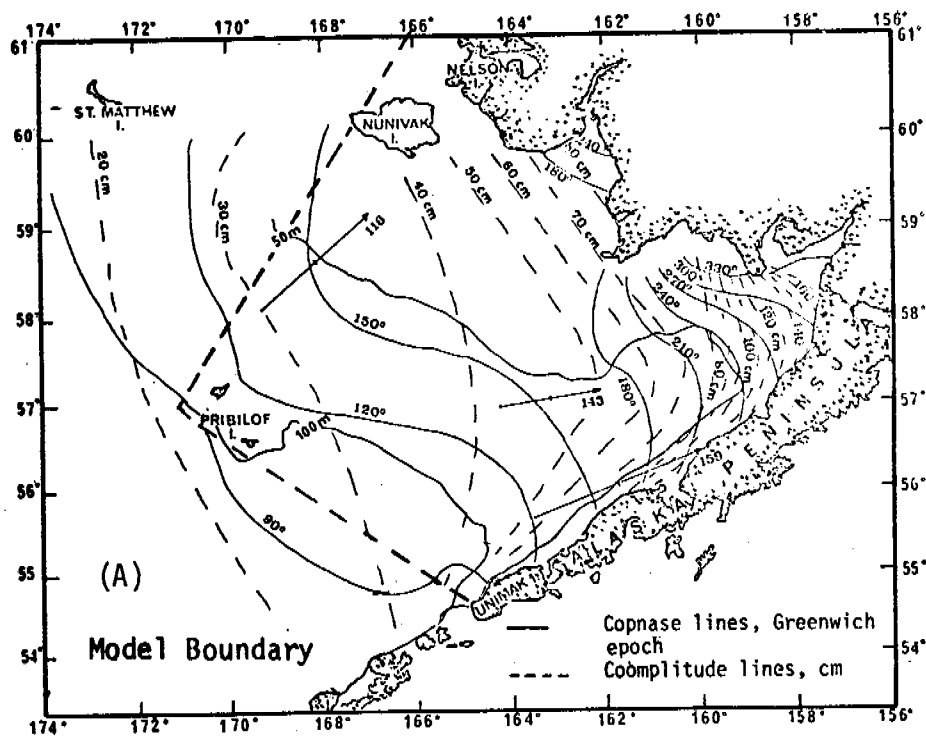


Fig. 9 --Comparison between the computed (B) amplitude and phase of the semidiurnal tide and a similar chart (A) derived from field data as compiled by the Pacific Marine Environmental Laboratory, National Oceanic and Atmospheric Administration. The observed chart does not show an amphidromic point at the cape west of Togiak Bay, as no data collection station was available.

MAINE & COASTAL HABITAT MANAGEMENT
ALASKA DEPT. OF FISH & GAME
333 Raspberry Road
Anchorage, Alaska 99502

MAINE
U.S.
ALASKA
1997

ADF&G HABITAT LIBRARY



3234500066325